

THE MONSOON TROUGH BOUNDARY LAYER

Edited by

R NARASIMHA
D R SIKKA
A PRABHU

INDIAN ACADEMY OF SCIENCES
BANGALORE

Special Issues of the Academy:
Earth and Planetary Sciences

	Title	Guest Editor	Price	
			India Rs.	Abroad US \$
1.	Seismology in India	J. N. Brune	100	25
2.	Experimental Petrology	A. K. Gupta	100	25
3.	Structure and Tectonics: The Indian Scene	K. Naha, S. K. Ghosh and D. Mukhopadhyay	100	25
4.	Geomagnetic Methods and Lithospheric Structure	B. P. Singh	100	25
5.	Climate and Global Warming	P. K. Das	100	25
6.	Biogeochemistry of the Arabian Sea	D. Lal	100	25
7.	Progressive and Superposed Deformations	S. K. Ghosh, S. Sengupta and N. Mandal	100	25

THE MONSOON TROUGH BOUNDARY LAYER

Edited by

R NARASIMHA
D R SIKKA
A PRABHU



INDIAN ACADEMY OF SCIENCES
BANGALORE 560 080

Editors

R NARASIMHA, *Centre for Atmospheric and Oceanic Sciences, Indian Institute of Science, Bangalore 560 012 and Jawaharlal Nehru Centre for Advanced Scientific Research, Bangalore 560 094.*

D R SIKKA, *Indian Institute of Tropical Meteorology, Pune 411 008.*

A PRABHU, *Centre for Atmospheric and Oceanic Sciences, Indian Institute of Science, Bangalore 560 012.*

COVER PICTURE: The 30 m mast erected at Kharagpur as part of the MONTBLEX Programme, against a background of a diagram from the well-known book *The Rainfall of India* by Blanford (1886). The diagram shows the mean isobars for India for the month of June 1877, clearly displaying the monsoon trough. (The values of the pressure are quoted in inches of mercury.)

Photograph of the mast by courtesy of Dr S V Kailas, *National Aerospace Laboratories, Bangalore 560 017.*

© 1997 by the Indian Academy of Sciences

Reprinted from *Proceedings of the Indian Academy of Sciences (Earth and Planetary Sciences)*, Volume 104, Number 2, June 1995; Volume 105, Numbers 1 & 3, March & September 1996

Phototypeset and printed at Thomson Press (I) Ltd., Faridabad 121 007
for the Indian Academy of Sciences.

Contents

Preface.....	iii
Genesis of the monsoon trough boundary layer experiment (MONTBLEX) <i>D R Sikka and R Narasimha</i>	1
Planning MONTBLEX – An overview..... <i>Sudarsh V Kailas and Malti Goel</i>	33
Synoptic meteorological observations and weather conditions during MONTBLEX-90..... <i>S K Srivastav</i>	51
Statistical analysis of the position of the monsoon trough..... <i>G Rajkumar and R Narasimha</i>	83
MONTBLEX tower observations: Instrumentation, data acquisition and data quality..... <i>S Rudra Kumar, S Ameenulla and A Prabhu</i>	97
Estimation of surface temperature from MONTBLEX data..... <i>K Narahari Rao</i>	125
Atmospheric boundary layer studies at Jodhpur during MONTBLEX using sodar and tower..... <i>B S Gera, S P Singal, Neeraj Saxena and Y S Ramakrishna</i>	141
Thermal and wind structure of the monsoon trough boundary layer..... <i>G Rajkumar, R Narasimha , S P Singal and B S Gera</i>	153
A study of turbulent characteristics of atmospheric boundary layer over monsoon trough region using Kytoon and Doppler sodar..... <i>K G Vernekar, M N Patil and B S Murthy</i>	171
Study of horizontal scales of motion observed over Kharagpur during MONTBLEX-1990..... <i>B Roy and U K De</i>	185
Wind profiles in the boundary layer over Kharagpur associated with synoptic scale systems..... <i>D K Paul, S P Ghanekar, B S Murthy and K G Vernekar</i>	199
Some observations from the data taken in and around Kharagpur during the onset of the monsoon, 1990..... <i>R Pradhan, B Roy, U K De and D K Rakshit</i>	209
Variability of the oceanic boundary layer characteristics in the northern Bay of Bengal during MONTBLEX-90..... <i>V S N Murthy, Y V B Sarma and D P Rao</i>	223
Roughness length and drag coefficient at two MONTBLEX-90 tower stations..... <i>Kusuma G Rao</i>	245
Estimation of drag coefficient over the western desert sector of the Indian summer monsoon trough..... <i>U C Mohanty, P S Parihar, T Venugopal and Parashuram</i>	261
An analysis of MONTBLEX data on heat and momentum flux at Jodhpur <i>Kusuma G Rao, R Narasimha and A Prabhu</i>	277
Estimation of surface heat flux and inversion height with a Doppler acoustic sounder..... <i>L K Sadani and B S Murthy</i>	293

Atmospheric surface layer parameters during different phases of monsoon over Varanasi from MONTBLEX-90.....	313
..... <i>D V Viswanadham and A N V Satyanarayana</i>	
Fluxes of heat and momentum over sea surface during the passage of a depression in the north Bay of Bengal.....	329
..... <i>S Sivaramakrishnan, M N Patil and K G Vernekar</i>	
Planetary boundary layer over monsoon trough region in a high resolution primitive equation model.....	339
..... <i>K V J Potty, U C Mohanty, B Nandi and K J Ramesh</i>	
The mean and turbulence structure simulation of the monsoon trough boundary layer using a one-dimensional model with $e-l$ and $e-\epsilon$ closures.....	359
... <i>Kusuma G Rao, V N Lykossov, A Prabhu, S Sridhar and E Tonkachev</i>	
Understanding the turbulent structure of the atmospheric boundary layer: A diagnostic approach.....	393
..... <i>M Chatterjee, G K Sen and D K Sinha</i>	
MONTBLEX data archival centre.....	411
..... <i>K G Vernekar and S S Aralikatti</i>	
Subject Index.....	419

Preface

This volume presents a collection of papers on the results of the Monsoon Trough Boundary Layer Experiment carried out in 1990. This national Experiment (called MONTBLEX hereafter), supported by the Department of Science and Technology, involved 20 scientific institutions from across the length and breadth of the country. The project, initiated in March 1987, appears to be the largest meteorological field experiment planned and executed within the country so far, and has yielded a wealth of information that has been analysed during the five years following the Experiment. We can confidently say that, in spite of the present volume and the papers that have appeared elsewhere in the national and international meteorological literature, there is still much work to be done before the results of the Experiment are completely digested.

More than a century ago, Blanford (1886), in his classic memoir *The Rainfall of India*, noted the existence of a “barometric trough which runs obliquely across Northern India, and is the chief seat of the convective ascent...”. This trough may be regarded as the equatorial trough of the northern summer in Indian longitudes, and extends from the region of moist convection centred near the head of the Bay of Bengal to the seasonal heat low at its western end in Rajasthan and Pakistan. The air mass to the south of the trough comes from over the Arabian Sea, while that to the north comes from the Bay of Bengal; or, as Blanford put it, the trough is located near the “debatable ground of the western and eastern branches of the monsoon”. Many cyclonic vortices are formed in the neighbourhood of the trough, and its position is closely associated with the pattern of rainfall in India, as has been discussed in detail by Rao (1976). Thus, the rainfall is a local minimum at the trough, presumably because of subsidence caused by anabatic winds from the Himalaya, and monsoon depressions tend to move along its southern edge, resulting in copious rainfall in their southern quadrants.

This in itself makes the monsoon trough an object worthy of study, but there is in addition the realization in recent years that the proper parameterization of eddy fluxes can play a crucial role in providing better simulations of the monsoon. There is very little field data on land against which such parameterization schemes can be tested: and it is against the background of these two considerations that the MONTBLEX project was conceived.

The genesis of the Experiment has been described in the first paper in the volume by Sikka and Narasimha. They trace briefly the history of atmospheric boundary layer studies in India, beginning with the kite ascents at Jhang and Karachi (both now in Pakistan) organized by J H Field in 1905, and culminating in some of the studies made during MONEX 1979 at Balasore and Digha and during the total solar eclipse of 1980. Given that the monsoon trough is the most important feature in the lower troposphere associated with weather and climate in India during the summer monsoon season, it seemed essential to study the role of the boundary layer in the area in which the trough is located.

The scientific objectives of MONTBLEX were thus chiefly to describe the structure of the atmospheric boundary layer across the entire extent of the trough, to study eddy fluxes and energetics, and, to the extent possible, formulate better parameterization schemes for boundary layer quantities to be used in large scale atmospheric modelling.

The planning of MONTBLEX was a major effort which has been described in the paper by Kailas and Goel. A large number of institutions and scientists were involved in the programme, which consisted of a pilot experiment at Kharagpur in 1989 and the

main experiment in 1990. The Experiment included observations from four surface layer masts, respectively at Jodhpur, Delhi, Varanasi and Kharagpur, ocean cruises by ORV *Sagarkanya*, observations over the network of the India Meteorological Department, sodar and tethered sonde measurements, and extensive aircraft flights carried out by the Indian Air Force.

S K Srivastav summarizes the features of the monsoon season in the year 1990. He notes that the rainfall during the season was the third highest during the preceding decade, being uniformly above normal in 32 out of 35 meteorological subdivisions. This rainfall however was associated with fewer depressions than normal (only four in the Bay of Bengal instead of the usual seven or eight, with none occurring in July). The onset was also earlier than usual, and no typical 'break' in the monsoon ever occurred during the whole season. Srivastav summarizes in addition the various weather events that occurred during the season, including the deep depressions of 13th–15th June and 14th–16th August, and the depression during 20th–24th August.

Rajkumar and Narasimha analyse the spectrum of the position of the monsoon trough during 1990. They find that the mean and standard deviation are in broad agreement with the earlier analysis of Paul and Sikka. The probability distributions of the trough position are generally skew, with the most probable location lying *north* of the mean and the median lying *south* of the mean. It looks as if there is a reasonably well-defined northern-most position that the trough likes to lock into, although it is away from it for considerable lengths of time. These features, in particular the extremes of the trough position, correlate well with the orography: the Himalayan range in the north and the Satpur-Vindhya ranges in the south.

Rajkumar and Narasimha find statistically significant peaks in the spectrum of the trough position with periods of 7–8 days and 2–3 days, which correspond respectively to the intervals between and the duration of weather systems during the monsoon. There is an indication of periods around 16 days and 40–50 days as well, respectively corresponding to the well-known biweekly period and the "40-day mode".

A major component of the MONTBLEX programme was the series of observations made on the four micro-meteorological towers already mentioned. Rudra Kumar, Ameenulla and Prabhu describe the various components in a typical MONTBLEX tower observatory and describe the experiments carried out in the surface layer at the four sites. Among the sensors that the towers carried were the following: cup anemometers, wind vanes, Gill and hot wire anemometers, sonic anemometers, resistance thermometer devices, humicaps and Lyman alpha sensors, sub-soil temperature sensors, rain gauge instruments and solar radiation sensors. The data were acquired through a slow data logger as well as a fast response PC-based data acquisition system. The towers at Jodhpur, Varanasi and Kharagpur were all located in farm fields. The Kharagpur tower, set up for the pilot experiment carried out during 1st–7th July 1989, was in an open and almost homogeneous site. The full scale surface layer observations for MONTBLEX were conducted at all four sites from the last week of May 1990 to the middle of September 1990. Data recorded were usually in stretches of 10–15 minutes every three hours, the frequency being increased to every hour during intensive observation periods. A series of seven checks, made to verify the quality of the data, established both qualitatively and quantitatively that the instrumentation system recorded various physical variables in the surface layer quite accurately.

The soil surface temperature was not available at any of the sites, but in view of its importance Narahari Rao has devised a method by which it can be inferred from the

measurements available at three depths below the soil surface. Using 30-minute averages he finds that the most reliable results are obtained from an analysis of the phases of the sub-soil temperature time series; this approach has the big advantage that it is independent of any errors that might arise in the calibration of the sensors. Using this method Rao estimates the surface temperature at all four sites. A comparison with true measured surface temperature at Pune shows that the method has considerable value, although differences of a few degrees may occur at certain times.

The next seven papers concern the structure of the atmospheric boundary layer. Gera, Singal, Saxena and Ramakrishna report on results from a monostatic sodar set up at Jodhpur. Their observations cover not only the MONTBLEX period in 1990 but also the period July 1992 to September 1993. They report that the erosion of the morning inversion layer by growing thermal plumes underneath was rarely seen except during the winter months. They conclude that the radiation inversion layer tends to be shallow at Jodhpur.

Rajkumar, Narasimha, Singal and Gera examine the thermal and wind structure of the monsoon trough boundary layer using both radiosonde and sodar data. They characterize the observed thermal structure in terms of neutral, stable and unstable sub-layers and find that in 90% of the radiosonde launches at 0530 hr, 48% of those at 1730 hr and 69% of those at 1100 hr, the first radiosonde layer near the ground is stable; the classical mixed layer was found in only 11% of the data set analysed. They therefore infer that, if a mixed layer is present under such conditions, it must have been less than 250 m in depth. Correlating radiosonde and sodar data, they conjecture that the lowest layer in the atmosphere during the monsoon, especially with heavy clouds or rain, is often stable, but there may be shallow plumes that penetrate such a layer during day-time. They also find a weak low level jet at Jodhpur at heights generally between 400 and 900 m with wind speeds of 6 to 15 m/s. It appears as if, during the monsoons, the norm, at least around the western end of the trough, may be closer to the nocturnal boundary layer than to the standard convective mixed layer.

Vernekar, Patil and Murthy analyse some characteristics of the atmospheric boundary layer at Kharagpur using Kytoon and Doppler sodar data. They attempt to evaluate structure functions from the Kytoon data and obtain qualitative information on the height and type of inversion and thermals from the sodar. Analysis is made of four data sets acquired on three days, namely 23rd and 24th May and 4th June 1990. The main conclusion is that the temperature structure function shows the expected power law behaviour on only two occasions out of four, and that the velocity structure function does not show a systematic variation.

Roy and De use data from the same sodar to estimate the characteristic wave length of the horizontal wind at Kharagpur. The data pertain to the onset and mid-monsoon phases of the season. Defining a dominant frequency they derive a length scale that is in general appreciably smaller than the values obtained during GATE over the sea surface.

Paul, Ghanekar, Murthy and Vernekar study wind profiles over Kharagpur associated with two synoptic scale systems that occurred during 20th to 24th August and 1st to 5th September 1990. The study shows that when a system was 200 to 250 km away from the site the boundary layer winds showed good agreement with the synoptic wind analysis up to 750 m from the surface. The sodar wind at 900 and 1500 m suggests a mesoscale cyclonic circulation within the boundary layer. When the system lay away from the station the wind field suggests convergence, but when the system lay over the

station there were significant descending motions; these conclusions agree with earlier studies that report that ascending motions are organized ahead of a monsoon system.

A study of the monsoon onset phase is made by Pradhan, Roy, De and Rakshit using data from four platforms: the micrometeorological tower, Kytoon, sodar and ceilometer. The data are generally consistent with each other but are not in complete agreement, which is not surprising as the averaging times for the different platforms vary from minutes to about an hour. They find that the cloud base often penetrates below the inversion height, and that the maximum inversion height occurs later than the maximum in the heat flux. The sensible heat flux estimated by the usual profile method is found to be high in the presence of a weather system and drops substantially as the system dissipates; the momentum flux also behaves in a somewhat similar way. The authors conclude that synoptic features and surface boundary layer characteristics, as well as the inter-relation of low cloud formation with the atmospheric boundary layer, have close linkages.

Murthy, Sarma and Rao study the variability of the oceanic boundary layer during 18th to 31st August and 9th to 19th September 1990. They find that with the development of a deep depression close to the study area, intense upwelling of sub-surface cold water is observed, but this is weakened as the depression moves away. By examining the rate of change of heat content in the upper 100 m and the net surface heat gain, they conclude that horizontal advective processes play an important role. These advective processes are attributed to the presence and movement of a warm core eddy through the study location.

The next six papers in this collection deal with eddy fluxes. Accurate estimates of surface roughness parameters are crucial for determining the surface drag and for parameterization of eddy fluxes between the earth and the atmosphere. Kusuma Rao makes a detailed analysis of the roughness length at Jodhpur and Kharagpur, based chiefly on measured average velocities under nearly neutral conditions. She finds that while at Kharagpur the estimates of roughness height are fairly consistent (average value 1.9 cm), at Jodhpur the site is basically non-homogeneous and has an average roughness length of 1.2 cm in a relatively open sector, and a somewhat higher value of 6.8 cm in the "rough" sector. She also finds that at Jodhpur the drag coefficient seems to increase rather rapidly at low wind speeds, whereas at Kharagpur (where incidentally the wind speeds rarely fell below 2 ms^{-1}) the drag coefficient appears to be less than at Jodhpur by nearly 50%. The low wind data at Jodhpur indicate drag coefficients higher than values postulated earlier over land or oceans.

Mohanty, Parihar, Venugopal and Parashuram analyse momentum flux at Jodhpur and present a regression formula for the drag coefficient as a function of wind speed and surface stability. They report that indirect methods of drag measurement underestimate the true fluxes as obtained from the eddy correlation technique. Thus the value of the drag coefficient they derive is some 35% higher than the average value for the neutral drag coefficient over tropical and subtropical land surfaces estimated by Garratt. The authors make a correction for stability in the form of a regression involving the temperature difference between 1 and 15 m levels in the surface layer (in addition to the wind). (Drag values at light winds, less than 2.5 ms^{-1} , were not examined).

Kusuma Rao, Narasimha and Prabhu continue with an extensive and detailed analysis of both heat and momentum flux at Jodhpur, especially at low wind speeds.

They find that the sensible heat flux varies with the $3/2$ or $4/3$ power of a characteristic temperature differential such as that between 1 and 10 m: the data in the open sector at Jodhpur provide particularly strong evidence for this scaling. The drag coefficient at low speeds seems to vary nearly in inverse proportion to the wind speed, suggesting that the drag itself is linear in the wind speed at low winds. They conclude that if the fluxes are parameterized by bulk aerodynamic coefficients, it is essential to take dependence on wind speed into account. They also recommend a parameterization of the sensible heat flux in terms of a suitable temperature differential. They note that the $3/2$ power law for the heat flux, which would be consistent with the Businger stability functions, fits the heat flux data as well as the $4/3$ power law does, but that estimates of friction velocity and temperature using the Businger flux relationships do not agree with observed values at low winds.

Sadani and Murthy study sodar data obtained at Kharagpur on four days, respectively representing pre-monsoon, dry, active and relatively weak phases of the monsoon. By using the vertical velocity variance and inversion height, both derived from sodar data, and using Wyngaard's relation for the middle mixed layer, they estimate surface heat fluxes. The values so derived are of the same order as those measured directly on the tower.

Viswanadham and Satyanarayana present results on atmospheric surface layer parameters during different phases of the monsoon over Varanasi. They choose five days for analysis and classify conditions into dry, weak, moderate and active phases. Various derived parameters, including the total kinetic energy, vertical velocity variance and Monin-Obukhov length, are presented. They note that whenever the monsoon is active the diurnal variation diminishes, and whenever there is a break or dry spell it becomes prominent. During the active phase the sky is generally overcast and moist winds are present, both of which tend to stabilize the atmosphere.

Sivaramakrishnan, Patil and Vernekar present data on eddy fluxes over the sea during the passage of a depression in north Bay of Bengal. The fluxes are computed by the profile method using meteorological data acquired on ORV *Sagarkanya*. They find that the fluxes of sensible and latent heat, water vapour and momentum show diurnal and synoptic scale variations depending on the weather. The fluxes increase considerably during the depression period. Furthermore, momentum, heat and evaporation flux coefficients are not equal to each other under convective conditions.

There are three papers connected with modelling. Potty, Mohanty, Nandi and Ramesh base their conclusions on a high resolution primitive equation model, with half-degree resolution and 16 levels in the vertical (seven of them within the boundary layer). The model is integrated using FGGE level IIIb analysis of the European Center for Medium-range Weather Forecasts. The study shows that the diurnal variation of the total kinetic energy (TKE) over land is a dominant feature in comparison with that over the ocean. Along the monsoon trough region the energy increases from the eastern end to the western, and is mainly associated with increase in sensible heat flux as one moves west along the trough. Furthermore, the model simulates the low level wind maximum which is a characteristic feature of the boundary layer over the monsoon region.

Kusuma Rao, Lykossov, Prabhu, Sridhar and Tonkachev use a one-dimensional model with $E-l$ and $E-\varepsilon$ closures to simulate the monsoon trough boundary layer. They find that the choice of the constants in the dissipation equation is a crucial issue, and suggest a set of values for them that avoids a common approximation for TKE

generation and actually simulates the turbulence structure better. They also find that $E-\varepsilon$ closure simulates the turbulence structure better than the $E-l$ model. Furthermore, the simulated temperatures compare quite well with observations if the boundary layer is neutral or unstable but not if it is stable. The moisture profile is also simulated as well but not wind.

Chatterjee, Sen and Sinha attempt a diagnostic approach to study the character of the atmospheric boundary layer using transilient turbulence and second-order closure models (both one-dimensional). The models are applied to a five-day period in June 1990 when Kytoon data were available. Using the approach of Stull and Driedonks, they estimate mixing potentials using Kytoon data on wind and temperature. The second-order closure model suggests two different levels at which turbulence is active.

Finally Vernekar and Aralikatti describe the data archived at the centre set up for the purpose at the Indian Institute of Tropical Meteorology.

In the introductory paper of Sikka and Narasimha, a list of the publications on MONTBLEX data that have appeared elsewhere in the meteorological literature is also provided.

From the analysis that has been carried out till now, some major conclusions seem to emerge. The investigations reported here show the presence of a low level wind maximum, frequent occurrence of relatively stable conditions near the surface, a rapid increase in the flux co-efficients at low winds and possible occurrence of a mesoscale eddy within a synoptic scale disturbance within the boundary layer. The analyses have also given some insight into the complicated process of ocean-atmosphere interactions under the influence of a monsoon depression, such as depression-generated up-welling and its decay as the depression moves away. The role of mixed layer dynamics in causing changes in SST over the Bay of Bengal is an important aspect which needs further study. These findings raise questions about implications for modelling the monsoon which still need to be tackled. Furthermore, they also raise certain fundamental questions about the monsoon trough boundary layer and its structure that seem to need more precise and more sharply focussed observation programmes before they can be satisfactorily resolved. As it often happens with scientific field programmes, MONTBLEX has resolved some of the issues on which it was focussed while others have been exposed. For example an interesting problem which needs to be investigated is the physical causes responsible for the frequent occurrence of stable conditions in the monsoon boundary layer in the presence of organized convection and rainfall. The connection between this phenomenon and soil wetness, soil temperature and the stabilization after the conditional instability has been released appear important to this problem. Another large scale aspect which requires closer scrutiny with diagnostic, theoretical and modelling approaches is the locking in of the monsoon trough close to the Satpura-Vindhya ranges during active monsoon conditions and near the foot-hills of the Himalaya or even north of it during the weak phases. Data along the Satpura-Vindhya-Aravallies complex as well as in the lower ranges of the Himalaya and across Nepal and Tibet would be needed to diagnose the possible mechanisms before theoretical and modelling approaches become fruitful. There are interesting and fundamental questions raised by the data on the eddy fluxes at low winds, and on the interaction between free convection and wind. There is a suggestion that proper parameterization may need account to be taken of soil moisture or other parameters. Some of the above mentioned problems may call for another MONTBLEX-type field programme with more ambitious and specific objectives.

In any case MONTBLEX has succeeded in generating considerable scientific interest in the meteorological community in India on pursuing multi-faceted atmospheric boundary layer studies with focussed objectives. It is gratifying that it has also generated a rich harvest of scientific publications analysing the data acquired during the Experiment and raising fascinating new questions that need to be answered.

It only remains for us to thank the Department of Science and Technology, in particular all the three Secretaries who held office during the period (Dr. V. Gowariker, Prof. P. Rama Rao and Prof. V. S. Ramamurthy), and their many officers who were connected with the project, for their enthusiastic support; all the investigators who responded so readily to our request for contributions to this special volume; and Prof. V K Gaur and the editorial staff at the Academy for their understanding and cheerful support during the nearly three-year period over which this volume has been under preparation.

R Narasimha
D R Sikka
A Prabhu
Guest Editors

References

- Blanford H F 1886 *The Rainfall of India* (Delhi: India Meteorological Department).
Rao Y P 1976 *Southwest Monsoon*. Met. Monograph 1/1976 (Delhi: India Meteorological Department).

Genesis of the monsoon trough boundary layer experiment (MONTBLEX)

D R SIKKA and R NARASIMHA*

Indian Institute of Tropical Meteorology, Pune 411 008, India

*Centre for Atmospheric Sciences, Indian Institute of Science and Jawaharlal Nehru Centre for Advanced Scientific Research, Bangalore 560 012, India

Abstract. This paper sets out the motivation for carrying out an observational experiment on the atmospheric boundary layer along the monsoon trough, in the light of earlier studies of the atmospheric boundary layer in India and elsewhere, and the significant role that the trough has been shown to play as a key semi-permanent feature of the southwest monsoon. The scientific objectives of the experiment are set out, and its planning and execution are touched upon. Some of the gains resulting from the experiment are mentioned, and lessons for the future about the conduct of such programmes are drawn.

Keywords. Atmospheric boundary layer; monsoon trough; MONTBLEX; observational programme.

1. Introduction

The atmospheric boundary layer (ABL) is perhaps best defined as that portion of the atmosphere next to the Earth's surface that is strongly influenced by interaction with the surface on time scales less than a day. This layer has depth and stability characteristics that vary temporally on the diurnal, meso, synoptic and seasonal scales and spatially due to changing characteristics of the surface and intensity of weather patterns. The layer is responsible for exchanging heat, moisture and momentum with the underlying land or ocean surface and is thus of crucial dynamical and thermodynamical importance. The primary mechanism for exchanging these properties is turbulence, which arises from instability and, once initiated, tends to maintain itself by horizontal and vertical shears of wind and by thermal convection in which surface properties play an important role.

When the boundary layer is neutrally stable its depth may be defined as the height where the frictional effects (as indicated say by the fluxes) are marginal, or the wind is given by the geostrophic balance between the Coriolis force and pressure gradient provided the horizontal acceleration is insignificant (Holton 1972). Under convectively unstable conditions, the top of the boundary layer is marked by a capping inversion; and under highly stable conditions (as e.g. at night) the height of the inversion at the surface gives perhaps the most convenient characteristic dimension for the boundary layer (although other more satisfactory definitions of the boundary layer height can be devised; e.g. Garratt 1992).

The depth of the ABL may range from a few tens of meters in highly stable nighttime conditions to even 3 km in thermal convective conditions during summer afternoons over the Indian land area, when the inversions and stable layers are absent

(Ananthakrishnan and Rangarajan 1963). For average conditions in the tropics the layer extends up to a depth of about 1 km. The boundary layer may be classified into stable, undisturbed convective and disturbed convective types. The stable layer is confined to the ground-based inversion and the undisturbed convective boundary layer is confined to low-level inversion or the base of low clouds. Observations over India and elsewhere in the tropics show that the disturbed boundary layer may extend to a considerable portion of the troposphere, particularly in the large scale convergent zones where organised convection prevails. Because of the dominance of moist processes and the smallness of the Coriolis force, the ABL in the tropics differs from those in the middle and high latitudes. The ABL also differs over land and ocean.

Since the work of Lettau (1932) atmospheric turbulence in the ABL has been extensively studied in the last 60 years, from theoretical and modelling considerations on the one hand and through field observations and laboratory measurements on the other. (See for recent work Garratt 1992; Betts and Beljaars 1993; Beljaars and Holtslag 1991; Holt and Raman 1988; Mahrt and Ek 1993). These studies have often been driven by practical problems such as the dispersal of pollutants, loads on tall structures, flow past obstacles (e.g. hills), spatial and temporal variations of refractive index by turbulence in the wind, and micro-climatic variations within growing crops and forest canopies (Garratt 1974; Panofsky and Dutton 1983). The necessity for parameterizing sub-grid scale boundary layer processes for large scale weather forecasting models and for simulation of the climate by general circulation models has added a new dimension to ABL research (Deardorff 1970, 1972; Mahrt 1983). The simulation of tropical circulation and convection has been shown to be particularly sensitive to the way the ABL processes are parameterized (Betts 1976, 1978; Holt and Raman 1988).

Most field experiments undertaken to-date for investigating turbulent processes in the ABL have been carried out either on land in the mid-latitudes (e.g. the Kansas (1968), Minnesota (1973) and Oklahoma (1983) Experiments in USA and the Wangara Experiment (1967) in Australia), or on the marine ABL over the tropical Pacific and Atlantic Oceans (e.g. the Line Island Experiment LIE 1967, the Barbados Meteorological Experiment (BO-MEX) 1969, the Atlantic Tropical Experiment (ATEX) 1969, the Global Atlantic Tropical Experiment (GATE) 1974 and the Airmass Transformation Experiment (AMTEX) 1974–75). Extensive literature is available on the marine ABL as a result of these experiments (Augstein *et al* 1973, 1974; Brummer *et al* 1974; Esbenson 1975; Riehl 1977, 1979). The monsoon boundary layer over the Arabian Sea has been critically reviewed by Young (1987) and observational studies provided by Rao and Hor (1990), Pant (1982) and Pant *et al* (1985). However, our information on the structure and characteristics of the ABL over the land-locked tropics has remained only rudimentary as large scale experimental studies over such areas have been virtually non-existent, exceptions being the Meteorological Experiment in Venezuela with emphasis on Hydrology (VIMHEX 1969–1972), and the Amazon Boundary Layer Experiment (ABLE) in 1984 to study special characteristics of the boundary layer over the Amazon forest.

The Indian summer monsoon trough region (to which we shall return below) provides a rather special meteorological environment within the tropics, wherein for the four-month period from June to September every year organised moist convection prevails over the sub-continental scale. Rao (1976) has discussed two important low level semipermanent features of the monsoon season – the heat low and the monsoon trough. The ABL over the region thus merits special study, and a large scale field

experiment called the Monsoon Trough Boundary Layer Experiment (MONTBLEX) was planned, organised and executed by the Indian atmospheric science community from 1987 to 1990 under the sponsorship of the Department of Science and Technology (DST), Govt. of India (Goel and Srivastava 1990).

This article describes the genesis of MONTBLEX and some of its achievements. Section 2 highlights briefly some relevant characteristics of ABL. A short account of previous ABL studies in India, providing the background to MONTBLEX, is offered in § 3. Section 4 deals with the special meteorological environment of the region relevant to the experiment. An account of the evolution of MONTBLEX and its scientific objectives is given in § 5. Planning, design, and the scientific management of the experiment, and the resources that were brought to bear, are discussed in § 6. A brief overview of the field phases of the experiment and the lessons learnt in carrying it out, as well as a summary of the research results and scientific gains from the experiment, are contained in § 7. Section 8 contains some concluding remarks.

2. Characteristics of ABL

The ABL is generally divided into three parts, namely the skin layer, the surface layer and the outer layer. The skin layer, generally only a few centimeters deep, is where molecular diffusion processes operate and viscosity causes the wind to approach zero at the surface; vertical wind shear and temperature gradients are high in this region. The surface layer, typically 10–100 m deep, is characterized by momentum and heat fluxes that may be assumed to be nearly constant (to within 10%, say: Panofsky and Dutton 1983), and insensitive to the Earth's rotation, with the wind structure being defined by surface friction and temperature gradient. There is diurnal variation in the thickness of the surface layer, from about 10 m during clear nights with light wind to about 100 m in day time. The outer layer may be a mixed layer or an Ekman layer, and extends from the top of the surface layer to the height of the ABL. Within the mixed layer, large scale convective motions are driven by surface friction, density gradient and the Earth's rotation. Typically, the eddy fluxes are large at the surface and decrease to zero near the top of the ABL.

The characteristics of the ABL over tropical oceans are somewhat different from those over land, and have been studied in detail for the Atlantic Ocean with the data collected under ATEX and GATE (Augstein and others, 1973, 1974). The essential feature revealed in these studies is the presence of convergence in the sub-cloud layer within the mixed layer which under disturbed conditions pumps energy to the disturbance through organised updrafts. The downdraft associated with the disturbance can in turn modify the sub-cloud layer and tends to arrest the energy source of the disturbance. In the wake of the disturbance the boundary layer recovers to undisturbed conditions.

The general characteristics of atmospheric turbulence in the boundary layer have been discussed in standard text books (Panofsky and Dutton 1983; Kaimal and Finnigan 1994 etc.). In the surface layer the turbulent eddies have a depth scale comparable to height above ground. Theoretical approaches based on Monin-Obukhov similarity concepts have resulted in the formulation of universal relationships for the statistical properties of turbulence in the surface layer, including in particular the wind profile for a wide range of stability conditions. In the mixed layer a different type

of scaling argument is used to determine the statistical properties of turbulence. The spectrum of boundary layer turbulence covers length scales from millimeters to kilometers and temporal scales from a fraction of a second to hours. Different characteristic length scales apply to different ranges and the governing laws are also different. Information on the spectra and co-spectra of ABL turbulence has been accumulated in the field experiments already mentioned and by study of data acquired on meteorological towers (e.g. at the Boulder Atmospheric Observatory in USA, Kaimal 1988; Kaimal and Finnigan 1994). A fairly unified picture of turbulence in the ABL has thus been gained as a result of critical comparisons of theoretical studies and experimental data.

3. Brief account of the development of ABL studies in India

Work on determining the thermal and wind structure in the lower atmosphere may be said to have begun in India when Field (1905) organised kite ascents at Jhang and Karachi (both now in Pakistan). Subsequently pilot balloon ascents began at Agra in 1917 and a regular Indian network was established in the 1920s and 1930s. Early workers also used comparison of temperatures at hill stations with near-by stations in the plains to determine the seasonal variation of lapse rates in the lower atmosphere. In the late 1920s and early 1930s the Royal Air Force also organised aircraft flights at Karachi, Peshawar, Bangalore and a few other stations to study the low-level structure of the atmosphere. These flights revealed the existence of low-level inversions over Karachi (Hariharan 1932; Krishna Rao and Bhatia 1937), particularly in the monsoon season, suggesting the shallowness of the moist monsoon current and the prevalence of subsidence over the region of the seasonal heat low over Sind (Pakistan). Boundary layer observations near the surface were carried out on a tower at the agrometeorological observatory, Poona by Ramdas and his colleagues (Ramdas and Atmanathan 1932; Ramdas 1932). One of the most intriguing findings of these early studies was the presence of a lifted temperature minimum on calm clear nights over bare surfaces, which has been theoretically explained only very recently by Vasudeva Murthy *et al* (1993). With the introduction of pilot-balloon flights, meteograph ascents, and self-recording anemographs at various stations and the expansion of the radiosonde network during the 1920s to 1950s, the scope of the studies expanded and a variety of investigations was undertaken on the diurnal variability of winds, land-sea breezes along the coasts and their penetration to inland stations, katabatic and anabatic wind flows in valleys, mountain waves, low level inversions and stable layers, the low-level jet stream over Peninsular India, profiles of mean static energy, etc. In the 1950s tethered balloons were used for research on the structure of low-level turbulence and diffusion characteristics for the aerodrome station at Ambala (Saha 1956 a, b). Drop-sondes, introduced in India under the International Indian Ocean Expedition (IIOE) programme, established (to the surprise of meteorologists) the existence of low-level atmospheric inversions over the west and central Arabian Sea that disappeared as the monsoon current approached the west coast of India (Colon 1964; Sikka and Mathur 1965). During subsequent monsoon experiments like the Indo-Soviet ISMEX-73 (Pant 1978, 1982; Pant *et al* 1985), Monsoon-77 and Monsoon-88 (Sadhuram *et al* 1989), radiosonde ascents on board research ships gave further insight into the Arabian Sea marine boundary layer. MONEX-79 made a focussed study of the Arabian Sea

monsoon boundary layer; and NCAR Electra aircraft gust probes were specially designed to study the fine structure of both free-air and cloud turbulence (Rao and Hor 1990). A preliminary study of the monsoon ABL, using 10 m masts, was made at the east coast stations Balasore and Digha by the Indian Institute of Science research group (Narasimha *et al* 1981).

Over land the Indian Institute of Tropical Meteorology (IITM) launched a special experiment in 1966-67 over the Palghat region off the Kerala coast to study the peculiar characteristics of the local ABL as the flow rushes through a large gap in the Western Ghats (Ramachandran *et al* 1980). Badri Narayanan (1978) used a gust sphere to measure atmospheric gusts near the ground during the SW monsoon season at Bangalore. He found that gusts have the characteristics of the eruptions observed in turbulent boundary layer flow. Tower instrumentation for study of boundary layer turbulence was first introduced in India in 1965 (Rao *et al* 1965) at the Equatorial Rocket Launching Station at Thumba (near Trivandrum), and later at a few nuclear power stations (Shirvaikar *et al* 1970). A low-altitude boundary layer tower was also used by IITM scientists (Vernekar and Sadani 1980) to study the micro-climate of crops at Pune. The total solar eclipse of 1983 gave another opportunity for the study of the response of the surface layer to rapid changes in solar radiation (Narasimha *et al* 1982). Aircraft probes of the boundary layer over the Deccan Plateau were organised by IITM as part of their warm cloud seeding programme in the 1980s, and the data studied by Parasnis and Morwal (1991). The Centre for Atmospheric Sciences of the Indian Institute of Technology, Delhi (IITD), in collaboration with the scientists of the University of North Carolina, USA, and IISc, Bangalore (Raman *et al* 1990), undertook the study of ABL turbulence in Delhi through tower instrumentation during 1986. Monostatic sodars were deployed initially by the scientists of National Physical Laboratory (NPL) Delhi in the 1980s (Singal *et al* 1982) to study stratified layers for application to line-of-sight microwave communication links in the country; subsequently the NPL group introduced this technique at several other stations too.

The IITM organised a Symposium on Environmental Physics and the Atmospheric Boundary Layer in 1981 (IITM 1982). IIT Delhi organised an International Conference on Tropical Micrometeorology and Air Pollution in 1988, and the papers were published in a special issue of *Atmospheric Environment* in 1990 (24A 723–858). The National Physical Laboratory, New Delhi organised an International Symposium on Acoustic Remote Sensing of the Atmosphere and the Oceans in 1990 (Singal 1990).

The above survey shows that, beginning in 1905, several studies were conducted in India to investigate different aspects of the lower layers of the atmosphere including the boundary layer over individual stations in India and over the Arabian Sea for a variety of scientific purposes and practical applications. Appendix 1 details some of these studies under broad heads and provides a bibliography on the subject to 1990. A cursory glance at this literature shows that the monsoon boundary layer over the landmass of India, and particularly over the monsoon trough region, has been hardly studied in any organised manner.

The problems connected with moist and dry convection within the convective boundary layer in the monsoon trough are unique in some respects. Convective instability has been extensively studied in India during the 1930s to the 1950s using radiosonde data (Normand 1938; Roy 1946; Raychoudhury 1952), but only with a view to forecast occurrence of severe thunderstorms. The role of the boundary layer and its interactions with the cloud layers hardly received any attention in that period even

though it was known that the roots of deep convection lie near the ground. Thus, a clear gap has existed in our knowledge about the boundary layer processes in the monsoon trough region and the role they play in organising moist convection within it. There was, therefore, a need to fill this gap and obtain a detailed picture of the ABL in the region and its linkage with the spatial and temporal variability of the large scale monsoon.'

4. Large scale meteorological environment of the monsoon trough region

The monsoon trough is the most important feature in the lower troposphere over India during the summer monsoon season (June to September), and has been known for over a century; indeed Blanford (1886) noted, "The seat of the barometric trough is a region of relatively low pressure, which is more or less persistent throughout the monsoon. Within this tract the easterly and westerly winds alternately hold sway; the former predominant to the north of the Ganges and Jamuna, the latter on the higher land to

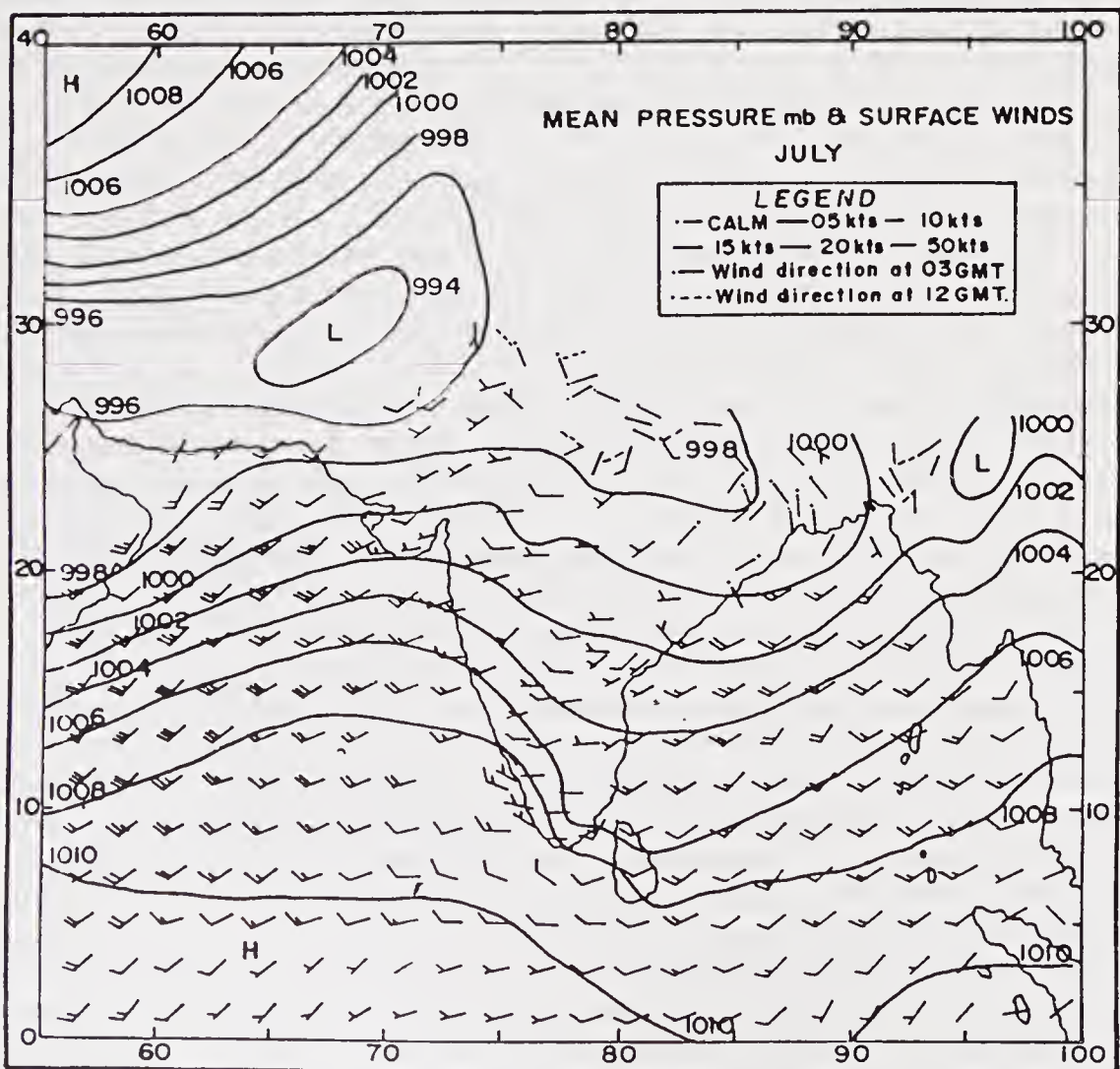


Figure 1a. Normal pressure distribution over India during the monsoon season (typically July).

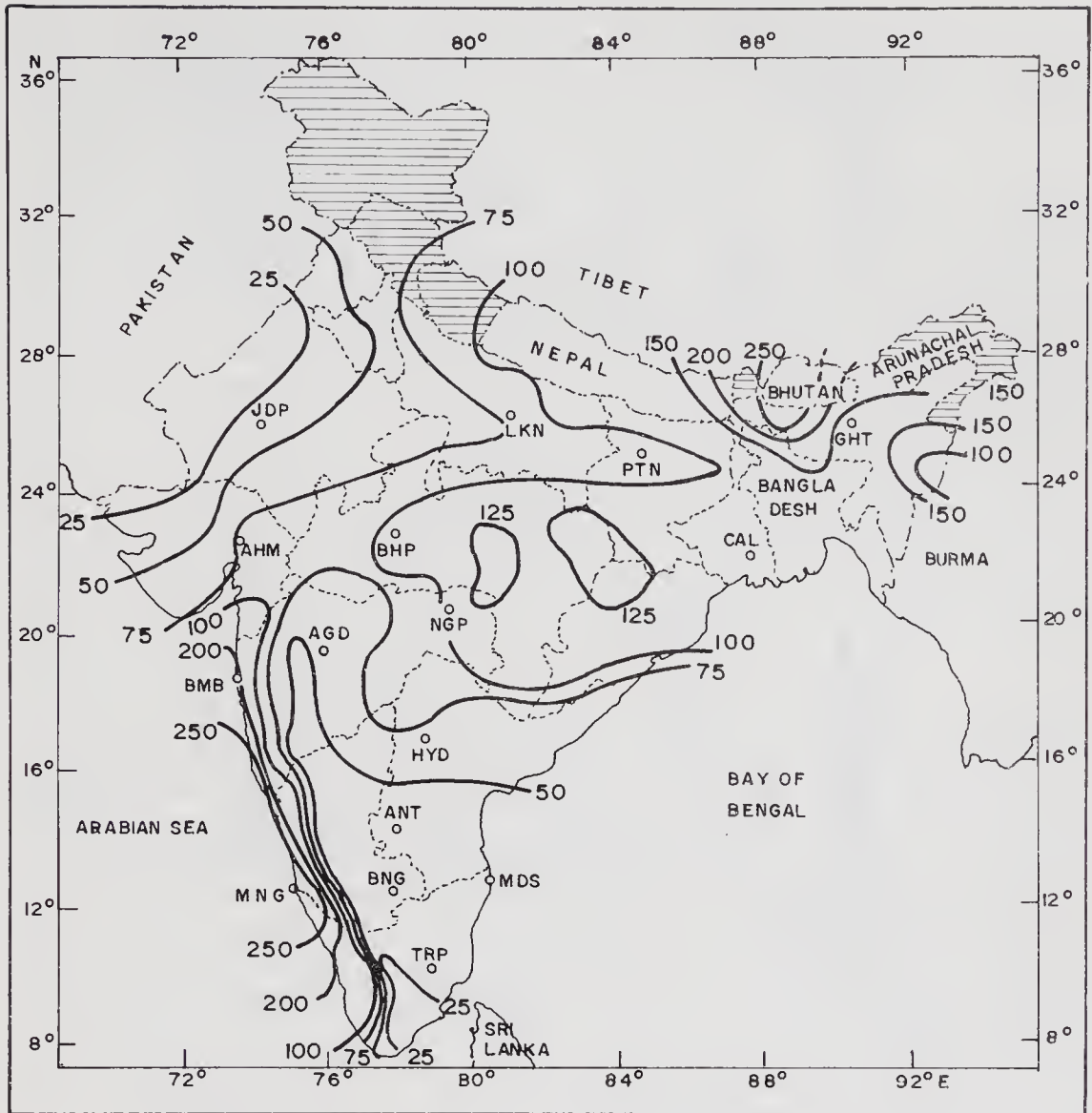


Figure 1b. Normal rainfall distribution over India (after Parthasarathy *et al* 1984: Shaded portions not considered).

the south". It is seen on the sea-level pressure chart (figure 1a) as a sub-continental scale feature stretching from west Rajasthan to the Head of the Bay of Bengal across the entire length of the Gangetic Valley. On the seasonal and monthly mean charts, strong westerly to south-westerly winds flow to the south of the trough and weak easterly to north-easterly winds flow to its north. Figure 1b gives the seasonal monsoon rainfall distribution over India.

There are major differences in the dynamical and convective characteristics of the eastern and western parts of the trough. The western end corresponds to a heat low with very shallow ascent and convergence limited to the lowest half kilometer or so and clear skies above (Sawyer 1947), whereas the eastern end is a so-called dynamic trough with convergence up to the mid-troposphere and moist ascent throughout the troposphere with intense convection and clouding (figure 2a). The eastern end of the trough also lies on the warm waters of the north Bay of Bengal which acts as a source of heat

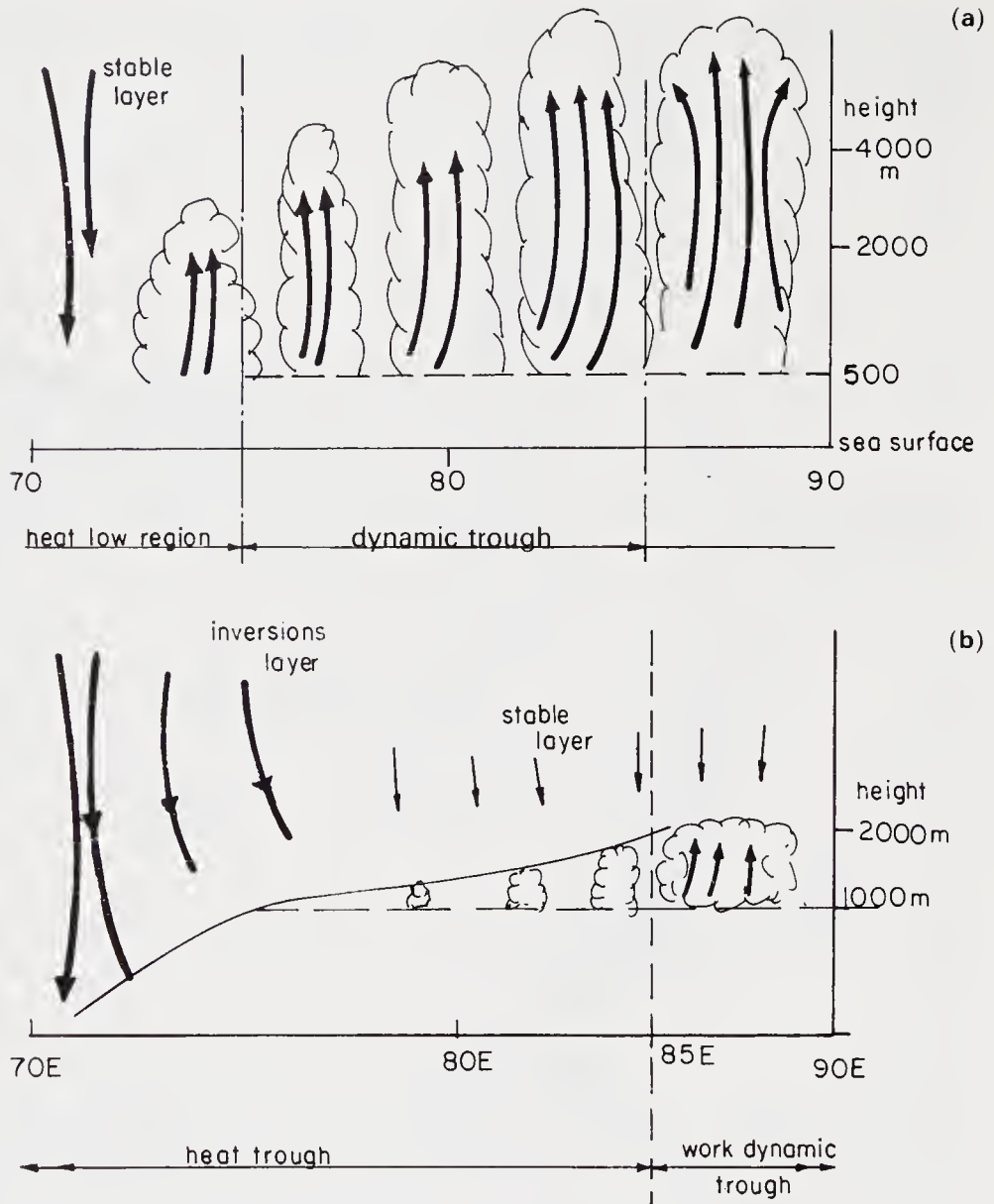


Figure 2a,b. Schematic clouds and vertical motion in east-west section across the monsoon trough for (a) active and (b) prolonged 'break' (lower) situation.

and moisture to the monsoon flow as it turns around the trough axis. Thus generally dry convection with shallow clouds occurs over west Rajasthan ($70-75^{\circ}\text{E}$), where stable conditions usually prevail with a shallow moist layer capped by a low level stable inversion layer (Hariharan 1932; Krishna Rao and Bhatia 1937; Sinha 1958 and Ananthakrishnan and Rangarajan 1963). The boundary layer in the western portion of the trough is generally of the undisturbed type. Alternation of deep moist convection and unsaturated moist processes occurs in the middle region of the trough, say $75-85^{\circ}\text{E}$. On the other hand the dynamic trough is characterized by moisture convergence and lower tropospheric cyclonic vorticity. Besides, conditional instability prevails over the entire region under normal conditions. The trough is located north of 20°N , where the Coriolis parameter is quite important. The resulting upward motion on top of the boundary layer due to Ekman pumping results in a secondary circulation

forced by frictional convergence (Holton 1972) in the dynamic trough region. This in turn results in conditional instability of the second kind (CISK) which is a dominant factor in the tropics, and, coupled with barotropic and baroclinic instability processes, is responsible for the formation of the monsoon disturbances (Shukla 1978) and the maintenance of the dynamic trough (Sikka and Gadgil 1980).

The sub-continental scale trough remains disturbed on different scales with periods ranging from the diurnal to 1–2 days, 3–7 days, 10–20 days and 30–50 days along the stretch of the trough east of 75°E. As the trough is a region of instability, vortices on the scale of 500–2000 km (cloud cluster, meso- and synoptic scales) form and move within the trough with quasi-regularity. These weather systems feed on the energy and moisture pumped across the boundary layer as the roots of convective clouds lie within the sub-cloud layer. Planetary, regional and local rain systems with condensation processes interact strongly, and the local boundary layer processes also appear to interact with the large-scale monsoon variability (Young 1987). This could be observed clearly in the slowing down of the prevailing winds when the instability is building up and the strengthening of the flow when the cloud downdrafts on the local scale occur in disturbed weather episodes. Also during such episodes the boundary layer close to the ground shows stabilization and drying whereas the cloud layer air above shows higher moistening and destabilization.

The kind of variations seen in the monthly/seasonal mean trough in the east-west direction, between the dynamic low at one end and the heat low at the other, is also seen in the temporal fluctuations. The major fluctuations on the supersynoptic scale are between the 'active' spells (in which the trough becomes dynamic over the subcontinental scale) and the weak spells or 'breaks'. In intense breaks, the entire trough except the extreme eastern end becomes a heat trough (figure 2b). Thus there are major transitions from a moist convective region with high cyclonic vorticity above the boundary layer to rather dry and undisturbed conditions with anticyclonic vorticity above the boundary layer. Figure 3(a,b) shows the circulation at 850 hPa and 700 hPa for active and break monsoon situations. During active monsoon conditions, when the low level flow has strong horizontal convergence, deep clouds frequently develop in the vicinity of the dynamic trough; local surface parameters have only a secondary effect. Large-scale horizontal and vertical wind shears are maintained externally by the large-scale dynamics of the flow in the monsoon trough, and thus the kinetic energy of the local turbulence may be expected to increase. During 'break' conditions, turbulent eddy transport is expected to be reduced. The change, if any, in the kinetic energy spectrum of the turbulent flow in the monsoon trough during disturbed events could only be conjectured as it was never systematically measured prior to MONTBLEX.

Besides these large-scale variations, the complex orography and land surface of the subcontinent results in forcing over a large range of spatial scales. Large-scale topography is marked by the high Himalayan barrier to the north of the trough axis and the shallow topography of the Vindhya and Satpura hills to its south. To the east are the hills of the Myanmar coast and NE India and to the west the rugged Aravalli range. Thick forests lie to the east, north and along central India and thin forests to the west across the Aravallis. Lush green vegetation during the monsoon season prevails over its entire length from Bengal to east Rajasthan, but western Rajasthan is relatively bare of vegetation. Swollen Himalayan rivers flow across the Gangetic Valley. The real landscape consists of an assemblage of hills and vegetation patches, which interact meteorologically and hydrologically through horizontal transfer of energy, water,

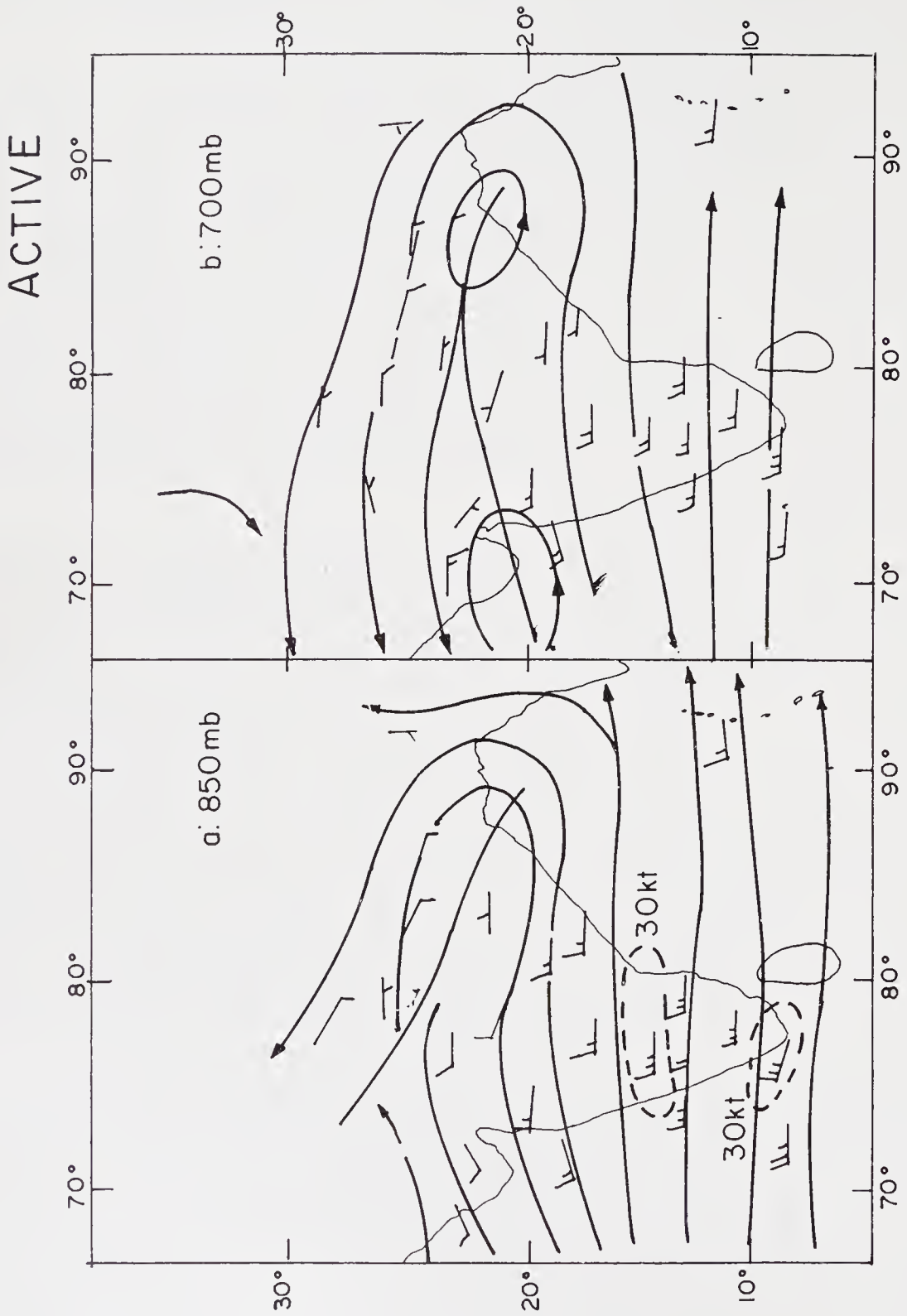


Figure 3. (Continued)

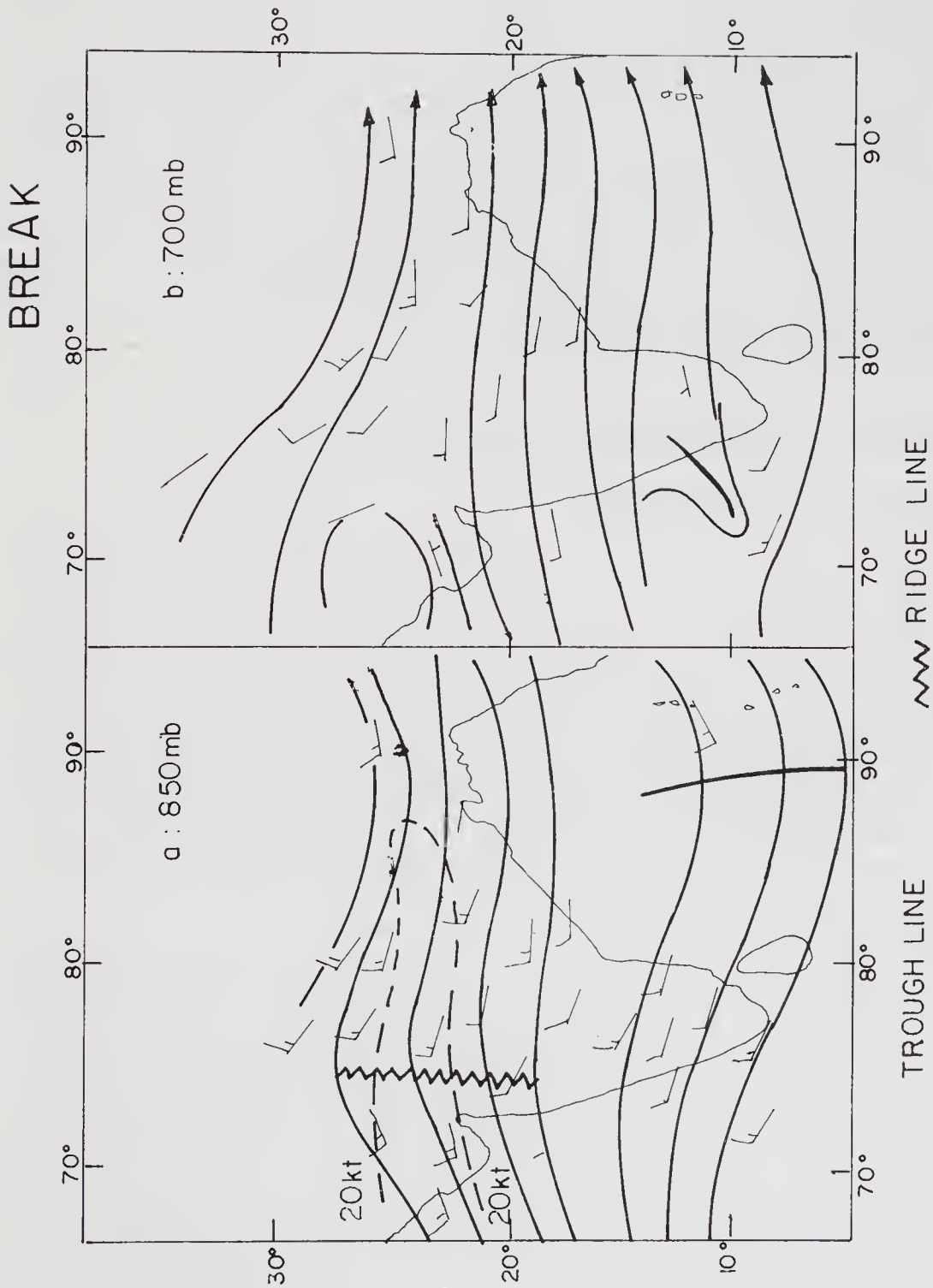


Figure 3. Streamlines at 850 hPa for active and 'break' monsoon situations.

carbon and nutrients. Thus *surface heterogeneity* prevails on the large scale which influences land-atmosphere interactions on different scales. Heavy rainfall occurs just to the south of the trough axis due to large scale convergence. Orographically induced vertical ascent occurs to its north and east along the foothills of the Himalayas and the hills of NE India respectively.

The soil in the Gangetic Valley is alluvial, and, after the onset of monsoon rains, contains high moisture east of 85°E, and medium moisture between 75 to 85°E. Sandy soil with little moisture exists at the western end. The wet soil inhibits sensible heat transfer but promotes exchange of latent heat to the boundary layer, whereas relatively dry soil transfers more sensible heat but less latent heat.

Besides the moisture-rich low-level monsoon flow, local evaporation from the soil and water bodies (viz. rivers, standing water-filled fields and pools), as well as evapotranspiration from standing vegetation, provides additional sources of local moisture along most of the trough region.

5. Evolution of MONTBLEX and its scientific objectives

5.1 Formulation of the experiment

On the large scale the monsoon boundary layer over the oceans is continuously evolving (Young 1987). The low level flow, just before crossing the equator, turns westwards. On its passage toward the west coast of India, it first flows over the cold waters off the Somalia Coast and then over the warmer east Arabian Sea. It strikes the Western Ghats, ascends on the wind-ward side and descends over the lee side. After passing over the landmass of Peninsular India, it again flows over the warmer waters of the Bay of Bengal, becomes more southerly, and then turning cyclonically along the monsoon trough, finally moves eastward along the Himalayan foothills. In its course over India, it passes over areas of torrential rain and over mountain complexes where its properties are modified due to planetary, regional and local rain systems and heterogenous ground surface.

The mechanisms underlying the monsoon are numerous: over a hundred years of research has unfolded only some of the intriguing aspects about the size and strength of the signals in large scale pressure, temperature and wind fields that generate and maintain the monsoon. The boundary layer in the large scale monsoon airstream encounters strong interactions across the highly complex surfaces of the ocean and solid land mass over which it flows; and it is important that these interactions are studied. The earlier monsoon experiments (IIOE (1963–65), ISMEX-73, Monsoon-77, Monsoon-88 and MONEX-79) focussed on the study of the Arabian Sea marine ABL. The challenging problem of the ABL over the monsoon trough region was yet to be tackled in any organised manner. Some workers (e.g. Krishnamurty and Bhalme 1976; Sikka and Gadgil 1980) had suggested that changes in lower tropospheric stratification and cloud radiation feed-backs could be of significant importance to the low frequency oscillations of the monsoon. Others (like Shukla 1978) invoked CISK as an important mechanism for the instability of the monsoon flow; and Mishra and Salvekar (1980) produced unstable disturbances by explicit high resolution integration of the boundary layer equations within the framework of quasi-geostrophic baroclinic theory. Thus the study of the monsoon ABL has been considered important from several angles.

As already mentioned a preliminary attempt was made during MONEX-79 by the atmospheric sciences group at IISc to study the surface layer of the monsoon at the east coast station of Balasore using turbulence measuring instruments installed on a 10 m high tower. In subsequent years (1980–86) the infrastructure and the scientific manpower for carrying out boundary layer measurements were strengthened in India.

During several informal discussions which the authors of this article had on the important problem of the role of the boundary layer in monsoon dynamics, it was considered desirable to undertake a major field experiment for the study of the ABL in the monsoon trough region. The Department of Science and Technology (DST) had in 1986 included ABL study as one of the thrust areas in its Atmospheric Science Programme. Besides, facilities for enabling numerical weather prediction over the medium-range scale were being contemplated at that time by DST as a major new initiative. It was necessary that ABL data should be collected for the special meteorological environment of the monsoon trough to develop and adopt realistic boundary layer parameterization schemes for the Indian region. The authors then felt that the time was ripe to launch a field experiment for the purpose and called it *MONTBLEX*. The IITM Pune, as a nodal agency, submitted a Project to the DST in 1987 for a co-ordinated study of the ABL under the title *MONTBLEX* with the sponsorship of DST and with multiagency participation. After a review of the project by a specially constituted group the Science and Engineering Research Council (SERC) finally approved execution of the project in 1988.

5.2 *Scientific objectives of MONTBLEX*

The scientific objectives of *MONTBLEX* were centred around:

- Description of the ABL structure variation in time and space under varying phases of the monsoon over the Gangetic Valley, and study of the ABL dynamics.
- Study of the role of eddy fluxes in the maintenance of the monsoon trough.
- Energetics of the monsoon trough.
- Determination and validation of ABL parameters for use in modelling.

It was considered that the fulfillment of these objectives should require the collection of the following data sets:

- Near-surface measurements of temperature, moisture and momentum fluxes at three places within different regimes of the monsoon trough, characteristic of dry/unsaturated/deep moist convection, as well as under disturbed and undisturbed conditions as the monsoon cycles through the onset, advance, active and break phases.
- Day-to-day and diurnal variability of the extent and characteristics of ABL as determined by sodars operating at different places at the location of the boundary layer towers.
- Wind, temperature and moisture soundings at the radiosonde stations located within the monsoon trough at 12 hourly or shorter intervals. More frequent soundings (3-6 hourly intervals) were required during the life history of an active disturbance (well marked low pressure area, monsoon depression) and in its close proximity.
- Wind vector profiles in the mixed layer using Doppler sodar and minisondes in the deep moist convective regime.

- Standard radiation observations available at stations located within the monsoon trough.
- Role of air-sea interaction and oceanic upper layer in north Bay of Bengal at the eastern end of the trough.
- INSAT cloud pictures/OLR and radar pictures within the monsoon trough.
- Tethersonde ascents in the deep-moist part of the monsoon trough to adequately describe the mixed layer fluctuations.

6. Planning, design and management of MONTBLEX

6.1 Planning

The programme was originally conceived and proposed by IITM, Pune and IISc, Bangalore. As it developed, several other institutions were involved in its implementation (as listed in Appendix 2). The participating institutions were assigned nodal responsibilities for different components of the programme with co-ordination among different institutions. These institutions submitted separate proposals for funds for their activities which were made available to them by the DST after peer-review.

Very early during project planning it was also conceived that there would be a pilot experiment in the summer of 1989 at Kharagpur at the eastern-most tower site. With the experience gained during the pilot experiment, the full programme with four tower sites, upgraded conventional network and aircraft missions was to be implemented in the operational phase during the summer monsoon of 1990. In order to execute the pilot and the operational phases a detailed implementation plan was prepared and distributed to all the participating institutions.

Details about the components of MONTBLEX and the accuracy requirements are given in the companion paper by Kailas and Goel in this volume.

6.2 Training of scientists

Even though a core team of scientists who were to implement the programme had good experience in boundary layer measurements and sufficient theoretical background, it was also planned to launch a training programme to induct young scientists to MONTBLEX from universities and research institutes engaged in atmospheric science in India. For this purpose, the following activities were carried out:

- A well organised training programme at IITM, Pune in which Dr J C Kaimal, Chief Scientist of the Boulder Atmospheric Observatory under the Wave Propagation Laboratory, NOAA, USA, who was a visiting Professor at the Institute during January – February 1988, delivered a series of lectures on ‘The Atmospheric Boundary Layer – Its structure and measurement’. The lecture notes (Kaimal 1988) were distributed among the participating institutions. Dr Kaimal also took part in several discussions with Indian scientists about selection of relevant sensors for tower measurements, accuracy requirements, data acquisition and processing, and data quality assessment procedures.
- A training workshop on the physics of the ABL was organised at IIT Kharagpur in April 1989, just prior to the pilot experiment. Experienced scientists delivered

lectures in this workshop on theoretical and experimental aspects of ABL, including data acquisition and retrieval techniques, to the younger scientists who were getting inducted into ABL work in India.

- A training course organised at IISc Bangalore during April – May 1990, just before the commencement of the full operational phase, emphasized the theoretical aspects of the ABL. It also helped to co-ordinate the efforts of participating scientists in the practical aspects of the experiment.

6.3 Design of MONTBLEX

6.3.1 *Observational Systems:* The observational systems deployed for the experiment consisted of the following.

- Four towers for the surface layer measurements of mean and turbulent quantities at different levels to provide profiles.
- Remote sensing for the mixed layer by using Doppler sodar at IIT Kharagpur and monostatic sodars at the four tower stations (Varanasi, Delhi, Jodhpur and Calcutta). Doppler sodar can give horizontal wind, vertical wind and temperature distribution to a height of 1.5 km within a radius of 60 km and the monostatic sodar can give the height of the boundary layer, stratified layers, thermals, plumes, wind shear layers and inversion layers.
- Tethered balloon flights at IIT Kharagpur during low wind conditions to determine wind, temperature and humidity in the boundary layer up to 1.0 km.
- Minisonde at IIT Kharagpur and low level radiosonde at selected IMD stations.
- Conventional surface and upper air observations over the operational weather network of the IMD within the monsoon trough zone, taken at an increased frequency during Intensive Observational Periods (IOPs).
- Aircraft flights of the Indian Air Force (IAF) from selected bases to measure the environmental wind and temperature at pre-designated flight levels and tracks whenever the need was felt.
- Special cruise of the Ocean Research Vessel (ORV) *Sagarkanya* from Visakhapatnam to a position 20°N 90°E over north Bay of Bengal. The ship took a quasi-stationary position at this location during August – September 1990. Radiosonde ascents and routine oceanographic observations including XBTs were launched in this programme.
- INSAT cloud pictures and OLR observations.
- Weather radar observations over the IMD network within the monsoon trough.

Figure 4 gives the distribution of the various observational systems used during the experiment within the monsoon trough.

6.3.2 *Data management:* All the data generating investigators and organisations were required to provide proper quality-controlled data sets – preferably on computer compatible systems like floppies, tapes or cartridges. All the tower data were to be quality-controlled by the IISc Bangalore group. For the final storage of data and for arranging its distribution to the investigators in India, a MONTBLEX Data Centre was established at IITM, Pune and the data were archived at the Centre by September 1992 (for details, see paper by Vernekar in this volume).

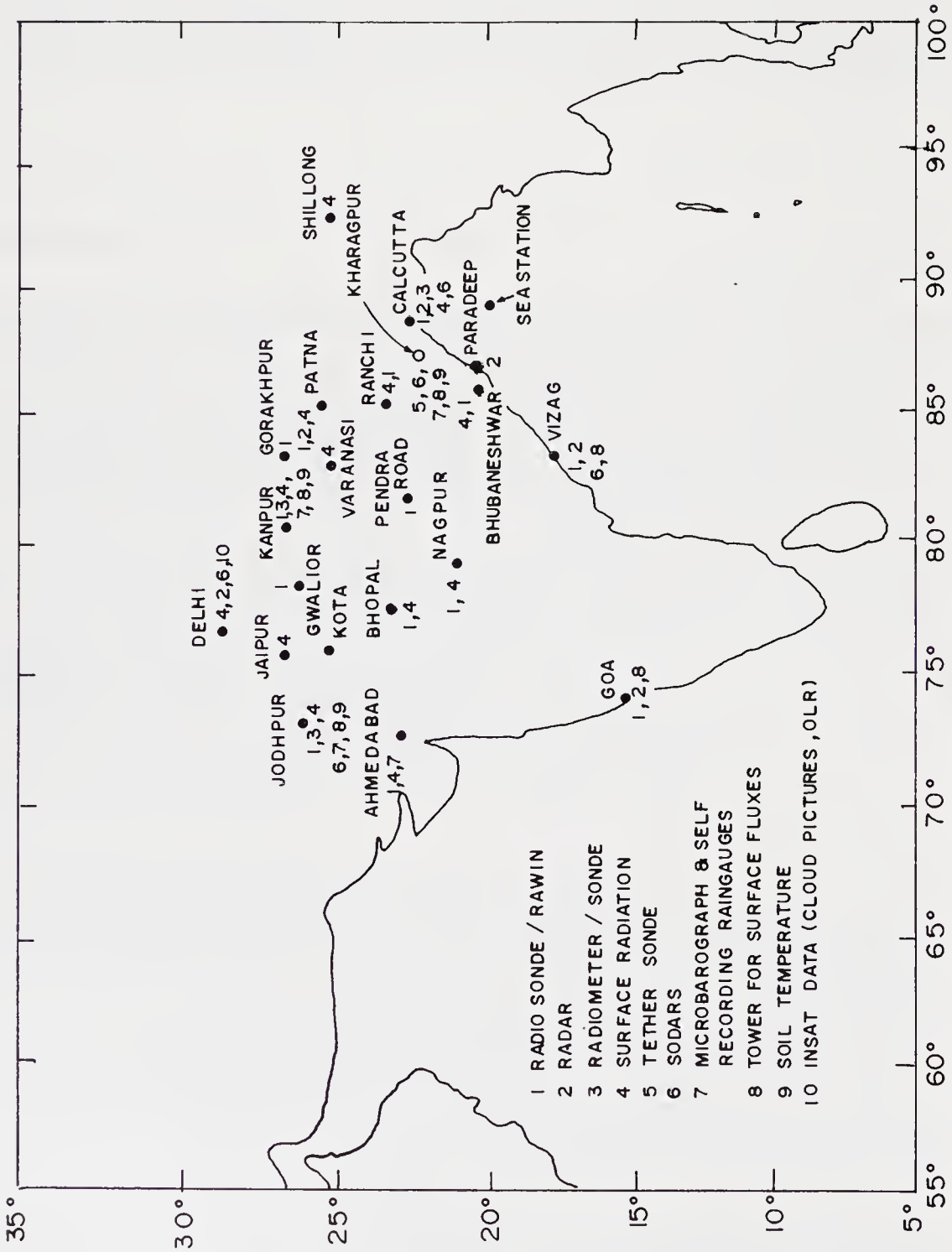


Figure 4. Observational systems deployed for MONTBLEX.

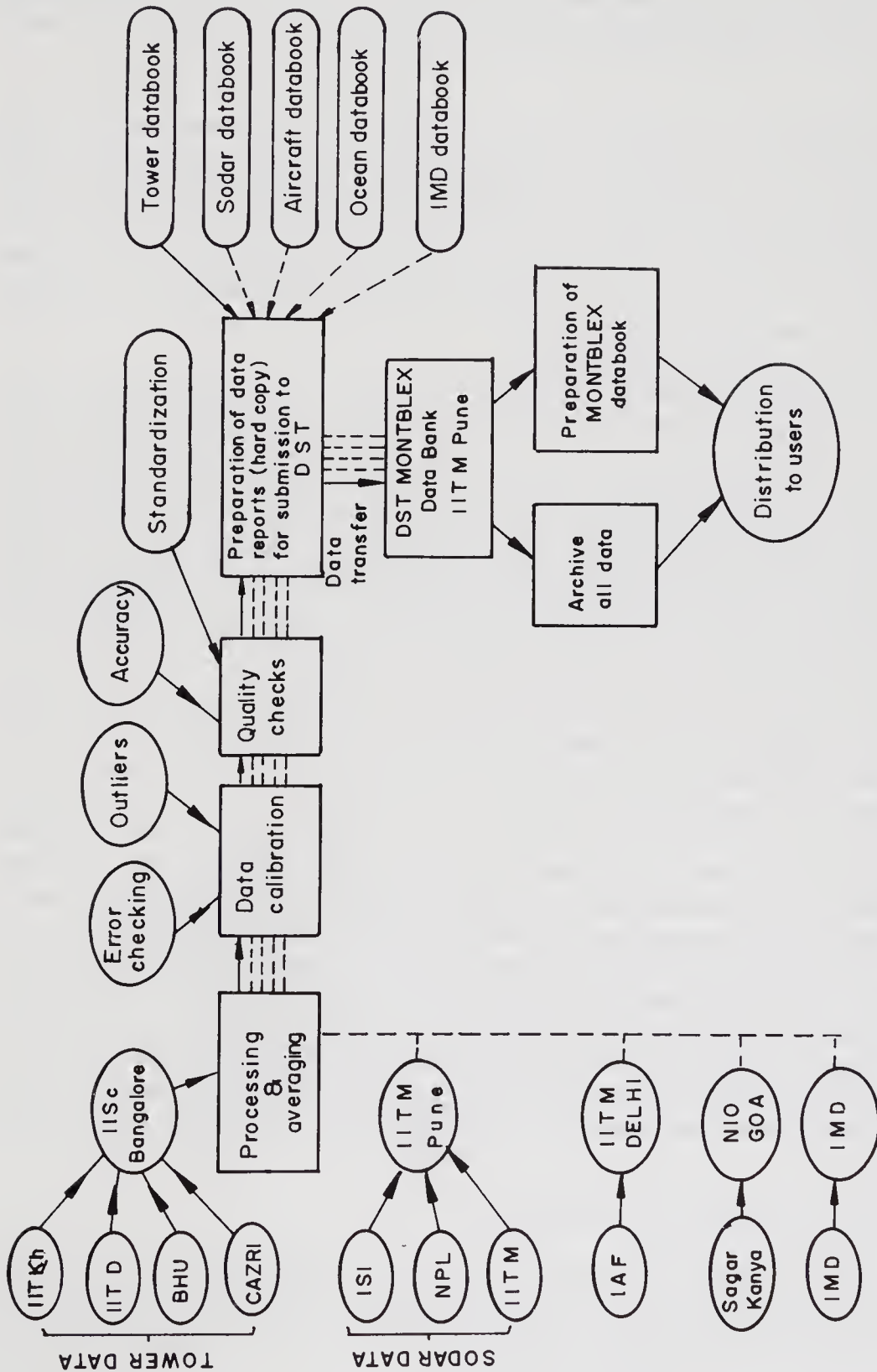


Figure 5. MONTBLEX data flow.

Distribution of quick-look data direct from the experimental groups began from 1990 for the pilot experiment and from 1991 for the full field experiment. The IITM Data Centre began distributing the quality-controlled data from 1992 onwards. Figure 5 gives the MONTBLEX data flow diagram.

6.3.3 Modelling: A modelling group was organised to facilitate the use of MONTBLEX data for the use of the modelling community. This group held several overview meetings and interacted with the data management and experimental groups in respect of their special needs. Although local surface soil evaporation could contribute significantly to moisture flux, this could not be determined precisely at all the tower stations as only soil temperature data below the surface were available. To that extent there remained a gap in information for modelling surface soil temperature in different environments within the trough zone.

From a modelling perspective, Garratt (1993) discusses ABL parameterization schemes as comprising three components: a surface component whose aim is to calculate surface fluxes; a mixing component, whose aim is to provide a profile of vertical fluxes throughout the ABL; and a cloud component whose aim is to obtain cloud cover and cloud properties. NWP models usually parameterize the surface fluxes over land in terms of Richardson number, roughness length, friction velocity, temperature, albedo and ground roughness, besides the forecast flow properties at the surface. The fluxes then modify the flow and the cycle goes on. The vertical eddy fluxes are often parameterized in terms of vertical eddy diffusion coefficients as functions of stability parameters. Similarity theory and K-theory, with first order, one-and-a-half order and second order closure assumptions for the mean flow and turbulent fluxes, are used in some of the parameterization schemes. Several models have been devised for use in GCMs, e.g. Deardorff (1972); Mellor and Yamada (1974); Yamada (1976); Blackadar (1977); Garratt (1992, 1993). The vertical eddy diffusion is assumed to vanish at the top of the boundary layer. The parameterizations involved assume the ABL to be quasi-stationary, its response to large scale forcing being rapid. The approaches utilising turbulence kinetic energy (TKE) closure (Holt and Raman 1988; Garratt 1992) use a prognostic budget equation for TKE which is given in terms of the diffusivity K containing an empirical length scale. The MONTBLEX data would provide an opportunity to validate parameterization schemes for the land-locked monsoon region. The modelling group, therefore, laid emphasis on comparisons of the measured fluxes with those based on standard models. For this purpose, the modelling group conducted in 1992 an intercomparison workshop for the fluxes in the surface layer by different techniques (profile, bulk aerodynamic and eddy correlation methods) by using fast response and slow response data for spells of active monsoon and no-rain cases.

6.4 *Scientific management and resources*

For the proper management of the inter-agency activities involved in the programme, the DST established several committees and groups. These groups were in particular responsible for arranging all infrastructure at the respective tower sites, and the planning and monitoring of the programme.

As the programme gained momentum and the Pilot Experiment phase approached, a bulletin called MONTBLEX News (Kailas 1990–92) was issued from IISc Bangalore to promote flow of MONTBLEX related information among all the scientific teams.

For the full field phase of the 1990 experiment a MONTBLEX Operations Control Centre (MOCC) was established in May 1990 by IITM at IMD, New Delhi.

The DST gave strong support to the programme through grants which covered major expenses. Besides this resource, without which the programme could not have been implemented, the participating institutions contributed significantly by providing expert scientific and technical manpower as well as other infrastructural facilities available with them. Very important contributions were made by the IAF Met. Branch in organising aircraft flights, IMD New Delhi for providing conventional surface and upper air observation as well as INSAT and radar data and the Department of Ocean Development in keeping ORV *Sagarkanya* exclusively at the disposal of the Programme for the period August – September 1990.

7. Operational field phase: Research results, scientific gains and lessons learnt

7.1 The pilot experiment – July 1989

For the MONTBLEX pilot experiment carried out at Kharagpur during 1–7 July 1989, an operational centre was established at the Meteorological Office in Calcutta with support from IMD. Data acquisition began on 2 July 1989. Slow and fast response tower instruments, minisonde, Lyman Alpha humidity measurements and the IMD conventional observing system were used in this experiment.

7.2 The full field experiment 1990

Active preparations for the full field experiment – 1990 began from March 1990 onward and the observational teams were positioned at the respective sites from April 1990.

All observational platforms participated in this phase. To co-ordinate the operations and observations in respect of changing synoptic situations within the monsoon trough region, MOCC undertook daily analysis of the monsoon situation, disseminated information to all special observational sites about the emerging synoptic situation every 2–3 days, alerted site-teams and the relevant IMD network about Intensive Observational Periods (IOPs), co-ordinated the research flights (twelve in all) from different IAF stations, kept communications open with ORV *Sagarkanya* during the ship observational programme and prepared weather summaries relevant to MONTBLEX operations. The scientists of IMD, IAF Met Branch and IIT Delhi participated in the discussions at MOCC on the day of issuance of each advisory. MOCC started functioning from the fourth week of May 1990 and continued its activities till mid-September. At the end of its operations a report about the whole operations and a detailed weather summary for the use of participating scientists were prepared and distributed to all research teams. Further details on the two field phases and the weather developments during the full field phase can be obtained in the companion papers in this volume by Kailas and Goel and by Srivastava.

From the point of view of synoptic development, the weather co-operated with the MONTBLEX design strategy enabling all types of situations to be adequately sampled at different sites by the observational groups. The ORV *Sagarkanya* also experienced active and weak monsoon spells. Even though it could reach its stationary position

only in mid-August it took excellent observations during the development of a monsoon depression during 18th–21st August 1990.

7.3 Research results

A workshop was organised at IISc Bangalore in January 1992 where preliminary MONTBLEX research results were presented by different teams. A second workshop was held at IITM Pune in April 1993.

The ultimate aim of MONTBLEX has been to promote research in ABL as relevant to our understanding and modelling of monsoon processes. Right from the conception of the programme, the participating scientific teams have emphasized the use of the experimental data for research and publications of their results in scientific media. Over the last 6 years, a body of scientific literature has appeared based on the research in the evolutionary phase of MONTBLEX (1987–1989), the pilot experiment 1989 and the full field phase 1990. The output has appeared in three forms: research reports, papers presented in scientific conferences and symposia and papers in refereed research journals. A fairly up-to-date list of publications in journals along with a number of papers in scientific symposia/conferences (apart from the papers published in the present special journal volume), is given in Appendix 3.

The research work using MONTBLEX data has proceeded with reference to some of the broad objectives of the programme such as the study of turbulence in the mixed layer, thermodynamic structure of the ABL during different synoptic situations prevailing in the monsoon trough, and modelling. Although considerable preliminary work has been done in the last 3–4 years, the full impact of MONTBLEX is expected to be felt in the next few years, provided research support is continued.

7.4 Scientific gains and lessons learnt

There have been some obvious gains from MONTBLEX. It was a unique effort in which the Indian research community on its own conceived the programme and implemented it successfully in all its phases. It provided an opportunity to test complex techniques of ABL measurements, compare and validate results and build confidence in a variety of systems. Many of the systems complemented each other and worked very well. In totality, the planning and implementation of the MONTBLEX accomplished several plus points. The problem of making precise measurements in the monsoon boundary layer is not trivial. The successful implementation of MONTBLEX provided useful lessons for carrying out in future similar field experiments which might well cover more ambitious objectives. Also, measurements on key parameters like surface soil moisture and surface energy balance with *in situ* radiation measurements, which were generally missing in MONTBLEX, must be included in future field studies.

MONTBLEX helped enormously in nucleating various groups engaged in ABL research within the country. The effort has certainly helped in training young scientific workers in all aspects of ABL research. Most of the instrumentation used in the experiment was indigenously developed and fabricated and this should help in the emergence of work in the exciting and complex field of atmospheric technology in India.

One operational difficulty was the non-availability of detailed information about the development of local weather events at all tower sites. This gap could be filled by

reports on the hourly weather events recorded by near-by airport weather stations. In future experiments of this nature it is imperative that a detailed weather diary is maintained by the local field units.

The weather environment at Kharagpur was hostile to sophisticated instruments due to the general prevalence of disturbed weather and antecedent deep convection. The abilities of the research team were put to severe test in managing the observational programme there. It is clear that more spares and a stand-alone power supply are mandatory in such an environment. The regular hoisting of Kytos turned out not to be feasible due to high winds at Kharagpur. With hindsight, it appears that this facility could have been better availed of at a location like Varanasi, where the prevailing winds in July – August are lighter and the lightning activity is also less frequent. There were also problems at Kharagpur for the supply of hydrogen gas as there was no IMD run pilot balloon observatory at the place. Similarly, transport problems also added to the difficulties of the scientists. However, excellent co-operation was provided by the host institutions without which it would not have been possible to accomplish the majority of the set goals.

At the time of this writing, the modelling component of the experiment has attracted only modest attention. This area needs more focussed attention during the coming years. Success here demands a continuous dialogue between modellers, synoptic meteorologists and boundary layer experimental scientists.

There is also a need to integrate the results obtained from field studies about understanding the surface-atmosphere exchanges to describe the large scale monsoon processes. More focussed investigations are needed to study the MONTBLEX data with that perspective so that the role of boundary layer and cloud processes in modulating the regional scale monsoon can be quantitatively determined. There is also a need to clearly spell out whether the scale invariants of the ABL theory work in all situations and are valid under all environments (as sampled by the four boundary layer towers).

8. Concluding remarks

The successful accomplishment of the inter-agency field programme has been due to the great enthusiasm and dedication of the participating teams. The results hold promise that the Indian atmospheric science community would forge itself vigorously in future on bolder initiatives in experimental areas to unfold the complex nature of atmospheric phenomena in and around the subcontinent. Observing the details of phenomena on varied scales and their mutual interactions, and modelling the resultant behaviour of the atmosphere, are both highly worthwhile and challenging tasks that need to be continuously pursued and supported.

Finally it is encouraging to find that the experiment has already yielded a good crop of research publications on ABL by Indian scientists (Appendix 3), and the present volume offers the latest outcome of these efforts.

Acknowledgements

It is our pleasure to thank DST, in particular Dr Malti Goel, and other participating institutions for the whole-hearted and unflinching support provided to MONTBLEX.

Many scientists, students, technicians and air and ship crews co-operated to make MONTBLEX possible. Our appreciation goes in particular to all the members of the experimental scientific teams who dedicated their efforts cheerfully in difficult field operations which led to the successful implementation of the programme.

The reference work for this article was done at the IMD Library in Pune for which thanks are due to the Meteorological Office, Pune. DRS specially thanks Prof R N Keshavamurty, Director and Shri K G Vernekar, Deputy Director, IITM Pune, for providing facilities for completing the first draft of this article. The authors express their thanks to Prof. S. Gadgil of the Indian Institute of Science, Bangalore, for her significant contributions in the early stages of the formulation of MONTBLEX, and for going through the present manuscript and giving useful suggestions. Finally, it is a matter of great satisfaction to both the authors to witness the successful implementation of a programme whose seeds lay in the exciting discussions they had during two decades of scientific interaction.

APPENDIX 1

Some references to scientific studies done on ABL in India

Broad purpose of study (station data used)	Instrumentation/ Techniques used	References
1. Comparison of winds derived from surface isobars with observed winds in first km above the surface (at Agra, Bangalore, Bombay)	Geostrophic/gradient wind balance	Ishaque (1927) Vittal Sarma (1952)
2. Diurnal variation of temperature in the surface layer and lapse rate in the lower atmosphere (Pune, Karachi, Cherat)	Screen thermograph data at different heights, aircraft flights and comparison of temperature at hill stations with those at near-by plains stations	Ramakrishnan (1930) Ramanathan (1930) Atmanathan (1931a,b) Hariharan (1932) Ramdas (1932) Ramdas and Malurkar (1932) Veryard (1934) Ramdas and Atmanathan (1932) Krishna Rao and Bhatia (1937) Desai and Mal (1937) Sreenivasaiah (1942) Saha (1977)
3. Land-sea breezes, diurnal variation of lower tropospheric winds, influence of topography on low-level	Anemographs, routine and special pilot balloon ascents	Atmanathan (1931c) Ramanathan and Ramakrishnan (1935) Sen Gupta and

winds, katabatic and anabatic winds (Pune, Bombay, Visakhapatnam, Allahabad, Ahmedabad, Sriharikota etc.)

4. Analysis of thermodynamic diagram for convective instability and thunderstorm forecasting, and study of convective boundary layer profiles of mean static stability (different stations over India)

5. Inversion and stable lapse rates, mixing depths for pollutant dispersal

6. Radioclimatology of different stations over India

7. Diffusion of horizontal momentum by turbulence (Ambala airport), growth of ABL Pune, diffusion studies at nuclear sites

Radiosonde ascents

Radiosonde data

Radar and radiosonde data

Tethered balloons, surface flux measurements at towers

Chakravarty (1940)
Raychoudhury (1946)
Agarwala (1951a, 1957)
Parthasarathy and Narayanan (1952, 1953)
Venkateswaran (1953)
Raghavan (1956)
Rao and Mukherjee (1958)
Mukherjee and Ghosh (1965)
Alvi (1967)
Thiruvengadathan *et al* (1985),
Sadhuram and Vittal Murthy (1986)

Normand (1938)
Basu and Ramsahay (1938)
Roy (1950)
Rao (1950)
Pisharoty (1945)
Raychoudhury (1951, 1952)
Anjaneylu (1969)
Pant *et al* (1985)
Parasnis (1990, 1991)
Kulkarni (1986)

Hariharan (1932)
Krishna Rao and Bhatia (1937)
Ananthakrishnan and Rangarajan (1963)
Sivaramakrishnan *et al* (1971)
Mandal and Padmanabhamurty (1979)
Manjukumari (1985)
Rangarajan and Eapen (1990)

De (1959)
Kulshrestha and Chatterjee (1966)

Saha (1956a,b)
Shirvaikar *et al* (1970)

Vernekar *et al* (1991, 1993)

8. Vertical wind shear at low-levels for equatorial rocket launching site (Thumba)	Low-altitude tower instruments	Rao <i>et al</i> (1965) Narayanan and Devatsey (1972) Narayanan and Sudhakaran (1980)
9. Surface layer sensible heat flux for evolving convective boundary layer (Thumba)	Doppler sodar and tower instrumentation	Sengupta <i>et al</i> (1986) Winston <i>et al</i> (1993)
10. Stratified layers and wind shear in the ABL (Delhi)	Monostatic sodar	Gera and Sarkar (1980) Singal and Agarwal (1982) Singal <i>et al</i> (1982, 1986a,b)
11. Special experimental study of boundary layer in Palghat gap	Pilot balloon ascents, self-recording surface weather instruments	Ramachandran <i>et al</i> (1980)
12. Inversion in Arabian Sea and the Arabian Sea monsoon boundary layer	Dropsonde data, aircraft gust probes	Colon (1964) Sikka and Mathur (1965) Ramakrishnan (1974) Ramanathan (1978) Meyer and Rao (1985), Kusuma Rao (1986) Pant (1977, 1978, 1982) Holt and Sethuraman (1985, 1986a) Rao and Hor (1990) Mohanty and Mohankumar (1990)
13. Low-level jet over Peninsular India and the Arabian Sea	Radiowind and pilot balloon data, dropsonde data	Joseph and Raman (1966) Pant (1982) Kanti Prasad <i>et al</i> (1985)
14. Downwind evolution of monsoon surface layer in the ABL (Orissa coast)	Low-altitude tower	Holt and Sethuraman (1986b) Narasimha <i>et al</i> (1981)
15. Surface layer flux studies	Low-altitude tower	Raman <i>et al</i> (1990)
16. Micrometeorology of crops	Surface layer flux measuring instruments	Vernekar and Sadani (1980).

BIBLIOGRAPHY TO APPENDIX 1

- Agarwala K S 1951 *Indian J. Meteorol. Geophys.* **2** 277
 Agarwala K S 1957 *Indian J. Meteorol. Geophys.* **8** 456

- Alvi S M A 1967 *Indian J. Meteorol. Geophys.* **18** 233
- Ananthakrishnan R A and Rangarajan S 1965 *Indian J. Meteorol. Geophys.* **16** 173–189
- Atmanathan S 1931a *IMD Sci. Note* **4** 40
- Atmanathan S 1931b *IMD Sci. Note* **40** 101–114
- Atmanathan S 1931c *IMD Sci. Note*, **46** 1–10
- Anjaneylu T S S 1969 *Tellus* **21** 64–74
- Bhatia K L 1941 *IMD Sci. Note*, **116** 11–18
- Basu S and Sahay Ram 1939 *IMD Sci. Note* **89** 67–76
- Colon J A 1964 *Indian J. Meteorol. Geophys.* **15** 183–200
- De A C 1959 *Indian J. Meteorol. Geophys.* **10** 295–299
- Desai B N and Mul S 1937 *IMD Sci. Note*, **87** 354
- Field J H 1905 *Mem. Indian Meteorol. Dept.*
- Gera B S and Sarkar S K 1980 *Indian J. Radio Space Phys.* **9** 86–90
- Hariharan A S 1932 *IMD Sci. Note*, **46** 41–48
- Hariharan A S 1987 *Mausam* **38** 171–176
- Holt T and Sethuraman S 1985 *Boundary-Layer Meteorol.* **33** 259–282
- Holt T and Sethuraman S 1986a *Boundary-Layer Meteorol.* **37** 71–87
- Holt T and Sethuraman S 1986b *Mon. Weather Rev.* **114** 2176–90
- Ishaque M 1927 *IMD Sci. Notes* **1** 1–12
- Joseph P V and Raman P L 1966 *Indian J. Meteorol. Geophys.* **17** 407–410
- Jambunathan R and Ramamurty K 1974 *Indian J. Meteorol. Geophys.* **25** 403–410
- Kanti Prasad, Gupta M G and Hingorani J K 1985 *Mausam* **36** 197–202
- Krishna Rao P R and Bhatia K L 1937 *IMD Sci. Note* **78** 119–130
- Kulkarni P L 1986 *Mausam* **37** 533–536
- Ramachandran G, Rao K V and Krishna K 1980 *J. Appl. Meteorol.* 881–888
- Kulshrestha S M and Chatterjee K 1966 *Indian J. Meteorol. Geophys.* **17** 367–384
- Mandal B B and Padmanabhamurty B 1979 *Indian J. Meteorol. Geophys.* **30** 473–478
- Manjukumari 1985 *Mausam* **36** 71–74
- Meyer W D and Rao G V 1985 *J. Atmos. Sci.* **42** 1929–1943
- Mohanty U C and Mohankumar N 1990 *J. Environ.* **A24** 823–825
- Mukherjee A K and Ghosh S K 1965 *Indian J. Meteorol. Geophys.* **16** 429–436
- Narasimha R, Prabhu A, Rao K N and Prasad C R 1982 *Proc. Indian Natl. Sci. Acad.* **A48** 175–186
- Narasimha R, Prabhu A, Rao K N, Adiga B S and Ameenulla S 1981 Project MOBLE, reports 81FM 1–5, Dept. Aero. Engg., IISc, Bangalore
- Narayanan V, Devatsey T L 1972 *Indian J. Meteorol. Geophys.* **23** 97
- Narayanan V and Sudhakaran N 1980 *Mausam* **31** 409–414
- Normand C W B 1938 *Q. J. R. Meteorol. Soc.* **64** 71–74
- Pant M C 1977 *Indian J. Meteorol. Geophys.* **28** 189–196
- Pant M C 1982 *Mausam* **33** 85–90
- Pant M C 1978 *Indian J. Meteorol. Geophys.* **29** 88–100
- Pant M C, Singh M S and Manohar Lal 1985 *Mausam* **36** 371–374
- Parasnis S S 1991 *J. Atmos. Sci.* 999–1002
- Parasnis S S 1990 *Boundary-Layer Meteorol.* **52** 69–74
- Parthasarthy S, and Narayanan J 1952 *Indian J. Meteorol. Geophys.* **3** 197–203
- Parthasarthy S and Narayanan S 1953 *Indian J. Meteorol. Geophys.* **4** 205–219
- Parthasarathy B, Sontakke N A and Kothawale D R 1984 *Curr. Sci.* **53** 94–96
- Pisharoty P R 1945 *IMD Tech. Note*, 13

- Raghavan K 1956 *Indian J. Meteorol. Geophys.* **7** 289–294
- Ramdas L A and Atmanathan S 1932 *IMD Sci. Note* **54** 89–96
- Ramdas L A 1932 *IMD Sci. Note* **41** 115–124
- Ramdas L A and Malurkar S L 1932 *Indian J. Phys.* **6** 495–508
- Raman S, Templeman B, Templeman S, Holt T, Murthy A B, Singh M P, Agarwaal P, Nigam S, Prabhu A and Ameenulla S 1990 *Atmos. Environ.* **A24** 723–734
- Ramanathan K R 1931 *IMD Sci. Note* **30** 131–134
- Ramanathan K R and Ramakrishnan P 1935 *IMD Sci. Note* **67** 214–222
- Ramanathan K R and Ramdas L A 1935 *Proc. Indian Acad. Sci.* **1** 822–8
- Ramakrishnan K P 1939 *IMD Sci. Note* **14** 46–63
- Ramanathan Y 1978 *Indian J. Meteorol. Geophys.* **29** 643–654
- Ramachandran G, Rao K V and Krishna K 1980 *J. Appl. Meteorol.* **19** 881–888
- Rangarajan C and Eapen C D 1990 *J. Atmos. Environment.* **A24** 849–852
- Rao D V and Mukherjee A K 1958 *Indian J. Meteorol. Geophys.* **9**, 313
- Rao K N 1950 *Indian J. Meteorol. Geophys.* **1** 17–23
- Rao G V and Hor T H 1990 *Mausam* **41** 213–216
- Rao Kusuma 1986 *Boundary-Layer Meteorol.* **36** 283–294
- Rao M S V, Sikdar D N and Chandrasekharan C 1965 *Indian J. Meteorol. Geophys.* **16** 221
- Roy A K and Mahalingam L S 1941 *IMD Sci. Note.* **117** 19–40
- Roy A K 1950 *Indian J. Meteorol. Geophys.* **1** 77
- Raychoudhury S N 1951 *Indian J. Meteorol. Geophys.* **2** 226
- Raychoudhury S N 1952 *Indian J. Meteorol. Geophys.* **3** 91–100
- Raychoudhury S N 1946 *IMD Sci. Note.* **119** 51–58
- Sadhuram Y and Vittal Murthy K P R 1986 *Mausam* **37** 187–192
- Saha K R 1956a *Indian J. Meteorol. Geophys.* **7** 145
- Saha K R 1956b *Indian J. Meteorol. Geophys.* **7** 353
- Saha S K 1977 *Indian J. Geophys.* **28** 493–498
- Sengupta P K and Chakravarty K C 1940 *IMD Sci. Note.* **108** 43–67
- Sengupta K, Kunhikrishnan A K, Radhika V and Nair K N 1986 *Atmos. Res.* **20** 119–123
- Shirvaikar V V, Kapoor R K, Sundarajan A, Sharma L N and Shastry P L 1970 *Indian J. Meteorol. Geophys.* **21** 361–366
- Sikka D R and Mathur M B 1965 *Proc. Met. Results of IIOE Symp, IITM Pune, 55–67*
- Singal S P, Gera B S and Ghosh A B 1982 *J. Inst. Engineers* **63** ETI 49
- Singal S P, Agarwal S K and Gera B S 1982 *Mausam* **37** 436–440
- Singal S P, Agarwal S K, Gera B S and Pahwa D R 1986 *Mausam* **37** 435–440
- Singal S P, Ojha V K, Tej Pal, Gera B S, Sharma M and Mohnan M N 1986 *Mausam* **37** 193–196
- Sivaramakrishnan M V and Mokashi A Y, *IMD Sci. Rep. no. 155*
- Sreenivasiah B N 1942 *IMD Sci. Note.* **106** 43–67
- Thiruvengadathan A, Rao C V V S and Iyer S S 1985 *Mausam* **36** 499–502
- Venkateswaran S V 1953 *Indian J. Meteorol. Geophys.* **4** 82–85
- Vittal Sarma V 1951 *Indian J. Meteorol. Geophys.* **2** 241–247
- Vernekar K G and Sadani L K (1980) *Indian J. Meteorol. Geophys.* **31** 125–132
- Vernekar K G, Sadani L K, Mohan B, Saxena S, Debaje S B, Pillai J S, Murthy B S and Patil M N 1991 *Indian J. Radio Space Phys.* **20** 312–315
- Vernekar K G, Mohan B, Saxena S, and Patil M N 1993 *J. Appl. Meteorol.* **32** 1426–1432

Veryard R G 1934 *IMD Sci. Note* **64** 87–113

Winston J, Prakash J, Ramakrishnan R and Kunhikrishnan P K 1993 *Q. J. R. Meteorol. Soc.* **119** 187–197

APPENDIX 2

Participating institutions in co-ordinated MONTBLEX programme

Institutions	Nodal responsibility
1. Indian Institute of Tropical Meteorology (IITM), Pune	Doppler Sodar, Tethersonde, low-level ascents; Data centre; R&D co-ordination and management.
2. Indian Institute of Science (IISc), Bangalore	Tower instrumentation for all towers; intercomparison of surface layer data; R&D co-ordination and management.
3. India Meteorological Dept. (IMD), New Delhi	Maintenance and enhancement of conventional weather observing system; INSAT imaging; radar observations; and data processing of all these data. Support to operational centre at Calcutta and to MOCC at New Delhi.
4. Indian Air Force (IAF), Meteorology Branch, New Delhi	Aircraft flights; data collection from their observing systems.
5. Indian Institute of Technology, Delhi (IITD)	Maintenance of instrumented tower on campus and supply of data; R&D modelling.
6. Indian Institute of Technology, Kharagpur (IITKh)	Maintenance of special observational setup for MONTBLEX on campus.
7. Indian Institute of Technology, Kanpur (IITK)	Modelling R&D.
8. Banaras Hindu University (BHU), Varanasi	Maintenance of instrumented tower and other facilities on campus; supply of data.
9. Central Arid Zone Research Institute (CAZRI), Jodhpur	Maintenance of instrumented tower and other facilities like Sodar on campus; supply of data.
10. National Physical Laboratory (NPL), New Delhi	Supply and maintenance of monostatic sodars at Delhi, Varanasi and Jodhpur, and processing and supply of data.
11. Indian Statistical Institute (ISI), Calcutta	Monostatic sodar facility at Calcutta, and supply of data.
12. National Institute of Oceanography (NIO), Panjim	ORV <i>Sagarkanya</i> ; observational programme in north Bay of Bengal and supply of data.

13. Naval Physical Oceanography Laboratory, Cochin	Participation in oceanographic cruises of <i>Sagarkanya</i> .
14. Physical Research Laboratory (PRL), Ahmedabad	Organisation of oceanographic observational programme and study of MONTBLEX data.
15. Calcutta University, Calcutta	Study of MONTBLEX data.
16. Jadhavpur University, Calcutta	Study of MONTBLEX data.
17. Jawaharlal Nehru University (JNU), New Delhi	Study of MONTBLEX data.
18. Andhra University (AU), Waltair	Study of MONTBLEX data.
19. Department of Ocean Development (DOD)	Providing ORV <i>Sagarkanya</i> facility for the oceanographic programme in the Bay of Bengal.
20. Department of Science & Technology (DST), New Delhi	Funding; overall co-ordination and management.

APPENDIX 3

Journal publications resulting from MONTBLEX programme

- Gera B S and Singal S P 1990 Tropical boundary layer studies during monsoon period using sodar. In: *Acoustic Remote Sensing* (ed) S P Singal (New Delhi: Tata McGraw-Hill) pp. 390–394
- Gera M and Srivastava H N 1990 Acoustic sounding of atmospheric boundary layer. In: *Acoustic Remote Sensing* (ed) S P Singal (New Delhi: Tata McGraw-Hill) pp. 407–412
- Gera B S, Singal S P, Ramakrishna Y S and Vasudev S 1993 Anomalous sodar observation at Jodhpur during monsoon period; *J. Acous. Soc. India* **21** 105–109
- Goel M and Srivastava H N 1990 MONTBLEX; *Vayu Mandal* **19** 1–8
- Goel M and Srivastava H N 1990 Monsoon trough boundary layer experiment (MONTBLEX); *Bull. Am. Meteorol. Soc.* **71** 1594–1600
- Goel M 1992 Some aspects of boundary layer processes in monitoring climate change in Indian monsoon region; *Proc. 5th International Meeting on Statistical Climatology*, Toronto pp. 191–194
- Goel M 1993 Montbllex and monsoon dynamics: Early results; *Vayu Mandal* **22** 45–51
- Goel M 1993 A report on the workshop on MONTBLEX research results; *Curr. Sci.* **65** 897–899
- Goel M 1994 Acoustic sounding work in India and its potential in environment impact assessment; *Proc. 7th International Symposium on Acoustic Remote Sensing and Associated Techniques of the Atmosphere and Oceans* Boulder, USA
- Goel M and Ramanathan Y 1995 Study of rain episode in the desert region of the Indian summer monsoon trough; *Atmos. Environ.* **29** 2191–2198

- Kusuma G Rao, Sethu Raman, Prabhu A and Narasimha R 1995 Turbulent heat flux variation over the monsoon-trough region during MONTBLEX-90; *Atmos. Environ.* **29** 2113–2129
- Kusuma G Rao, Narasimha R and Prabhu A 1996 Estimation of drag coefficient at low wind speeds over the monsoon trough land region during MONTBLEX-90; *Geophys. Res. Lett.* **23** 2617–2620
- Parashuram, Venugopal T and Mohanty U C 1994 Simulation of the thermodynamic structure of atmospheric boundary layer over Calcutta with a 1 D TKE closure PBL model; *Mausam* **45** 107–114
- Parasnis S S and Goyal S S 1990 Thermodynamic features of the atmospheric boundary layer during summer monsoons; *Atmos. Environ.* **24** 743–752
- Parasnis S S and Morwal S B 1991 Convective boundary layer over Deccan plateau of India, during summer monsoon; *Boundary-Layer Meteorol.* **54** 59–68
- Parasnis S S, Morwal S B and Vernekar K G 1991 Convective boundary layer in the region of monsoon trough – A case study; *Adv. Atmos. Sci.* **8** 505–509
- Parasnis S S 1991b Convective mixing in the monsoon boundary layer; *Boundary-Layer Meteorol.* **48** 59–68
- Prabhu A and Vernekar K G 1990 Monsoon trough boundary layer experiment: Preliminary results; *Mausam* **41** 209–212
- Pradhan R, De U K and Sen P K 1994 Surface sensible heat flux over a deep moist convective region and its interplay with synoptic and mesoscale features; *Proc. Indian Acad. Sci. (Earth Planet. Sci.)* **103** 353–367
- Seetharamayya P, Parasnis S S, Nagar S G and Vernekar K G 1993 Thermodynamic structure of the boundary layer in relation to a monsoon depression over the Bay of Bengal – A case study; *Boundary-Layer Meteorol.* **65** 307–314
- Singh I P 1992 Surface fluxes and the cyclogenesis over north and adjoining north Bay of Bengal during MONTBLEX 1990; *Mausam* **43** 399–402
- Singal S P, Gera B S and Ojha V K 1993 Sodar studies of the monsoon trough boundary layer at Jodhpur (India); *Mausam* **44** 9–14
- Sivaramakrishnan S, Saxena S and Vernekar K G 1992 Characteristics of turbulent fluxes of sensible heat and momentum in the surface boundary layer during the Indian summer monsoon; *Boundary-Layer Meteorol.* **60** 95–108
- Surendra S P and Savita B M 1994 A convectively-driven boundary layer in the monsoon trough; *Boundary-Layer Meteorol.* **71** 197–204
- Surendra S P, Mrudula K K and Vaishali A K 1995 On the thermodynamics of downdrafts in the monsoon trough region; *Boundary-Layer Meteorol.* **73** 195–201
- Tripathy S K, De A K and Das J 1992 Computer analysis of atmospheric plume structures; *Indian J. Radio Space Phys.* **21** 321–328
- Tripathy S K, De A K and Das J 1993 A computer algorithm of noise removal in acoustic radar echograms; *Indian J. Radio Space Phys.* **22** 301–305
- Tyagi A, Mohanty U C and Ramesh K J 1994 Planetary boundary layer structure in the monsoon trough region; *Mausam* **45** 213–222
- Vernekar K G, Sadani L K, Mohan Brij, Saxena S, Debaje S B, Pillai J S, Murthy B S and Patil M N 1991 Structure and growth of atmospheric boundary layer as observed by tethered balloon payload; *Indian J. Radio Space Phys.* **20** 312–315
- Vernekar K G, Mohan Brij, Saxena S and Patil M N 1993 Characteristics of the atmospheric boundary layer over a tropical station as evidenced by tethered balloon observations; *J. Appl. Meteorol.* **32** 1426–1432

References

- Ananthakrishnan R and Rangarajan S 1963 *Indian J. Meteorol. Geophys.* **14** 173–189
- Augstein E, Riehl H, Ustapoff H and Wagner V 1973 *Mon. Weather Rev.* **101** 101–111
- Augstein E, Schmidt H and Postapuff 1974 *Boundary-Layer Meteorol.* **6** 129–150
- Badri Narayanan M A 1978 *Indian J. Meteorol. Hydrol-geophys.* **29** 459–466
- Beljaars A C M and Holtslag A A M 1991 *J. Appl. Meteorol.*, **30** 327–341
- Betts A K 1976 *J. Atmos. Sci.* **33** 1000–1020
- Betts A K 1978 Meteorology over the Tropical Oceans; *Q. J. R. Met. Soc.* **108** 105–132
- Betts A K and Beljaars A C M 1993 Estimating effective roughness length for heat and momentum from FIFE data; *Atmos. Res.* **30** 251–261
- Blackadar A K 1977 *High resolution models of planetary Boundary Layer*, *Adv. Sci. & Eng.* (Gordon & Breach, Sci. Publishers)
- Blanford H F 1886 *The Rainfall of India Met. Memoir* (Indian Meteorological Department)
- Colon J A 1964 *Indian J. Meteorol. Geophys.* **10** 295–299
- Brummer B, Augstein E and Riche H 1974 *Q. J. R. Meteorol. Soc.* **100** 109–121
- Colon J A 1964 *Mausam* **15** 183–200
- Deardorff J W 1970 *J. Atmos. Sci.* **27** 1211–1213
- Deardorff J W 1972 *Mon. Weather. Rev.* **100** 93–106
- Esbenson S 1975 *J. Atmos. Sci.* **32** 1921–1933
- Field J H 1905 *Mem. India Meteorol. Dept.*
- Garratt J R 1974 *Q. J. R. Meteorol. Soc.* **104** 199–211
- Garratt J R 1993 *J. Climate* **6** 419–449
- Garratt J R 1992 *The Atmospheric Boundary Layer* (U. K.: Cambridge University Press) 316 pp.
- Goel M and Srivastava H N 1990 *Bull. Am. Meteorol. Soc.* **71** 1594–1600
- Hariharan A S 1932 *India Met. Dept. Tech. Note* **50** 41–48
- Holton J R 1972 *An Introduction to Dynamic Meteorology* (Chapter Planetary Boundary Layer) (Academic Press Inc.)
- Holt T and Raman S B 1988 *Rev. Geophys.* **26** 761–780
- IITM 1982 *Proc. Symp. Environmental Physics and Atmospheric Boundary-Layer*, IITM, Pune
- Kailas S V (ed) 1990–92: *MONTBLEX News*, Indian Institute of Science, Centre for Atmospheric Sciences, Bangalore
- Kaimal J C 1988 *The atmospheric boundary layer – its structure and measurements*, Lecture notes, IITM, Pune
- Kaimal J C and Finnigan J J 1994 *Atmospheric Boundary Layer Flows* (Oxford: Oxford University Press) 289pp
- Krishnamurty T N and Bhalme H N 1976 *J. Atmos. Sci.* **33** 1937–1954
- Krishna Rao P R and Bhatia K L 1937 *IMD Sci. Note.* **78** 119–130
- Lettau H 1932 *Atmosphaerische Turbulenz* (Leipzig: Akademische Verlagsgesellschaft)
- Mahrt L 1983 *Rev. Geophys. Space Phys.* **21** 1042–1048
- Mahrt L and Ek M 1993 *Boundary Layer Meteorol.* **65** 381–400
- Mellor G C and Yamada T 1974 *J. Atmos. Sci.* **31** 1791–1806
- Mishra S K and Salvekar P S 1980 *J. Atmos. Sci.* **37** 384–394
- Monin A S and Obukhov A M 1954 Basic laws of turbulent mixing in the ground layer of the atmosphere; *Trans Geophys., Inst. Akad. Nauk USSR*, **151** 163–187
- Narasimha R, Prabhu A, Rao K N, Adiga B S and Ameenulla S 1981 *Project MOBLE. Reports 8IFM I 5*. (Dept. Aero Engg., IISc, Bangalore)
- Narasimha R, Prabhu A, Narahari Rao K and Prasad C R 1982 *Proc. Indian. Natl. Sci. Acad.* **A48** 175–186
- Normand C W B 1938 *Q. J. R. Meteorol. Soc.* **64** 71–74
- Panofsky H A and Dutton J A 1983 *Atmospheric Turbulence* (New York: John Wiley and Sons)
- Pant M C 1978 *Indian J. Meteorol. Geophys.* **29** 88–100
- Pant M C 1982 *Mausam* **33** 85–90
- Pant M C, Singh M S and Manohar Lal 1985 *Mausam* **38** 371–374
- Parasnis S S and Morwal S B 1991 *Boundary-Layer Meteorol.* **52** 69–74
- Ramdas J A and Atmanathan S 1932 *Beit. Geophys.* **37** 116–117
- Ramdas L A 1932 *Indian Meteorol. Dept. Sci. Note* **41** 115–124
- Ramachandran G, Rao K V and Krishna K 1980 *J. Appl. Meteorol.* **881–888**

- Raman S, Templeman B, Templeman S, Holt T, Murthy A B, Singh M P, Agarwal P, Nigam S, Prabhu A, Ameenulla S 1990 *Atmos. Environ* **24** 723–34
- Rao G V and Hor T H 1990 *Mausam* **41** 213–216
- Rao Y P 1976 *Southwest Monsoon, Met. Monograph 1/1976*. India Met. Deptt., 36pp
- Rao M S V, Sikdar D N and Chandrasekharan C 1965 *Indian J. Meteorol. Geophys* **16** 221
- Raychoudhury S N 1952 *Indian J. Meteorol. Geophys.* **3** 91–100
- Riehl H 1979 *Climate and Weather in the tropics* (Academic Press) 611pp
- Riehl H 1977 *Mon. Weather Rev.* **105** 1402–1420
- Roy A K 1946 *India Meteorol. Dept. Tech. Note* **16**
- Sadhuram Y, Krishnamurthy L and Babu M T 1989 *Boundary-Layer Metereol.* **48** 333–344
- Saha K R 1956a *Indian J. Meteorol. Geophys.* **7** 145
- Saha K R 1956b *Indian J. Meteorol. Geophys.* **7** 353
- Sawyer J S 1947 *Q. J. R. Meteorol. Soc.* **73** 346–369
- Shukla J 1978 *J. Atmos. Sci.* **35** 495–508
- Shirvaikar V V, Kapoor R K, Sundarajan A, Sharma L N and Shastri P L 1970 *Indian J. Meteorol. Geophys.* **21** 361–366
- Sikka D R and Mathur M B 1965 *Proc. Symp. Meteorol. Results of IIOE, IITM, Pune* 55–67
- Sikka D R and Gadgil S 1980 *Mon. Weather Rev.* **108** 1840–1853
- Sinha K L 1958 *Indian J. Meteorol. Geophys.* **9** 251
- Singal S P 1990 *Acoustic Remote Sensing*. Proc. 5th Intl Symp. Tata-McGraw Hill, New Delhi.
- Singal S P, Agarwal S K and Gera B S 1982 *Mausam* **37** 436–440
- Vasudeva Murthy A S, Srinivasan J and Narasimha R 1993 *Philos. Trans. R. Soc. London* **A344** 183–206
- Vernekar K G and Sadani L K 1980 *Indian J. Meteorol. Geophys.* **31** 125–132
- Yamada T 1976 *J. Atmos. Sci.* **33** 781–792
- Young J A 1987 In *Monsoon Meteorology* (eds) C P Chang and T N Krishnamurti (London: Oxford University Press)

Planning MONTBLEX – An overview

SUDARSH V KAILAS and MALTI GOEL*

Centre for Civil Aircraft Design and Development, National Aerospace Laboratories,
Bangalore 560 017, India

*Department of Science and Technology, New Delhi 110 016, India

Abstract. The multi-institutional experiment MONTBLEX aimed at sensing and studying the atmospheric boundary layer over the monsoon trough region of the northern plains of India during the summer monsoon of 1990. Four core facilities consisting of micro-meteorological towers and state-of-the-art instrumentation were created along the trough axis. This overview emphasizes the key features of project planning, management and execution, and provides details of all the experimental observation sites.

Keywords. MONTBLEX; monsoon trough; micrometeorological towers; atmospheric sensing.

1. Introduction

The Monsoon Trough Boundary Layer Experiment, acronymed MONTBLEX, was an intense multi-institutional effort sponsored by the Department of Science and Technology (DST), Government of India, intended to probe the atmospheric boundary layer (ABL) over the monsoon trough region of the Gangetic Plains. The project, initiated in March 1987, may be described as the largest meteorological field experiment originating from India and one among the largest atmospheric boundary layer projects carried out anywhere.

Atmospheric boundary layer processes affect cumulus convection, sub-cloud layer convergence, pollution dispersal, land-air and air-sea interaction etc. The monsoon trough (figure 1) is the seat of cyclonic vorticity in the lower troposphere, particularly along its eastern end over the north Bay of Bengal where organized moist convection prevails during the monsoon months. The disturbances move westwards and cause rain all over the Gangetic Plains. The western end of the monsoon trough is over west Rajasthan and adjoining Pakistan and is characterized by dry convection with shallow clouds. Very little information is available on the effects of boundary layer processes associated with the deep moist and the unsaturated, near-dry processes that respectively take place over the length of the monsoon trough as it extends inland, although understanding such processes is of primary importance for the investigation of monsoon dynamics.

A brief account of the genesis of the project appears in Sikka and Narasimha (1995). The project evolved from various discussions between different scientists, most notably R Narasimha, D R Sikka, A Prabhu and S Gadgil. Based on the recommendation of a scientists' meeting on implementation of the expert panel report on atmospheric sciences, held on 5th April 1984, DST constituted an expert group on atmospheric boundary layer studies chaired by R Narasimha, which after a number of meetings submitted a report on a co-ordinated study of the atmospheric boundary layer. This was

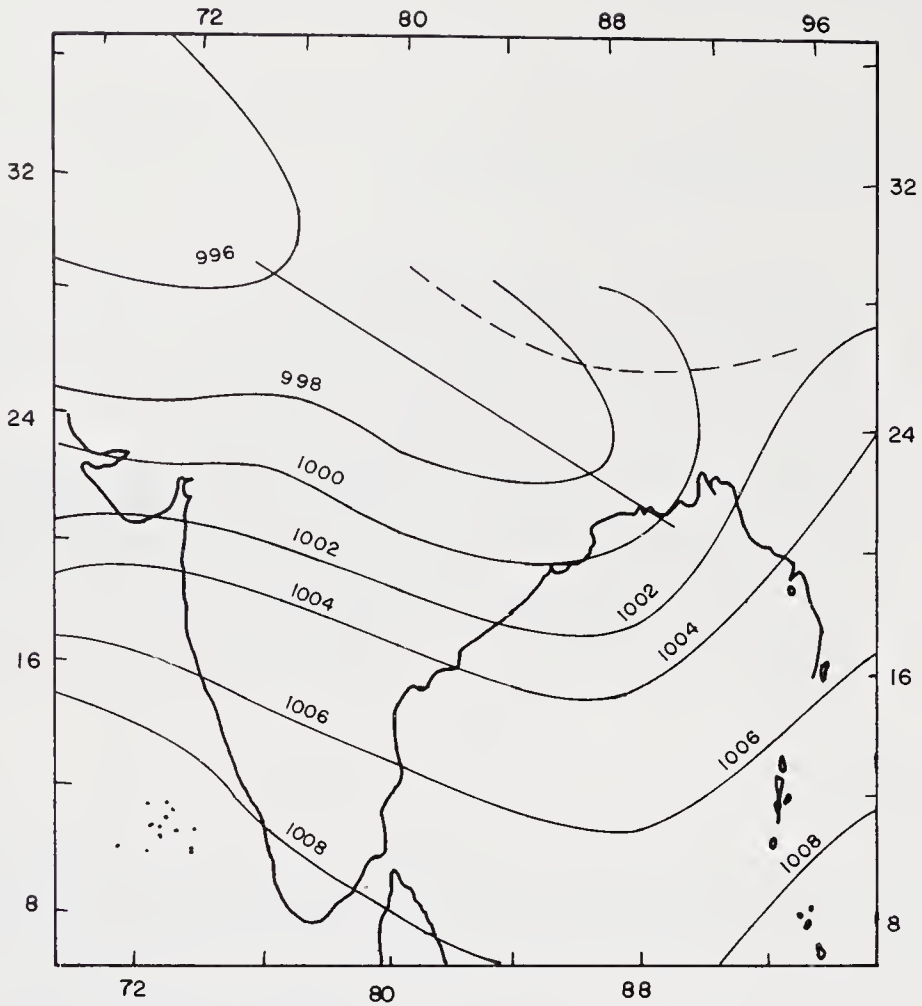


Figure 1. The position of the monsoon trough. The thick line indicates its position during active monsoon periods and the dashed line shows its northward shift during 'breaks' in the monsoon.

reviewed by the Project Execution and Monitoring Committee of the DST under the chairmanship of R P Sarkar, the then Director General of the India Meteorological Department (IMD), and the concept of MONTBLEX was accepted in July 1987. Three projects under the auspices of the Indian Institute of Tropical Meteorology, Pune (IITM), Indian Institute of Science, Bangalore (IISc) and the Indian Institute of Technology, New Delhi (IITD) respectively were approved as parts of a co-ordinated project on boundary layer studies on 25th March 1988.

2. Objectives, scope of the project and the organizations involved

The objective of the experiment was to collect comprehensive data on both mean and fluctuating atmospheric parameters from stations along the location of the monsoon trough and selected adjoining areas including the Bay of Bengal during the period of the 1989 monsoon. These dates were later modified so that a pilot experiment could be conducted during the 1989 monsoon with the full-fledged main experiment slated for 1990.

The main component of the project was the construction of three micro-meteorological towers at Kharagpur, Varanasi and Jodhpur and augmenting an existing tower at the IIT, Delhi. These towers were equipped with state-of-the-art fast-response instrumentation and data acquisition systems for sensing and recording the mean and fluctuating wind speed, wind direction, temperature and humidity in the ABL and soil temperature (Rudrakumar *et al* 1995; Narahari Rao 1995).

Complementing the towers were extensive observations of the state of the atmosphere with an array of sensing systems including sodars, pilot balloons, tether sondes, radiometer flights, radar and ground observations from weather stations at the tower sites and the existing networks of IMD and the Indian Air Force (IAF). Simultaneous oceanographic and meteorological observations during cruises by ORV *Sagarkanya* of the Department of Ocean Development in the Bay of Bengal and aircraft flights by the IAF over the trough region were also conducted.

The responsibility for the tower stations, from design to collection and validation of data, was with A Prabhu and his group from the Centre for Atmospheric Sciences (CAS), IISc. The group from IITM led by K G Vernekar conducted sodar, tether sonde and pilot balloon experiments from Kharagpur and took part in the ship cruises. The IMD and the Met. Division of the IAF conducted ground and pilot balloon measurements. The IMD was also in charge of radiometer, radar, satellite and upper air observations while the IAF also conducted instrumented aircraft flights.

The National Institute of Oceanography (NIO) conducted the special MONTBLEX cruise of the ORV *Sagarkanya* during which measurements were made by scientists from IITM, IMD, the Naval Physical and Oceanographic Laboratory (NPOL) and NIO.

The National Physical Laboratory (NPL) installed a monostatic sodar and conducted measurements at Jodhpur while the Indian Statistical Institute (ISI) did so at Varanasi.

Goel and Srivastava (1989, 1990) have earlier discussed the limitations in the current knowledge of the monsoon system and the scope for additional observations that led to the concept and objectives of MONTBLEX, the design of the experiment and future data needs.

3. Project planning

The planning and execution of the project was carried out through various committees and groups, with the composition shown in Appendix 1. The progress of the project was continually reviewed by the MONTBLEX Monitoring Committee (MMC). A Science Advisory Group (SAG) assisted the MMC in scientific matters. A modelling group took care of advising the MMC on the specialized requirements of data for monsoon modelling, one of the primary objectives of MONTBLEX. Plan documents (see below for details) on operations and data management were prepared. A MONTBLEX Operations Control Centre (MOCC), set up in the offices of the IMD, New Delhi, identified periods for intensive observation and informed all data collecting platforms about the progress of the monsoon. A MONTBLEX Operations Director (MOD) performed the critical task of setting up and running the MOCC. On completion of the project a data centre was established where all data were collated and stored centrally. A data users meeting assessed data needs and archiving options from the point of view

of the users of MONTBLEX data. Various workshops were conducted on the basic physics of the atmospheric boundary layer, the science (and art) of its measurement and on the results of analysis of the data acquired. Reports were prepared on the various aspects of MONTBLEX including studies using data acquired from its different observation platforms. *MONTBLEX News*, a newsletter sponsored by DST, was published from IISc detailing the progress of the project. The DST earth and atmospheric sciences section was the primary administrative node for all the inter-institutional co-operative efforts.

3.1 *Monitoring MONTBLEX*

This was in the charge of MMC, which met five times from 1988 till 1992 at various places including IIT Kharagpur, IISc and DST Delhi, to monitor the health of the project and decide on the future course of action at each stage of the project. On 19th – 20th September 1988, MMC took various preparatory steps, including the establishment of a data management cell, the publication of a MONTBLEX bulletin, the organization of a winter school for participants and observers, and the constitution of the Scientific Advisory Group. On 19th May 1989, it was decided to conduct a pilot experiment during 1st to 7th July 1989 and in this connection to establish an operations centre at Calcutta. On 19th September 1989 the pilot experiment was reviewed, and it was decided to go ahead with the main experiment in 1990, including a ship observation plan. On 12th April 1990 the state of preparedness for the main experiment was reviewed.

On completion of the main experiment, the results were reviewed on 23rd January 1991 and it was decided that all data should, on completion of processing, be transferred to a MONTBLEX Data Centre to be set up at IITM.

3.2 *Scientific Advisory Group*

This group (SAG) prepared the observation strategy for MONTBLEX. It guided the project on positioning the ORV *Sagarkanya* over the head of the Bay of Bengal, the need for supplementary aircraft observations and the preparation of a detailed map of the observation system to study the monsoon circulation. The group also formulated the detailed observational programme to be implemented by IMD and other participating institutions, for an area of radius 400 km centred around the Kharagpur tower, with an area within a radius of 200 km being a core region.

On 3rd July 1991, upon the completion of the experiment, SAG suggested that the infrastructure created under MONTBLEX continue to be operational. A spin-off has been the formulation of a programme on Radio Acoustic Sounding System (RASS) for which a RASS core group has been constituted to suggest an action plan.

3.3 *The modelling group*

The MONTBLEX modelling group met at DST on 21st March 1990, reviewed the results of the pilot experiment and made recommendations on calibration of sensors and on collection of additional soil data.

3.4 Plan documents

As part of the planning process, two plan documents, on operations and data management respectively, were prepared and submitted to the monitoring committee.

3.4.1 *The MONTBLEX operations plan:* This document (Kusuma Rao and Prabhu 1988) summarized the scientific objectives, specific tasks and data requirements to be fulfilled by MONTBLEX, listed the participating agencies and identified the MONTBLEX area of operations. Based on these proposals, the plan identified the operations schedule at the different experimental sites and components for 1989 and 1990.

The observational programme was divided into a core programme and a supplementary programme. The core programme included measurements of surface turbulent fluxes at the four tower locations representative of various distinct physical processes that take place in the region of the monsoon trough; and radiosonde, radiometer, sodar, tetheredsonde, radiation, radar, ship and satellite information which are to be collected from identified stations along with standard synoptic data. A supplementary programme was to have included tower observations at NIO, Goa and INCOR, Visakhapatnam but this unfortunately had to be abandoned. A work plan showing the responsibilities of each participating group was described in considerable detail. The specifications of the measuring sensors were also set out in the plan.

The concept of the MONTBLEX operations centre (later to become the MOCC) was introduced and its role identified. This centre was planned to consist of operational forecasting, scientific planning, operations control, administrative services and data management. Key components of the MOC were a forecast centre located at IMD Delhi, a support centre housing the data management group at Bangalore, and an intensive operations period advisory group.

At the suggestion of the MMC, a design and operation plan for MONTBLEX-90 was prepared by D K Rakshit. The plan highlighted the objectives and goals of the experiment, identified 18 institutions and agencies to be involved in the data collection, analysis and modelling, listed observational requirements and allocated specific tasks.

3.4.2 *Data management plan:* This plan (Kailas and Prabhu 1988) considered various aspects of data collection, quality control and archiving of all the data recorded during the operational periods of the different segments of the MONTBLEX data acquisition system. In particular, the plan included the following: summary of all data acquisition platforms including the instrumentation; data expected to be available from the above and the responsibility of data collection and transmission to the data centre; periodic checking of data for quality control and feed-back to the collecting agency; quick dissemination of data while events are fresh in the minds of MONTBLEX participants and other user groups; ensuring a centralized and well-documented archive of all data under the MONTBLEX data centre, and preparation of a catalogue of the MONTBLEX data base called the MONTBLEX data book.

A time table was also formulated to help the investigators plan the various stages of the experiment well in advance, and to bring out the data book.

3.4.3 *Ship observation plan:* Following various earlier discussions, the ship observation plan was finalized on 18th August 1989. It was decided that the ORV *Sagarkanya*

would be on a MONTBLEX cruise between 10th June and 31st July 1990 in the north Bay of Bengal during different monsoon conditions coinciding with the major observational phase of MONTBLEX. The period was later changed to 10th August to 30th September 1990 based on the availability of the ship. Scientists from IMD, IITM, NIO and NPOL Cochin, participated in the cruise. It was decided to acquire surface meteorological observations every hour, radiosonde observations twice a day as routine and four times a day during the intensive observation periods, along with XBT and thermistor chain data and omegasonde readings.

3.5 *The MONTBLEX operations control centre*

This centre, with its own operations director, was set up to co-ordinate all operations and advise on the intensive observation periods during the MONTBLEX main experiment, viz., 15th May to 30th September 1990. The centre was established as an extension of one of the field units of IITM Pune, at the office of the Director General of Meteorology, New Delhi, utilizing the extended weather charts and other facilities for monitoring the evolution of the monsoon systems available there. MOCC was under the overall guidance of the MMC. M G Gupta, the Director of MOCC, received support from IMD scientists at the Northern Hemisphere Analysis Centre (NHAC), New Delhi, scientists of the MONTBLEX modelling group and representatives of the Indian Air Force in discharging his operational responsibilities. The day-to-day progress of the monsoon was critically reviewed in periodic discussions (normally tri-weekly). Extended weather charts, cloud pictures recorded by INSAT, rainfall summary prepared by NHAC and other relevant information were used in these discussions to assess the prevailing weather systems relevant to the monsoon and their likely behaviour during the next 2–3 days. Based on these, advisories were finalized for the observation programme with the specific intent to identify Intensive Observation Periods (IOPs) and aircraft tracks.

The IOPs identified during MONTBLEX 1990 are listed by Srivastav (1995). The withdrawal of the monsoon did not commence till 14th September 1990 when MOCC discontinued issue of operational messages.

3.6 *Data users meeting*

Immediately after the successful completion of the main experiment, the following five groups were formed by data users to co-ordinate data processing, with IISc handling the surface and tower data; IITM, Pune the sodar data; IITM, Delhi the IAF data; and NIO the ORV *Sagarkanya* observations. Also a data archiving and distribution centre was established at IITM. A data catalogue based on the WMO format with INSAT pictures included in the synoptic report was prepared by the MOCC.

3.7 *The data centre*

This centre has been set up at IITM, and is described separately by Vernekar (1995).

3.8 Training programmes

A training-cum-orientation workshop for MONTBLEX participants was organized by the Department of Physics and Meteorology at IIT Kharagpur from 3rd to 7th April 1989. Using the first MONTBLEX tower as it was getting ready, various scientific groups, particularly the observational and experimental teams, were trained on various data-collecting methods and procedures used in the project. An intensive course on the atmospheric boundary layer and turbulence was conducted at IISc from 25th April to 4th May 1990. Over thirty participants were introduced to MONTBLEX tower instrumentation and related hardware and software, for which purpose a small micro-meteorological tower was erected.

3.9 News about MONTBLEX

A news letter on MONTBLEX provided a useful record of the activities of the many different groups, institutions and data platforms, and acted as a forum for exchange of information and messages. Five issues of the news letter were issued from May 1989 to January 1992. Articles in scientific journals (Goel and Srivastava 1989, 1990) presented the details and scope of MONTBLEX to a wider audience.

4. Experiments conducted

4.1 The pilot experiment

In July 1988, the IISc team along with the IITM instrumentation group and IIT Kharagpur scientists set up the first of the 30 m MONTBLEX towers in the farmland near the southeastern boundary of IIT Kharagpur. The tower site enjoys an uninterrupted fetch of over 500 m towards the south, the region of the prevailing monsoonal winds. The tower (set up in two weeks) had instruments to measure slow winds (1 Hz), humidity, temperature and direction at 6 levels: 1, 2, 4, 8, 15 and 30 m. In addition, fast response (around 8 Hz), wind speed and temperature sensors were installed at 4 and 15 m. At 15 m a hot wire anemometer was also installed. A PCM telemetry system transferred the data signals conditioned by translators housed at the foot of the tower to a PC kept in a room some 200 m away. For details on the instrumentation see Rudra Kumar *et al* (1995).

The instruments withstood the vagaries of the tempestuous weather at the site in 1989, and the team had an opportunity to learn about possible problems when the data acquisition system failed due to lightning, power failure or theft of a section of the linking cable. Some of the data were analysed by the Bangalore group and presented at a project monitoring committee meeting at Kharagpur in September 1989.

With this tower ready and operational, the pilot experiment was conducted during 1st–7th July 1989. The objectives of the experiment were to test all the tower instruments and the data acquisition system, initiate an operations centre at IMD Calcutta, activate the communications network for data transfer, and gear up the data management centre for large scale data processing and replication; in other words, to

test if the system worked well as an integrated whole. The observation platforms included for this experiment were the tower at IIT, Kharagpur, the 20 m tower at IIT, Delhi and the IMD network over the trough region.

The IISc group reached Kharagpur on 1st July and, after calibrating and checking out the whole system, began data acquisition on 2nd July 1989. Three-minute averages of slow tower data were recorded on cassettes, and fast data on the hard disk of a PC-XT. The IITM group installed a Lyman-alpha humidity meter and launched minisondes. There were many improvements incorporated, notable among them being the complete automation of the data acquisition making it possible to record data automatically for a specified period at specified intervals. For details on the tower, sensors and on the data availability see Prabhu *et al* (1990).

4.2 *The main experiment*

4.2.1 *The 1990 monsoon:* A brief discussion of the progress of the 1990 monsoon over India appears in Srivastav (1995). It is seen that the monsoon advanced into the south Andaman Sea and adjoining southeast Bay of Bengal on 19th May, one day ahead of the normal date. It set in over Kerala on 28th May four days ahead of the normal date, and reached Bombay ten days ahead of the normal date.

The progress in the East was only slightly slower, setting in over Calcutta and most of the northeast on 6th June, close to the normal date. Further advance came with the depression of 14th–15th June and its westward movement. Subsequent lows that developed in the monsoon trough region and moved west-northwest, maintained the progress of the monsoon into northwest India. Delhi witnessed its arrival on the normal date of 29th June. The pace then quickened and the entire country was covered by 1st July, two weeks in advance of the normal date. In short, the progress of the onset of the monsoon from Kerala to northwest India took 35 days, less than the normal 45 days. It arrived 7–10 days ahead of normal onset over most of the country, and two weeks ahead in many places in northwest India.

During most of July, the monsoon trough was fairly active and a number of embedded lows were formed. These travelled as usual in a west-northwest direction and were generally associated with an upper air circulation extending to mid-tropospheric levels. The few western disturbances of that year also moved across the northern part of the country causing a temporary 2–3 day northward shift of the monsoon trough. Interestingly, break conditions in the monsoon, when the entire trough axis shifts to the Himalayan foothills, did not develop in the July–August period.

August was remarkable for the strong variations in the synoptic conditions. The upper troposphere in the northern extratropical regions of the country was affected by the meridional flow displacing the sub-tropical high northward. This led to weak surface pressure gradients, so much so that the monsoon trough was not discernible for a few days till a depression developed in the west central Bay of Bengal and travelled across central India. A few days later another depression with a life span of 5 days formed in the north Bay. The passage of the remnant of Typhoon Becky into the northeast Bay across the Arakan Coast towards the end of August and its progress west-northwest helped in the continuance of the mid-monsoon phase, which was 3–4 weeks longer than normal over many parts of NW India, probably being the cause of the above-normal rainfall.

Normally the June–September monsoon season is punctuated by 9–10 depressions (1–2 in June, 2–3 each in the following months). The 1990 monsoon saw only 4 depressions – one each in June and September and two in August (see table 3 in Srivastav 1995).

The early onset along with the absence of break conditions and the late withdrawal provided a longer than normal mid-monsoon phase. Rainfall was fairly well distributed in time and space with no report of severe flood conditions anywhere in the country. The country thus experienced good rainfall (6% above normal, among the best three of the decade, the other two being 1983 and 1988) during the southwest monsoon season of 1990. An overall review of the season is presented by Srivastav (1995).

4.2.2 *The tower sites:* The instrumentation group at CAS, IISc set up the two towers at Banaras Hindu University (BHU), Varanasi and Central Arid Zone Research Institute (CAZRI), Jodhpur in January 1990. At Jodhpur, the whole system was also tested and all links checked out in January; this early operationalization was beneficial, for it took just three days to reactivate it for the main experiment (which began only some months later). The system worked uninterrupted except when severe floods in late June forced a shut-down for a few days. Though the Varanasi tower could not be made operational till early June due to various local problems, once these were sorted out, the system ran satisfactorily though not as spectacularly. The Jodhpur tower over-looked a large 400 m swath of desert flats while the Varanasi tower overlooked nearly 300 m of flat (and at that time fallow) farmland with trees in the distance.

The fast-response sensors, complementary signal conditioning electronics and data acquisition software, all developed for the experiment, worked satisfactorily. All the towers had Lyman-alpha fast-response humidity sensors developed in-house at CAS, IISc with the collaboration of IITM. A fast-response infra-red humidity meter was also developed but could not be made operational for MONTBLEX due to difficulty in procuring certain critical imported sensors. As the dates for the main experiment neared, the group had upgraded the 32-channel PCM transmitter-receiver system to handle 64 channels and vastly improved its electronics and reliability. The instrumentation at each tower is discussed by Rudra Kumar *et al* (1995).

The Kharagpur tower was made operational for the main experiment on 25th May 1990 by the IISc team. The slow data from 32 channels of the tower sensors were continuously recorded on cassette tape of a Campbell data logger as three-minute averages. Fifteen minutes of fast data from 32 channels were recorded on the hard disk of a PC-XT every three hours (0530, 0830, 1130, 1430, 1730, 2030, 2330 hrs UTC) and transferred on to a cartridge tape.

At Varanasi, the slow data acquisition system was tested (after drawing a temporary cable over a distance of nearly 400 m) at the time of setting up the tower in January 1990. After the team returned to Varanasi on 26th May, a temporary shed housed the data acquisition computer, and data acquisition was begun on 8th June after considerable teething trouble. Because of the lack of time for a thorough running-in of the system and the extreme heat, less data could be acquired than at the other sites. The system was otherwise identical to that at Kharagpur.

At Jodhpur the tower was installed in late December 1989. Most of the instruments were mounted and both the slow and fast data acquisition were checked out in early January itself. All the systems were rechecked in April.

The whole system was quickly made operational in June. The configuration of the system was the same as at Kharagpur and Varanasi. The system broke down due to unprecedented floods (the worst in a 100 years) in Rajasthan, with Jodhpur being among the worst hit. Despite the incessant rain and water-logging the system was reactivated in near entirety within a few days. The early operationalization of the tower is reflected in the fact that this tower provided the cleanest and largest amount of data.

The Delhi tower, identical to the other towers, was made operational in May 1990 with data being acquired from early June.

The tower data have been discussed by Rudra Kumar *et al* (1995). A series of eight checks were made on both profile and turbulence data. These consist of:

- time traces from various sensors;
- comparative plots of data from sensors measuring the same variable;
- wind and temperature profile plots;
- calculation of roughness lengths;
- statistical parameters;
- stability parameters and their diurnal variation;
- probability density plots; and
- energy spectra.

The data analysed were selected randomly from sonic, hotwire and Gill anemometers, slow and fast platinum temperature sensors, humicaps and windvanes. Plots of time series helped eliminate data that is too spiky or having signal drop-outs or having poor correlation between different levels. Comparison of traces of different sensors measuring the same physical variable helped in the data reliability assessment and faulty sensors are listed. If the number of spikes are few it is reported as 'spiky' or the actual number of spikes are listed in an appendix that is attached to the data report (Rudra Kumar *et al* 1991). If the data is very bad, either due to too many spikes or because the sensor was not working for a major part of the time, that data set is not stored.

Traces of horizontal velocity from the sonic and Gill anemometers were compared to that of the cups and mismatches reported.

Comparison was made of fast temperature from the platinum thermometer and the sonic anemometer. Only Lyman-alpha data which matched data from the nearest humicap sensor were stored.

Profile plots of averages helped indicate offset errors in different sensors which would show up as kinks in the otherwise smooth profile. Statistical parameters like standard deviations, fluxes and correlation coefficients were determined and checked for expected values as quoted in the literature. Diurnal variation of the gradient Richardson number, the flux Richardson number, the Monin-Obukhov length, fluxes, eddy coefficients etc. were computed and checked for expected trends. Probability distributions were checked for deviation from the standard Gaussian. The spectra of the velocity components from the different fast sensors, and of the temperature and humidity, were plotted and checked for the existence of the Kolmogorov drop-off in the inertial sub-range.

The data are checked for invalid values (e.g., negative values when the sensor is off), and wrong entries by the collecting personnel. It is finally organized into files containing all available data of *one variable* from one station along with useful notes and comments on the various data sets available.

Table 1. Special IMD stations for radiosonde/radiowind observations for MONTBLEX-90.

Station	No. of RS/RW ascents	No. of low level soundings	Total
Calcutta	261	70	331
Bhubaneswar	170	70	240
Ranchi	214	57	271
New Delhi	262	46	308
Jodhpur	249	46	295

Table 2. Special IMD stations for pilot balloon ascents.

Stations	Number of ascents
Jamshedpur	350
Raipur	399
Gopalpur	399
Balasore	425
Jharsuguda	277
Gaya	474

The tower team consisted of A Prabhu, S V Kailas, S Ameenulla, S Rudra Kumar, H P Srinivasan, S Vasudev, B Madhu, Chikke Gowda, H Raja and K Shiva Shankar from IISc and A Chandrashekar, Badrinath and Rajkumar from IIT, Kharagpur took part.

4.2.3 The IMD component: The IMD conducted extensive observations from 15th May to 22nd September. These included upper air, pilot balloon (PB), surface and radar observations (see Srivastav 1995).

In addition to the routine observations carried out by the upper air network, additional observations were required from various network stations. Hence besides the usual 0 and 12UTC radiosonde/radiowind observations, five stations (Calcutta, Bhubaneswar, Ranchi, New Delhi and Jodhpur) were earmarked to take special observations at 6 and 18UTC using low level sondes and these are listed in table 1. Similarly, in addition to routine observations from a number of PB stations in the area of interest, the six stations at Jamshedpur, Raipur, Gopalpur, Balasore, Jharsuguda and Gaya carried out additional PB observations all of which are listed in table 2.

The Calcutta centre conducted one radiometersonde ascent per week during the IOPs, whereas Bhubaneswar and Jodhpur conducted routine fortnightly ascents. In all, 10 ascents were made at Calcutta and 6 each at Jodhpur and Bhubaneswar.

Weather radar observations, three-hourly or more frequent, were taken from the X-band radars at Calcutta and Ranchi. The Calcutta radar made 1503 observations while the one at Ranchi made 289.

The IMD scientists on board ORV *Sagarkanya* on the MONTBLEX cruise (11th August – 23rd September 1990) carried out three-hourly surface observations in

addition to one daily radiosonde (00 UTC) and low level ascent. In all 275 surface observations, 33 radiosonde and 30 low level soundings were taken during the cruise.

All the stations which conducted PB ascents also recorded three-hourly surface observations.

The participants from IMD are too numerous to be listed here but the contributions of the teams led by S K Srivastav and others have been extensive.

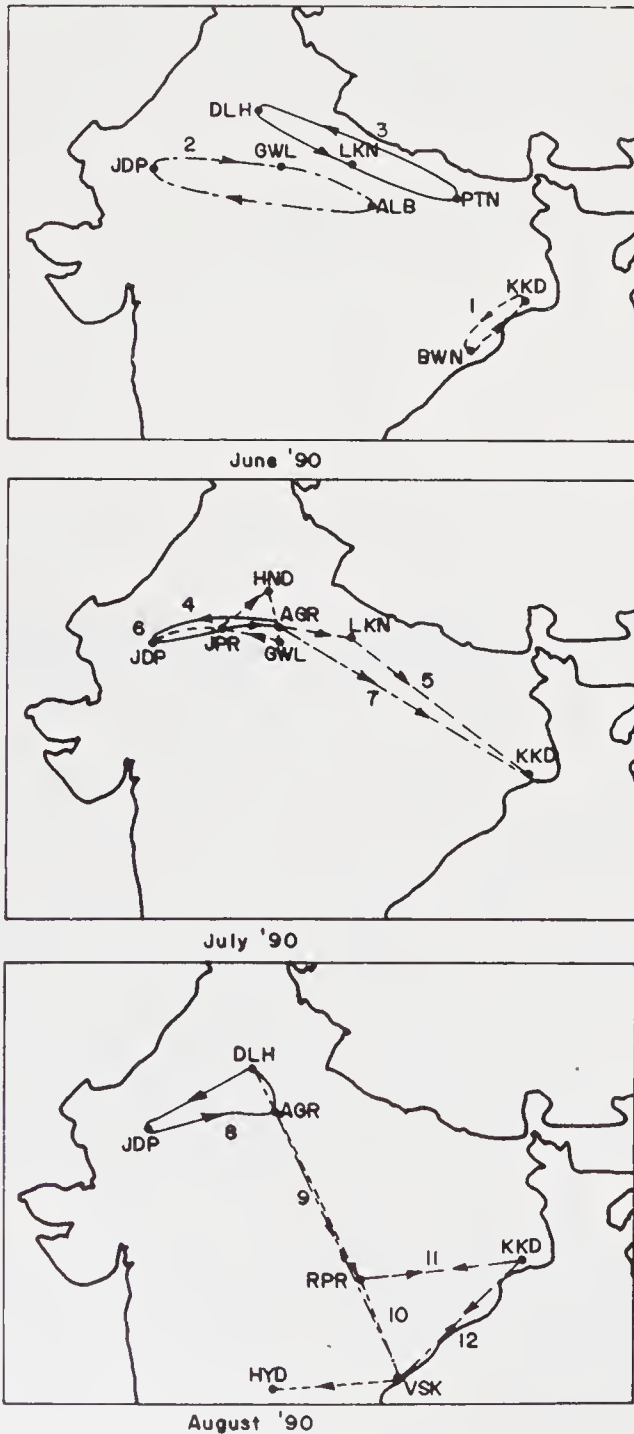


Figure 2. The paths of the aircraft flights. In all, 12 flights were made over the monsoon trough region and sometimes beyond.

4.2.4 *The IAF contribution:* The Indian Air Force collected surface and pilot balloon data along the monsoon trough from their in-house observatories besides undertaking rather extensive aircraft flights for MONTBLEX.

Twelve IAF met. sections, viz., Kalaikunda, Allahabad, Kanpur, Lucknow, Gorakhpur, Hindon, Agra, Jodhpur, Gwalior, Bareilly, Suratgarh and Bhatinda took surface observations from 1st May to 15th September 1990. Surface observations were recorded at three hourly intervals at the synoptic hours. During IOPs, surface observations were recorded by the hour UTC.

Pilot balloon observations were recorded at four stations, Kalaikunda, Agra, Suratgarh and Bhatinda at 00 and 12UTC, with 06UTC recorded additionally during IOPs.

Cloud ceiling readings were recorded at Kalaikunda, Gwalior, Agra and Jodhpur using laser ceilometers and ceilographs.

Twelve An-32 sorties (42 hours in all) were flown by IAF from Allahabad, Hindon, Agra, Kalaikunda and Jodhpur (with one Met. Officer on board on all the flights). In-flight observations of wind direction, wind speed and air temperature were taken every 10 minutes. All the sorties were arranged with a notice of 48 hrs. The sorties covered the areas of meteorological interest determined by MOCC. Figure 2 shows the tracks of these flights.

AVM. N Natarajan, Air Cmde. K C Varma and Gp. Capt. O P Madan, besides many observers from the different centres, took part in this effort.

4.2.5 *The ocean observations:* Cruise 56 of the ORV *Sagarkanya* sailed from Marmugao at 12UTC on 11th August 1990 for MONTBLEX observations in the north Bay of Bengal. Surface meteorological observations were started from 15UTC on 11th

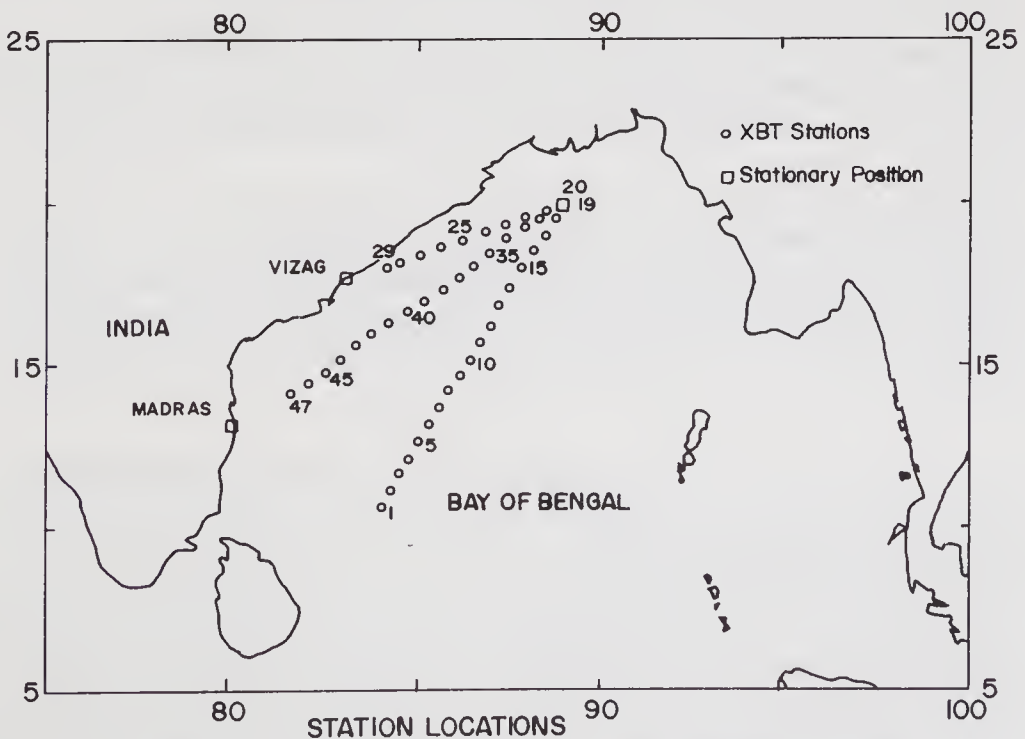


Figure 3. The path of the ORV *Sagarkanya* during its MONTBLEX cruise showing XBT stations.

Table 3. Observations made on ORV *Sagarkanya*.

Parameter	No. of observations
CTD	251
STD	210
Upper air ascents	73
XBT	48

August and were repeated at 3-hour intervals. Upper air ascents were begun from 15th August when the vessel entered the Bay of Bengal, and were repeated at the synoptic hours. The vessel reached the stationary position 20°N/89°E at 2230UTC on 17th August, at which time observations on oceanographic and meteorological parameters were started; they continued till 2330UTC on 1st September. The vessel reoccupied the same position from 1640UTC on 8th September till 2330UTC on 19th September after a trip to Visakhapatnam for provisions and bunkers. Figure 3 shows the track of the ORV *Sagarkanya*.

The observations made at the synoptic hours consisted of CTD up to 100 m, STD up to 300m, surface and micrometeorological observations (with sensors fixed on a 5 m long boom projecting into the sea from the bow of the vessel), upper air ascents at 00 and 12UTC, continuous measurements of atmospheric electricity and precipitation current measurements when rain occurred. XBT launches were made at 3-hourly intervals when the vessel was cruising from 10, 34.2°N/84, 02.2°E up to 20°N/89°E during 15th–17th August, from 20°N/089°E up to Visakhapatnam during 1st–3rd September and from 20°N/089°E up to Madras during 19th–22nd September. Table 3 lists the number of observations made at the synoptic hours. Three additional radiosonde ascents were made at 06UTC during 23rd–25th August.

During the cruise the vessel experienced four low pressure systems of which two were weak. The observations were completed on 19th September at 2330UTC and the cruise concluded at 08UTC on 22nd September when the vessel reached Madras.

The cruise participants were D P Rao with Y V B Sarma, G Nampoothiri, A M Michael, R Vaithyanathan and P Chodankar (all from the Physical Oceanography Division of NIO), Y E A Raj, P P Butala, P Sridharan, Kuldip Wali, P M Jagmohan Rao and S V Lambat (from IMD), P Seetharamaiah and C G Deshpande (from IITM), K V Sanil Kumar, N Mohankumar and M X Joseph (from NPOL) and 7 graduate trainees.

4.2.6 Studies by IITM: The instrumentation group at the Indian Institute of Tropical Meteorology, Pune operated a Doppler sodar, a Kytton and minisondes at the Kharagpur core station during MONTBLEX.

The Doppler sodar was made operational on 15th May 1990 and collected data up to 8th September 1990, operating continuously during IOPs, but was restricted to day time observations during other periods, except during 1200–1500 h UTC and during power failures.

Data on the three wind components and their standard deviations, echo intensity, reliability of data etc. were recorded and are available on IBM compatible floppies recorded in ASCII or as facsimile records of the return echo.

The tethersonde system was operated at Kharagpur from 22nd May to 28th June. The number of flights had to be restricted due to high wind, rain, lightning and other constraints. In all 28 flights were recorded. Data are available as a computer printout for wind speed and direction, dry and wet bulb temperatures and pressure. Other derived parameters like relative humidity, mixing ratio, potential temperature, dew point etc. are also available.

Data of temperature versus height from 42 minisondes with an ascent rate of 100 m/min during the IOP in July were recorded as graphs and tables.

The IITM team included K G Vernekar, S Sivaramakrishnan, L K Sadani, Brij Mohan, S B Debaje, S Pillai, B S Murthy, M N Patil, Subrato Sinha, Seethramayya and S S Parasnis.

4.2.7 The NPL sodar experiments: The MONTBLEX core station of Jodhpur, representative of the dry convection in the desert region in the west, was equipped with a monostatic sodar which was designed and set up by the acoustics section of the National Physical Laboratory, New Delhi.

The instrument worked automatically and almost continuously (70% of the time) from 30th May to mid-September 1990, needing very little personal attention and recording the thermal structure of the ABL up to a height of 700 m.

Shear echoes from nocturnal inversions with flat tops and tall spiky tops of the undulating kind have been seen. Day time thermal echoes showing the formation of thermal plumes due to solar heating of the earth's surface were also observed. The erosion of the nocturnal stable layer structure soon after sunrise has also been recorded. The height of the structures can be measured and the changes in the structures due to various weather phenomena can be studied (Singal *et al* 1993).

S P Singal, B S Gera and V K Ojha from NPL took part in the experiments.

4.2.8 The ISI monostatic sodar: The Indian Statistical Institute (ISI), Calcutta set up a monostatic sodar at Varanasi from 28th May 1990 to 3rd September 1990. Inversion heights, types of inversions and thermals were recorded as hardcopies. J Das took part in the experiment.

4.2.9 Studies by NPOL: Three scientists (see section 5.2.5) from the Naval Physical and Oceanographic Laboratory, Cochin took part in the MONTBLEX cruise of ORV *Sagarkanya*. Time series of vertical profiles of temperature and salinity were measured to understand the heat and salt budgets of the mixed layer.

5. The post-MONTBLEX workshops

After the completion of MONTBLEX, results of the analyses of the data were presented at two workshops. The first, titled 'Workshop on preliminary scientific results of the MONTBLEX programme', was held on 16th–17th January 1992 at IISc, while the next titled 'The second monitoring workshop on the MONTBLEX research results' was held on 26th–27th March 1993 at IITM. Proceedings of these workshops were brought out and are available at DST and IITM respectively. A report on the second workshop appeared in Goel (1993). These workshops were occasions for all those who had used MONTBLEX data to share their results and experiences from the analysis of the data,

Table 4. Consolidated picture of data acquired during MONTBLEX 1990.

Slow response tower data.....	on all days with few interruptions
Fast response tower data.....	70%
Soil temperature.....	90%
Doppler sodar (Kharagpur).....	worked very well
Monostatic sodars (Jodhpur, Calcutta).....	good
IMD radiosonde.....	500 ascents
IMD radar.....	2 stations
IMD radiometeorology data.....	90%
Kytoon flights (Kharagpur).....	28
Miniradiosonde flights (Kharagpur).....	42
XBT profiles (Bay of Bengal).....	47
IAF upper air observations.....	12 stations

e.g., an intercomparison experiment for validating the methodology for computation of surface fluxes was conducted and the results presented in the second workshop.

6. Conclusions

MONTBLEX collected a vast amount of data, a consolidated picture of which is listed in table 4.

The set of extensive, simultaneous data collected over a vast region will probably continue to be analysed for a long time, hopefully revealing various facets of the Indian monsoon hitherto unknown to us.

Acknowledgements

It is a pleasure to acknowledge the strong support given to this project by Dr. V Gowariker and Dr. P Rama Rao, successive Secretaries in DST during the course of the project; by Drs. M N Qureshi, H N Srivastava and H K Gupta, Advisers on Earth Sciences at DST; and by D T Vengayil and D R Ram who helped M G in co-ordinating the project effort at DST.

APPENDIX 1

The execution of the project was carried out through the following working groups and committees.

■ **MONTBLEX Monitoring Committee:** S K Dube (IITD), M Goel (DST, Convenor), R N Keshavamurthy (PRL), R Narasimha (IISc, Chairman), D K Rakshit (Delhi, Co-ordinator), Y Ramanathan (IITK), S N Sengupta (IMD), D R Sikka (IITM), D K Sinha (Calcutta Univ.), S K Srivastav (IMD).

- **Science Advisory Group:** S Gadgil (IISc), Malti Goel (DST, Convenor), D K Rakshit (IIT Kh), Y Ramanathan (IITK), D P Rao (NIO), S N Sengupta (IMD), D R Sikka (IITM, Chairman).
- **Data Users Groups:** R K Datta (NCMRWF), S K Dube (IITD), Malti Goel (DST, Convenor), Harsh Gupta (DST), M G Gupta (IMD), U C Mohanty (IIT), A Prabhu (IISc), D K Rakshit (DST/IIT Kh), Y Ramanathan (IITK, Chairman), D P Rao (NIO), D R Sikka (IITM), S P Singal (NPL), S K Srivastav (IMD), Doyil T Vengayil (DST), K G Vernekar (IITM).
- **MONTBLEX Modelling Group:** Malti Goel (DST, Convenor), U C Mohanty (IIT), Y Ramanathan (IITK, Chairman), K J Ramesh (IIT), M Shankar Rao (IISc), D R Sikka (IITM), D K Sinha (Calcutta Univ.), S K Srivastav (IMD).
- **MONTBLEX Operations Control Centre:** M G Gupta (IMD, Director), Gp. Capt. O P Madan (IAF), G S Mandal (IMD), U C Mohanty (IIT).
- **Editorial Board of MONTBLEX News:** Sudarsh V Kailas (IISc, Editor), R Narasimha (IISc, Advisor).

References

- Kailas S V and Prabhu A 1988 The MONTBLEX data management plan; MONTBLEX document No MD1, CAS, IISc, Bangalore
- Kusuma Rao and Prabhu A 1988 The MONTBLEX operations plan; MONTBLEX document No MD2, CAS, IISc, Bangalore
- Goel M and Srivastava H N 1989 MONTBLEX; *Vayumandal* **19** January–June 1–8
- Goel M and Srivastava H N 1990 Monsoon Trough Boundary Layer Experiment; *Bull. Am. Meteorol. Soc.* **71** 1594–1600
- Goel M 1993 A report on the workshop on MONTBLEX results; *Curr. Sci.* **65** 897–899
- Narahari Rao K 1995 Estimation of surface temperature from MONTBLEX data; *Proc. Indian Acad. Sci. (Earth Planet. Sci.)* **104** 257–271
- Prabhu A, Narahari Rao K, Kusuma Rao, Kailas S V, Rudra Kumar S, Ameenulla S and Srinivasan H P 1990 MONTBLEX pilot experiment, 1989 – tower component; CAS Report No. 90 AS 2, CAS, IISc, Bangalore
- Rudra Kumar S, Srinivasan H P, Sathyadev H N, Ameenulla S and Prabhu A 1991 Surface layer data from MONTBLEX-90; MONTBLEX document No. 91 MD 2, CAS, IISc, Bangalore
- Rudra Kumar S, Ameenulla S and Prabhu A 1995 MONTBLEX tower observations: Instrumentation, data acquisition and data quality; *Proc. Indian Acad. Sci. (Earth Planet. Sci.)* **104** 221–248
- Sikka D R and Narasimha R 1995 Genesis of the monsoon trough boundary layer experiment (MONTBLEX); *Proc. Indian Acad. Sci. (Earth Planet. Sci.)* **104** 157–187
- Singal S P, Gera B S and Ojha V K 1993 Sodar studies of the monsoon trough boundary layer at Jodhpur (India); *Mausam* **44** 9–14
- Srivastav S K 1995 Synoptic meteorological observations and weather conditions during MONTBLEX-90; *Proc. Indian Acad. Sci. (Earth Planet. Sci.)* **104** 189–220
- Vernekar K G 1995 MONTBLEX data archival centre; *Proc. Indian Acad. Sci. (Earth Planet. Sci.)* **104** 249–256

Synoptic meteorological observations and weather conditions during MONTBLEX-90

S K SRIVASTAV

India Meteorological Department, Pune 411 005, India

Abstract. In the present paper a review of meteorological observations conducted by India Meteorological Department during MONTBLEX-90, including intensive observation periods, has been made. Also, an exhaustive weather summary, discussing the special weather features that occurred during the MONTBLEX observational period, is presented. The paper has been prepared to provide a ready reference of the synoptic features to research workers who are utilizing MONTBLEX data for their studies.

Keywords. MONTBLEX; radiosonde/radiowind; storm detection radars; cyclone detection radars; INSAT; pilot balloon; radiometersonde; intensive observation periods.

1. Introduction

1.1 *IMD observational network*

Though a part of IMD's total network of observatories situated around the normal position of monsoon trough participated in the MONTBLEX observational programme, it will be useful, first, to have an idea of the total observational network of IMD.

1.1.1 *Surface observational network:* The surface observational network of IMD consists of 562 stations. The network density is adequate (as per WMO standard) in most parts of the country excepting the Rajasthan desert and the hills of northern India.

1.1.2 *Upper air network:*

(a) *Pilot balloon observatories:* There are 62 stations in the pilot balloon observational network of the IMD as shown in figure 1. Two to four observations of upper wind are taken daily from each station at main synoptic hours using optical theodolite.

(b) *Radiosonde/radiowind (RS/RW) observatories:* The RS/RW observational network comprises 34 radiosonde/radiowind stations and one radiosonde station (figure 2). Two observations per day are taken from these stations at 0000 and 1200 GMT. X-band radars and radiotheodolite (401 MHz and 1.6 GHz) are used as ground equipment for recording upper air data.

1.1.3 *Storm detection radar stations:* Figure 3 shows the network of storm detection radar stations. Except for Sriganganagar and Jaisalmer, which have S-band radars, all the others have X-band radars and are primarily used for observing and reporting

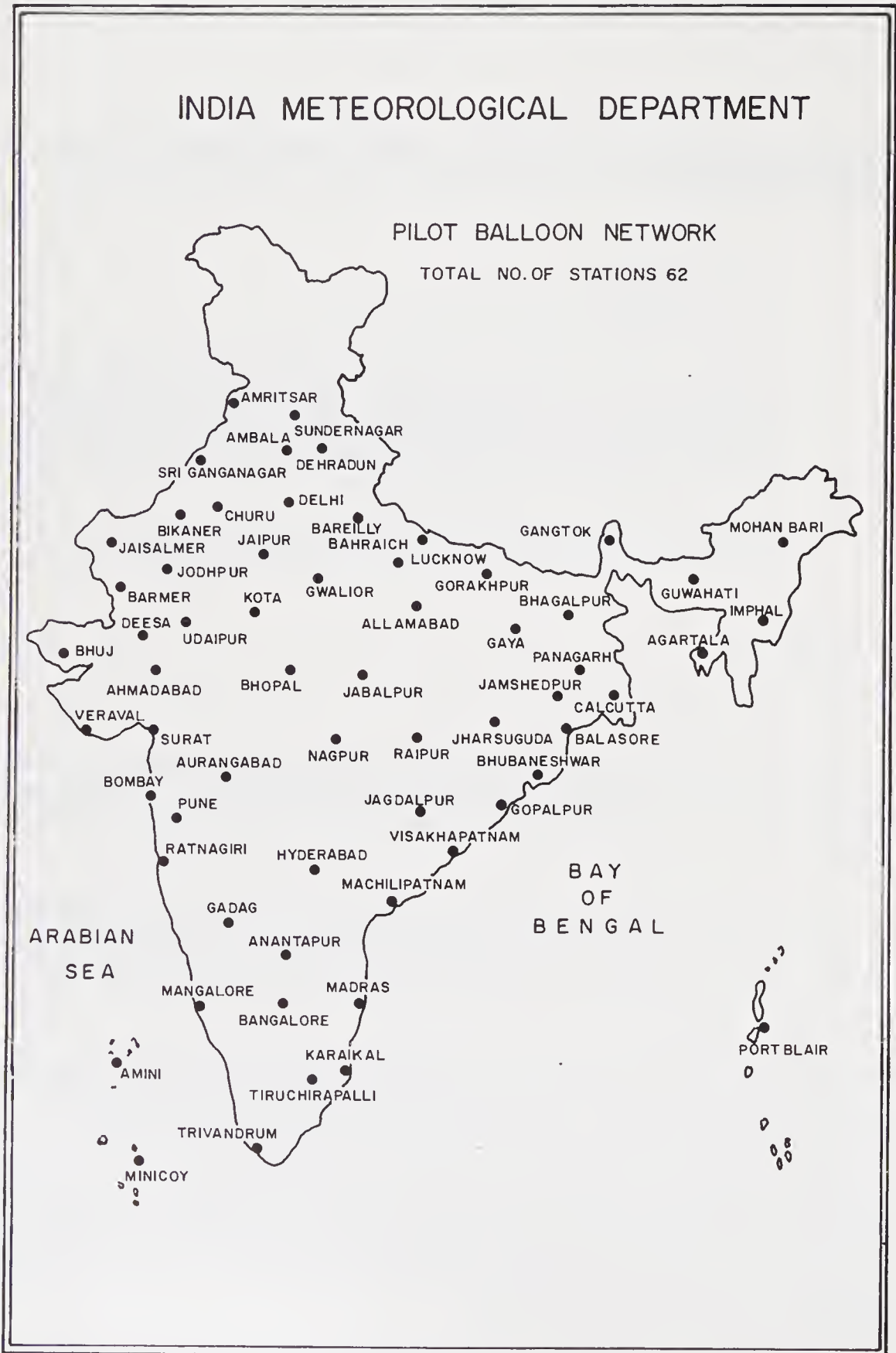


Figure 1.

INDIA METEOROLOGICAL DEPARTMENT

UPPER AIR NETWORK

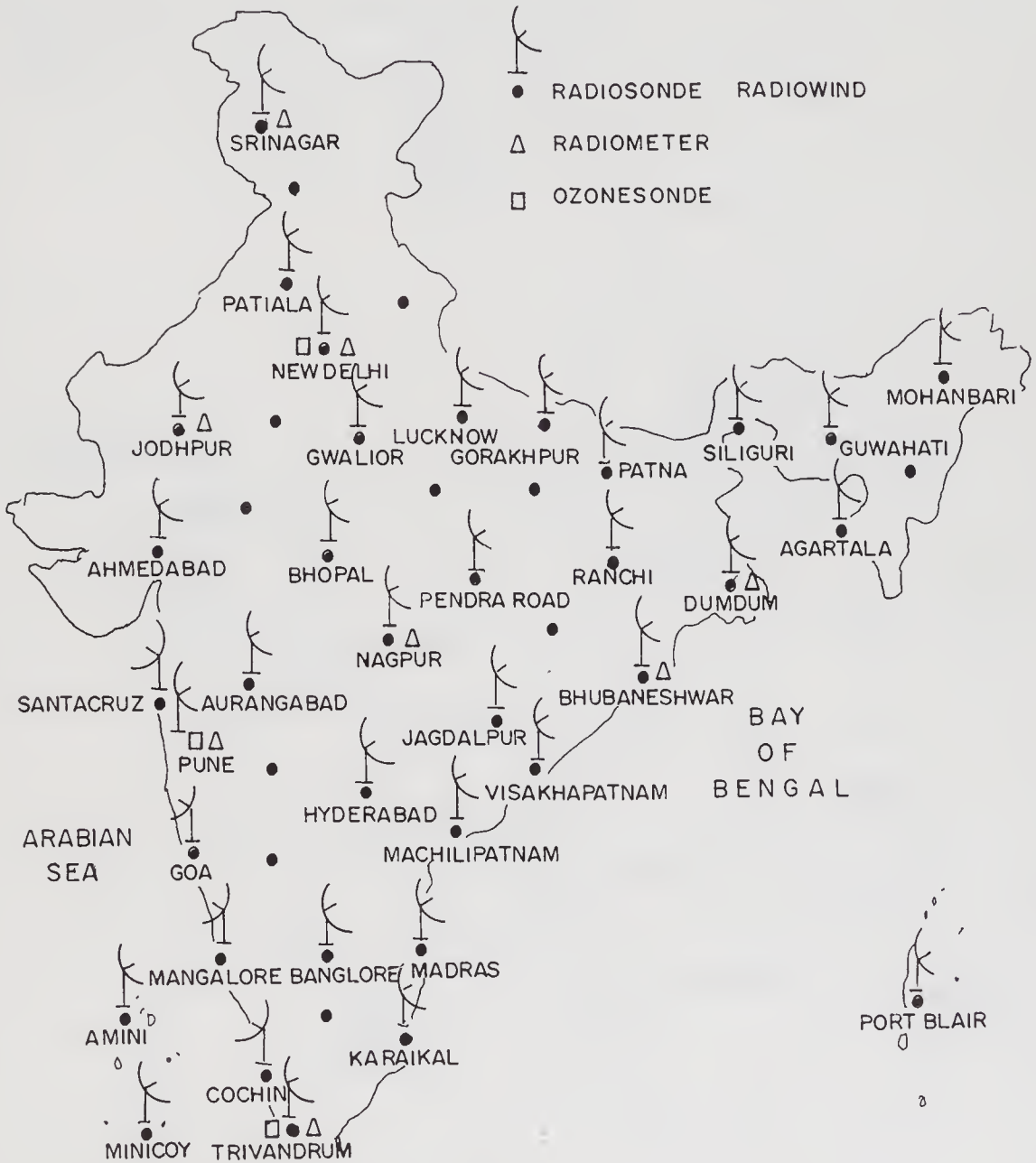


Figure 2.

cloud echoes up to 100 km around airports for aviation purposes. The information is also used for local forecasts in the respective cities where these are located.

1.1.4 *Cyclone detection radar stations:* A chain of 10 high-powered S-band radars located on the east and west coasts are used for the detection of cyclones/severe thunderstorms. These radars have overlapping ranges so that any cyclone over the sea will be detected and tracked by at least two or more radars thereby increasing accuracy of detection (figure 4).

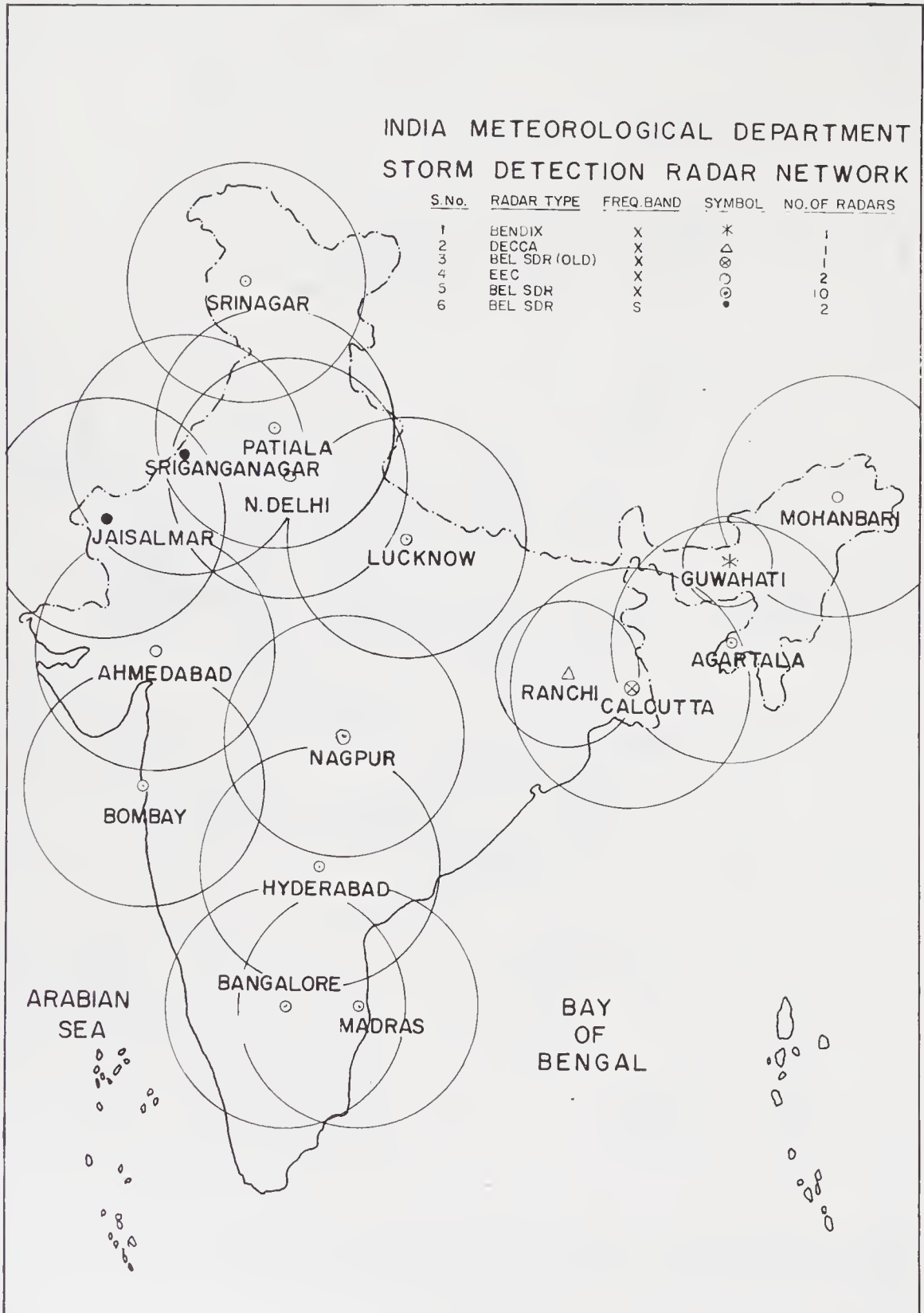


Figure 3.

INDIA METEOROLOGICAL DEPARTMENT

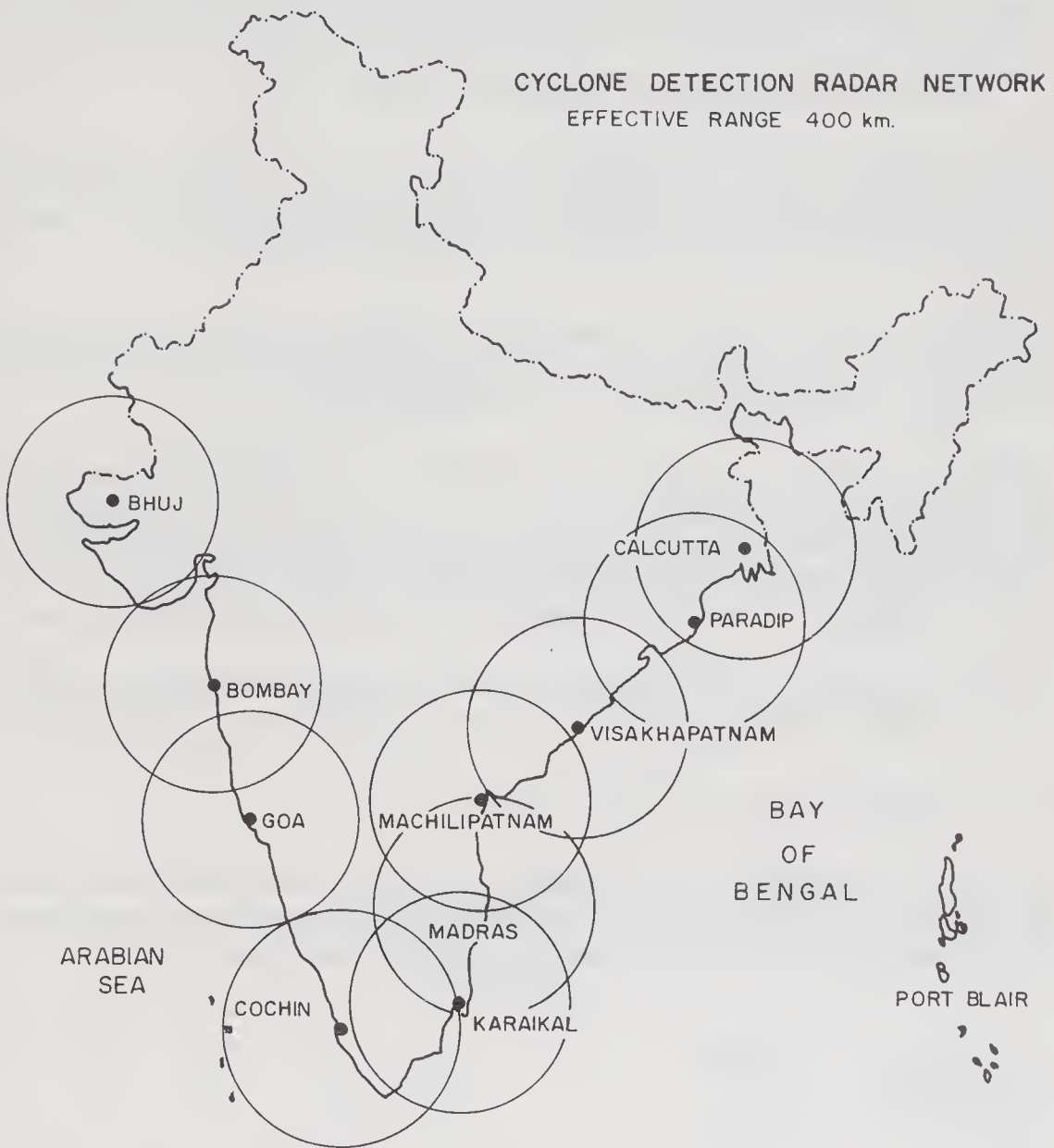


Figure 4.

1.1.5 *Satellite picture transmission stations:* These stations receive the cloud cover pictures taken and transmitted by the polar orbiting satellites operated by various countries. However, the frequency is limited to generally one or two pictures a day depending on its traverse over the Indian region. Compared to cloud pictures of INSAT, they have a higher resolution but are not available whenever desired.

1.1.6 *INSAT observations:* All the three geostationary satellites, 1D, 2A and 2B have the capability of taking cloud pictures both in visible and infra-red bands. The frequency of observation could be as high as every half-an-hour.

1.1.7 *Data collection platforms*: In inaccessible areas, surface observations can be collected through installation of automatic data collection platforms. Data are transmitted to INSAT in pseudo-random burst mode which are then re-transmitted and can be received at any location on an INSAT-compatible ground station. 100 such platforms have been installed and more are planned for the future.

1.1.8 *Non-departmental raingauge stations*: For collecting rainfall data, a large number (9512) of raingauge stations are being maintained by various state agencies. About half of these report rainfall data at synoptic hours; the remaining are of the non-reporting type, whose data are archived and can be received once a month.

1.1.9 *Radiation observations*: For recording of total incoming and outgoing radiation, 45 radiation observatories have been set up. These observations are extremely useful for calculations of the heat budget of the atmosphere (figure 5).

1.1.10 *Ozone observatories*: India has one of the best ozone observation networks in the world. This consists of surface ozone, total ozone and Umkehr observing stations, and ozonesonde stations. Recently two Brewer spectrophotometers have been inducted into the network. This sophisticated equipment is capable of recording NO_x , SO_2 , concentrations and UV radiation, in addition to normal total ozone measurement.

1.1.11 *Others*: Apart from the above, there are many other observatories set up to collect atmospheric data like pollution, atmospheric electricity etc.

1.2 MONTBLEX-90 observation network

1.2.1 *Surface observation network*: Figure 6 shows the surface observatories which participated in the MONTBLEX-90 special (enhanced) observational programme. Three-hourly observations of the following parameters were taken:

	<u>Accuracy</u>
■ Temperature	$\pm 0.1^\circ\text{C}$
■ Pressure	$\pm 0.1 \text{ hPa}$
■ Humidity	$\pm 1.0\%$
■ Rainfall	$\pm 1 \text{ mm}$

These data were taken on self-recording instruments, so continuous records are available.

1.2.2 *Upper air observational network*: Figure 7 shows the upper air observatories which participated in the special MONTBLEX programme.

(a) *Pilot balloon observatories*: Four observations per day were taken at eleven stations. In addition, eight RS/RW stations also took additional pilot balloon observations at 0600 and 1800 hrs UTC every day.

(b) *RS/RW observatories*: Eleven stations took routine ascents at 00 and 12 UTC.

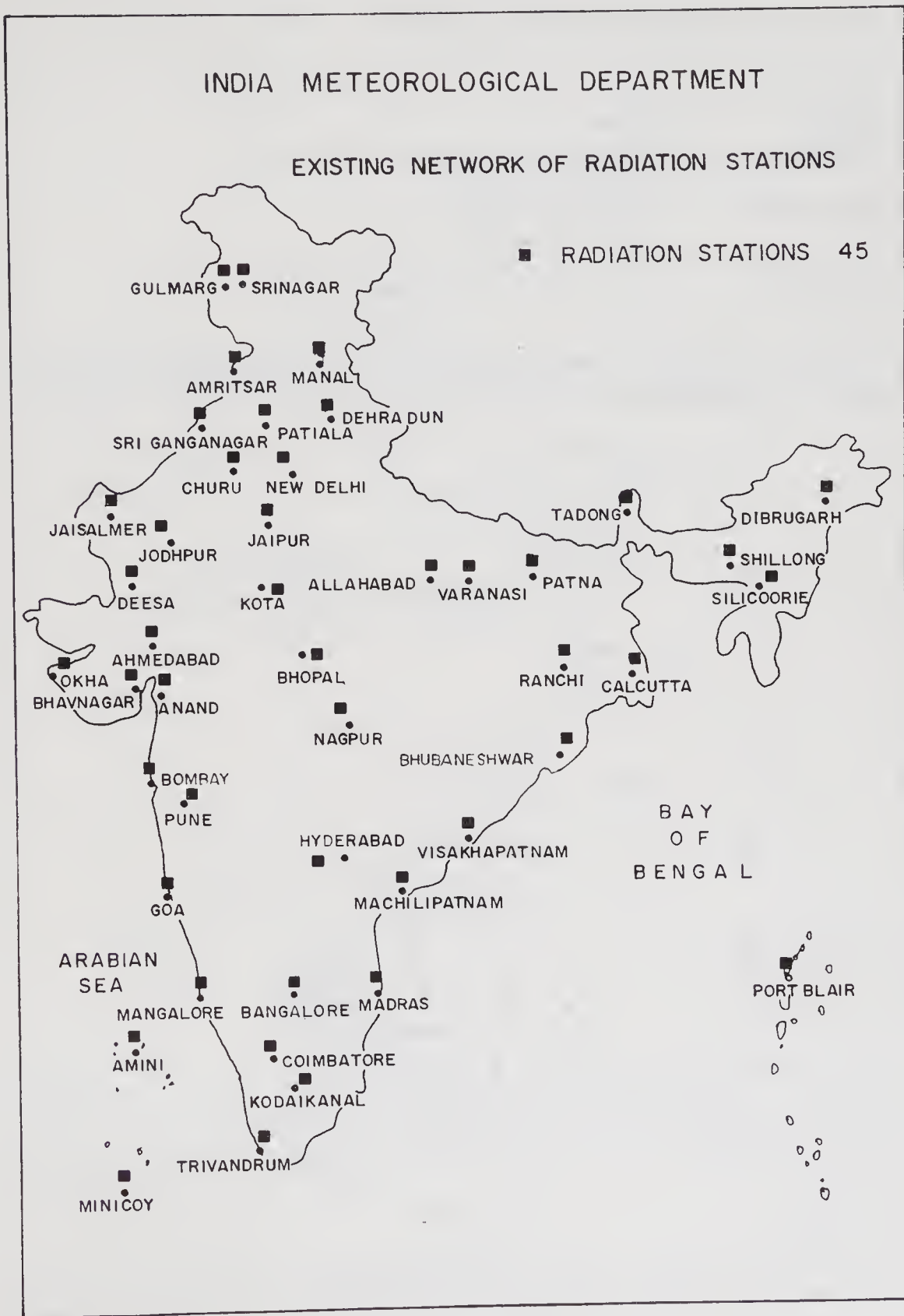


Figure 5.

Data accuracy of radiosonde used is given below:

■ Temperature	$\pm 0.5^{\circ}\text{C}$.
■ Pressure	$\pm 1\text{ hPa}$.
■ Humidity	$\pm 5\%$ up to tropopause or 300 hPa 00 hPa whichever is lower.
■ Wind speed	$\pm 1\text{ m/s}$ below 10 m/s. $\pm 10\%$ above 10 m/s
■ Wind direction	$\pm 5^{\circ}$ for wind speeds above 25 m/s $\pm 10\%$ for lower wind speeds.

(c) *Low-level observations:* IMD has designed and developed a low-level sonde capable of yielding high resolution data on pressure, temperature and humidity up to

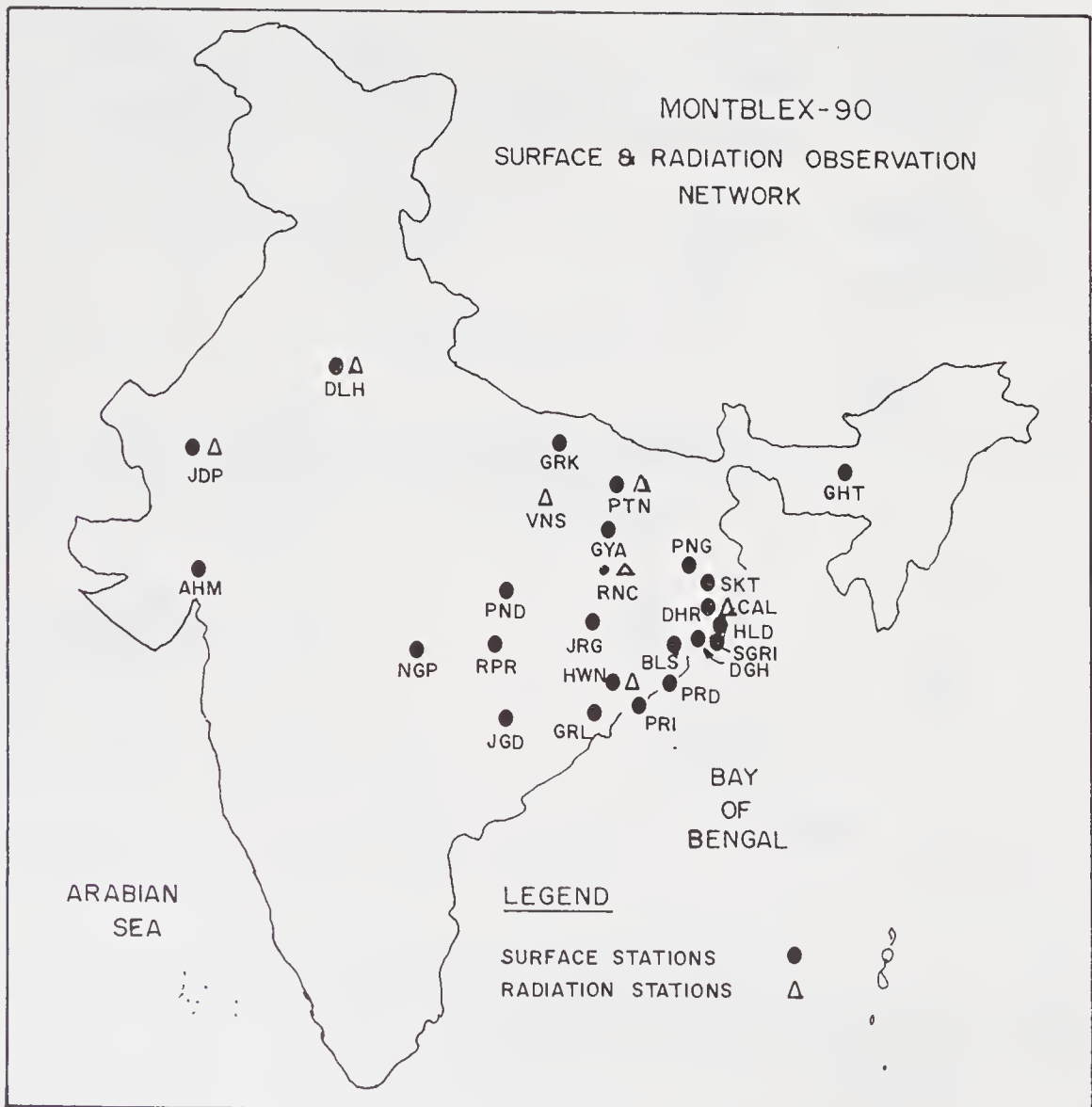


Figure 6.

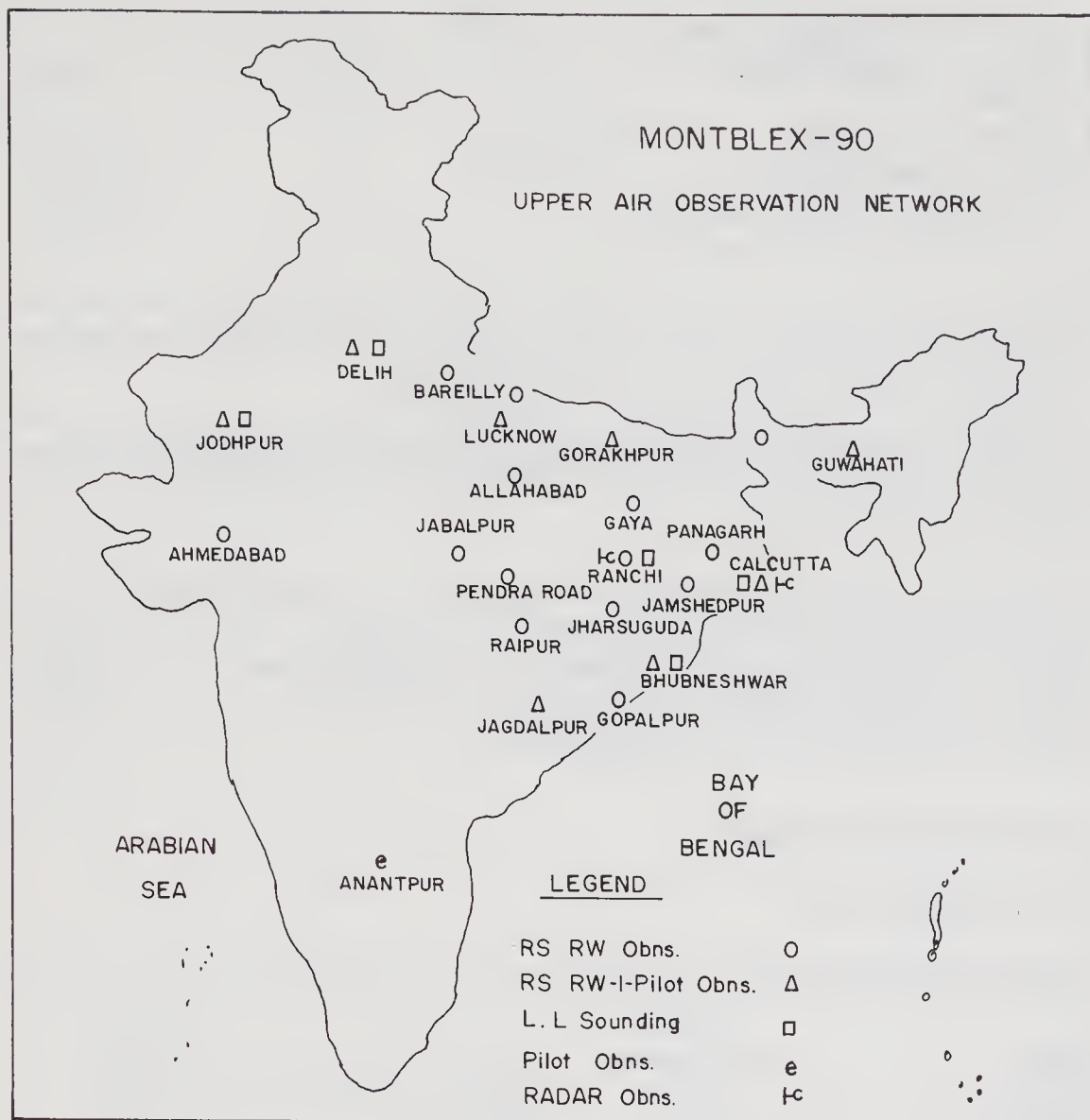


Figure 7.

about 3 km height. The sonde is released with a very slow rate of ascent (2 m/s) as compared to 5 m/s of normal radiosonde. The measurement accuracy of the data is ± 0.5 hPa, $\pm 0.5^\circ\text{C}$ and $\pm 2\%$ for pressure, temperature and humidity respectively. These low-level high resolution observations were taken at Calcutta, Bhubaneswar and Ranchi at 06 and 18 UTC every day.

1.2.3 Radiation observations:

(a) Surface measurements: From seven stations, special radiation observations were recorded. The following parameters were measured:

<u>Parameter</u>	<u>Accuracy</u>
■ Intensity of solar radiation	$\pm 2\%$

■ Global and diffuse solar radiation	$\pm 2\%$
■ Effective outgoing long wave radiation	$\pm 2\%$
■ Duration of sunshine	$\pm 5\%$
■ Difference between the total incoming and outgoing radiation	$\pm 2\%$

(b) *Radiometersonde measurements*: Calcutta took special radiometersonde ascents once every week during intensive observation periods. Bhubaneswar and Jodhpur conducted routine fortnightly ascents during the period.

1.2.4 *Radar observations*: X-band storm detection radar stations at Ranchi and Calcutta were utilized for recording three-hourly cloud echoes around the station along with their vertical extent.

1.2.5 *INSAT data*: During the MONTBLEX-90 period, INSAT-1B has provided cloud imagery in the visible channel (0.55–0.75 μm) round the clock. The satellite imagery is the only continuous meteorological data base available over the Indian Ocean and can enable continuous monitoring of the southwest monsoon right from its onset over Kerala coast in May, to its withdrawal.

2. Total MONTBLEX data

2.1 Surface observations

Station	<u>No. of observations</u>	Station	<u>No. of observations</u>
Jodhpur	1048	Diamond Harbour	1048
Delhi	1048	Sagar Island	1048
Ahmedabad	1048	Guwahati	1048
Nagpur	1048	Puri	1048
Gorakhpur	1048	Calcutta	1048
Pendra Road	1048	Balasore	1048
Patna	1048	Jharsuguda	800
Ranchi	1048	Gaya	1038
Bhubaneswar	1048	Gopalpur	1048
Paradip	1048	Jamshedpur	1048
Panagarh	1048	Raipur	1038
Shantiniketan	1048		

2.2 Pilot balloon observations

Out of eleven PB stations which took routine PB ascents twice a day, the following stations took additional ascents as indicated below:

<u>Station</u>	<u>No. of observations</u>	<u>Station</u>	<u>No. of observations</u>
Gaya	101	Jharsuguda	31
Jamshedpur	111	Balasore	113
Bhubaneswar	62	Panagarh	107
Gopalpur	130		

2.3 RS/RW observations

Eleven RS/RW stations, as shown in figure 11, took regular RS/RW observations twice a day. At selected stations additional ascents were taken using low-level sondes.

2.4 Low-level observations

<u>Station</u>	<u>No. of observations</u>	<u>Station</u>	<u>No. of observations</u>
Calcutta	70	New Delhi	46
Bhubaneswar	70	Jodhpur	46
Ranchi	57		

2.5 Radiation observations

Seven radiation stations (figure 12) took special 3-hourly radiation observations during the entire MONTBLEX-90 period.

2.6 Radiometer observations

<u>Station</u>	<u>No. of observations</u>
Calcutta	10
Jodhpur	6
Bhubaneswar	6

2.7 Radar observations

Weather radar observations, three-hourly or more frequent, were taken from the X-band radars at Calcutta (1503 observations) and Ranchi (289 observations) during the period.

3. Intensive observation periods (IOPs) during MONTBLEX-90

Table 1 gives the period along with the area of IOP and also the synoptic situation

Table 1. Intensive observation periods (IOPs) during MONTBLEX-90
(First two digits in the period column indicate the month and the next two are the dates).

IOP No.	Period	Area	Synoptic weather situation
1.	0601-0617	Eastern part	Monsoon trough in formative stage with easterlies over NE India.
2.	0605-0612	Varanasi	
3.	0623-0703	Delhi Jodhpur	Shift in the monsoon trough as a result of western disturbances.
4.	0705-0712	Eastern part Varanasi	Intensive convective clouds and trough fluctuation.
5.	0717-0721	Jodhpur	Western disturbances moving across Himalayas.
6.	0726-0801	Eastern parts Varanasi Raipur	Monsoon trough variations and possibility of break monsoon conditions.
7.	0803-0808	Delhi Jodhpur	Passage of well-marked low over south-west Rajasthan.
8.	0814-0818	Eastern parts Varanasi Raipur	Formation of depression and passage across central parts of the country.
9.	0818-0820	Delhi Jodhpur	Seasonal low over south Rajasthan and adjoining areas, axis passing through Jodhpur.
10.	0820-0825	Eastern parts Varanasi Raipur	Formation of deep depression centred in the North Bay of Bengal.
11.	0828-0831	Eastern parts Varanasi	Marked change in the position of monsoon trough and southward shift.
12.	0901-0904	Eastern parts	Formation of depression near eastern parts.
13.	0903-0907	Varanasi	Passage of land depression over central parts.
14.	0906-0908	Delhi	Temporary shift of the eastern part of the axis from Nepal to north Bay of Bengal.

which warranted the observations. These were decided by the MONTBLEX Operational Centre at Delhi. However, these observations could not always be exactly implemented by concerned field stations because of lack of immediate communication. The actual periods of IOP when the observations were taken are shown in figures 11 to 14 along with the weather phenomena existing at that time.

4. Southwest monsoon 1990

4.1 General

The 1990 monsoon rainfall (i.e. rainfall from 1st June to 30th September 1990 over the country) ranks the third best during the last decade. Another unique feature of the southwest monsoon season of 1990 is that, inspite of the absence of many classical features, the total rainfall has been uniformly above normal in 32 out of 35 meteorological sub-divisions.

4.2 *Characteristic features of the season*

The following were the characteristic features of the southwest monsoon of the year 1990:

- Most of the depressions/well-marked low pressure areas were initially observed as upper air circulations.
- Only four depressions formed in the season as against a normal of 7 to 8 in the Bay of Bengal.
- No depression developed over the Arabian Sea during the season.
- During the entire month of July 1990, no depression formed in the Bay of Bengal.
- One depression in August moved as far west as west Rajasthan. The remnants of other depressions in August and a few low pressure areas also moved up to west Rajasthan.
- Onset of monsoon over Kerala took place as early as 19th May 1990. No onset vortex was observed during the onset phase.
- Cross equatorial flow in the lower tropospheric levels off Somalia coast was observed from the month of May.
- There was regular movement of mid-latitude troughs in westerlies across extreme north India and Tibetan plateau resulting in the shifting of the Tibetan anticyclone to the southern latitudes.
- Typical 'break monsoon' condition, i.e. monsoon trough moving north to the foothills of Himalayas, was absent during the entire season.
- Most of the drought-prone areas received normal rainfall during the season.
- Duration of the monsoon period, particularly over northwest India, was above normal.
- No severe floods occurred in the normal flood-prone areas of the country.

4.3 *Onset and advance*

In 1990, the monsoon set in over Kerala and extreme southern parts of Tamil Nadu on 19th May. By 21st May, it rapidly advanced to parts of north interior Karnataka, South Konkan and Goa. It further advanced into north Konkan, south Madhya Maharashtra, more areas of north interior Karnataka and the rest of Rayalaseema on 31st May. The advance, therefore, was extremely rapid and it was early by 4 to 7 days compared to the normal.

By 6th June, the monsoon further advanced into north Madhya Maharashtra, Marathwada, Vidarbha, rest of Andhra Pradesh, southeast Madhya Pradesh and south Orissa. In the last phase it advanced over west Uttar Pradesh, Haryana, Rajasthan and north Gujarat. Date-wise advance of the southwest monsoon 1990 is shown in figure 8. Over the monsoon trough region the advance was near the normal dates.

However, in certain areas the onset was delayed: for example, by 15 days in north Gujarat region and Saurashtra and Kutch and by 4 to 5 days in Madhya Pradesh, east Rajasthan and south Gujarat.

4.4 *Withdrawal*

The withdrawal of southwest monsoon-1990 commenced by the end of September. It withdrew from Jammu and Kashmir, west Rajasthan and parts of Punjab on 27th September. It further withdrew from Himachal Pradesh, northwest Uttar Pradesh,

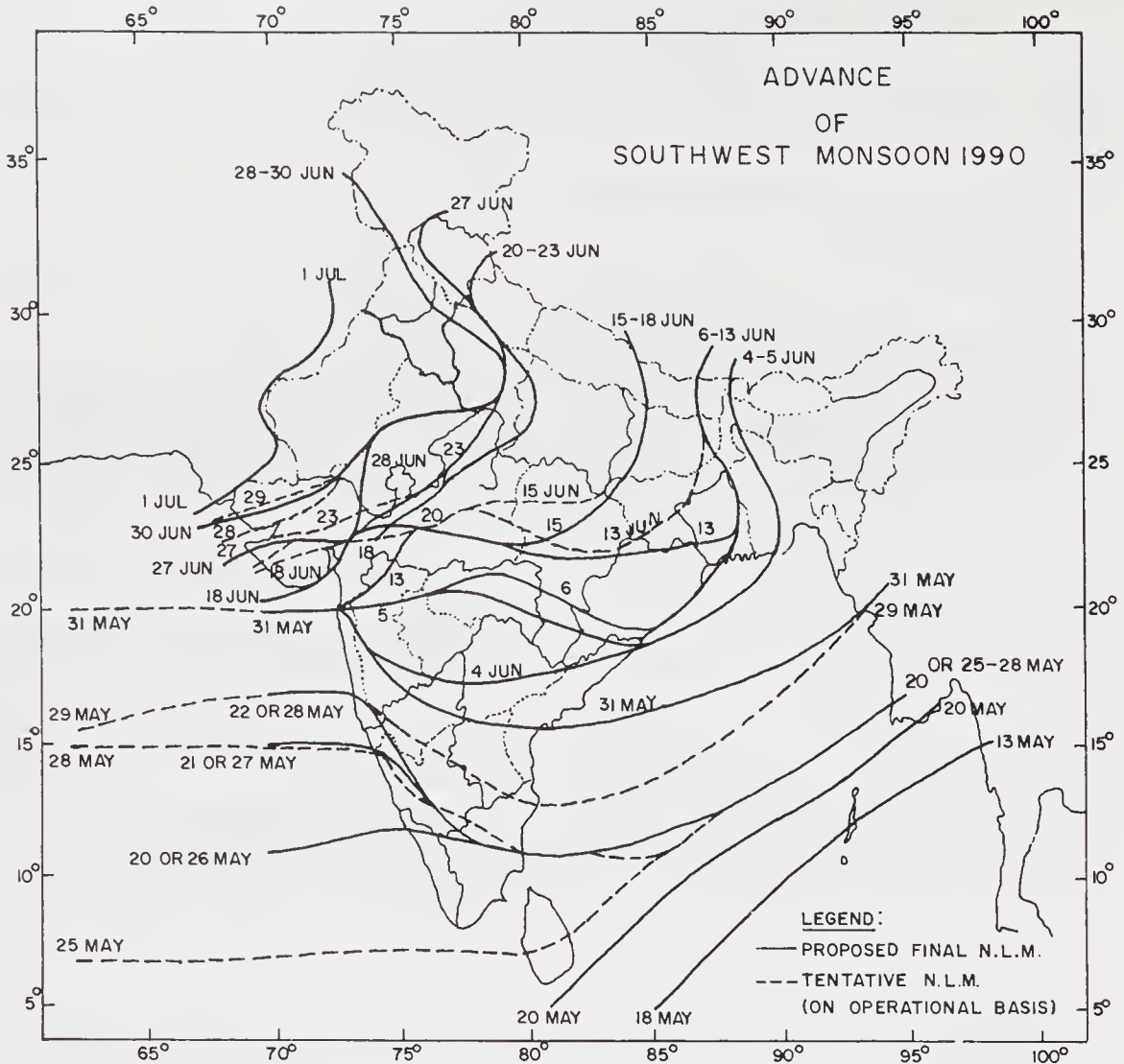


Figure 8.

Haryana and rest of Punjab on 28th September. During the first week of October, it withdrew from the rest of west Uttar Pradesh, east Rajasthan, Gujarat, northwest Madhya Pradesh and western parts of east Uttar Pradesh. The withdrawal of the monsoon was late by about 10 days in most parts of the monsoon trough region.

4.5 Break monsoon

During monsoon-1990, no such classical break condition was seen. The upper end of the monsoon trough did move northwards for a few days but no prolonged dry spell was observed.

4.6 Rainfall during monsoon-1990

The rainfall distribution over time has been uniformly above normal. However, spatial distribution over the country has not been uniform. Certain areas did not receive adequate rainfall. Departures as high as -60% occurred over central Orissa. Figure 9

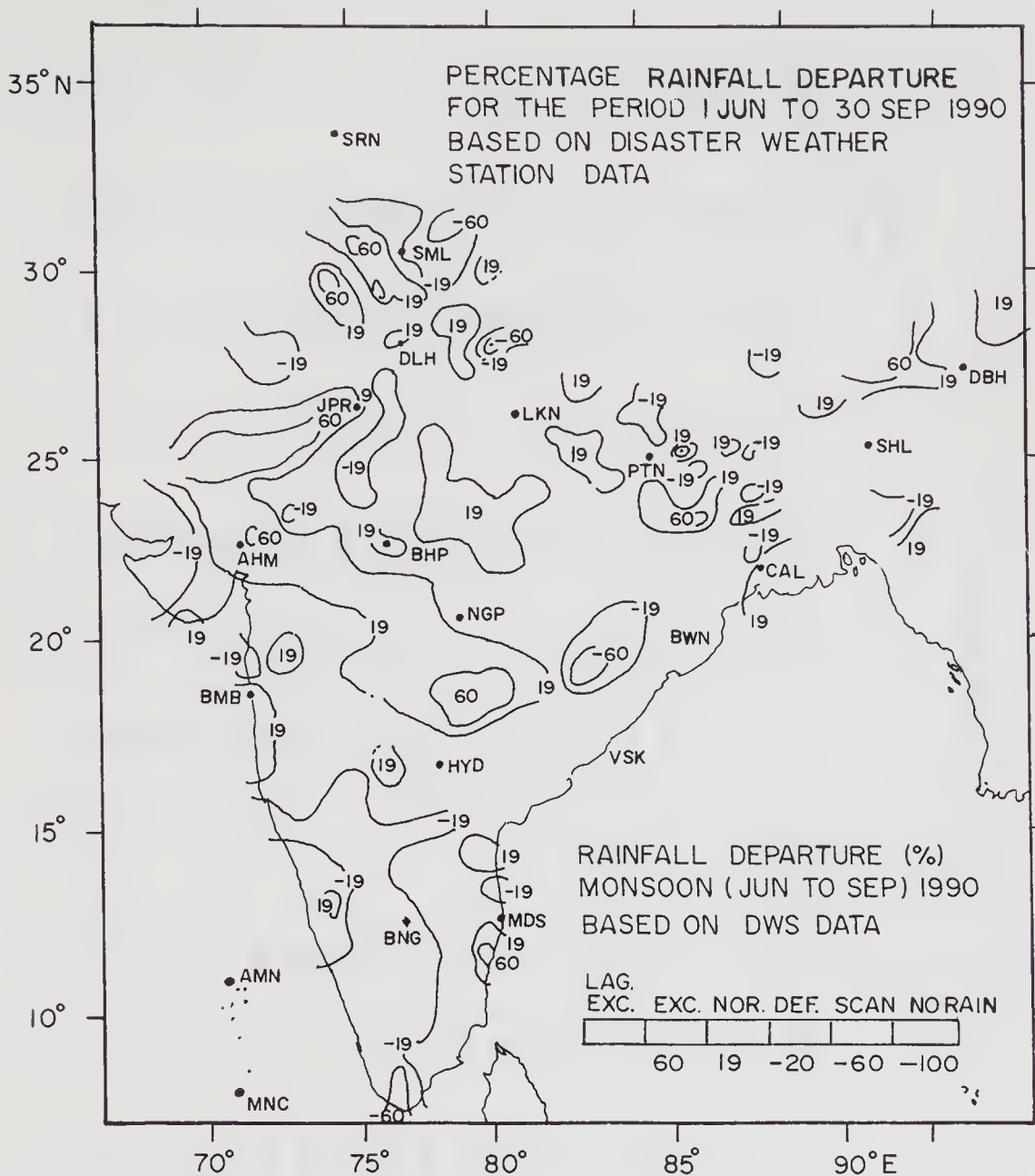


Figure 9.

shows the percentage departure for the period 1st June to 30th September. For classification of rainfall distribution, the following norms are used:

<u>Classification</u>	<u>Percentage departure of rainfall from normal</u>
Excess	+ 20 or more
Normal	+ 19 to - 19
Deficient	- 20 to - 59
Scanty	- 60 or less
Dry	- 100.

Table 2. Sub-divisional means of rainfall (mm) for each month and season as a whole. June to September 1990.
(Based on the Disaster Weather Station data).

Sub-divisions	Jun		Jul		Aug		Sep		Season Jun to Sep		
	Act.	%Dep.	Act.	%Dep.	Act.	%Dep.	Act.	%Dep.	Act.	%Dep.	
A. and N. Island	255	-46	196	-46	238	-34	330	-19	1019	1598	-36
Arunachal Pradesh	771	37	721	20	358	10	656	16	2507	2052	22
Assam and Meghalaya	519	4	514	-5	311	-25	501	50	1845	1791	3
Nag., Mani., Mizo., and Tri.	339	-11	388	19	329	3	238	3	1294	1254	3
Sub-Him. W. B. and Sikkim	567	6	501	-18	635	27	456	11	2160	2062	5
Gangetic W. B.	227	-11	431	39	262	-14	280	13	1200	1118	7
Orissa	221	1	255	-30	344	-3	258	4	1078	1185	-9
Bihar plateau	247	28	551	64	254	-22	267	21	1319	1075	23
Bihar plains	167	-2	498	59	210	-33	196	-12	1071	1021	5
East U.P.	97	-6	474	51	188	-32	162	-15	959	890	7
Plains of west U.P.	38	-15	345	31	199	-21	244	44	849	782	8
Hills of west U.P.	92	-10	439	10	351	-4	189	-3	1131	1104	2
Har., Chand. and Delhi	26	-51	245	24	141	-19	219	98	632	536	18
Punjab	18	-57	274	46	189	12	215	115	695	498	40
Himachal Pradesh	100	6	355	-4	342	0	245	46	1042	972	7
Jammu and Kashmir	13	-79	141	29	164	2	103	38	421	406	4
West Rajasthan	29	7	213	106	194	67	50	-1	486	298	63

East Rajasthan	75	33	196	-19	204	-19	219	43	693	705	-2
West M.P.	185	59	293	-12	360	20	307	63	1145	936	22
East M.P.	303	80	356	-12	296	-21	338	48	1294	1177	10
Gujarat Reg., Daman, Dadra and Nagar Hav.	84	-33	253	-35	593	121	244	44	1173	953	23
Saur., Kutch and Diu	98	19	35	-83	277	112	88	-3	498	502	-1
Konkan and Goa	778	14	734	-35	1069	57	373	5	2953	2852	4
Madhya Maharashtra	150	-1	233	-18	337	78	103	-37	823	789	4
Marathwada	223	54	117	-13	372	102	107	-41	819	715	15
Vidarbha	301	81	321	-4	506	83	126	-38	1254	983	27
Coastal A.P.	96	-14	118	-31	182	12	159	-8	554	616	-10
Telangana	199	43	187	-22	385	84	110	43	881	780	13
Rayalaseema	52	-16	61	-31	81	-18	141	5	335	384	-13
Tamil Nadu and Pondi.	30	-43	41	-43	78	-20	126	22	275	327	-16
Coastal Karnataka	933	7	996	-15	1027	50	269	12	3226	3037	6
N. Interior Karnataka	156	59	95	-36	186	53	72	-52	507	520	-3
S. Interior Karnataka	168	17	200	-29	266	42	82	-42	732	755	-3
Kerala	512	-26	630	-17	361	-17	104	-58	1607	2131	-25
Lakshadweep	166	-46	336	20	124	-35	99	-39	725	941	-23

Monsoon activity was normal or above normal in 18 meteorological sub-divisions for 11 weeks and in 16 meteorological sub-divisions for 7 weeks. The monsoon trough region received normal seasonal monsoon rainfall. Monthly performance of rainfall sub-divisionwise and over the season as a whole may be seen in table 2. Twenty five sub-divisions received normal rainfall, 7 received excess and 3 sub-divisions were deficient. There was no sub-division in the scanty category. The seasonal rainfall departures analysed on the basis of individual station rainfall are shown in figure 10.

4.7 Disturbances over Indian region during monsoon-90

Normally, various disturbances like depressions, well-marked low pressure regions

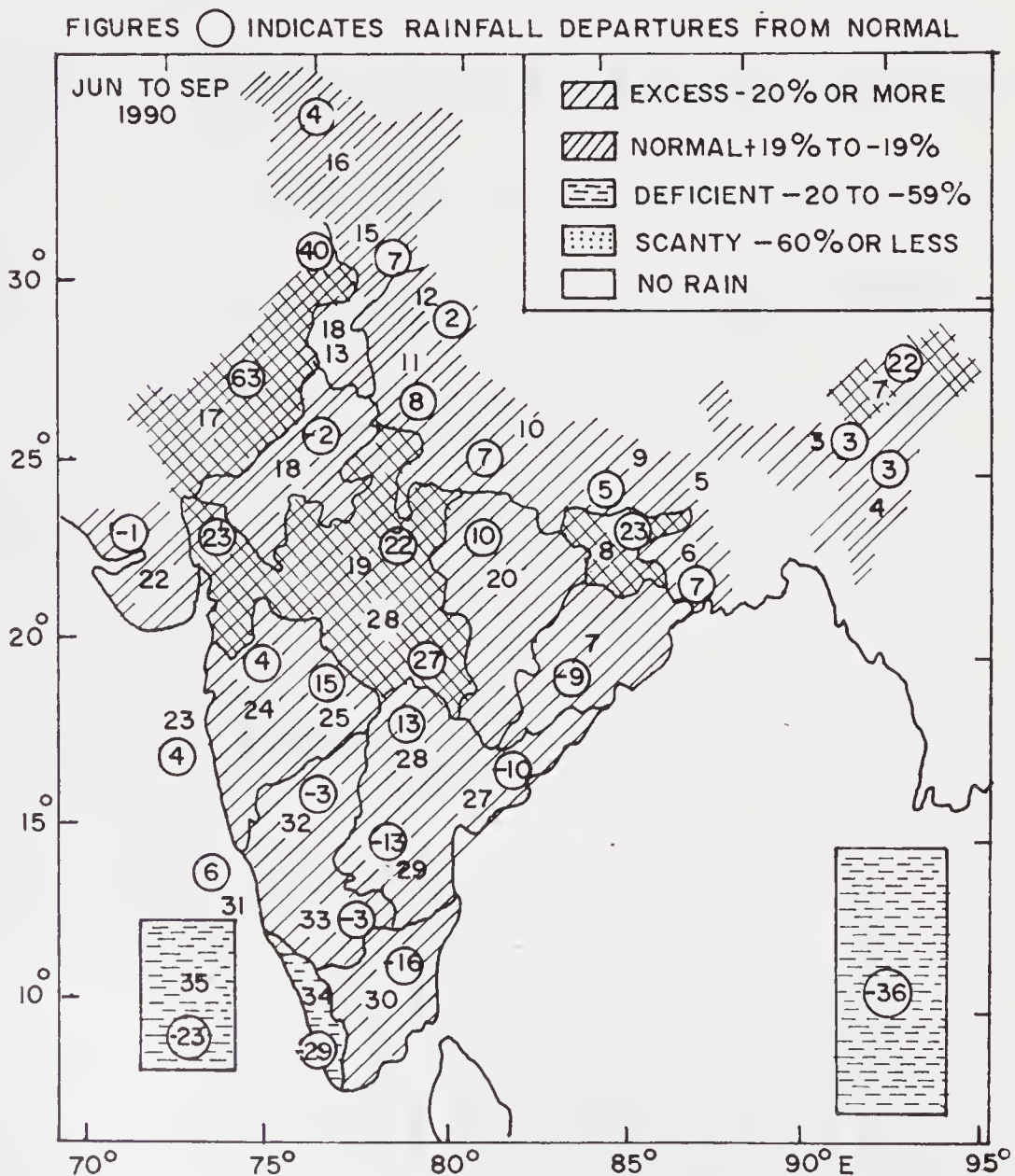


Figure 10. Percentage departure of rainfall from normal for June to September 1990 (Figures outside the circles indicate serial number of met. sub-divisions)

and a trough in the mid-latitude westerlies develop during the monsoon, heralding either increased activity or acceleration in the progress of monsoon onset over the country. Their location, persistence and movement play a vital role in the rainfall distribution over the country.

In the monsoon season of 1990, even these systems were fewer in number as compared to normal and yet the monsoon rainfall was above normal in most of the country. This was due to the fact that the monsoon trough remained situated close to its normal position on most of the days in the 1990 season.

Table 3 gives the total number of various types of disturbances that developed during monsoon 1990. Month-wise breakup of these systems is given in table 3. Figures 11 to 14 depict these systems vis-a-vis the intensive observation periods (IOP). Tracks of depressions during the year 1990 including MONTBLEX-90 period are shown in figure 15.

Some of these systems are discussed in detail below.

4.7.1 Deep depression: 13th–15th June 1990: The system initially appeared as an upper air disturbance over west central Bay on 7th June. Under its influence a low pressure area formed on 10th, which subsequently concentrated into a depression over the northwest Bay on 13th evening. It moved in a west-northwesterly to westerly direction and crossed the north Orissa and West Bengal coasts and weakened over north Orissa and adjoining east Madhya Pradesh on 15th evening.

The depression lay centred at 1200 UTC of 13th near 21.0°N, 89.0°E. At this hour Sandheads and Khepupara (Bangladesh) reported surface winds NNW/25 kt and E/15 kt respectively. At 0.9 km a.s.l., the winds at Calcutta and Bhubaneswar were ENE/35 kt and N/25 kt respectively at 0000 UTC of the day. The satellite classification at 0300 UTC was T 1.0. At 0300 UTC of 14th, it became a deep depression over the northwest Bay and neighbourhood, centred near 21.5°N, 87.5°E. The system crossed the coast near Contai on the afternoon of 14th and weakened into a depression and was centred about 50 km north-northeast of Keonjhar at 1200 UTC of 14th when Keonjhar reported WNW/20 kt wind. At 0300 UTC of 15th the depression lay centred about 50 km south of Rourkela. Thereafter, the system weakened by evening of 15th into a well-marked low pressure area over north Orissa and adjoining Bihar plateau and east Madhya Pradesh. The remnant remained stationary over the area for a couple of days and became unimportant over northeast Madhya Pradesh and neighbourhood on 18th. INSAT pictures of the depression may be seen in figures 16a to 16c.

Due to this system, the southwest monsoon advanced over Orissa, West Bengal, Bihar and adjoining east Madhya Pradesh. The maximum pressure change of

Table 3. Month-wise break-up of systems.

Systems	Jun	Jul	Aug	Sep	Total
Depression/deep depression	1	Nil	2	1	4
Low pressure area/well-marked low pressure area	1	3	3	3	10
Cyclonic circulation	4	7	5	6	22
Western disturbances	3	1	Nil	Nil	4

IOP & DETAILS OF WEATHER SYSTEMS DURING
JUNE 1990

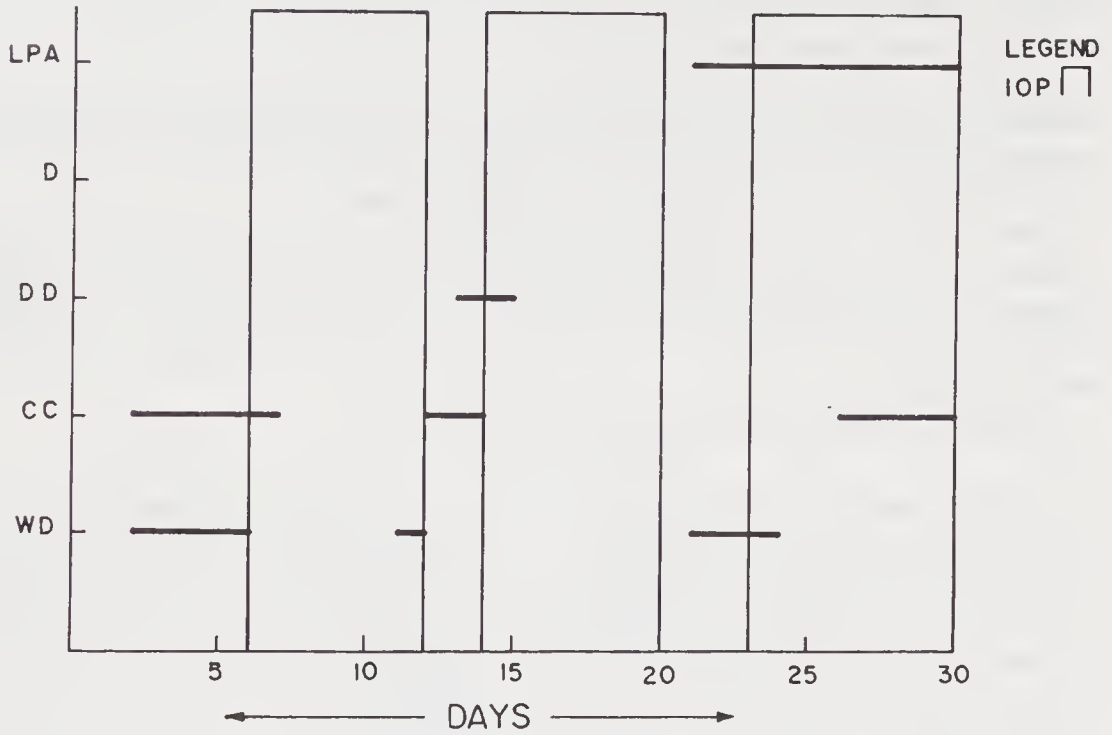


Figure 11.

IOP & DETAILS OF WEATHER SYSTEMS DURING
JULY 1990

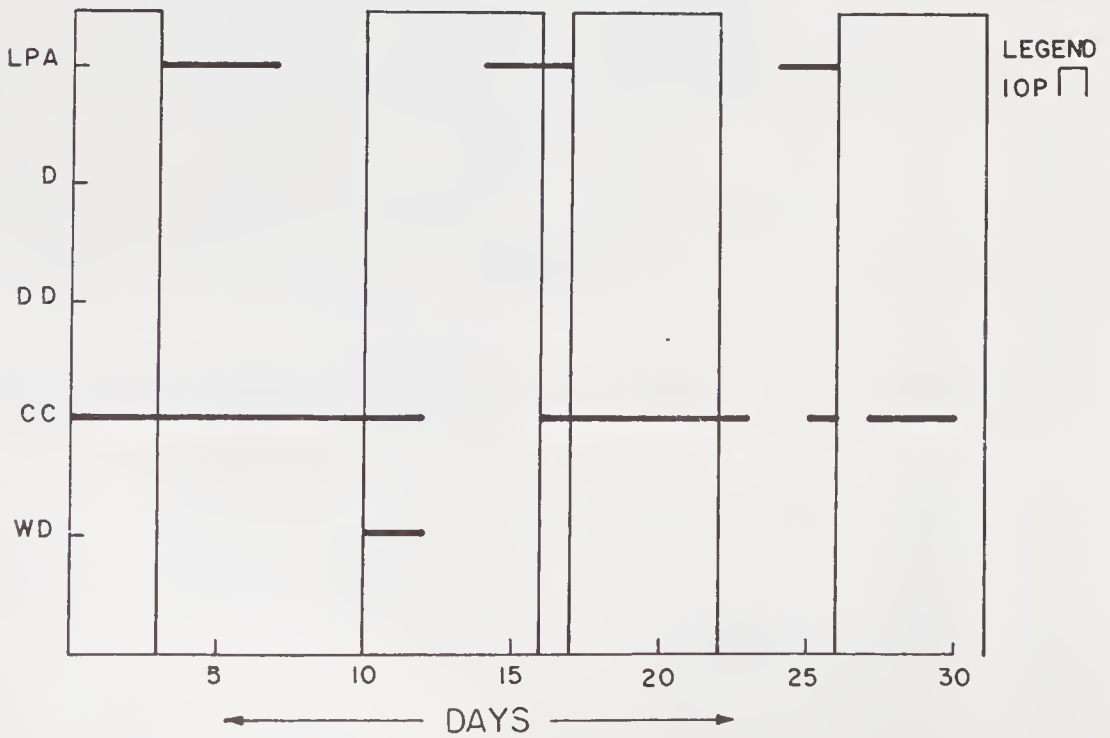


Figure 12.

IOP & DETAILS OF WEATHER SYSTEMS DURING
AUGUST 1990

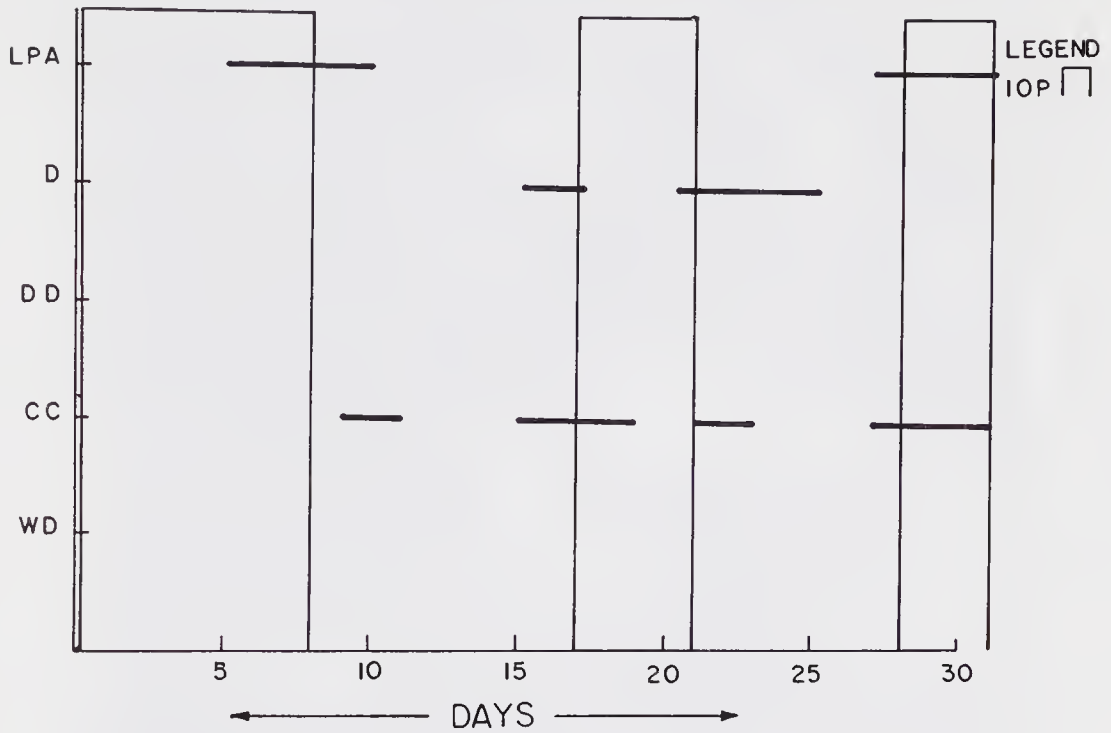


Figure 13.

IOP & DETAILS OF WEATHER SYSTEMS DURING
SEPT. 1990

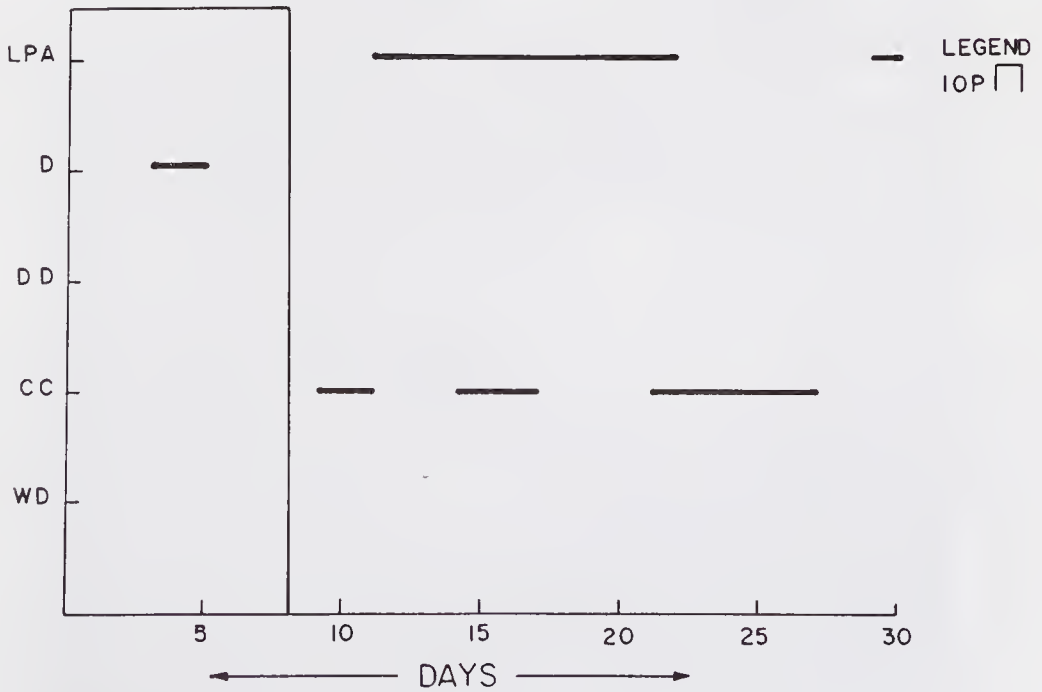


Figure 14.

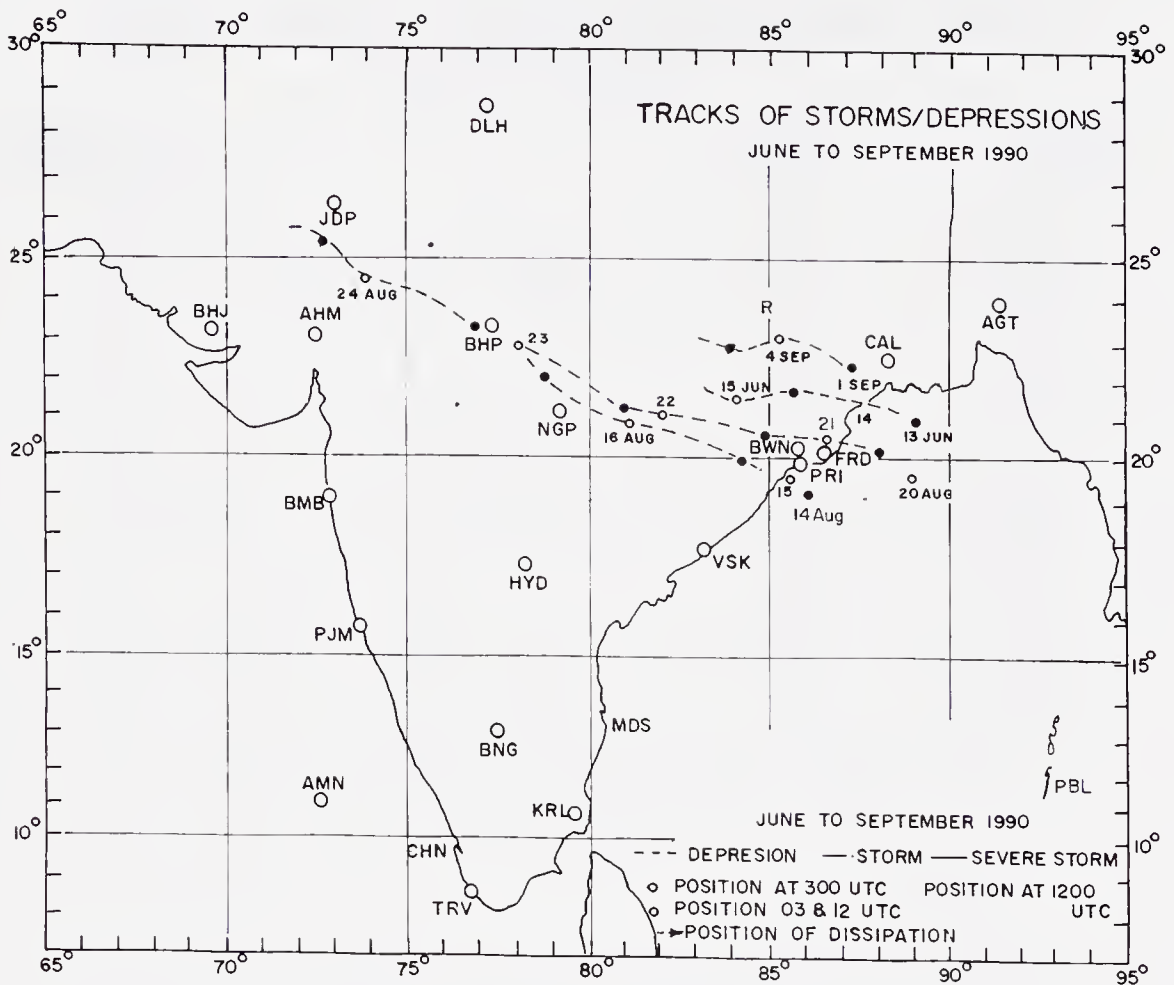


Figure 15.

– 7.6 hPa and pressure departure of – 11.8 hPa were recorded at Sandheads at 0300 UTC on 14th. The circulation of the system extended up to 9.5 km a.s.l. on 14th morning whereas on other days it extended up to middle tropospheric levels only.

The fall-out of this system in terms of rainfall on 16th and 17th June, when the system affected the eastern end of the monsoon trough, is shown in figures 17 and 18 respectively.

4.7.2 Depression: 14th–16th August 1990: The system was initially seen as an upper air disturbance over west central and adjoining northwest Bay on 12th and further into a depression on 14th evening. Moving west-northwestwards, it crossed south Orissa coast between Gopalpur and Puri around 15th noon and weakened over southwest Madhya Pradesh and adjoining Vidarbha on 16th night. On the evening of 14th, when the system concentrated into a depression over northwest and adjoining west central Bay, centred near 19.0°N, 86.0°E, the surface winds at Puri and Bhubaneswar were E/15 and NE/10 kts. The 24-hour pressure changes and pressure departures at the coastal stations between Kalingapatnam and Puri were – 3 to – 5 hPa and – 3 to – 6 hPa respectively. Moving slightly northwestwards, the depression lay at 0300 UTC of 15th August close to the coast, centred near 19.5°N, 85.5°E. At this hour, Puri and Gopalpur reported SE/10 kt and NW/10 kt surface winds respectively. However, at

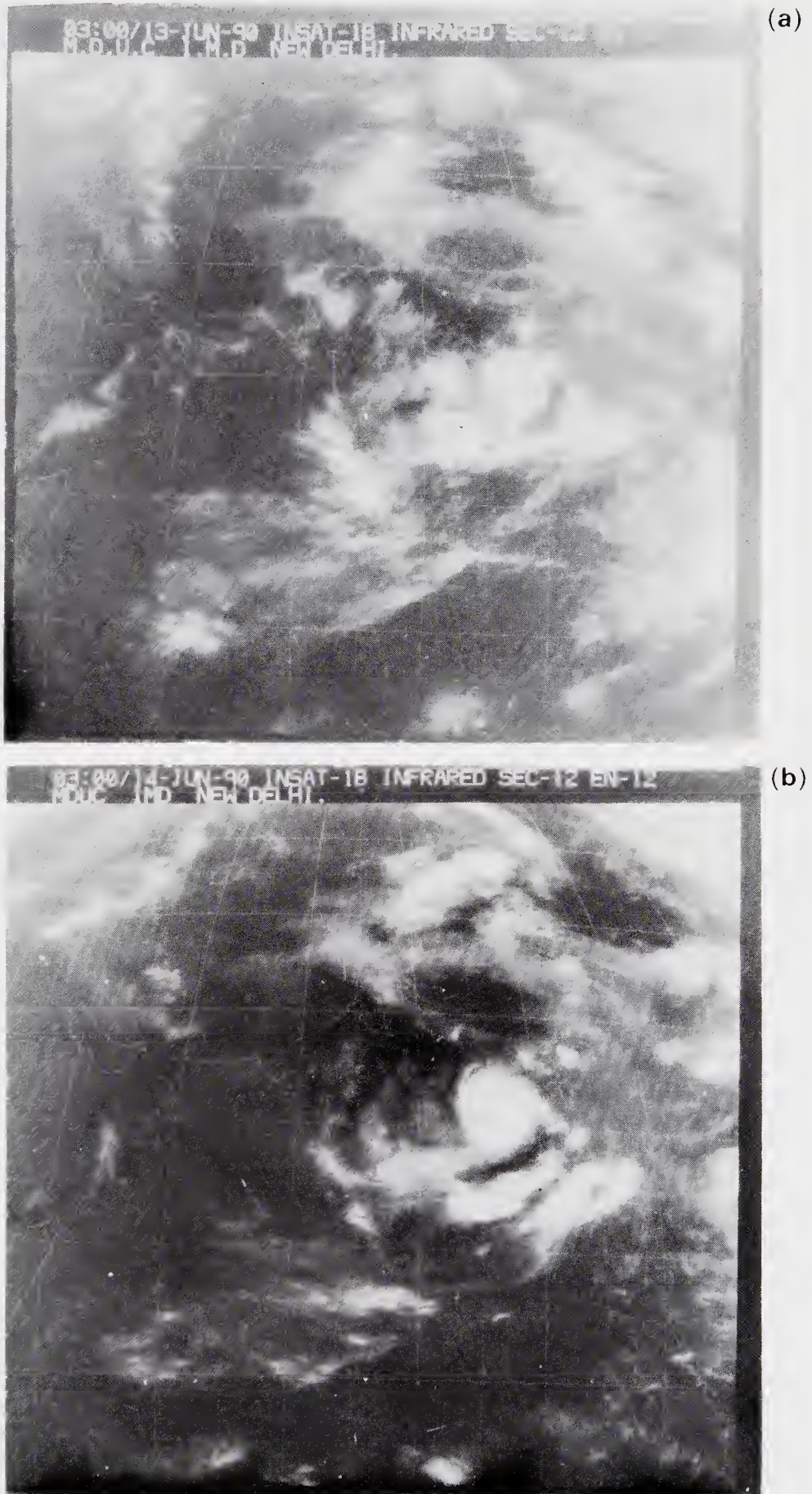


Figure 16(a & b).



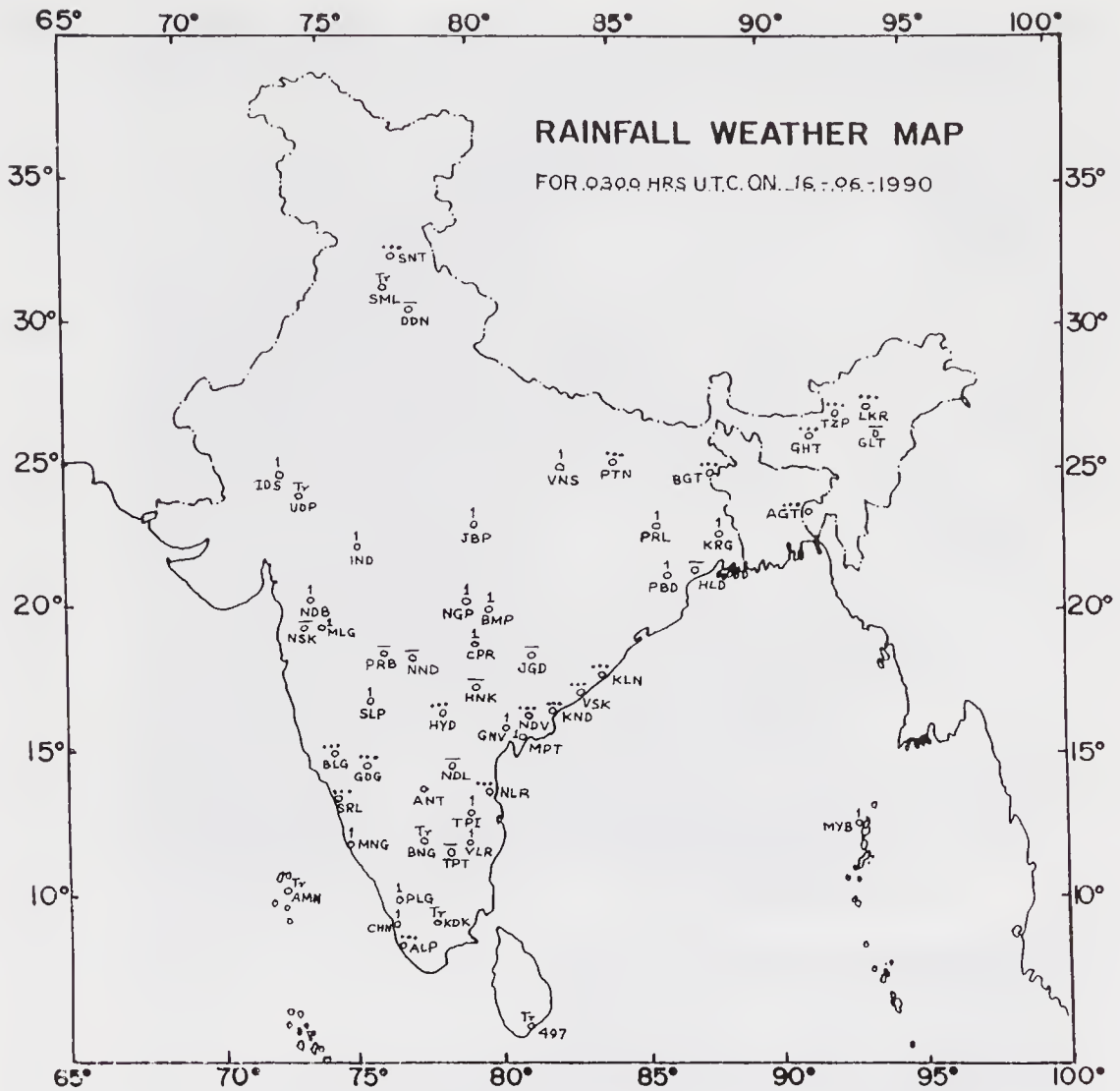
Figure 16(c).

0600 UTC a ship lying about 100 km east of the depression centre reported $190^{\circ}/29$ kt wind.

Moving in a west-northwesterly direction, the system crossed south Orissa coast between Gopalpur and Puri around noon of 15th and lay at 1200 UTC over Orissa centred near 20.0°N , 84.0°E (about 90 km east of Bhawaniputra, figure 15). In the evening, the system lay over central Madhya Pradesh and adjoining Vidarbha close to Chindwara. Continuing to move in a west-northwesterly direction, it weakened into a well-marked low pressure area over southwest Madhya Pradesh and neighbourhood on 17th morning. The system further moved westwards and merged with the seasonal low over south Pakistan and adjoining west Rajasthan on 19th August. INSAT pictures of the depression may be seen in figures 19a to 19c.

Figures 20 to 22 show rainfall map over the country during 15th to 17th August. It is observed that this depression gave rainfall over several stations within the trough region.

4.7.3 Deep depression: 20th–24th August: A depression was formed on the morning of 20th August out of an upper air cyclonic circulation over north adjoining central Bay. It crossed north Orissa coast around noon of 21st as a deep depression and further moving in a west-northwesterly direction weakened and merged with the seasonal low over west Rajasthan.

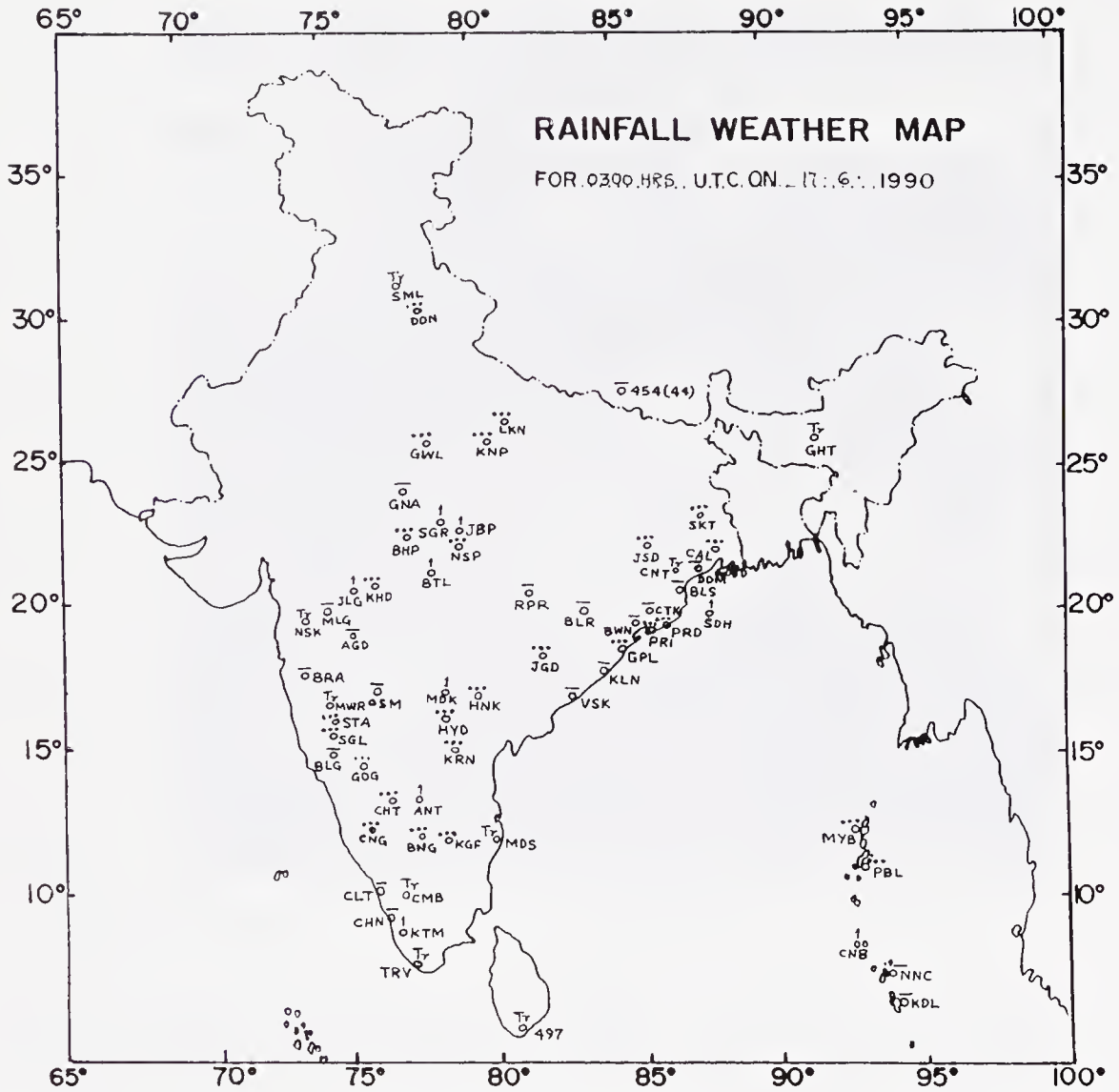


RAINFALL DATA

VERY HEAVY (12 cm)	Gangtok	4 cm	Hutbay	2 cm	Cuddalore	3 cm	Purlia	1 cm	
Bombay(Santacruz)	15 cm	Jalgaon	4 cm	Masulipatnam	1 cm	Varanasi	1 cm	Diamondharbar	1 cm
Calcutta	42 cm	Vengurla	4 cm	Yotmal	2 cm	Asansol	3 cm	Krishnanagar	1 cm
HEAVY (7-12 cm)	Pondicherry	5 cm	Chanderpur	1 cm	Midnapur	2 cm			
Ratnagiri	7 cm	Goa (Panjim)	4 cm	Tandong	3 cm	Mayabandar	1 cm		
Kozhikode	8 cm	MODERATE (1-3 cm)	Sholapur	1 cm	Long Island	2 cm			
Bhira	8 cm	Calcutta (DD)	3 cm	Malegaon	1 cm	Dohad	3 cm		
Mahabaleshwar	7 cm	Indore	1 cm	Ramagundam	3 cm	Veraval	1 cm		
Gondia	7 cm	Mangalore	1 cm	Palghat	1 cm	Raichur	2 cm		
Bijapur	7 cm	Vellore	1 cm	Osmanabad	3 cm	Cannur	3 cm		
RATHER HEAVY (4-6 cm)	Jabalpur	1 cm	Wardha	2 cm	Kottayam	2 cm			
Bhubaneswar	4 cm	Ganavaram	1 cm	Navdurbar	1 cm	Punalur	2 cm		
Pendra	5 cm	Cochin	1 cm	Brahmapuri	1 cm	Medak	3 cm		
Karawar	6 cm	Nagpur	1 cm	Baripada	1 cm	Nizamabad	2 cm		
		Carnicobar	2 cm	Jawai Damsitel	1 cm	Karnool	2 cm		
						Tirupathi	1 cm		
						Purlia	1 cm		
						Diamondharbar	1 cm		
						Krishnanagar	1 cm		

Figure 17.

On 20th morning, the disturbance concentrated into a depression over northwest and adjoining central Bay centred near 19.5°N, 89.0°E (figure 15). Moving in a west-northwesterly direction the depression lay at 1200 UTC centred near 20.8°N, 88.0°E.



RAINFALL DATA

MODERATE (1-3 cm)		Akola	5 cm	Nanded	7 cm
Sand head	1 cm	RATHER HEAVY (4-6 cm)		Pusad	7 cm
Carnicobar	1 cm	N. Lakhimpur	6 cm	Mahabaleshwar	9 cm
Anantapur	1 cm	Bombay (SCZ)	6 cm	Nizamabad	7 cm
Jalpaiguri	2 cm	Mangalore	4 cm	Cannanore	2 cm
Buldana	2 cm	(Airport)		Kottayam	1 cm
Medak	1 cm	Mangalore	5 cm	Khammam	3 cm
Nidadavala	2 cm	(Panambur)		Narsingpur	1 cm
Meracara	2 cm	Kakinada	5 cm	Jalgaon	1 cm
Balurghat	2 cm	Dibrugarh	4 cm	Navdurbar	4 cm
Gangtok	2 cm	HEAVY (7-12 cm)		Parbhani	2 cm
Bijapur	3 cm	Nagpur	9 cm		
		Amroli	9 cm		

Figure 18.

By 0300 UTC of 21st, the system had intensified into a deep depression and lay centred close to Paradip.

Based on winds recorded by the high wind speed recorder at Paradip, the deep depression crossed close to Paradip on the morning of 21st August. At 0300 UTC of

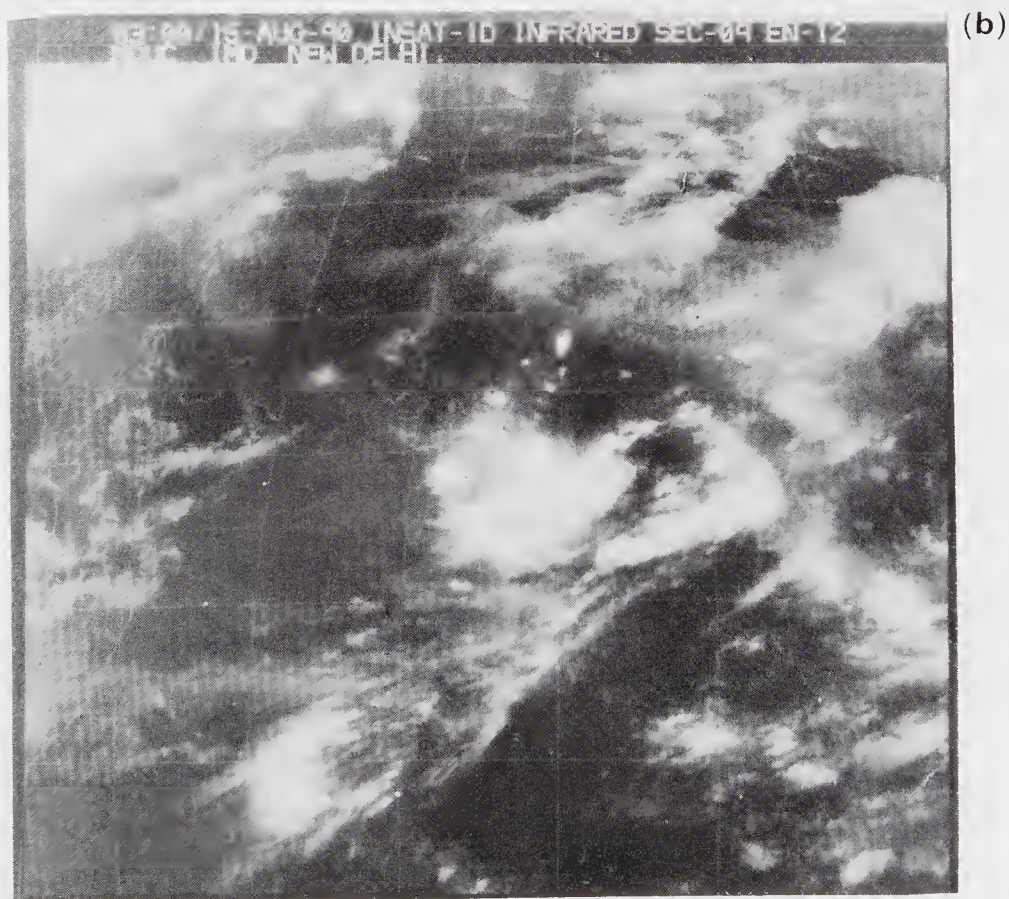
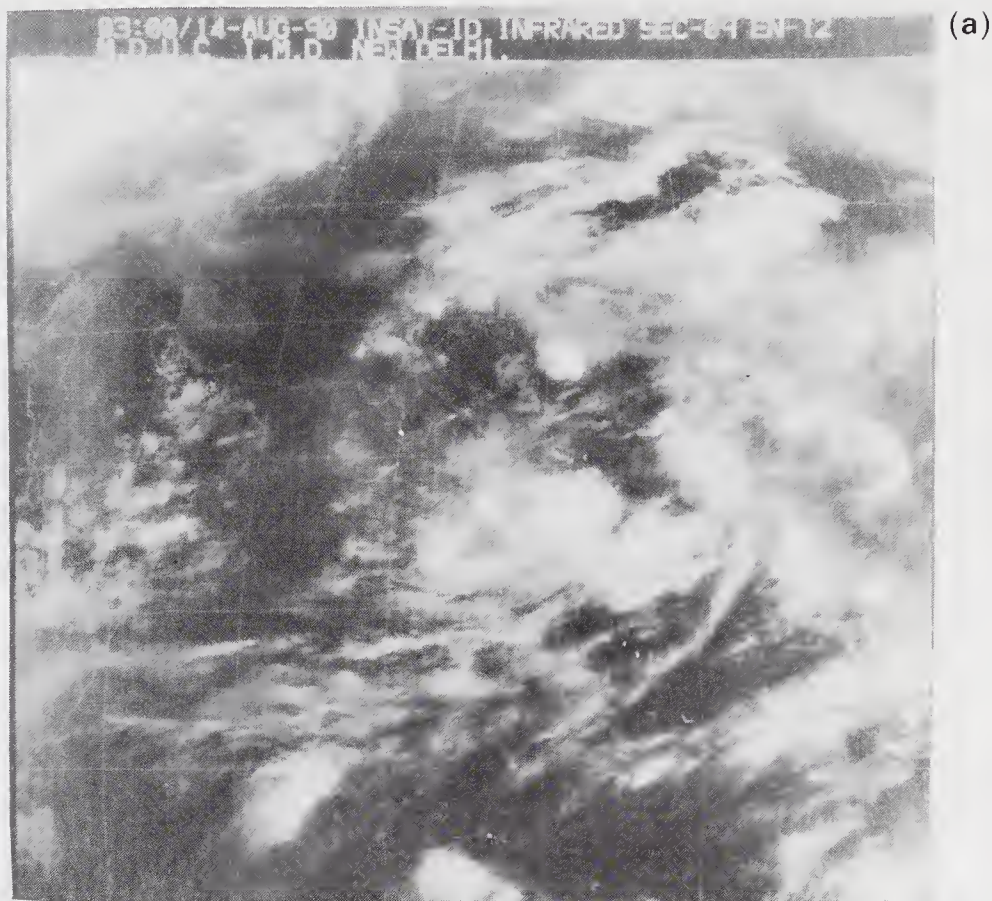


Figure 19(a & b).

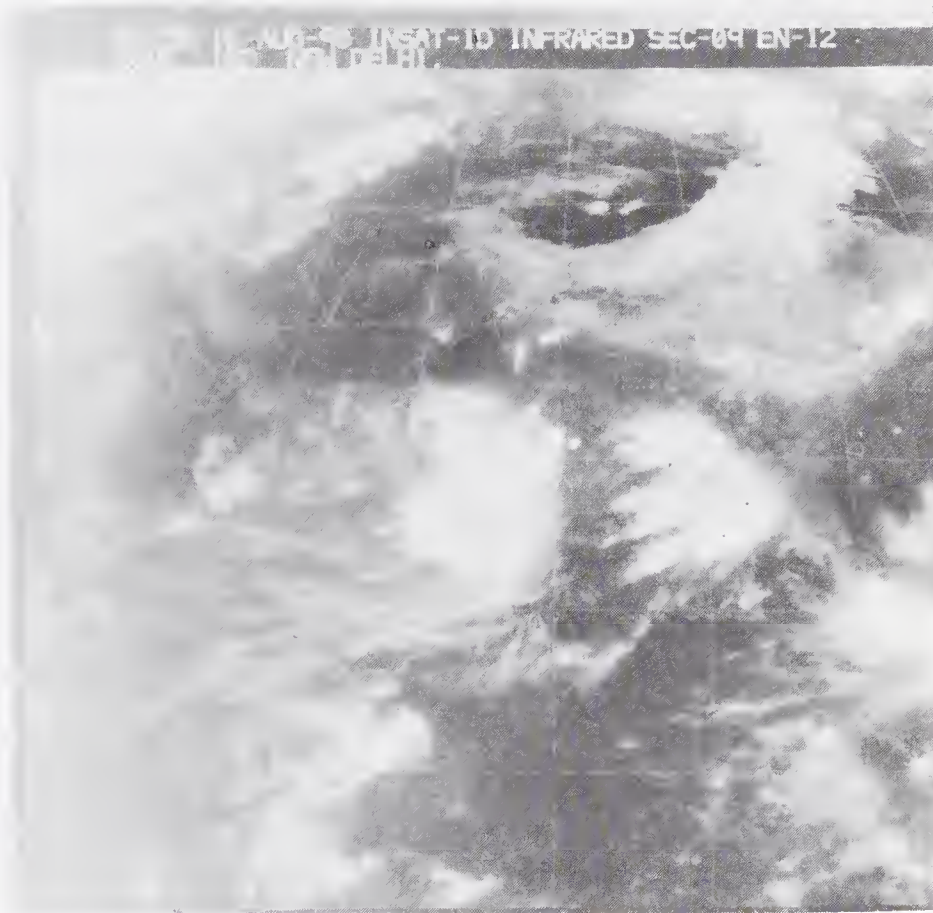


Figure 19(c).

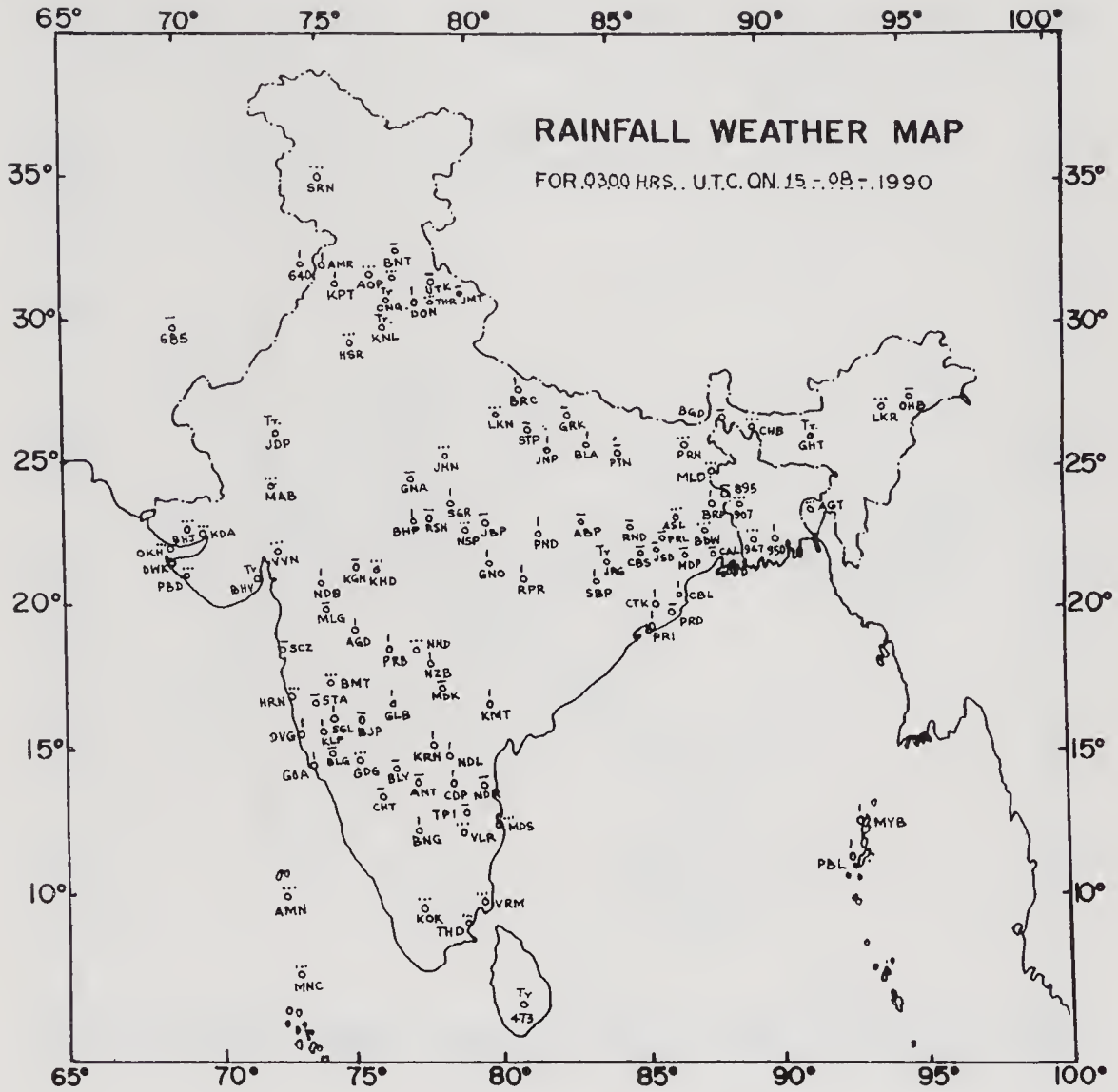
22nd, it weakened to a depression over southeast Madhya Pradesh and neighbourhood, centred about 70 km ESE of Raipur. At 1200 UTC of 23rd the depression was centred about 60 km west of Raipur and at 0300 UTC of 23rd about 30 km northwest of Panchmari. The depression moved in a northwesterly direction along the monsoon trough up to west Rajasthan by 25th and weakened further and merged with the seasonal low by 26th August.

In association with the system, the lowest pressure of 991.1 hPa was recorded at Paradip at 0300 UTC of 21st. Maximum pressure change (-8.9 hPa) and the pressure departure (-10.6 hPa) were also observed at 0300 UTC of 21st at Bhubaneswar. On all days, the associated cyclonic circulation extended up to 7.6 km a.s.l. with southerly tilt with height except on 21st when the circulation had hardly any tilt with height.

The system caused very heavy rainfall in Orissa, Madhya Pradesh, Maharashtra, Gujarat and in the Telangana region of Andhra Pradesh.

5. Data source

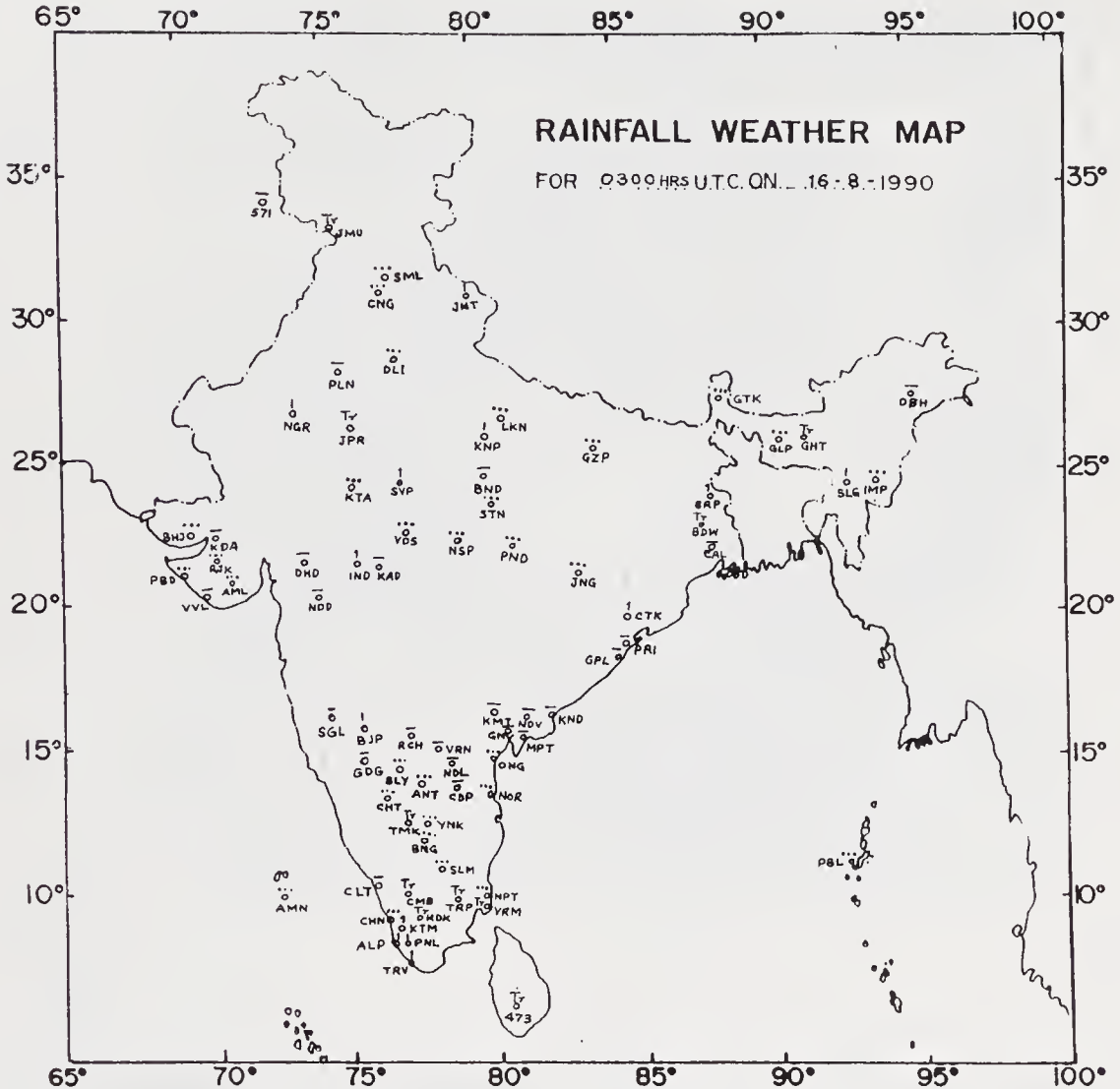
A data bank has been established at Indian Institute of Tropical Meteorology, Pune. Details of data available in the bank are given in a companion paper by Vernekar and



RAINFALL DATA

VERY HEAVY (12 cm)	Ratnagiri	4 cm	Machilipatnam	1 cm	Punalur	2 cm	Chandbali	1 cm
Bombay(Colaba)	Sand heads	5 cm	Bangalore	1 cm	Kozhikode	2 cm	Ujjain	2 cm
Bhica (43062)	Nidadavale	6 cm	Goa (Panjim)	1 cm	Mayabunder	1 cm	Bapatla	5 cm
HEAVY (7-12 cm)	Indore	4 cm	Aurangabad	1 cm	Long island	2 cm	Parbhani	1 cm
Santa Cruz	Chanderpur	5 cm	Brahmapuri	2 cm	Port Blair	1 cm	Dharmasala	3 cm
Mercara	Agumbe	6 cm	Gondla	1 cm	Gulbarga	1 cm	Disha	2 cm
Shirali	Karwar	6 cm	Pendra	1 cm	Balasore	3 cm	Nizamabad	1 cm
Alibag	Mahabaleshwar	5 cm	Bhubaneswar	2 cm	Bhopal	1 cm	Cuddapah	1 cm
RATHER HEAVY (4-6 cm)	Chamba	4 cm	Puri	1 cm	Nagpur	3 cm	Sangli	1 cm
Ongle	Jhelawar	6 cm	Dehradun	1 cm	Raipur	1 cm	Deogarh	1 cm
Mangalore	Osmanabad	4 cm	Jammu	2 cm	Nandigama	1 cm	Cuttak	1 cm
Jagadlpur	Rentachintla	4 cm	Amritsar	1 cm	Mehboobnagar	5 cm		
Kalingapatnam	Gannavaram	4 cm	Halwara	1 cm	Nandyal	1 cm		
Visakhapatnam	MODERATE (1-3 cm)		Cochin	2 cm	Sagar	1 cm		
Kakinada	Panambur	3 cm	Solapur	2 cm	Hosangabad	2 cm		
	Hyderabad	2 cm	Kolhapur	1 cm	Sambalpur	1 cm		

Figure 20.

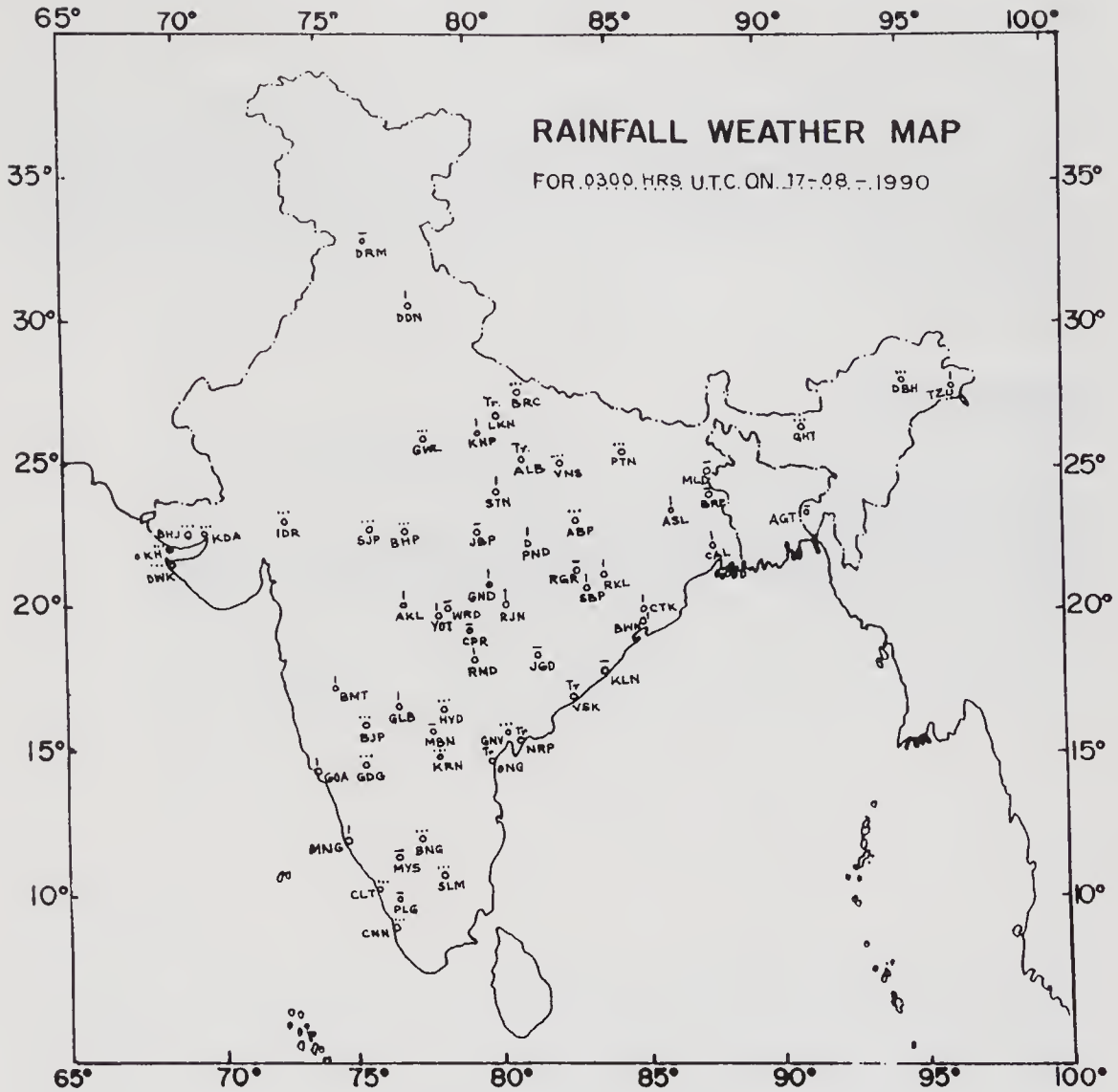


RAINFALL DATA

VERY HEAVY (> 12 cm)	Nizamabad 10 cm	Hakimpet 5 cm	Balasure 3 cm	Uttarkashi 2cm	Kottayam 1cm
Bhira 37 cm	Medak 9 cm	N.Lakhimpur 4 cm	Bijapur 1 cm	Joshinath 1cm	Kothagudem 3cm
Mahabaleshwar 21 cm	Osmanabad 7 cm	Golaghat 4 cm	Kanwar 2 cm	Cuttack 1cm	Berhampare 1cm
Alibag 13 cm	Madurai 7 cm	Raipur 5 cm	Gulbarga 3 cm	Paradip 2cm	Rajnandgaon 3cm
Wardha 13 cm	Ramgundam 8 cm	Venguda 4 cm	Karwar 2 cm	Kenughagarh 3cm	Shirpuri 1cm
Agumbe 14 cm	Chandrapur 10 cm	MODERATE (1-3 cm)	Belgum 3 cm	Baripada 3cm	Rajgarh 2cm
Harnai 13 cm	Yeotmal 12 cm	Aurangabad 2 cm	Chickmagalur 2 cm	Ahmednagar 3cm	Rajgarh 2cm
HEAVY (7-12 cm)	Amraoti 6 cm	Palghat 2 cm	Satara 1cm	Indore 1cm	
Bombay (Santacruz) 8 cm	RATHER HEAVY (4-6cm)	Punalur 1 cm	Hanamkonda 2cm	Jalgaon 2cm	
Bombay/Colaba 9 cm	Jagdalpur 6 cm	Ranchi 3 cm	Bulsar 3cm	Beed 2cm	
Ratnagiri 7 cm	Shirali 5 cm	Nagpur 1 cm	Silchar 1cm	Kanpur 1cm	
Sholapur 7 cm	Nanded 7 cm	Khondwa 2 cm	Akola 3cm		
Nagpur 9 cm	Parbhani 5 cm	Ujjain 4 cm	Buldana 4cm		
Jabalpur 11 cm	Mahabubnagar 5 cm	Midnapore 2 cm	Mangalore 2cm		
Mercara 7 cm	Gondla 4 cm	Baramati 3 cm	Baramati 3cm		
		Satara 1 cm	Honavar 2cm		

Figure 21.

Aralikatti (1995). It may be mentioned that in addition to the above, data from the regular stations of IMD are also available from the Additional Director General of Meteorology (Research), India Meteorological Department, Pune 411 005.



RAINFALL DATA

VERY HEAVY (12 cm)	Bhanwar	8 cm	Sangli	5 cm	Contai	3 cm	Nizamabad	2 cm	
Ratnagiri	28 cm	Surat	10 cm	Parbhani	5 cm	Raipur	2 cm	Rangundam	1 cm
Baroda	14 cm	Amreli	7 cm	Nanded	6 cm	Veravel	3 cm	Asansol	1 cm
Bhavnagar	13 cm	Naudurbar	9 cm	Amraoti	8 cm	N.Lakhimpur	3 cm	Bramhapuri	2 cm
Bhira	21 cm	Valsad	7 cm	MODERATE (1-3 cm)				Khandwa	3 cm
Mahabaleshwar	12 cm	Broach	8 cm	Kalaikunda	2 cm	Goa	1 cm	Satna	1 cm
Jalgaon	17 cm	RATHER HEAVY (4-6 cm)				Dehradun	1 cm	Ahmedabad	3 cm
V.V. Nagar	15 cm	Bombay(Scz)	4 cm	Calcutta-DD1	1 cm	Akola	1 cm	Gulbarga	1 cm
HEAVY (7-12 cm)		Pune (LHG)	4 cm	Delhi(PLM)	2 cm	Pendra	1 cm	Gelgaum	3 cm
Bombay (Colaba)	7 cm	Pune	5 cm	Imphal	2 cm	Nagpur	2 cm	(Samhra)	
Kolhapur	7 cm	Aurangabad	4 cm	Solapur	2 cm	Tezu	1 cm	Karwar	3 cm
Malegaon	8 cm	Balashore	4 cm	Kanpur	1 cm	Cuttack	1 cm	Sambalpur	1 cm
Mahan	7 cm	Alibag	6 cm	Mangalore	1 cm	Phulbani	3 cm	Jharsuguda	1 cm
Rajkot	7 cm	Satara	6 cm	Bhubaneswar	1 cm	Rajnandgaon	1 cm	Baramati	1 cm
Tezpur	7 cm	Paradip	6 cm	Tadong	2 cm	Yeotmal	1 cm		
				Purulia	2 cm				

Figure 22.

Acknowledgements

The author is grateful to Dr N Sen Roy, Director General of Meteorology for his encouragement and for extending facilities for preparation of this paper. Special thanks are due to Shri P Rajesh Rao, Director, Office of the Deputy Director General of Meteorology (Upper Air Instruments), New Delhi, for his help in preparation of the manuscript. The author is also grateful to Prof R Narasimha for inviting him to contribute this paper.

Suggested Reading

Anon. 1991 *Mausam* **42** 309–328

Goel M 1993 *Vayu Mandal* **23** 3–4

Gupta G R, Desai D S and Biswas N C 1991 *Mausam* **42** 219–226

Vernekar K G and S S Aralikatti 1995 *Proc. Indian Acad. Sci., Earth Planet. Sci.* **104** 249–256

Statistical analysis of the position of the monsoon trough

G RAJKUMAR and R NARASIMHA*

Jawaharlal Nehru Centre for Advanced Scientific Research, Jakkur P.O., Bangalore 560 064, India

Abstract. Using surface charts at 0330GMT, the movement of the monsoon trough during the months June to September 1990 at two fixed longitudes, namely 79°E and 85°E, is studied. The probability distribution of trough position shows that the median, mean and mode occur at progressively more northern latitudes, especially at 85°E, with a pronounced mode that is close to the northern-most limit reached by the trough. A spectral analysis of the fluctuating latitudinal position of the trough is carried out using FFT and the Maximum Entropy Method (MEM). Both methods show significant peaks around 7.5 and 2.6 days, and a less significant one around 40–50 days. The two peaks at the shorter period are more prominent at the eastern longitude. MEM shows an additional peak around 15 days. A study of the weather systems that occurred during the season shows them to have a duration around 3 days and an interval between systems of around 9 days, suggesting a possible correlation with the dominant short periods observed in the spectrum of trough position.

Keywords. Monsoon trough; statistics; spectrum; MONTBLEX.

1. Introduction

It is well known that the position and intensity of the monsoon trough have a vital bearing on the monsoon rainfall of India (e.g., Rao 1976; Sikka and Narasimha 1995). In particular, fluctuations in the position of the trough (which can move by as much as 5° latitude in a day) are related to the short-period variations of rainfall. Thus, when the axis of the trough moves north and lies close to the Himalaya, rainfall weakens over most of north India (a condition characteristic of the so-called break in the monsoons, although widespread and heavy rains occur in the northeast, the Himalayan foothills and the southeast peninsula); correspondingly when the trough moves south there tends to be heavy rains in the north Indian plains and the monsoon becomes 'active' (with the opposite trend in the other areas already mentioned). It is therefore of great interest to study the fluctuations of the monsoon trough.

Rao (1976) quotes studies by Srinivasan and Ramakrishnan (1970) on the position of the trough in July and August. The trough is found to be in the "near-normal" position on only 30–47% of the occasions, and "more frequently to the north of the mean position" at 77°E. It is not clear how the "normal" position is defined, as the table accompanying the discussion (Rao 1976, p. 94) shows that, at 77°E, the trough is more often north of the normal position in both July and August; the "normal" does not coincide with any of the well-known statistical location parameters, like the mean, the median and the mode. A possible explanation is that the normal position is based on monthly averages of the *surface pressure* (Joseph P. V. 1996,

*Also at Centre for Atmospheric Sciences, Indian Institute of Science, Bangalore 560012.

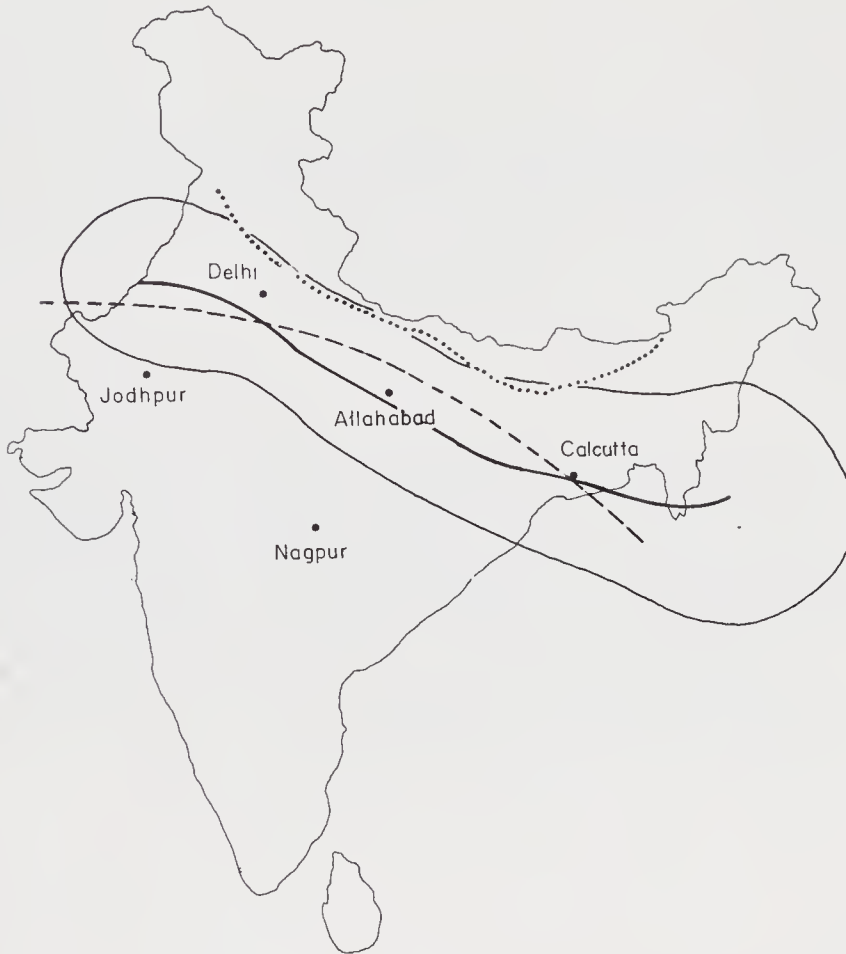


Figure 1. Typical monsoon trough positions during active (dashed line) and weak (dotted line) phases, with region of one standard deviation (enveloping continuous line) around the mean from Paul and Sikka (1976).

private communication) and so weighs the pressures differently from a monthly average of *trough position*.

Paul and Sikka (1976) analysed the mean and standard deviation in the latitudinal position of the trough at nine longitudes ranging from 73.25°E to 93.75°E . The trough position was determined using both pressure and wind direction data over a period of 20 years (0300 GMT during July and August, 1946–65). The analysis showed that the mean position varied from 28.9°N at 73.25°E to 21.6°N at 93.75°E (see figure 1); the standard deviation was nearly constant at about 2.6° up to about 87°E , but increased rapidly eastwards to 3.9° at 93.75°E .

In their study of the oscillations of the monsoon system, Krishnamurthy and Bhalme (1976) investigated nine characteristic parameters including the mean sea-level pressure over the monsoon trough, with a sample of 92 days covering the months of July, August and September in the year 1967 (which had near-normal rainfall). A spectral analysis was made using the direct FFT technique. The analysis revealed a salient oscillation at a period of about 11.5 days, and another at 4.5 days. From an analysis of the other eight parameters as well, the authors concluded that the monsoon system exhibits a “quasi-bi-weekly” oscillation with a period of 14 ± 2 days, and a short-period fluctuation on a scale of 2–6 days. It was suggested that while the latter

might be a reflection of local instabilities or passage of local disturbances, the quasi-bi-weekly oscillation could be due to winter-hemisphere or planetary scale waves, or a manifestation of a natural cycle in the monsoons involving cloud/radiation/stability interactions.

The objective of the present note is to provide a brief statistical analysis of the monsoon trough position during the MONTBLEX year 1990, with a view to determining the relevant time scales in its dynamics (and possibly also of the monsoon trough boundary layer). It is proposed to supplement the present analysis by examining data from other years as well.

2. Determination of the trough position

In this paper, we determine the trough position as a curve drawn from the seasonal low over the Pakistan area eastward to Gangetic West Bengal, demarcating the regions where the winds have an easterly component to the north from those where they have a westerly component to the south, and taking into account surface pressure. The frequent presence of a low pressure region to the east helps to fix the position of the trough. For the purpose of the present study two longitudes where the trough is almost always well-defined were selected, namely 79°E and 85°E respectively towards the two ends of the trough. These longitudes are separated by around 660 km. Outside this range the trough is frequently difficult to define and (especially near the Bay) may not even have a unique position; as gaps in the time series may vitiate the spectral analysis we shall describe below, we have limited ourselves to the two selected longitudes. The data on the surface pressure and wind were taken chiefly from the Indian Daily Weather Report. The position so determined is accurate to within about 1 degree latitude at both longitudes.

Except for four days at the eastern end, trough positions at both selected longitudes could be determined unambiguously and objectively on all days from 4th June to 14th September 1990. On one day (10th August) the eastern end of the trough was difficult to identify, because there were no closed isobars locating a low pressure region and the surface wind did not show the characteristic change in direction. In the present analysis, the position for this day has been taken as the mean of the positions on the previous and on the next day, taking account of the overall wind and pressure patterns. On 17th June and 31st August, the trough could not be drawn beyond 83°E longitude; on 8th August it could be drawn only up to 82°E . On these three occasions, the position was determined by extrapolation to 85°E longitude. On all other days the trough was clearly defined.

Figure 1 shows the trough position on a typical day (25th August 1990) when it was close to the Himalayan foothills (weak monsoon activity), as well as on another day (1st July 1990) when it was over the central parts of the country with the eastern end dipping into the Bay of Bengal (active monsoon). For comparison, the mean \pm standard deviation position of the trough as found by Paul and Sikka (1976) for July and August (over a 20-year period) is also shown in figure 1; the two data sets are clearly consistent.

The daily position of the trough during June, July and August 1990 has been plotted for both the selected longitudes in figure 2(a, b and c). By and large the fluctuations at the two longitudes appear to be in phase. It will be seen that the position fluctuates from 21.4°N (17th August) to 32.0°N (27th August) at 79°E longitude, and from 15°N

(8th August) to 27°N (25th June) at 85°E longitude. The extremes in the trough position over land correlate well with the orography: the Himalayan range in the north, and the Satpura-Vindhya ranges in the south.

3. Probability distributions

Table 1 lists the mean and standard deviation in the latitude of the trough at both longitudes. The data are in broad agreement with the figures quoted by Paul and Sikka (1976) as averages over a 20-year period, also shown in the same table. The extreme positions generally occur during the month of August, which is consistent with the high standard deviation for that month as can be seen from table 1. Indeed, as figure 2 indicates, the fluctuations in the trough position appear most vigorous in August, which experienced two depressions and three low-pressure areas (Srivastav 1995). Furthermore, during August the trough was significantly southward of its mean position during the [rest of the] season.

The position of the trough, at the two longitudes selected, has been placed in 2-degree (latitude) bins and their frequencies calculated. The resulting probability histograms are shown in figure 3. The distributions reveal a striking skewness: the mode, at both longitudes, is north of the mean; but there is a relatively sharp cut-off northwards of the mode; on the other hand each distribution shows a long southward tail. The mean is not necessarily the best indicator of the location in such cases. Table 2 presents the median, mean, and mode at both longitudes: it will be seen that they occur at respectively more northern latitudes, and that the differences between them are rather larger at the eastern end of the trough.

These data imply that care is needed in describing the location of the trough. Thus, at both longitudes but more markedly at the eastern end, the most probable location is

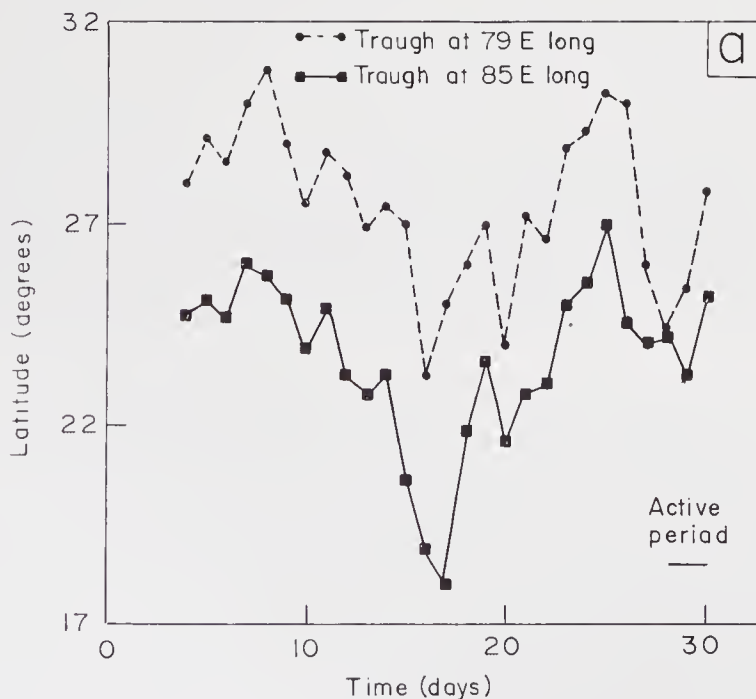


Figure 2(a). Latitudinal positions of the monsoon trough in June 1990.

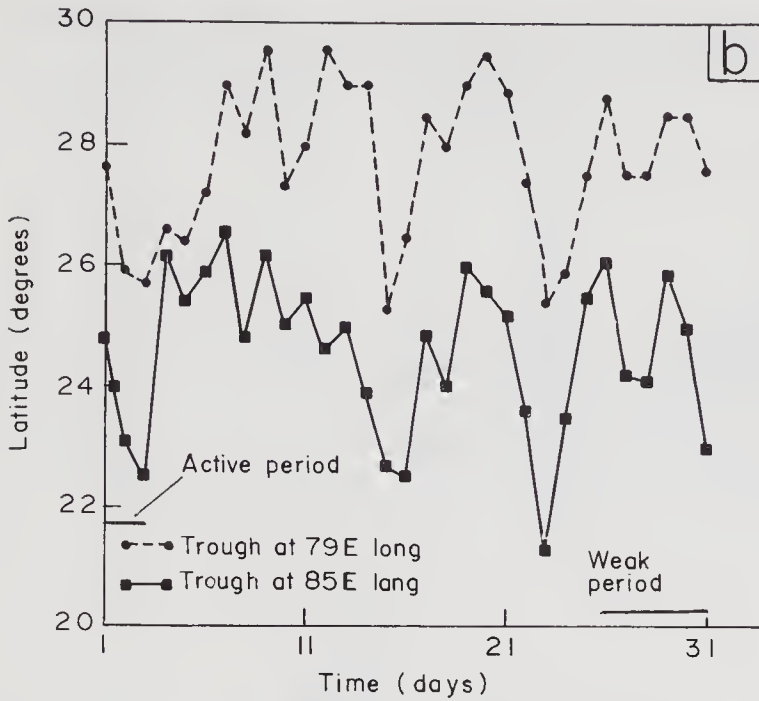


Figure 2(b). Latitudinal positions of the monsoon trough in July 1990.

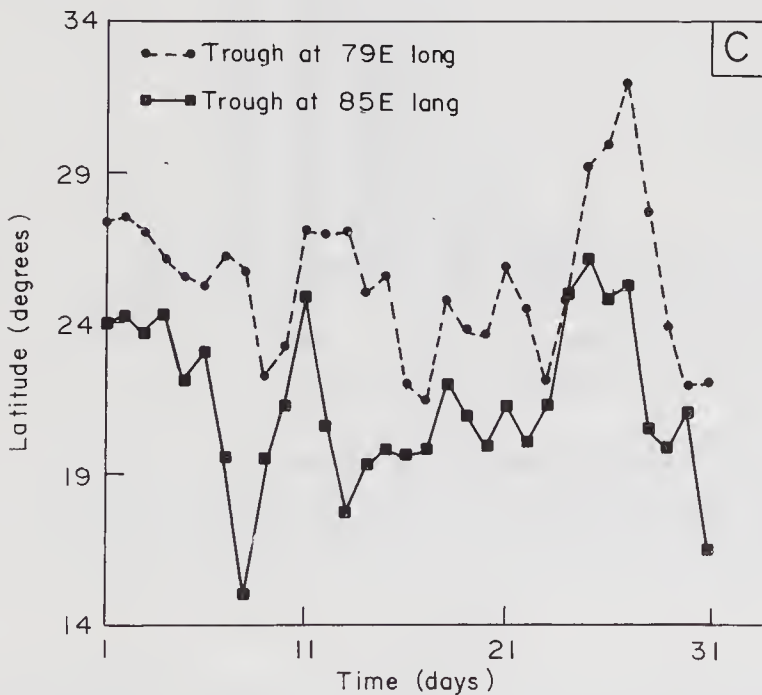
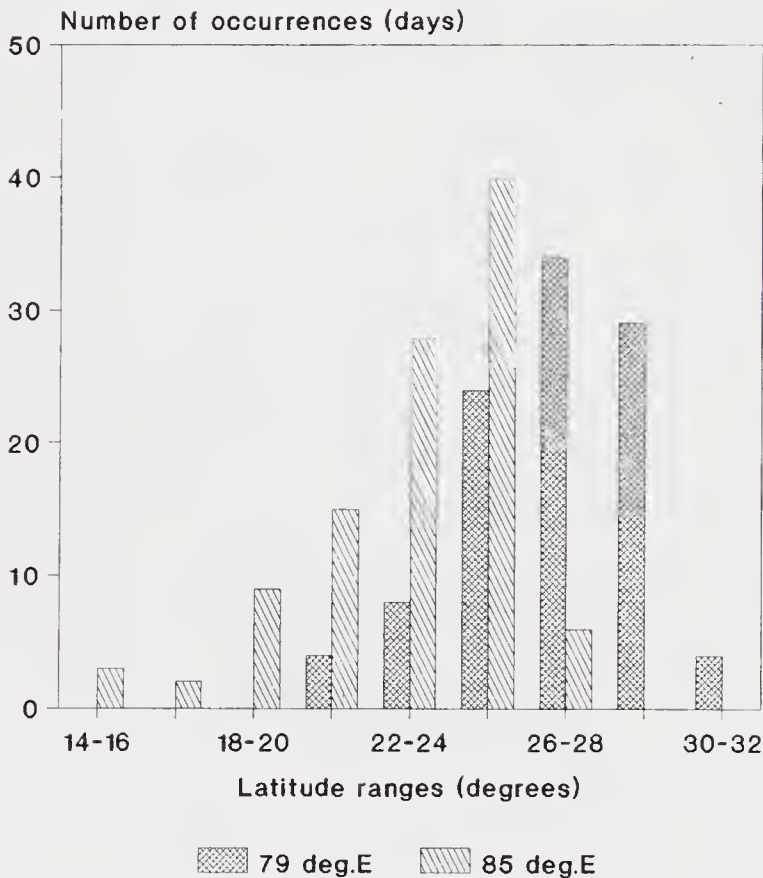


Figure 2(c). Latitudinal positions of the monsoon trough in August 1990.

north of the mean but more than half the time the trough is south of the mean! Another way of putting it is that there is a well-marked, northern-most position that the trough prefers to lock into, although it is away from it for appreciable lengths of time. This is particularly true during July, when the trough is very active and touches its northern limit frequently, as is visually clear from figure 2(b).

Table 1. Statistical parameters of the position of the monsoon trough.

Period	Position at 79°E		Position at 85°E	
	mean	s.d.	mean	s.d.
June	27.50	1.98	23.62	2.08
July	27.72	1.27	24.60	1.32
August	25.39	2.52	21.37	2.66
September	27.26	2.11	23.31	1.55
June – September	26.9	2.22	23.20	2.38
Paul and Sikka	26.8	2.3	23.0	2.6

**Figure 3.** Frequency distribution of the position of the monsoon trough.

4. Spectra

It is interesting to study the spectral characteristics of the fluctuations in the position of the trough, based on the time series of latitudinal position shown in figure 2.

Spectral analysis can be carried out by any of several methods; these have been critically discussed by Press *et al* (1986) and MacDonald (1989). We adopt here two independent methods.

The first is a simple method following WMO (1966), which is an approach similar to that developed by Blackman and Tukey (1958). In this method, one starts with a given time series of N equally spaced values, and computes all serial covariances for lags from 0 to m time units, where m is some number less than the number of data points N . Then

Table 2. Location of monsoon trough.

Longitude deg. East	Median deg. North	Mean deg. North	Mode deg. North
79	26.7	26.9	27.0
85	21.0	23.2	25.0

one computes the cosine transform of the resulting $m + 1$ lag covariance values, obtaining raw spectral estimates. These estimates are then smoothed to obtain consistent estimates of the final power spectrum, and evaluated for statistical significance. To do this, we fit a null hypothesis continuum to the spectrum. Assuming r_1 to be the lag-one correlation coefficient for the population, the following expression is evaluated for various choices of the harmonic number k between 0 and m :

$$S_k = \bar{s} \left[\frac{1 - r_1^2}{1 + r_1^2 - 2r_1 \cos(\pi k/m)} \right].$$

Here \bar{s} is the average of all the $m + 1$ raw spectral estimates.

Tukey (1950) has found that the ratio of the magnitude of the spectral estimate to the local magnitude of the continuum is distributed as chi-square divided by the degrees of freedom. Thus, given the degrees of freedom, the critical percentage point levels can be found from standard statistical tables. In other words a desired percentage confidence level for the null continuum is given as a second spectrum whose value for any wavelength is equal to a certain fixed multiple of the value of the null continuum at that wavelength. We compute in this way the continuum at 99 and 95 per cent confidence levels and plot them along with spectral estimates.

The spectra using this method are shown in figures 4 and 5 for the time series of trough position at 79°E and 85°E respectively; the prominent peaks are listed in table 3. One peak showing a periodicity of 7.7 days is seen clearly, and is significant at better than 99%. At 79°E two other peaks at 3.7 and 2.7 days are significant at 95% whereas at 85°E two different peaks at 2.9 and 2.6 days are significant at 99% and one at 4.5 days above 95% level. Peaks of the same periodicity viz., 7.7 and 2.7 days are seen at both longitudes, suggesting that they are robust characteristics of the fluctuating trough. A peak is also seen at 51.5 days though it is above the 95% significance level only at 85°E. It should be interpreted with some caution since the length of the data is only 2 cycles.

A smoother spectrum may be obtained by the maximum entropy method (MEM). We first standardize the variables by considering

$$\eta = \frac{y - \bar{y}}{\sigma_y},$$

where y is the latitudinal position (deg.) of the trough on any day and \bar{y} and σ_y its mean value and standard deviation evaluated over the whole data stretch (= 103 days). Associated with MEM is a parameter called its order, which Press *et al* (1986, p. 433) recommend should be "a few times the number of sharp spectral features that one desires it to fit". Keeping the results of figures 4 and 5 in mind, we have first tried order $M = 15$. The spectra are seen to be smoother than the FFT results. At $M = 20$ the sharp spectral peak at period $T = 7$ days is already split, suggesting that increasing the order

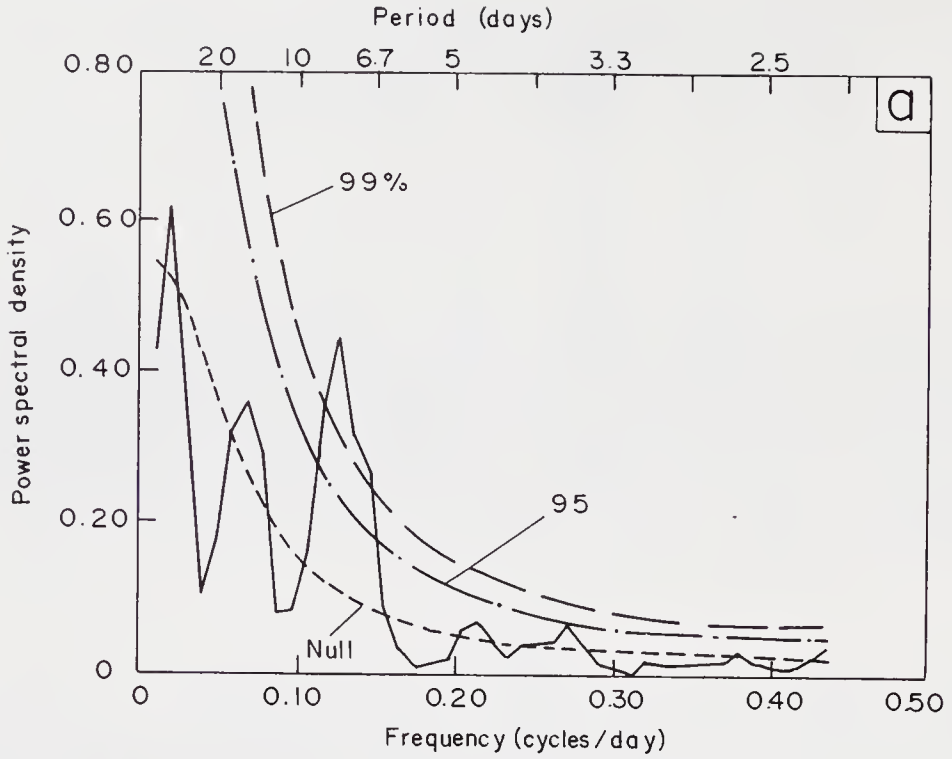


Figure 4(a). Power spectral estimates with confidence limits at 79°E (with smoothing).

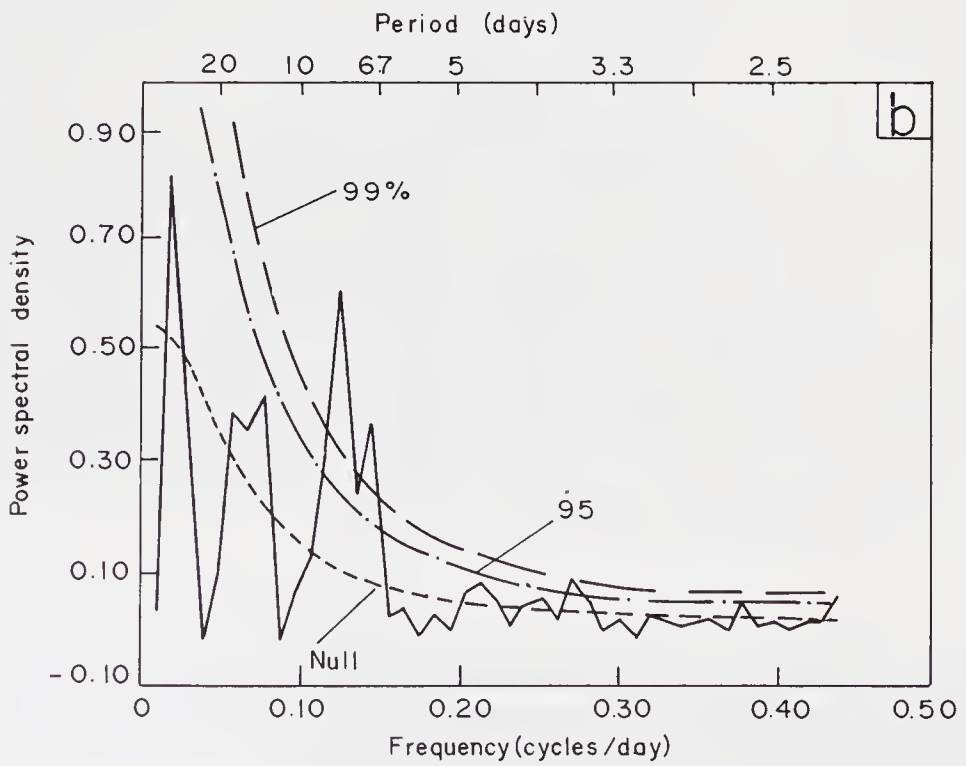


Figure 4(b). Power spectral estimates with confidence limits at 79°E (without smoothing).

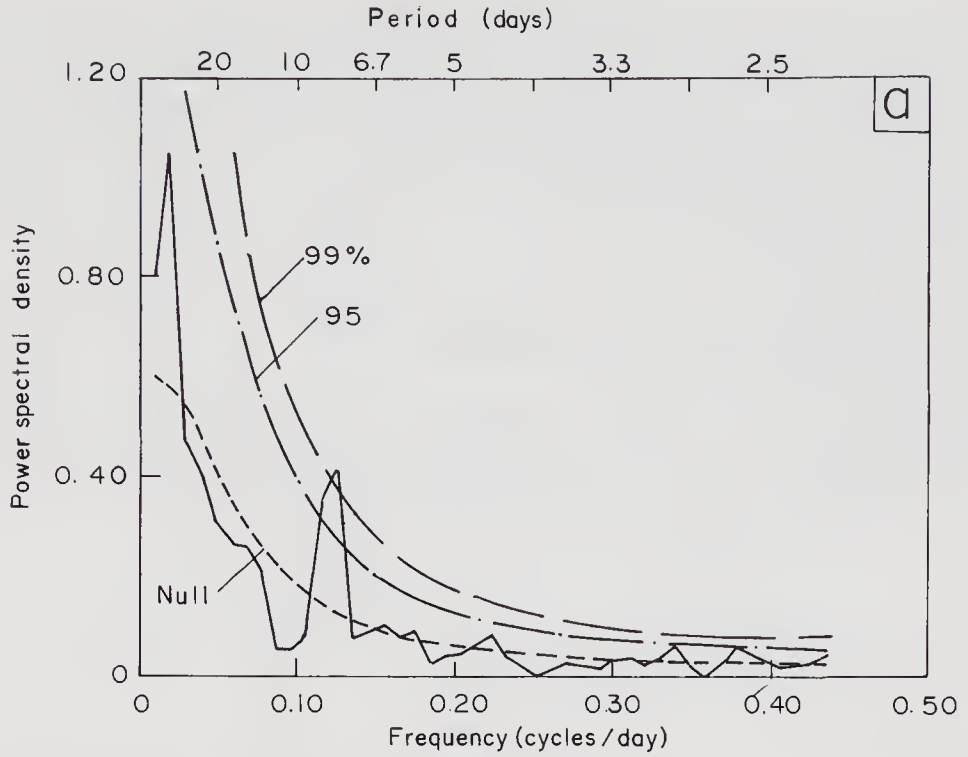


Figure 5(a). Power spectral estimates with confidence limits at 85°E (with smoothing).

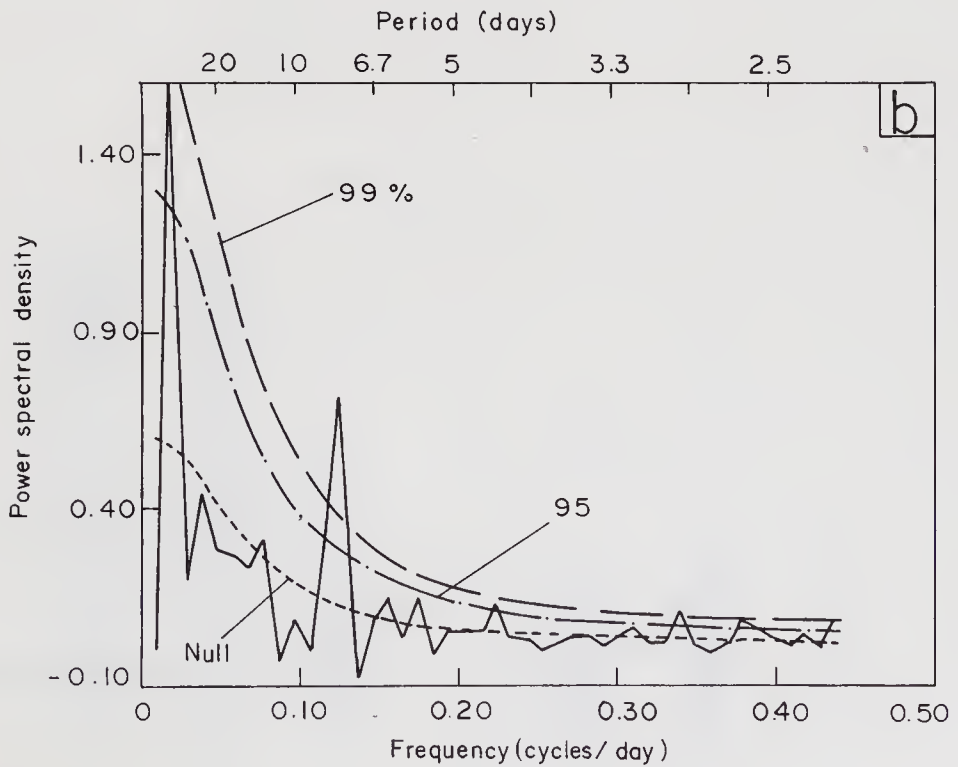


Figure 5(b). Power spectral estimates with confidence limits at 85°E (without smoothing).

further would lead to spurious spectral peaks, as noted by Press *et al.* However, at $M = 40$, a new peak appears at $T = 40$ days, but this should again be viewed with caution, as there would be less than 3 cycles of this period in the data stretch examined here.

In the light of this discussion the spectrum evaluated with $M = 15$ appears most appropriate, but results with $M = 15, 20$ and 25 are all shown for both the selected longitudes (figures 6 and 7). In these spectra two peaks viz., one at 7.3 days and another at 14.9 days stand out clearly.

An interesting feature of these spectra is that the peaks at the higher frequencies are more prominent at 85°E longitude than at 79°E , and occur at nearly the same frequencies in both methods.

To study the meteorological significance of these periods, we note that, during the monsoon, periods of clear days alternate with days of disturbed weather due to synoptic

Table 3. Prominent spectral peaks in fluctuations of monsoon trough position.

Longitudes deg. (East)	Periods (days)	Confidence level (%)
79	7.7	99
	3.7	95
	2.7	95
	51.5	> 75
85	7.7	99
	2.9	99
	2.6	99
	4.5	95
	51.5	> 95

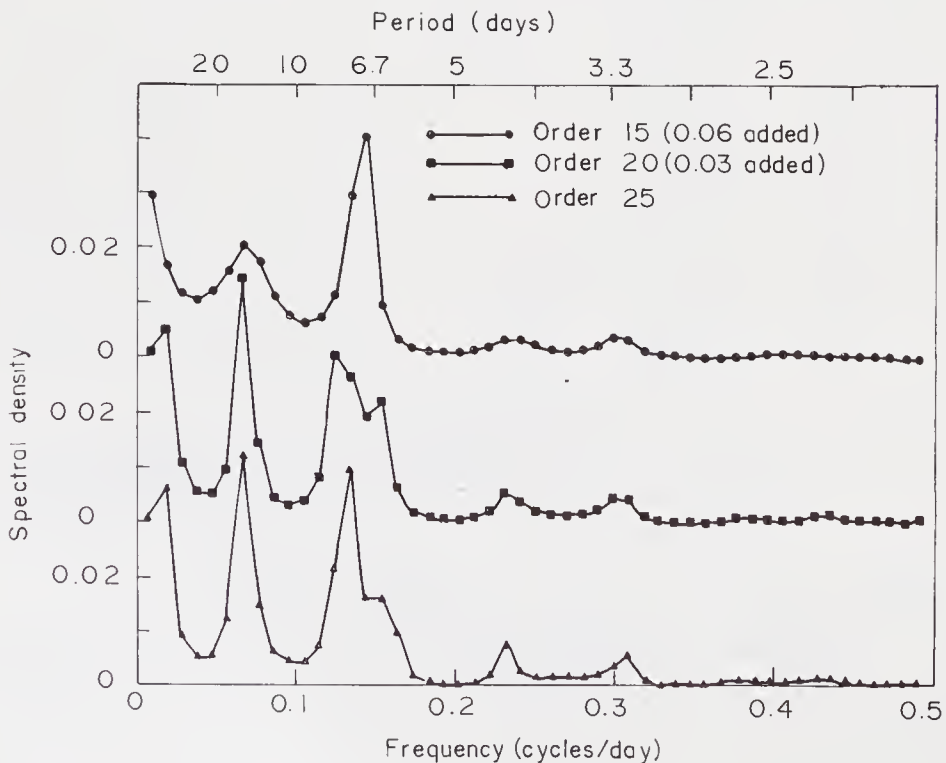


Figure 6. Power spectral estimates using MEM at 79°E .

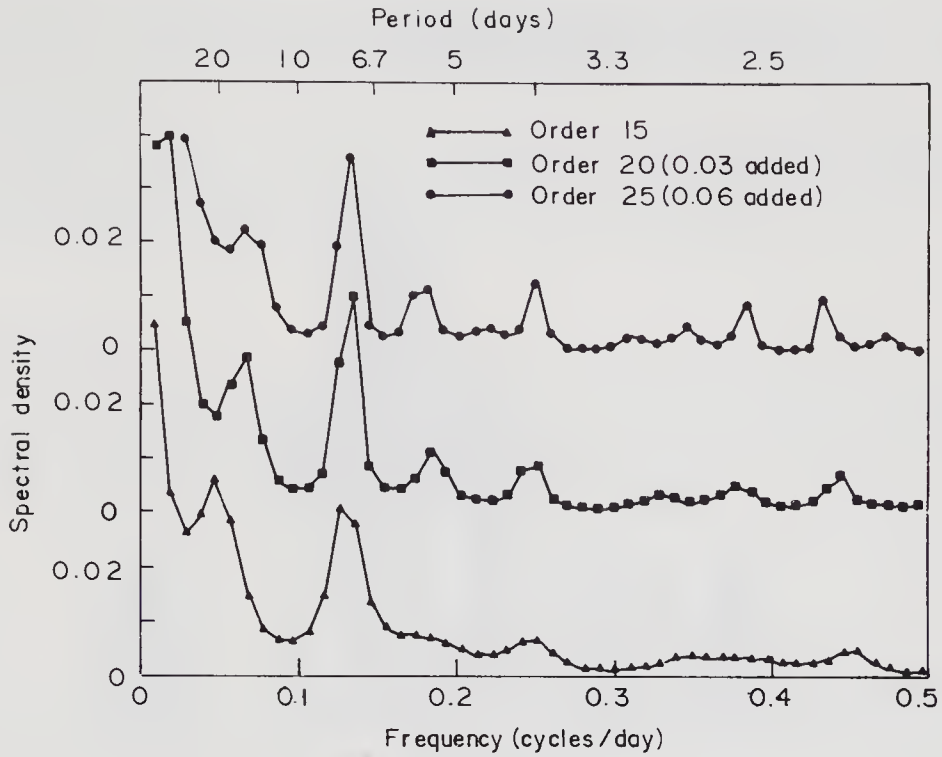


Figure 7. Power spectral estimates using MEM at 85°E.

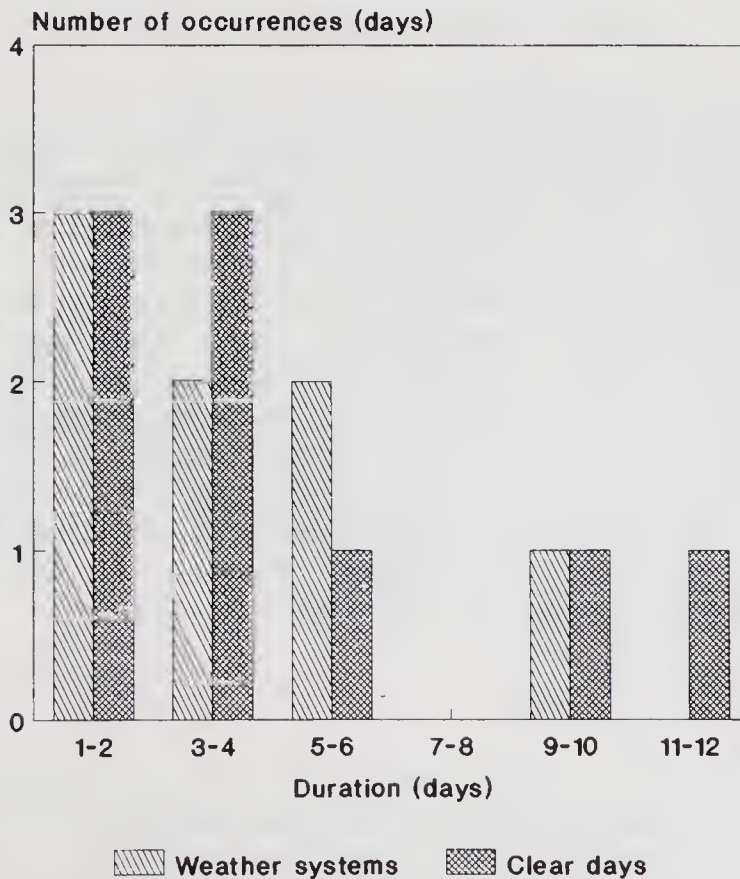


Figure 8. Frequency distribution of the life span of synoptic system or period of clear days.

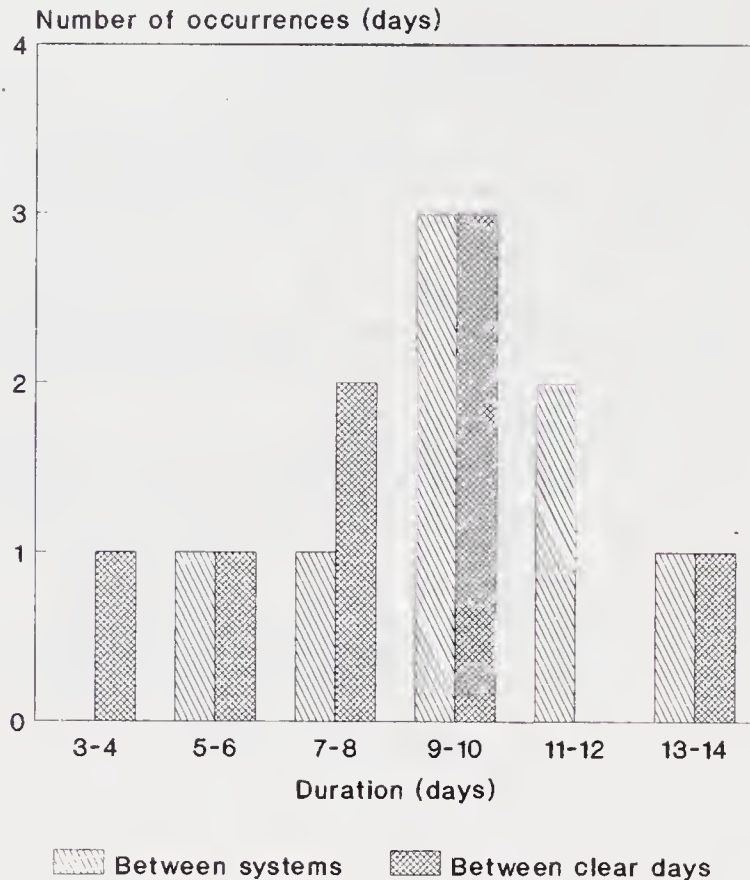


Figure 9. Interval between synoptic systems/stretch of clear days.

systems. The frequency distributions of the life of such weather systems and the duration of periods of clear days are shown in figure 8. It can be noted that the duration of such synoptic systems or clear periods is around 3 days. This correlates with the spectral peaks at 2.7 and 3 days in figure 5. The reason that these high frequency peaks are seen less prominently at 79°E longitude could be that most systems weaken considerably as they penetrate inland. (The available moisture is much less on land when compared to the sea.) The weather systems usually last for a period of about 3 days as can be seen from figure 8, followed by a similar period of dry days. The time interval between one such system and the next is shown in figure 9. The mode is around 9 days. This correlates well with the peak at 7.7 days in the spectra. The bi-weekly peak mentioned by Krishnamurti and Bhalme (1976) is seen only in the MEM spectra, and is more prominent at 79°E . There is evidence of a peak at 40–50 days in some of the spectra, and although their statistical significance is low because of the short record length (only 3 periods or less), they are consistent with the occurrence of the well-known 40-day mode (e.g., Sikka and Gadgil 1980).

5. Conclusions

The monsoon trough positions during the MONTBLEX-90 period show a highly skewed distribution, with a mode well north of the mean. Because of this skewness one needs to be cautious in defining a 'normal' position for the trough.

Hidden periodicities are sought in the time series of trough position by computing spectral densities using two different methods. Both methods show peaks around 7 to

8 days, and 2 days and 3 days, the latter being more prominent at 85°E longitude. MEM shows a period around 16 days as well. Both methods suggest there might be a peak around 40–50 days.

The 1990 season was characterized by the absence of any true break in the monsoon (Srivastav 1995), so to obtain a complete picture of the statistics of the trough some other years also need to be studied. Such a study is now on hand.

Acknowledgements

We thank Dr P V Joseph, Prof S Gadgil and Dr D R Sikka for their helpful comments on an earlier version of this manuscript. This work was supported by a grant from the Department of Science and Technology, Government of India.

References

- Blackman R B and Tukey J W 1958 The measurement of power spectra. (New York: Dover Publications)
- Krishnamurty T N and Bhalme H N 1976 Oscillations of a monsoon system. Part I: Observational aspects; *J. Atmos. Sci.* **33** 1937–1954
- MacDonald G J 1989 Spectral analysis of time series generated by nonlinear processes; *Rev. Geophys.* **27** 449–469
- Paul D K and Sikka D R 1976 Extended range forecasting – categorization of weather charts. Part I: Monsoon sea level pressure field. Project report no: ERF/1, 34 pp. (Indian Institute of Tropical Meteorology, Pune)
- Press W H, Flannery B P, Teukolsky S A and Vetterling W T 1986 Numerical Recipes. (Cambridge University Press)
- Rao Y P 1976 The southwest monsoon. (India Meteorological Department)
- Sikka D R and Gadgil S 1980 On the maximum cloud zone and the ITCZ over Indian longitudes during the southwest monsoon; *Mon. Weather Rev.* **108** 1840–1853
- Sikka D R and Narasimha R 1995 Genesis of the monsoon trough boundary layer experiment (MONTBLEX); *Proc. Indian Acad. Sci. (Earth Planet. Sci.)* **104** 157–187
- Srinivasan V and Ramakrishnan A R 1970 Location of the monsoon trough over India in the lower troposphere during July–August. Proc. Symp. Tropical Meteorology; *Am. Meteorol. Soc.* 2–11 (University of Hawaii, Honolulu)
- Srivastav S K 1995 Synoptic meteorological observations and weather conditions during MONTBLEX-90; *Proc. Indian Acad. Sci. (Earth Planet. Sci.)* **105** 189–220
- Tukey J W 1950 The sampling theory of power spectrum estimates. Symposium on *Applications of autocorrelation analysis to physical problems*; U.S. Office of Naval Research NAVEXOS-P-735 pp. 47–67 (Washington D.C.)
- WMO 1966 Some methods in climatological analysis; *WMO Tech. Note No. 81* 53 pp. WMO (Geneva)

MONTBLEX tower observations: Instrumentation, data acquisition and data quality

S RUDRA KUMAR*, S AMEENULLA and A PRABHU

Centre for Atmospheric Sciences, Indian Institute of Science, Bangalore 560012, India

*Now at Experimental Aerodynamics Division, National Aerospace Laboratories, Bangalore 560017, India

Abstract. Tower platforms, with instrumentation at six levels above the surface to a height of 30 m, were used to record various atmospheric parameters in the surface layer. Sensors for measuring both mean and fluctuating quantities were used, with the majority of them indigenously built. Soil temperature sensors up to a depth of 30 cm from the surface were among the variables connected to the mean data logger. A PC-based data acquisition system built at the Centre for Atmospheric Sciences, IISc, was used to acquire the data from fast response sensors. This paper reports the various components of a typical MONTBLEX tower observatory and describes the actual experiments carried out in the surface layer at four sites over the monsoon trough region as a part of the MONTBLEX programme. It also describes and discusses several checks made on randomly selected tower data sets acquired during the experiment. Checks made include visual inspection of time traces from various sensors, comparative plots of sensors measuring the same variable, wind and temperature profile plots, calculation of roughness lengths, statistical and stability parameters, diurnal variation of stability parameters, and plots of probability density and energy spectrum for the different sensors. Results from these checks are found to be very encouraging and reveal the potential for further detailed analysis to understand more about surface layer characteristics.

Keywords. Atmospheric surface layer; sensors; tower instrumentation; data quality.

1. Introduction

The tower platform has now been established as a standard and most convenient facility to make experiments in the surface layer, and to some extent beyond it, in the Atmospheric Boundary Layer (ABL). There are permanent tower observatories established for a continuous programme of boundary layer research, like for example the 300 m tower of the Boulder Atmospheric Observatory (BAO), Colorado, USA (see Kaimal and Gaynor 1983 for details) and the 200 m tower of KNMI, Cabauw, Netherlands (see Driedonks *et al* 1978 for details).

The variables of greatest interest to boundary layer meteorologists are the mean and fluctuating components of wind velocity, temperature and humidity. The stability of the layer at any time is obtained mainly using mean parameters, and the fluctuating quantities are required to describe the turbulence structure within the layer. The adequate measurement of these quantities in the surface layer makes stringent demands on the instrumentation system used to probe the layer.

Sensors for measuring the time-averaged properties of the flow should have a high degree of absolute accuracy and long-term stability. Sensors for measuring turbulent properties of the flow should have a broad frequency response to account for all the eddy scales contributing to the process. The response time for mean sensors can be as

long as a minute but for the fluctuation sensors it should be no more than 0.1 s. The above requirements have been kept in mind while designing the instrumentation system for MONTBLEX.

It is a well known fact now that our understanding of the ABL has to depend in large part on observational studies. The Kansas and Minnesota experiments (see Kaimal and Wyngaard (1990) for details) are regarded as important milestones in boundary layer research. As far as tower observations in India are concerned, a beginning was made by the pioneering efforts of a group from the Indian Institute of Science (A Prabhu, R Narasimha and their co-workers), who carried out observations for the first time in India using an instrumented 10 m tower (Narasimha *et al* 1981) on the shores of the Bay of Bengal (near Balasore, Orissa) as a part of MONEX in 1979. This led to a growing interest in the understanding of ABL processes in the Indian monsoon region, and provided a strong base and motivation to MONTBLEX.

A careful experiment in the atmospheric boundary layer demands a variety of measurements involving various atmospheric parameters on different time scales, including in particular multi-point observations spread over the height of the ABL which itself varies in time and space.

Preparation and observation phases of the MONTBLEX lasted from 1987 to 1990, with a pilot experiment in 1989 and the full-scale experiment during the monsoon period in 1990. The group from the Indian Institute of Science (IISc) was responsible for installation and carrying out tower observations at three stations, viz. Kharagpur, Varanasi and Jodhpur. IIT Delhi upgraded an earlier platform to the standard 30 m tower for MONTBLEX and experiments during the observational phase were assisted by the IISc group. Thus there were in all four 30 m towers for surface layer observations. The tower sites were selected so that they covered the deep moist convective region (Kharagpur) at one end of the monsoon trough, the dry convection in the desert region (Jodhpur) at the other end, and the transition zone in-between (Varanasi, Delhi).

Conducting a field experiment in the atmosphere is itself an enormous exercise. The interpretation of the data acquired, recorded through various sensors and instrumentation, is equally important in deriving an understanding of the physics of the atmosphere. First of all, it is essential that data from the field experiments are thoroughly checked and validated before using them for detailed analysis. A section is devoted to the discussion of results obtained during such an assessment of the quality of the MONTBLEX tower data including many of the checks suggested by Kaimal (1990) for the validity of the field data on ABL, but we begin with the tower instrumentation-set up used in the experiment.

2. Tower instrumentation

The complete tower instrumentation system used for the experiment may be broadly grouped into three components, viz. the tower platform, sensors and signal conditioning units, and the data acquisition system. The block schematic of a typical tower instrumentation system is shown in figure 1.

2.1 *The tower platform*

The tower is a 30 m high, guyed, uniform triangular lattice structure designed to

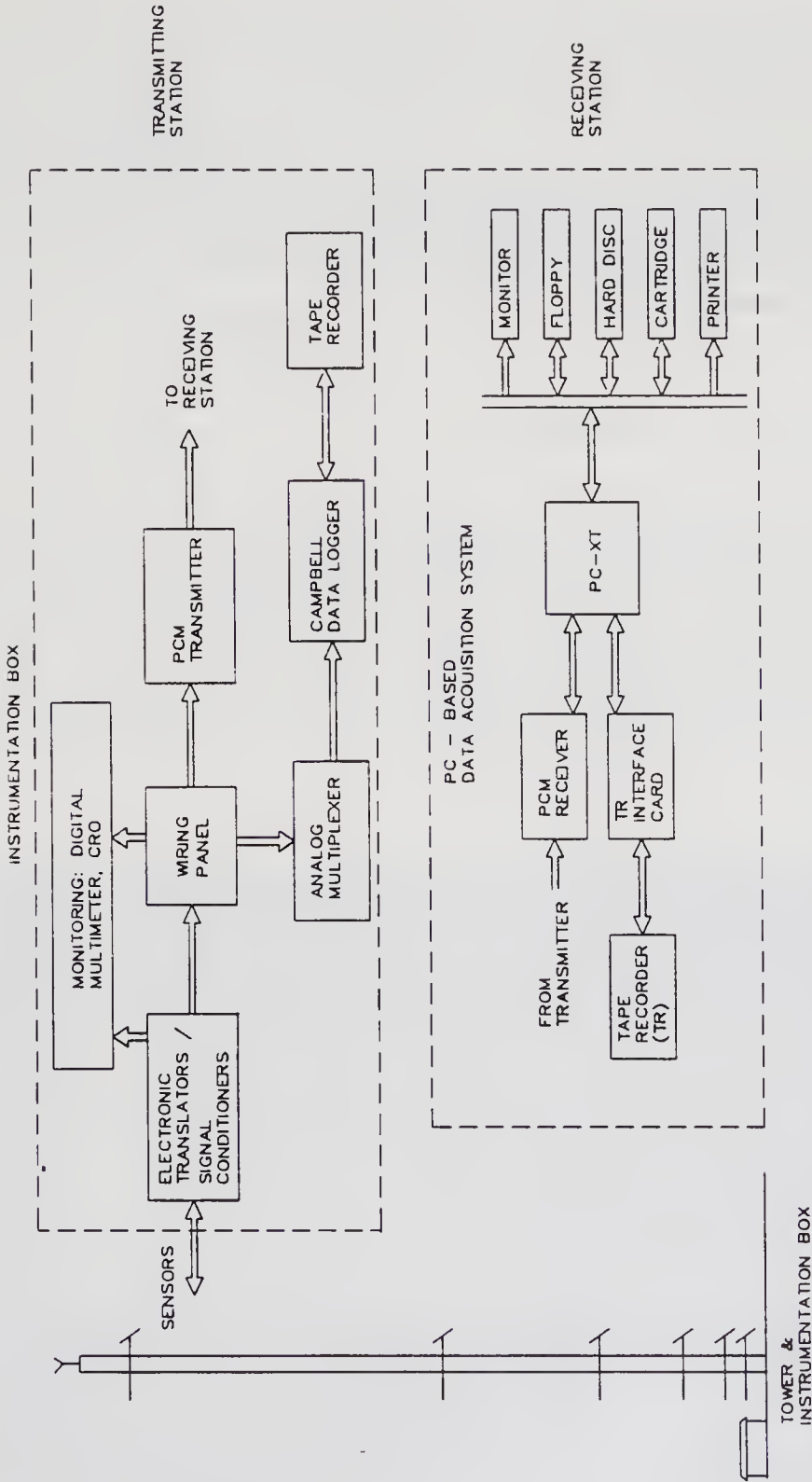


Figure 1. Block schematic of a tower instrumentation system.

withstand a windspeed of 180 km/hr. Booms are fitted at 6 levels (1, 2, 4, 8, 15, 30 m) with horizontal arms attached to these booms at a distance of about 1.3 m from the body of the tower. On these horizontal arms instrument posts are placed for mounting the sensors. Figure 2 shows a picture of an instrumented boom. The booms are designed so that they can be partially rotated about the vertical and horizontal axes to facilitate the orientation of the sensors towards the prevailing wind of the season and to ensure the horizontality of the instrument posts. This rotational facility also makes the mounting of the sensors on the instrument post easier. This is the improved version of an earlier simple boom which could be moved only in a direction perpendicular to the tower and without any rotating facility.

2.2 Sensors and signal conditioning units

The sensors mounted on the instrumentation posts of the booms are connected to their respective electronic translators (signal conditioning units) which are racked in a weather-proof instrumentation container at the foot of the tower. This container is placed permanently on one side of the tower opposite the mean direction of the prevailing wind of the season. The translators contain the electronics to process the signal output from each sensor and to convert it to the dynamic range of the data acquisition system. Translators also supply power to the small electronic circuit attached to the sensor, and are equipped with built-in electronics for calibration.



Figure 2. Picture of an instrumented boom.

The set of sensors/instruments used and the parameters they measure are listed below.

- Cup anemometer – horizontal wind speed.
- Wind vane – wind direction.
- Gill and hotwire anemometers – three components of wind velocity.
- Sonic anemometer – three components of wind velocity and temperature.
- Platinum resistance thermometer devices (RTDs) – mean and fluctuating temperature.
- Humicaps – relative humidity.
- Lyman-alpha – absolute humidity.
- Soil temperature sensors (encapsulated platinum wire).
- Rain-gauge instrument.
- Solar radiation sensor.

Among these, the cup, Gill and hotwire anemometers, the wind vane, the platinum wire thermometers, and the relative humidity and Lyman-alpha instruments were made by Sunshine Enterprises, Bangalore. The sonic anemometers were imported from USA (made by Applied Technologies, Colorado). The rain-gauges were from Dynalab, Pune, India and the solar radiation sensors were from LI-COR Inc., USA. A brief description of each of these sensors, together with their specifications, is given in the following paragraphs.

2.2a Cup anemometer: The 3-cup anemometer works on the principle that the rotational speed of the rotor due to differential drag on the cups is directly proportional to the wind speed perpendicular to the rotor axis (i.e. horizontal wind speed). The electronic conditioning unit is designed to accommodate wind speeds in the range 0–50 m/s. The sensor has a low starting threshold of 0.5 m/s, an accuracy of 1.5–2% full scale and a distance constant of less than a metre.

2.2b Wind vane: This consists of a vane that rotates on a vertical shaft to orient itself in equilibrium to the mean direction of the wind. The variation in resistance of a 10 K potentiometer coupled to the shaft is converted to voltage, which is then proportional to the wind direction in the range 0–360 degrees. This instrument has an accuracy of ± 3 degrees, a threshold of 0.5 m/s and a distance constant of 5 m.

2.2c Temperature: Mean and fluctuating components of both air and soil temperature are measured using RTDs. Standard RTDs are thin platinum wires of about $12.5 \mu\text{m}$ diameter and are usually encapsulated in ceramic. They have a known and constant coefficient of temperature. The change in resistance of the device with temperature is measured on a precision bridge and converted to a linearly varying dc voltage proportional to the temperature.

These RTDs have a response time of 3 s or better, and an accuracy of 0.2% of the full scale range of 0–50 degree centigrade. Their sensing elements (platinum wires), when used without encapsulation, measure the fluctuating component of the temperature with a response time of approximately 0.01 s. We have used both the types to measure the mean and the fluctuating components of temperature. These sensors are mounted on the tower boom with a self-aspirated radiation shield.

2.2d *Relative humidity*: Relative humidity is measured by humicap sensors made by Vaisala, Finland, with the characteristic that the capacitance of the sensor changes linearly with change in the relative humidity. The change in capacitance in turn varies the frequency of an oscillator, which is then converted to a varying voltage using a signal conditioning electronic circuit. The accuracy of the instrument is $\pm 2\%$ in the range 10–90% relative humidity, and the response time is 10 s for 5% to 90% change in the relative humidity. The sensing element is provided with a self-aspirated radiation shield.

2.2e *Gill anemometer*: This is a three-component wind speed measuring instrument, but employs polystyrene foam propellers moulded in the form of true helicoids. The propeller provides one revolution for each 30 cm of passing wind and responds only to that component of the wind which is parallel to the axis of rotation of the propeller. The number of revolutions per second of each propeller is used to generate an analog output proportional to the magnitude of the wind component along the respective axis, the direction of rotation being used to get the direction of the wind component.

The accuracy, threshold, distance constant and range are respectively $\pm 1\%$, nearly equal to zero, 0.6 m and ± 20 m/s.

2.2f *Sonic anemometer*: This is a three-axis sonic wind system from Applied Technologies, Inc., USA (model SWS-211/3KE). It uses a pair of ultrasonic transducers for each axis and operates on the principle of measuring the transit time difference between ultrasonic pulses travelling a known distance (15 cm in this case) along and against the wind component parallel to the axis. From these transit times, the u , v and w components of the wind velocity are computed. The streamwise component of velocity can be computed as $(u^2 + v^2)^{1/2}$. The virtual temperature of the air is also obtained from the transit times for the w axis. The basic sampling frequency in the system is 100 Hz, which is then brought down to 10 Hz by averaging over 10 samples. The instrument can be used as a stand-alone unit, and its serial output directly connected to any monitor screen with a serial interface. Analog signal outputs can be obtained with the help of a separate unit also supplied by the manufacturer. These can be recorded along with analog outputs from other instruments through a common data acquisition system, to be described in §2.3. The accuracy of this instrument is ± 0.05 m/s for velocity components and $\pm 1\%$ for temperature measurements. This is designed for a range of ± 20 m/s in horizontal directions (u, v) and ± 5 m/s in the vertical direction (w). Temperature range is -20 to $+50$ degree C.

2.2g *Hotwire anemometer*: The hotwire anemometer used is of constant temperature type, i.e. the temperature of the wire (sensing element) is kept constant by using a servo-amplifier and an electronic feedback. The wire used is usually of platinum or tungsten with a diameter of the order of $0.5 \mu\text{m}$ to $25 \mu\text{m}$ and length of the order of a few millimeters. It consists of three hot wires lying on the generators of a cone, two of them to measure the horizontal velocity components and the third to resolve the vertical velocity. They are designed to measure wind components up to 10 to 15 m/s and have a high frequency response of 10 kHz.

2.2h *Rain gauge*: The principle used in this instrument from Dynalab, Pune (Model RRR-100) is as follows. The rain water collected through 112.8 mm diameter collector

area is converted into approximately equal-sized drops in air medium and counted electronically, sensing by means of two electrodes. The resolution is 1/100 mm of rain. The output is an analog voltage equivalent of rain rate and is refreshed at a prefixed interval of time.

2.2i *Solar radiation*: The sensor is a silicon photovoltaic detector supplied by LI-COR Inc., USA for measuring the incoming solar radiation. The current produced by the sensor is converted to a voltage proportional to the incident solar radiation. The sensor has a sensitivity of 0.08 Am²/kW (typical), linearity of 1% up to 3 kW/m² and a response time of 10 μs.

2.3 Data acquisition system

The data acquisition system is a vital link in the tower instrumentation system. The voluminous amount of data acquired by the various sensors is made available only through this link which, apart from data logging, also provides the facility of on-line monitoring of various parameters for quick-look evaluation of the quality of the data. We used two logging systems in our experiment: a small compact data recorder placed at the tower base for recording mean data (based on Campbell's data logger), and an IBM-compatible PC-based system mainly for recording fast response sensor data using a pulse-code modulated (PCM) telemetry system. The conditioned outputs from the translators are given simultaneously (whenever required) to both the Campbell data logger and the fast data acquisition system with the help of a wiring panel. From figure 1 it may be noted that the sensors, the signal conditioners, the wiring panel, the data logger multiplexer and the cassette tape recorder form the slow data link. The fast data link departs after the wiring panel and goes through the PCM transmitter, the transmission link, the receiver card and the PC with storage devices such as hard disk and the cartridge tape recorder.

2.3a *The data logger*: This data logger (type 21X micrologger) from Campbell Scientific, Inc., USA, used to record data from all the slow response sensors, can take a maximum of 16 channels. To accommodate more channels, six of the 16 channels are multiplexed to take six additional channels each, providing in all 36 + 10 channels. The data logger has its own instruction set using which it can be programmed to sample each channel at a specified interval, average the data over a specified number of sample points, convert them into engineering units using specified multiplication factors and store them on audio cassette tapes. The display on the data logger facilitates on-line monitoring of atmospheric variables being recorded.

2.3b *Fast response data acquisition system*: This PC-based system intended to record data from fast response sensors was fully developed at the Centre for Atmospheric Sciences, IISc. It consists of a PCM telemetry system interfaced to the PC and a user-friendly data acquisition software which runs on the computer. Both PCM telemetry system and the data acquisition software are described in detail in separate reports (Rudra Kumar *et al* 1990a, b), so they are discussed only briefly here.

The PCM telemetry system consists of a transmitter, a transmission link and a receiver. Both transmitter and receiver are designed around the Intel 8 bit microprocessor

8085A. The block schematics of the transmitter and the receiver are shown respectively in figures 3 and 4.

■ *Transmitter:* The transmitter can be programmed through a DIP switch to take a specified number of analog channels in the range 1–64. It selects these channels one at a time using analog multiplexers (CD 4051), and encodes them in digital form using PCM with the help of an analog-to-digital converter (AD574) of 12 bit resolution. The converted digital data are then read into the microprocessor at regular intervals determined by the sampling rate, using a programmable input/output device (8155), and presented in a form acceptable to a parallel-to-serial converter (8251A) for serialisation. The serialised data are driven by a line driver (8T13) onto the transmission link. A 12-bit synchronising code is also sent in the beginning of each data set to demarcate successive data sets. The complete operation of the transmitter is governed by the software programmed into a 4 kbyte program memory (EPROM 2732A). The input parameters, namely number of channels (user selectable) and the frequency of transmission (set to 10 kHz using another DIP switch), are read into the system using another programmable input/output device (8255A). The timer section of 8155A is appropriately programmed to generate a 10 kHz square wave. Also the memory (256 bytes) of this IC chip is used as a scratch pad for intermediate storage and stack operations.

The transmitter is usually placed inside the instrumentation box at the tower. The transmission link is a twisted pair of wires carrying the serial output from the transmitter to the receiver in a computer room usually located at a distance of 100 to

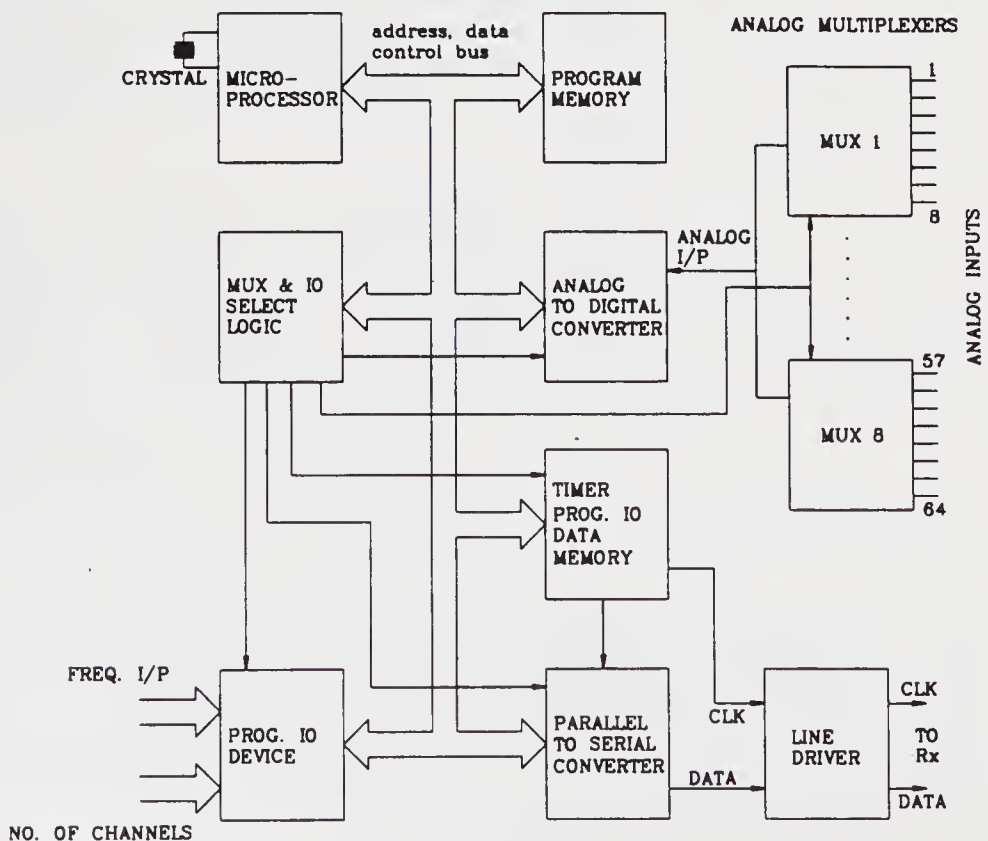


Figure 3. Block schematic of the PCM transmitter.

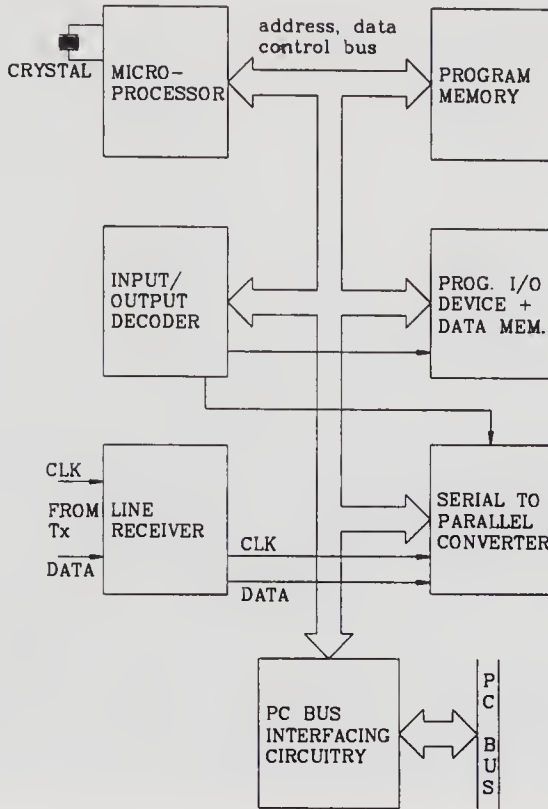


Figure 4. Block schematic of the PCM receiver.

200 m from the tower. The electronics at the transmitter is designed to drive the signal to a maximum of 200 m.

■ *Receiver:* The receiver is designed to sit directly on the PC peripheral bus as an add-on card. The first unit on this card is a line receiver (8T14) which receives the incoming serial data and presents it to the next stage of serial-to-parallel conversion. The clock used for the conversion is the same signal that is generated and used at the transmitter end, and is brought to the receiver through a line driver and a line receiver on a separate line. The on-board microprocessor (8085A) with software burnt into a 4 kbytes memory (EPROM 2732A) programs appropriately the ICs 8251A and 8155A. The 8251A converts the received serial data to parallel form and presents them to the microprocessor. The processor first detects the synchronising code and then onwards, interrupts the PC after every serial to parallel conversion of 12 bits, which is the resolution of the analog-to-digital converter used in the transmitter and corresponds to the output of one sensor. The PC, in its interrupt service routine, reads the data available at the output port of the 8155A and stores it for further processing. Here also, the memory available in the 8155A chip is used for intermediate storage and stack operations.

2.3c *Data acquisition software:* The data acquisition software which runs on the computer is user-friendly, menu-driven and flexible, and provides various convenient features. Variables like the number of channels, number of data samples to be averaged on each channel before storing, time interval to display on the screen (on-line) the mean values of a set of sensor outputs and the duration of the data acquisition can all be

programmed prior to the beginning of the acquisition experiment. The channel table, which gives details such as channel number, the sensor connected, units of measurement and multiplication factor, can be viewed and if necessary appropriately modified according to the actual physical connections of sensors on the tower. Date, start time and end time of acquisition are automatically stored using the real time clock facility of the PC. Any additional signatures like the experiment number and the synoptic conditions (which are useful during post-processing) around the tower may also be entered using the appropriate options of this menu-driven data acquisition software.

The option of automatic recording (unattended data acquisition) is also provided, using which the data can be recorded in the absence of the experimentalist. This option is particularly useful to record data during night. When this is exercised the additional input of duration between successive experiments is to be entered. The data acquisition software finally stores the data on the PC hard disc in binary form; this is necessary because the higher sampling rate needs large memory, and binary data converted to engineering units requires larger area for storage. However the facility of on-line monitoring of a set of variables (6 channels at a time) in engineering units on the screen of the computer provides the check that is necessary in this kind of experiment. The data stored on the hard disc can be transferred regularly to cartridge tapes through the cartridge tape drive (TVSE make TD 1060i) connected to the PC.

3. Sites

Before going into the details of the observations made at all the four tower stations, a brief look around the tower platforms is given below.

The towers in Kharagpur, Varanasi and Jodhpur are located in farm fields. From the point of view of a clean fetch Kharagpur is perhaps the best site among all, as it has a long stretch of open and flat surface towards the south (nearly 1 km), which is the mean direction of prevailing wind during the season. Figure 5 shows a picture of terrain and fetch at this site. The data acquisition computer is placed in a small room of about 3 m height situated at a distance of about 150 m north-east from the tower.

The Varanasi tower also has an open field towards the south and a small building of 3 m height, situated at a distance of about 15 m towards the west of the tower, which houses the data acquisition computer. There is a wind mill (8 m high) towards the south-west at a distance of about 25 m. Figure 6 shows a picture of this site.

At the Jodhpur tower (figure 7) we see fairly good open space around the tower with a few small plants of less than 0.5 m height grown for research purposes towards the west and north-west. A few, small bush trees of 1 to 2 m height, present closer to the tower during the installation (seen in the picture), were cut before the experiment started. A 6 m-high building is located at about 100 m from the tower towards the west and the data acquisition computer is placed inside this building.

At the Delhi tower, the nearest structure, located towards the east at a distance of about 15 m, is a small room of 3 m height, in which the computer and the data logger are placed. Raman *et al* (1990) have described this site with a picture of the tower (when it was 20 m high).

The pictures presented in this section are taken from the album of pictures photographed during the installation of tower platforms by the IISc group at Kharagpur (1988), Varanasi and Jodhpur (1989–90).



Figure 5. A picture of the Kharagpur site showing fetch and terrain.



Figure 6. Terrain and fetch at the Varanasi tower.

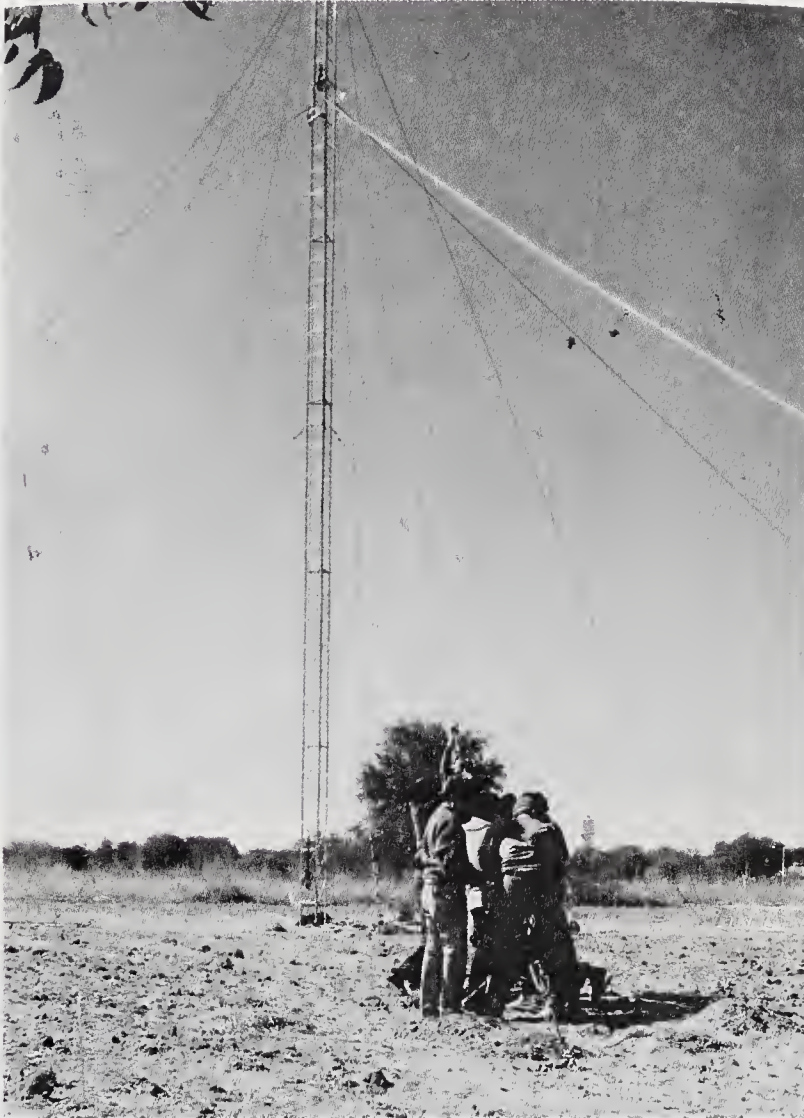


Figure 7. A picture of the Jodhpur site during tower erection.

4. The experiment

Preparations began in 1987 with the selection of suitable sites at Kharagpur, Varanasi and Jodhpur for the installation of the towers. The hardware and software for the PC-based data acquisition was designed and developed at the CAS, IISc. In the summer of 1988 a 30 m tower was installed in the air field at IISc and a preliminary exercise was carried out. The tower was later transported to Kharagpur.

4.1 Pilot experiment at Kharagpur

The Kharagpur tower was installed in the agricultural research field on the IIT Kharagpur campus in the last week of July 1988. The pilot experiment was carried out in 1989 for a week (1st to 7th July) mainly to test all the instruments and the data acquisition system. The observations made during this experiment have been reported

by Prabhu *et al* (1990). This experiment was carried out amidst severe thunderstorm activity. There were a few break-downs of the data acquisition system due to some electronic component failures, suspected to have been caused by induced electromagnetic fields during lightning. Also, there was a frequent problem in the synchronising logic of the receiver, which forced a redesign of the PCM telemetry system (Rudra Kumar *et al* 1990b). The pilot experiment proved to be a very useful exercise as invaluable operational experience was gained during highly-disturbed meteorological conditions and enabled the Instrumentation Group at CAS, IISc to incorporate necessary protection against the lightning hazard in the instrumentation system.

4.2 Main phase observations

Installation of tower platforms at Varanasi and Jodhpur was completed by the end of January 1990. The full scale surface layer observations for MONTBLEX were conducted at all four places from the last week of May 1990 to the middle of September 1990. This duration (approximately three and a half months) was chosen to include pre-monsoon, as well as active and break periods.

4.2a Sensor configuration on the tower: Figure 8 shows the tower-sensor configuration at all four sites. It is seen that in general there are 6 levels of cup anemometers and wind vanes, 4 levels of slow response temperature sensors, 3 or 4 levels of relative humidity sensors, 2 levels of fast response temperature sensors, one level of sonic, Gill and hotwire anemometers, one level of Lyman-alpha instrument, 3 levels of soil temperature sensors

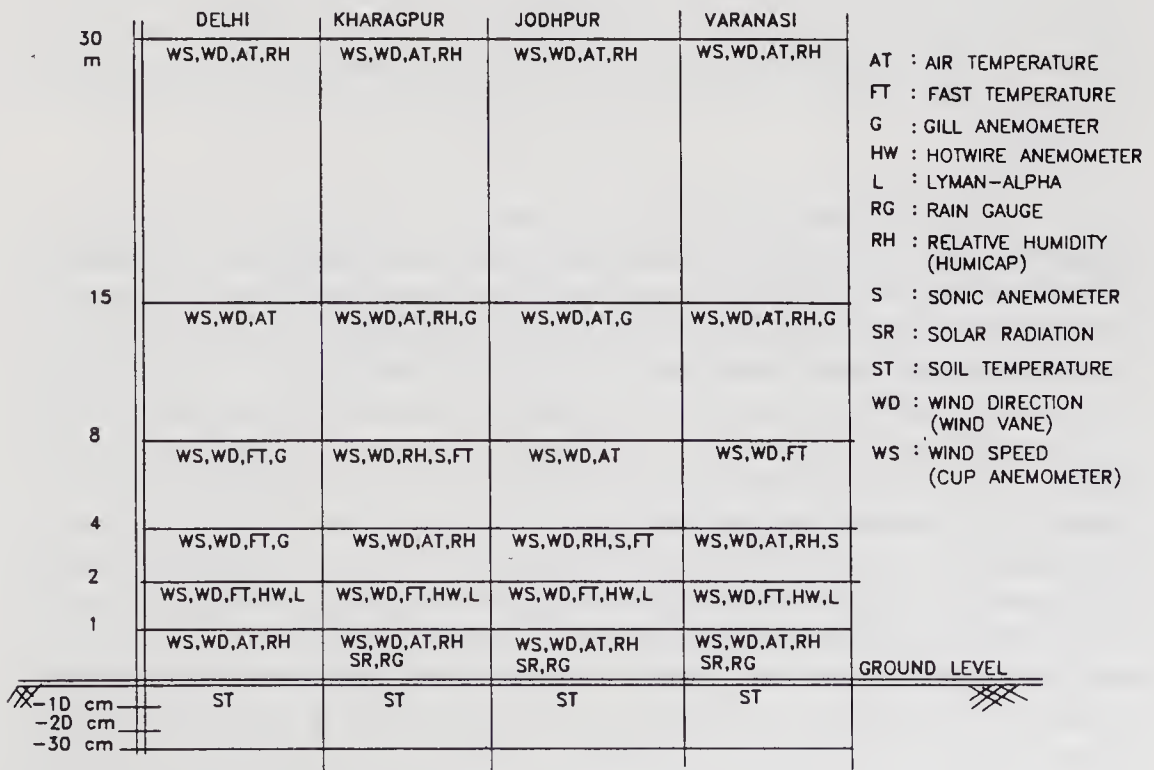


Figure 8. Tower-sensor configuration at the four field stations.

and one each of a rain gauge and solar radiation measuring instrument. At the Delhi tower there is no sonic anemometer, rain gauge or solar radiation instrument. Also it may be seen that there is a small variation in the height at which the different sensors are on the tower among the four stations.

4.2b Data acquisition: The slow response sensors connected to the Campbell data logger were sampled at a frequency of 1 Hz and averaged for 3 minutes before being finally stored on audio cassette tapes. Occasionally 1 minute averaging has also been selected by the local data acquisition personnel. Data have been acquired round the clock on this data logger. Both slow and fast sensors were connected to the PCM telemetry system. Only 32 channels were used on the PCM transmitter with a known (constant) value of DC voltage connected to channel 1 as a quantitative check on the incoming data through the complete link of the PC based PCM telemetry system. Data have been recorded on this logging system in stretches usually of 15 minutes (sometimes 10 minutes when the back-up facility was not available) every hour during Intensive Observational Periods (IOPs), and every three hours at other times. The acquisition sampling rate was 8.41 Hz. This number arises from the following parameters: transmission clock rate of 10 kHz, 33 channels (including one channel for the sync. word) of 12 bit resolution, and averaging done over 3 data samples on each channel. At the Delhi tower there was no PCM telemetry system; instead, there was a 16 channel acquisition card (from Keonics Ltd., Bangalore) on the PC, to which all the fast response and a few slow response sensor outputs were connected.

The IOPs were declared from time to time, depending on the importance of special events during the monsoon, by the MONTBLEX operation control centre (MOCC) who were closely watching the movements of the monsoon. The personnel engaged in the acquisition were advised to enter the synoptic conditions around the tower with the option provided in the menu-driven data acquisition software before acquisition of each data set. The total data files recorded on the fast response data acquisition system with the synoptic and other details have been compiled in a report by Rudra Kumar *et al* (1991a).

4.2c A glimpse of field experience: Simultaneous observations at different places for a duration of three and a half months was quite a challenging task. All the earlier exercises including the pilot experiment were of much shorter duration and confined to one station. Some of the difficulties which were actually faced by the observational team were not anticipated before the experiment. At each of the tower stations a group of trained personnel was engaged in acquiring the data according to the instructions from the core team. There was one expert team of instrumentation engineers (SRK and SA were among them) travelling to and fro from east (Kharagpur) to north-west (Jodhpur) and attending to faulty instruments and break-downs (if any) in the data acquisition system. There were a few break-downs in the data acquisition system at Kharagpur and Varanasi mainly due to the failure of the PCs at these places. The only break-down at Jodhpur was due to an unusual spell of rain in the first week of July when the tower and the instrument box were in water (max of about 10 cm) for 2 to 3 days. Even at Varanasi, the instrument box had to be lifted up due to water at the site. The time required to set right break-downs at any place depended chiefly on the current location of the expert team along the network of the tower stations! The gaps in both the fast and slow data were mainly due to the delay in the expert team reaching the

required field station. Nevertheless, the data acquired at each of the tower stations covers varied stability conditions and all special events of the monsoon.

4.2d *Calibration at site:* Mean temperature and relative humidity at all levels were frequently checked against psychrometer readings and the difference was recorded in the log book. Also wind vanes were aligned to the true North once in fifteen days. The sonic anemometer was calibrated as instructed by the manufacturer (using zero-wind tubes) whenever there was a change in the transducers. Hot wire probes were calibrated at the tower using portable wind tunnels.

5. Post-processing and final format of the data

The data files from all the tower stations were brought to Bangalore for editing and post-processing. The fast data recorded on the PCM telemetry system (referred to as the fast data files), which were in binary form after acquisition on site, were converted to the respective engineering units and stored in ASCII format. Each fast data file was then transferred to a separate directory in which all the variables are stored as separate files. The name of the directory contains codes for the field station, month, date and time of the day as given below.

Data file : SMDDTTTT

where S : Station code

(K = Kharagpur

V = Varanasi

J = Jodhpur

D = Delhi)

M : Month number

DD : Date

TTTT : Start time of acquisition.

For example, the J6150900 directory (or the binary file) represents the data recorded on June 15th at Jodhpur, with the acquisition started at 0900 hrs. The names of the files stored under each of these directories give the variables with a level code attached to them (1, 2, 3, etc.), indicating the level at which the corresponding sensor was mounted on the tower. There are about 900 fast data files available for Jodhpur, 450 for Delhi, 350 for Varanasi and 300 for Kharagpur stored in about 65 cartridge tapes of 40 Mbytes capacity.

During the process of conversion of fast data files from binary form to the respective engineering units, the time trace of all the variables and the comparative plots of outputs from different sensors measuring the same variable have been visually inspected. Any discrepancies like presence of spikes, signal drop-outs and offset errors, or any other unusual behaviour seen in any variable have been separately reported (Rudra Kumar *et al* 1991b). Various quality checks have been made on randomly picked data sets to validate the data, and are reported in detail in a separate report (Rudra Kumar and Prabhu 1991).

For the mean variables recorded on the Campbell data logger (referred to as slow data), all the valid data corresponding to a channel, on all available days and times (for

the whole experiment), are concatenated and stored in a separate file. The name of the file contains the station information, the variable and the level at which the sensor is mounted. For sample, Temp 1. kgp represents temperature data at level 1 from Kharagpur (.bhu, .del and .jdp have been used respectively for Varanasi, Delhi and Jodhpur). The mean variables are stored in 4 cartridge tapes of 40 Mbytes capacity.

6. Quality analysis

Here, we present the important results from the quality assessment exercise using various checks. A detailed technical report has been made on the assessment of quality of tower data from MONTBLEX-90 (Rudra Kumar and Prabhu 1991). The data have been selected randomly and the details such as file names and variables are printed on the figures themselves.

The first obvious check is to visually see the time series plot of the data to find out if there are any spikes or signal drop-outs. When there is more than one sensor measuring the same variable it is a good check to plot them to the same scale and check how they compare. Profile plots for mean quantities are best to see if there are any kinks indicating faulty or offset drifted sensors. Then from computed values like roughness height from the windspeed profile, stability parameters and their diurnal variation etc., the data quality may be ascertained. This distribution of data (especially the turbulence quantities) over their mean gives another check of the quality. The energy spectrum of the turbulence quantities may be seen to look for the slope of the energy decay in the inertial sub-range.

6.1 *Visual inspection of the time series data*

Time traces from various sensors are plotted to look for spikes and signal drop-outs. While plotting data recorded in the fast data files an averaging time of 1 s is used, i.e. each point on the plot is an average over one second.

Examples:

- Figure 9 shows time traces of cup anemometer data at all 6 levels plotted simultaneously with the origin of the successive levels shifted on the y-axis by a fixed value to look at any coherent structures that might be present over the height of the tower.
- Figures 10 and 11 show examples of traces of all three wind velocity components from sonic and Gill anemometers respectively.
- Figures 12a and 12b show time series plots of mean values of temperature and relative humidity (averaged for 3 minutes) at 30 m (level 6) for one complete day at Kharagpur.

As illustrated by figure 9, cup data are spike-free. Incidentally we clearly discern a coherent structure over the height of the tower. The wind components from sonic and Gill anemometers (figures 10, 11) are also seen to be spike-free, but the Gill w component (at all stations) is often found to have one or two spikes in 10/15 minutes stretch of data (Rudra Kumar and Prabhu 1991). The w component is much smaller than the u and v components, and has a mean close to zero. The strong correlation between temperature and relative humidity variations seen in figure 12 suggests that the

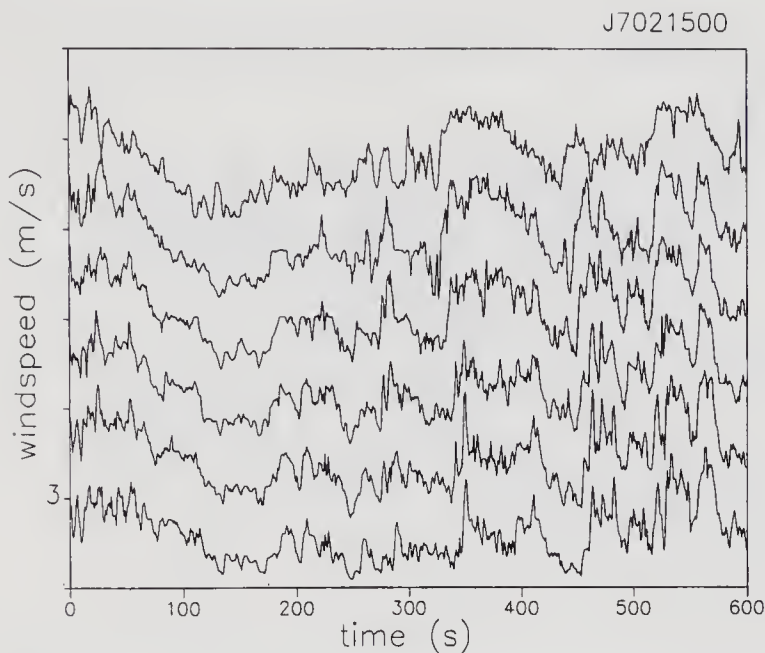


Figure 9. Time trace of cup anemometer data at all 6 levels.

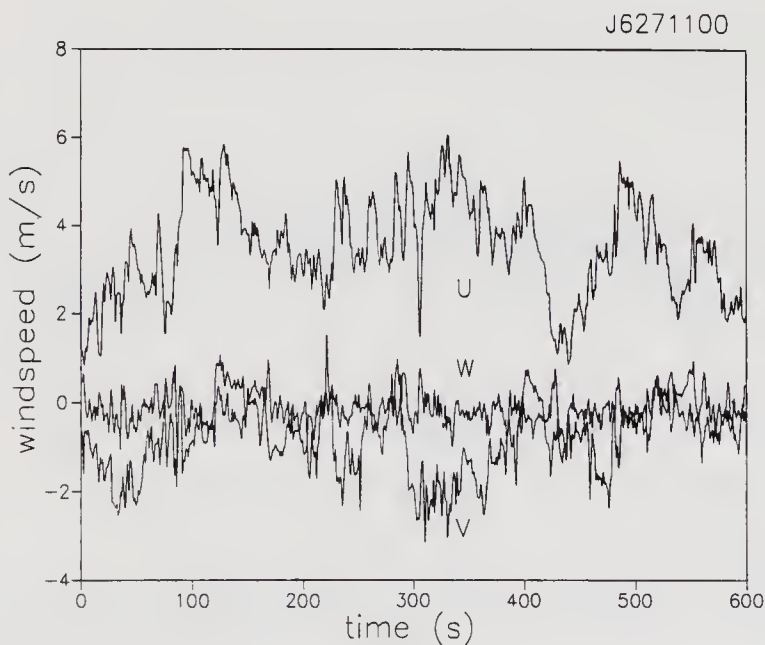


Figure 10. Time series plot of velocity components from a sonic anemometer.

different sensors and the instrumentation system are effectively recording true physical processes in the atmosphere.

6.2 Comparison of data from different sensors measuring the same physical variable

Figures 13 and 14 show time traces of the horizontal velocity $\sqrt{(u^2 + v^2)}$ computed

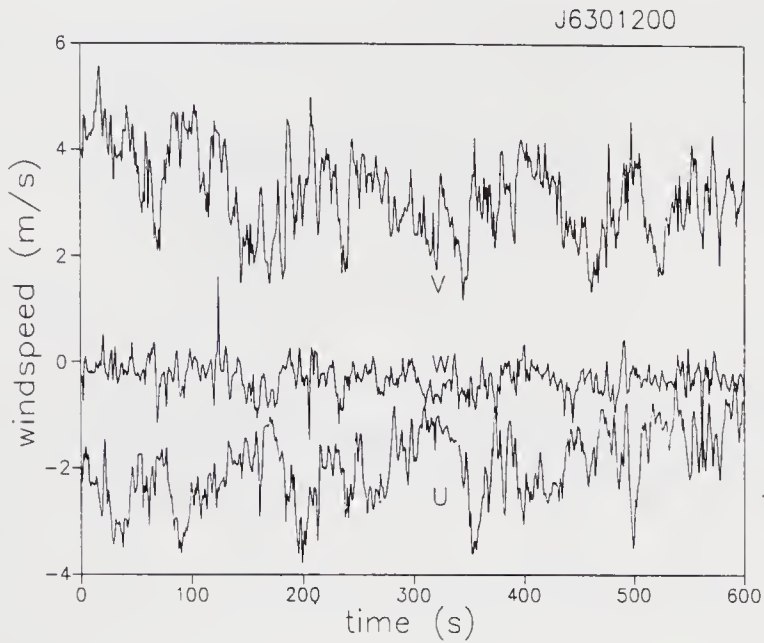


Figure 11. Time series plot of velocity components from a Gill anemometer.

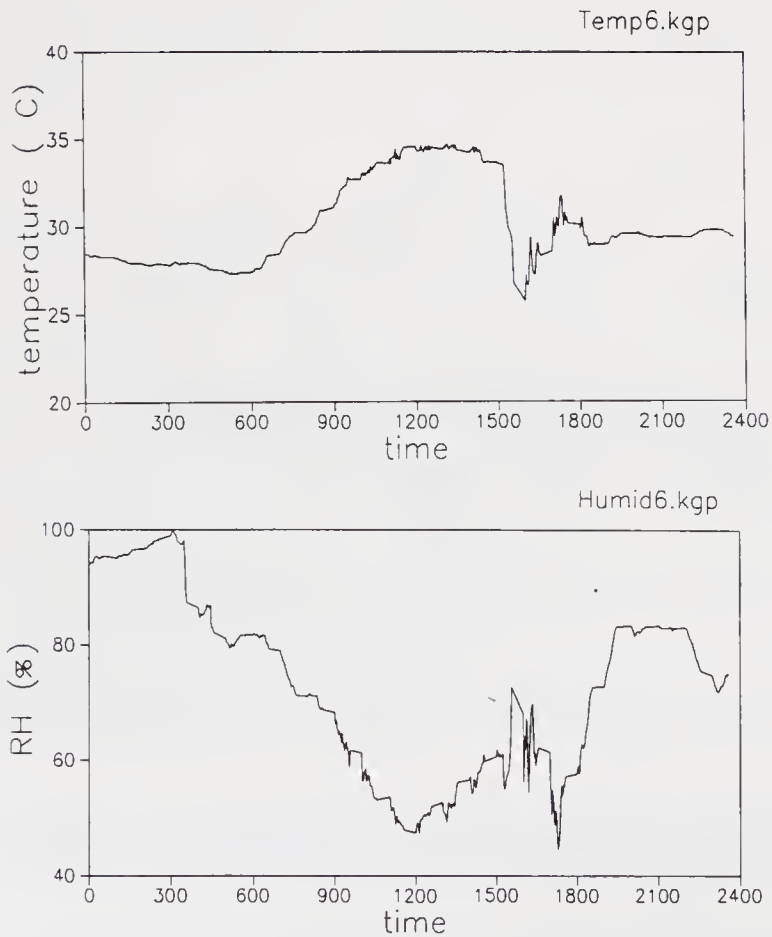


Figure 12. Three-minute averaged temperature and relative humidity data plot for one full day.

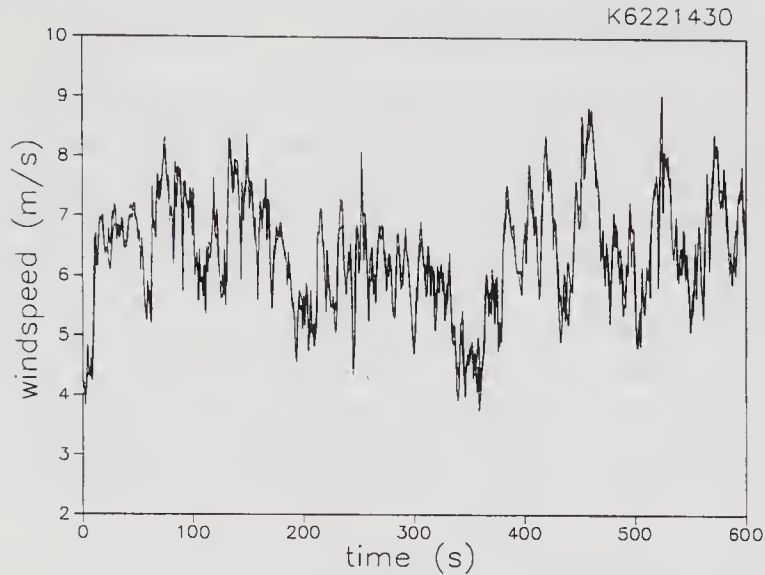


Figure 13. Simultaneous plot of horizontal windspeed from cup and sonic anemometers mounted at the same level on the tower.

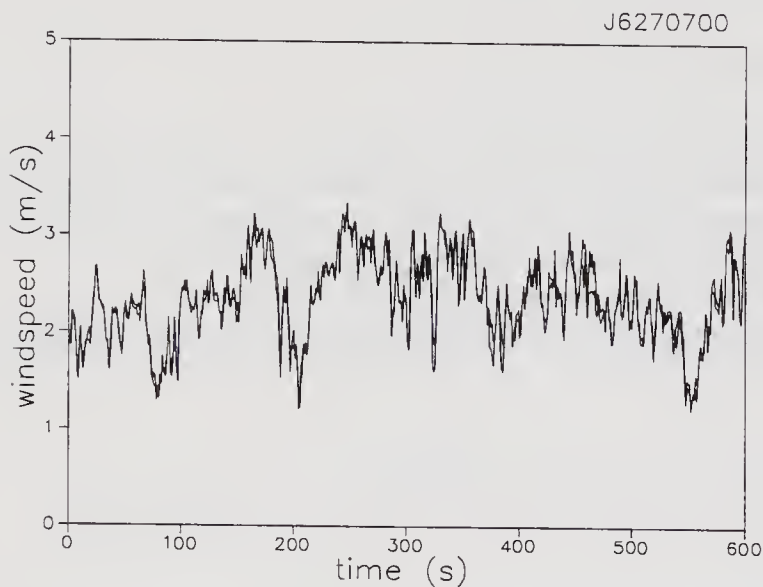


Figure 14. Simultaneous plot of horizontal windspeed from cup and Gill anemometers mounted at the same level on the tower.

from the u and v components recorded by the sonic and Gill anemometers, plotted over the wind speed from the cup anemometers at the respective levels on the tower.

Considering the different designs, response times and calibration procedures underlying the different sensors, the comparison made above between the sonic and Gill anemometer data with that of the cup anemometer must be considered very good. Such agreement between different sensors measuring the same physical variable (wind in the above case) proves quantitatively that these instruments are quite accurate and that the data recorded represent closely the true value of the wind in the atmosphere.

6.3 10/15 minute averages of time series data

From the fast data files, the data are averaged over the complete duration (10 or 15 minutes) and plotted against the height to see if there are any kinks in the vertical profile. By this method we can obtain indications of a faulty sensor or drift in calibration at one or more levels. Here, the data from the cup anemometer and the temperature sensors (which are available at all the levels and stored in the fast data file) have been considered.

Figure 15 shows a temperature profile (solid line) without the data from the levels where fast temperature sensors are mounted (2 m and 4 m in this case of Jodhpur). These points are also indicated in the figure and the discrepancy is reported as due to an offset error in the mean value of the fast temperature sensor (Rudra Kumar and Prabhu 1991). Figure 16 shows two wind profiles using the cup anemometer data.

From the above profile plots it is seen that care should be taken in obtaining temperature profiles. Fast temperature sensors may have an offset error in their mean level and therefore should be used with caution; they may however be used with confidence to get fluctuations. Cup data again show good reliability by the smooth structure exhibited in the vertical profile.

6.4 Mean wind profiles and calculation of z_0

Mean wind profiles when the stability conditions are neutral or near-neutral are plotted against height on log-linear scales and a least-squares straight line is fitted. The value of z_0 (roughness height) is obtained by extrapolating the profile linearly to zero wind and should typically be a few centimeters in open areas.

Figure 17 shows two cases (near-neutral), one each from Kharagpur and Jodhpur respectively. The value of z_0 (2.5 cm, in both cases) is of the same order as widely quoted

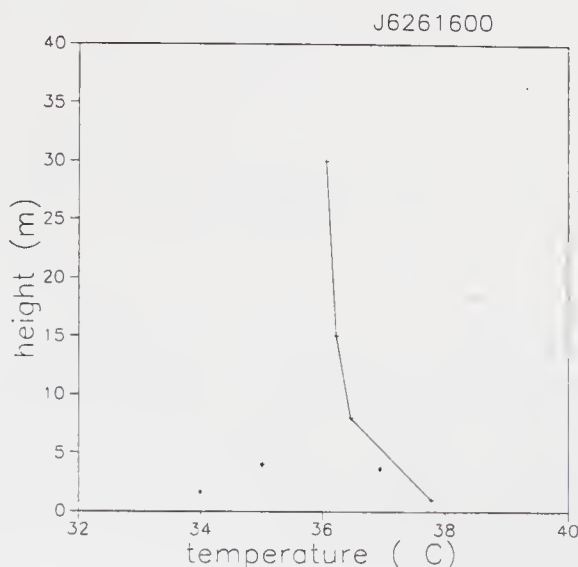


Figure 15. A temperature profile using 10-minute averaged data from slow response sensors. Points not connected at 2 m and 4 m correspond to fast response sensors.

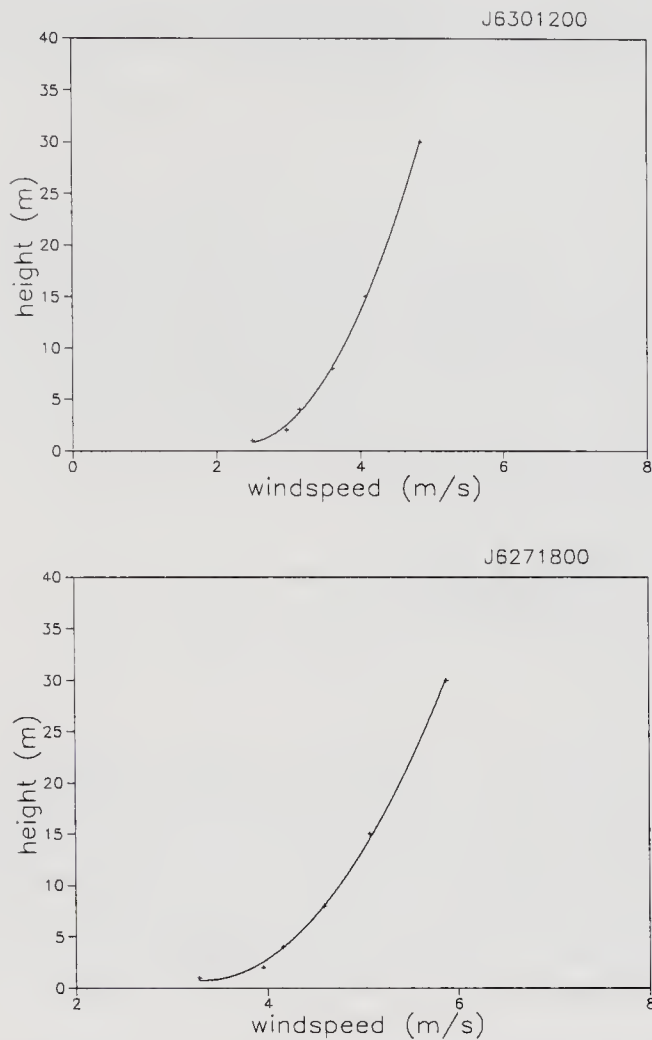


Figure 16. Typical wind profiles constructed from 10-minute averaged cup anemometer data.

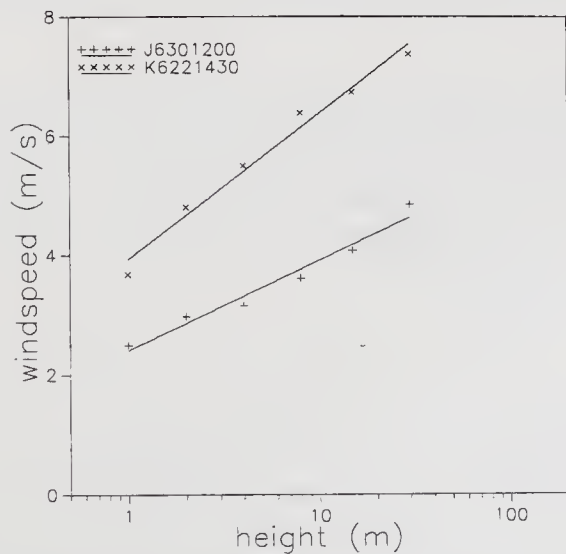


Figure 17. Log-linear plot of wind profile data (two near-neutral cases).

for open areas (Panofsky and Dutton 1984). Both Jodhpur and Kharagpur have fairly good open space around the observational platform.

6.5 Diurnal variation of various parameters

We show here data from Jodhpur for one full day during an IOP (observation every hour), to examine the diurnal variation of various stability and statistical parameters. The data cover the time period from 0600 hours on 26 June to 0600 hours on 27 June 1990 without two data sets (1300 hrs data on 26th has not been recorded possibly due to power failure and 0400 hrs data on 27th is not considered as it was found unreliable). The following parameters are determined and plotted in figures 18 to 20:

- Gradient Richardson number – Ri (1–15 m).
- Gradient Richardson number – Ri (1–30 m).
- Flux Richardson number – Rf (at 4 m).
- Ratio of height to Monin-Obukhov length – z/L .
- Ratio of std. dev. of vertical velocity (w) to friction velocity – σ_w/u_* .
- Correlation coefficient – R_{uw} .
- Correlation coefficient – R_{wT} .

A clear diurnal variation can be seen in various stability parameters like Ri, Rf and z/L . As reported from earlier investigations using data from the Kansas experiment (Haugen *et al* 1971), here also we notice that σ_w/u_* stays around 1.3 for near neutral conditions and increases for strong unstable conditions. R_{uw} from the expected value of around -0.3 for near neutral conditions drops to lower values during strong unstable conditions and R_{wT} varies from -0.4 for stable conditions to 0.7 for unstable conditions, roughly the same range as reported by Haugen *et al* (1971).

6.6 Probability density of data from various sensors

The probability density of some of the variables was also examined to check the distribution pattern. Figure 21 shows the distribution of u and w components from a sonic anemometer.

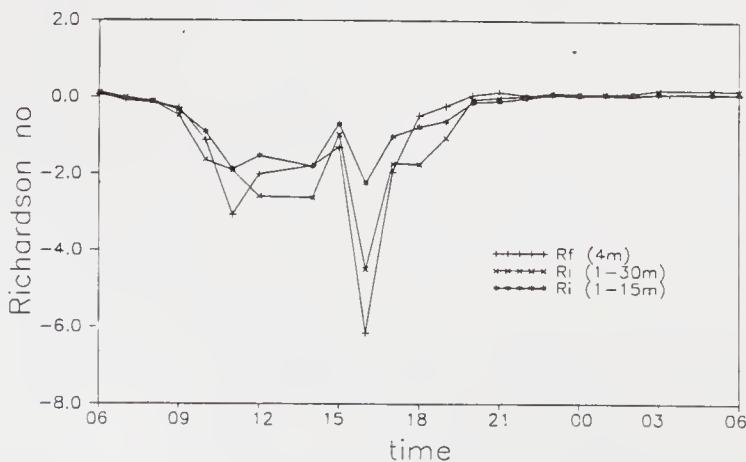


Figure 18. Diurnal variation of Ri(1–15 m), Ri(1–30 m) and Rf computed at 4 m.

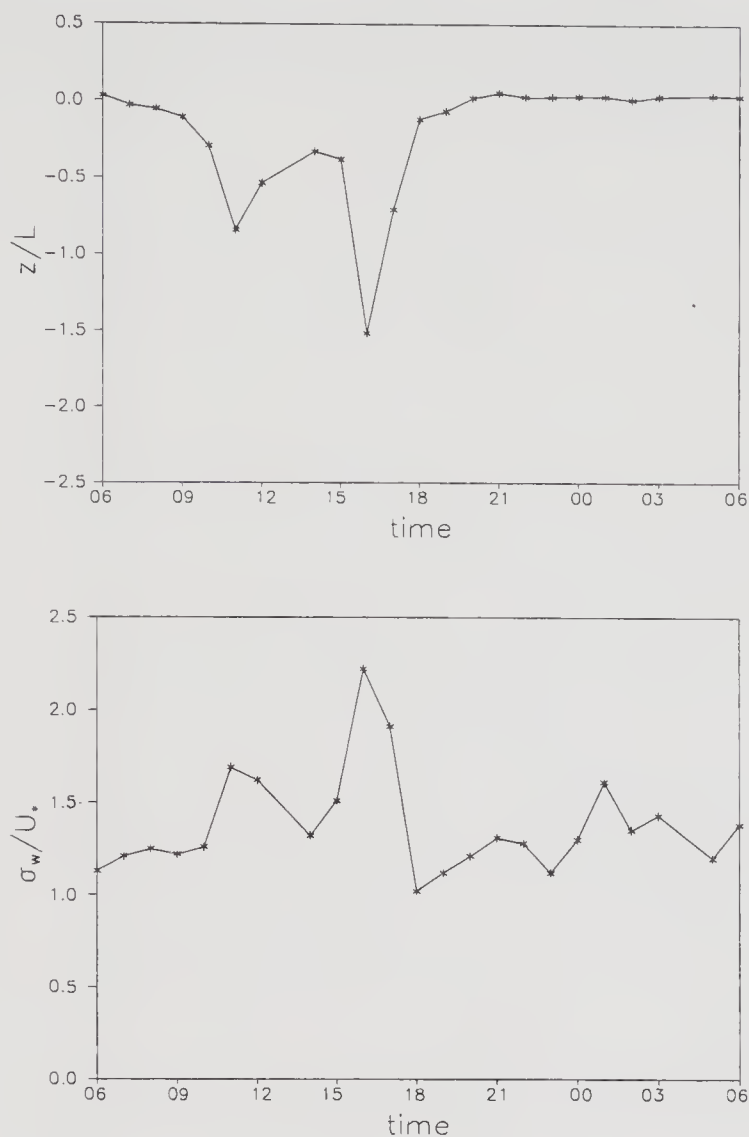


Figure 19. Diurnal variation of z/L and σ_w/u_* .

It is seen that the data points lie mostly within a $\pm 3\sigma$ band around the mean (central line). Along with the distribution of the actual data (shown by symbols), the Gaussian function with the same standard deviation (shown by the full curve) is also plotted in each of the figures. It is seen that the distribution of the data closely follows the standard Gaussian over the range of observed values.

6.7 Power spectral density

It is well known that the spectrum of velocity, temperature and humidity fluctuations in the atmosphere decay with respect to the frequency with the Kolmogorov slope of $-5/3$ in the inertial sub-range. To check this we have looked at u and T components from the fast response sonic anemometer, and humicap data whose response time is greater than one second. These are respectively shown in (a), (b) and (c) of figure 22.

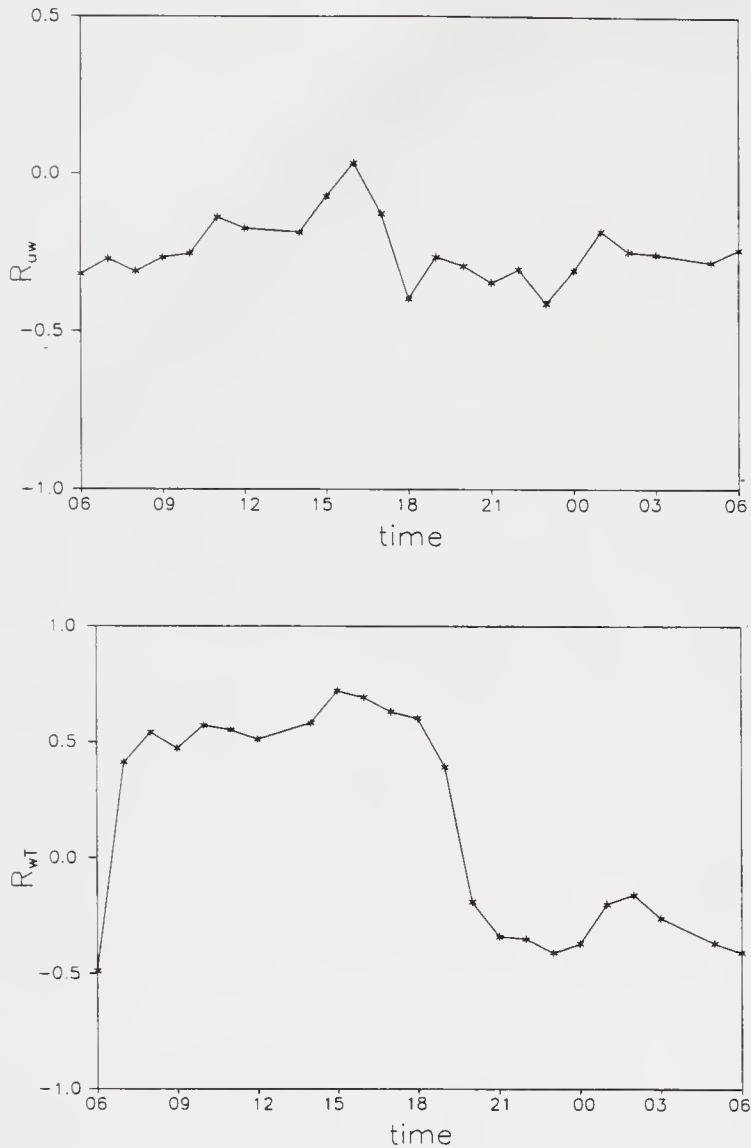


Figure 20. Diurnal variation of R_{uw} and R_{wT} .

The line drawn in each figure gives the Kolmogorov slope of $-5/3$. Spectra of data from the faster response sonic anemometer (figure 22a, b) show the Kolmogorov slope at higher frequencies (up to 1 Hz and beyond). However, the spectra of data from the relatively slower sensor such as the humicap (figure 22c) show approximately the Kolmogorov slope below 1 Hz, and deviate at higher frequencies (above 1 Hz), presumably due to inadequate high frequency response and noise.

7. Conclusions

A typical tower instrumentation system which integrates both indigenous and imported sensors with an in-house data acquisition system has been described. The tower, the Campbell data logger, the PCM telemetry system and the PC/XT with the cartridge tape drive form the main basis of the instrumentation system. The

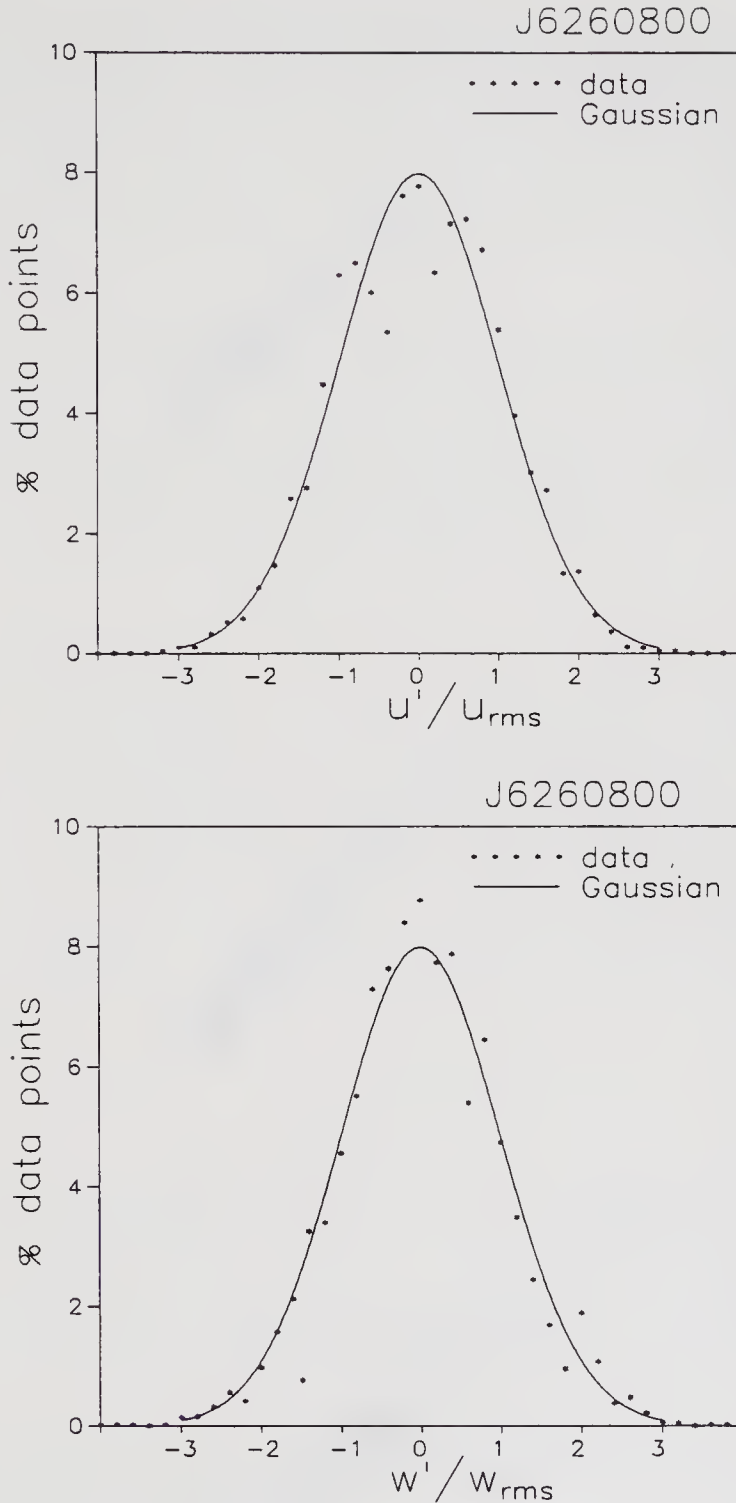


Figure 21. Distribution of u and w data from a sonic anemometer.

system has been configured in such a way that a large number of physical parameter sensors can be used in the experiment. The user-interactive software written on the PC as well as on the Campbell data logger enables the user to designate and identify the sensor and provides the option of entering the appropriate calibrations for these sensors.

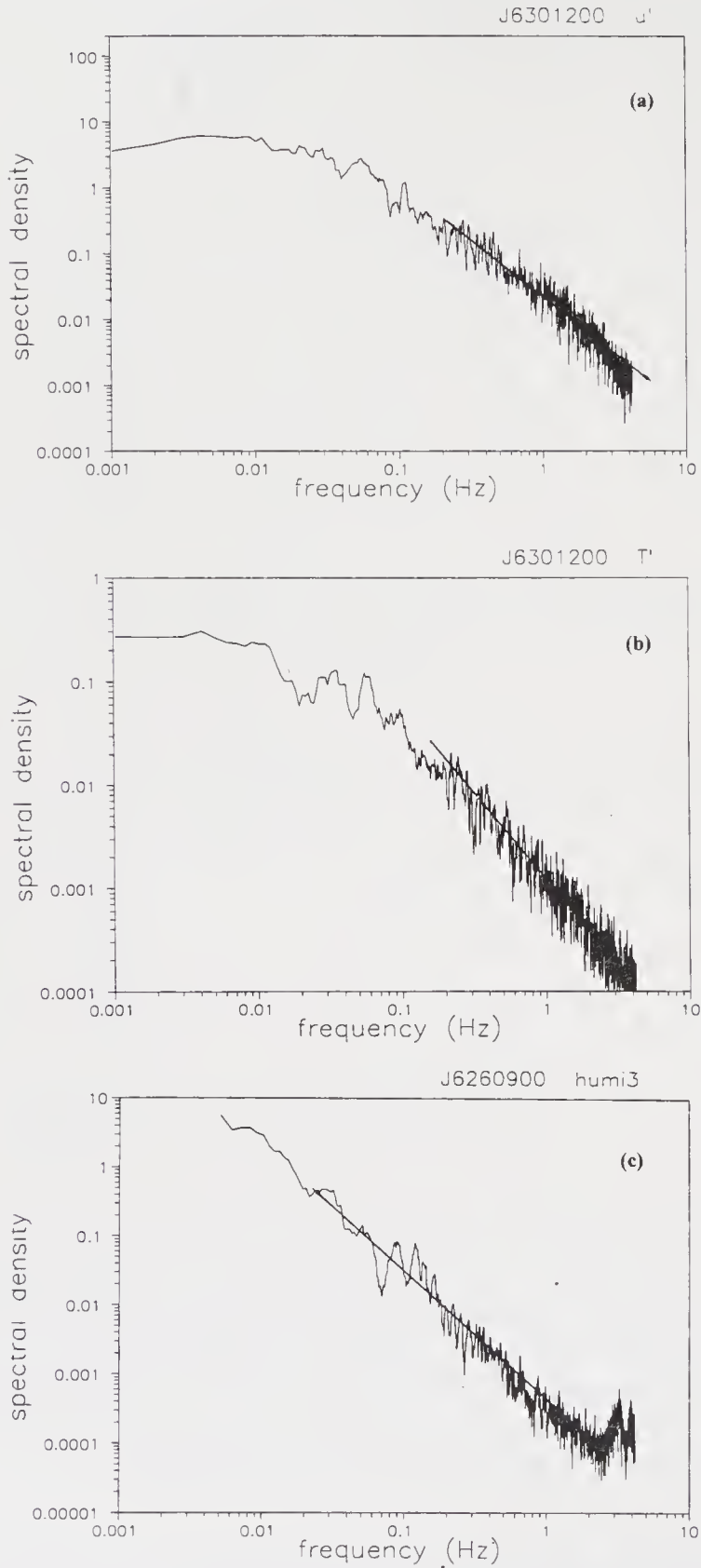


Figure 22. Power spectral density plot of (a) u component and (b) T data from a sonic anemometer and (c) data from a humicap sensor.

Tower observations carried out in the different convective zones of the monsoon trough during 1990 have resulted in the acquisition of a valuable set of atmospheric data under varied stability conditions. The instrumentation system, most of which was built indigenously (including the in-house built data acquisition system), functioned well in probing the atmospheric surface layer using 30 m tower platforms. The experience gained from this massive field experiment has been valuable. On the whole, observations at Jodhpur were the most successful in terms of number of good sets of continuous data.

A series of seven checks was made in order to verify the quality and validate the tower data from the field experiment carried out in the surface layer during MONTBLEX (1990). This quality analysis has established both qualitatively and quantitatively that the instrumentation system has recorded various physical variables in the surface layer quite accurately and has revealed the strong potential for further detailed analysis to understand the various aspects of boundary layer processes.

Acknowledgements

We thank all our colleagues at the Centre for Atmospheric Sciences, IISc for their excellent contributions during the observational programme. We thank all the scientists and technicians from other participant institutes who rendered help during the experiment. We also thank the host institutes for providing all the necessary support.

We thank Prof. R Narasimha for his continuous encouragement and guidance throughout the experiment. We thank Dr Kusuma Rao, Dr Narahari Rao and Dr Kailas for their active participation and useful suggestions. We also thank Mr. H P Srinivasan for his contribution in the development of software programs for the data analysis.

References

- Driedonks A G M, Van Dop M and Kohsiek W H 1978 Meteorological observations on the 213 m mast at Cabauw, in the Netherlands; *Prepr. 4th AMS Symp. Meteor. Obs. Instr. (Denver)* 41–46
- Haugen D A, Kaimal J C and Bradley E F 1971 An experimental study of Reynolds stress and heat flux in the atmospheric surface layer; *Q. J. R. Meteorol. Soc.* **97** 168–180
- Kaimal J C and Gaynor J E 1983 Boulder Atmospheric Observatory; *J. Appl. Meteorol.* **22** 863–880
- Kaimal J C and Wyngaard J C 1990 The Kansas and Minnesota experiments; *Boundary-Layer Meteorol.* **50** 31–47
- Kaimal J C 1990 Basic tests for checking validity of field data. WPL Application note no. 5.
- Narasimha R, Prabhu A, Rao K N, Adiga B S and Ameenulla S 1981 Project MOBLE – A monsoon boundary layer experiment at Balasore, July 1979. Report 81 FM 1. Department of Aerospace Engineering, IISc, Bangalore
- Panofsky H A and Dutton J A 1984 *Atmospheric turbulence* (New York: Wiley Inter-Science Publications)
- Prabhu A, Rao K N, Kusuma G R, Kailas S V, Rudra Kumar S, Ameenulla S and Srinivasan H P 1990 The MONTBLEX pilot experiment. Report 90 AS 2; Centre for Atmospheric Sciences, IISc., Bangalore, India
- Raman S, Templeman B, Templeman S, Murthy A B, Singh M P, Agarwal P, Nigam S, Ameenulla S and Prabhu A 1990 Structure of the Indian southwesterly pre-monsoon and monsoon boundary layer observations and numerical simulation; *Atmos. Environ.* **A24** 723–734
- Rudra Kumar S, Sahu B R and Prabhu A 1990a The data acquisition software for the PC-based PCM telemetry system. Report 90 MD 4; Centre for Atmospheric Sciences, IISc, Bangalore, India
- Rudra Kumar S, Srinivasan H P, Ameenulla S and Prabhu A 1990b PCM telemetry system. Report 90 MD 5; Centre for Atmospheric Sciences, IISc. Bangalore, India

- Rudra Kumar S, Srinivasan H P, Srikrishna R, Ameenulla S and Prabhu A 1991a Available tower data from MONTBLEX-90. Report 91 MD 1; Centre for Atmospheric Sciences, IISc, Bangalore, India.
- Rudra Kumar S, Srinivasan H P, Satyadev H N, Ameenulla S and Prabhu A 1991b Surface layer data from MONTBLEX-90. Report 91 MD 2; Centre for Atmospheric Sciences, IISc, Bangalore, India
- Rudra Kumar S and Prabhu A 1991 Quality assessment of the tower data from MONTBLEX-90. Report 91 MD 3; Centre for Atmospheric Sciences, IISc, Bangalore, India

Estimation of surface temperature from MONTBLEX data

K NARAHARI RAO

Centre for Atmospheric Sciences, Indian Institute of Science, Bangalore 560012, India

Abstract. It is observed that the daily mean temperature of the soil is linear with depth and the variation of the temperature is sinusoidal with a period of a day. Based on these observations the one-dimensional heat conduction equation for the soil can be solved which gives the amplitude and phase variation of the temperature wave with depth. Given the temperature data at three levels below the surface, the amplitude and phase variation and hence the surface temperature variation over the day are estimated. The daily mean temperature of the surface is estimated from linear extrapolation of the daily means at the three levels below the surface. Estimated values of soil thermal diffusivity show a substantial change after sudden and heavy rains.

Keywords. Soil and surface temperature; diurnal variation; phase and amplitude of temperature waves; thermal diffusivity.

1. Introduction

Because of the importance of the surface layer in determining the eddy fluxes of mass, momentum and energy, the Monsoon Trough Boundary Layer Experiment (MONTBLEX) conducted during the monsoon of 1990 gave particular importance to the surface layer measurements. The locations chosen for such observations lie along the trough, and are:

- IIT Kharagpur (KGP),
- Banaras Hindu University at Varanasi (BHU),
- IIT Delhi (DEL), and
- CAZRI at Jodhpur (JDP).

30 m masts were erected at each site with the required instrumentation at six levels (1, 2, 4, 8, 15 and 30 m) above ground level to measure vertical and horizontal velocities, wind direction, temperature and humidity (Rudra Kumar *et al* 1991).

The soil temperature was measured at three levels (0.1, 0.2 and 0.3 m) below the ground using resistance thermometers of 12.5 microns diameter platinum wire encapsulated in ceramic. These were sampled at 1 Hz, averaged over one minute or three minutes and stored on audio cassette tape through a Campbell data logger. For a proper analysis of these data, it is important to have precise information about surface parameters such as roughness length, temperature, moisture etc. To estimate the surface temperature, which is the purpose of the present analysis, we use 30 minute averages of soil temperature obtained from the logged data.

2. Equations for the surface layer

The wind and temperature profiles in the surface layer are governed by the following equations:

$$u(z) = (u_*/\kappa)(\ln(z/z_0) - \psi_M(z)), \quad (1)$$

$$\theta(z) - \theta_0 = (0.74 \theta_*/\kappa)(\ln(z/z_0) - \psi_H(z)), \quad (2)$$

where $u(z)$ = mean wind speed at height z , m/s

u_* = characteristic (friction) velocity, m/s

z = vertical height, metres

z_0 = roughness length, metres

κ = von Karman constant = 0.41

$\theta(z)$ = temperature at height z , degrees

θ_* = characteristic temperature, degrees

θ_0 = surface temperature, degrees

ψ_M, ψ_H = correction factors for u and θ in the log law.

The surface temperature, which is not an easy quantity to measure, was not directly measured during MONTBLEX. However, since the soil temperatures have been recorded at three levels below the ground, θ_0 can in principle be inferred from this data.

3. Evaluation of surface temperature

We first assume that temperature is governed by the one-dimensional heat conduction equation in the soil,

$$\partial\theta/\partial t = D \partial^2\theta/\partial z^2, \quad (3)$$

where

$D = K/\rho C$, thermal diffusivity of the soil, m^2/s

ρ = density of soil, kg/m^3

C = specific heat of soil, $\text{cal kg}^{-1} \text{deg C}^{-1}$

K = conductivity of the soil, $\text{cal m}^{-1} \text{s}^{-1} \text{deg C}^{-1}$.

We can in principle obtain the thermal diffusivity using equation (3). One approach is the following: The time derivative of temperature at the middle level can be obtained from

$$\partial\theta/\partial t = (\theta(t+1) - \theta(t-1))/2\Delta t. \quad (4)$$

The second derivative at the middle level is obtained from the three temperature measurements at z_1, z_2 and z_3 as:

$$\partial^2\theta/\partial z^2 = (\theta(z_3) - 2\theta(z_2) + \theta(z_1))/(\Delta z)^2, \quad (5)$$

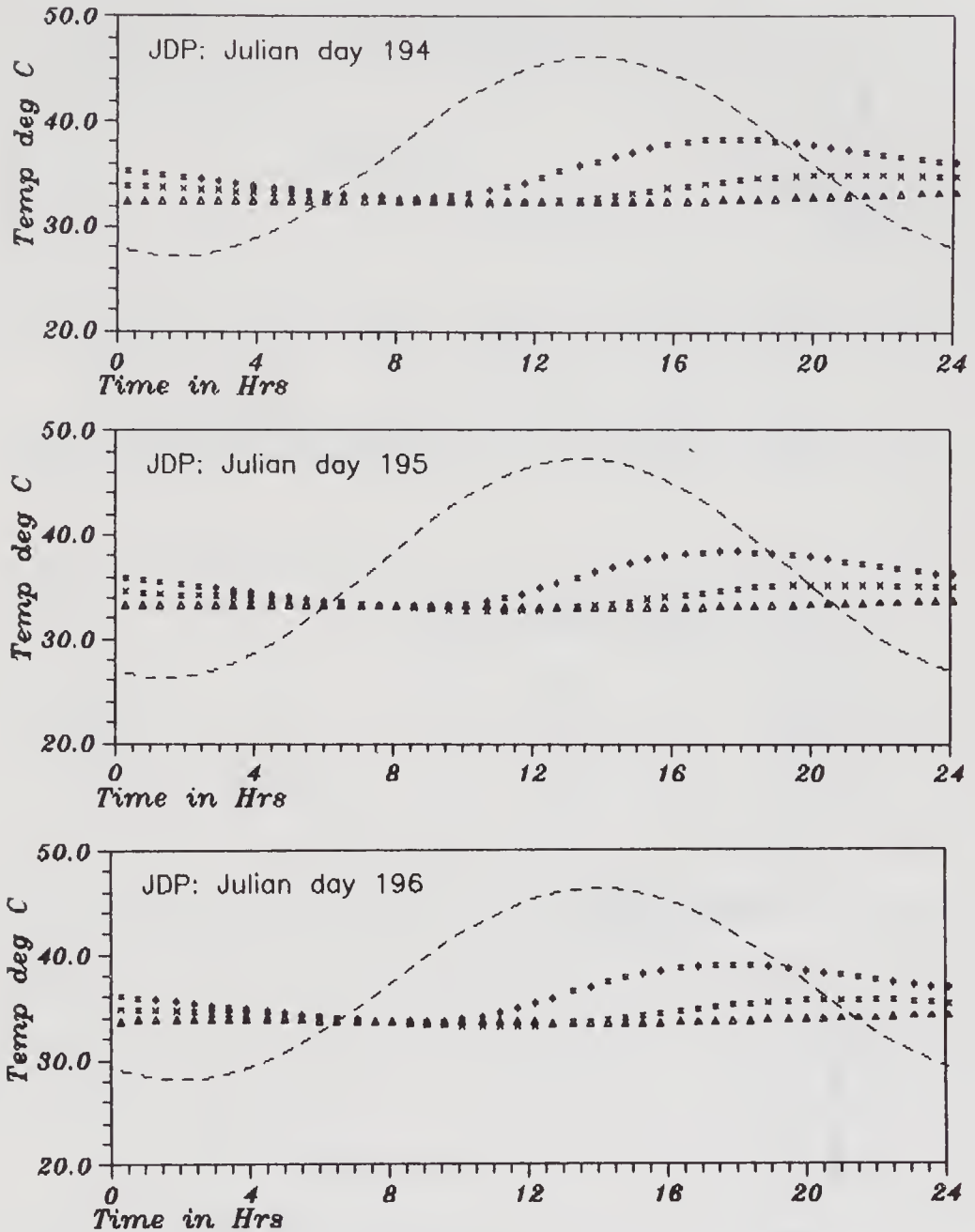


Figure 1. Variation of temperature over the day (* - 0.1 m, x - 0.2 m, Δ - 0.3 m and ——— surface).

and substituting from equations (4) and (5), D can be evaluated from equation (3). Once D is known, applying the equations to the first level it is possible to evaluate the surface temperature θ_0 .

Computations however show that, many times during the day, the sign of $\partial\theta/\partial t$ evaluated as above does not agree with that of $\partial^2\theta/\partial z^2$, implying a negative coefficient of diffusion! The derivatives depend heavily on the accuracy of the temperatures measured, which in turn depends on the calibration constants and drifts. The difficulties of obtaining derivatives numerically are well known, and it was felt that this method is not the appropriate one to use here in the present situation.

Measurements show that the temperature variation of the soil is approximately a sine wave with a period of one day at all three levels below the surface, with a phase

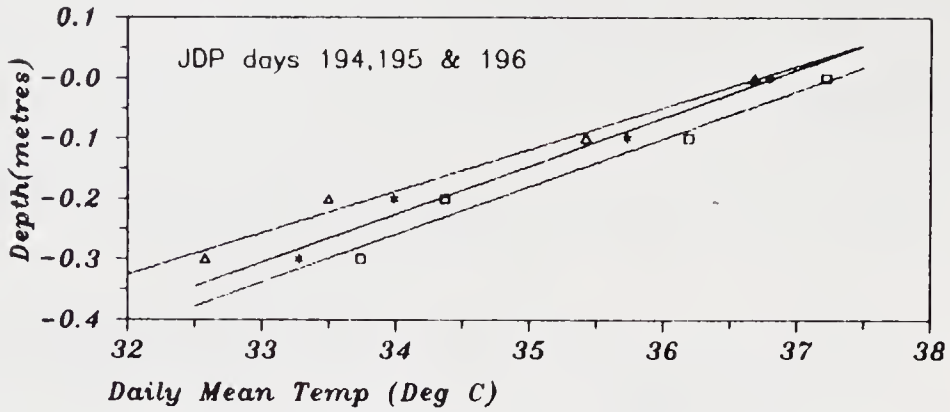


Figure 2. Variation of daily average temperature with depth at JDP. (Δ - day 194; * - day 195 and \square - day 196).

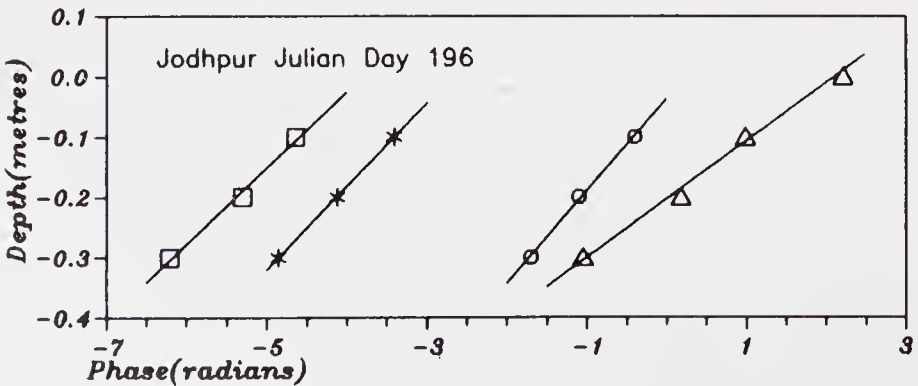
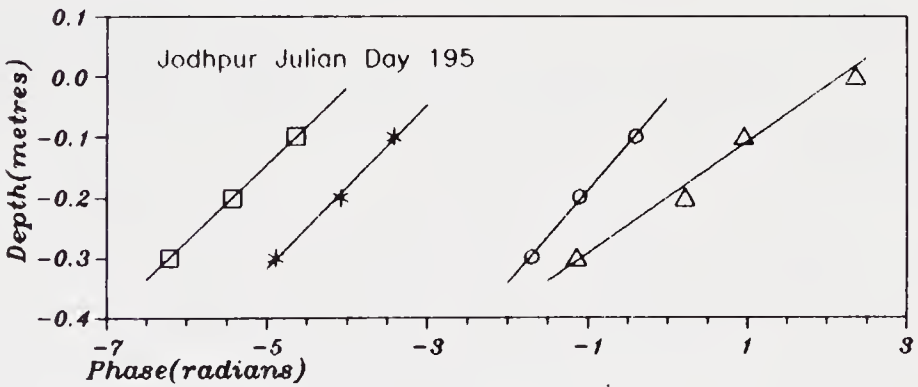
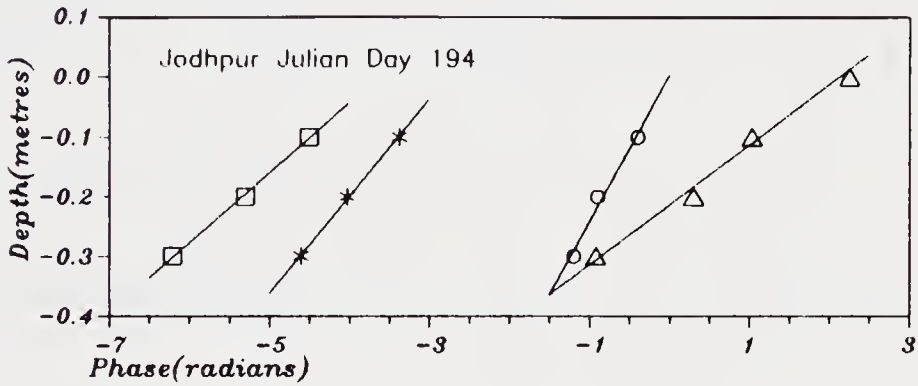


Figure 3. Variation of the phase with depth (\square - beginning, * - mid, o - maximum and Δ - logarithm of the amplitude).

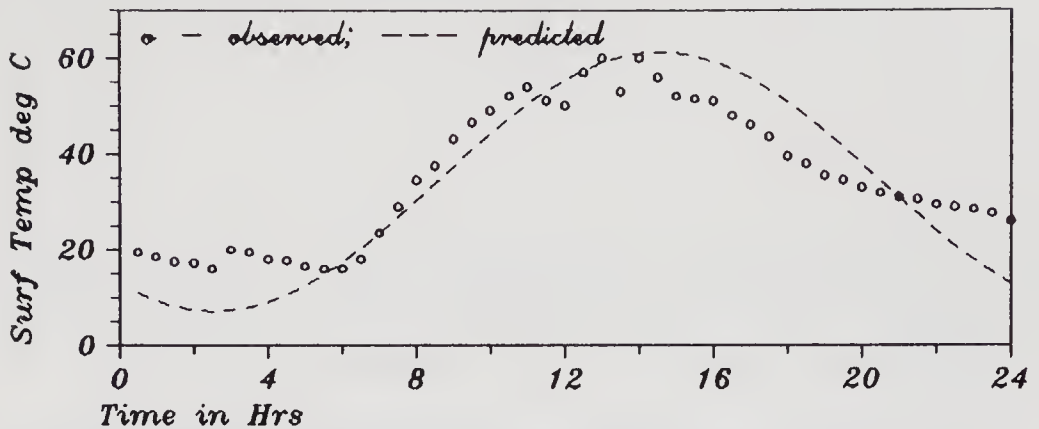


Figure 4. Comparison of computed and measured surface temperatures – data from Pune, 4th–6th May 1992.

Table 1. Variation of alpha.

	BHU	DEL	JDP	KGP
No of pts:	60	43	64	54
Mean alpha:	3.54	6.82	6.63	4.98
Std. Dev.:	1.31	1.90	1.77	1.68
Limit for 95% confidence:	0.34	0.59	0.44	0.46

difference between different levels (figure 1). With this condition, the solution of equation (3) can be obtained as (Kirkham and Powers (1972)):

$$\theta(z, t) = \bar{\theta}(z) + \tilde{\theta} e^{-\alpha z} \sin(\omega t - \alpha z), \quad (6)$$

where $\bar{\theta}$ is the mean temperature at depth z over the day, $\tilde{\theta}$ is the amplitude of the sine wave at the surface,

$$\alpha = \sqrt{(\omega/2D)} \text{ and has the units metre}^{-1},$$

$$\omega = 2\pi/P \text{ in radians/hr, and}$$

$$P = 24 \text{ hrs, the period of the sine wave.}$$

It is also observed that the mean temperature over the day varies linearly with depth (figure 2). Hence, a value of $\bar{\theta}$ at $z = 0$ can be obtained from extrapolation, and is shown there in figure 2.

In equation (6), one finds that the amplitude decreases like $e^{-\alpha z}$ and the phase of the sine wave shifts by αz with depth z . Therefore, from the measurements, α can be determined in two ways – one from the amplitude and the other from the phase.

In the first method the maximum and minimum of the temperature wave, the difference between which gives twice the amplitude, is determined. With temperature measurements at three levels below the ground level, knowing that the amplitude varies like $e^{-\alpha z}$, we can evaluate α . Figure 3 shows the variation of the logarithm of the amplitude with depth; the slope of the straight line in these plots gives α . The value shown at $z = 0$ is from extrapolation. It may be noted that the amplitude at the lowest

Table 2. Computed daily mean surface temperature, amplitude and alpha.

Day	Varanasi			Delhi			Jodhpur			Kharagpur		
	TM	AMP	ALF	TM	AMP	ALF	TM	AMP	ALF	TM	AMP	ALF
144	—	—	—	—	—	—	—	—	—	30.6	1.4	4.4
145	—	—	—	—	—	—	—	—	—	30.5	3.1	5.3
146	—	—	—	—	—	—	—	—	—	29.1	2.5	6.4
147	—	—	—	—	—	—	—	—	—	28.7	3.4	6.9
148	—	—	—	—	—	—	—	—	—	30.3	2.9	6.0
149	—	—	—	—	—	—	—	—	—	30.4	2.4	7.3
150	—	—	—	—	—	—	—	—	—	28.0	3.0	7.3
154	—	—	—	—	—	—	—	—	—	30.0	2.3	6.5
155	—	—	—	—	—	—	—	—	—	30.2	2.5	6.7
156	—	—	—	—	—	—	—	—	—	28.9	2.6	6.5
157	—	—	—	—	—	—	—	—	—	28.0	1.1	2.0
158	—	—	—	—	—	—	—	—	—	28.4	2.2	4.8
159	—	—	—	—	—	—	—	—	—	29.0	2.0	5.4
160	—	—	—	38.1	5.2	8.3	—	—	—	28.9	2.3	6.4
161	41.9	5.0	3.7	37.6	7.5	9.2	—	—	—	28.5	2.9	6.3
162	42.3	10.6	8.0	38.0	7.2	9.4	43.6	1.6	5.6	28.7	1.4	2.8
163	44.0	10.6	7.3	35.8	4.2	6.5	39.4	—	—	30.5	2.4	4.9
164	42.7	6.5	5.5	35.4	7.4	9.1	37.7	4.2	7.8	29.6	1.4	5.5
165	43.5	1.7	5.0	36.5	8.0	8.4	41.8	—	—	—	—	—
166	—	—	—	37.5	8.3	8.8	41.7	5.1	7.8	26.6	1.2	5.9
167	—	—	—	38.0	7.7	8.6	42.3	4.4	6.6	26.7	1.1	5.9
168	—	—	—	38.9	7.5	8.4	43.5	3.9	7.0	26.9	0.8	6.4
169	—	—	—	38.3	3.4	5.1	43.1	3.5	7.6	27.3	1.8	5.6
170	—	—	—	38.5	6.5	9.1	42.3	1.9	3.9	27.4	1.4	5.3
171	—	—	—	35.3	4.1	6.7	41.9	—	—	26.9	—	—
172	—	—	—	36.0	6.7	9.0	42.0	—	—	27.1	1.1	5.5
173	—	—	—	34.0	—	—	41.3	—	—	27.6	1.2	4.4
174	—	—	—	34.7	1.3	2.6	40.8	2.4	6.3	27.7	1.2	4.4
175	—	—	—	34.2	5.3	8.7	40.2	1.9	4.0	27.0	0.6	4.4

Table 2. (Continued)

Day	Varanasi			Delhi			Jodhpur			Kharagpur		
	TM	AMP	ALF	TM	AMP	ALF	TM	AMP	ALF	TM	AMP	ALF
211	—	—	—	—	—	—	36.4	—	—	—	—	—
212	—	—	—	—	—	—	37.0	4.5	8.2	—	—	—
213	35.6	0.7	2.6	—	—	—	37.4	3.8	8.2	—	—	—
214	—	—	—	—	—	—	37.6	3.5	7.1	—	—	—
215	34.6	1.0	3.6	—	—	—	35.0	3.1	3.5	—	—	—
218	37.2	0.8	2.5	—	—	—	—	—	—	—	—	—
219	37.6	1.6	4.6	—	—	—	—	—	—	—	—	—
220	37.7	1.0	4.2	—	—	—	—	—	—	—	—	—
221	37.7	0.9	3.9	—	—	—	—	—	—	—	—	—
222	38.8	1.1	2.7	—	—	—	32.6	3.1	6.0	—	—	—
223	37.9	1.2	3.2	—	—	—	33.4	2.7	5.4	—	—	—
224	35.6	—	—	—	—	—	32.4	—	—	—	—	—
225	35.9	1.0	3.8	—	—	—	31.2	—	—	—	—	—
226	35.0	—	—	—	—	—	32.4	3.4	7.0	—	—	—
227	37.6	0.9	3.4	—	—	—	34.5	4.4	5.8	—	—	—
228	37.2	0.8	3.8	—	—	—	36.8	4.3	5.4	—	—	—
229	37.2	1.4	3.8	—	—	—	37.4	3.1	5.7	—	—	—
230	38.2	1.9	3.7	—	—	—	37.8	3.6	7.2	—	—	—
231	38.5	1.1	3.0	—	—	—	37.9	3.6	6.7	—	—	—
232	37.3	0.4	3.1	—	—	—	36.0	4.2	7.8	—	—	—
233	40.0	1.0	2.8	—	—	—	34.8	4.0	8.1	—	—	—
234	38.0	0.9	3.5	—	—	—	34.4	3.4	8.7	—	—	—
235	38.1	1.3	4.1	—	—	—	33.3	3.6	8.3	—	—	—
236	38.1	1.6	3.0	—	—	—	32.8	—	—	—	—	—
237	38.1	1.9	3.1	—	—	—	31.0	—	—	—	—	—
238	37.1	1.0	2.8	—	—	—	29.9	—	—	—	—	—
239	36.2	1.4	7.1	—	—	—	30.0	2.3	8.5	—	—	—
240	37.6	1.2	2.9	—	—	—	30.8	3.3	6.9	—	—	—

241	36.6	0.8	3.6	—	—	32.4	3.3	6.1	—	—	—	—
242	37.5	1.2	2.9	—	—	32.6	1.1	4.1	—	—	—	—
243	38.2	2.3	4.0	—	—	32.1	3.7	8.6	—	—	—	—
244	36.6	0.2	1.2	35.8	0.6	32.9	2.7	6.5	29.2	3.0	5.4	—
245	—	—	—	37.9	5.1	32.2	4.2	9.7	—	—	—	—
246	—	—	—	37.0	8.6	31.8	—	—	—	—	—	—
247	—	—	—	36.4	—	32.0	4.3	8.4	30.2	0.5	1.2	—
248	—	—	—	—	—	33.6	4.9	6.6	—	—	—	—
249	—	—	—	36.8	3.9	35.2	4.5	6.2	27.8	1.9	0.2	—
250	—	—	—	39.0	2.9	33.0	1.0	3.1	26.1	2.1	1.8	—
251	—	—	—	36.3	2.5	32.8	4.6	9.3	—	—	—	—
252	—	—	—	40.6	3.0	32.9	4.8	8.7	—	—	—	—
253	—	—	—	38.3	—	33.5	3.9	6.5	—	—	—	—
254	—	—	—	37.9	3.8	32.8	0.6	1.2	—	—	—	—
255	—	—	—	36.3	2.3	—	—	—	—	—	—	—
256	—	—	—	35.8	1.7	—	—	—	—	—	—	—
257	—	—	—	36.1	1.4	—	—	—	—	—	—	—
261	—	—	—	34.3	1.3	—	—	—	—	—	—	—
262	—	—	—	37.6	—	—	—	—	—	—	—	—
263	—	—	—	37.4	—	—	—	—	—	—	—	—
264	—	—	—	36.6	—	—	—	—	—	—	—	—

Day – Julian day; TM – Daily mean temperature at the surface; AMP – Amplitude of the temperature wave at the surface; ALF – Alpha.

level does not fit into the trend. This may be due to difficulty in accurate evaluation of a small amplitude or in the calibration constant for that sensor.

The phase differences between the three waves below the ground can be found in four different ways. Since the sine wave has a period of a day, we can determine the phase from the point where the wave crosses the mean. This happens at two points during every cycle. However, it is found from experience that the crossings around midnight are more difficult to determine than the middle one, which is simply due to the fact that the wave crosses the mean with a distinct positive slope around midday. Figure 3 shows the variation of phase determined from both the midnight and midday crossings with depth. The fourth method is to determine the time when during the day the temperature

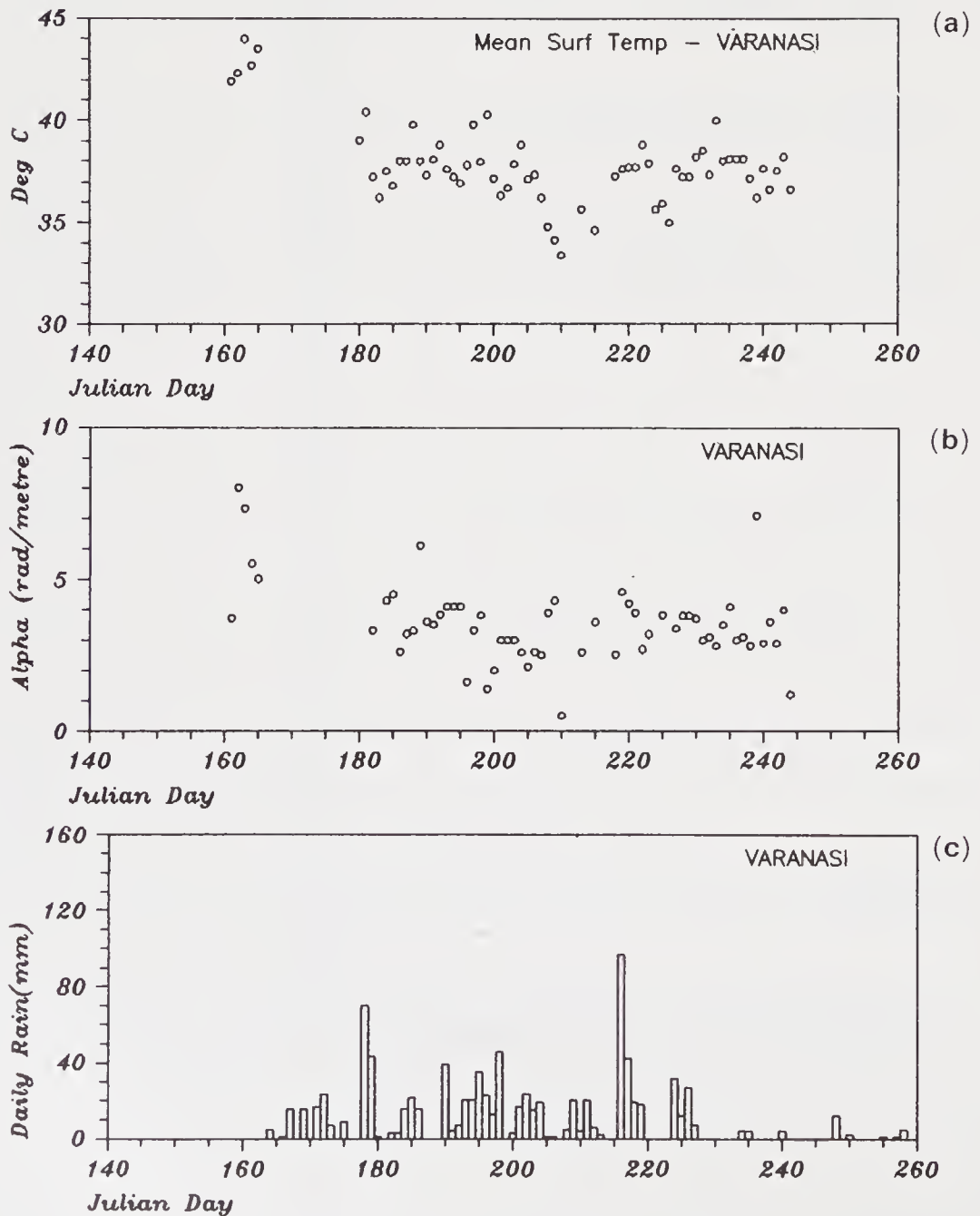


Figure 5. (a) Surface mean temperature; (b) α ; and (c) rain at BHU.

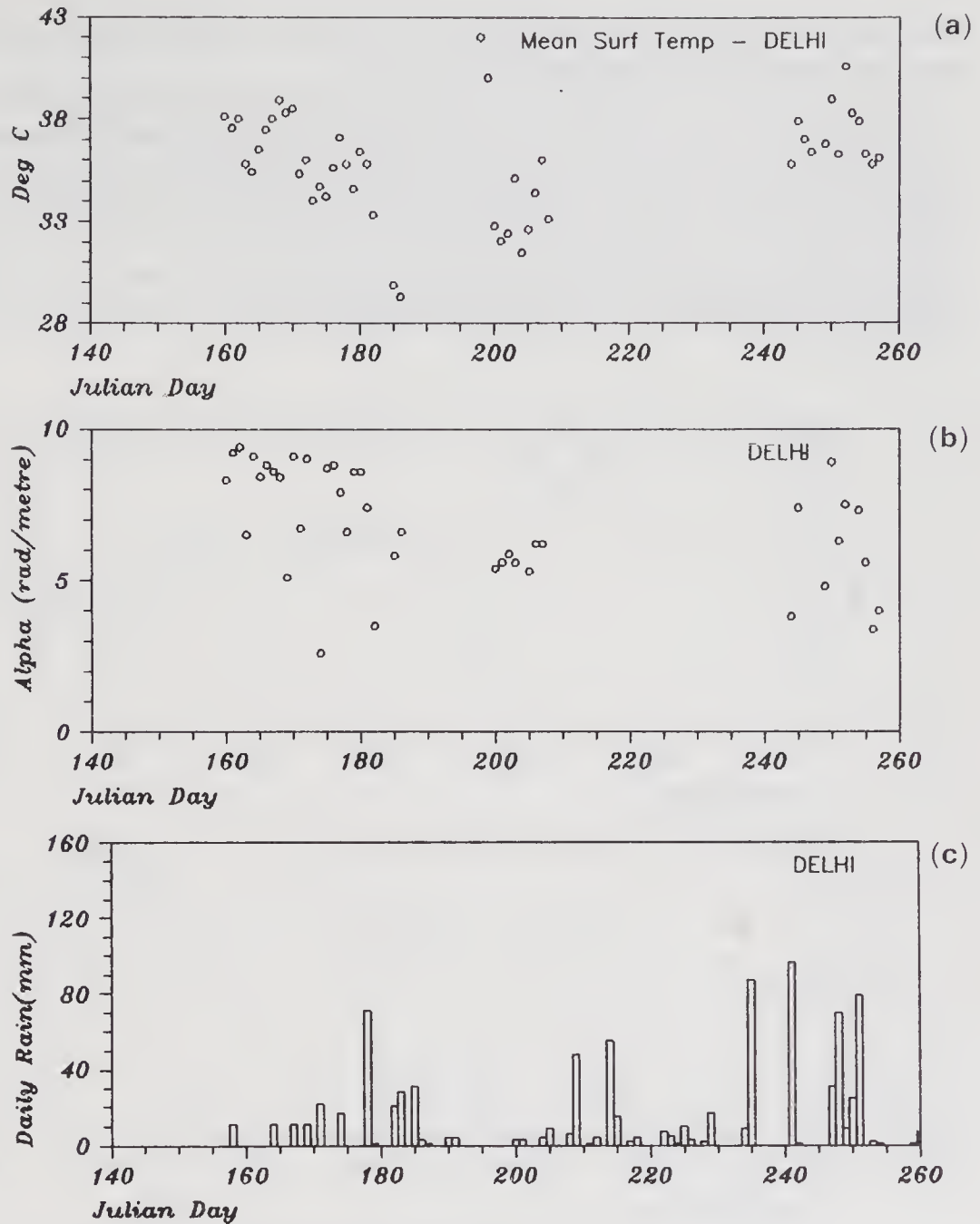


Figure 6. (a) Surface mean temperature; (b) α ; and (c) rain at DEL.

waves have a maximum, which is also a measure of the phase of the wave. In principle, this is more difficult as the time at which the maximum occurs is not sharply defined, since a sine wave has zero slope at this point. However, it can be seen from figure 3 that this method also gives a reasonable estimate of α .

It may be noted here that the value of the temperature measured within the soil depends on the calibration constant and drift (if any) of the instrument; so does the amplitude. On the other hand, the phase does not depend on either of the above, and hence should actually give the most reliable information about α .

It is possible that α cannot be estimated by all the four methods mentioned above, mainly because of the discontinuity in data at some stretches during the day. α obtained

from different methods is averaged for further analysis. If α cannot be estimated by two methods at least, such data has been discarded.

Knowing the mean temperature at three levels below the ground a straight line can be fitted through those three points and extrapolated to get the mean temperature at the surface (figure 2). The phase difference and the amplitude of the surface temperature can be computed from α and the temperature data at the first level below the surface. The temperature of the surface for the whole day can be computed. The dotted line in figure 1 shows the result. Taking into account the longer day at Jodhpur during that time, this temperature wave crosses the mean around the same time delay after sunrise and sunset.

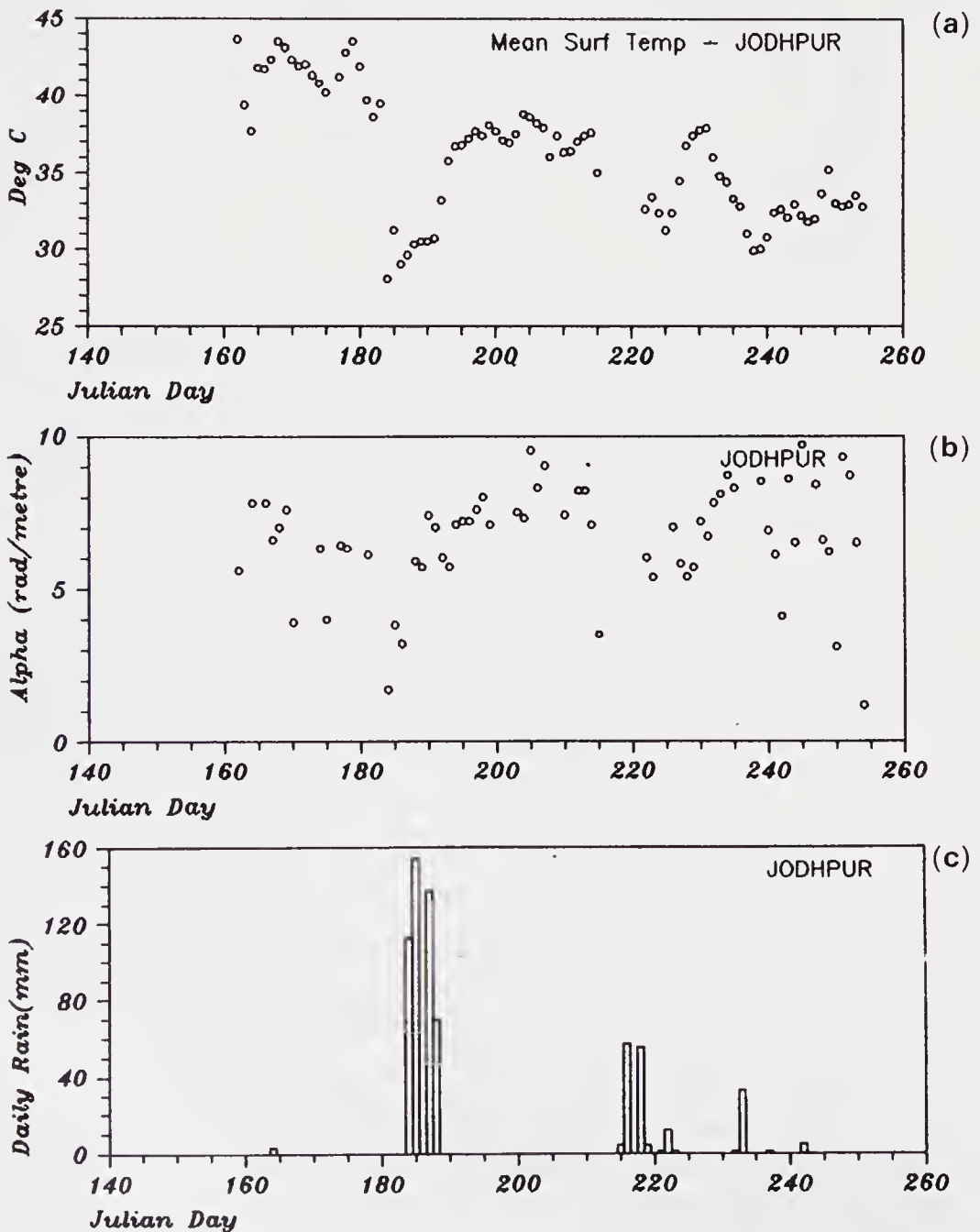


Figure 7. (a) Surface mean temperature; (b) α ; and (c) rain at JDP.

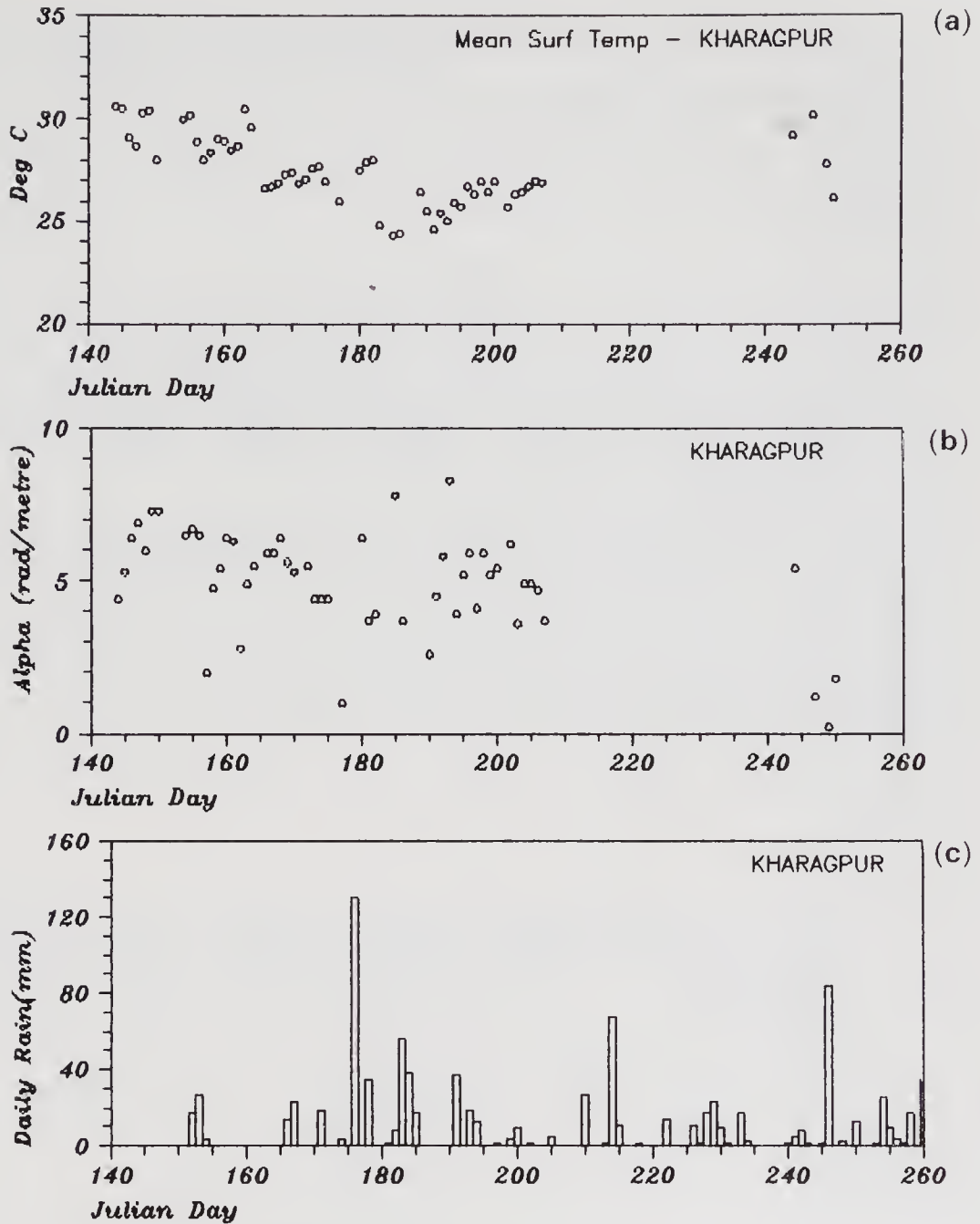


Figure 8. (a) Surface mean temperature; (b) α ; and (c) rain at KGP.

Figure 4 gives the observed surface temperature along with the surface temperature computed as explained above from the data at three levels below the ground during 4th to 6th May 1992 at Pune (kindly supplied by Dr. Verneker, IITM). The agreement is very good, giving us confidence in the present procedures for obtaining the surface temperature.

4. Conclusions and recommendations

Table 1 gives the mean, standard deviation and 95% confidence levels for the mean of α for all the four stations. The values are seen to be different for different stations. The spread seems to be large (about 25 to 30% of the mean). The values of the thermal

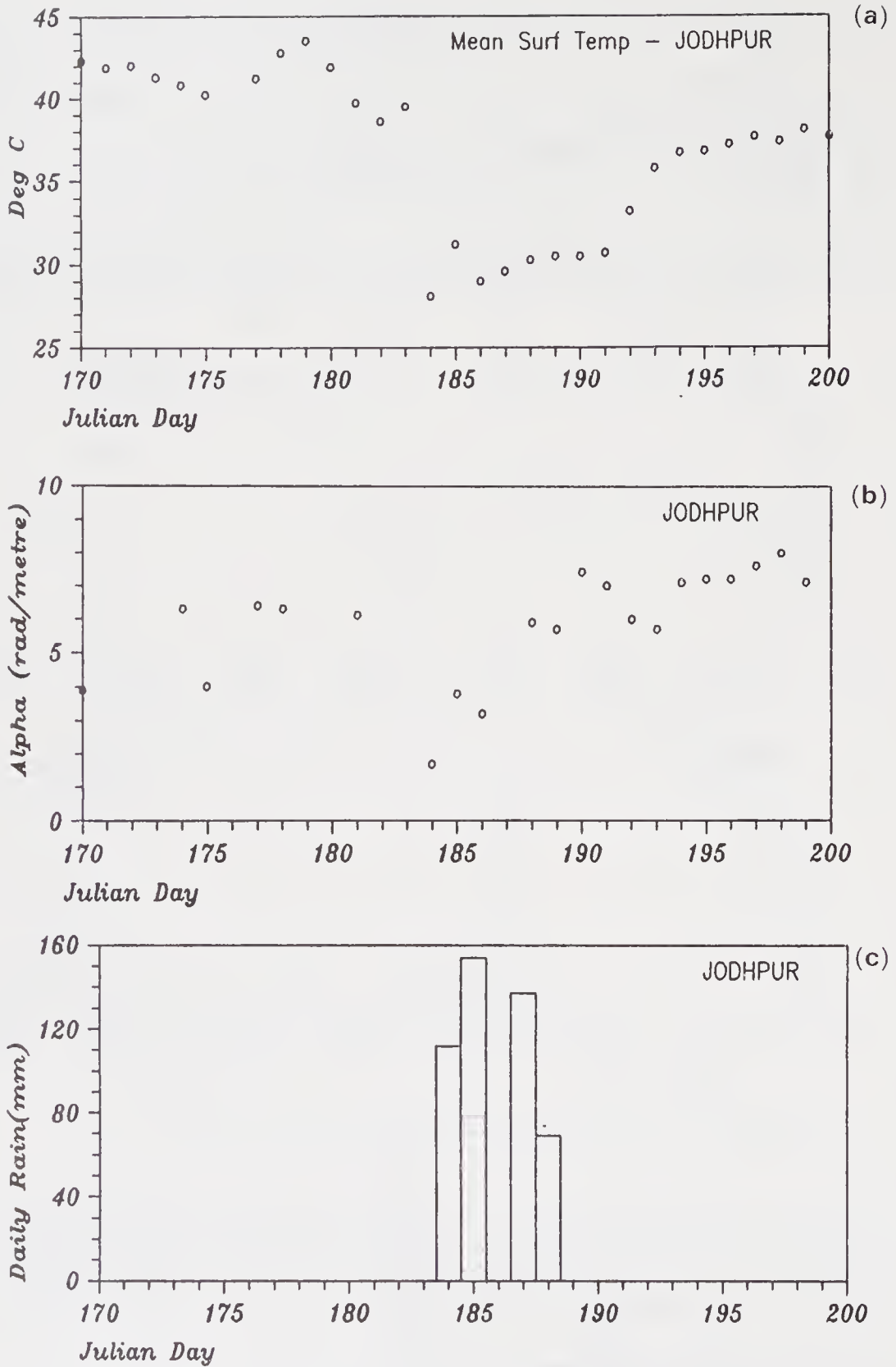


Figure 9. (a) Surface mean temperature; (b) α ; and (c) rain at JDP around a heavy rainfall.

diffusivity calculated from α are in the range (about 0.1×10^{-6} to 1.3×10^{-6} m²/s) reported by Kirkham and Powers (1972).

The mean surface temperature over the day, the amplitude of the temperature wave at the surface and α are computed over the period of the experiment and are given in table 2 which can be used for getting the surface temperature at any time of the day. The daily mean surface temperature, α and the rainfall at all the four stations are presented in figures 5 to 8.

It can be seen from the Jodhpur data (figure 7) that the α and the mean surface temperature change appreciably following heavy rains. To illustrate this more clearly, figure 9 shows the period of such an event at Jodhpur. At this station, the mean α over the full duration of the experiment is 6.63 rad/m with a standard deviation of 1.77 rad/m. Following rain on day 183, the value of α drops to about 1.7 rad/m on day 184 and the mean surface temperature over the day falls drastically from 39.5°C on day 183 to 28.1°C on day 184. It is observed during the experiment that the air temperature during the early hours of day 184 was around 25°C. From the data, the estimated probability of α attaining this low value is less than 1%. A similar trend was observed around day 220. It is therefore clear that the thermal diffusivity and the surface temperature of the soil must have changed substantially after sudden, very heavy rains.

At other sites, the rainfall was almost uniformly spread over the period of experiment; so no sudden changes can be observed. However, as long as the temperature waves are sinusoidal and the mean temperatures are linear with depth, the present analysis should still hold good.

References

- Kirkham D and Powers W L 1972 *Advanced Soil Physics* (Wiley Interscience)
Rudra Kumar S, Srinivasan H P, Srikrishna R, Ameenulla S, Prabhu A (1991) Available tower data from MONTBLEX 1990, Rep 91 M D 1 CAS, IISc, Bangalore 12.

Atmospheric boundary layer studies at Jodhpur during MONTBLEX using sodar and tower

B S GERA*, S P SINGAL*, NEERAJ SAXENA* and
Y S RAMAKRISHNA**

*National Physical Laboratory, New Delhi 110012, India.

**Central Arid Zone Research Institute, Jodhpur, India.

Abstract. A monostatic sodar was set up at Jodhpur, near the western end of the monsoon trough, to investigate the atmospheric boundary layer dynamics. A 30 m instrumented tower was also located close to the sodar antenna. Data were collected from June to August during the monsoon period of 1990, as also from July 1992 to September 1993.

Thermal plumes, surface-based stable layers (both flat or short spiky top and tall spiky top), elevated/multi-layers with or without undulations and dot echo structures were seen; however, erosion of the morning inversion layer in the form of a rising layer with growing thermal plumes under it was rarely seen, and that too only during the winter period. The observed structure of the stable layer with tall spikes and its depth have been found to be correlated with the intensity of the monsoon spell; the dot echoes have been found to be correlated with the approach of a monsoon depression near Jodhpur; and the elevated/multilayers have been attributed to the formation of a subsidence (shear instability).

Keywords. Sodar; MONTBLEX; monsoon trough; boundary layer; atmosphere; thermal structure; rainfall.

1. Introduction

To investigate the atmospheric boundary layer dynamics at Jodhpur, near the western end of the monsoon trough, a monostatic sodar was set up in the plain grounds of the Central Arid Zone Research Institute, Jodhpur, as part of the multi-institutional, DST co-ordinated research programme called 'Monsoon Trough Boundary Layer Experiment' abbreviated as MONTBLEX (Goel and Srivastava 1989). A 30 m instrumented tower was also located adjacent to the sodar antenna.

The objectives of the investigation were to monitor the diurnal and day-to-day variability of the planetary boundary layer and to identify the characteristic changes associated with the thermal structure of the monsoon trough boundary layer.

2. The site and the investigational systems

The experimental site was the Central Arid Zone Research Institute located on the outskirts of Jodhpur city. It has vast plain grounds.

Jodhpur ($26^{\circ}18'N$, $63^{\circ}04'E$) is in a dry zone in the Thar desert, on the Aravalli range, and has a hill and valley terrain. Rainfall at Jodhpur is normally very low. During summer monsoon months, the days are extremely hot and are followed by sudden nocturnal cooling.

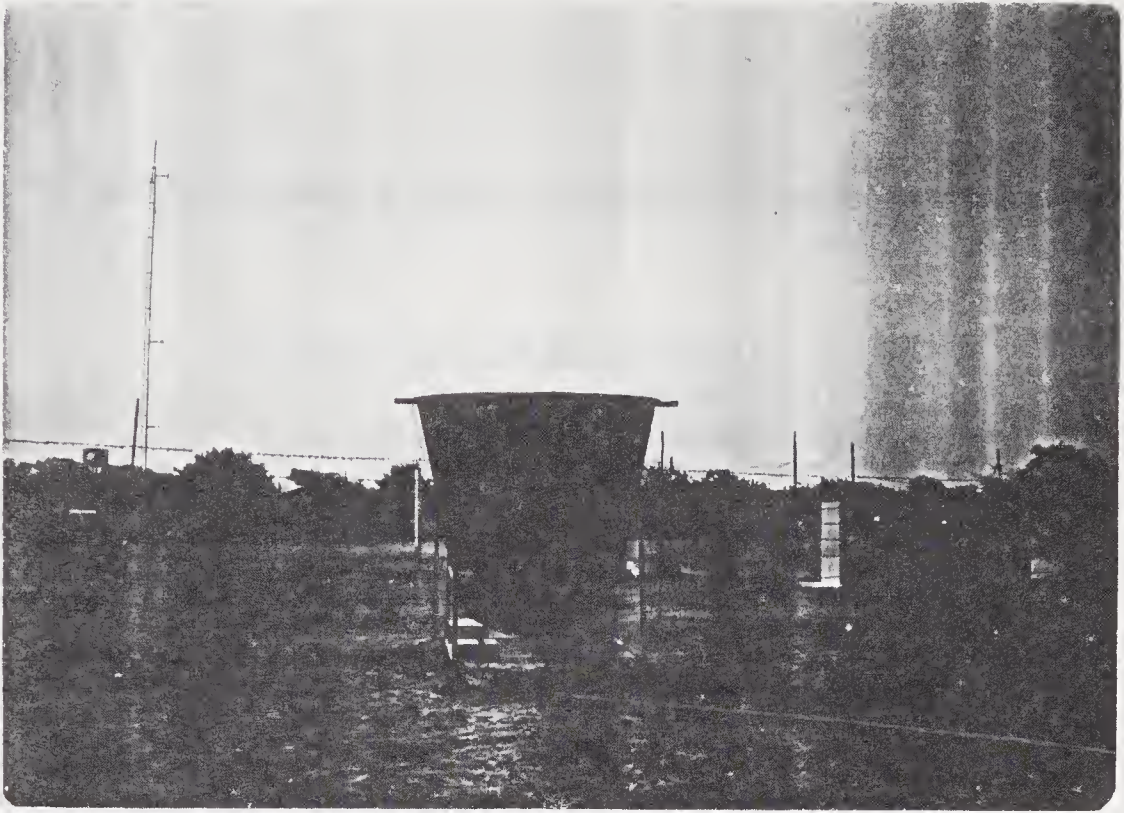


Figure 1. A view of the sodar antenna placed in the vast plain grounds of CAZRI, Jodhpur. In the background, the instrumented tower can also be seen.

The sodar system, indigenously designed, developed and fabricated (Singal and Gera 1982), consisted of a paraboloid antenna, trans-receive low noise electronics and a facsimile display device. The paraboloid antenna was specially designed to give a powerful directional beam in the vertical direction at a frequency of 2.2 kHz. Structurally, it was made up of a 1.2 m paraboloid with its focus at a height of 0.4 m, jointed at its periphery with a 2 m-high conical shield. It was made of a 5 mm-thick fibre-glass mixed with lead powder. The shield has been further pasted from inside with a 10 cm-thick high density polyurethane foam. This helps to shield the ambient noise being received by the antenna as also to reduce the noise pollution due to the sounder. At the focus of the paraboloid a 50 W acoustic transducer was mounted to act as an acoustic transmitter and receiver. The whole assembly was housed in a rectangular angle iron frame (figure 1). This antenna system could give a narrow acoustic beam of width $\pm 10^\circ$ and a 90° sidelobe rejection of 55–60 dB at a frequency of 2 kHz.

The system's electronics was used to transmit sound pulses of 80 ms duration at 2.2 kHz frequency vertically upwards every four seconds, after amplification from a power amplifier to emit acoustic tonebursts of 10 acoustic watt power. These tonebursts after reflection from the thermal inhomogeneities in the atmosphere were received by the same antenna. The received signal was suitably amplified, range-compensated, filtered, detected and displayed on a facsimile recorder. The facsimile recorder handled signals in the voltage range of 2–10 volts and could display the thermal structure of the lower atmosphere up to a height of 700 m as a function of time. The complete characteristics of the sodar system are given in table 1.

The antenna was kept on plain ground in the open, facing up, while the electronic instrumentation and facsimile recorder were housed in a single-storeyed observatory

Table 1. Characteristics of NPL monostatic sodar system.

Transmitted power electrical	: 40 watts.
Transmitted power acoustical	: 10 watts.
Pulse-width	: 60 ms.
Pulse repetition period	: 4 sec.
Operational range	: 700 m (approx.).
Receiver bandwidth	: 50 Hz.
Frequency of operation	: 2200 Hz.
Acoustic velocity	: 340 m/s (average).
Ambient temperature	: 300 K (average).
Transmit-Receive antenna	: Parabolic reflector surrounded by acoustic cuff.
Receiver area	: 2.5 sq. m.
Preamplifier sensitivity	: Fraction of a microvolt.
Recorder	: Facsimile recorder.

building 100 m away from the antenna. Data were collected from June to August during the monsoon period of 1990, the actual planned study period of the MON-TBLEX, as also from July 1992 to September 1993 to further understand the structure of the atmospheric boundary layer. Observations were continued throughout the day without interruption except for periods of power or instrumentation breakdown.

The tower, also indigenously designed, developed, fabricated and maintained by the Indian Institute of Science, Bangalore was established in the same grounds. The tower had 6 levels of slow and fast instrumentation sensors of temperature, humidity, wind-speed and wind direction at 1, 2, 4, 8, 15 and 30 m heights. The slow data from 32 channels of the tower sensors were being continuously recorded on the cassette tape of a Campbell data logger as three-minute averages. Fifteen minutes of fast data (8 Hz) from 32 channels were being recorded on the hard disk of a PC-XT every three hours (0530, 0830, 1130, 1430, 1730, 2030, 2330 and 0230 hrs IST) and transferred on to a cartridge tape. A convenient high-roofed room was provided for the tower computer as also for the sodar instruments.

3. Results and discussion

Typical shear echo and thermal echo structures (figure 2), as well as no-echo periods, were seen almost daily on the facsimile records. Shear echoes were constituted of ground-based layer structures (both flat or short spiky top and tall spiky top), multi/elevated layer structures with and without undulations superposed over them, and dot echoes. Thermal echoes were constituted of vertically growing thermal plumes with broad to thin bases. Shear echoes represented night-time stable layer structures, thermal echoes represented day-time convective conditions and no-echo structures represented the presence of almost neutral conditions commonly found during the evening transition period. The elevated/multi-layer structures were mostly seen under disturbed weather conditions.

The ground-based thermal plume structure started developing with daybreak with shorter plumes growing into taller plumes achieving a maximum height of 300–400 m during 1200–1400 hrs IST. Erosion of the nocturnal ground-based layer usually observed in the form of a morning rising layer above the thermal plumes was rarely seen

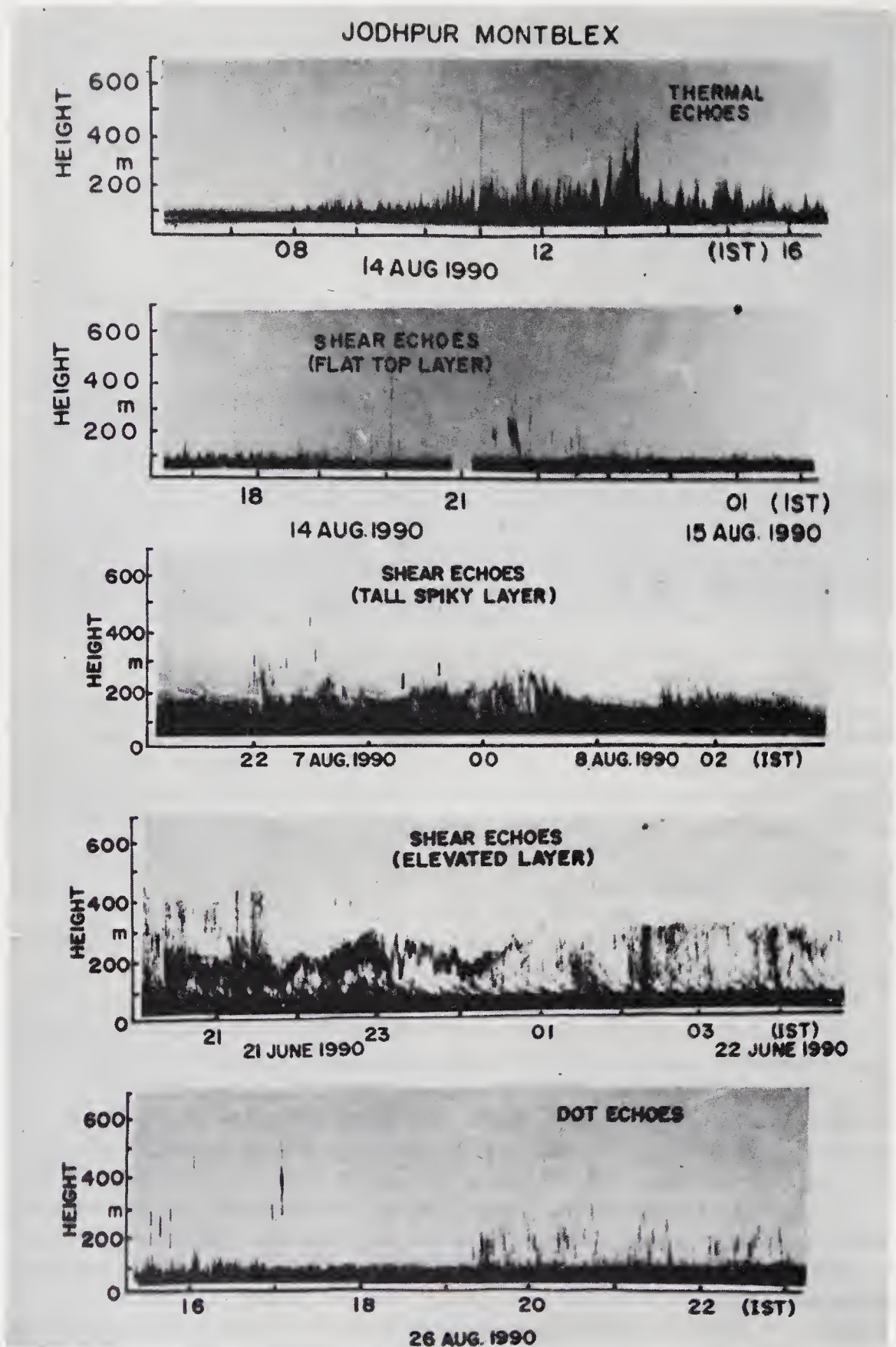


Figure 2. Typical shear echo and thermal echo structures seen in the atmospheric boundary layer at Jodhpur.

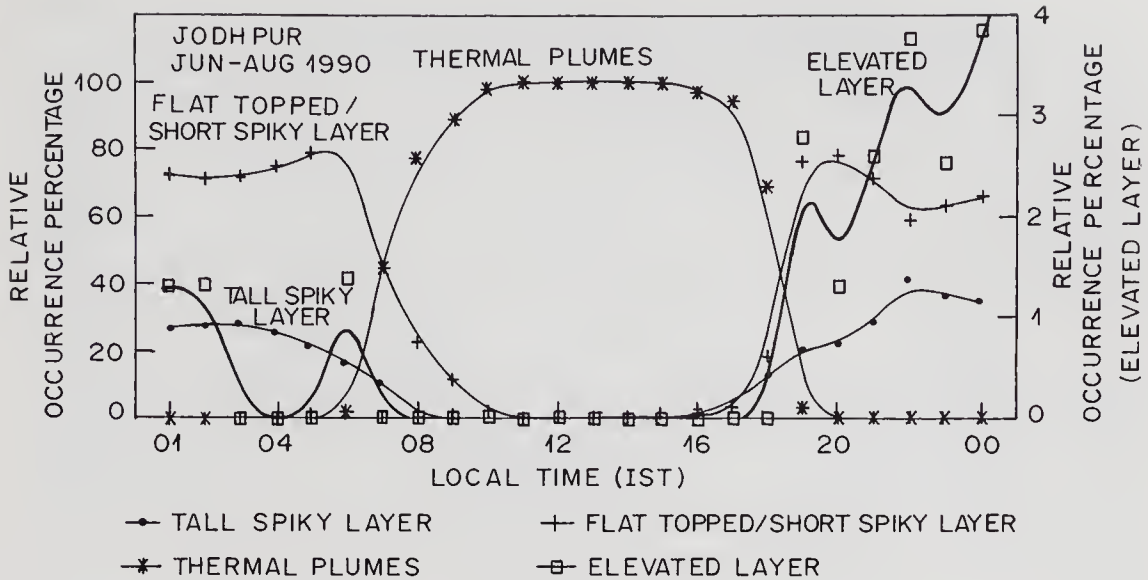


Figure 3. Plot of the diurnal distribution of the various sodar structures. The occurrence percentage is only relative for all the structures.

(only during winter months) for the atmospheric boundary layer at Jodhpur indicating that the radiational inversion layer is weak and shallow, a result which has been corroborated by a study of the Jodhpur tower data by Singh *et al* (1992). The height of the thermal plumes started decreasing in the afternoon and vanished during the evening transition period. Since acoustic echoes are due to turbulence in the lower atmosphere (Brown and Hall 1978), a measure of the height of the echoes gives a measure of the height of the turbulent atmospheric boundary layer. However, a measure of the height of the thermal plumes on sodar is an underestimate since sodar sensitivity is poor during the day-time due to the prevailing excessive ambient noise which limits the processing of the genuine signal only up to a few hundred metres close to the ground surface.

Shear echoes appear on the sodar echogram during the evening hours preceded by a blank transition period of no echoes for about half an hour. The nocturnal stable layer most often develops up to midnight but sometimes keeps on growing throughout the night. On clear days, it is mostly the ground-based layer which is seen. It has a depth of 150–200 m. On disturbed days, elevated/multilayers with or without undulations or dot echoes over and above the ground-based layer have also been seen as also reported earlier for Delhi (Singal *et al* 1985). Undulating layers have sometimes also been observed on clear days.

The diurnal distribution of the various structures during the monsoon period is shown in figure 3. It may be seen that only during the day-time the thermal plumes have been seen. The flat-topped ground-based layer is mostly seen during the period from 2000 hrs in the evening through 0600 hrs in the morning. The elevated layer has been most often seen during the early night hours up to midnight when it has the maximum occurrence. Tall spiky layers (ground-based) have been seen for about 30% of the nocturnal occurrence period.

The occurrence percentages of various sodar structures during the MONTBLEX period have also been studied and are shown in table 2. It may be noted that thermal

Table 2. Occurrence percentages of the various sodar structures (both stable and unstable) during the monsoon months of 1990, monthwise as well as total.

Month	Stable structures (ground-based)		Unstable structures	Additional structures	
	TS (%)	SS/FT (%)	CP (%)	EL/ML (%)	DE (%)
	(out of 100%)			(out of total)	(out of total)
June 1990	18.17	23.83	58.00	2.00	0.00
July 1990	18.69	32.94	48.37	0.00	0.00
August 1990	5.00	51.32	43.68	0.15	1.32
Monsoon period	13.77	36.54	49.69	0.67	0.44

TS – Tall spiky.
CP – Convective plumes.

SS – Short spiky.
EL – Elevated layer.
DE – Dot echoes.

FT – Flat topped.
ML – Multilayer.

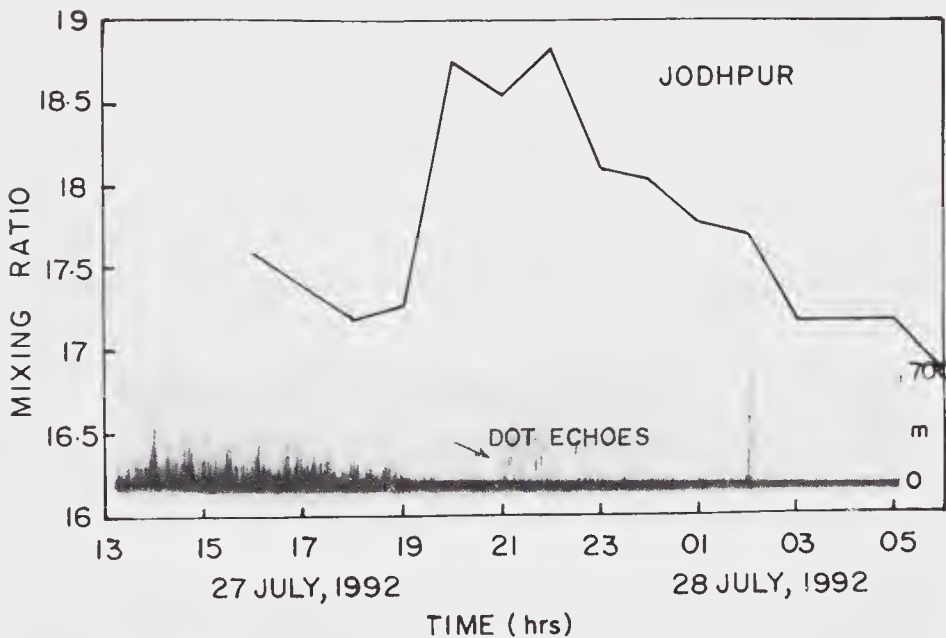


Figure 4. Plot of the mixing ratio as a function of the day-time on 27th July, 1992 at Jodhpur with an inset of the simultaneously varying thermal structure as observed by sodar.

plumes occur about 50% of the time, flat-topped/short spiky structures about one-third of the time while tall spiky structures occur for about 14% of the time. It is interesting to note that the frequency of occurrence of tall spiky structures is low during the month of August when dot echoes have been seen, a result of low winds and high moisture content in the atmosphere. The elevated/multilayers occur more often during June, which may be due to cyclonic circulations from the Gulf.

Dot echoes have been seen only on the days of monsoon depression when excess moisture content is present in the atmosphere. The correlation of the dot structures with the moisture content has been confirmed with the help of the tower data and can be seen from a plot of the mixing ratio and observed dot echoes as a function of the time of the day in figure 4.

A study of the occurrence of nocturnal sodar structures in the form of elevated/multilayers, gusts and dot echoes has been conducted on the days of monsoon depressions and is shown in table 3. It may be seen that elevated/multilayer and gust structures may be formed during the period when a depression is progressing towards Jodhpur from the Bay of Bengal, and culminate in the formation of dot echoes when the depression comes closer to Jodhpur. Since depressions are linked with the presence of excess moisture accompanied with strong winds and the presence of dot echoes is linked with high moisture content (Singal *et al* 1985), it appears that dot echoes may be used as an indicator for an approaching depression.

A study of the occurrence of tall spiky structures and the relative changes in the depth of the turbulent boundary layer in terms of the intensity of the major rainfall spells has also been conducted and is shown in figure 5. It may be seen that the extent of the cumulative fortnightly rainfall spells is responsible for the large relative occurrence percentage of tall spiky structures while the extent of weekly rainfall is responsible for a relative increase in the depth of the stable turbulent boundary layer. It may be noted that tall spiky structures are associated (Singal *et al* 1986) with strong surface winds which is a usual feature of the rainfall spell.

3.1 Unusual features during the monsoon season of 1992

The sodar was operated at the Jodhpur station in the monsoon season even after the MONTBLEX programme. During this extension period, an unusual observation in the form of an elevated multilayer structure on the sodar echograms was made (figure 6) during the period Sept. 15th–18th, 1992. In the early hours of Sept. 15th, a faint elevated layer structure existed beyond the height of 600 m. This elevated structure became stronger and turned into multilayers and undulations during the early morning (nocturnal) hours when stable conditions prevailed on Sept. 16th and 17th, and receded during the early hours of Sept. 18th. There was no rainfall during this period and the sky was more or less clear.

To interpret this unusual observation and to look into its linkages with the weather phenomena, an analysis of the meteorological data, both micrometeorological and synoptic, was made.

Surface pressure over Jodhpur started increasing from Sept. 12th, 1992 onwards. It remained more or less steady during the period Sept. 14th–17th, when it started increasing again. As compared to this local observation, the synoptic weather map of Jodhpur showed the existence of a trough between 1.5 and 3.0 km on the west side of Jodhpur during Sept. 14th–18th, responsible for the cyclonic circulation up to 300 m on Sept. 15th. The wind flow pattern became anticyclonic on Sept. 19th, in agreement with the increase in surface pressure.

Wind speed at 2100 hrs was increasing at both 15 m and 30 m levels up to Sept. 15th, 1992. It became steady (between 1.5 and 2.5 m/s) for the next three days, with a slight increase later on. Wind direction at 2100 hrs was southwesterly up to Sept. 14th, when it changed direction and became westerly. On the synoptic scale also, a similar behaviour in agreement with the tower measurements was noticed.

Mixing ratio was continuously decreasing from Sept. 10th onwards for a number of days. It became steady during the period Sept. 15th–17th, and had a sudden fall on Sept. 17th, a trend which continued for the next few days.

Table 3. Sodar structure during the intensive synoptic observation period.

Intensive observation period	Days of deep depression	Time of observation of specific structures (IST)	Specific sodar observation in addition to ground-based layer				Remarks
			Elevated/Multi-layer/waves	Gust	Dot Echoes		
14th–15th June 1990	14th June	—	—	—	—	Depression remained far away from Jodhpur.	
	15th June	—	—	—	—		
15th–19th August 1990	15th August	—	—	—	—	Depression progressed towards Jodhpur but started dissipating from Nagpur onwards.	
	16th August	—	—	—	—		
	17th August	1900	No	No	Yes		
	18th August	2000	No	No	Yes		
20th–24th August 1990	19th August	—	—	—	—		
	20th August	1900	Yes	No	No	Depression progressed towards Jodhpur and reached relatively closer.	
	21st August	—	—	—	—		
	22nd August	1900	No	Yes	No		
	23rd August	1900	No	No	Yes		
24th August	—	—	—	—	—		

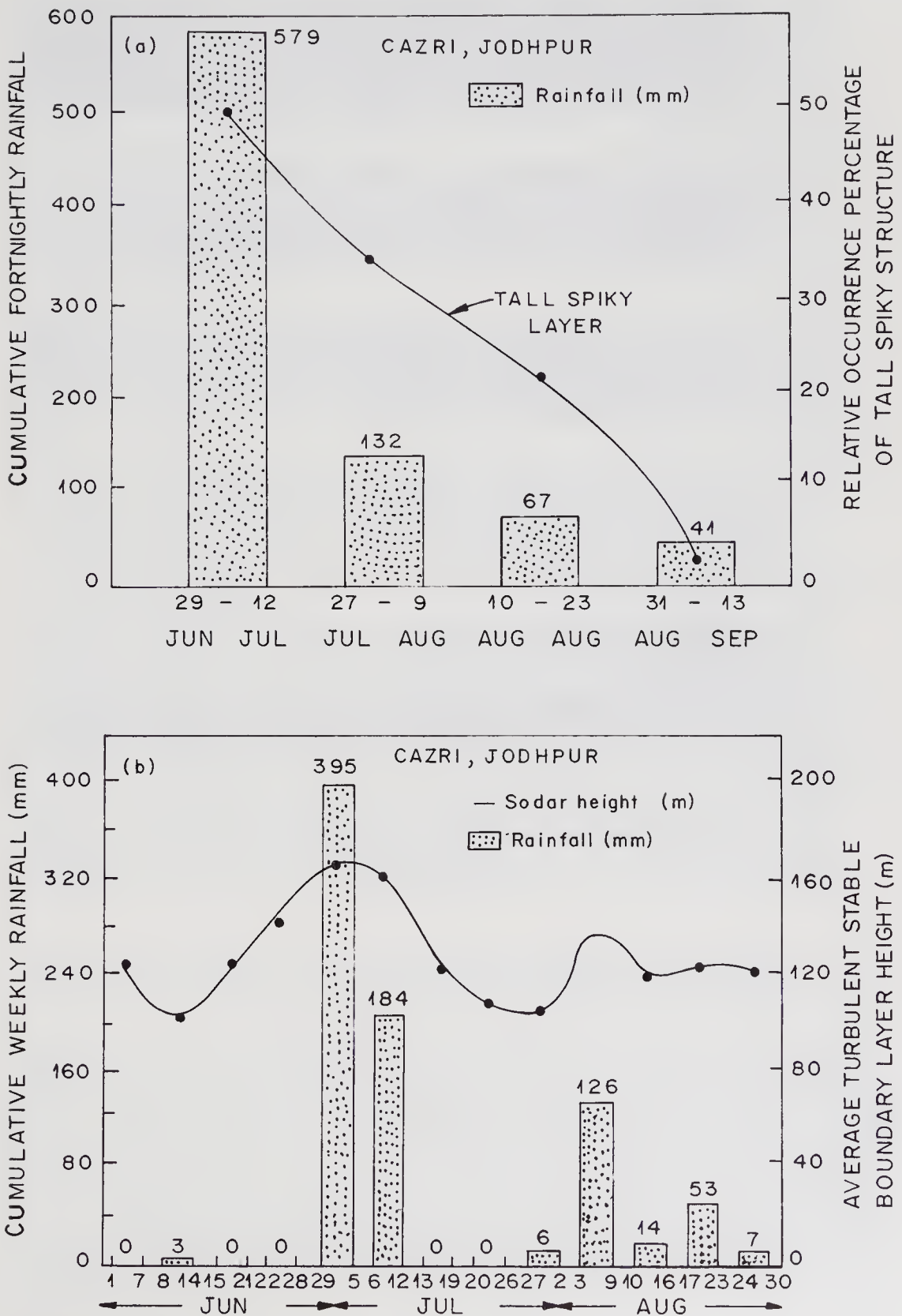


Figure 5. A plot of the cumulative: (a) fortnightly rainfall and relative occurrence of the tall spiky structures, and (b) weekly rainfall in relation to the depth of the turbulent stable boundary layer during the period June to August 1990 at Jodhpur.

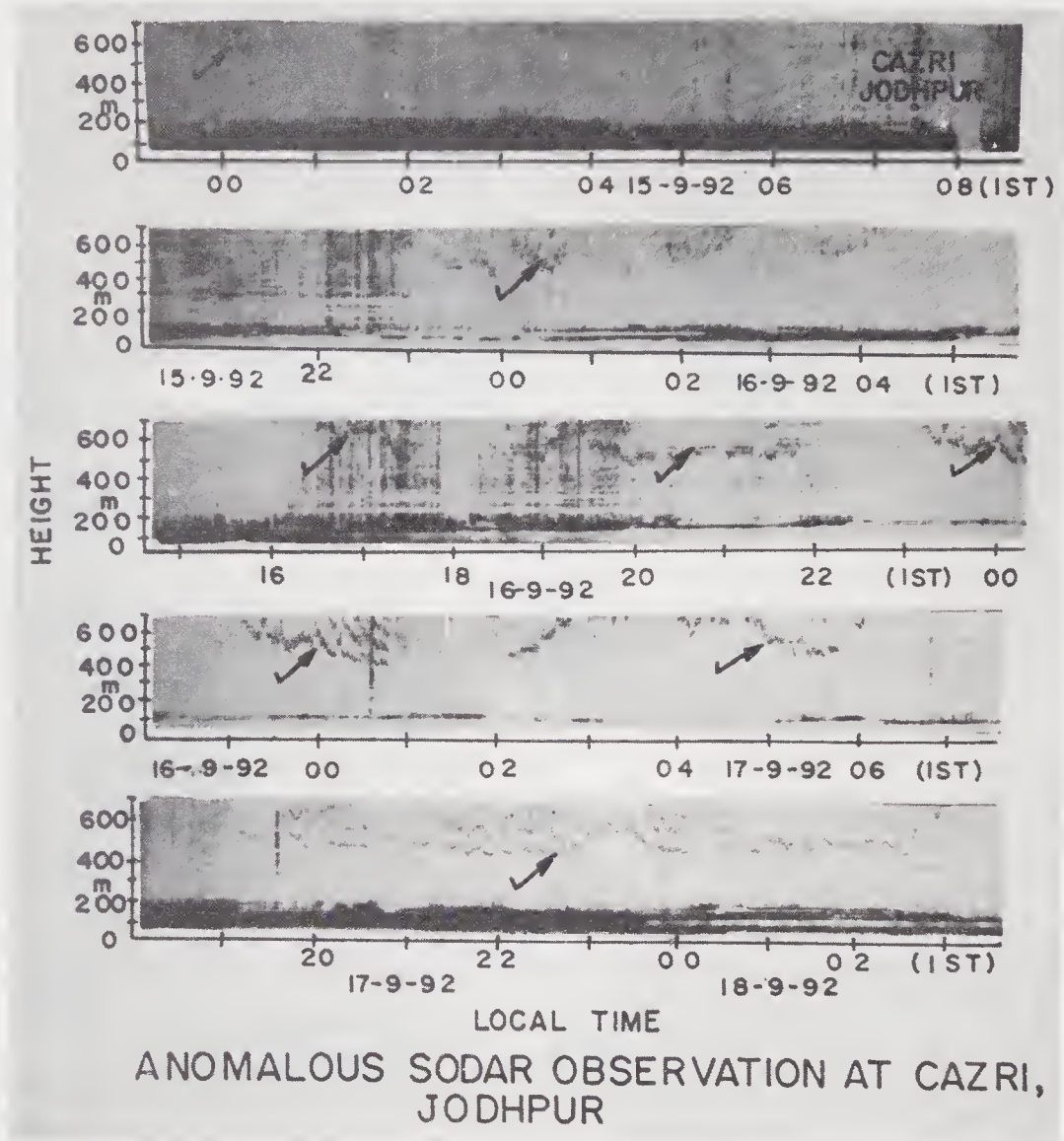


Figure 6. Sodar echograms during the stable period of September 15th–18th, 1992 at Jodhpur. The observed elevated/multilayer structures have been marked to show their distinct characteristic and persistence.

The Richardson number had a value of 12 at 2100 hrs on Sept. 10th, 1992, which decreased to a value of less than 2 on Sept. 14th, and to about 1 on Sept. 15th, a value which it maintained for the next three days (figure 7). At 0300 hrs on Sept. 12th, the Richardson number was more or less equal to zero. On subsequent days it started increasing and attained a value of 7 on Sept. 15th. Further on, it started decreasing and reached a value of about 0.2 on Sept. 17th when it started increasing again.

A look at the weather data shows that a cyclonic circulation lay near Jodhpur during the night of Sept. 14th–15th, 1992, when the weather from the less stable atmosphere at 2100 hrs became more stable in the early hours of the morning as shown by the prevailing Richardson number. The weather was cyclonic up to Sept. 18th, however the moisture content was low. The weather became anticyclonic from Sept. 19th onwards when the shear instability ceased to exist and the withdrawal of the monsoon current was reported by the India Meteorological Department.

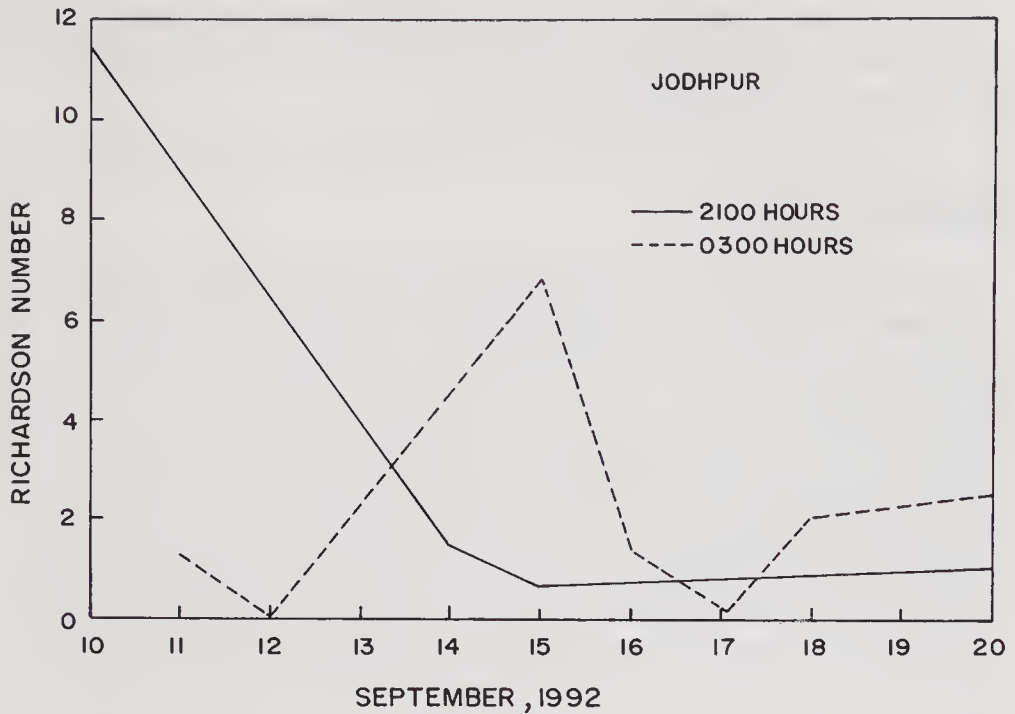


Figure 7. A plot of the Richardson number during Sept. 10th–20th, 1992 at 2100 and 0300 hrs (IST) at Jodhpur.

The elevated/multilayers on the sodar echograms during the period Sept. 15th–18th, 1992 are the reflex images of the subsiding air-mass, while the lower values of the Richardson number (less than or close to the critical value) during Sept. 16th–17th, are responsible for the generation of shear instability/undulations (Gossard and Hooke 1975).

4. Conclusion

It has been seen that sodar provides valuable information about the depth and the nature of the thermal structure of the turbulent atmospheric boundary layer. It has also been seen that a detailed analysis of the sodar echograms vis-a-vis meteorological data can be used as indicators of monsoon characteristics.

The absence or fast disappearance of the morning rising layer indicates that the radiation inversion layer is shallow at Jodhpur. To probe it further, highly resolved boundary layer data within the lowest 100 m of the atmosphere may be useful, an exercise which can be accomplished inexpensively on a continuous real-time framework through the use of acoustic remote sensing Doppler mini sodar system. This device will not only give highly resolved data of the height of the thermal boundary layer from 10m onwards but will also provide wind information in the lower atmosphere.

Acknowledgements

The authors are thankful to the Department of Science and Technology, Govt. of India for financial grant to accomplish the above work in the MONTBLEX programme. The

authors are also thankful to the Director, National Physical Laboratory, New Delhi for permission to publish the above work. One of the authors (NS) gratefully acknowledges the financial support of CSIR, New Delhi.

References

- Brown E H and Hall F F Jr 1978 Advances in atmospheric acoustics; *Rev. Geophys. Space Phys.* **16** 47–110
- Goel Malti and Srivastava H N 1989 MONTBLEX; *Vayu Mandal*, **20** 1–8
- Gossard E E and Hooke W H 1975 *Waves in the Atmosphere*, (New York: Elsevier)
- Singal S P and Gera B S 1982 Acoustic remote sensing of the boundary layer; *Proc. Indian Acad. Sci. (Engg. Sci.)* **5** 131–157
- Singal S P, Gera B S and Aggarwal S K 1985 Studies of the sodar observed dot echo structures; *Atmosphere–Ocean* **23** 304–312
- Singal S P, Gera B S, Pahwa D R and Aggarwal S K 1986 Studies of sodar surface based shear echo structures; *Atmos. Res.* **20**, 125–131
- Singh R S, Ramakrishna Y S, Rao A S, Prabhu A and Vasudev S 1992 Quantification of some weather features in arid surface boundary layer; *Proc. of Workshop on Preliminary Scientific Results of MONTBLEX*, 16th–17th January, 1992, I.I.Sc., Bangalore, pp. 35–43

Thermal and wind structure of the monsoon trough boundary layer

G RAJKUMAR, R NARASIMHA, S P SINGAL* and B S GERA*

Jawaharlal Nehru Centre for Advanced Scientific Research, Bangalore 560064, India

*National Physical Laboratory, New Delhi 110012, India

Abstract. Radiosonde data from Jodhpur, taken at 0530, 1730 and around 1100 hr IST during MONTBLEX 1990, reveal that the distribution of virtual potential temperature θ_v below about 500 hPa has a structure characterized by up to three layers each of approximately constant gradient. We are thus led to introduce a characterization of the observed thermal structure through a sequence of the symbols *N*, *S* and *U*, standing respectively for neutral, stable or unstable conditions in the different layers, beginning with the one closest to the ground. It is found that, of the 29 combinations possible, only the seven classes, *S*, *SS'*, *SNS'*, *NS*, *NSS'*, *USS'* and *UNS* are observed, where *S'* stands for a stable layer with a different gradient of θ_v than in the layer *S*. It is also found that, in 90% of the launches at 0530 hr, 48% of the launches at 1730 hr and 69% of the launches around 1100 hr, the first radiosonde layer near the ground is stable; the classical mixed layer was found in only 11% of the data set analysed, and, if present on other occasions, must have been less than 250 m in height, the first level at which radiosonde data are available. Supplementing the above data, sodar echograms, available during 82% of the time between June and August 1990, suggest a stable layer up to a few tens of metres 48% of the time. A comparative study of the radiosonde data at Ranchi shows that the frequent prevalence of stability near the surface at Jodhpur cannot be attributed entirely to the large scale subsidence known to be characteristic of the Rajasthan area. Further, data at Jodhpur reveal a weak low level jet at heights generally ranging from 400 to 900 m with wind speeds of 6 to 15 m/s. Based on these results, it is conjectured that the lowest layers in the atmosphere during the monsoons, especially with heavy clouding or rain, may frequently be closer to the classical nocturnal boundary layer than to the standard convective mixed layer, although often with shallow plumes that penetrate such a stable layer during daytime.

Keywords. Atmospheric boundary layer; monsoons; thermodynamic structure.

1. Introduction

The classical picture of the convective boundary layer in the lower atmosphere suggests the following pattern (see e.g., Stull 1988). In the lowest hundred meters or less from the surface, in the region called the surface layer, the fluxes and the stresses vary by less than 10% of their value at the surface. A super-adiabatic temperature lapse rate and strong wind shears are not uncommon here. Above this layer is a mixed layer where the turbulence is convectively driven, and heat, moisture and momentum are well mixed. The mixed layer grows with time over the day and reaches its maximum height late afternoon. Usually the top of the mixed layer is a stable inversion layer in which the virtual potential temperature increases with height. This layer acts as a lid to thermals rising from the ground. At this height entrainment into the mixed layer occurs. Towards the evening transition the mixed layer collapses, and at night a stable nocturnal boundary layer develops near the surface.

Previous work on the height of the mixed layer at Indian stations has been largely based on radiosonde data, generally available only at 0000 GMT (0530 IST) and 1200 GMT (1730 IST). The data consist of temperature, dewpoint and wind direction

and speed, at various pressure/height levels. By plotting the virtual potential temperature profile, the boundary layer height is estimated as extending to the base of the capping inversion above the zero gradient region indicating the neutral or well-mixed layer. To define neutrality a threshold gradient is usually set; this value was chosen as 2 K km^{-1} by Parasnis and Goyal (1990) over land, and about 1 K km^{-1} by Holt and Raman (1985) over the oceans. During daytime, when radiosonde data are not available, mixed layer heights were estimated following Holzworth (1962) using the morning 0530 hr radiosonde ascent and the surface temperature data at the given time (e.g., Padmanabhamurty and Mandal 1979). The mixed layer heights so estimated over Indian stations are listed in table 1.

The present work examines the structure of the lower atmosphere especially over the western side of the monsoon trough region, based largely on radiosonde and sodar data. Some studies have also been made of data from Ranchi and Delhi to provide comparisons. Although the accuracy of Indian radiosonde data has sometimes been questioned (e.g., Ananthakrishnan and Soman 1992), it is noted that there has been no suggestion of errors at the low altitudes we are considering here.

Table 1. Mixed layer heights from various studies over Indian stations.

Investigators	Site	Mixed layer height
Gamo <i>et al</i> (1994)	New Delhi	3000 m during premonsoon. 5000 m during monsoon. 2000 m during postmonsoon. < 1000 m during winter season.
Holt and Raman (1987)	MBL over northern Bay of Bengal	400 m to 500 m.
Holt and Raman (1985)	East central Arabian Sea	800 m to 1500 m.
Padmanabhamurty and Mandal (1976)	New Delhi	1000 m (December). 2000 m (March).
Parasnis and Morwal (1994)	Kharagpur	100 m (0600 am). 900 m (1200 pm).
Parasnis and Goyal (1990)	Pune	850 mb (active monsoon). 780 mb (break monsoon).
Raman <i>et al</i> (1990)	Bangalore Delhi Delhi	900 m (convective conditions). 2500–3000 m (maximum). 4700 m (with a weaker inversion at 2500 m).
Raman (1982)	Raichur	2800 m (during NE monsoon).
Kusuma <i>et al</i> (1991)	Monsoon trough region	approximately 500 m and 3000 m during active and break monsoon respectively.

The data used for the study are from radiosondes over Jodhpur (26.18N, 73.08E) taken during MONTBLEX-90. The data are available at intervals of 50 hPa usually and 20–30 hPa during intensive observation periods (IOP). The weather during such periods is summarized in table 2. The data were available up to 200 hPa, but in the present study only data up to 500 hPa are considered. Using these data the virtual potential temperature has been computed using the standard methods (Iribarne and Godson 1973). In analysing these distributions, it has been useful to identify two special weather conditions that we shall call dry and wet situations, defined as follows. A dry situation is said to occur when at least five preceding days go without receiving any rain. When more than 10 mm rainfall occurs each day for two or more days continuously, we term it a ‘wet’ situation. (The soil may be expected to be respectively dry and wet during these situations.) Jodhpur was an ideal station for this study since there were days with all the following situations occurring sometime or other during the season (indeed we had eight samples for each case): (i) days when the wet situation prevailed, (ii) days when the dry situation prevailed, (iii) days when the trough was over the station and (iv) days when it was more than 500 km from the station. The days so selected for analysis are listed in table 3. Jodhpur may of course be considered representative of the western side of the monsoon trough region.

As the radiosonde data are available only at specific hours during the day, the need was felt to supplement the present analysis with an examination of sodar data, which were

Table 2. Weather situation during intensive observation periods.

Period	Weather system
29th June to 3rd July	Monsoon onset phase.
17th July to 22nd July	Weak monsoon in that area.
4th August	Passage of well-marked low across south Rajasthan, organized clouds.
18th August to 20th August	Period of monsoon depressions/low pressure systems.

Table 3. Days selected for analysis as representing various weather situations.

Weather situations	Periods
Heavy rain	July: 2, 3, 4, 5, 6. August: 2, 3, 4, 5, 6 and 20.
No rain	June: 18, 19, 20, 21, 28, 29, 30. July: 26, 27, 28, 29.
Trough very near/ over the station	July: 4, 5, 24. August: 6, 17, 23, 31.
Trough far from station	June: 7, 8, 24, 30. August: 25. September: 2, 10.

available on a virtually continuous mode at Jodhpur. The instrument was a monostatic sodar designed and developed at the National Physical Laboratory (Singal and Gera 1982). Sound pulses of 80 ms duration were sent every 4 s and the backscattered signal, after proper amplification, filtering and detection, was displayed on a facsimile recorder as an 'echogram'. The operating frequency was 2200 Hz and the maximum range was 700 m. In an earlier study of the monsoon boundary layer over Jodhpur (Singal *et al* 1993) the following echo patterns were observed in the echograms recorded by the sodar: shear echo, thermal echo, and multiple/elevated layered structures. During the three months June – August, shear echoes corresponding to a stable layer were seen 46% of the time, thermal echoes corresponding to an unstable layer were seen 36% of the time and 18% of the time no echoes were received. However this analysis was not segregated into the different weather situations mentioned above and no direct correlation with radiosonde data was attempted. We have therefore re-examined the data again in detail.

2. Method of analysis

In general our experience has been that the classical mixed layer (convective boundary layer capped by an inversion) is not often revealed by radiosonde ascents at a place like Jodhpur. To demonstrate that there are such cases, figure 1 shows one instance at 1100 hr on 18th August 1990 over Jodhpur where a mixed layer, with constant virtual potential temperature, is observed up to a height of about 900 hPa. Also shown in figure 1 are data from a Kyttoon ascent at Kharagpur (1700 hr, 3rd June 1990), showing a mixed layer (height ~ 450 m) with an overlying stable layer.

However, while mixed layers like those in figure 1 are rare, an extensive examination of the available radiosonde data at Jodhpur shows that the distribution of virtual potential temperature can almost always be characterized as consisting of up to three layers of approximately constant gradient in each layer (figure 2). In all of the charts in figure 2, the first point in the profile is the surface air temperature at screen height. As the second point from the radiosonde (i.e., the first above screen height) is usually at a height of 950 hPa, it is of course not possible to resolve a mixed layer that is shallower than this height. Nevertheless, it is clear from the profiles shown in figure 2 that the

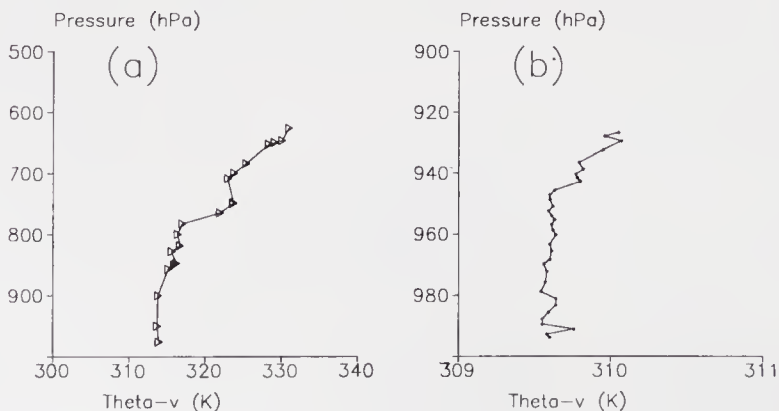


Figure 1. Virtual potential temperature profiles showing mixed layer heights on (a) 1100 hr, 18th August 1990 at Jodhpur using radiosonde data, (b) 1700 hr, 3rd June 1990 at Kharagpur, using Kyttoon data.

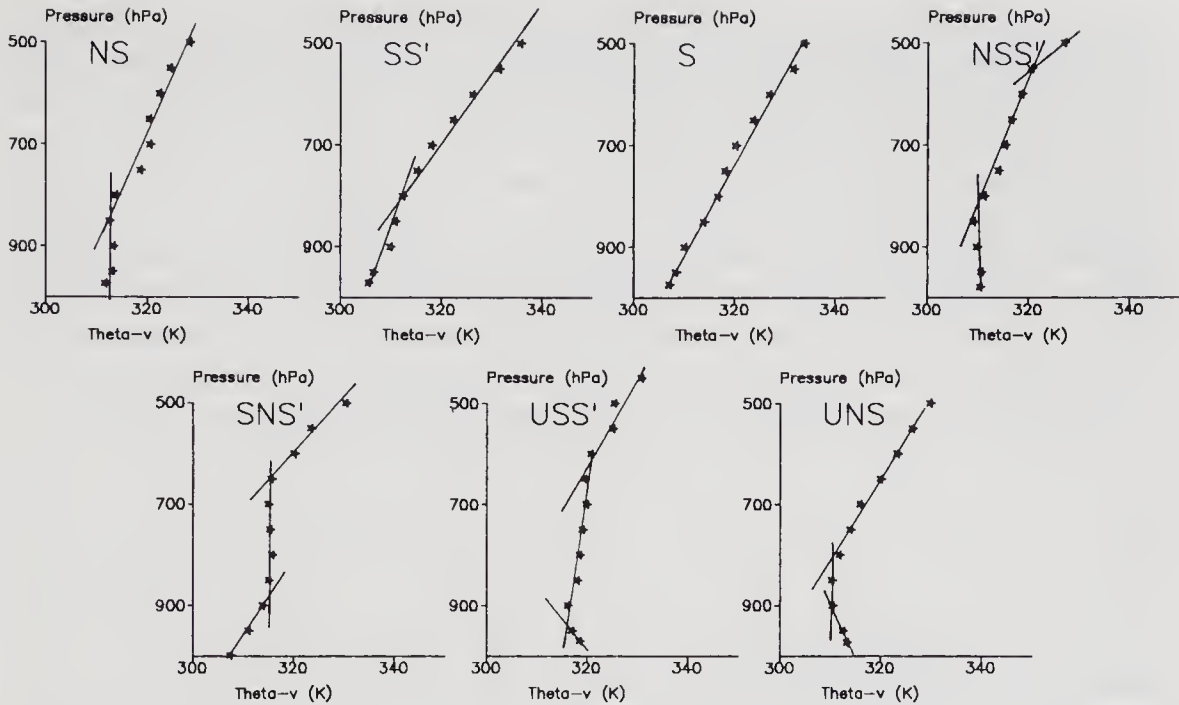


Figure 2. Seven types of virtual potential temperature profile observed over Jodhpur during 1990. Clockwise from top left: 1700 hr, 28th July; 1730 hr, 5th August; 1730 hr, 6th August; 1730 hr, 10th September; 1730 hr, 4th August; 1730 hr, 19th June; 1730 hr, 23rd August.

simplest way to describe the thermal structure of the lower troposphere (up to 500 hPa) is that it consists of up to three layers in each of which the gradient of the virtual potential temperature θ_v is approximately constant (to within 2 K km^{-1}). We may designate each such structure by a set of three symbols S , N , U , standing respectively for stable, neutral and unstable conditions; if there is more than one layer belonging to the same stability category but with a distinctly different potential temperature gradient, we denote it by a primed symbol (thus SS' denotes two stable layers with different θ_v gradients). A major finding of the analysis is that all the available data can be classified into one of the seven types shown in figure 2. In the system of classification proposed here, these types are designated as S , SS' , SNS' , NS , NSS' , USS' and UNS ; the symbols are arranged in the order of their occurrence with increasing height from the surface. Of a total of 29 combinations possible, as many as 22 (namely $SS'S''$, $SS'N$, $SS'U$, SN , SNU , SU , SUS' , SUN , SUU' , N , NSN' , NSU , U , US , USN , USU' , UN , UNU' , UU' , $UU'S$, $UU'N$, and $UU'U''$) were not seen in the data examined here. (We are of course not in a position to assert that these structures are not possible, but they certainly seem rare during the monsoons.)

In this study we look at the first two layers from the surface. A probability distribution of their occurrence is computed during wet and dry situations, as well as when the trough is either over the station or away from it. The wind velocity has also been plotted during the various situations.

Also the sodar echograms taken in Jodhpur have been examined in detail to derive information about stability (Singal *et al* 1983; Singal 1990), since within its limited range (700 m), the resolution of the sodar is much better than that of the radiosonde. At any given time, one of the following structures could be observed: (i) stable, (ii) neutral,

(iii) plumes, (iv) elevated stable layers, (v) rain or (vi) dust. For each day a chart was then prepared, indicating the echogram type at different times of day; a sample is shown in figure 3. The symbol 'na' (not available) indicates periods when the data were not available or the echoes were not legible.

An attempt was then made to identify the stability class appropriate to each echogram. This subject has received considerable attention in the literature. Singal (1989, 1993) describes efforts made to associate an appropriate Pasquill stability class with the echogram type. It turns out however that such a scheme correlates with tower data only about 50% of the time. On the other hand, a less elaborate classification into just three types, namely stable, neutral and unstable, produces excellent correlation between sodar and tower data. We have therefore opted for this simple scheme.

In general, thermal plumes indicate the presence of an unstable layer; surface based shear echoes a stable layer; and no echoes a possible neutral layer. There was hardly any observation of neutral echoes at Jodhpur. Among the other types of echoes observed were the elevated stable layer and waves, both of which could be clearly seen on the echograms. They represent stable layers. There is some ambiguity in interpreting dot echoes from an echogram alone, but it probably represents water vapour clusters (Singal *et al* 1985). The presence of continuous echoes in the echograms, from top to bottom of the chart, usually indicates drizzle or rain, since the scattering of sound waves by the water droplets would extend throughout the scanned area. On most such

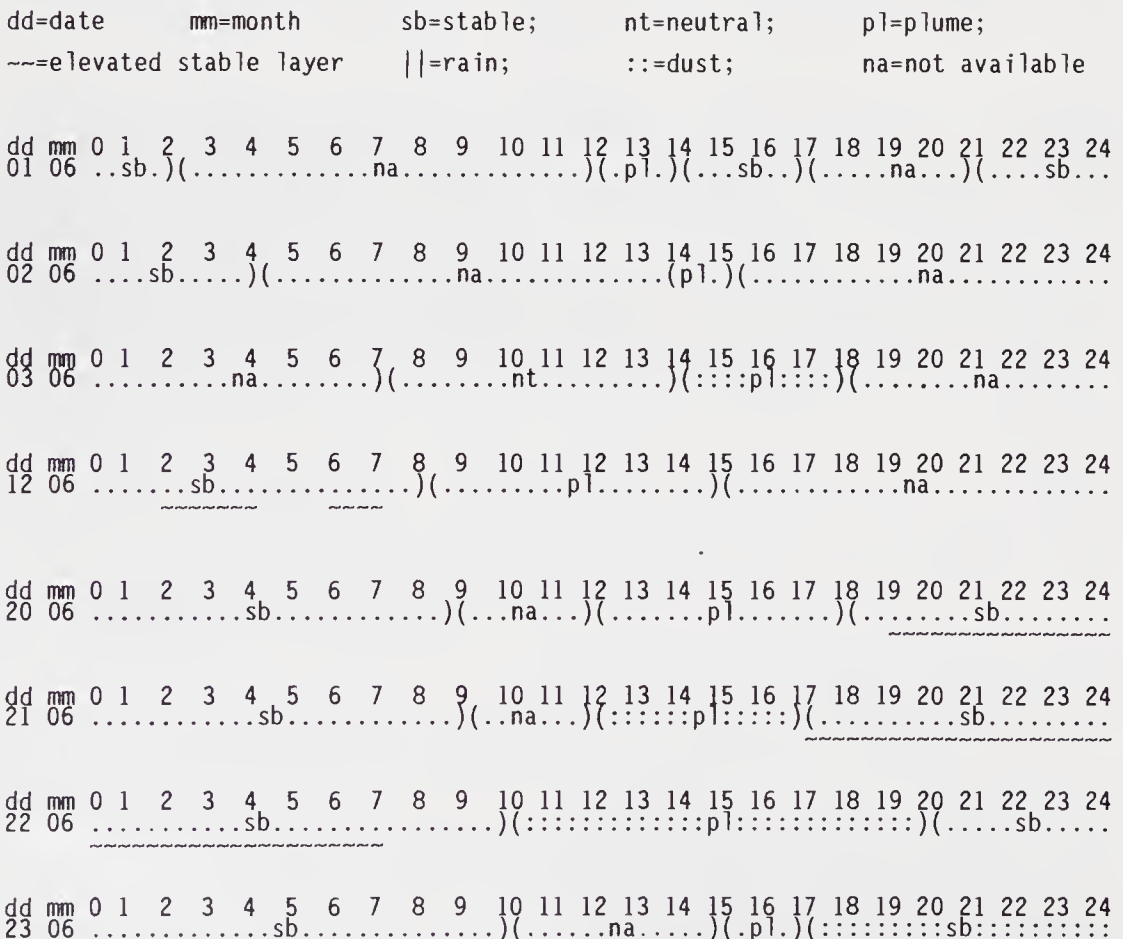


Figure 3. A sample representing identification of echogram types during different times of day.

occasions (e.g., 3rd, 15th, 21st–23rd June), plumes can be clearly seen almost immediately after the cessation of the continuous rain-like echoes. These occasions are therefore classified as unstable. However on 4th and 6th June continuous rain-like echoes were seen but with no plumes; furthermore the Indian Daily Weather Report does not mention any rain at Jodhpur on those days. On the other hand the weather summary prepared by the MONTBLEX team on site (Rudra Kumar *et al* 1991) recorded the occurrence of a sand storm. Since the presence of denser particles suspended in the atmosphere tends to have a stabilizing effect on the flow (Wamser and Lykossov 1995), such instances have been classified as stable.

Using the interpretations described above, we have classified all available data into one of three conditions, stable (*S*), neutral (*N*) or unstable (*U*), at any given time.

4. Results and discussion

4.1 Radiosonde data

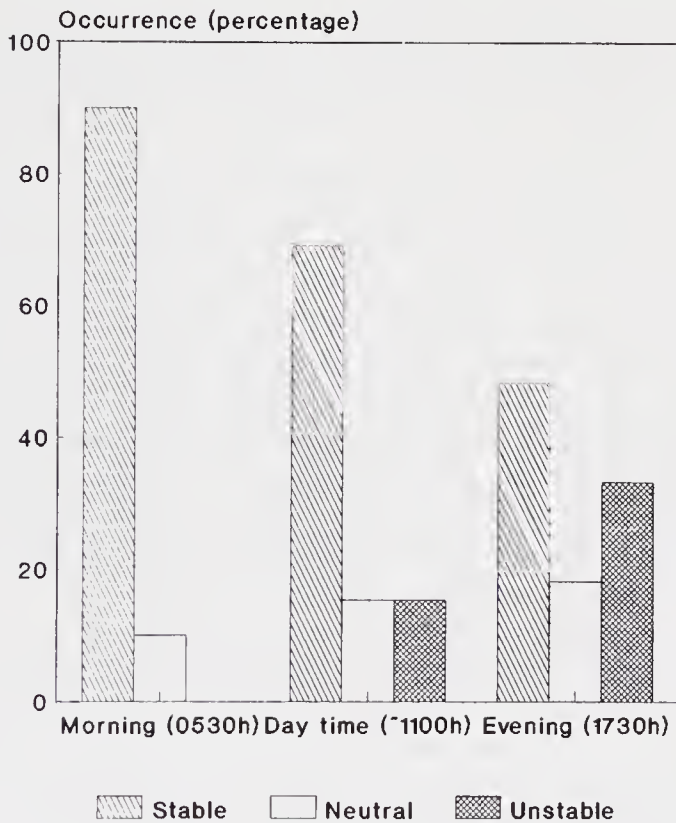
The results obtained during the different weather situations mentioned in section 2 are listed in table 4. Among the days when dry and wet situations prevailed, the frequency of occurrence of the various stability classes in the first two layers of the lower atmosphere is examined. When it was wet both layers were stable during morning 0530 hr and evening 1730 hr, whereas around noon the layer close to the surface was stable and the layer above that was neutral (*SN*). During dry situations in the morning the lowest layer is usually stable, and the layer above that is either stable or neutral (*SS'* or *SN*). In the evenings it is usually unstable or neutral capped by a neutral or stable layer (*US* or *NS*). Around noon the lowest layer was again stable but the layer above that is often neutral (*SN*). Unfortunately data were available only for 13 days during daytime, and this might at first seem to be a biased sample, as the daytime radiosonde launches occurred only during IOPs. However, as the IOP were determined based on weather towards the eastern region of the monsoon trough, the weather at Jodhpur was often undisturbed on these days; in fact on 9 of these 13 days, there was no rain. We believe that the results presented here do therefore indicate the general trend, but clearly more data and analysis are required to draw firm conclusions.

The thermal structure has also been examined when the trough was over the station and when it was away by more than 500 km. As can be seen from table 4, no clear pattern seems to emerge. When the trough is over the station, during the mornings the first layer from the surface is usually stable and the second neutral or stable; during the evenings all the stability classifications are observed in the first layer, whereas it is mostly stable in the second layer. When the trough is far away, the first layer is again stable during the mornings in most of the cases studied, whereas in the evenings the second layer is neutral or stable even though the first layer can be unstable, neutral or stable.

To summarize, it appears as if, irrespective of the weather situation being wet or dry, and the monsoon trough being over the station or far away from it, the lowest layer is almost always stable. Considering the data from 76 radiosonde launches which includes all the weather situations mentioned before, the lowest layer of constant gradient from the surface is stable 90% of the time in the morning at 0530 hr, 69% during daytime (around 1100 hr) and 48% during the evenings at 1730 hr (figure 4).

Table 4. Stability classes of the first two layers of constant gradient during various weather situations using radiosonde data over Jodhpur.

Weather	Time of radiosonde flight	Stability classes				
		<i>US</i>	<i>NS</i>	<i>SN</i>	<i>SS'</i>	<i>S</i>
Dry situation	0530		1	5	3	1
	1730	5	3	1	1	
Wet situation	0530		1	2	4	2
	1730	1	1	2	4	2
Trough over Jodhpur	0530		1	2	3	1
	1730	2	1	1	2	1
Trough far from Jodhpur	0530		1	4	3	4
	1730	2	3	3		

**Figure 4.** Percentage occurrence of the different types of stability of the lowest layer of constant gradient from the surface in Jodhpur.

Mixed layers have been observed at Jodhpur only during 11% of the time, and when observed they have a depth between 400 and 900 m.

The general prevalence of a stable layer near the ground at Jodhpur may at first appear to be related to the large-scale subsidence of air characteristic of the northwest of India (see e.g., Das 1962; Rao 1976, pp. 86–88). To ascertain whether the stable layer

over Jodhpur is due to this subsidence, data over Ranchi, (23·21N, 85·20E) a station much further to the east where mild convergence is believed to occur at the surface, are considered. Ranchi has the advantage of being an elevated region (606 m above mean sea level), and would be free from the effects of other advective flows such as the sea breeze that may affect stations not so well inland. Here again, using radiosonde data, virtual potential temperature profiles are plotted. The stability of the first layer of constant gradient is noted. Frequency distributions of different stability conditions are derived at 0530, 1100 and 1730 hr. As can be seen from figure 5, the frequency of stable conditions in the lowest layer was 85% in the morning, 60% around noon, and 80% during the evening. These results over Ranchi strengthen the observations from Jodhpur that during the monsoon season a stable layer near the surface is observed more often than was expected.

A similar analysis at Delhi shows that the frequency of a stable first layer is 95·8%, 26·3% and 52·2% at 0530, 1100 and 1730 hr respectively.

Typical profiles of wind speed and direction observed at Jodhpur at 0530 and 1730 hr are shown in figures 6 and 7 respectively. It is seen that there is a maximum in the wind speed at around 950–850 hPa level, and that there is a change in wind direction by only ± 20 degrees as wind speed changes from about 12 to 5 m/s through the maximum. Judging by the criteria used by Joseph and Raman (1966) this is a low level jet, although relatively weak as wind speeds are generally lower than 15 m/s. More specifically, the low level jet has the following characteristics. The jet axis is at heights varying from 950 to 850 hPa during a dry situation, and the maximum velocity varies from 6 m/s to

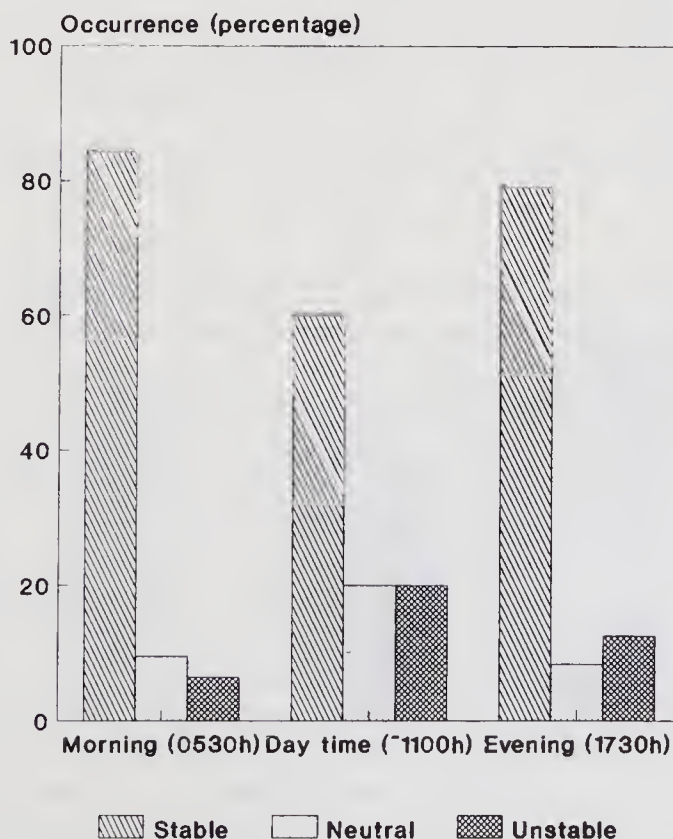


Figure 5. Percentage occurrence of the different types of stability of the lowest layer of constant gradient from the surface in Ranchi.

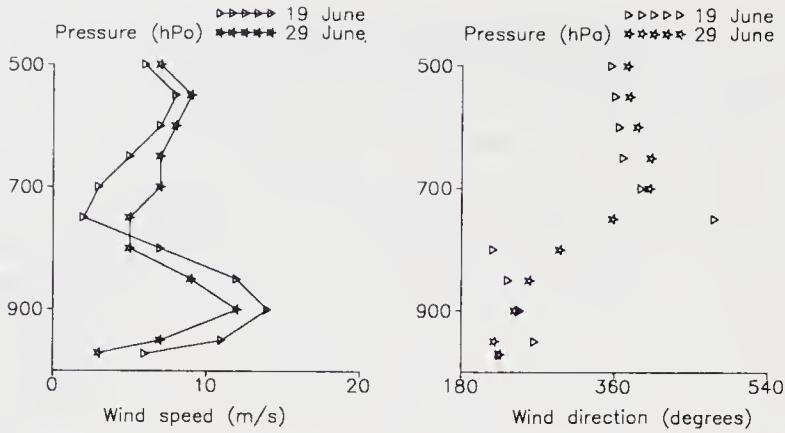


Figure 6. Typical profiles of wind speed and direction at 0530 hr over Jodhpur, during 1990.

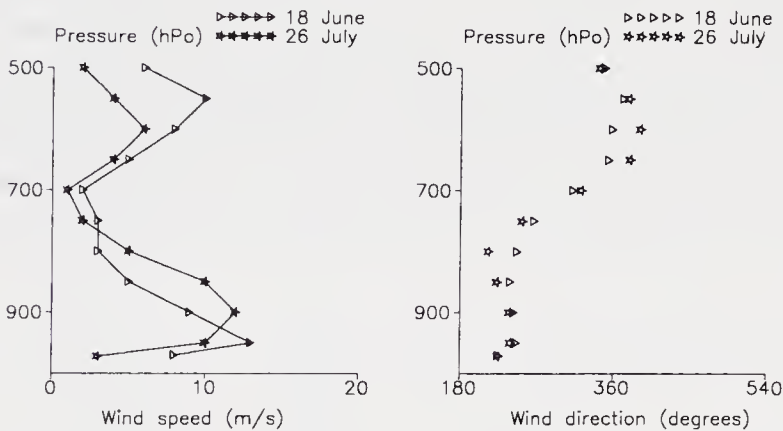


Figure 7. Typical profiles of wind speed and direction at 1730 hr over Jodhpur, during 1990.

15 m/s. But during wet situations the jet is found to be better organized; its axis is around the 950 hPa level, and the velocities are between 4 and 8 m/s both morning and evening (figures 8a and b). It is well known that a low level jet occurs over peninsular India during the monsoons (Joseph and Raman 1966; Rao 1976), as an extension of the Findlater jet (Findlater 1969) over the Arabian Sea; this jet, usually located around 15°N , is generally observed at central and southern stations south of 20°N . Although the presence of such a jet at latitudes beyond 20°N does not appear to have been studied, it is possible to interpret the data, such as from figure 3 in Sikka and Narasimha (1995), as indicating a westerly jet over Jodhpur, especially during a break in the monsoon. There was no classical 'break' in 1990 (Srivastav 1995); at any rate it is generally considered that at the latitude of Jodhpur such a jet, even if present, will be weak. At higher altitudes, the wind over Jodhpur changes direction, from approximately southwesterly to northeasterly, with a very weak wind maximum of 5–10 m/s. It is essential to study whether these characteristics of the wind seen at Jodhpur are local or extend over a wider region. While this question is outside the scope of the present paper, it appears that, in the light of the present observations, the low level jet of figure 8 could be different from the well-known low level jet over the peninsula.

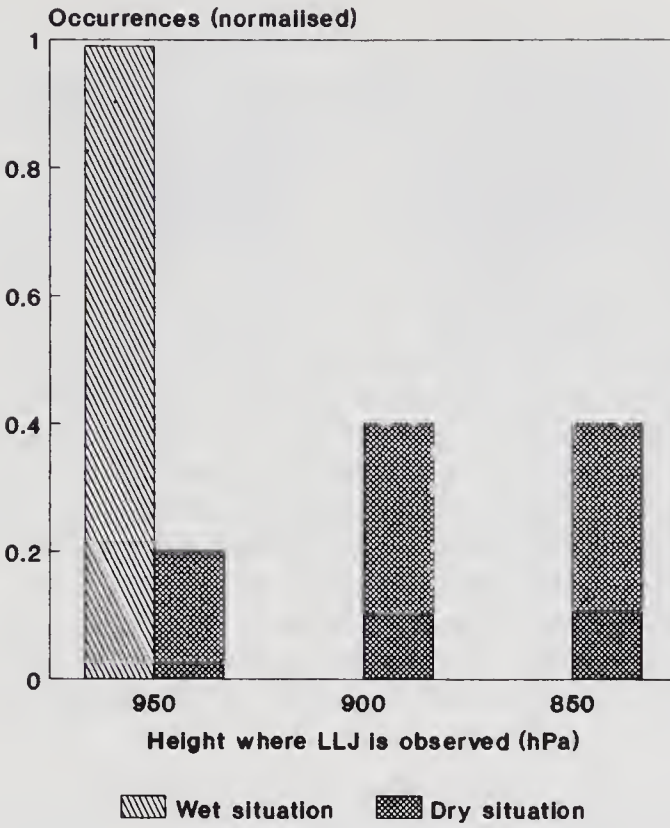


Figure 8(a). Height of low level jet during wet and dry situations.

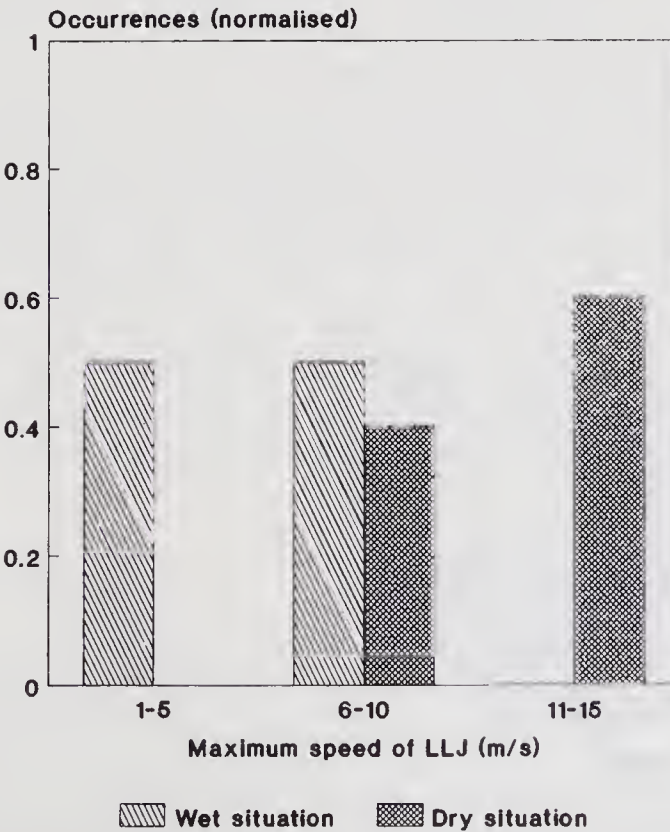


Figure 8(b). Maximum wind speed in the low level jet during wet and dry situations.

4.2 Sodar data

The echograms for the month of June, July and August 1990 have been examined using methods following Shaw (1974), Brown and Hall (1978) and Singal (1990) for the various structures mentioned elsewhere. Two distinct time intervals were considered: (i) 1000 to 1600 hr, when usually thermal plumes are expected, and (ii) times other than (i) i.e., from 1600 to 1000 hr when stable, neutral and even unstable conditions can be expected. The situation considering the whole day from 0000 to 2400 hr is also examined. Table 5 shows the frequency of occurrence of stable and unstable conditions for the above time periods during the individual months June, July and August 1990, and also during the whole season from June to August. Figure 9 shows an analysis of the data (considering the whole day) for the entire period June to August 1990. An analysis based on the weather situation indicates that, during wet-situation days 74% of the available data shows the region near the surface to be stable. Even when the situation is dry and less than half the sky is covered with cloud, as much as 60% of the data available shows stable stratification (figure 10).

Considering the entire monsoon season in the year 1990, stable layers occurred during 48.3% of the time according to the sodar data, whereas the radiosonde data (from all daytime launches during a variety of weather situations listed in section 2),

Table 5. Frequency of occurrence of various stability situations during different time periods over Jodhpur as observed from SODAR echograms (*S* – stable; *U* – unstable; *NA* – data not available).

Time period	10–16 hours			00–10 hours and 16–24 hours			00–24 hours		
	<i>S</i>	<i>U</i>	<i>NA</i>	<i>S</i>	<i>U</i>	<i>NA</i>	<i>S</i>	<i>U</i>	<i>NA</i>
June	7.2	57.8	35.0	56.5	10.6	32.9	40.1	26.3	33.5
July	9.1	81.2	9.7	76.9	16.9	6.2	54.3	38.3	7.4
August	9.1	76.3	14.5	71.1	16.5	12.5	50.4	36.4	13.3
June to August	8.5	71.9	19.6	68.3	14.7	17.0	48.3	33.8	17.8

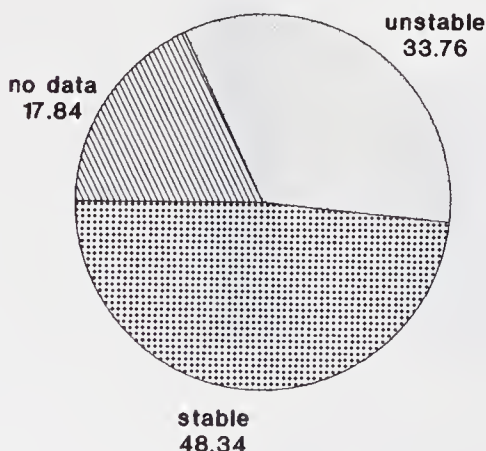


Figure 9. Stability classifications using echograms, monthwise and for the entire period (June–August, 1990) over Jodhpur.

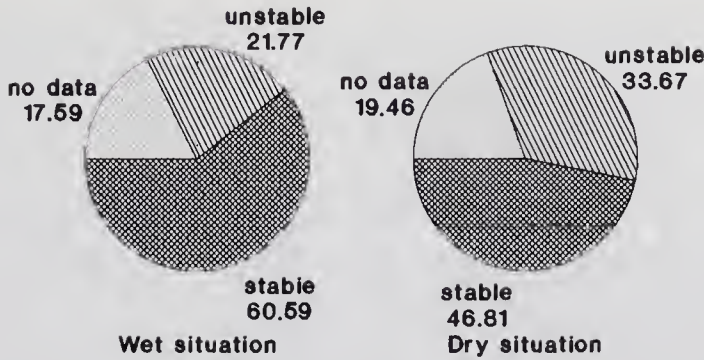


Figure 10. Stability shown by the echograms for wet and dry situations.

indicated a stable layer during a larger percentage (66%) of the time. In order to examine this difference, θ_v profiles from radiosonde data and the sodar echograms both taken at the same time have been compared in detail for two cases. Figures 11(a and b) show the sodar echogram and θ_v profile at 1235 hr on 17th July 1990 over Jodhpur. The θ_v profile belongs to the *SN* class, and shows the lower atmosphere to be stable up to 250 m and neutrally stable from 250 to 1200 m above the surface. Data are not available between screen height (1.2 m) and 250 m, so the presence of an unstable layer below 250 m cannot be ruled out. Plumes are seen on the echogram up to nearly 400 m. At 1135 hr during 20th July 1990 (figure 12b), the θ_v profile (again *SN*) shows the lower atmosphere to be stable up to 720 m (900 hPa) and neutral above. At the same time the sodar echograms (figure 12a) show the presence of plumes up to 200 m. Although it is difficult to draw firm conclusions without knowing the temperature distribution below the first level of observation provided by the radiosonde, figure 12 provides some indication that, even if plumes are present in the echogram, the lower atmosphere appears stable from the radiosonde data. A possible explanation is the following. During daytime the ground temperature can go very high, up to 5 to 10° warmer than the temperature at screen height at Jodhpur. This temperature gradient, which is up to two orders of magnitude higher than that elsewhere in the lower atmosphere, can initiate strong plumes. From figures 11(a) and 12(a) it seems that such plumes will penetrate into a possibly stable layer above, to a height that depends on the intensity of the plume and the stability of the overlying layer. The presence of plumes underneath a statically stable layer suggests that the height of plumes cannot be unambiguously converted into the height of a mixed layer, as the latter may be shallow in spite of indications of some buoyant transport above it by sodar echograms.

5. Conclusions

The structure of the lower atmosphere over Jodhpur has been studied using radiosonde and sodar data. Depending on the rainfall over the station dry and wet situations are defined. When the situation was wet the atmosphere was predominantly stable during mornings and evenings; whereas during afternoons there is often a stable layer underneath a neutral layer. During a dry situation the picture is almost the same during mornings, in the first layer from surface; during evenings it is neutral or unstable in both the layers, and during afternoons the second layer above the ground is usually

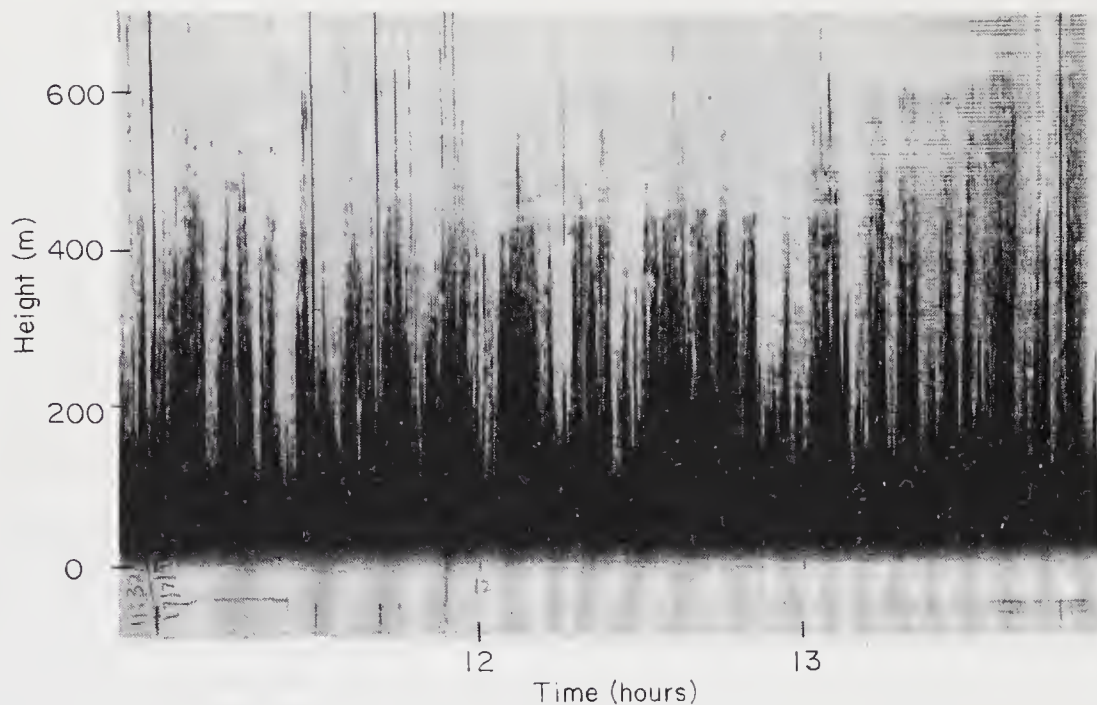


Figure 11(a). Echograms showing plumes on 17th July 1990 over Jodhpur.

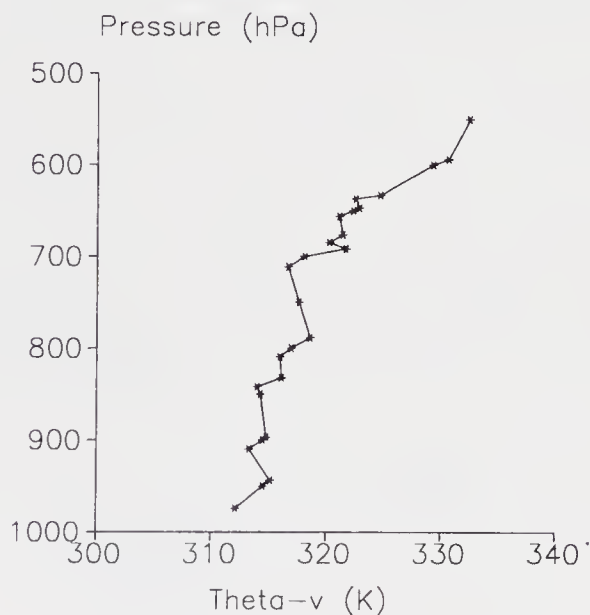


Figure 11(b). Virtual potential temperature profile at 1235 hr, 17th July 1990 over Jodhpur showing stable layer up to 250 m.

neutral.

The classical mixed layer was rarely found; given that the available radiosonde data have a resolution of only 50 hPa it is possible that a mixed layer existed within the first reported level of radiosonde data, implying that, if present, it must generally be shallow (less than 250 m). Occasionally, however, the mixed layer was found to extend up to 900 m at noon.

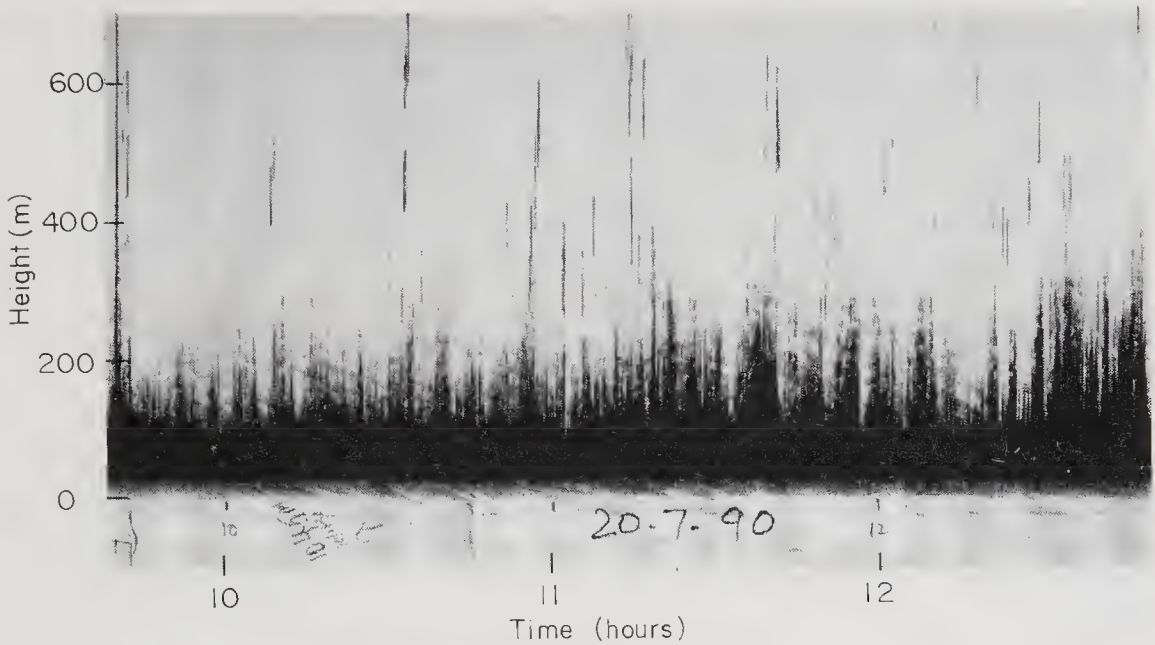


Figure 12(a). Echograms showing shallow plumes on 20th July 1990 over Jodhpur.

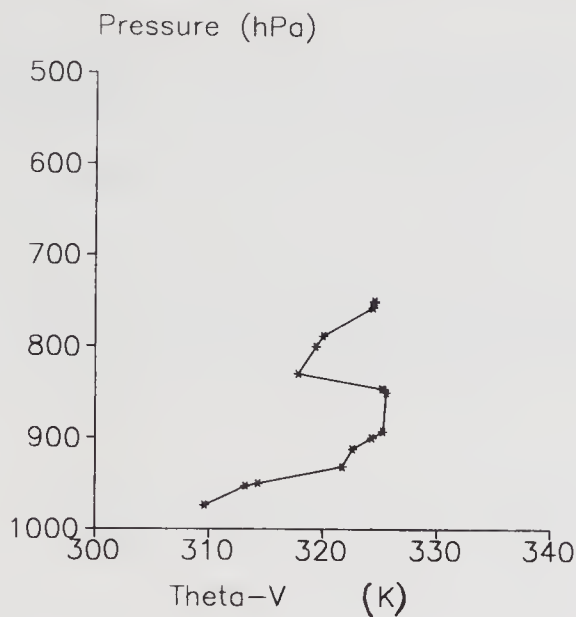


Figure 12(b). Virtual potential temperature profile at 1135 hr, 20th July 1990 over Jodhpur showing stable layer near the surface.

A low level jet is observed at Jodhpur even though the latitude is north of 26°N , to be compared with the Findlater jet which is generally considered to occur mostly south of 20°N . During dry situations the jet was stronger, and occurred at a height varying from 950 to 850 hPa.

A detailed examination of sodar records showed that, during wet situations, the lowest layer was stable nearly 75% of the time; even on dry situations without cloud, it is most often stable. A critical comparison with radiosonde data shows the presence of plumes even when the lowest radiosonde layer indicates stability. It is conjectured that the high

temperature gradients very near the surface (100 times that of rest of the boundary layer) can give rise to shallow plumes which penetrate an otherwise stable layer above.

Thus the presence of stable conditions most of the time in the lower most part of the atmosphere (first layer of constant gradient), as inferred from radiosonde and sodar data, and of the low level jet, suggests that the typical monsoonal boundary layer may be closer to a nocturnal boundary layer rather than to the classical well-mixed layer, especially when the ground is wet and the sky is overcast.

Acknowledgements

This work is supported by a grant from the Department of Science and Technology. We are grateful to Dr. D R Sikka for illuminating comments on an earlier draft of this paper. We also thank Ms. Shweta Nagi, Summer Research Fellow at JNC from Miranda House, Delhi, for assistance in radiosonde data reduction for Ranchi and Delhi

References

- Ananthkrishnan R and Soman M K 1992 Inconsistencies in the mean fields of temperature, geopotential height and winds over the Indian aerological network during July – August; *Mausam* **43** 199–204
- Brown E H and Hall F F Jr. 1978 Advances in atmospheric acoustics; *Rev. Geophys. Space Phys.* **16** 47–110
- Das P K 1962 Mean vertical motion and non-adiabatic heat sources over India during the monsoon; *Tellus* **14** 212–220
- Findlater J 1969 A major low level air current near the Indian Ocean during the northern summer; *Q. J. R. Meteorol. Soc.* **95** 362–280
- Gamo M, Goyal P, Manjukumari, Mohanty U C and Singh M P 1994 Mixed layer characteristics as related to the monsoon climate of New Delhi, India; *Boundary-Layer Meteorol.* **67** 213–227
- Holt T and Raman S S 1978 A comparison of the significant features of the marine boundary layers over the east central Arabian Sea and the north Central Bay of Bengal during MONEX-79; *Mausam* **38** 171–176
- Holt T and Raman S S 1985 Aircraft and ship observations of the mean structure of the marine boundary layer over Arabian Sea during MONEX-79; *Boundary-Layer Meteorol.* **33** 259–282
- Holzworth G C 1962 A study of air pollution potential for western United States; *J. Appl. Meteorol.* **1** 366–382
- Iribarne J V and Godson W L 1973 Atmospheric Thermodynamics; *Geophysics and Astrophysics Monographs* **6** pp. 222
- Joseph P V and Raman P L 1966 Existence of low level westerly jet stream over peninsular India during July; *Indian J. Meteorol. Geophys.* **17** 407–410
- Kusuma G R, Raman S S and Prabhu A 1991 Boundary-layer heights over the monsoon trough region during active and break phases; *Boundary-Layer Meteorol.* **57** 129–138
- Padmanabhamurty B and Mandal B B 1976 A note on pollution potential at Delhi during October 1975 – March 1976; *Vayu Mandal* **6** 58–60
- Padmanabhamurty B and Mandal B B 1979 Climatology of inversions, mixing depths and ventilation coefficients at Delhi; *Mausam* **30** 473–478
- Parasnis S S and Goyal S B 1990 Thermodynamic features of the atmospheric boundary layer during the summer monsoon; *Atmos. Environ.* **A24** 743–752
- Parasnis S S and Morwal S B 1994 A convectively-driven boundary layer in the monsoon trough; *Boundary-Layer Meteorol.* **71** 197–204
- Raman S S 1982 Dynamics of the atmospheric boundary layer during the 1980 total solar eclipse; *Proc. Indian National Sci. Academy* **A48** 187–195

- Raman S S, Templeman B, Templeman S, Holt T, Murthy A B, Singh M P, Agarwaal P, Nigam S, Prabhu A and Ameenulla S 1990 Structure of the Indian southwesterly premonsoon and monsoon boundary layers observations and numerical simulations; *Atmos. Environ.* **A24** 723–734
- Rao Y P 1976 Southwest monsoon; *Meteorological Monograph, Synoptic meteorology* 1/1976 Indian Meteorological Department pp. 367
- Rudra Kumar S, Srinivasan H P, Satyadev H N, Ameenulla S and Prabhu A 1991 Surface data from MONTBLEX-90; *Report no. 91MD2*, Centre for Atmospheric Sciences, Indian Institute of Science, Bangalore 560012, India
- Shaw N A 1974 Observations of atmospheric structure using an acoustic sounder; ANL/RER/75-2 *Radiological and Environmental Research Division*, Argonne National Laboratory, IL 60439, USA, pp. 37
- Sikka D R and Narasimha R 1995 Genesis of the monsoon trough boundary layer experiment (MONTBLEX); *Proc. Indian Acad. Sci. (Earth Planet. Sci.)* **104** 157–187
- Singal S P 1989 Acoustic sounding stability studies; *Encyclopedia of environment control technology: Air pollution control* (ed) Cheremissinoff (Houston (Texas): Gulf Publishing) **2** 1003–1061
- Singal S P 1990 Need for acoustic sounding (SODAR) monitoring of the atmospheric boundary layer for environmental pollution management, in environmental planning and management in India; *New world environment series*, (New Delhi: Ashish Publishing House) **1** 77–105
- Singal S P 1993 Monitoring air pollution related meteorology using SODAR; *Appl. Phys. B (Photo and Laser Chemistry)* **57** 65–82
- Singal S P and Gera B S 1982 Acoustic remote sensing of the boundary layer; *Proc. Indian Acad. Sci. (Engg. Section)* **5** 131–157
- Singal S P, Gera B S and Aggarwal S K 1983 Studies of the boundary layer at Delhi using sodar; *Proc. 2nd Int. Symp. on Acoustic Remote Sensing of the Atmosphere and Oceans*, Rome, Italy, 29th August – 1st September **xiii** 1–8
- Singal S P, Gera B S and Aggarwal S K 1985 Studies of sodar-observed dot echo structures; *Atmosphere-Ocean* **23** 304–312
- Singal S P, Lewthwaite E W D and Wratt D S 1989 Estimating atmospheric stability from monostatic acoustic sounder records; *Atmos. Environ.* **23** 2079–2089
- Singal S P, Gera B S and Ojha V K 1993 Sodar studies of the monsoon trough boundary layer at Jodhpur (India); *Mausam* **44** 9–14
- Srivastav S K 1995 Synoptic meteorological observations and weather conditions during MONTBLEX-90; *Proc. Indian Acad. Sci. (Earth Planet. Sci.)* **104** 189–220
- Stull R B 1988 An introduction to boundary layer meteorology, Kluwer Academic Publishers, pp. 666
- Wamser C and Lykossov V N 1995 On the friction velocity during blowing snow; *Beitr. Phys. Atmosph.* **68** 85–94

A study of turbulent characteristics of atmospheric boundary layer over monsoon trough region using Kytoon and Doppler sodar

K G VERNEKAR, M N PATIL and B S MURTHY

Indian Institute of Tropical Meteorology, Pune 411 008, India.

Abstract. As a part of the MONTBLEX-90 observational programme, Kytoon and Doppler sodar observations were taken at Kharagpur. These data are analysed to study the turbulent characteristics of the atmospheric boundary layer in terms of stability, temperature structure function (C_T^2) and velocity structure function (C_V^2). C_T^2 follows a $Z^{-4/3}$ law on most of the days, whereas the variation of C_V^2 is not systematic. C_V^2 and C_T^2 values are found to vary between 10^{-5} – $10^{-1} \text{ m}^{4/3} \text{ s}^{-2}$ and 10^{-5} – $10^{-2} \text{ }^\circ\text{C}^2 \text{ m}^{-2/3}$ respectively.

Keywords. Temperature structure parameter (C_T^2); velocity structure parameter (C_V^2); turbulent dissipation (ϵ); mixing ratio.

1. Introduction

During the main phase of the Monsoon Trough Boundary Layer Experiment 1990 (MONTBLEX-90) a Doppler sodar manufactured by M/s Aerovironment, USA, Model 2000, was operated at Kharagpur during May–September 1990. The Doppler sodar measures all the three components (u, v, w) of wind in the height range of 45–1050 m. Along with Doppler sodar, a Kytoon payload was hoisted on 28 occasions. Using Doppler sodar and Kytoon data, structure functions estimated during early morning and evening hours are discussed with respect to the boundary layer pattern observed by Doppler sodar. The features of nocturnal boundary layer observed by Doppler sodar are also discussed.

2. Experimental details

To start with, a brief description and specifications of both the Doppler sodar and Kytoon are given.

2.1 Doppler sodar specifications

Specifications are shown in table 1. The total wind speed and its east-west, north-south and vertical components are printed at a height interval of 30 m beginning at 45 m and reaching up to 1050 m.

2.2 Specifications of Kytoon payload

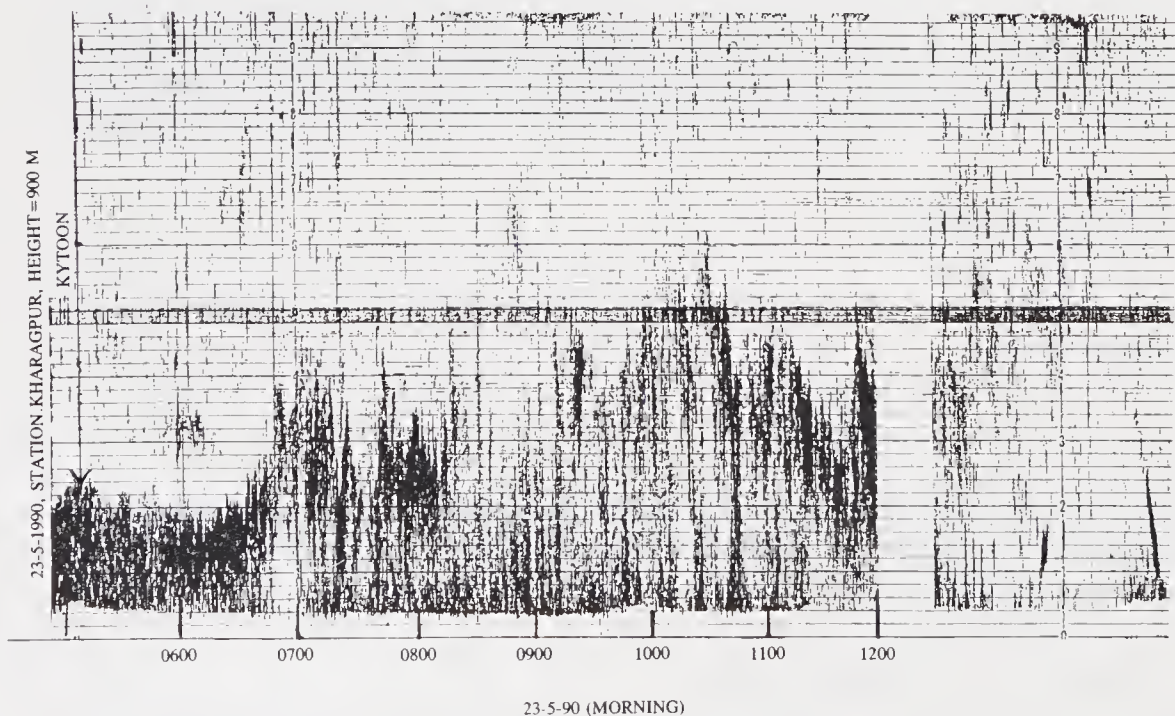
The Kytoon system consists of a 2.3 m^3 aerodynamically shaped balloon which can be raised to a height of 1500 m with the help of a tether. The payload consists of sensors for

Table 1. Specifications of Doppler sodar.

No	Wind component	Measurement range	Accuracy
1.	Horizontal wind speed	0 to ± 25 m/s	0.2 m/s
2.	Vertical wind speed	0 to ± 3.7 m/s	0.1 m/s
3.	Horizontal wind direction	0 to 359 deg.	5 deg for wind speed > 1.5 m/s

Table 2. Specifications of Kytoon payload.

Sensor	Resolution	Response time
Temperature (dry)	0.01 °C	3 s
Temperature (wet)	0.01 °C	12 s
Humidity	0.1%	
Pressure	0.1 mb	
Wind speed	0.1 m/s	
Wind direction	1°	
Weight of the entire payload	200 g	

**Figure 1.** Sodar echogram on 23-5-90 morning.

wind, wind direction, pressure, dry bulb temperature and wet bulb temperature. The data from these sensors can be transmitted on 401 MHz telemetry to the ground receiver. The receiver has a microprocessor and with an initial input of data from five sensors, about 30 derived parameters are evaluated. Specifications of the payload are shown in table 2.

2.3 Description of the Sodar and Kytoon data

The Doppler sodar, though a versatile instrument that gives entire wind data, with all three components, standard deviations and the backscatter intensity, was not supplied

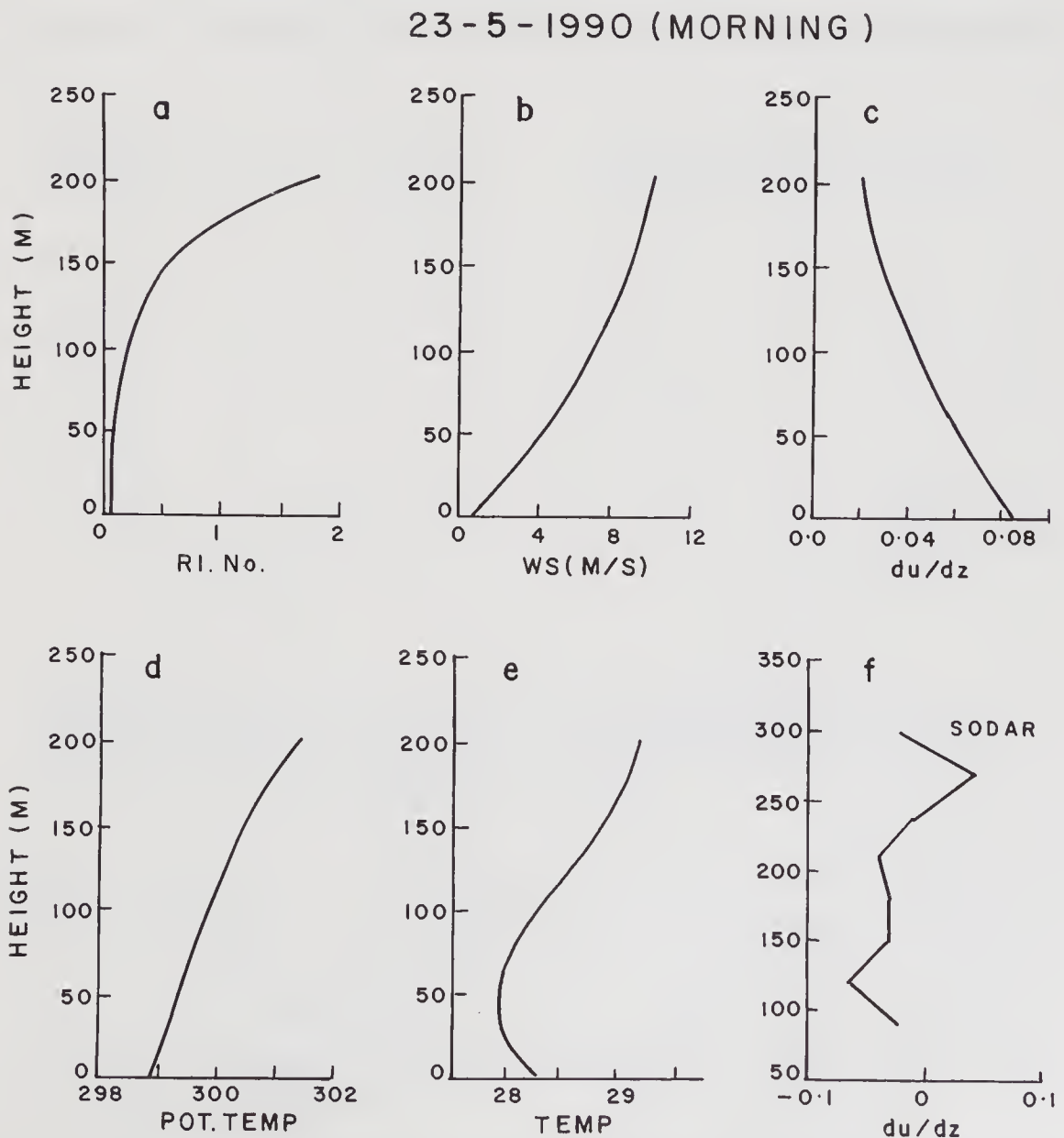


Figure 2(a)-(f). (a) Vertical variation of Richardson no (Ri) on 23-5-90 using Kytoon data; (b) for wind speed; (c) for wind speed gradient (du/dz); (d) for potential temperature; (e) for dry bulb temperature; (f) same as in figure 2(c) using sodar data.

with the necessary software for evaluating the temperature structure functions. The alternative is to use output power and backscattered power values and then evaluate the necessary structure functions, which is a rather difficult task and was not possible at Kharagpur. Hence, an attempt is made to evaluate structure functions using Kytoon data in this paper. The sodar data are used for obtaining qualitative information on the boundary layer, like type of inversion, height of inversion and thermals.

The Kytoon data were available in terms of height versus temperature, potential temperature, mixing ratio and pressure. The data were printed every 20 seconds and smoothed using a spline technique.

3. Temperature and velocity structure functions in the boundary layer

The structure constants, C_v^2, C_T^2 i.e. the r.m.s differences in the values of the instantaneous

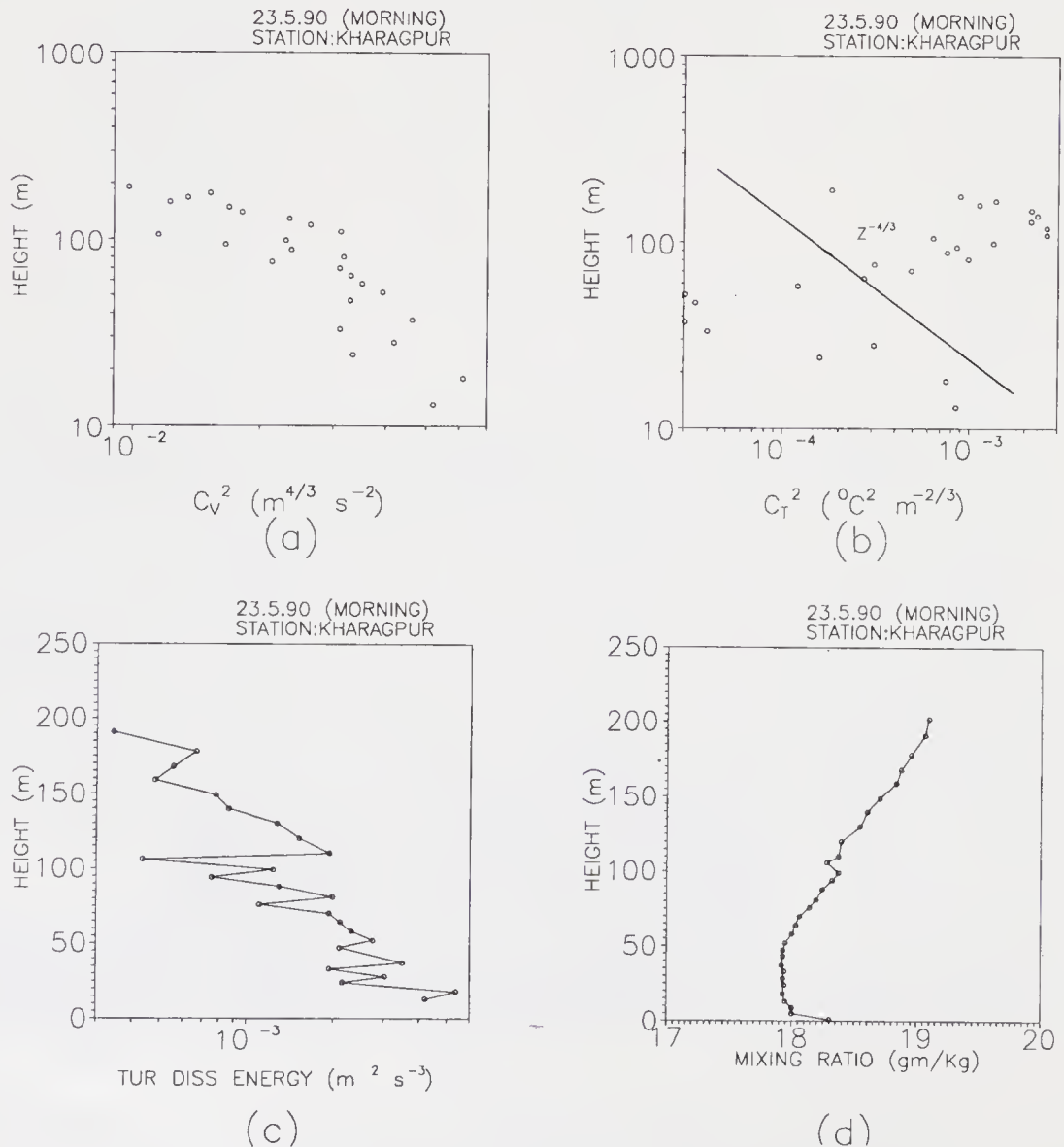


Figure 3(a-d). (Continued)

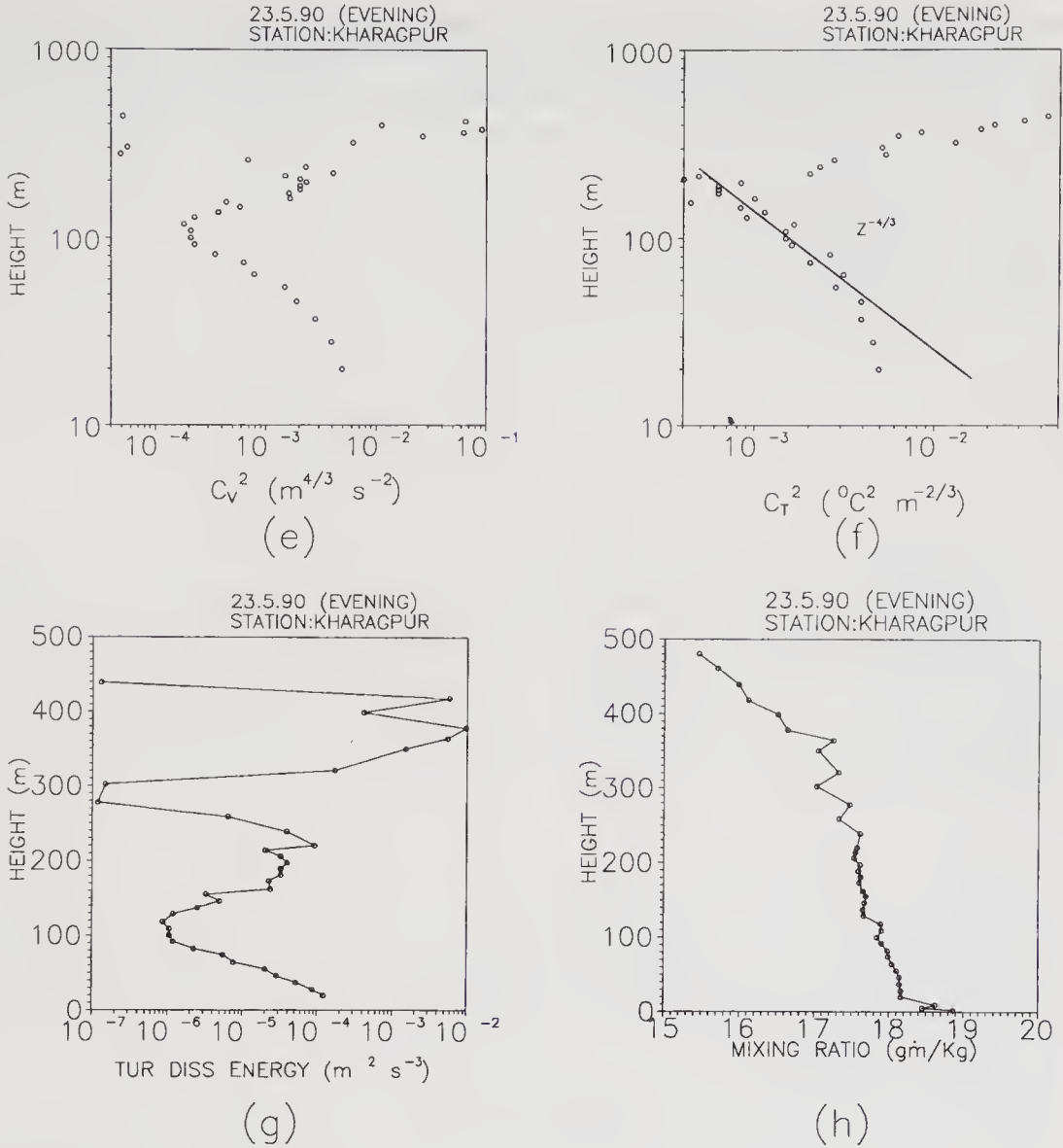


Figure 3(a)–(h). (a) Vertical variation of C_V^2 on 23-5-90 morning using Kytoun data; (b) same, but for C_T^2 ; (c) same, but for ϵ ; (d) same, but for mixing ratio; (e) same as in figure 3(a) but on 23-5-90 evening; (f) same as in figure 3(b) on 23-5-90 evening; (g) same as in figure 3(c) on 23-5-90 evening; (h) same as in figure 3(d) on 23-5-90 evening.

velocity or temperature at two points in the atmospheric volume separated by unit distance, are given by

$$C_V^2 = \frac{[V(x) - V(x + \Delta x)]^2}{(\Delta x)^{2/3}}, \tag{1}$$

$$C_T^2 = \frac{[T(x) - T(x + \Delta x)]^2}{(\Delta x)^{2/3}}, \tag{2}$$

where Δx is the separation between two sensors lying within the inertial subrange of velocity fluctuations. C_V^2 and C_T^2 define the turbulence intensity in the atmosphere. Higher the values of C_V^2 and C_T^2 , higher is the turbulence. Brown and Clifford (1976) have studied

the variation of C_v^2 and C_T^2 with respect to boundary layer height for day time under unstable conditions. For stable atmospheres C_v^2 becomes small except for large values in layers of large shear associated with winds. Measured values of temperature structure parameter C_T^2 have been found to obey the following relation with the altitude:

$$C_T^2 = aZ^{-4/3}, \tag{3}$$

while the C_v^2 obeys the relation,

$$C_v^2 = b + cZ^{-2/3}, \tag{4}$$

23-5-1990 (EVENING)

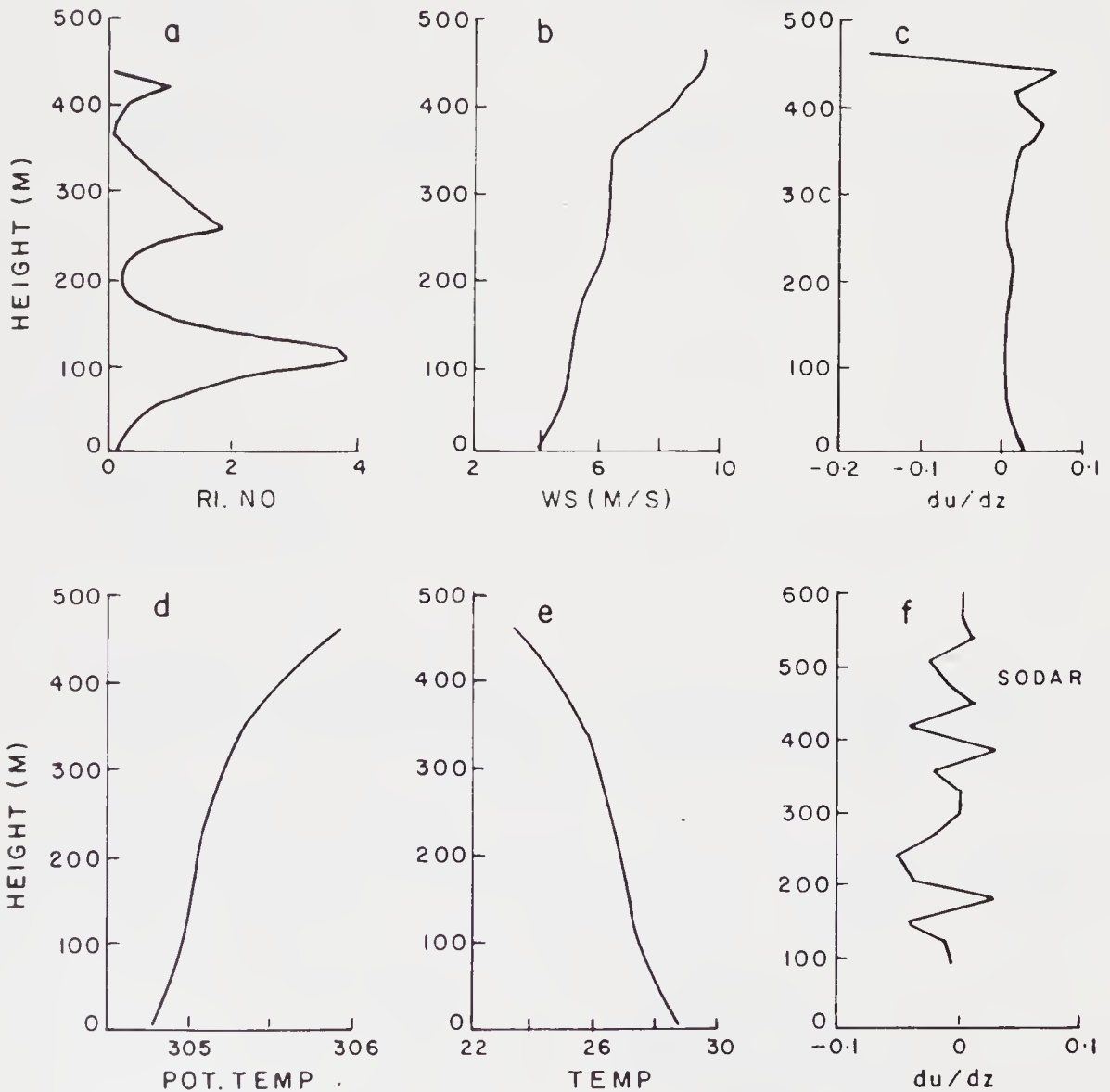


Figure 4(a)-(f). (a) Same as in figure 2(a) on 23-5-90 evening; (b) same as in figure 2(b) on 23-5-90 evening; (c) same as in figure 2(c) on 23-5-90 evening; (d) same as in figure 2(d) on 23-5-90 evening; (e) same as in figure 2(e) on 23-5-90 evening; (f) same as in figure 2(f) on 23-5-90 evening.

where a, b, c are constants and Z is the altitude. Measurements of C_v^2 and C_T^2 using sodar data have been reported by Gaynor (1977). Variations in the temperature structure parameter have been studied by Neff (1975) and Singal *et al* (1982) as a function of the height of the morning rising inversion.

Frisch and Clifford (1974) have shown that C_v^2 is nearly constant with height throughout the mixing layer not exhibiting a falloff with height as does C_T^2 . Frisch and Ochs (1975) have shown from *in situ* measurements that the C_T^2 decreases with height as $-4/3$ power extending atleast up to 80% of the convective mixed layer. C_T^2 lies in the range $10^{-5} - 10^{-2}$ between 90 and 400 m range with variable integration (6–60 minutes). C_v^2 lies in the range $10^{-5} - 10^{-1}$ in the similar height range with similar integration period.

Also in the inertial subrange, it is observed that,

$$2\varepsilon^{2/3} = C_v^2, \varepsilon = \left(\frac{1}{2}C_v^2\right)^{3/2}, \tag{5}$$

where ε is the rate of destruction of the turbulent kinetic energy ($m^2 s^{-3}$) (Tatarskii 1971). Caughey *et al* (1978) have computed the variations of the dissipation parameter ε from the sodar derived values of the structure parameters. Thomson *et al* (1978) have also reported the time and altitude variation of ε . Gaynor (1977) reported variation of ε with respect to stability conditions. Comparison of C_T^2 obtained with sodar and ε values obtained with balloon at Sgnlok mountain has been reported by Guryanov *et al* (1987), who observe that the sodar estimates are regularly higher, about twice the balloon estimates during

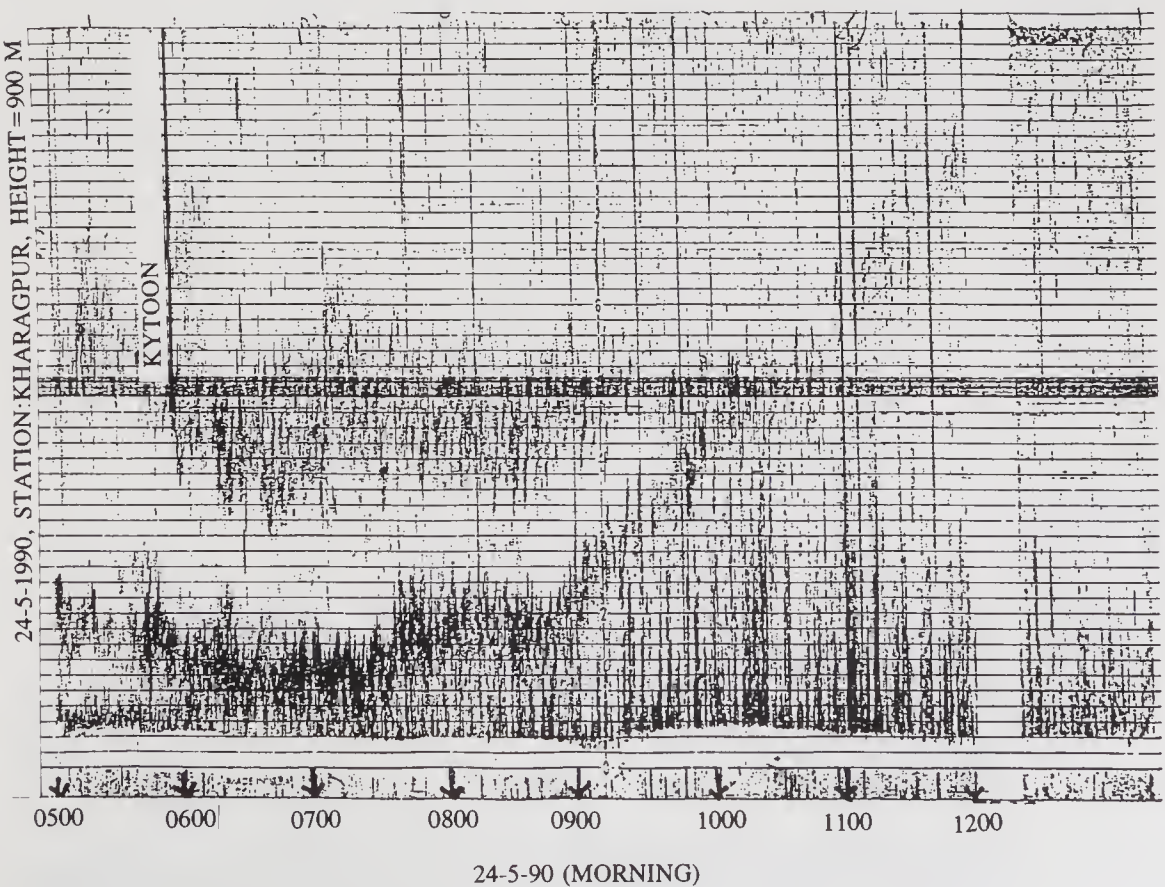


Figure 5. Sodar echogram on 24-5-90 morning.

night time. These discrepancies have not found any suitable explanation. In these experiments the scatter of C_T^2 as observed by sodar and Kytoon was between 10^{-7} and 10^{-2} . In the present paper an attempt is made to study the boundary layer and evaluate the structure parameters C_T^2 , C_V^2 and dissipation of energy ϵ with respect to synoptic conditions prevailing at Kharagpur.

4. Analysis of data

The smoothed Kytoon data are utilised to evaluate the Richardson number, C_T^2 , C_V^2 and ϵ . The smoothed data on potential temperature and mixing ratio have also been

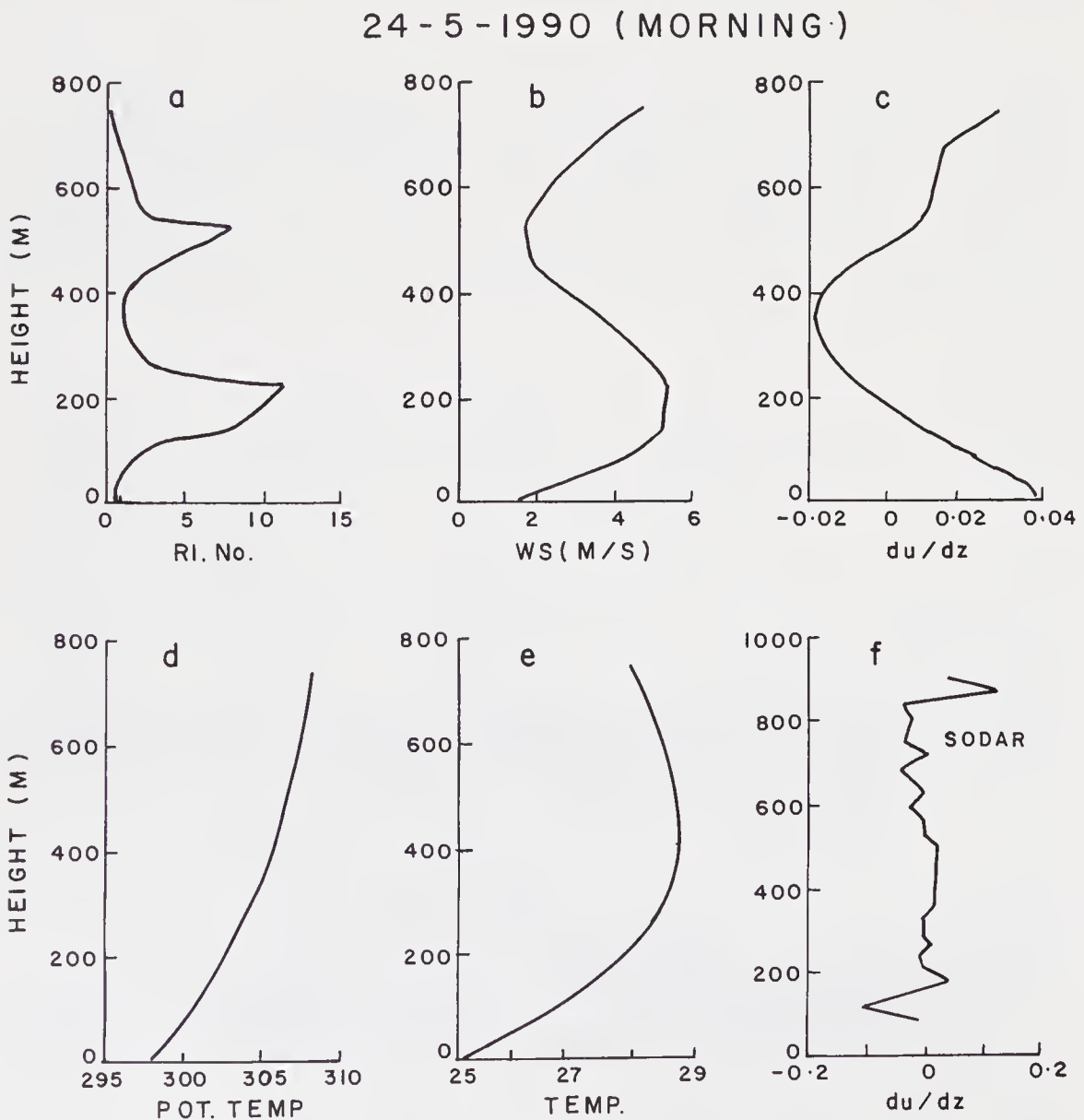


Figure 6(a)-(f). (a) Same as in figure 2(a) on 24-5-90 morning; (b) same as in figure 2(b) on 24-5-90 morning; (c) Same as in figure 2(c) on 24-5-90 morning; (d) same as in figure 2(d) on 24-5-90 morning; (e) same as in figure 2(e) on 24-5-90 morning; (f) same as in figure 2(f) on 24-5-90 morning.

utilised to plot the respective profiles on the day of interest. Only a few specific cases are discussed. As the Kyttoon data are available during synoptic hours, only the simultaneous data available on the Doppler sodar are looked into. Basically, the dynamics of the early morning boundary layer formation at Kharagpur are analysed in terms of stability in the boundary layer.

As mentioned earlier, only 28 flights of Kyttoon were possible and only the data pertaining to three limited flights are used in the analysis.

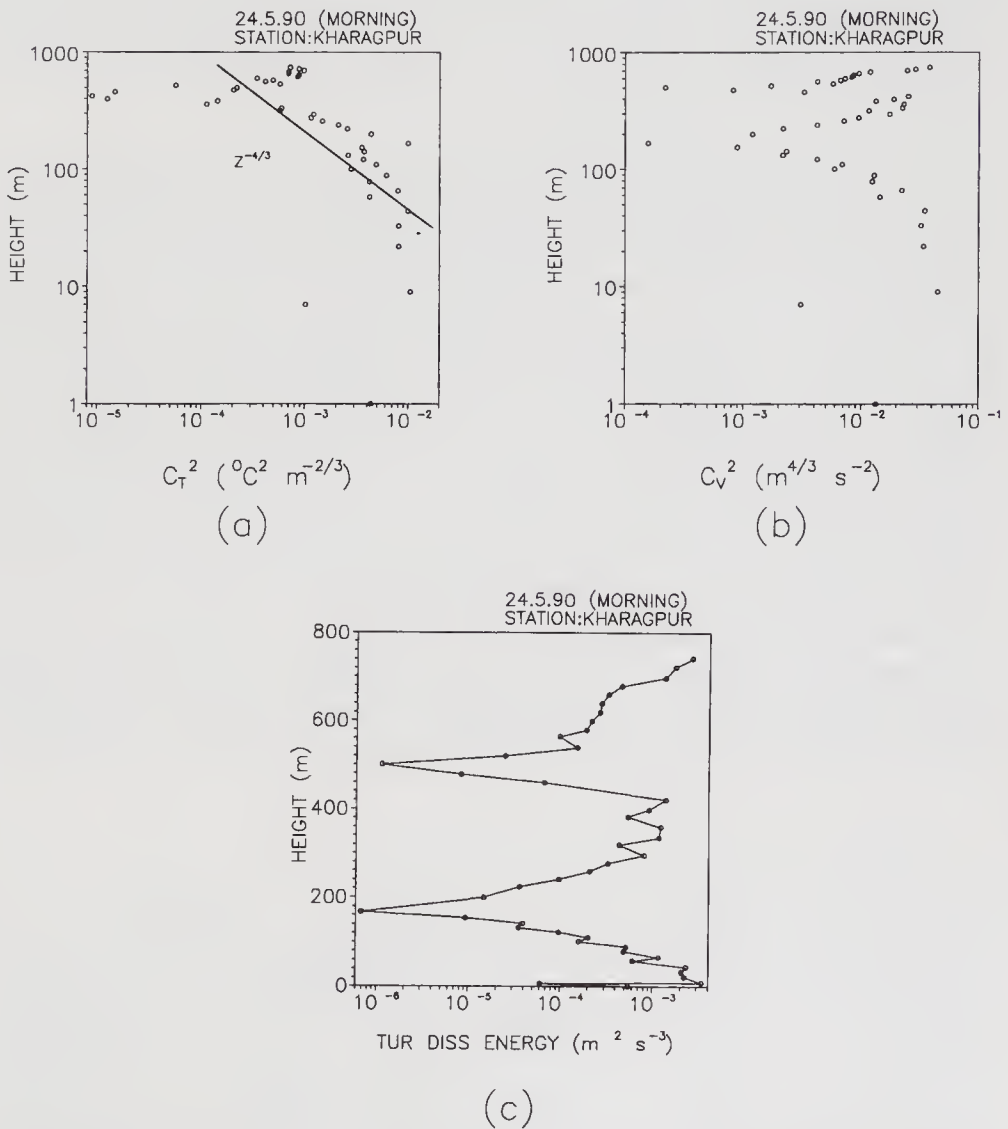


Figure 7(a)–(c). (a) Same as in figure 3(a) on 24-5-90 morning; (b) same as in figure 3(b) on 24-5-90 morning; (c) same as in figure 3(c) on 24-5-90 morning.

4.1 Intercomparison of echogram and the Kyttoon derived parameters

Only three-days data pertaining to Kyttoon flight which are of interest because of some abnormalities observed at the time of hoisting are analysed. The sodar data are utilised qualitatively. The data on following dates are looked into:

No	Date	Period	Time	Max. height reached by Kytoon	Availability of Sodar data
1.	23.5.1990	Morning	0529 hrs, IST	202 m	Available.
2.	23.5.1990	Evening	1652 hrs, IST	480 m	Insufficient.
3.	24.5.1990	Morning	0551 hrs, IST	763 m	Available.
4.	4.6.1990	Morning	0606 hrs, IST	590 m	Available.

Each flight is dealt with separately.

4.1.1 *23.5.90 morning flight (synoptic conditions: clear sky)*: During this flight the sodar echogram (figure 1) showed a ground-based inversion around 220 m. The Kytoon could reach only 202 m. The nocturnal boundary layer height increased upto 400 m around 0700 hrs and after this it decreased until 0800 hrs. Later the routine evolution of the boundary layer took place. With lapse of time the Kytoon observed Richardson number (figure 2a) was around zero indicating neutral stability up to 50 m. Later the Richardson number started increasing and reached a value of 2, showing a stable layer which is again established by the potential temperature profile (figure 2d). Winds increased steadily and reached a speed of 10 m/s at 200 m (figure 2b). Wind gradients (figure 2c) at ground level are of relatively small amplitude but decreased with height attaining a value 0.02 s^{-1} at 200 m. Figure 2f shows the sodar observed wind gradients, which are also small in amplitude but vary between -0.1 and $+0.1$.

C_V^2 and C_T^2 profiles are shown in figures 3a and 3b respectively. C_V^2 follows a $-4/3$ law whereas C_T^2 does not. A minimum in C_T^2 is observed at 30 m and a maximum at 100 m. Figure 3c shows the dissipation of turbulent energy which decreases steadily with height. Figure 3d shows the mixing ratio profile for the same launch. The surface

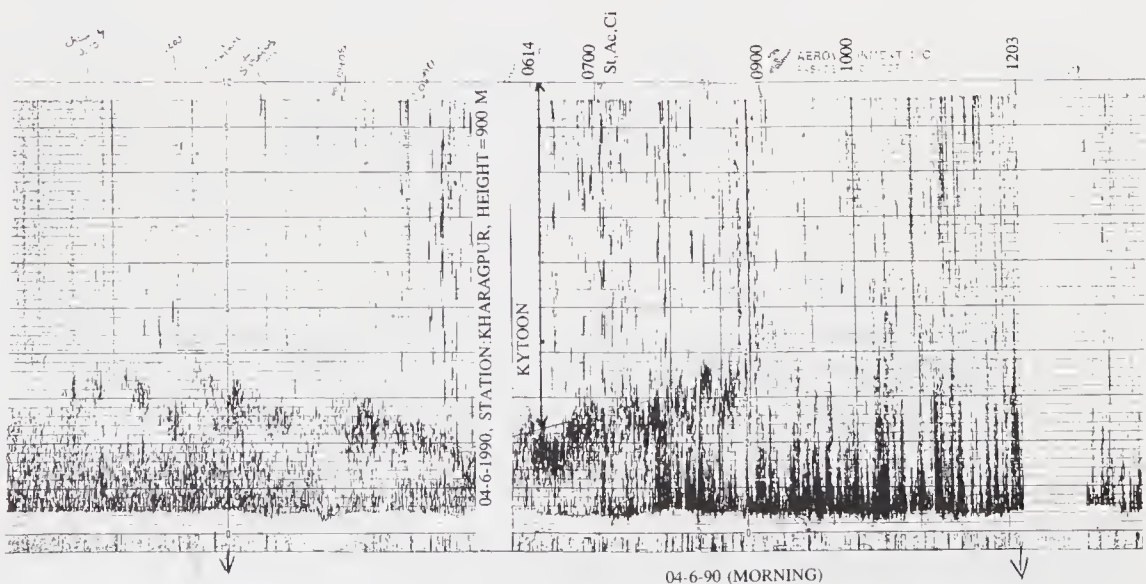


Figure 8. Sodar echogram on 04-6-90 morning.

value is around 18.3 g/kg and gradually increases to 19.0 g/kg at 200 m. This increase can be explained in terms of advection of moisture from the surrounding area.

4.1.2 23.5.90 evening flight (synoptic conditions: cloudy): During this launch the Doppler sodar was not functioning properly. The Kytoon could reach a height of 480 m. The Kytoon observed Richardson number (figure 4a) shows a strong stability ($Ri \approx 4.0$) around 100 m and similar peaks at 200 and 380 m with lesser amplitude. Winds (figure 4b) steadily increase up to 10 m/s at 480 m. Wind gradients (figure 4c) are near zero up to a height of 350 m, but beyond this height they are negative and steep. Potential temperature (figure 4d) shows a steady increase again confirming a stable layer. The sodar observed wind gradients (figure 4e) are varying between $+0.05$ and -0.05 s^{-1} .

4 - 6 - 1990 (MORNING)

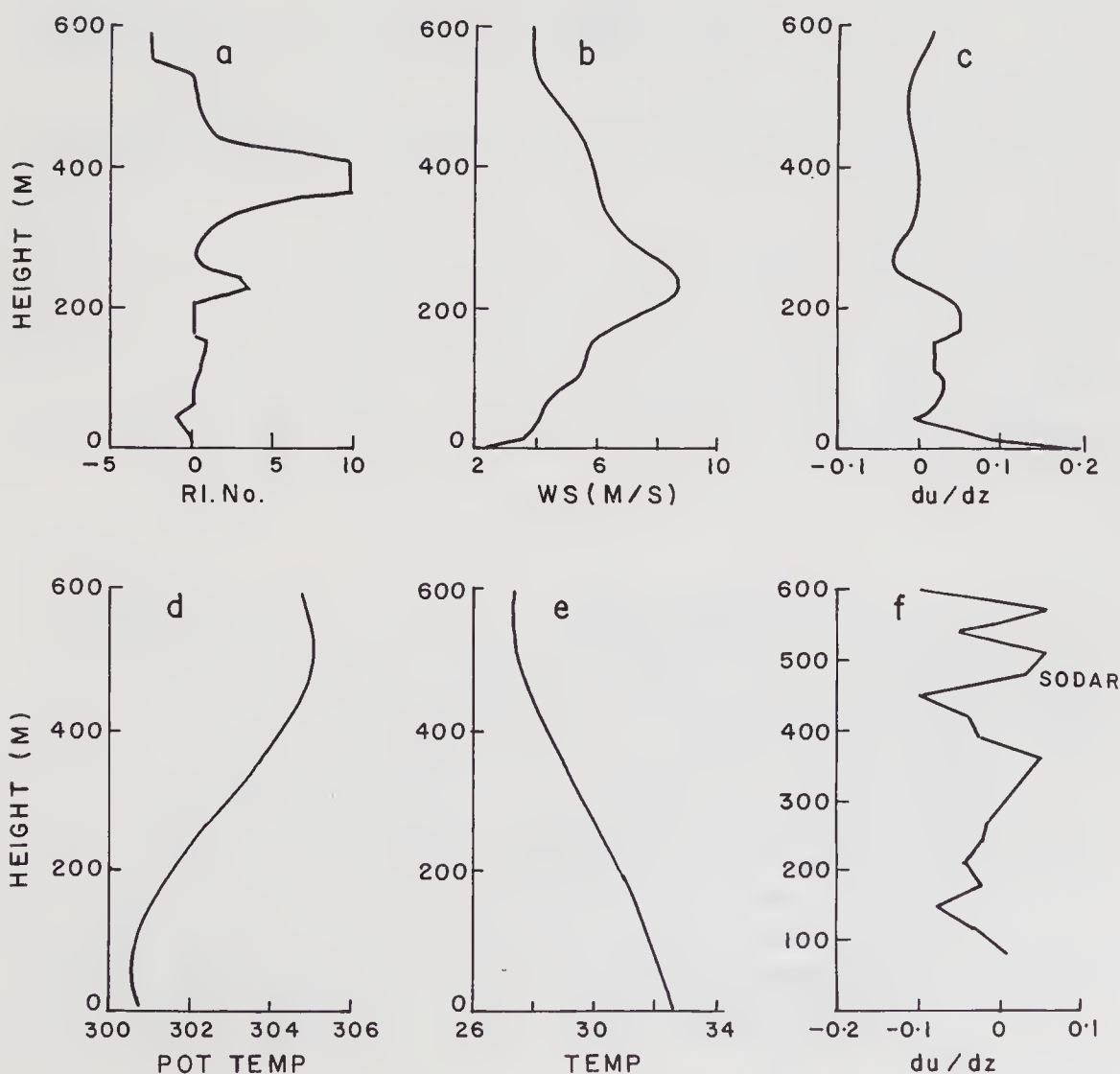


Figure 9(a)–(f). (a) Same as in figure 2(a) on 04-6-90 morning; (b) same as in figure 2(b) on 04-6-90 morning; (c) same as in figure 2(c) on 04-6-90 morning; (d) same as in figure 2(d) on 04-6-90 morning; (e) same as in figure 2(e) on 04-6-90 morning; (f) same as in figure 2(f) on 04-6-90 morning.

Referring to figure 3e and 3f, C_V^2 and C_T^2 profiles follow $-4/3$ law and show a decreasing trend with height up to 200 m. A minimum at 200 m is found for both the profiles. Figure 3g (dissipation of turbulent energy, ϵ) shows a minimum at 300 m and increases beyond that height. The mixing ratio (figure 3h) exhibits the usual steady decrease from 18.5 g/kg at ground to 15.5 g/kg at 480 m.

4.1.3 24.5.90 morning flight (synoptic conditions: clear sky): Figure 5 shows the echogram for 24.5.90 morning flight. The ground-based inversion had a trend typical of the nocturnal boundary layer. Right from 0500 hrs another inversion developed and was floating around 500 m, till it merges with the ground-based one at 1000 hrs. After 1030 hrs the routine evolution of boundary layer takes place. Figure 6a shows the profile of Richardson number clearly indicating two stable regions at 200 and 460 m respectively corresponding to the two inversions observed on the echogram. Wind

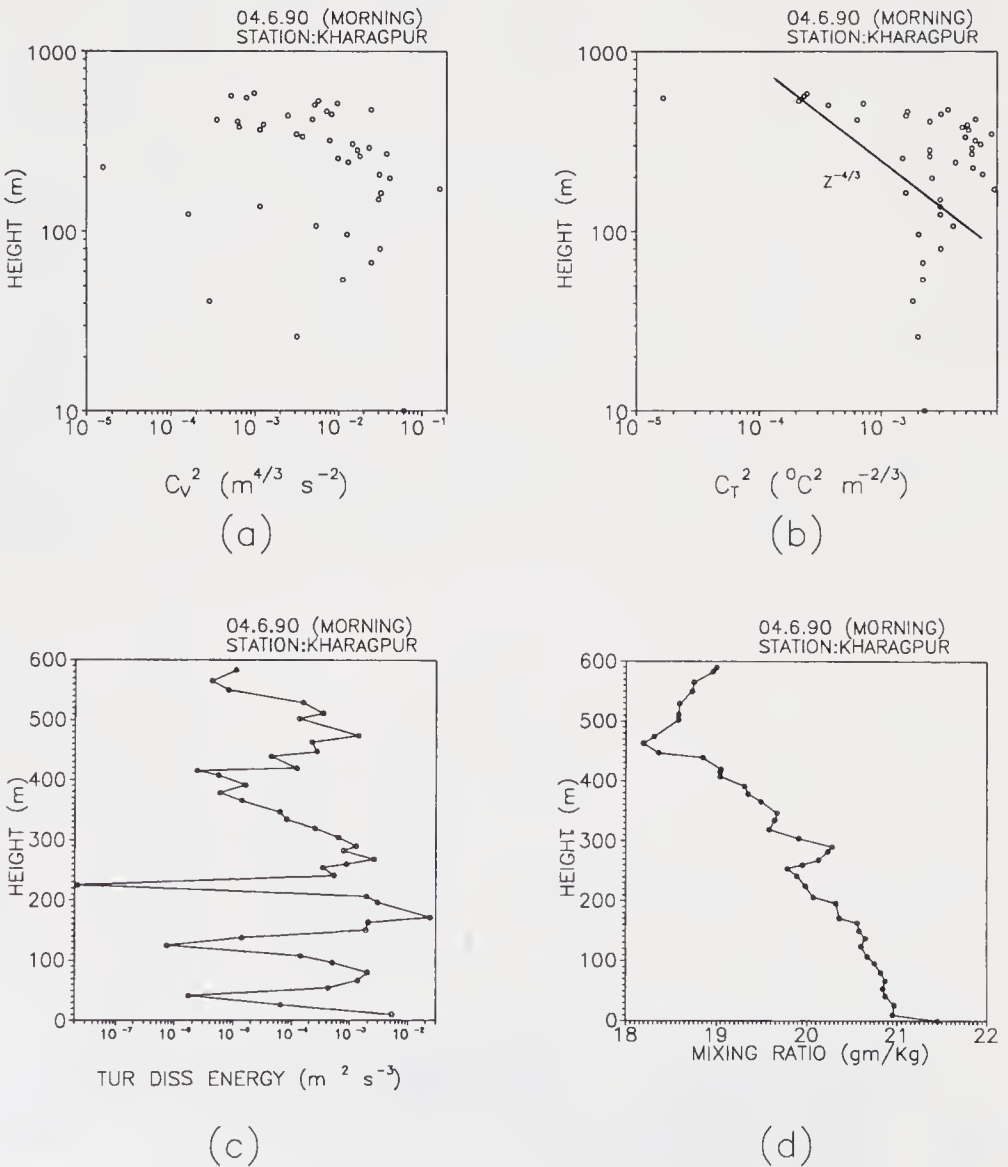


Figure 10(a)-(d). (a) Same as in figure 3(a) on 04-6-90 morning; (b) same as in figure 3(b) on 04-6-90 morning; (c) same as in figure 3(c) on 04-6-90 morning; (d) same as in figure 3(d) on 04-6-90 morning.

speed (figure 6b) and wind gradients (figure 6c) do not show significant variations. But the wind speed is minimum at 460 m, the second inversion level. The dry bulb temperature (figure 6e) profile shows a temperature strata between 200 and 400 m. Thus the region between two inversions has a nearly constant temperature. During this Kytoon flight the wet bulb sensor was not working and hence the mixing ratio parameter is not available.

Variations of C_T^2 and C_V^2 and dissipation of turbulent energy are shown in figures 7a, 7b and 7c respectively. Figure 7b shows clearly two minima at the inversion heights 200 and 460 m. In the case of C_T^2 a falloff with $-4/3$ power law is observed to follow up to 500 m whereas for C_V^2 two minima are observed at 200 and 460 m. These minima in the C_V^2 and Richardson number profiles coincide with the minima observed in the ϵ profile.

4.1.4 04.6.90 morning flight (synoptic conditions: slightly cloudy): Figure 8 shows the sodar echogram on 4.6.90. The Kytoon was hoisted at 0606 hrs. On this day the nocturnal boundary layer height varied between 300 and 500 m. At 0530 hrs its height reduced to 180 m and then it started increasing.

The Kytoon data analysis shows a strong stability $Ri \approx 10$ (figure 9a) around 400 m. This may be because of steep gradients of potential temperature (figure 9d) at 400 m and minimum wind gradients (≈ 0) (figure 9c) around 400 m. In general on this day the wind gradients were low. The sodar derived wind gradients (figure 9f) also showed variations around zero.

Figures 10a, b, c and d show C_V^2 , C_T^2 , ϵ and mixing ratio profiles respectively for 4.6.90. The C_V^2 profile (figure 10a) is highly scattered, and the C_T^2 profile (figure 10b) does not obey the $-4/3$ law. Between 20 and 200 m region C_T^2 is almost constant. Above 200 m a falloff is observed. The dissipation of turbulent energy (figure 10c) shows a steady decrease. The sudden decrease in ϵ observed at 220 m is an isolated point which may be wrong. Figure 10d shows the mixing ratio profile showing a steady decrease from a surface value of 21.5 g/kg.

5. Conclusions

- The nocturnal boundary layer height decreases in the early morning hours and then increases followed by another decrease and again followed by a routine increase.
- On 24.5.90 two inversions are observed and at these inversions, the Richardson number is very high, whereas C_V^2 showed two dips at the inversion heights. Consequently the turbulent energy dissipation also showed two minima at the inversion heights.
- A steady decrease in mixing ratio was observed on all launches of Kytoon except on 23.5.90 morning when a small increase with height was observed up to 200 m. This may be due to the advection of moisture from the surrounding area.
- The C_T^2 profile follows a $-4/3$ law up to 200 m on two days, i.e. 23rd and 24th May 1990. C_V^2 variations are not systematic. Sometimes C_V^2 is found to obey a $-4/3$ law. The $-4/3$ law is not obeyed for both C_T^2 and C_V^2 on 4th June.
- C_V^2 and C_T^2 values lie in the range 10^{-5} – 10^{-1} and 10^{-5} – 10^{-2} respectively.

Acknowledgement

The authors wish to thank the Department of Science and Technology, Government of

India for financing the MONTBLEX-90 programme and the Director, Indian Institute of Tropical Meteorology, Pune for constant encouragement throughout this work.

References

- Brown E H and Clifford S F 1976 On the attenuation of sound by turbulence; *J. Acoust. Soc. Am.* **68** 788–794
- Caughey S J, Crease B A, Asimakopoulou D N and Cole R S 1978 Quantitative Bistatic Acoustic sounding of the atmospheric boundary layer; *Q. J. R. Meteorol. Soc.* **104** 147–161
- Frisch A S and Clifford S F 1974 A study of convection capped by a stable layer using Doppler radar and Acoustic echo sounder; *J. Atmos. Sci.* **31** 1622–1628
- Frisch A S and Ochs G R 1975 A note on behaviour of the structure parameter in a convective layer capped by a marine inversion; *J. Appl. Meteorol.* **14** 415–419
- Gaynor J E 1977 Acoustic Doppler Measurement of atmospheric boundary layer velocity structure functions and energy dissipation rates; *J. Appl. Meteorol.* **16** 148–155
- Guryanov A E, Kallistratova M A, Martvel F E, Pecur M S, Petenco I V, Time N S and Shurygin Ye A, *Izvestiya* 1987 Comparison of sodar and microfluctuations measurements of the temperature structure parameter in mountainous terrain; *Atmos. Oceanic Phys.* **23** 685–691
- Neff W D 1975 Quantitative evaluation of acoustic echoes from the planetary boundary layer, NOAA Technical Report ERL 322, WPL 38
- Singal S P, Gera B S and Aggarwal S K 1982 Determination of structure parameter using sodar, *Boundary-Layer Meteorol.* **23** 105
- Singal S P, Gera B S, Pahwa R and Aggarwal S K 1986 Studies of surface based shear echo structure. *Atmos. Res.* **20** 125–131
- Thomson D W, Coulter R L and Warhoff Z 1978 Simultaneous measurement of turbulence in the lower atmosphere using sodar and aircraft; *J. Appl. Meteorol.* **17** 723–734
- Tatarski V I 1971 The effect of the turbulent atmosphere on the wave propagation, Israel Program for Translation

Study of horizontal scales of motion observed over Kharagpur during MONTBLEX-1990

B ROY and U K DE

Physics Department, Jadavpur University, Calcutta 700 032, India

Abstract. Characteristic wavelengths for the u and v components of wind are studied using the Monsoon Trough Boundary Layer Experiment (MONTBLEX) data obtained from a Doppler Sonic Detection and Ranging System (sodar) over the land station Kharagpur (near sea-coast). The principal stability parameter (Z_i/L_o) is used to infer the behaviour of the non-dimensional form of the characteristic wavelength (L_H) within the entire stability range occurring during the sounding periods. This is compared with GATE – 1974 results (over the sea surface) published by Fitzjarrald (1978).

Keywords. Monsoon; range-bin; range; micrometeorological; sodar; MONTBLEX, acoustic; Doppler; backscatter.

1. Introduction

Frisch *et al* (1976), Fitzjarrald (1978) and Best *et al* (1981) estimated the horizontal scale of free convection applying Taylor's hypothesis and reported it to be of the order of several kilometers. From experiments in Rayleigh convection and also from the measurements by use of a Doppler acoustic sounder and tower-mounted instrumentation, Fitzjarrald (1976) earlier reported that the dominant scale of free convection was about six times the depth of the convective layer. Later on, working further with the Global Airmass Transformation Experiment (GATE) data of free convection, Fitzjarrald (1978) concluded that the non-dimensional dominant scale of convection depends upon the extent of the Atmospheric Boundary Layer (ABL) principal stability parameter. Kaimal *et al* (1976) found the 3-dimensional turbulent scale to be of the order of $1.5Z_i$ during free convection, i.e. for $Z_i/L_o > 100$ where Z_i is the inversion depth in the ABL and L_o is the Monin-Obukhov length in the surface layer of the ABL, which is also representative of the shear and buoyancy forces within the surface layer.

We use the Doppler acoustic sounder (Aerovironment model V-2000) data to infer the horizontal characteristic wavelength (L_H) for the u and v components in the ABL over station Kharagpur ($22^\circ 18'N$, $87^\circ 12'E$) and then compare the results with those reported from the GATE data. Henceforth we abbreviate the Kharagpur observation station as KGP. In this study we use the surface layer stability parameter obtained from slow response micrometeorological data-sets from a 30 m high tower and sampled at 1 Hz. The tower was located near the sodar site at Kharagpur. Data used in this analysis pertain mostly to the 'onset' phase of monsoon (June 04–24, 1990) and also during the mid-monsoon phase (August 28– September 08, 1990). Average values of L_H/Z_i for the stable and the unstable cases were obtained separately.

2. Data understanding

The Doppler sodar was a 3-axis, monostatic type operated at a frequency of 1500 Hz, with a pulse repetition rate of 14 s. Total range of the sounder was 1500 m and range interval was 30 m. The first 60 m data were not available in the data-sets. The data acceptance tests performed within the sounder identify and reject much of the erroneous data. However, a data reliability code prescribed with each sounding range was also used to accept or reject the sodar backscatter intensity data (as per the technical instruction manual of the sodar manufacturer).

The effective range of the Doppler sodar at a particular site depends primarily upon the meteorological conditions at the site and the intensity of background noise. The meteorological conditions determine the number of thermal scatterers and therefore the strength of the return signal. The signal strength however decreases with altitude due primarily to spherical spreading and atmospheric attenuation of the transmitted and reflected energy. This signal must overcome background noise in order to be detected by the sounder. The statistical significance of sodar data often depends upon the number of samples taken during the entire averaging interval. This is particularly useful in case of evaluation of the wind component standard deviations. In general, between 50 and 70 transmit pulses per active antenna are considered to be the minimum required to assure adequate data capture in the lower altitudes. More transmit pulses are generally required when we attempt to extend the range of the sounder.

The Doppler sounder provides backscatter intensity data (in arbitrary units) and also wind velocity information (in m/s) pertaining to the entire vertical range of the stable and the well-mixed layer, and frequently in the lower cloud layer. In this paper we represent the sodar intensity as I_v . As described earlier by Mandics and Hall (1976) these data delineate dynamic changes that have profound effects on the tropical moist mixed layer. This has relevance to the moist ABL over the observation station KGP. From the output file of sodar data we have the total number of samples (f_k) received at each range of interest i.e. between 60 and 1500 m at an interval of 30 m. This is the total number of pulses received as a result of 255 active sound pulses sent every 60 minutes.

Fitzjarrald (1978) pointed out that small-scale humidity fluctuations are found to contribute approximately 30% of the acoustic return intensity but the rest is due to fluctuations in temperature in the inertial sub-range of turbulence.

We consider the Doppler sodar to be a perfectly Eulerian sensor, i.e. it is truly able to measure the flow aloft. From the return pulse we infer that events causing the backscatter are thermal in nature and the disturbances actually causing such a return may be due mostly to advection of wind during the stable ABL condition. This may be justified on the ground that during stable ABL occurrence wind shear is the prime driving source and may cause mixing in the vertical. Under such a process it is likely that small-scale temperature fluctuations will arise. However, unstable situations are also influenced by the events of horizontal wind advection but thermal forcing of the ABL from the surface would mostly dominate over shear generation. For the present purpose of our investigation, we consider that horizontal advection of air would induce fluctuations in temperature which would result in sodar backscatter. Such a phenomenon would eventually cause a return signature only over the vertical antenna of the sodar system.

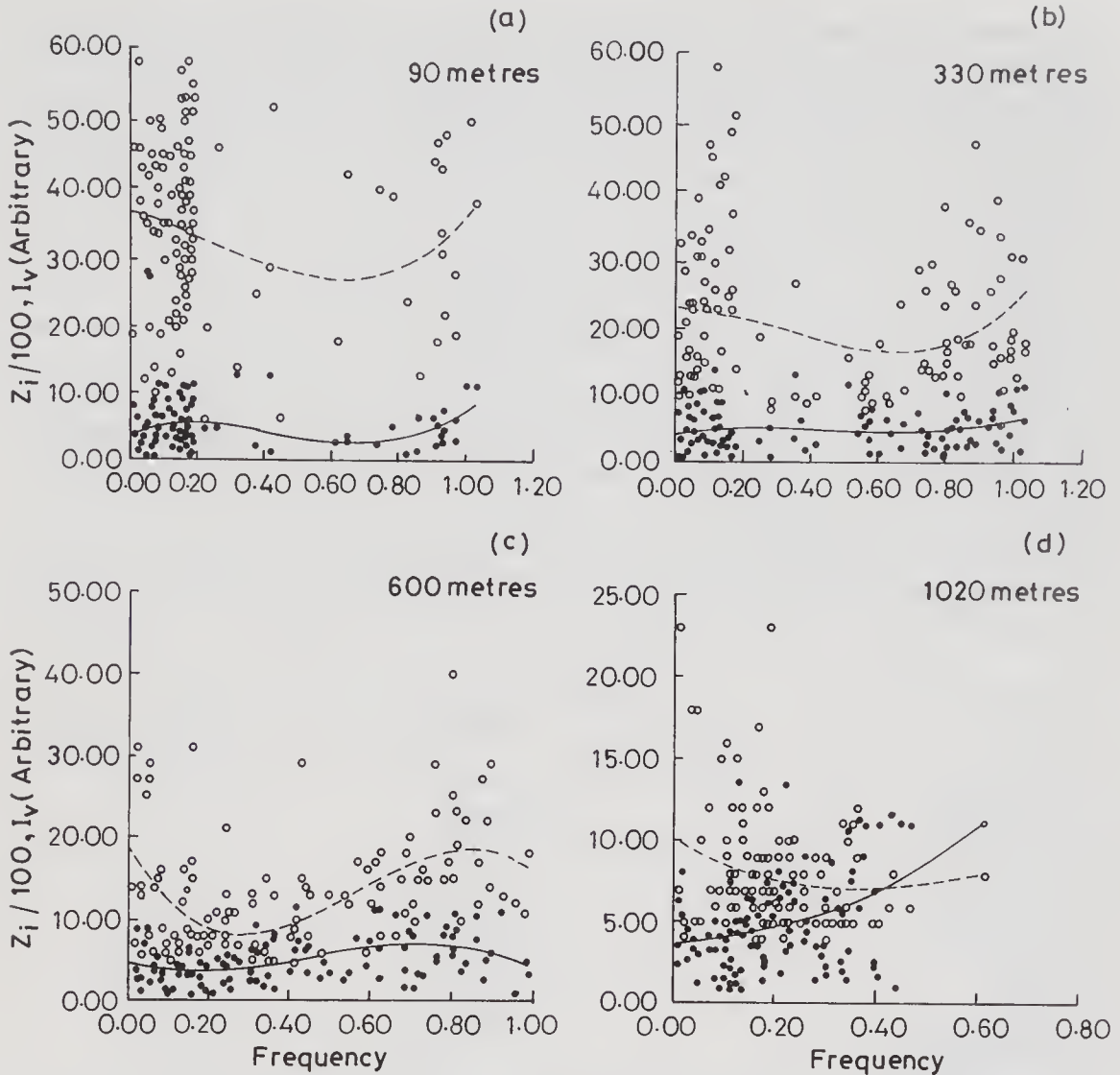


Figure 1(a)–(d). Shows frequency (per minute) characteristics of variation in backscatter intensity I_v (dashed line), and inversion depth fraction ($Z_i/100$) for 90, 330, 600 and 1020 m ranges for the stable ABL cases (solid line). The lines are obtained by fitting over the scatter of points (\square representing I_v , and * representing the inversion height).

3. Data analysis

3.1 Echo intensity

The sampling frequency (k) at each range (i.e. 90, 330, 600 and 1020 m) during the stable and unstable ABL cases may be written in terms of the ratio

$$k = \frac{\text{Total number of samples received in one averaging interval}}{\text{Illumination time (acoustic) in each interval}}$$

The illumination period is the total exposure time, of the particular range in consideration, to acoustic energy. This is almost constant, i.e. illumination time = effective pulse width (vertical) \times 255, because 255 pulses are sent out every 60 minutes (or during one averaging cycle).

We make range-bins Δk each of about 0.2 per minute and then plot I_v and the one-hundredth part of the sodar measured inversion depth ($Z_i/100$) in order to assimilate all data in a perceptible range for a common plot as shown in figures 1 and 2 for the stable and unstable cases respectively. One reason for looking into such plots is to realise the effect of inversion height changes at different reception frequency ranges (of the number of acoustic pulses received) on the actual scatter power at the respective ranges, and to see if there is any positive correspondence between the two.

Postulating I_v to be a direct measure of the virtual temperature fluctuation within a range of vertical separation, we find from figures 1(a)–(d) and 2(a)–(d) that the fluctuations in I_v at each range-bin have a higher correlation with the inversion depth Z_i when the ranges are below 1020 m above ground level (AGL). This signifies that the sodar effective range height is between 60 and 600 m AGL for both the cases of stability. This also suggests that at around 330 m the Doppler sounder receives minimum noise and maximum signal. Such a strong signature may perhaps be due to horizontal advection of air that apparently causes a sharp change in the temperature structure which in turn results in consistently better scattering at the 330 m range. From figures 1(a)–(d) we also find that at around 330 m the samples are evenly distributed over all frequencies.

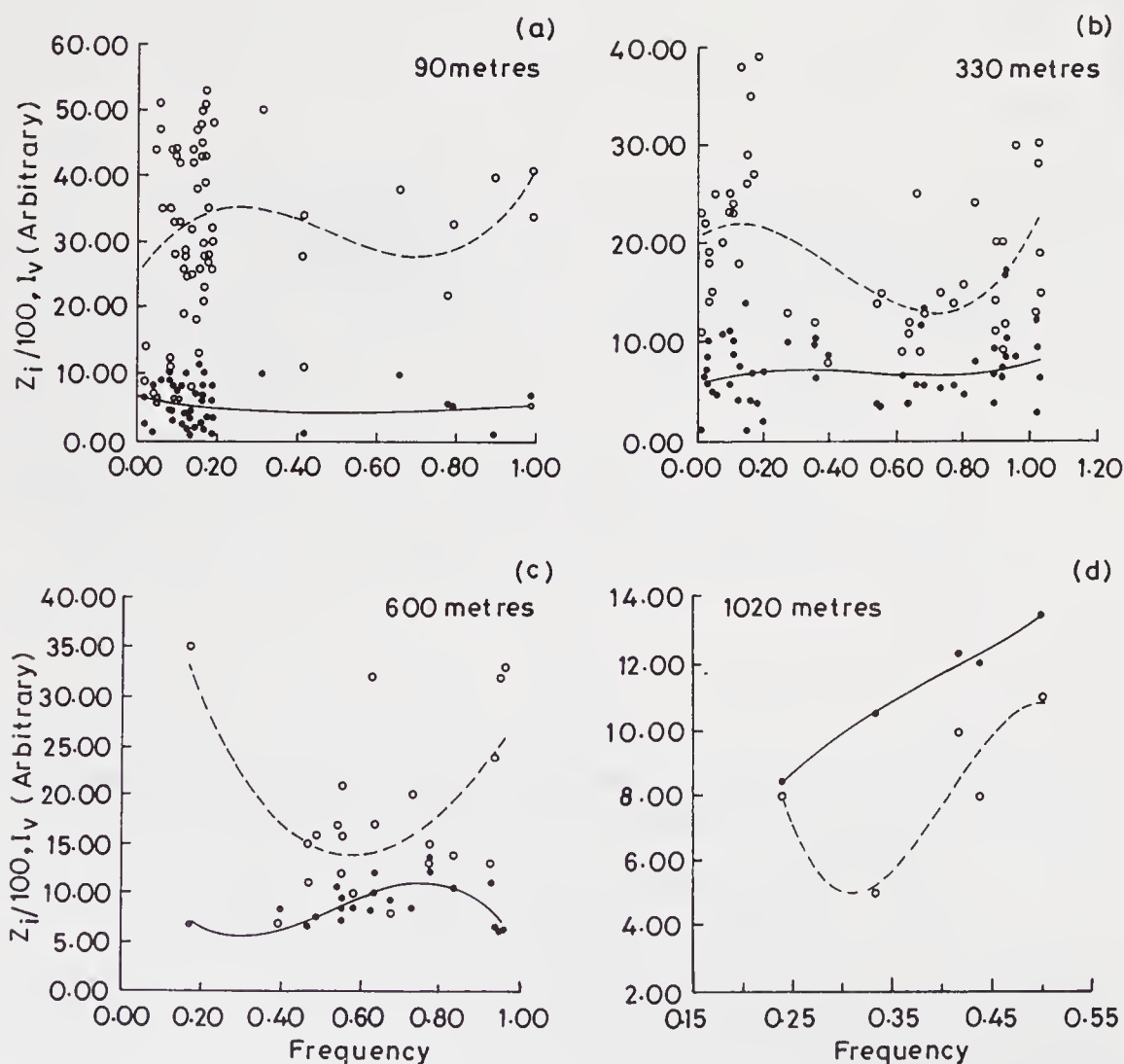


Figure 2(a)–(d). Same as in figure 1 but for the unstable ABL cases.

Table 1(a). Pearson's correlation coefficient between Z_i and I_v at different ranges and at each frequency range for stable cases.

Range height (m)	Frequency interval (per minute)	Number of samples	Correlation coefficient
90	0.0-0.2	56	0.014
	0.2-0.4	10	0.10
	0.4-0.6	10	0.09
	0.6-0.8	3	0.697
	0.8-1.0	3	-0.170
330	0.0-0.2	22	-0.031
	0.2-0.4	4	-0.012
	0.4-0.6	15	-1.00
	0.6-0.8	10	-0.352
	0.8-1.0	10	0.231
600		No samples	
1020		No samples	

Table 1(b). Pearson's correlation coefficient between Z_i and I_v at different ranges and at each frequency range for unstable cases.

Range height (m)	Frequency interval (per minute)	Number of samples	Correlation coefficient
90	0.0-0.2	95	0.169
	0.2-0.4	5	-0.312
	0.4-0.6	3	0.640
	0.6-0.8	4	0.310
	0.8-1.0	13	0.479
330	0.0-0.2	57	-0.067
	0.2-0.4	7	0.708
	0.4-0.6	11	0.749
	0.6-0.8	15	-0.083
	0.8-1.0	27	-0.380
600	0.0-0.2	39	0.290
	0.2-0.4	28	0.380
	0.4-0.6	18	0.174
	0.6-0.8	20	-0.088
	0.8-1.0	17	-0.040
1020	0.0-0.2	39	0.290
	0.2-0.4	28	0.380
	0.4-0.6	18	0.174
	0.6-0.8	20	0.088
	0.8-1.0	17	-0.040

This is also evident from figure 2(b) for the unstable case. The sample linear correlation coefficients between I_v registered at each of the selected sodar ranges and the inversion depth (Z_i) for each Δk are given in tables 1(a) and 1(b) for the stable and unstable ABL cases respectively. It is to be noted from table 1(a), that at the 90 m range the correlations are all positive except for the frequency range 0.8-1.0 per minute. This

may be explained as follows: The 90 m range lies mostly within the sodar sensed inversion depths occurring during the stable hours. Within the inversion depth any fluctuation in temperature is expected to be due to shear-induced mixing processes. This would cause a larger scatter signature as compared to the ranges that tend to lie outside the inversion depth. The negative correlations occurring in table 1(a) at levels other than the 90 m range during the stable cases is possibly due to a decrease in the magnitude of fluctuation of virtual temperature over ranges outside the inversion height during the stable ABL conditions. This would occur even if the extent of the stable boundary layer alters. In table 1(b) the correlation coefficients are found to be positive. This is explained on the basis that the enhancement of Z_i would mean a stronger convection and hence more fluctuation in the virtual temperature resulting in an increase in the backscatter intensity with the rise in Z_i . In general, from table 1(a)



Figure 3. (Continued)

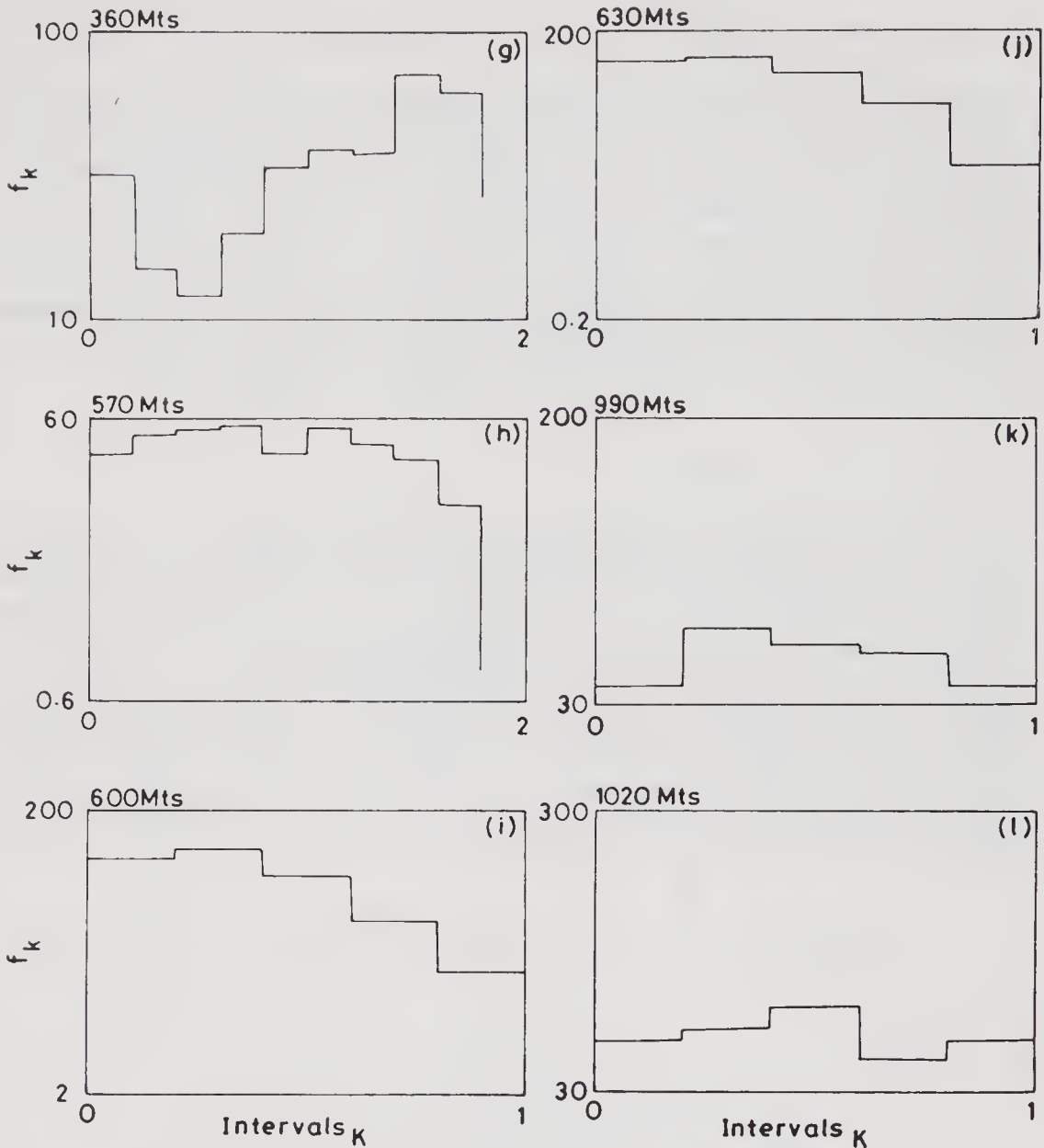


Figure 3(a)–(l). Number of received pulses from each sodar range during the entire sounding period and their histogram with occurrence frequencies for the stable ABL. f_k is number of pulses received in frequency step (interval) $_{\kappa}$, which is of size roughly 1/10th of the total frequency range in each plot.

and (b) it is to be noted that the correlation between I_v at 330 m AGL and Z_i is best obtained particularly at smaller Δk than those found for the other ranges of sounding. This excludes however a few sampling frequency ranges where the correlations are poor. In table 1(b), it is also found that at the 330 m range, the correlation is high in the frequency range 0.2–0.6 per minute and negative for the other frequency ranges. This signifies the fact that the scatter intensity at these sampling frequencies bears signatures of stronger temperature fluctuations with the rise in the inversion depth. This would also mean that the temperature fluctuations occurring due to horizontal flow during such cases bear almost direct correlation with the sodar backscatter power at those sampling frequencies.

3.2 Pulse frequency range

The number of pulses received at each frequency range-bin is considered here as discussed in § 3.1 and then the occurrence frequency histograms for the received pulse at each of the selected ranges are constructed, i.e. at 90, 120, 210, 270, 300, 330, 360, 570, 600, 630, 990 and at 1020 m AGL for the stable ABL cases (see figures 3a–l) and at 90, 330, 600 and 1020 m AGL for the unstable cases (see figures 4a–d). From figure 3 we find that at lower ranges of frequency the histogram plots show a wider range of the number of pulses received in each range-bin, whereas as we go higher up, the histogram yields a smoother cumulative characteristic. In case of the unstable ABL we also find a relatively smoother version at the 330 m range, but with a wider response as compared to the others.

3.3 Frequency weighted echo intensity

We select 90, 330, 600 and 1020 m backscatter intensity data and then make a frequency weighted echo-intensity series. In this series we take the variance of the frequency weighted intensity for each range and then plot against their corresponding occurrence frequencies expressed per minute. The Frequency Weighted Echo Intensity Variance = $\sum_i k_{\Delta k} (I_r)_{\Delta k} / n$ where n is the fraction of the total number of received pulses registered in the range-bin Δk and i is the component in the range-bin that is summed over. These are plotted in figures 5(a) and 5(b) for the stable ABL, and in figure 6 for the unstable ABL. From these plots we select the dominant frequencies (ν_m) for the 330 m range. For the stable case ν_m is 0.3/minute and for the unstable case it is 0.9/minute at

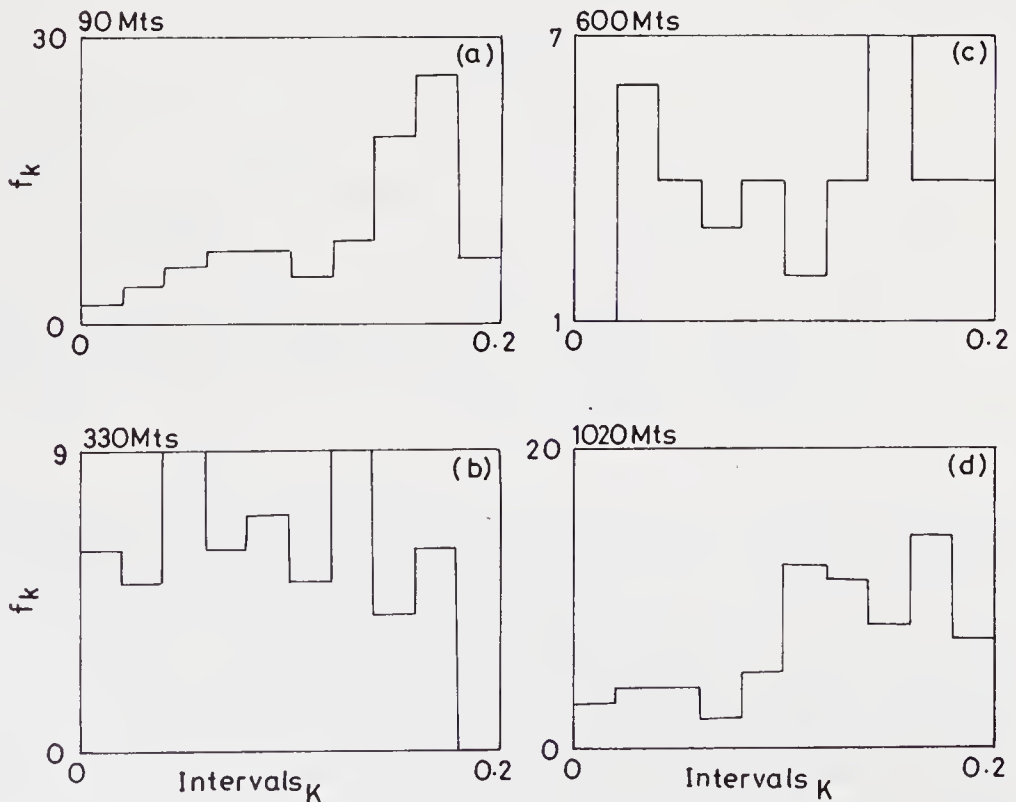


Figure 4(a)–(d). Same as in figure 3 but for the unstable ABL cases.

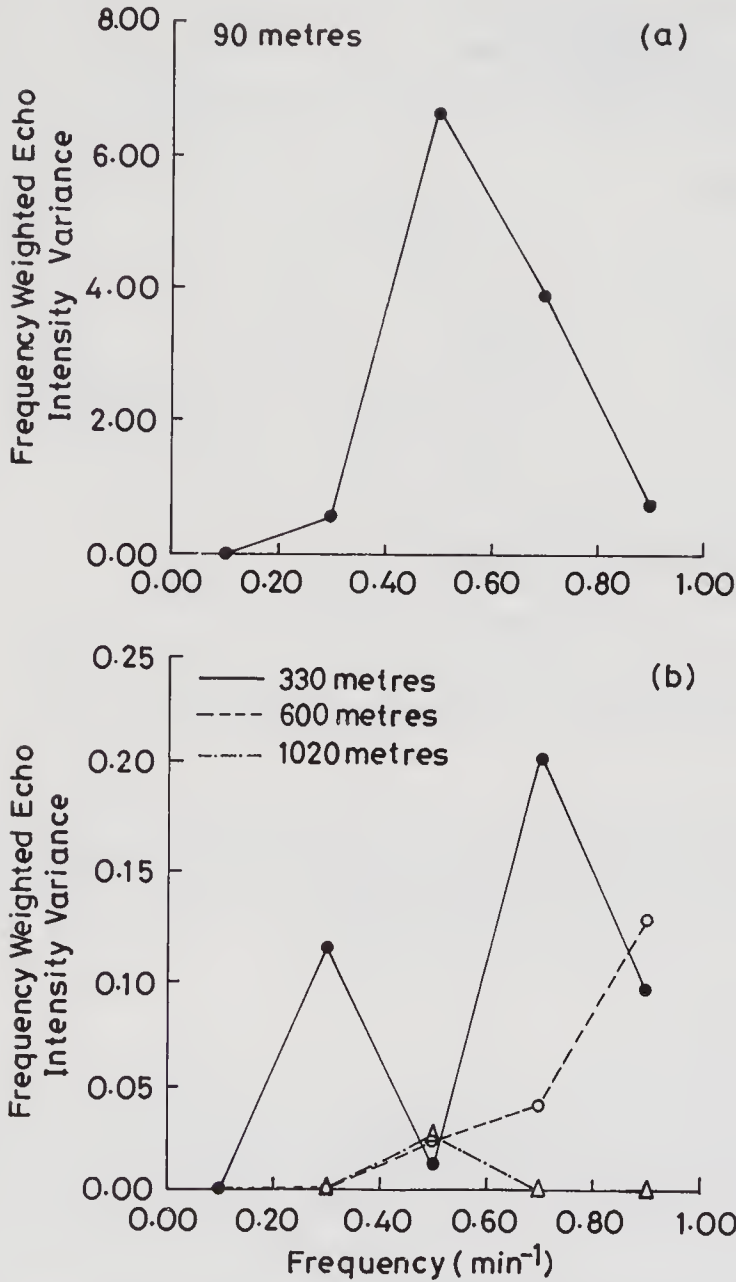


Figure 5a and b. Variance of frequency weighted echo intensity plotted against frequencies of occurrence (per minute) of return pulse at (a) 90 m range and (b) at other ranges of interest for the stable ABL cases. ν_m corresponds to a dominant frequency of the variance series.

the 330 m range. Horizontal wind speeds at 330 m range for both the cases of stability are taken from the sodar data-set. In this way we are able to express the horizontal wavelength for the u and v components of horizontal wind (L_H) as:

$$L_H = U_H / \nu_m \quad \text{where} \quad U_H = (\bar{u}^2 + \bar{v}^2)^{1/2}.$$

4. Characteristics of non-dimensional L_H during the monsoon period

Doppler sodar data were used to find the horizontal scale of motion (L_H) by use of the

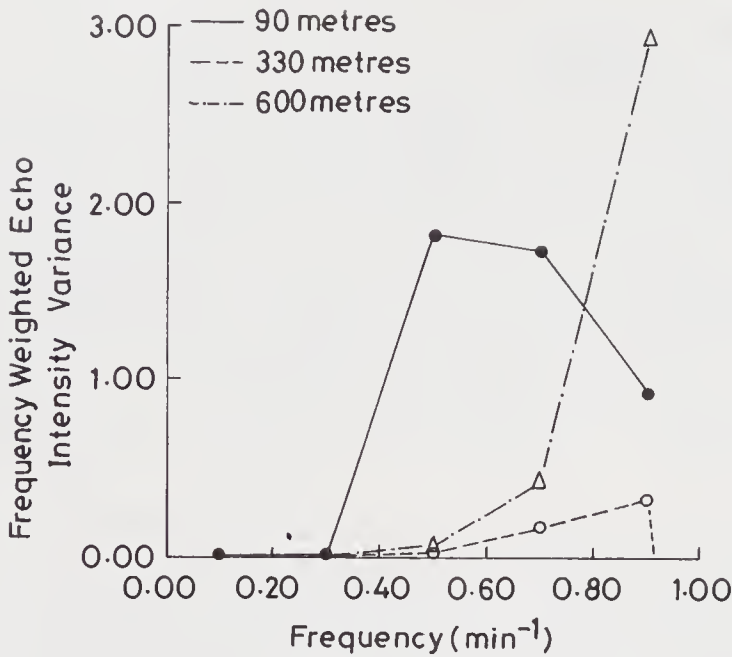


Figure 6. Same as in figure 5 but for the unstable ABL cases.

method described in the preceding section, and the magnitudes of the non-dimensional ratio L_H/Z_i were plotted along with the principal stability parameter Z_i/L_o . Z_i is measured by the Doppler sodar as essentially the height where the backscatter intensity peaks in the vertical. L_o is mathematically expressed as:

$$L_o = \frac{u_*^2}{\kappa(g/\theta_{v_o})\theta_{v*}}$$

where u_* is the surface layer friction velocity in metres per second, θ_{v*} is the reference virtual potential temperature of the surface layer expressed in degree Kelvins, θ_{v_o} is virtual potential temperature just over the surface of the earth in degree Kelvins, g is acceleration due to gravity and κ is the Von-Karman constant ($=0.4$). These are determined using a linear super-imposition technique for the wind and temperature profiles in the surface layer (Paulson 1970) after choosing a standard similarity relation for the profile (Dyer and Bradley 1982). Once θ_{v*} and u_* are evaluated, L_o may then be evaluated from the equation cited above, iteratively for each case of stability. Convergence in the evaluation of L_o was obtained in most cases within 5–10 iterative steps.

From a plot (shown in figure 7) we find that there occurs a flatter response of L_H/Z_i during cases of stable and unstable ABL over the station KGP, i.e., the magnitudes of L_H/Z_i cover a wider range of the principal stability parameter (Z_i/L_o) as compared with the results obtained over the sea-surface and published by Fitzjarrald (1978) by use of the Global Airmass Transformation Experiment (GATE-1974) data. Power fits obtained from the computed data as shown in figure 7 may be written as follows:

$$\text{GATE (over sea)} \quad \frac{L_H}{Z_i^{0.62}|L_o|^{0.38}} \cong 8.8,$$

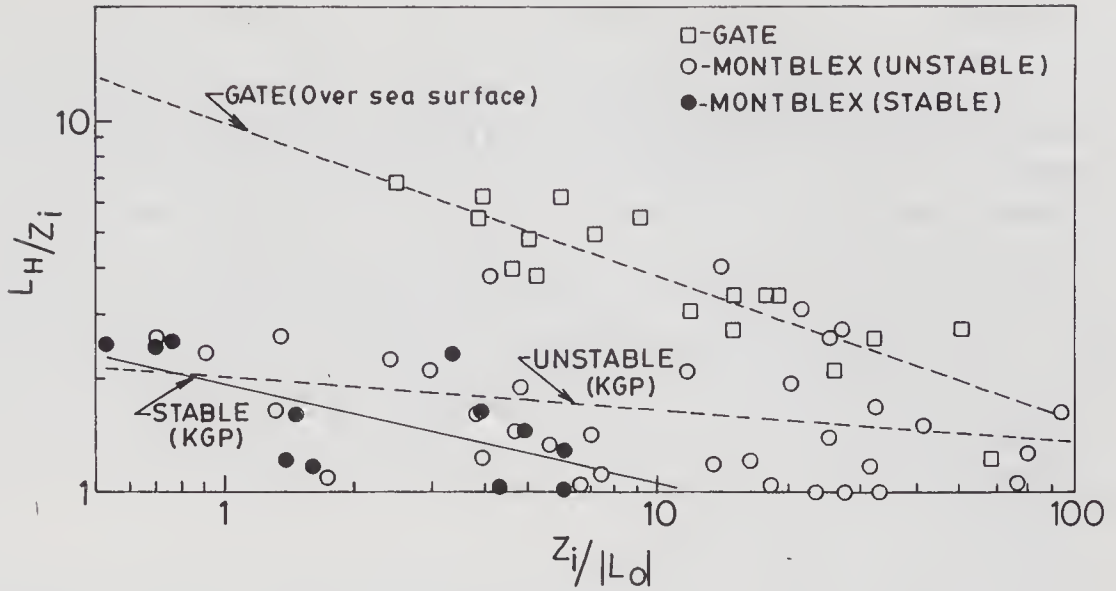


Figure 7. Horizontal scale of wind components (non-dimensionalised by Z_i) shown as a function of the principal ABL stability parameter. Note a flatter response of non-dimensional L_H as observed over inland station KGP than that reported over the sea surface (Fitzjarrald 1978).

Stable ABL (KGP)
$$\frac{L_H}{Z_i^{0.74} L_o^{0.26}} \cong 1.932,$$

Unstable ABL (KGP)
$$\frac{L_H}{Z_i^{0.90} |L_o|^{0.1}} \cong 2.033.$$

These relations in general show that the values obtained separately for the stable and the unstable conditions are not significantly different. The GATE values are about four times greater than those found at the station KGP. However, it is also to be noted that the GATE results used include data of the stable as well as the unstable cases together. From these fits it is seen that during the unstable ABL condition, the magnitude of $L_H/Z_i = 1.796$ when $Z_i/|L_o|$ is greater than 20 (indicating a range of moderate convection). For the stable case L_H/Z_i has an average value of 1.681 when Z_i/L_o is between 2 and 20. It is also evident that a change in L_H would be seen as adjustment in the ratio by Z_i and L_o so that the ratio is constant. Mahrt (1981) also pointed out that horizontal motions do impart a pressure gradient that indirectly transports momentum across the interfacial layer (between Z_i and free air aloft). This explanation may also be found applicable here. From these relations it is also obvious that the magnitude of L_H is significantly dependent on the characteristic frequency (v_m) because the horizontal wind speed is expected not to be significantly different in terms of its magnitude occurring over the sea surface than that occurring over the land surface. It may be interestingly pointed out here that the longer L_H values obtained over the sea surface are mostly due to occurrence of a significantly lower peak frequency of the echo intensity variance series than that found over the land station KGP. In this connection it is also necessary to point out that the peak frequency of the echo intensity variance series is also representative of the rapidity in the virtual temperature fluctuations.

5. Discussion

It was reported by Fitzjarrald (1978) that the dominant horizontal scale observed over the sea surface is around twice that of Z_i at high instabilities, and about 6 times Z_i at low instabilities. In this study we find that L_H when non-dimensionalised by Z_i as well as L_o together appearing in the denominator with different fractional powers (as in the respective power fits), the ratio is around 2.0 for the stable as well as for the unstable cases. A similar approach to resolve a power-fit of the GATE data reveals that the ratio is 8.8. This also implies that there occurs a wider coverage of the non-dimensional form of L_H on the principal stability parameter (see figure 7). In the case of the stable condition L_H/Z_i will tend to fall at a faster rate when compared with the same for the unstable case. This is because in the case of the stable boundary layer Z_i/L_o has higher power (0.26) than in the case of the unstable condition (0.1). This is quite consistent with the observations shown in figure 7.

We earlier saw an inter-relation between the mixing depth and the inversion depth in ABL observed over the station KGP. The inter-relation is through an empirical form of the surface stability parameter (Roy *et al* 1993). The inter-relation also points out that any change in the mixing depth also accounts for a change in the inversion depth. In this study we find that when Z_i is small compared to L_H then it may be that an increase in stress in the surface layer (due to advection of wind) results in a stronger mixing in the ABL hence a rise in the inversion height. This study has revealed the fact that with increase or decrease in the magnitude of the advective wavelength of horizontal wind over the station KGP, Z_i and L_o adjust differently magnitudewise because they have different exponents. This is true since the ratio is almost the same for both the cases of stability. During unstable conditions, the results obtained for station KGP indicate that for a change in magnitude of L_H , Z_i is expected to change more sharply than L_o . This is because the power of Z_i is 0.9 compared to the power of L_o , i.e. 0.1. GATE results signify that Z_i and L_o together absorb the changes almost equally since the powers of Z_i and L_o are about 0.6 and 0.4 respectively.

Acknowledgements

The authors are thankful to the Department of Science and Technology, New Delhi, for the research grant under the MONTBLEX programme that enabled them to pursue this work.

References

- Best P R, Ewald J and Ranowski M 1981 The estimation of pollutant dispersal from Queensland power stations; *Proc. 7th Int. clean air conference*, Clean Air Society of Australia and New Zealand, Adelaide, Australia (eds) K A Webb and A I Smith, August 24–28 pp. 429–448
- Dyer A J and Bradley E F 1982 An alternative analysis of flux-gradient relationships at the 1976 ITCE; *Boundary-Layer Meteorol.* **22** 3–19
- Fitzjarrald D E 1976 A field observation of atmospheric free convection; *J. Appl. Meteorol.* **15**, 259 pp
- Fitzjarrald D E 1978 Horizontal scales of motion in atmospheric free convection observed during GATE experiment; *J. Appl. Meteorol.* **17** 213–221

- Frisch A S, Chadwick R B, Moninger W R and Young J M 1976 Observations of boundary layer convection cells measured by dual – Doppler radar and echo sonde and by microbaro- graph array; *Boundary-Layer Meteorol.* **10** 259 pp.
- Kaimal J C, Wyngaard J C, Haugen D A, Cote O R, Izumi Y, Caughey S J and Reading C J 1976 Turbulence structure in the convective boundary layer; *J. Atmos. Sci.* **33** 2152 pp.
- Mahrt L 1981 Circulations in a sheared inversion at the mixed layer top; *J. Met. Soc. Jpn.* **59** 238–241
- Mandics P A and Hall F F Jr 1976 Preliminary results from GATE acoustic echo sounder; *Bull. Am. Meteorol. Soc.* **57** 1142–1147
- Paulson C A 1970 The mathematical representation of wind speed and temperature profiles in the unstable atmospheric surface layer; *J. Appl. Meteorol.* **9** 856–861
- Roy B, De U K and Rakshit D K 1993 On surface dependence of mixing depth in ABL – Case study using Doppler sodar data; *Proceedings of the 3rd International conference on advances in pattern recognition and digital techniques*, December 28–31 (Calcutta) p. 581–588

Wind profiles in the boundary layer over Kharagpur associated with synoptic scale systems

D K PAUL, S P GHANEKAR, B S MURTHY and K G VERNEKAR

Indian Institute of Tropical Meteorology, Pune 411 008, India

Abstract. Doppler sodar wind data for the boundary layer over Kharagpur obtained during MONTBLEX-1990 at a height interval of 30 m from surface up to 1500 m have been analysed for the periods when intense synoptic scale disturbances from north Bay of Bengal moved along the eastern end of the monsoon trough. The variation in the vertical wind profile in the lower boundary layer over Kharagpur during the passage of synoptic scale disturbances has been discussed in the paper. The analysis indicates that the mean winds over Kharagpur veered with height in the lower boundary layer near the surface suggesting divergence over Kharagpur when the system lay south/southwest of the station. No such veering has been noticed when the centre of the system lay very close to the station.

Keywords. Atmospheric Boundary Layer; synoptic systems; wind profile; veering.

1. Introduction

The Monsoon Trough Boundary Layer Experiment (MONTBLEX) was conducted during April – September 1990. 30-m instrumented towers were erected at Kharagpur, Varanasi, New Delhi and Jodhpur. Special instruments like Doppler sodar and Kyttoon were operated at Kharagpur. Other than these main stations, the India Meteorological Department arranged special observations at stations around the main tower stations. The main objective of the MONTBLEX programme was to study the Atmospheric Boundary Layer in the monsoon trough region during monsoon 1990.

The axis of the monsoon trough, under normal monsoon conditions, stretches from northwest India to north Bay of Bengal across the Gangetic plains. Kharagpur is situated close to the eastern end of the monsoon trough and lies within the moist convective regime of the trough. The synoptic features prevailing over the eastern part of the Indian region prior to and during the formation of synoptic scale systems showed the eastern end of the monsoon trough dipping into north Bay of Bengal, giving rise to low level cyclonic vorticity over the region (Sikka 1977). The low level monsoon westerlies after crossing south peninsula turn cyclonically around the eastern edge of the trough axis, and become southeasterly to easterly. Kharagpur lies in the stream of moist easterly winds when the disturbance lies to the south/southwest of it. With the shift of the trough axis towards the foothills of the Himalayas as the system moves northward, the station comes under the grip of westerly winds in the lower troposphere to the south of the trough.

In this study the Doppler sodar winds in the boundary layer over Kharagpur (22.3°N, 87.2°E) have been analysed and the boundary layer profiles have been studied under different situations, when the synoptic scale systems during their westward movement lay very close to the station or at some distance away from the station. The

sodar winds in the boundary layer over Kharagpur have also been compared with the synoptic wind analysis at the standard levels viz., 300, 600, 900 and 1500 m above sea level.

2. Data and method of analysis

The Doppler sodar was operated at Kharagpur during April – September 1990. The Doppler sodar determines the winds at 30 m intervals up to 1500 m. The winds averaged over a period of one hour were obtained. The Doppler sodar gives the total wind and its three components, their standard deviations, backscatter intensity and vertical wind gradient over 30 m.

Hourly Doppler sodar wind data at Kharagpur are analysed in time sections for each day. The analysis (not shown) does not indicate any well-defined diurnal variations of the boundary layer winds at Kharagpur except that winds are stronger and more steady in the early hours of the day than during the rest of the day. The zonal (u), meridional (v) and vertical (w) components of sodar winds are averaged for early morning hours from 0500 to 0900 instead of taking a fixed hour of observation which is rather discontinuous due to occasional missing data. The mean sodar winds for the morning hours are thus taken to correspond to morning synoptic wind observation of 00 UTC (0530 hrs IST). It may be noted that the sign convention of sodar wind components is opposite to that of the meteorological sign convention. For sodar data negative u and v correspond to westerly and southerly wind components and negative w corresponds to descending motion over the station. We have however converted the signs of sodar wind data to the usual meteorological sign convention. The wind components are analysed in the vertical time section for the days of the disturbances. Daily vertical profiles of wind components are also examined. The synoptic upper air wind data obtained from Radiosonde and Pilot balloon observations for 00 UTC at standard levels of 300, 600, 900 and 1500 m are analysed over the Indian region.

3. Synoptic scale systems under study

The boundary layer wind profile over Kharagpur in association with three intense synoptic scale disturbances (two monsoon depressions and a well-marked low) which formed over north Bay of Bengal during the later half of August till early September 1990 are studied in this paper. These situations correspond to active monsoon over the region. The tracks of these two depressions from their formative to dissipation stages and the location of a well-marked low pressure area on 29th August are shown in figure 1. It can be seen from figure 1 that the track of the depression of 20th–25th August has passed south of Kharagpur at a perpendicular distance of about 200 km from it and that of the other, of 1st–5th September, has passed almost across the station. The former system formed as a well-marked low over north Bay of Bengal about 250 km southeast of Kharagpur on the morning of 20th August (Indian Met. Dept., 1990). It concentrated into a depression by the same evening, crossed the eastern coast on 21st August, moved westwards and dissipated on 25th August. The second system had formed as a well-marked low pressure area and lay about 250 km southwest of Kharagpur on 29th August 0300 UTC (0830 hrs). The third system was the remnant

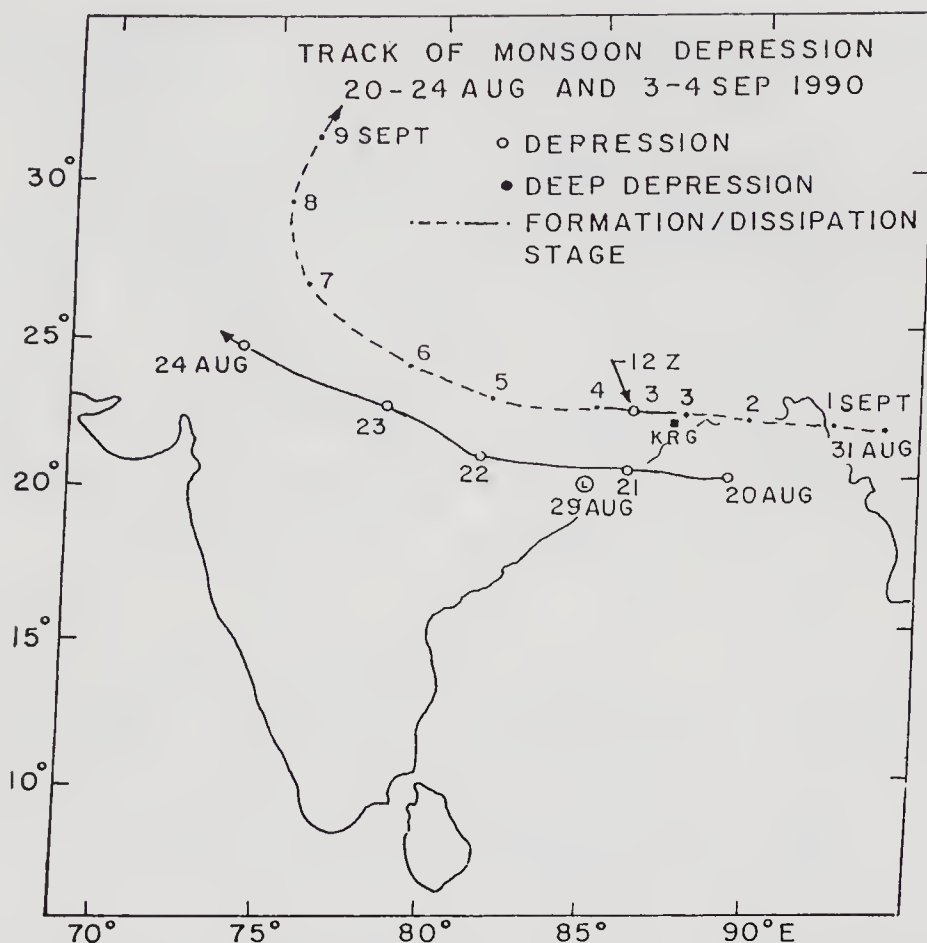


Figure 1. Track of lows/depressions during (i) 20th–24th August, 1990 and (ii) 31st August – 7th September, 1990 with the location of the well-marked low pressure area on 29th August, 1990.

of the west Pacific typhoon Becky, which on emerging to the extreme northeast Bay on 1 September moved westwards and lay as a well-marked low almost over Kharagpur on the morning of 3rd September. The location of the system at 0300 UTC (0830 hrs IST) can be seen from figure 2. It intensified to a depression by the afternoon of 3rd September and remained so till 4th September as it moved west of Kharagpur. Moving further westwards it weakened to a well-marked low and lay about 450 km west of Kharagpur on 5th September.

4. Results and discussion

The synoptic wind analysis at 600 and 1500 m for 00 UTC for three representative days of these systems, viz., 21st August, 29th August and 5th September, are shown in figure 3. The wind flows at 300, 600 and 900 m for 3rd September, when the system was located almost over the station, are shown on the bottom panel of the figure (figure 3). The sodar winds obtained at the respective height level are plotted in the chart at the location of Kharagpur. The mean sodar winds in the boundary layer over Kharagpur matched well with the prevailing synoptic wind flows up to 600 m on 21st August and 5th September for the depression cases and up to 450 m for the weaker system on 29th

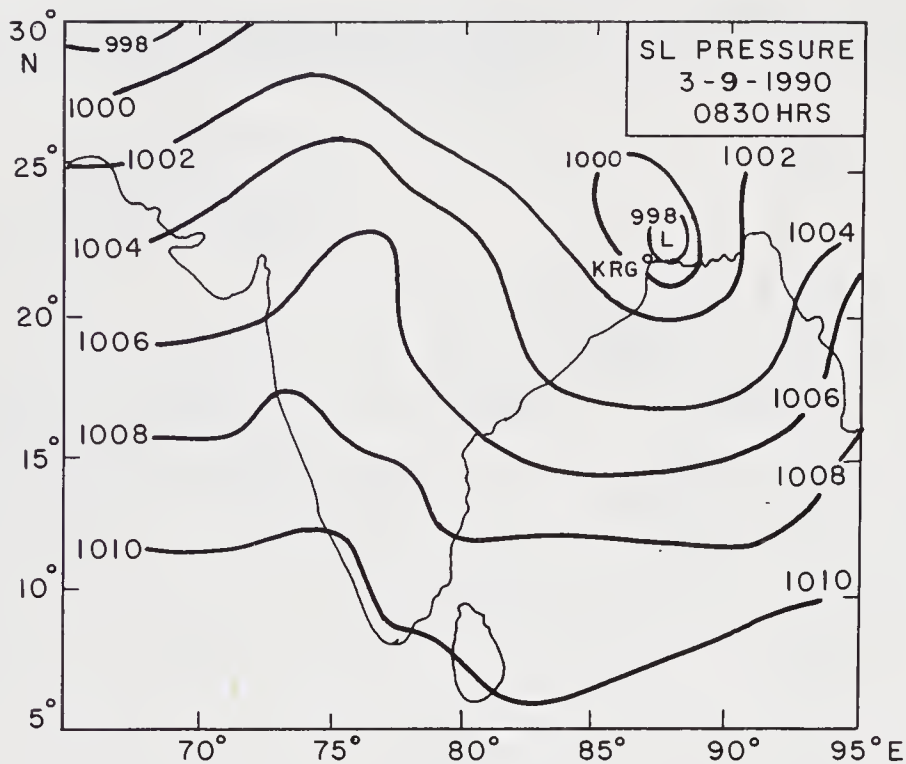
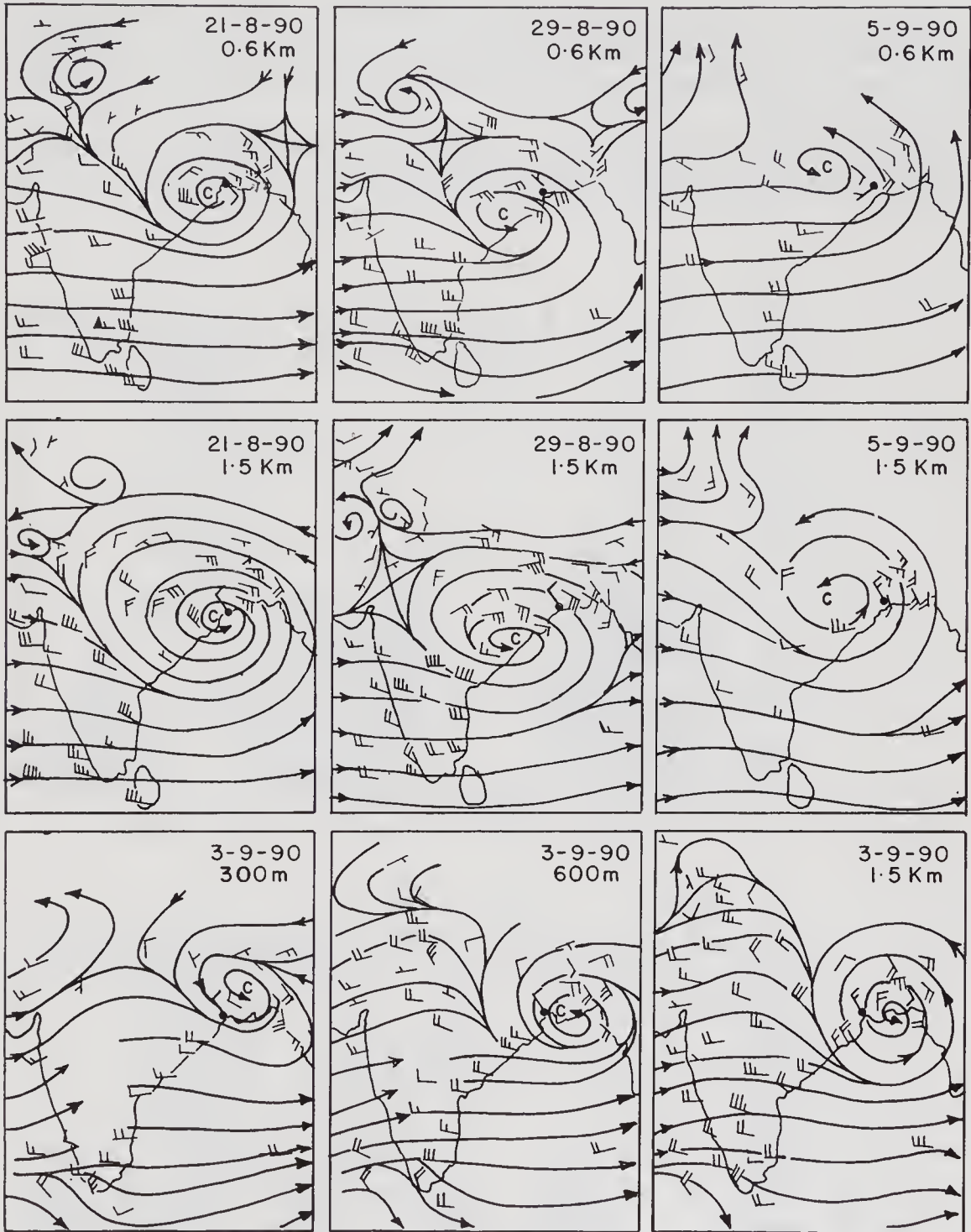


Figure 2. Sea level pressure analysis for 0830 hrs IST of 3rd September, 1990 showing the location of the low pressure system almost over the station Kharagpur.

August. It did not match at 900 and 1500 m levels where the sodar wind together with the nearby synoptically observed winds suggested formation of a meso-scale cyclonic circulation near Kharagpur. The mean morning time sodar winds thus agree with the instantaneous synoptic winds up to about 600 m for intense systems like depressions, beyond which the agreement between the two is not good.

The daily morning mean zonal and meridional components of the sodar winds are analysed in vertical time sections for the three cases: ■ 18th–24th August; ■ 27th–31st August and ■ 1st–7th September, 1990. Figure 4 shows the vertical time section of sodar winds for the periods 18th–24th August and 27th August – 7th September. Strong easterly winds over Kharagpur are observed up to about 750 m during the first two cases when the depressions were located away from the station and southwards by 200–250 km during their westward passage. The westerly winds above 750 m were rather weak. The lower level easterly winds, in the case of the first disturbance, rapidly weakened by early morning of 22nd August and changed to westerlies as the system moved further away from the station. The westerly winds dominated the entire boundary layer during 23rd–26th August till the second system formed on 26th August.

In the second case, the easterlies persisted till 31st August as the system moved slowly northwestwards. Strongest easterlies are observed on 21st August and 28th–29th August when the systems lay closer to the station within a distance of about 200–250 km. Contrary to this, the boundary layer winds in the third disturbance showed a different profile. On 3rd September the system lay almost over Kharagpur within 50 km and the westerly winds penetrated downwards through the boundary layer up to the surface level. Westerlies above 750 m were also stronger (> 10 m/s) compared to the



• KHARAGPUR

Figure 3. 0530 IST synoptic wind at 600 m (top), 1500 m (middle) for 21st, 29th August and 5th September 1990 and the same at 300, 600, 900 m for 3rd September 1990 (bottom).

other systems. Easterlies in the lower level up to 450 m were observed on 5th September when the system moved about 450 km away from the station.

The meridional winds over Kharagpur also showed similar characteristics with weak southerlies in the lower levels up to 750 m and northerlies aloft, when the systems were

moving westwards of the station during 21st–24th August, 29th–31st August and 4th–7th September. Northerlies dominated the boundary layer during the rest of the period. On 3rd September strong northerlies penetrated downwards up to the surface level over the station.

The profile of zonal and meridional winds for the days 21st August, 29th August and 3rd and 5th September representing the three cases of disturbances mentioned above

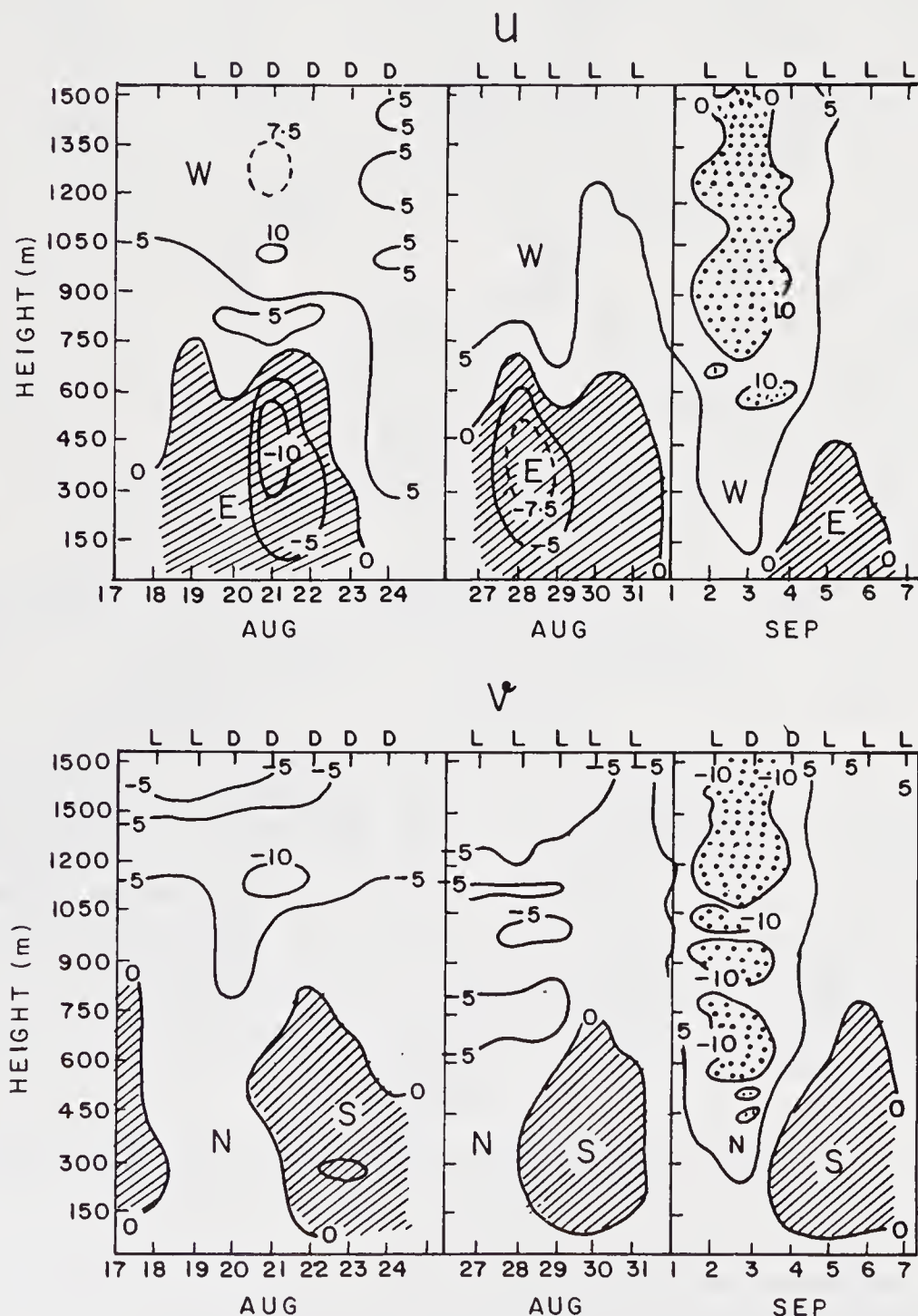


Figure 4. Vertical-time section of sodar wind at Kharagpur for the periods, 18th–24th August and 27th August – 7th September, 1990.

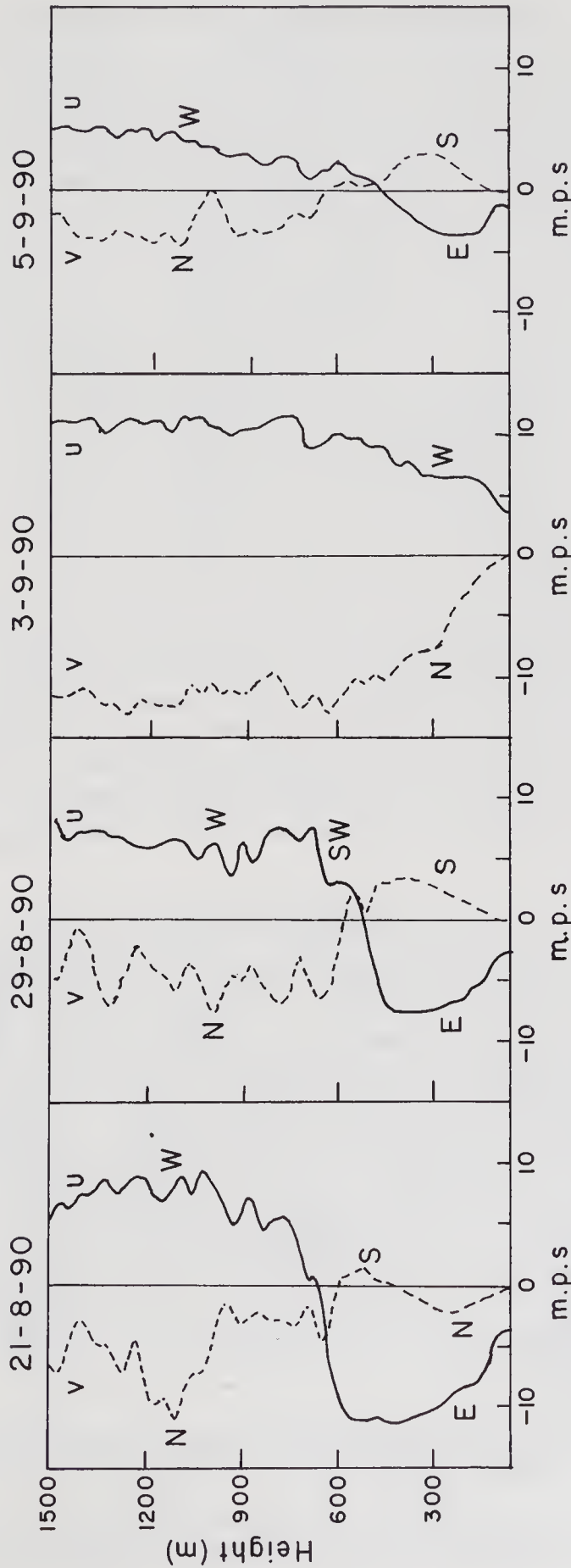


Figure 5. Vertical profile of zonal (u) and meridional (v) winds over Kharagpur for 21st August, 29th August, 3rd and 5th September 1990.

are shown in figure 5. The figure shows that the winds in the boundary layer over Kharagpur veered with height from northeasterly to southeasterly and then to northwesterly in the first two cases on 21st and 29th August and also on 5th September in the case of the third disturbance. No such veering is observed on 3rd September when the centre of the system lay over Kharagpur. The veering of winds with height in the lower boundary layer near the surface suggests boundary layer convergence over Kharagpur when the system lay south/southwest of the station.

The vertical component of the winds over Kharagpur is also analysed. Figure 6 shows a time section of vertical components of winds in the boundary layer over Kharagpur for the three cases of disturbances. While weak descending motions (< 1 m/s) are seen above 750 m in the case of the first two disturbances, the third case has shown strong descending motion of > 2 m/s on 3rd September. Figure 7 shows a profile of vertical wind component over the station for the three representative days of 21st, 29th August, 3rd and 5th September. Strong downward motion at the rate of $1.5 - 2.5$ m/s is seen above 200 m in the profile of vertical motion on 3rd September. The vertical velocity for the other two cases showed weak descending motion of the order of less than 1 m/s.

Sikka and Paul (1975) from their study of the structure of monsoon depressions have shown that the vertical velocity for the boundary layer is mainly due to the effect of the frictional term. The differential vorticity advection and thermal advection terms of the quasi-geostrophic omega equation produce weak upward motion near the centre and ahead of it and weak downward motion to the east of the centre. Kharagpur lay to the northeast of the centre of the systems on 21st and 29th August. On 3rd September the centre was over the station itself where strong descending motion at the centre of the system dominated. The weak downward motion over Kharagpur lying to the northeast of the centre of the system during 21st and 29th August is understood. However, the

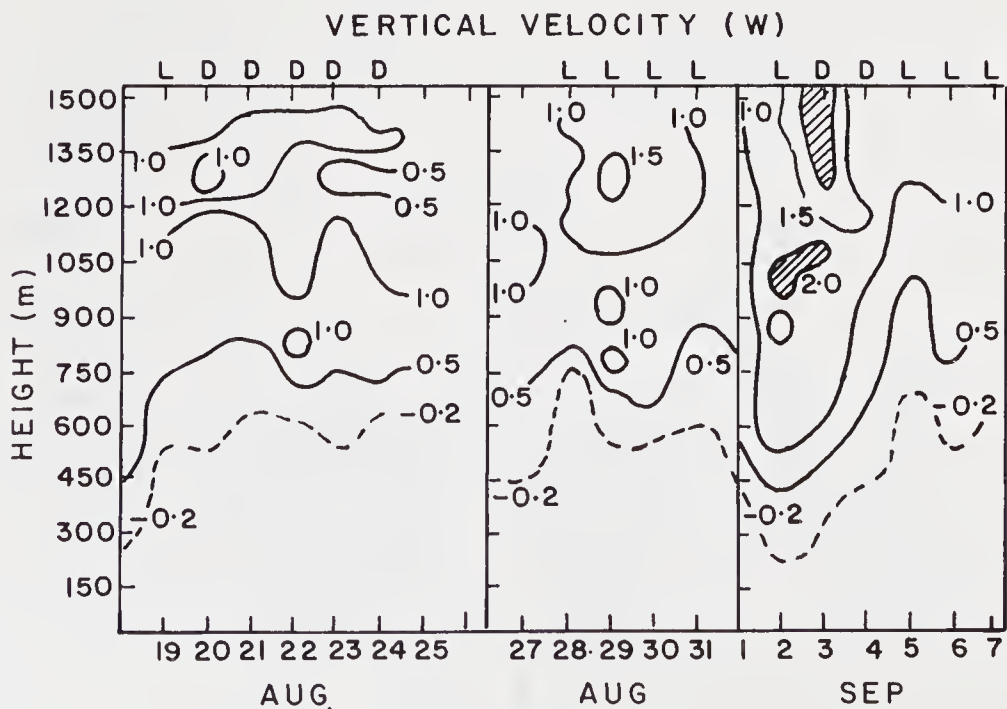


Figure 6. Same as figure 4, but for the vertical component of winds (w).

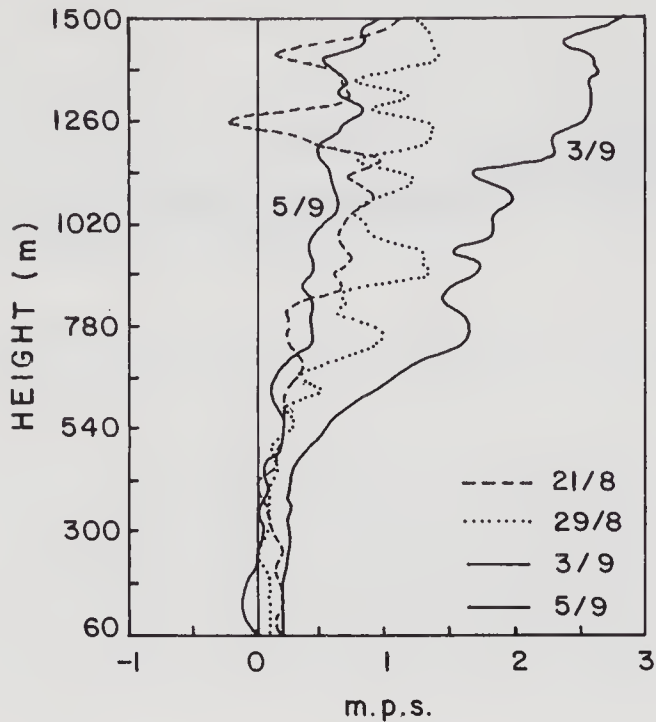


Figure 7. Same as figure 5, but for the vertical component of winds (w).

cause of the strong descending motion over Kharagpur close to the centre of the system on 3rd September needs further investigation.

5. Concluding remarks

The wind profiles in the boundary layer over Kharagpur in association with intense synoptic scale systems have been studied based on Doppler sodar wind data obtained during MONTBLEX 1990. The study showed that when the synoptic scale system lay somewhat SSW from Kharagpur at a distance of about 200–250 km, the boundary layer winds show good agreement with the synoptic wind analysis up to 750 m from the surface, beyond which there is no agreement. The sodar wind at 900 and 1500 m at Kharagpur together with some neighbouring synoptically observed winds suggests a meso-scale cyclonic circulation within the boundary layer near Kharagpur.

The study also showed that the mean wind over Kharagpur veered with height in the lower boundary layer suggesting divergence over Kharagpur, as the system lay to south/southwest of the station. No veering of winds is observed when the system lay over the station as on 3rd September 1990. The vertical wind components showed strong (weak) descending motions over Kharagpur when the systems are located very close to the station. The cause of such strong descending motion in the boundary layer near the centre of the systems needs further investigation.

Acknowledgement

The authors are thankful to the Department of Science and Technology, and also to colleagues of IITM who participated in the MONTBLEX programme.

References

Sikka D R 1977 *Pageoph* **115** 1501–1529

Sikka D R and Paul D K 1975, Lecture Notes: Geophysical fluid dynamics workshop on topics in Monsoon Meteorology, IISc, Bangalore, Vol. 1, 241–307

India Meteorological Department, 1990: *Daily Weather Reports*. July – September 1990.

Some observations from the data taken in and around Kharagpur during the onset of the monsoon, 1990

R PRADHAN, B ROY, U K DE and D K RAKSHIT

Department of Physics, Jadavpur University, Calcutta 700032, India

Abstract. During MONTBLEX 1990, various observational platforms were operated at Kharagpur and the nearby Kalaikunda Air Base. Using the data from all the platforms, one can draw the following conclusions. The temperature and wind data obtained from various sensors have overall compatibility. Sodar wind data indicate the presence of a low level jet at around 300 m above ground. The inversion height may be evaluated from the vertical profile of the sodar back-scatter echo intensity. The sub-synoptic or synoptic scale convergence modulates the inversion height and the presence of cloud-base within the inversion height in turn modulates the sensible heat and momentum fluxes.

Keywords. Boundary layer; inversion height; back-scatter intensity; surface parameters; convective instability; low level cloud-base height.

1. Introduction

In terms of global balance of energy, the surplus energy of the tropical region is transported from the surface of the earth to the upper atmosphere through two distinct processes, i.e., by radiation and by convection. In the process of convection eddy diffusion plays a decisive role, and occurs through the boundary layer. This diffusion (in the vertical direction) is controlled by the corresponding thermal as well as wind profiles over the region. In reality, the boundary layer influences the overall atmosphere to a great extent through parameters like the vertical gradients of potential temperature and the wind velocity.

In the present work the data generated at Kharagpur ($22^{\circ}18'N$, $87^{\circ}12'E$) observational station and that supplied by the nearby Kalaikunda (KLK) Air Base (3 to 4 km away from Kharagpur tower site) are utilized. At Kharagpur, a 30 m-high micro-meteorological tower with six levels of instrumentations (at heights 1, 2, 4, 8, 15, and 30 m) was erected. Besides, other observational facilities like an Aerovironment-make 3-axis, monostatic Doppler Sonic Detection and Ranging (sodar) system and some flights of a tether sonde were available. Surface and upper wind data and cloud-base heights observed with the help of a laser ceilometer were collected at the Kalaikunda Air Base and these data were also available.

In the present study, however, attention is confined to the monsoon onset phase only. The nature of the boundary layer during the onset phase is expected to be interesting, especially over a deep moist convective region like Kharagpur. The monsoon onset phase at Kharagpur in 1990 was June 1st – 17th.

First, we have utilized all available data during the period June 4th – 9th at Kharagpur and Kalaikunda to sketch the thermal and dynamical vertical structure from the surface up to the maximum available height. Simultaneous data from all the

above-mentioned sources were available only during the period June 4th – 9th. It has been found that the vertical profile of horizontal wind velocity components and temperature available from the various sources have overall compatibility.

Second, the vertical profiles of back-scatter echo intensity from the sodar system are presented for various times. In ten out of twelve cases, the inversion height supplied by the sodar coincides with the first peak in back-scatter echo intensity profile, but in two cases the coincidence is better with the second peak. Lastly, the time series for the surface parameters like sensible heat flux and momentum flux have been constructed for the period June 4th – 9th. The base of low level cloud supplied by a laser ceilometer at Kalaikunda Air Base has been correlated with the inversion height supplied by the sodar. It has been observed that the sensible heat flux shows a high value whenever the base of the low level cloud overhead lies within the inversion height or a wind convergence appears either in synoptic or sub-synoptic scales.

2. Data

The following sets of data are utilized in the present study.

2.1 Data from 30 m micrometeorological tower located at the IIT campus of Kharagpur

The instrumented tower had both slow as well as fast response sensors. In the present work, only 3-minute averaged slow response data available from MONTBLEX data bank are directly used.

2.2 Data from tether-sonde (kytoon) flights

The Atmospheric Instrumentation Research Inc. (USA)-make kytoon was flown at Kharagpur. Such flights could be accomplished only from the end of May 1990 to the end of June 1990. Altogether 29 flights were taken, out of which 20 were in the morning hours (between 0500 IST and 0600 IST) and the rest were in the afternoon hours (between 1400 IST and 1600 IST).

On an average the kytoon reached a height of about 350 m above ground, but on a few occasions it soared much higher. One of the reasons for its low level operation was the high wind conditions prevailing over Kharagpur during the month of June (Roy 1994).

Basic parameters like temperature, wind velocity, wind direction, relative humidity and the pressure heights were sensed directly by a data acquisition system attached to the kytoon.

2.3 Data from acoustic sounder or sodar

The 3-axis monostatic Doppler sodar operated during the MONTBLEX period has a sounding height ranging from 60 m to 1500 m; operation times were from 0530 IST to 1230 IST and again from 1430 IST to 1930 IST. However, during the intensive observation periods the sodar was operated for 24 hours. The sodar mostly provided the hourly averaged data, but in some cases 30-minute average data were also available.

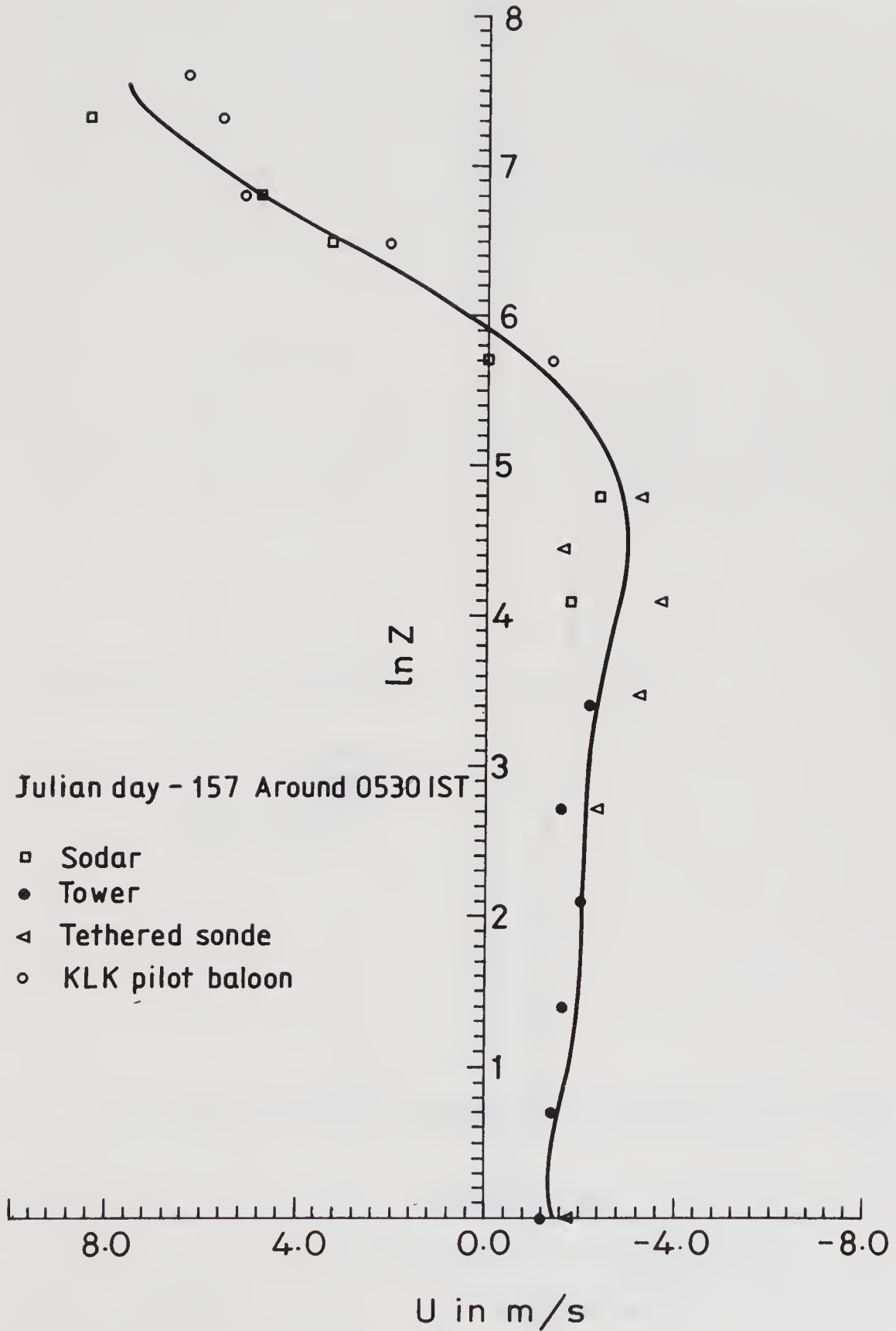


Figure 1(a). Mean vertical profile of zonal wind.

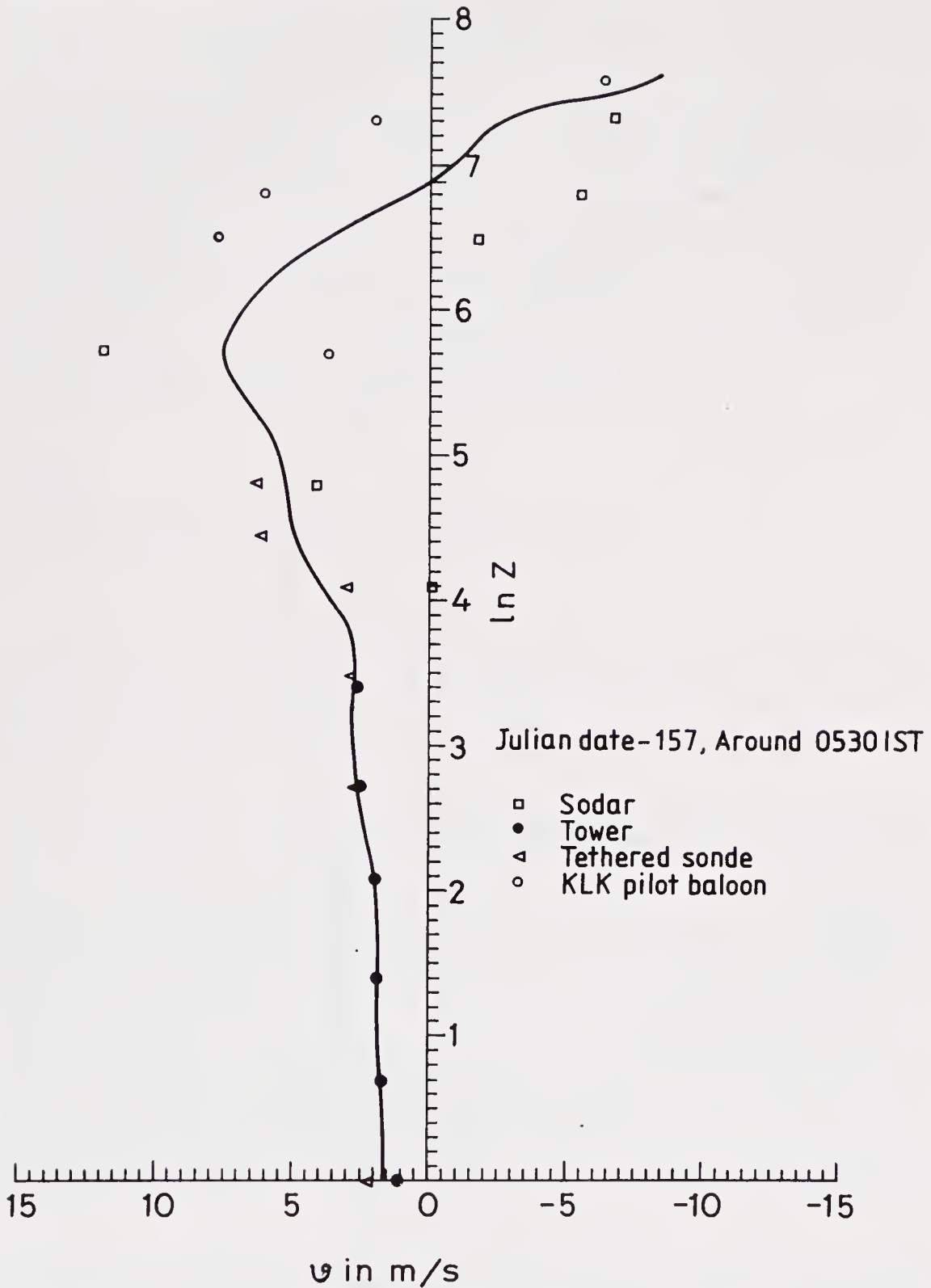


Figure 1(b). Mean vertical profile of meridional wind.

2.4 Pilot balloon data from Kalaikunda

In general pilot balloon observations were taken during four synoptic hours i.e., 00 UTC, 06 UTC, 12 UTC and 18 UTC. Although the observations were taken from

Kalaikunda Air Base, the upper wind data may be taken as almost representative for Kharagpur which is within a distance of 5 km.

It should be noted that all the four above-mentioned sensors provided wind data though the averaging periods were different. Besides, the height range of the tower and kytoon overlapped but the sodar ranges were much beyond; and lastly pilot balloon and the sodar data overlapped over a range of height, though the pilot balloon soared to a much greater height. Thus the wind data available from four different sensors have overlapping ranges but different averaging times.

However, temperature data were available only from the tower and kytoon, so these comparisons remain limited to the tower height.

2.5 Ceilometer data from KLK

The laser ceilometer was operated from the KLK Air Base at one-hour intervals during day-time. Data were available from 0700 IST to 1800 IST. These data provide the low level cloud-base height for the present study. The ceilometer cloud-base height at a particular hour is actually the mean of the two readings taken in a 10-minute interval.

Table 1. Dry bulb temperature in °C.

Date	Time (IST)	Height (metre)	Tower	Kytoon	Kalaikunda surface
04.06.90 (155)	0606	01	27.38	—	28.0
		10	—	27.08	
		26	—	26.91	
		30	27.17	—	
		41	—	26.81	
05.06.90 (156)	0627	01	27.82	27.84	27.6
		12	—	27.69	
		30	27.88	—	
		37	—	27.5	
06.06.90 (157)	0539	01	25.38	24.78	25.0
		15	—	24.73	
		30	24.8	—	
		32	—	24.6	
07.06.90 (158)	0530	01	25.61	—	26.4
		05	—	25.89	
		18	—	25.55	
		30	25.91	—	
		42	—	25.52	
09.06.90 (160)	0554	01	27.52	—	28.0
		09	—	27.1	
		29	—	26.96	
		30	27.63	—	
		36	—	26.90	

3. Analysis of wind and temperature data

Both zonal (u) and meridional (v) components have been studied taking data from all four platforms. A representative profile of each component is presented in figure 1(a and b) respectively. In fact, the mean profile during all these days is always a smooth curve, though the curve is drawn step-wise for each layer taking mean of all the available data within that layer.

Considering the profiles on all the days from June 4th – 9th, 1990, some general conclusions may be drawn:

- A low level jet existed at around 300 m level in sodar data during the morning hours on all these days. The jet velocity never fell below 12 m/s and has a dominant southerly component. Above the jet-level, a strong veering of wind exists.
- Around 300 m the first pilot balloon data are available, and on some occasions the kytoon reaches a height around 350 m. But from these platforms there is no concrete evidence for the existence of the low level jet on all these days.
- Compared to the tower data, the kytoon always gives a more negative u -component. So, the easterly component of wind dominates in the kytoon.
- Looking at the sodar and kytoon data structures one can conclude that the v -component of the sodar wind starts going above the corresponding component of the kytoon wind at a height which varies from 100 m to 200 m. However, one should remember that the averaging times for different platforms are completely different. Pilot balloon data are instantaneous, but the averaging time for the tower data is 3 minutes, for the kytoon it is almost instantaneous; on the other hand it goes to one hour in case of the sodar.

Table 1 shows good agreement in the temperature profile between tether sonde and tower data, though the tower temperatures are in general slightly higher. It has already been pointed out that there exists a sharp variation in temperature gradient in the

Table 2. Fourteen days comparison of sodar-reported inversion depth and back-scatter echo intensity.

Julian day	Sodar sounding period in IST	Sodar-reported inversion depth	Sodar-reported back-scattered echo intensity
144	0600–0700	150 m	1st... 150 m
145	0600–0630	390 m	1st... 200 m
146	0544–0600	210 m	1st... 210 m
155	0600–0700	210 m	1st... 210 m
156	0600–0700	210 m	1st... 200 m
160	0600–0700	240 m	1st... 230 m
168	0500–0600	90 m	1st... 87 m
168	1700–1800	660 m	1st... 210 m 2nd... 640 m
169	0500–0600	600 m	1st... 140 m
170	0519–0600	90 m	1st... 100 m
170	0524–0600	180 m	1st... 120 m
172	0511–0607	450 m	1st... 400 m
174	0518–0600	Not available	1st... 400 m 2nd... 1040 m
175	0535–0600	Not available	1st... 120 m

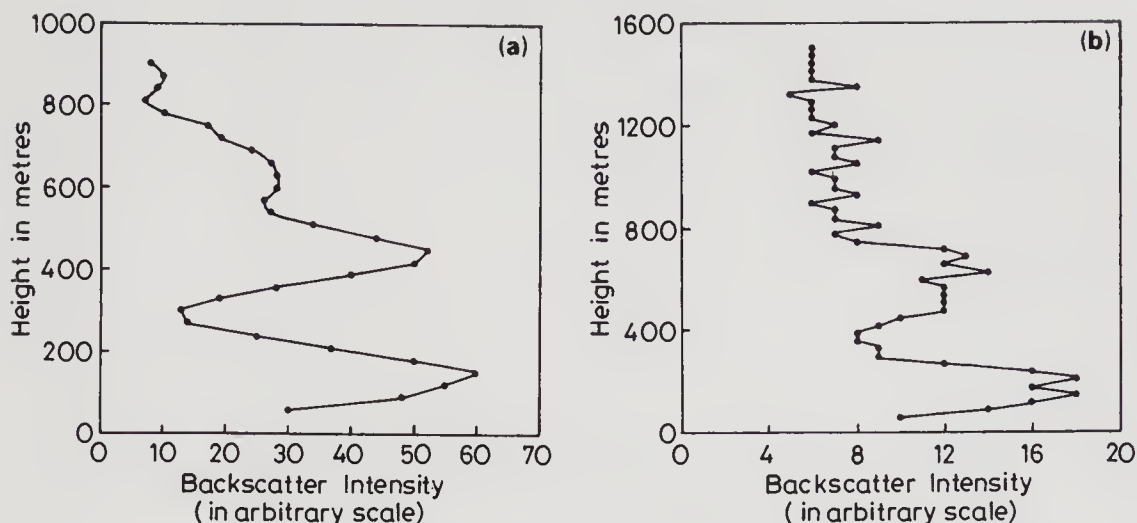


Figure 2. Vertical profile of back-scatter echo intensity as provided by sodar on (a) Julian day 144, 0600–0700 IST and (b) Julian day 168, 1700–1800 IST.

tower data (Pradhan *et al* 1994a) over 30 m height. Hence in the present study that sharp variation has been neglected by taking the temperature at the lowest level (1 m) and at the highest level (30 m) only. Tether sonde data are being presented up to a height which is nearest to but above 30 m height. Incidentally KLLK surface temperature data are included in the last column of table 1. From the table it is evident that the temperature data from different platforms are compatible.

It is also evident from table 1 that kytoon shows local surface instability on all the days. But the tower shows instability on Julian days 155 and 157 and the situation is nearly stable on all other days. Again, the lapse rate obtained from the tower data is quite comparable with that obtained from the tether sonde data on day 155. But on day 157, the lapse rate from the tower is appreciably higher. The magnitude on day 157 is higher than even the dry adiabatic lapse rate. It should be mentioned that this super-adiabatic situation has been observed in some cases. This situation is not at all unusual specially in the surface layer (Webb 1982).

It should be pointed out here that such irregularity in the thermal structure exists in many cases when the entire data set is analysed.

4. Some observations from sodar data only

The sodar provides the back-scatter echo intensity (in arbitrary units) from various ranges above the ground level, and also an inversion height with the help of an in-built algorithm. In the present work the vertical profile of the back-scatter echo intensity (I_v) is drawn and its peaks are compared with the inversion height (Roy 1994).

It is found that in eighty per cent of the cases the first distinct peak of back-scatter intensity coincides with the inversion height but in the rest (twenty per cent) the match is distinctly better with the second peak. In the latter cases, the first peak is apparently due to some noise.

In table 2, fourteen sets of data are presented covering about a month starting from May 24th, 1990. The second peak of back-scatter intensity is indicated in the table

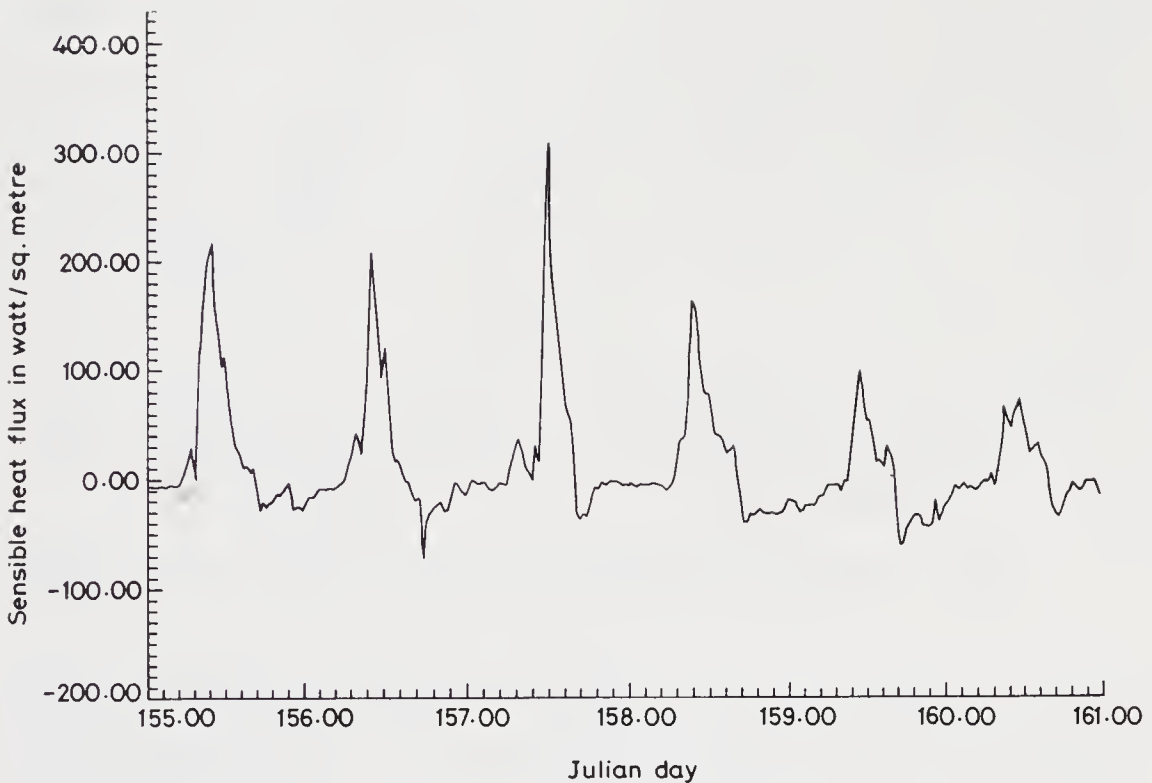


Figure 3. Time series of surface sensible heat flux from Julian day 155 to 160.

where it coincides with the sodar-reported inversion depth. All the data sets except one are during morning hours. Two representative vertical profiles of back-scatter echo intensity are being presented in figure 2(a and b). The inversion height given by the sodar system coincides with the first peak in figure 2(a) and the second peak in figure 2(b).

5. Synoptic situations, surface parameters and inter-play of low level cloud and inversion height

One can evaluate surface parameters like sensible heat flux, momentum flux and scaling temperature using the flux-profile and similarity relations of wind and temperature (Pradhan *et al* 1994b). The variations of the sensible heat flux and the momentum flux for the period of study are presented in figures 3 and 4. It should be noted that in these figures the day is indicated by Julian day and starts from 0000 IST and ends at 2400 IST.

The inter-relation of the cloud-base height from the ceilometer and the inversion height from the sodar are presented in figure 5. It is interesting to note that on June 4th, 5th and 6th (day 155 to 157) the cloud-base remains within the inversion height for varying durations of time. It is also to be noted that on those three days the maximum of the sensible heat flux also shoots up. In table 3, the time of occurrence of the maximum instability, the momentum flux and the sensible heat flux is presented. Besides, information about the temporal growth of the inversion height is also included in the 'remarks' column.

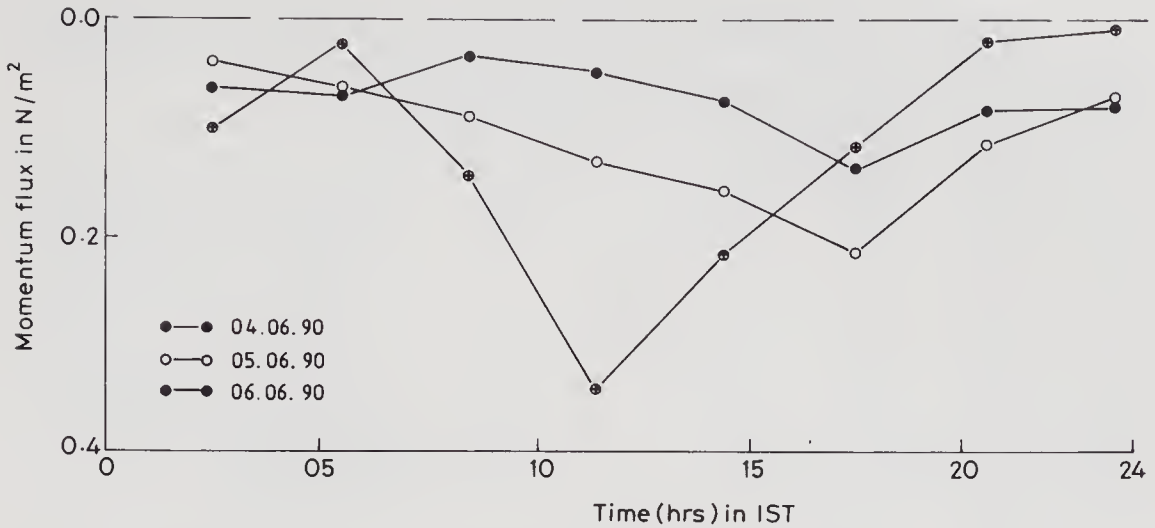


Figure 4. Diurnal variation of momentum flux from Julian day 155 to 157.

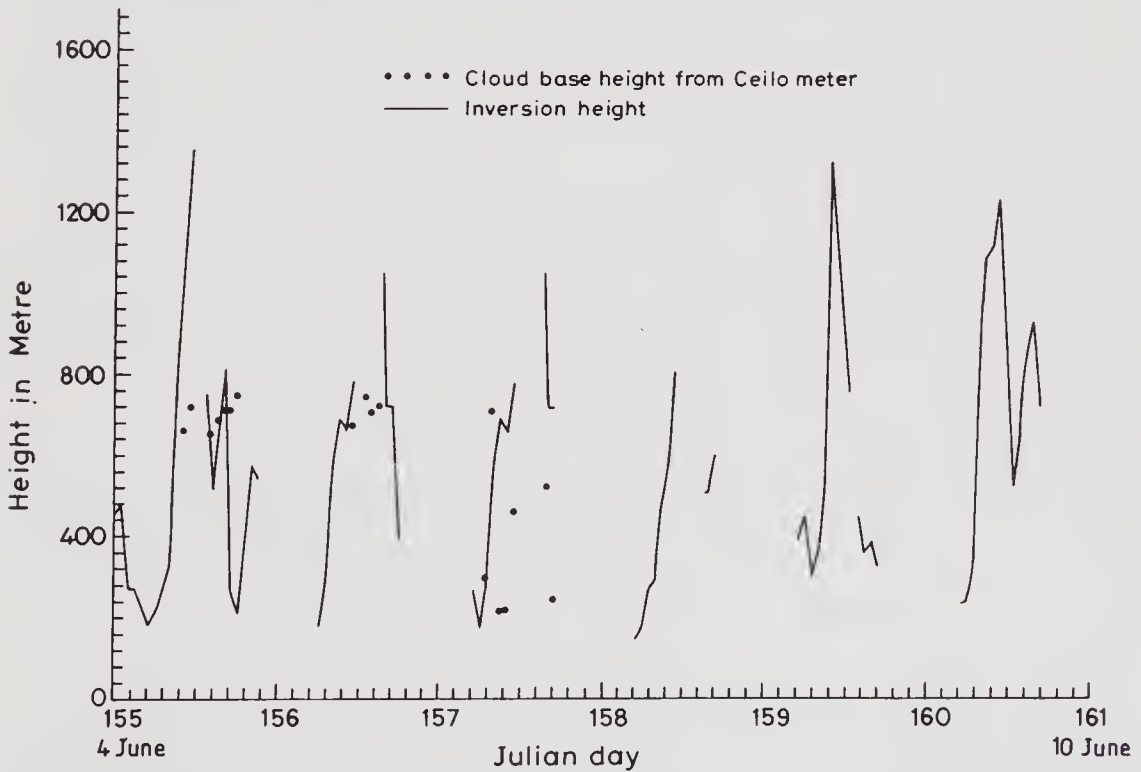


Figure 5. Simultaneous presentation of inversion depth obtained from sodar and lowest cloud-base height from laser ceilometer.

One finds that the maximum of heat flux always occurs earlier than the maximum of the inversion height. In fact the inversion height rises in the wake of rising heat flux; whenever the heat flux rises sharply, the inversion height also shoots up. But it also happens that on the three days under consideration the inversion height is no longer available from the sodar after it reaches a sufficiently high value. There are then two possibilities. First, the inversion height may rise above 1500 m which is the maximum range of the sodar being used; second, it might also happen that the inversion may not exist at all.

Table 3. Unstable condition. Time (in IST) of occurrence of maximum value in diurnal variation.

Julian day	Max. of ζ at hrs.	Max. of τ at hrs.	Max. of H at hrs.	Maximum inversion height at hrs.	Remarks
155	0930 to 1000	1600 to 1630	0930 to 1000	1100–1200	Inversion height starts rising from 0800–0900 hrs. Maximum value is 1350 m. No inverted height is available from 1200–1400 hrs.
156	1000 to 1030	1430 to 1530	1000 to 1030	1524–1600	Inverted height starts rising from 0800–0900 hrs. and reaches maximum value of 1050 m AGL. No inverted height is available from 1200–1524 hrs.
157	1200 to 1230	1130 to 1200	1200 to 1230	1524–1600	Awake of inverted height starts from 0800–0900 hrs. Maximum value is 1050 m AGL. No inverted height is available from 1200–1524 hrs.
158	0930 to 1000	1600 to 1630	0930 to 1000	1100–1200	Awake of inverted height starts from 0800–0900 hrs. Maximum value is 0810 m AGL. No inverted height is available from 1200–1534 hrs.
159	—	—	—	1039–1100	Availability of surface layer data is scattered in morning time and up to 1130 hrs. Maximum value of inverted height is 1320 m. No inverted height is available from 1200–1406 hrs.
160	1030 to 1100	1400 to 1430	1130 to 1200	1100–1200	Inverted height starts rising from 0700–0800 hrs. Maximum value is 1230 m AGL. No inverted height is available throughout the unstable period.

It is known that during unstable conditions the boundary layer is usually capped by an elevated inversion layer, and then one may accept that the depth of the boundary layer may be approximated by the inversion depth. In a stable situation, however, the inversion height signifies the top of the ground-based inversion. Many boundary layer meteorologists accept the concept that the inversion height gives the boundary layer height. But one can always claim that in either case the inversion height is closely related to the boundary layer depth.

Thus, during June 4th–6th, 1990 one can claim that the cloud penetrated the boundary layer and it is extremely important to check the peculiarities of these days.

Lastly, one can look at the synoptic situation and attempt to understand the impact of the surface parameters on the synoptic features and the inter-play between the low-lying clouds and the boundary layer depth. During the period of study, there were mesoscale phenomena like thunderstorm developments which are mentioned here, but

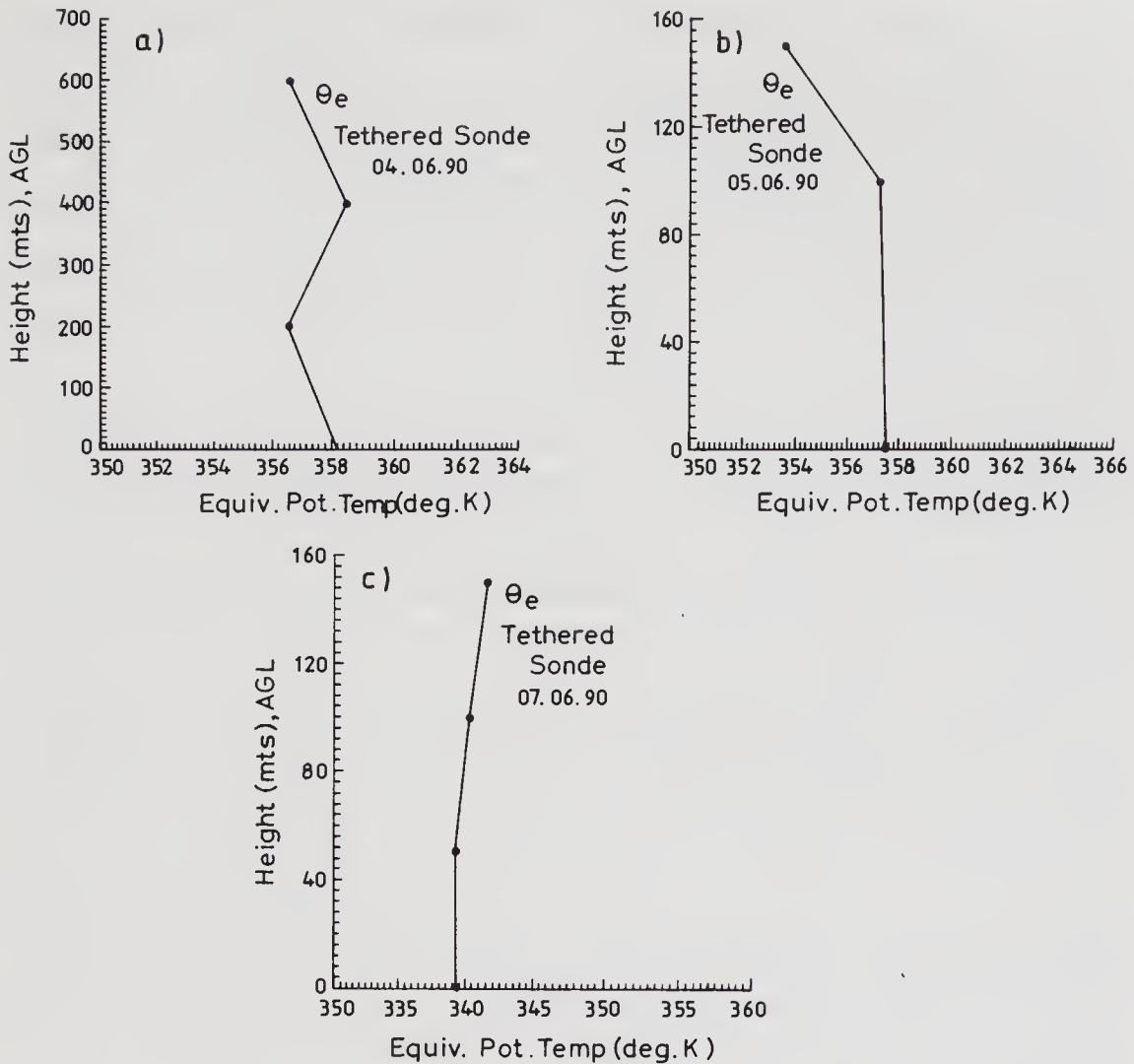


Figure 6. Vertical profile of equivalent potential temperature on Julian day (a) 155; (b) 156; and (c) 158 obtained from the morning flight of tether sonde.

the inter-relation between these events and the surface parameters are discussed elsewhere (Pradhan *et al* 1994b).

Incidentally, the period of the present study involved some atmospheric systems. Synoptically, from June 4th – 7th, there were middle and lower tropospheric cyclonic circulations over west central Bay of Bengal. On June 6th (day 157) a sub-synoptic cyclonic circulation centred over Gangetic West Bengal, after June 7th, the system dissipated. A low pressure system on June 10th lay over the north and west-central Bay of Bengal.

Incidentally, the tether sonde data provide the overall thermal structure of the atmosphere up to the sensed height. The thermal stability may be understood from the vertical profile of potential and equivalent potential temperature.

The inter-play of various features may be better realized if those features are compared day-by-day.

On June 4th (day 155), the cloud-base was below the inversion height at 1000 IST, 1100 IST and 1600 IST. However, inversion height data were not available from 1200 to 1420 IST. Again, ceilometer data were not available beyond 1800 IST. The average cloud-base height was near 700 m. Cumulus and strato-cumulus types were observed.

The inversion height varied from 800 m to 1400 m, when low clouds penetrated the inversion height.

There was surface convective instability since the morning as revealed by the tether sonde data (figure 6a). The sensible heat flux was high and the diurnal maximum was the second highest of the six days of time series presented (figure 3). As the momentum flux was low throughout the day (figure 4), the surface-scaling temperature (sensible heat flux divided by the square root of the momentum flux) was found to reach the maximum of the six days concerned. The maximum surface instability ζ (Stull 1988) was nearly -5.0 .

On the same day, a thunderstorm was reported at Kharagpur with a precipitation of 4.3 mm in the period between 2130 and 2359 IST.

On June 5th (day 156), the low cloud-base was distinctly below the inversion height at 1100 IST and 1600 IST. The inversion height data were not available from 1200 to 1524 IST. Average cloud-base height was nearly 750 m, whereas the inversion height varied from 750 m to 1000 m. There was a ground-based stable layer in the morning. This is inferred from a profile of the equivalent potential temperature (figure 6b). The surface sensible heat flux is high but the diurnal maximum was less than on the previous day and the scaling temperature shows a decreasing trend. The maximum surface instability ζ was -0.69 .

There was a widespread thunderstorm over Gangetic West Bengal, the Bihar plateau and many parts of northeast India. The thunderstorm struck Kharagpur at about 2220 IST on June 5th and persisted till 0010 IST of the next day with a precipitation of 6.8 mm.

On June 6th (day 157), for most of the time of the ceilometer observation, the low cloud was found to have penetrated the inversion height. The average cloud-base height of the penetrating low cloud was as low as 300 m, whereas the corresponding inversion height varied from 500 m to 1000 m. As indicated previously, a local convergence field developed over Gangetic West Bengal during the afternoon hours. In its wake, the momentum flux shot up to the highest value (figure 4) during the entire period of observation. Associated with this, the highest sensible heat flux (figure 3) is also found to occur, in spite of the scaling temperature showing a further downward trend in its diurnal maximum. Another notable feature was that whereas on all other days the momentum flux maximum occurred in the afternoon, on this day it occurred during the interval 1130 IST to 1200 IST. The maximum diurnal instability was -0.15 .

In fact on this day, the cloud was so low that no pilot balloon flight could be undertaken.

After June 6th, the symptoms of dissipation of the cyclonic vorticity in the Bay of Bengal were appearing. In fact no low cloud overhead at KLK Air Base was recorded by the ceilometer during June 7th – 9th. Sensible heat flux started to fall continuously. The diurnal maximum on June 7th was even less than that on June 5th. The diurnal maximum of momentum flux fell from the June 6th value by about 25% and then settled at a steady value because of a strong wind field during June 7th – 9th. So scaling temperature fell further though the maximum instability during this period did not differ much from the June 6th magnitude.

6. Conclusions

One can conclude that the temperature and wind field data obtained from different sources at and around Kharagpur have overall compatibility. The most notable feature

is the presence of a low level southerly jet in the morning hours sensed by the sodar at around 300 m above ground.

The inversion height supplied by the Aerovironment sodar and the first peak observed in the vertical profile of the back-scatter intensity are in general, closely related. However, in some cases the second peak is better correlated with the inversion height.

It seems that the synoptic features and the surface parameters as well as the inter-relation of the low cloud formation with the atmospheric boundary layer have a close linkage. It is evident from the analysis of these few days that whenever the low clouds can penetrate the boundary layer or inversion height, the surface sensible heat flux rises appreciably. On the other hand such a situation dominates whenever there is a convergence field, on either the synoptic or the sub-synoptic scale. In the presence of convergence, momentum flux shoots up because of high shear in the wind field. Thus, the sub-synoptic or synoptic scale convergence modulates the inversion height and the presence of cloud-base within the inversion height, which in turn modulates the sensible heat and momentum fluxes. However, it must be mentioned that to come to a firm conclusion, one must undertake more extensive studies of similar situations.

One should note that the monsoon advanced over northeast India on June 4th and the onset for Calcutta was declared on June 6th (Gupta 1990). But it did not advance much further beyond that date (Gupta 1990). This is evidently supported by the usual pattern of variation of the sensible heat flux as well as the inversion height as on an undisturbed day. Again this is supported by the rainfall distribution over Kharagpur (Pradhan *et al* 1994b). Apparently the monsoon over Kharagpur advanced with the depression which intensified from a low to this state over the Bay of Bengal on June 13th and crossed land on June 14th.

Lastly, it should be mentioned that on June 4th, the boundary layer was of the free convective type (as is evident from high scaling temperature and high negative value of ζ), but with the passage of time it converted first to a mixed convective type and then finally settled towards a forced convective situation (Thom 1975).

Acknowledgements

The authors are thankful to DST, Govt. of India for the sanction of a research project and the present work is a part of that project.

References

- Gupta M G 1990 MOCC Brief report, India Meteorological Department (New Delhi, India)
- Pradhan R, De U K and Sen P K 1994a Estimation of roughness length at Kharagpur micrometeorological tower site during monsoon onset of 1990; *Mausam* **45** 184–186
- Pradhan R, De U K and Sen P K 1994b Surface sensible heat flux over a deep moist convective region and its interplay with synoptic and mesoscale features; *Proc. Indian Acad. Sci. (Earth Planet. Sci.)* **103** 353–367
- Roy B 1994 Doppler acoustic sounding studies of some atmospheric boundary processes in a moist convective region; *Ph.D. Thesis* submitted to Jadavpur University, Calcutta (India) 248 pages
- Stull R B 1988 An introduction to boundary-layer meteorology (Kluwer Academic publishers) pp 180–183
- Thom A S 1975 *Momentum, mass and heat exchange of plant communities, vegetation and the atmosphere*, Principles, (ed) J L Monteith (London: Academic Press) **1** 57–109
- Webb E K 1982 Profile relationships in the superadiabatic surface layer; *Q. J. R. Meteorol. Soc.*, **108** 661

Variability of the oceanic boundary layer characteristics in the northern Bay of Bengal during MONTBLEX-90

V S N MURTY, Y V B SARMA and D P RAO

National Institute of Oceanography, Dona Paula, Goa 403 004, India

Abstract. Variability of the ocean surface boundary layer characteristics on daily time-scale is studied utilizing the 3-hourly hydrographic data collected at a stationary location (20°N, 89°E) in the Bay of Bengal during August (18th – 31st) and September (9th – 19th), 1990 under MONTBLEX-90 field programme. The daily variations of temperature, salinity, σ_θ , mixed layer thickness, stability, heat content and rate of change of heat content in the upper 100 m are discussed in relation to prevailing weather (depressions) and hydrographic conditions (influx of fresh water, presence of eddies). The mixed layer thickness is examined through temperature- and σ_θ -based criteria considering also the surface salinity in the latter. The T -based mixed layer thickness is always higher than that of σ_θ -based thickness. The rate of change of heat content is also computed up to the depth of 20°C and 14°C isotherms which takes into account the vertical motion and hence divergence. With the development of a low into a deep depression close to the study area, intense upwelling of subsurface cold waters is noticed from 100 m to the bottom of the surface mixed layer (20 m) from 18th to 20th August. The upwelling is weakened by 21st August when the depression moved away from the study location. This variation of upwelling is supported by the variation of surface mixed layer thickness, static stability at 30 m depth, heat content in the upper 100 m and the heat content up to the depth of 20°C isotherm from 18th to 21st August. The rate of change of heat content in the upper 100 m and up to the depths of 20°C and 14°C isotherms leads to net heat storage during August and to net heat depletion during September. This together with the net surface heat gain lead to an import (197 Wm^{-2}) and export (233 Wm^{-2}) of heat during August and September respectively through horizontal advective processes. These advective processes are attributed to the presence and movement of a warm core eddy through the study location.

Keywords. Ocean boundary layer; Bay of Bengal; heat budget; heat content; warm core eddy; southwest monsoon; MONTBLEX-90.

1. Introduction

Upper oceanic boundary layer studies are important for understanding the momentum and heat energy exchanges between the ocean and overlying atmosphere. These exchange processes are further influenced by the prevailing weather disturbances. This is particularly true during southwest monsoon in the northern Bay of Bengal where many monsoon lows/depressions are formed/developed under the influence of the 'monsoon trough' which in general, lies along an axis passing through northwestern India up to the head of the Bay of Bengal. In order to understand the variability of the atmospheric as well as marine boundary layer in detail in relation to the monsoon trough (during the period of southwest monsoon of 1990 on the land and in the northern Bay of Bengal), an extensive observation program acronymed MONTBLEX (MONsoon Trough Boundary Layer EXperiment) was organized by the Department of Science and Technology (DST) in association with various national laboratories, institutions and universities. The important synoptic weather features like the shift in

the location of the monsoon trough, cyclonic disturbances and the activity of the monsoon during the MONTBLEX-90 period have been documented by Gupta (1990). Rao and Murty (1992) studied the temporal variability of air temperature and water vapour content in the lower troposphere (up to 600 mb) over the northern Bay of Bengal at a stationary location utilizing the upper air data collected during MONTBLEX-90. Similarly, Sarma *et al* (1992) analyzed the surface meteorological data collected during the same experiment and showed that the sea surface gained heat during the observation period (18th – 31st August and 9th – 19th September, 1990) in spite of many cyclonic weather disturbances that prevailed in the study area. Murty *et al* (1993) studied the variability of upper (100 m) layer heat content and showed that the upper ocean lost 110 Wm^{-2} of heat during 18th – 20th August, 1990 and 1000 Wm^{-2} during 12th – 13th September, 1990 under the influence of depression/low during these periods. In addition, the presence of meso-scale eddies in the Bay of Bengal (Swallow 1983; Cutler and Swallow 1984; Rao *et al* 1987; Babu *et al* 1991) would also contribute to the variability in the heat and salt contents of the upper ocean. In this paper, we examine the temporal variability of the oceanic boundary layer characteristics in the northern Bay of Bengal during MONTBLEX-90 in relation to the prevailing weather and hydrographic conditions.

2. Data and methodology

The water temperature and salinity data collected using CTD probe (make: Sea Bird model SBE-11, USA) at 3-hourly intervals in the northern Bay of Bengal at a stationary location (20°N , 89°E ; figure 1) onboard ORV *Sagarkanya* during the southwest monsoon period (18th – 31st August and 9th – 19th September) of 1990 under MONTBLEX-90 programme have been utilized. The accuracies of the CTD temperature and salinity sensors are $\pm 0.005^\circ\text{C}$ and ± 0.002 PSU (Practical Salinity Unit) respectively. The data quality control procedures are detailed in Anon (1990). The daily averages of temperature,

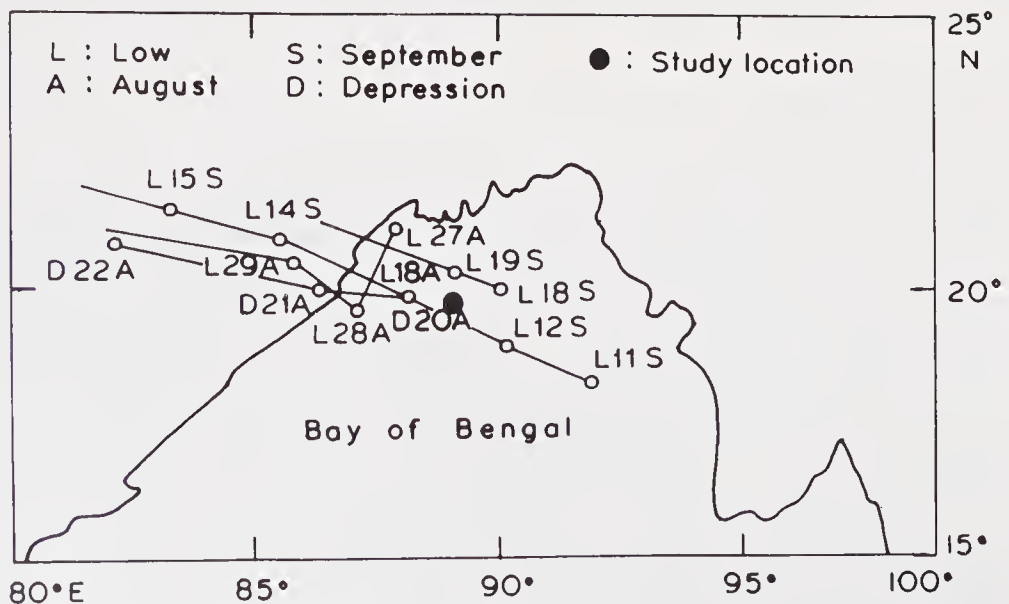


Figure 1. Area of study with trajectories of depressions.

salinity and σ_θ are obtained for the upper 100 m depth during August and September. The thickness of the surface mixed layer is obtained through two criteria. In the first criterion (temperature based) the thickness of the mixed layer is chosen as the depth where the water temperature is less by 1°C from the sea surface temperature following Murty *et al* (1992). Since the study area comes under the influence of a huge influx of fresh water and precipitation during the southwest monsoon, considerable variations in the salinity field occur which in turn affect the upper layer stratification thereby the mixed layer thickness. Hence, an alternative criterion based on σ_θ variation is adopted (Suga and Hanawa 1990) for determining the thickness of the surface mixed layer. This is the depth where the density is the surface density plus a chosen value. The chosen value is the increment in density obtained when the surface temperature is reduced by 1°C with salinity held constant.

The water stability (E) in terms of the Brunt-Vaisala frequency is computed from the changes in the daily averages of *in situ* density over a 10 m thick slab using the following equation (Pollack 1954):

$$E = g/\bar{\rho}[d\rho/dz - g\bar{\rho}/C^2],$$

where g is the acceleration due to gravity (9.8 ms^{-2}), ρ is the sea water density (kgm^{-3}), $\bar{\rho}$ is the mean density in the water column of dz , z is the depth (m) and C is the sound velocity (ms^{-1}) in sea water (Chen and Millero 1977).

The heat content of the upper water column is computed up to the fixed depth (100 m) and up to the depths of 20°C and 14°C isotherms using the following equation:

$$HC = \bar{\rho}C_p \int_0^D \Delta T dz,$$

where C_p is specific heat of sea water at constant pressure, ΔT is mean temperature of the layer of thickness dz and D is the depth of the water column considered. The heat content above the chosen isotherm which takes into account the vertical motion and hence divergence in the water column (Emery 1975) is useful for the upper layer heat budget and correlates well with the net heat flux at the sea surface.

From the daily mean values of HC , the rate of change of heat content is estimated as:

$$HS = dHC/dt = (HC_{(i+1)} - HC_i)/(24 \times 3600),$$

where the subscript 'i' represents the day.

3. Results and discussion

3.1 Salient weather features

The weather during 18th – 25th August is dominated by monsoon depressions and low pressure systems over the north/northwestern Bay (Gupta 1990). A low was formed on 18th August about 150 km to the west of the study location and developed there into a deep depression by the 20th and crossed the coast near Paradeep on the morning of 21st (figure 1). The monsoon trough shifted to the foot of the Himalayas during 24th – 26th August and shifted southward during 27th – 30th August. During 10th – 11th September

temporary northward shift of the monsoon trough was noticed and during 12th – 13th September a low passed over the study area (figure 1).

3.2 Surface meteorological conditions

The influence of the above weather conditions is clearly reflected in the daily variation of the surface wind field during August and September (figures 2a and 2b). With the development of deep depression the wind speed increased from 2 m/s on 18th August to 8 m/s on 20th August (figure 2a). The direction of wind was southwesterly initially, but under the influence of the deep depression exhibited a variation from southwesterly to southeasterly and southerly. With the northward shift of the monsoon trough the wind speed showed a gradual decrease from 21st to 26th August. A second maximum in wind speed with southerly direction was noticed on 29th August when the monsoon trough extended southward. During September also the higher speeds were associated with southerly winds (figure 2b) under the influence of a passing low.

The daily march of latent heat flux (Q_E) and the net heat flux (Q_N) at the sea surface during August (figure 3a) exhibited variations in accordance with the above weather conditions. Large latent heat flux (140 Wm^{-2}) and lower (60 Wm^{-2}) net heat gain (positive heat flux) occurred at the time of deep depression. It is also seen that the heat gain is decreased by about 80 Wm^{-2} from 18th to 20th August due to enhancement of latent heat flux by similar magnitude during the same period. As the monsoon trough moved northward the latent heat flux decreased and hence the net heat gain increased. Similarly with the southward shift of the monsoon trough the latent heat flux picked up and the net heat gain exhibited a decrease from 27th to 31st August. During September also, the latent heat flux and the net heat flux exhibited variations due to the prevailing weather conditions.

3.3 Temperature

The daily variation of temperature at selected depth levels (surface, 10, 30, 50, 75, 100 m) in the upper 100 m is shown in figures 4a and 4b for August and September respectively. The SST showed a gradual decrease of about 0.3°C from 29.1°C to 28.8°C under the influence of the low and deep depression from 18th to 21st August (figure 4a). The influence of this weather disturbance is felt up to a depth as deep as 100 m as seen from relatively lower temperatures up to 100 m depth from 18th to 22nd August. These lower temperatures are due to intense upwelling of cold waters in the upper 100 m water column. Gopalakrishna *et al* (1993) also reported storm-induced upwelling from about 80 m depth at a distance of around 110 km from the storm-centre. The slightly higher temperature differences between the surface and 30 m on 18th and 19th August are clearly due to the upwelling reaching the sea surface. After the disappearance of the depression from the study area, the SST slowly increased to 29.1°C by 25th August coinciding with the northward shift of the monsoon trough and consequent increase in net surface heat flux. With the increase of net heat gain and the reduction in the turbulent mixing due to winds, the temperature difference (between surface and 30 m) becomes minimum and leads to a thick isothermal layer occupying the top 30 m between 22nd and 31st August. Below this layer, the temperature increased rather rapidly from 22nd to 28th August at all the depth levels.

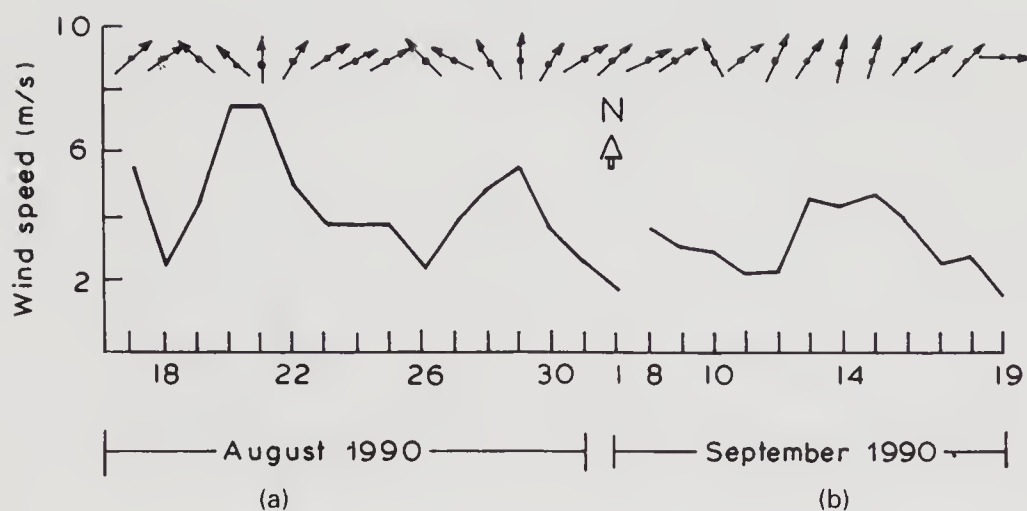


Figure 2. Variation of surface wind field during MONTBLEX-90 for August and September.

In September, the thick surface isothermal layer continued till the end of the observation period (figure 4b). Below this layer the temperature showed a gradual decrease from 11th to 17th at 50 m and 75 m depths. The temperature difference between surface and 50 m is low from 9th to 12th September and gradually increased to a higher value on 18th September. At 100 m the temperature varied between 21°C and 22°C.

While the decrease of SST is 0.2°C under the influence of a deep depression that developed close to the study area, the decrease of SST is 0.1°C when a low passed over the study area (12th – 13th September).

3.4 Salinity

In August, the daily variation of salinity shows a thin (10 m) isohaline layer in the top 10 m water column with its salinity increasing gradually from 31.9 PSU on 18th to 33.2 PSU on 26th August and then decreasing to 32.2 PSU by 31st August (figure 5a). The low salinity on 18th is due to the influence of fresh water influx from the northern Bay against the prevailing southwesterlies. The increase of salinity of the isohaline layer from 18th to 26th August could be due to mixing between the less saline fresh water and the relatively saline waters moving northward from the south of the study location (Murty *et al* 1992) under the influence of strong southeasterly/southerly winds associated with the depression and persistence of mixing after the cessation of strong winds. Large salinity differences are noticed from surface to 30 m depth on 18th only due to overlying low-salinity waters. At and below 30 m, salinity is slightly high (compared to the salinity on the next few days) from 18th to 21st supporting the upward movement of subsurface saline waters during the intense upwelling process as mentioned above. At 100 m salinity is uniform at 34.9 PSU. The minimum salinity difference between surface and 30 m depth from 23rd to 29th August suggests the thickening of the surface isohaline layer which is characterized by relatively high salinity.

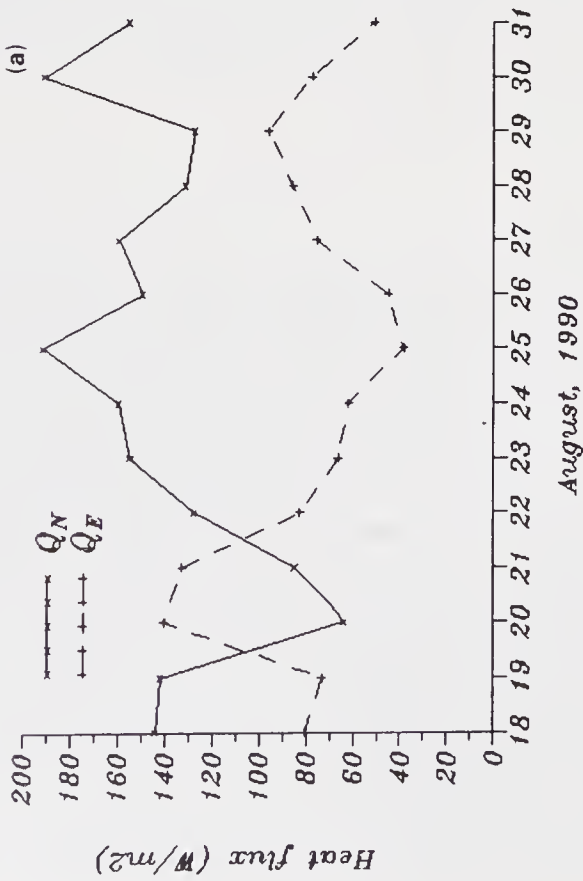
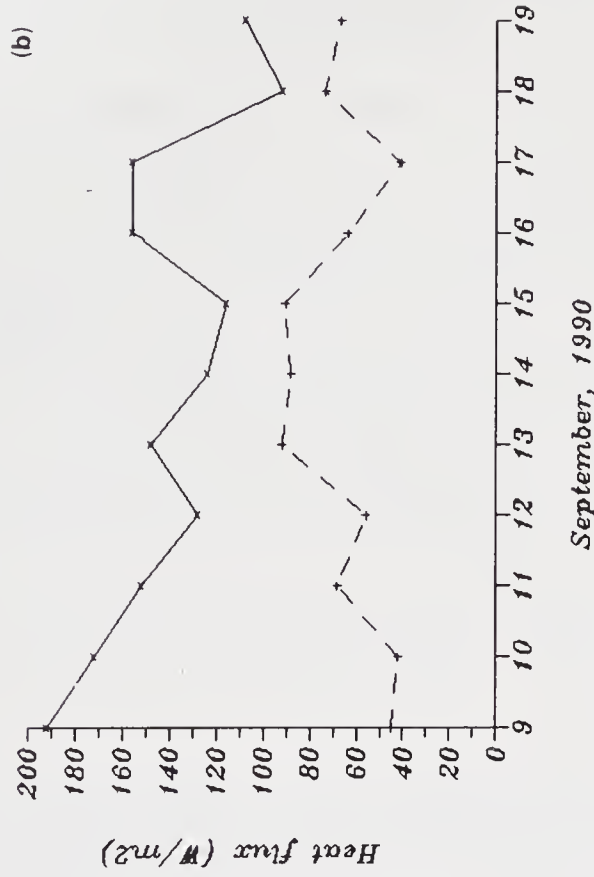


Figure 3. Variation of net surface heat gain (Q_N) and latent heat flux (Q_E) during MONTBLEX-90 for August and September.

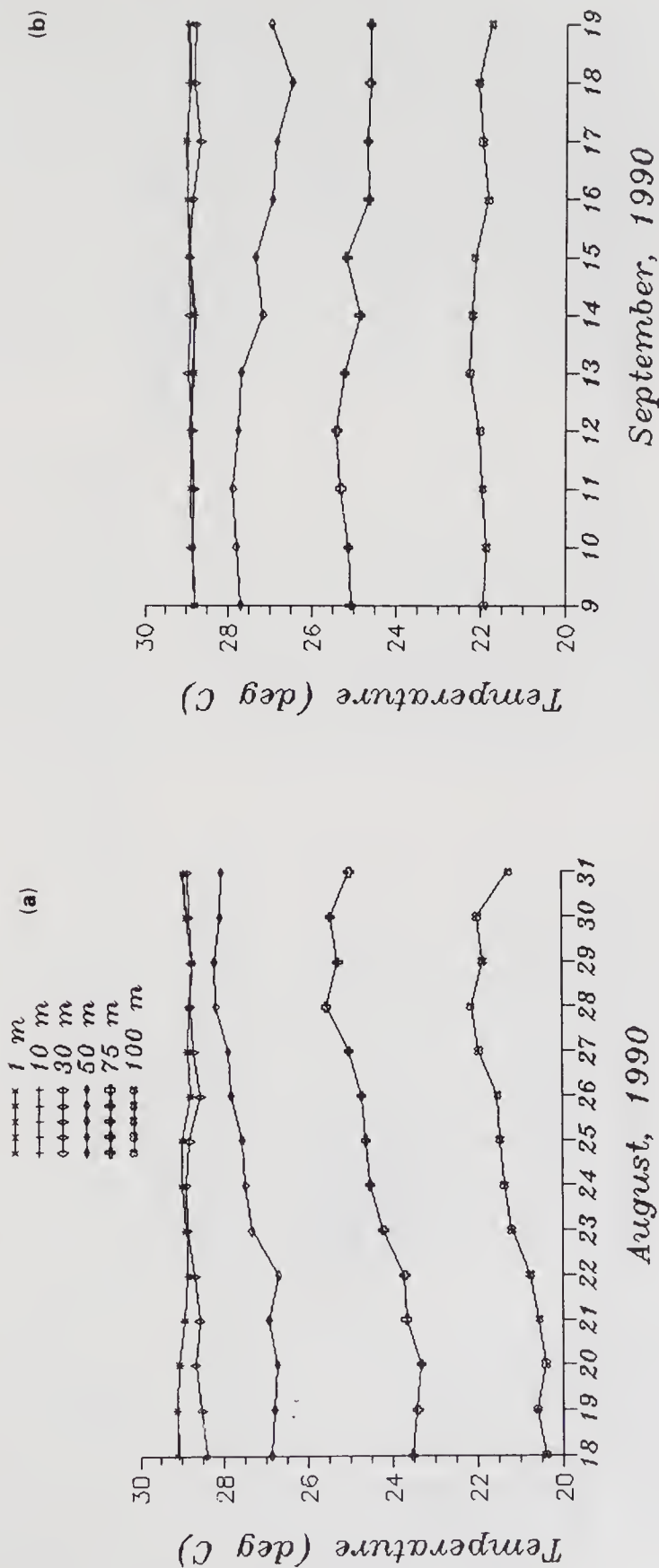


Figure 4. Temperature distribution in the upper 100 m during MONTBLEX-90 for August and September.

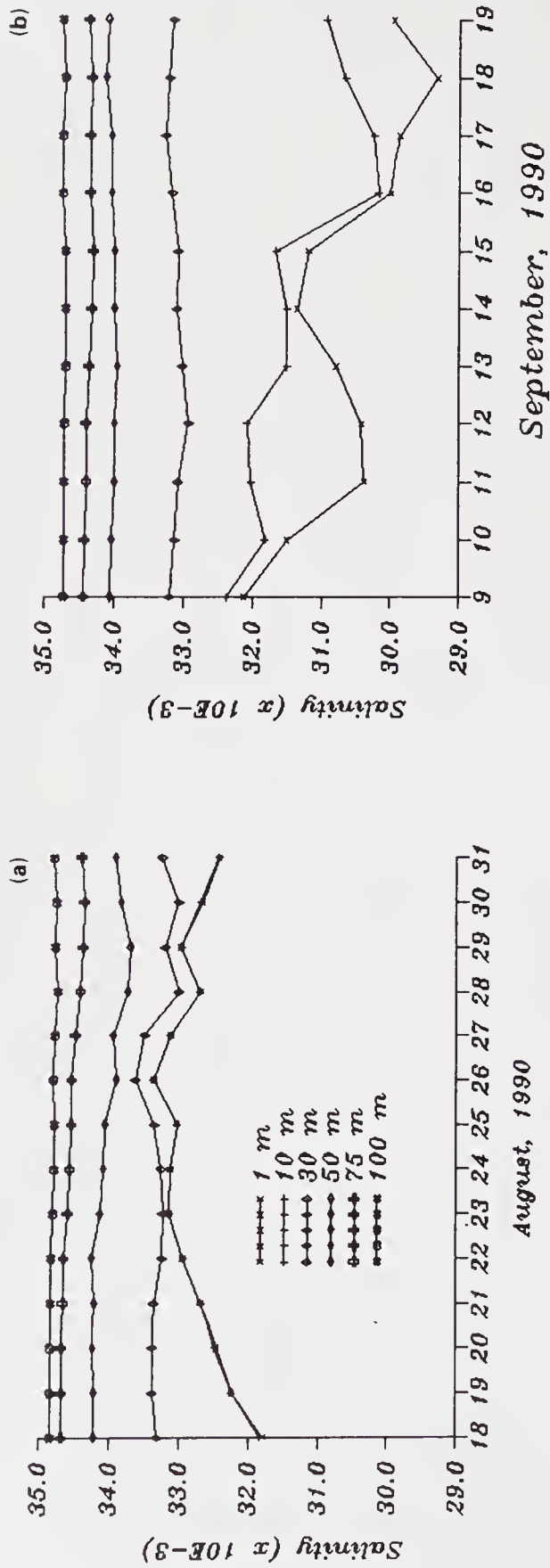


Figure 5. Salinity distribution in the upper 100 m during MONTBLEX-90 for August and September.

During September, a decrease of salinity in the top 10 m is clearly seen from 9th to 18th September coinciding with the period of the passing of a low and the relatively higher speeds of southwesterly/southerly winds (figure 5b). The salinity distribution at the surface and 10m indicates greater influx of fresh water towards the study location when compared to that in the top 10 m during August. The occurrence of slightly saline waters in the top 10 m from 13th to 15th September, indicates the northward movement of southern saline waters and their mixing with the fresh waters of the north Bay.

The fresh waters at the study location are in general noticed at the times of lower winds both during August and September, though the southwesterly winds persisted. It can be noted that in general the thin isohaline layer is embedded within the thick (30 m) surface isothermal layer. At and below 30 m depth, the daily variations of salinity are small.

3.5 Density anomaly (σ_θ)

In the upper 30 m, the density variations are very closely related to the salinity variations both in August and September (figures 6a and 6b). Below 30 m, the dominant influence of temperature on the density distribution is noticed as salinity variations become small. The occurrence of denser waters at subsurface depths from 18th to 22nd August could largely be due to the intense upwelling processes under the influence of the development of a deep depression close to the study area. The decrease in density at 50 m, 75 m and 100 m depths from 22nd to 29th August indicates the presence of warm waters at these depths.

3.6 Mixed layer thickness (MLT)

The MLT obtained through the σ_θ -based criterion is lower than that obtained by the T -based criterion. The large differences between the two MLTs become more clear from the scatter plots (figures 7a and 7b) of the mixed layer thicknesses computed following the two criteria. During August, two types of clusters can be seen in the scatter plot (figure 7a); one cluster shows near linear relation when the fresh water influx is insignificant while the second cluster exhibits large scatter indicating the effect of stratification on σ_θ -based MLT. During September, the influx of fresh water has dramatically worsened the relation between the MLTs with σ_θ -based MLT remaining much lower than the T -based MLT. This underlines the importance of stratification in the northern Bay of Bengal in the mixed layer dynamics; any effort to model the mixed layer should invariably include salinity.

The daily variation of MLT during August and September is shown in figures 8a and 8b respectively. In August, both the criteria showed lower MLTs on 18th and increased very little by 20th August. The σ_θ -based MLT increased steeply to about 32 m from 21st to 24th August when wind speed exhibited a decrease. The variation of σ_θ -based MLT is in accordance with the wind speed between 27th and 31st August. The σ_θ -based MLT can be considered as the layer of dominant turbulent mixing due to winds at the surface as it coincided nearly with the thickness of the surface isothermal layer. In that case, the lower MLTs from 18th to 20th August indicate the dominance of the upwelling process over the turbulent mixing, though winds are strong during this period under the influence of the developing deep depression. The T -based MLT exhibited a gradual

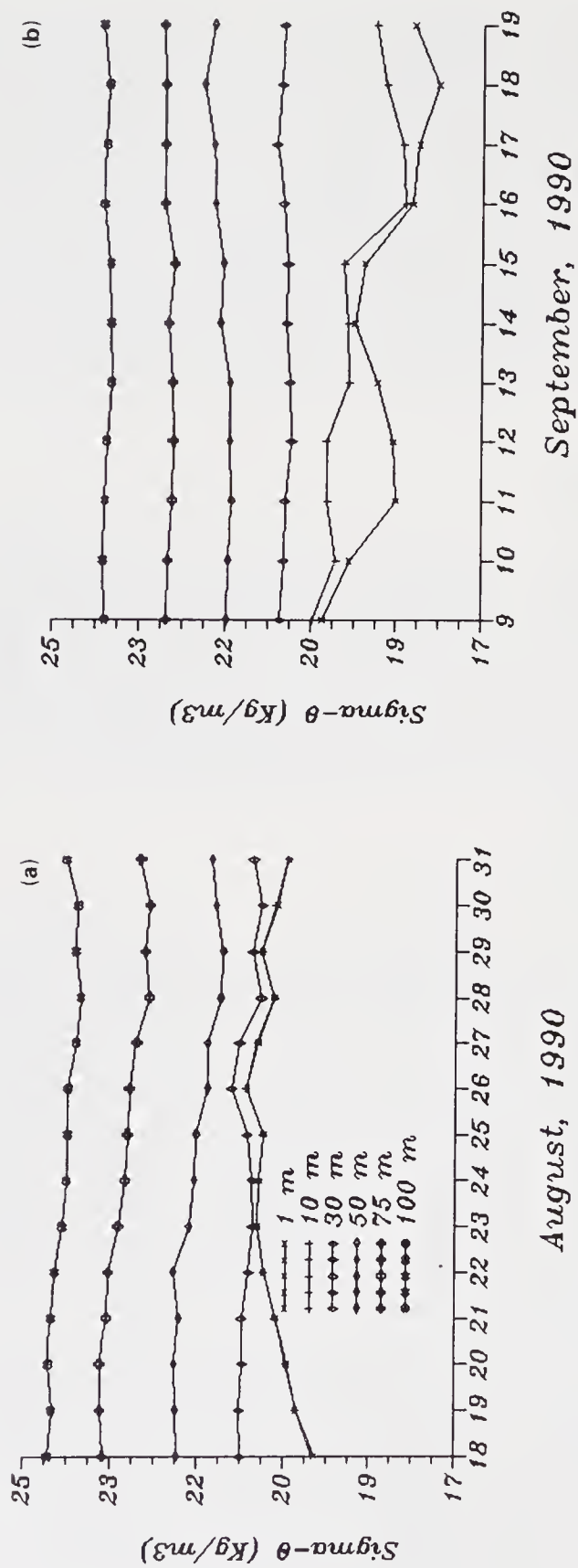


Figure 6. σ_θ distribution in the upper 100 m during MONTBLEX-90 for August and September.

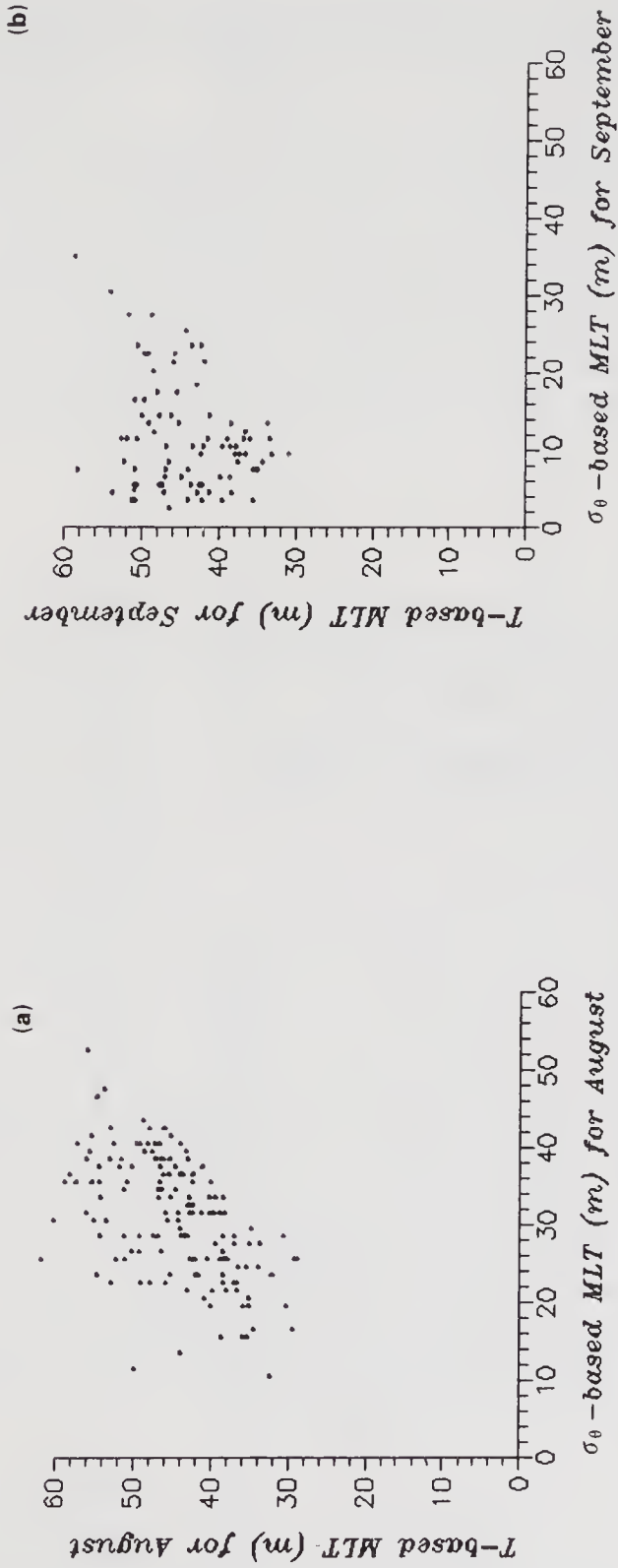


Figure 7. Scatter plot of T-based and σ_θ -based mixed layer thickness for August and September.

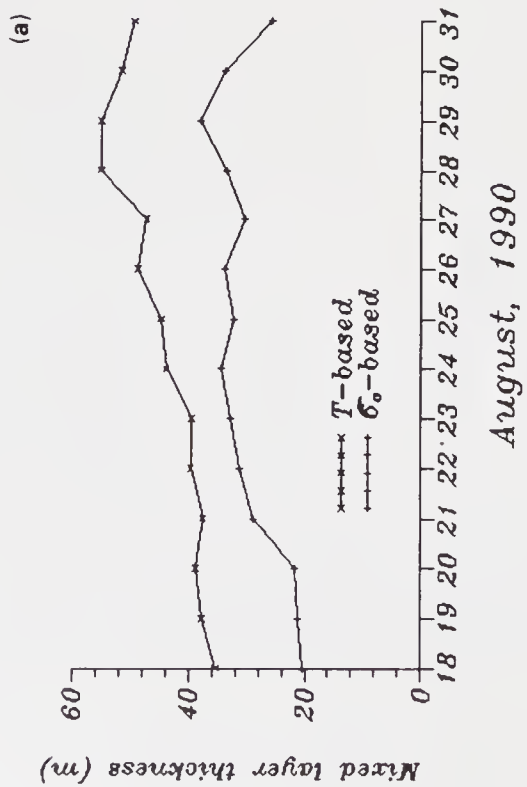
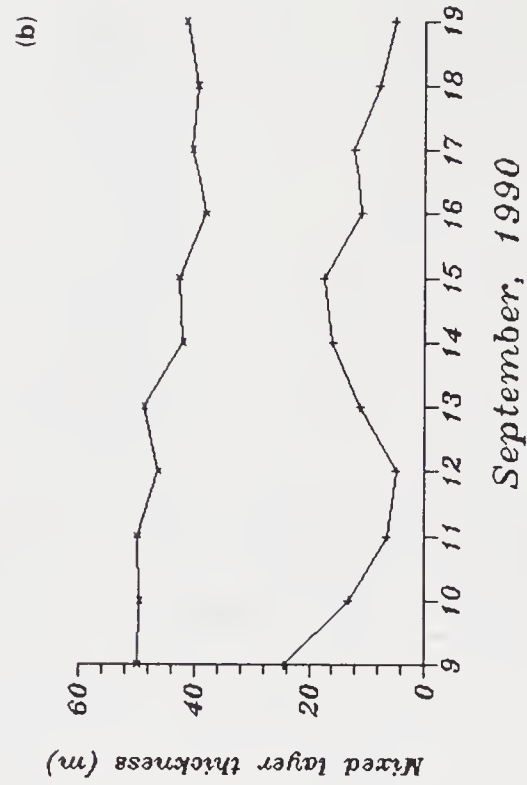


Figure 8. Variation of T-based and σ_θ -based mixed layer thickness during MONTBLEX-90 for August and September.

increase from 21st to 29th August and the differences in both the MLTs increased beyond 24th August. The increase of T -based MLT indicates warming below the σ_θ -based mixed layer.

During September, the σ_θ -based MLT variation is in accordance with the wind speeds at the surface. The higher the wind speeds the higher the σ_θ -based MLT. Also, on the days of fresh water influx the MLT is low. The σ_θ -based MLT decreased from 24 m on 9th September (figure 8b) to 6 m on 11th September in association with low salinity waters at the surface. The increase of MLT during 12th – 14th September is due to vertical mixing under the influence of higher winds of the passing low. One can notice large differences between σ_θ -based and T -based MLTs though the latter exhibits a gradual decrease. This decrease in T -based MLT indicates the cooling below the σ_θ -based mixed layer as SST was stable throughout the period from 9th to 19th September.

3.7 Stability

The stability of the water column over a 10 m slab at various depth levels is shown in figures 9a and 9b for August and September respectively. In August, very low stability is noticed at 10 m depth as this depth lies within the surface mixed layer (figure 9a) in which vertical gradients of density are low. The stability is considerably high ($9.5 \times 10^{-4} \text{ s}^{-2}$) on 18th at 30 m depth (25 – 35 m slab) just below the σ_θ -based MLT and is associated with intense upwelling of colder waters giving rise to higher vertical density gradients. This higher stability at 30 m restricts the upwelling effect reaching the sea surface. The rapid decrease of stability at 30 m depth after 18th August is followed by an increase of stability at 50 m depth indicating the deepening of the mixed layer thickness. This suggests that the turbulent mixing is strong and influences a deeper water column. At 75 m and 100 m depths the stability is relatively lower than that at 50 m depth. This shows that the vertical density gradients are lower at these depths compared to those at 50 m. These weak density gradients must be due to warming at subsurface depths suggesting the active role of horizontal advective processes.

During September, the stability at 10 m and 30 m depths exhibited opposite variation (figure 9b) and their daily variation is closely related to the daily variation of mixed layer thickness. The high variability in stability at 10 m is a result from the large density gradients generated by freshwater influx. The stability at 50 m, 75 m and 100 m depths varied within a narrow range and the stability at 100 m lies in between that at 50 m and 75 m depths. The gradual increase of stability at 100 m from 13th to 19th September suggests the increase in vertical density gradients which in turn shows that the horizontal advective processes are dominant.

3.8 Upper layer heat content

Figures 10a and 10 b represent the daily variation of upper layer heat content during August and September respectively. In August, the upper layer heat content is low ($109 \times 10^8 \text{ Jm}^{-2}$) from 18th to 22nd and exhibits a decrease by about $0.2 \times 10^8 \text{ Jm}^{-2}$ from 18th to 20th under the influence of the development of the deep depression. The corresponding heat loss would be about 110 Wm^{-2} in 48 hours. It appears that this heat loss has been utilized for the enhancement of latent heat flux by nearly up to the same magnitude at the air-sea interface during 18th to 20th August (figure 3a),

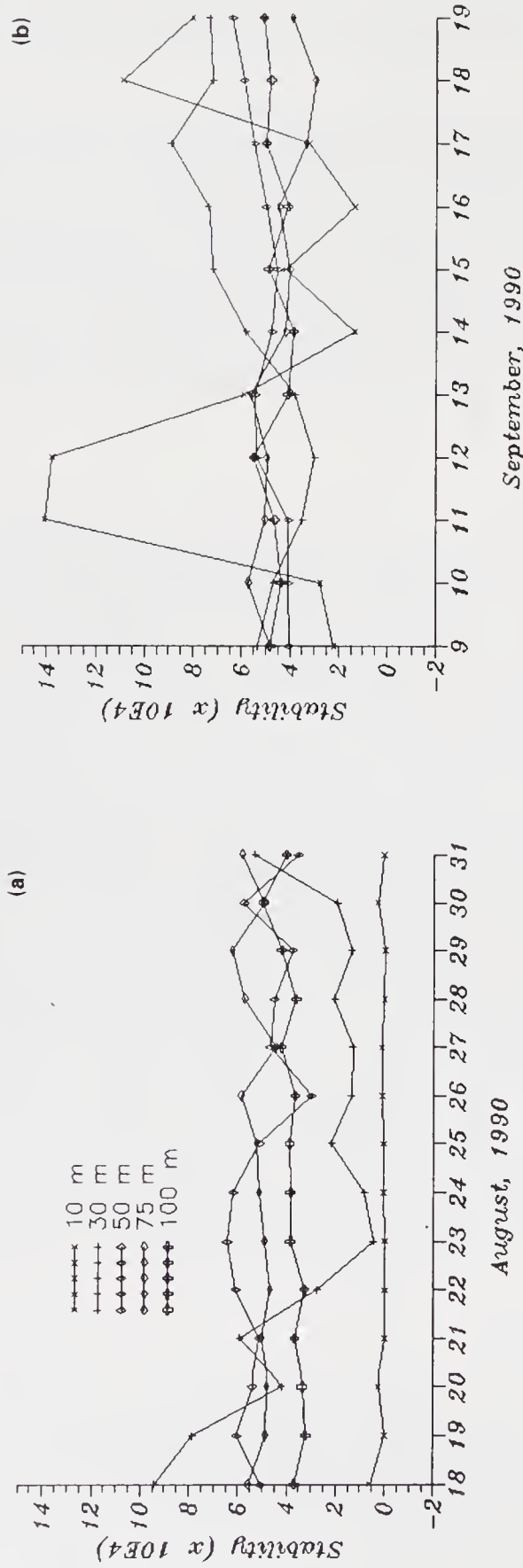


Figure 9. Stability distribution in the upper 100 m during MONTBLEX-90 for August and September.

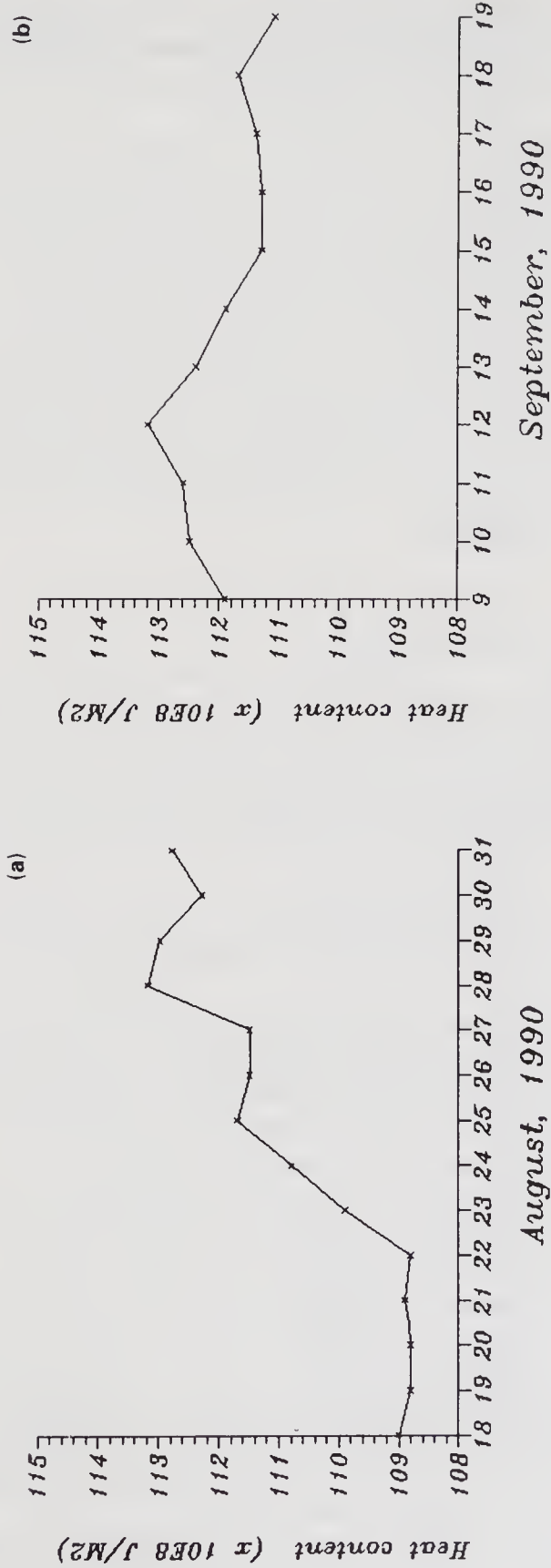


Figure 10. Variation of heat content in the upper 100 m during MONTBLEX-90 for August and September.

suggesting that the air-sea interaction is active with a positive feed-back from sea to air in the study area during this period. The heat content is invariant for the next two days, i.e. from 20th to 22nd August, and increased rapidly from 23rd to 25th August and gradually thereafter.

During September, the heat content in the upper layer increases from $111.8 \times 10^8 \text{ Jm}^{-2}$ on 9th to $113.5 \times 10^8 \text{ Jm}^{-2}$ on 12th September (figure 10b). It has decreased rapidly by 13th September when a low passed over the study location. However, the decrease of heat content is continued for the next two days, i.e. from 13th to 15th September, and exhibited an increase beyond 15th September.

When the variation of the upper layer heat content during August and September is examined in relation to the net heat flux at the sea surface during August and September, it is noticed that the increase (decrease) in the heat content is not entirely due to the increase (decrease) of net surface heat gain. It is also seen that the decrease of heat content at the time of depression and low is continued up to the next two days both during August and September. Further, at the time of decrease in the net heat gain the upper layer heat content is increased.

3.9 Rate change of upper layer heat content

The daily variations of rate of change of upper layer heat content during August and September are shown in figures 11a and 11b respectively. The surface layer loses (negative values) heat energy initially from 18th to 19th August and gains (positive) heat energy from 20th to 21st August due to the development of deep depression. This shows that the intense upwelling on 18th is weakened by 21st. Heat gain is dominant from 22nd to 28th August.

During September, heat gain in the upper layer is noticed initially and heat loss dominates from 12th to 15th. This is followed by weak heat gain and subsequently heat loss.

The mean values of the net heat flux (Q_N) at the sea surface, the rate of change of heat content up to a fixed depth of 100 m (Q_T), up to the depth of 20°C isotherm (Q_{T20}) and up to the depth of 14°C isotherm (Q_{T14}) for August and September are presented in table 1. During August the 20°C isotherm varied between 103 m and 117 m with the mean temperature of the column up to this isotherm varying from 25.55°C to 26.19°C. During September the 20°C isotherm varied between 107 m and 122 m with the mean temperature of the column varying from 25.66°C to 25.93°C. From the table, it is noticed that the sea surface gains heat energy to the tune of 141 Wm^{-2} both during August and September. The rate of change of heat content up to 100 m depth, however, indicates that the water column experiences a heat gain of 338 Wm^{-2} during August and heat loss of 93 Wm^{-2} during September. The rate of change of heat content computed up to the depth of 20°C isotherm (Q_{T20}) also shows a heat gain of about 950 Wm^{-2} during August and a heat loss of 170 Wm^{-2} during September. Extending the computations up to the depth of 14°C isotherm (Q_{T14}) also resulted in a heat gain during August and heat loss during September respectively.

The above mean values reveal that the water column considered receives excess heat energy over the net heat input at the surface during August and gives away more heat energy during September, though there is a net heat input at the surface. This suggests that there is import of heat towards the study location and export of heat from the study

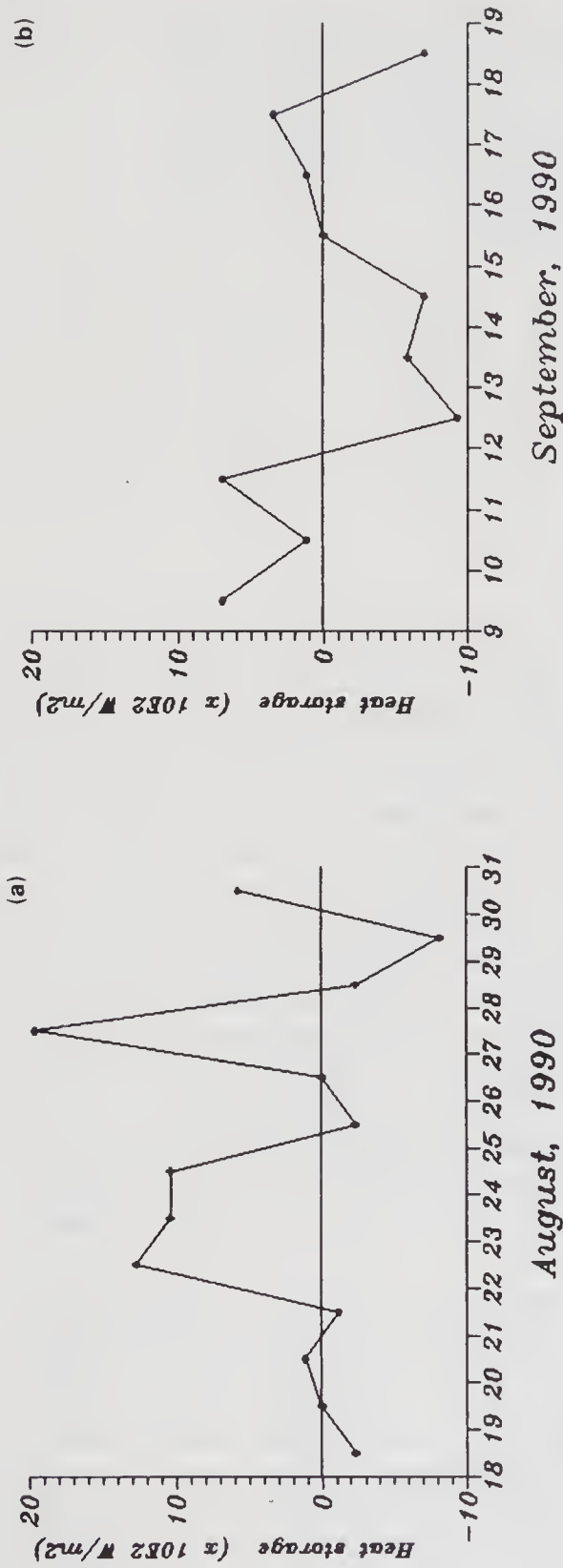


Figure 11. Variation of heat storage in the upper 100 m during MONTBLEX-90 for August and September. Positive (negative) indicates heat gain (loss).

Table 1. Upper ocean heat budget in the northern Bay of Bengal during southwest monsoon of 1990 (Q_N – net surface heat gain at the sea surface; Q_T – net heat storage in the upper 100 m; Q_A – heat import (+ ve)/export (– ve) due to lateral advective processes in the upper 100 m; Q_{T20} – net heat storage up to the depth of 20 °C isotherm; and Q_{T14} – net heat storage up to the depth of 14 °C isotherm). Units.: Wm^{-2}

Heat budget parameters	August	September
Q_N	141	140
Q_T	338	– 92
Q_A	197	– 233
Q_{T20}	950	– 169
Q_{T14}	1039	– 427

location due to lateral advective processes. On an annual scale the net heat input at the surface may be balanced by lateral heat export leaving out no local heat storage in the water column (Hastenrath and Lamb 1979a). However, on the seasonal or on shorter time scales it can be realised that the net heat gain at the sea surface (Q_N) will be utilized for the local heat storage (Q_T) and lateral heat export or import (Q_A) within the ocean (Hastenrath and Lamb 1979a), thus $Q_N = Q_T + Q_A$. From the mean values of Q_N and Q_T it can be estimated that the heat import during August amounts to 197 Wm^{-2} and heat export of 233 Wm^{-2} during September due to lateral advective processes (table 1) in the upper 100 m water column. Similarly, the Q_{T20} and Q_{T14} also indicate heat import during August and heat export during September, however with larger magnitudes compared to those in the upper 100 m water column. This shows that the trend of heat import during August and heat export during September are not altered even if the heat content computations were carried out up to a fixed depth level (100 m) or up to the depth of an isotherm, though the latter case takes into account the vertical movement of the isotherm and hence the vertical motion and the divergence in the water column above an isotherm. This suggests that the estimated heat import and export are mainly due to the lateral advective processes.

The above estimated heat import and export could be substantiated from the abrupt increase of mean temperature of the upper 100 m by about 0.8°C from 22nd August to 13th September and a decrease by about 0.2°C thereafter (figures 12a and 12b). The depths of the 26°C isotherm and 34.0 PSU isohaline have also shown a gradual deepening from 22nd August to 13th September and a gradual shoaling thereafter (figures 12c and 12d). A critical examination of the vertical movement of isotherms and isohalines in the upper 200 m water column during August and September reveals a similar trend of variation as that of the 26°C isotherm and 34.0 PSU isohaline. From these figures one can safely assume that the mean depths of occurrence of the isotherms and isohalines remained more or less unchanged from 31st August to 8th September though no data were available during this period. This observed deepening of isotherms and isohalines from 22nd August to 13th September indicates the advection of warm and less saline waters into the study area during this period which also gets its

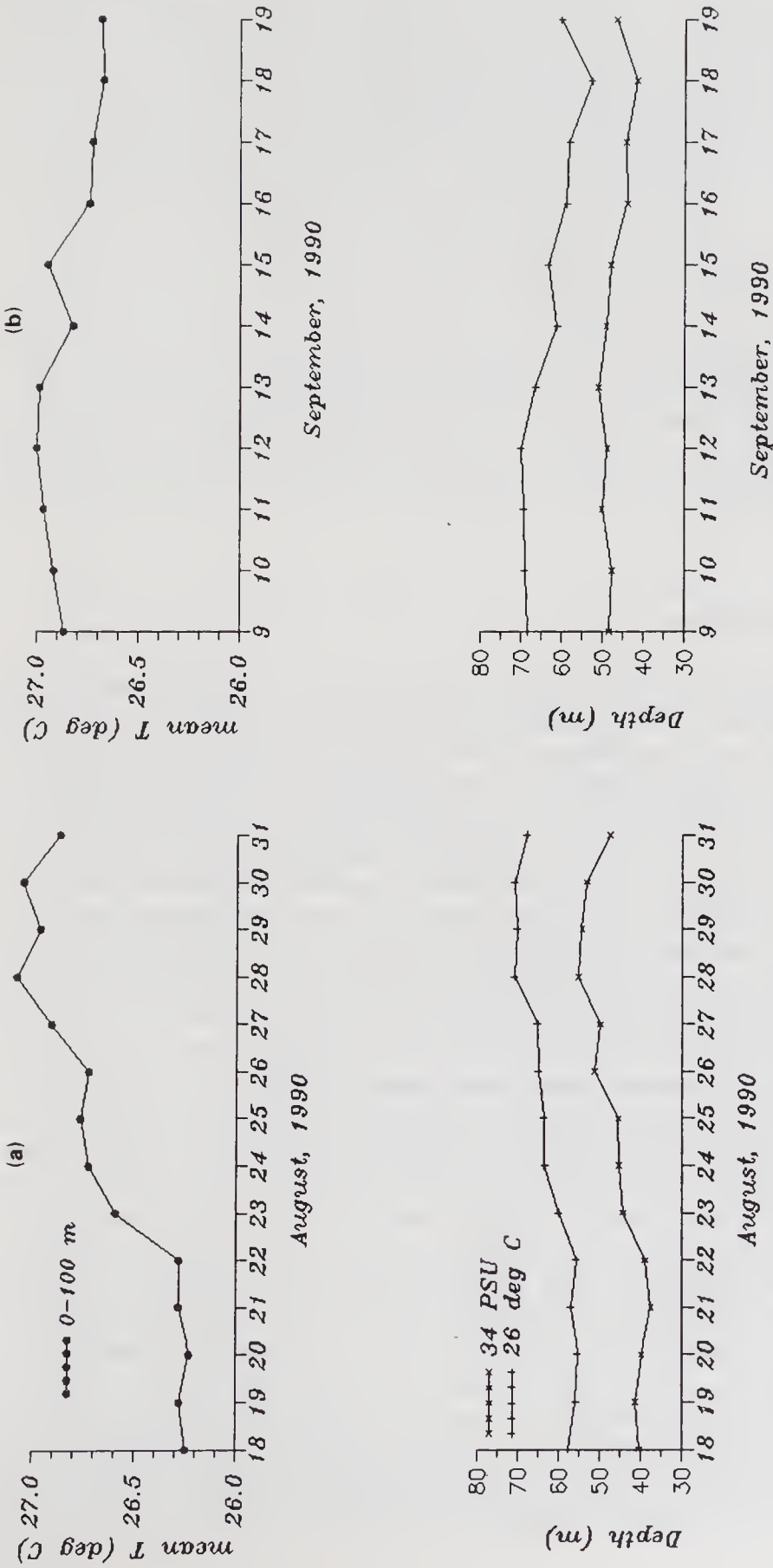


Figure 12. Variation of mean layer temperature and depths of 26°C isotherm and 34 PSU isohaline during MONTBLEX-90 for August and September.

support from the estimated heat import during August. The climatological wind stress curl (Hastenrath and Lamb 1979b; Babu 1987; Singh 1993) is positive which is conducive to divergence and hence to upwelling of cold waters. This rules out warm water sinking at the surface during this period. Hence, it can be inferred that the observed warming of the upper layers is due to the movement/advection of a warm core eddy (anticyclonic rotation) during 22nd August – 13th September towards the study location. The occurrence of peak values of depths of isotherms and isohalines on 28th August indicates that the core of the eddy was present at the study location on that day. Similarly, the decrease in the mean temperature in the upper 100 m, and the shoaling of the 26°C isotherm and 34.0 PSU isohaline beyond 13th September together with the estimated heat import during September can be attributed to the movement of the warm core eddy away from the study location. Earlier studies of Rao *et al* (1987) based on current meter measurements in the shelf region also infer the presence and movement of warm, less saline anticyclonic eddy in the northwestern Bay of Bengal during the southwest monsoon. However, more field observations are required to substantiate and adequately describe this oceanic feature in the northern Bay of Bengal during the southwest monsoon.

4. Summary and conclusions

The analysis of the data at a stationary location in the northern Bay of Bengal during the southwest monsoon of 1990 revealed two prominent events by which the oceanic upper layer characteristics are affected. Firstly, the intense subsurface upwelling of colder waters from a depth of 100 m is noticed during the development of deep depression at a distance of about 150 km from the study area from 18th to 20th August. The effect of depression-induced upwelling, however, has reached up to the base of the surface homogeneous layer. Because of this, the observed changes in SST are not large during the development period of deep depression. It is also highlighted that active air-sea interaction with positive feed-back from the sea to air prevailed during the development of deep depression wherein the heat loss from the surface layer is utilized to enhance the latent heat flux. Secondly, the advection of a warm core eddy, characterized by relatively less saline waters at its centre, towards the study area is inferred from the gradual increase of mean temperature of the upper layer, mixed layer thickness, and depths of the 26.0°C isotherm and 34.0 PSU isohaline from 22nd August to 13th September with the eddy centre at the study location on 28th August. The net heat loss from the upper layer during September without significant changes in the surface heat fluxes (when compared to August values) is then due to the movement of the eddy away from the study location on 13th September, which might also be aided by the passing low during 12th – 13th September. The lateral advective processes affecting the ocean boundary layer characteristics of the study area by bringing in heat during August and removing it during September are then clearly due to the presence and movement of the warm core eddy (through the study area) during the southwest monsoon – an important feature that has emerged from the MONTBLEX-90 programme in the northern Bay of Bengal. In order to adequately describe this oceanic feature and understand its role on the oceanic boundary layer characteristics more field observations in the northern Bay of Bengal during the southwest monsoon are suggested.

Acknowledgements

The authors are grateful to the Director, NIO for his support and are thankful to the Department of Science and Technology, New Delhi for sanctioning a grant-in-aid project under MONTBLEX programme. The authors express their sincere thanks to the anonymous reviewers for their critical comments on the manuscript towards improvement of the paper.

References

- Anon 1990 Oceanographic and meteorological data report of ORV *Sagarkanya* cruise 56 (MONTBLEX-90), National Institute of Oceanography, Dona Paula, Goa
- Babu M T 1987 Hydrography and circulation of the waters of Bay of Bengal during post monsoon season; M.Sc. thesis, University of Bombay, Bombay p. 78 (unpublished)
- Babu M T, Prasannakumar S and Rao D P 1991 A subsurface cyclonic eddy in the Bay of Bengal; *J. Mar. Res.* **49** 403–411
- Chen C T and Millero F J 1977 Speed of sound in sea water at high pressures; *J. Acoust. Soc. Am.* **62** 1129–1135
- Cutler A N and Swallow J C 1984 Surface currents of the Indian Ocean (To 20°S, 100°E): Compiled from historical data archived by Meteorological Office; Bracknell, U.K., *International Oceanographic Sciences Report No. 187* pp. 36 charts
- Emery W J 1975 The role of vertical motion in the heat budget of the upper ocean; Ph.D. dissertation, Hawaii Institute of Geophysics, University of Hawaii, USA, 81 pp.
- Gupta M G 1990 Brief report from Monsoon Trough Boundary Layer Experiment Operations Control Centre (MOCC), India Meteorological Department, New Delhi.
- Gopalakrishna V V, Murty V S N, Sarma M S S and Sastry J S 1993 Thermal response of upper layers of Bay of Bengal to forcing of a severe cyclonic storm – A case study; *Indian J. Mar. Sci.* **22** 8–11
- Hastenrath S and Lamb P J 1979a Climatic atlas of the Indian Ocean. Part II – The oceanic heat budget; University of Wisconsin Press, Wisconsin 93 charts
- Hastenrath S and Lamb P J 1979b Climatic atlas of the Indian Ocean. Part I – Surface climatic and Atmospheric circulation; University of Wisconsin Press, Wisconsin 97 charts
- Murty V S N, Sarma Y V B, Rao D P and Murty C S 1992 Water characteristics, mixing and circulation in the Bay of Bengal during southwest monsoon; *J. Mar. Res.* **50** 207–228
- Murty V S N, Rao D P and Sarma Y V B 1993 Variability of the marine boundary layer characteristics in the northern Bay of Bengal during MONTBLEX-90 (Abstract); Presented at the *Second Monitoring Workshop on MONTBLEX Research Results* held at IITM, Pune during 26–27 March, 1993.
- Pollack M J 1954 Static stability parameters in oceanography; *J. Mar. Res.* **13** 101–112
- Rao D P and Murty V S N 1992 Variability of temperature and water vapour content in the lower troposphere of the northern Bay of Bengal during MONTBLEX-90; In: *Proceedings of workshop on preliminary results of MONTBLEX* held at IISc Bangalore during 16–17 January, 1992, DST & MST, Technology Bhavan, New Delhi, 185 pp
- Rao K H, Antony M K, Murty C S and Reddy G V 1987 Gyres in the NW Bay of Bengal – Some observed evidences; *Indian J. Mar. Sci.* **16** 9–14
- Sarma Y V B, Seetharamayya P and Rao D P 1992 Ocean-atmosphere interaction in the vicinity of monsoon trough over the head of the Bay of Bengal; In: *Montblex News – A Bulletin of the MONTBLEX team*, Bangalore, 5, January, 1992
- Singh O P 1993 Variability of wind stress and wind stress curl over the north Indian Ocean during pre-monsoon and monsoon seasons of 1987 and 1988; *Mahasagar – J. of Limnology and Oceanography* **26** 9–14
- Suga T and Hanawa K 1990 The mixed layer climatology in the northwestern part of North Pacific subtropical gyre and formation of subtropical mode water; *J. Mar. Res.* **48** 543–566
- Swallow J C 1983 *Eddies in the Indian Ocean*; In *Eddies in marine science*, (Ed.) A R Robinson (Springer-Verlag, Berlin) p. 200–208

Roughness length and drag coefficient at two MONTBLEX-90 tower stations

KUSUMA G RAO

Jawaharlal Nehru Centre for Advanced Scientific Research, Jakkur P.O., Bangalore 560 064, India

Abstract. Using MONTBLEX-90 mean velocity data, roughness lengths and drag coefficients are estimated at Jodhpur and Kharagpur. At Jodhpur, since the surface is not uniform the roughness length is estimated separately in three different subsectors within the range of prevailing wind directions and averages to 1.23 cm in the sector between 200° and 230° which is relatively flat with no obstacles on the ground. At Kharagpur, where the terrain is more nearly homogeneous, the average value (for all prevailing wind directions) is 1.94 cm.

The drag coefficient C_D at Jodhpur shows variation both with the roughness subsector and with wind speed, the average over all directions increasing rapidly as the mean wind speed \bar{U}_{10} at 10 m height drops according to the power law $C_D = 0.05 \bar{U}_{10}^{-1.09}$ in the range $0.5 < \bar{U}_{10} < 7 \text{ m s}^{-1}$. At Kharagpur, the drag coefficient is smaller than at Jodhpur by nearly 50% for the same range of wind speeds ($> 3 \text{ m s}^{-1}$).

Keywords. Monsoon trough; boundary layer; roughness length; drag coefficient.

1. Introduction

Accurate estimates of surface roughness parameters are crucial for determining the surface drag and for parameterization of turbulent transport of heat, momentum and moisture between the earth and the atmosphere. Earlier studies using certain similarity hypotheses (Dyer and Hicks 1970; Businger *et al* 1971) introduce explicitly a local surface roughness length z_0 which for many purposes is an adequate characterization of the roughness. Recently Wieringa (1993) has emphasized the importance of a correct knowledge of the surface roughness of the earth in the description, modelling and forecasting of the behaviour of averaged winds and turbulence on all scales. He has presented a set of objective criteria required to be fulfilled in the experimental estimation of roughness lengths for any given homogeneous terrain situation, and has drawn valuable conclusions by an examination of fifty well-documented experiments that satisfy such criteria.

The most widely used bulk aerodynamic formula for the momentum transport requires specification of the value of a drag coefficient, which can be estimated from the turbulence measurements made in a field experiment. There are several experiments over the oceans that provide such drag coefficients and also many over the land region, but there is very little data over the monsoon region. The main aim of the present paper is to estimate values for the roughness length and drag coefficient for two tower stations where the Monsoon Trough Boundary Layer Experiment (MONTBLEX-1990) was carried out during the southwest monsoon season of the year 1990 (Goel and Srivastava 1990). A description of the terrain situation at the two stations is presented in the next section.

2. Tower site description

An account of the instrumentation and data acquisition systems, as well as an assessment of the quality of the tower data archived during MONTBLEX-90, is given by Prabhu *et al* (1990), Kusuma and Prabhu (1992) and Rudra Kumar *et al* (1995). We analyse data at two sites, namely Jodhpur (26°N , 73°E) and Kharagpur (22°N , 87°E) at either end of the monsoon trough, as the data here appear to be of the highest quality. A detailed account of the tower site at Jodhpur and Kharagpur stations is given here based in part on data available in the form of video movies and photographs taken at each site.

2.1 Jodhpur

The tower was installed on a farm field in the campus of the Central Arid Zone Research Institute. The surface was covered with small pebbles in the initial phase of the experiment but turned green in the first week of July with patches of grass as the experiment continued with the advance of the monsoon. The prevailing direction of



Figure 1. The site at Jodhpur tower looking southwest.

wind at the tower was from a sector between southeast and west. The terrain situation is illustrated in figure 1. To the west of the tower there were several trees about 5 to 6 m high, and a building about 6 m high was located about 100 m from the tower; the data acquisition system was placed in this building. To the south of the tower at about 100 m there was a water tank about 25 m high. Between east and southeast of the tower there were several trees 5 to 6 m high at a distance of 100 m. A couple of bush-like trees were found present at the north of the tower. The land stretch between 200° and 230° was fairly flat without any obstacles on the ground.

2.2 Kharagpur

The tower was installed on a farm field in the campus of the Indian Institute of Technology, figure 2 shows the terrain situation. The field was covered with wild grass reaching a height of 30–60 cm. In the prevailing wind direction, which was between southwest and southeast, the fetch was vast, open and flat over a long distance of about 1 km. The data acquisition system was placed in a building about 4 m high, located about 150 m to the northeast of the tower. On the western and northern sides there were many buildings and trees.

3. Data selected for analysis

The periods selected for analysis are from 15th June to 12th July and from 26th July to 10th August for both Jodhpur and Kharagpur. Data selected here comprise the

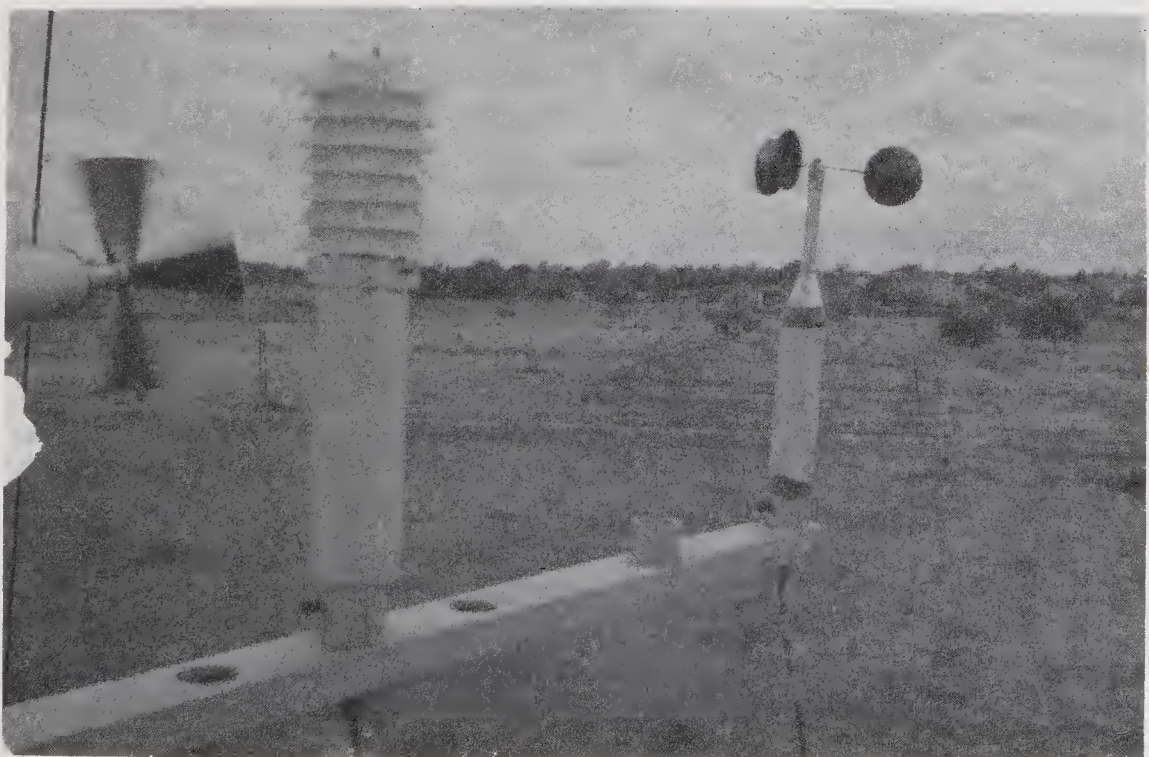


Figure 2. The site at Kharagpur tower looking south.

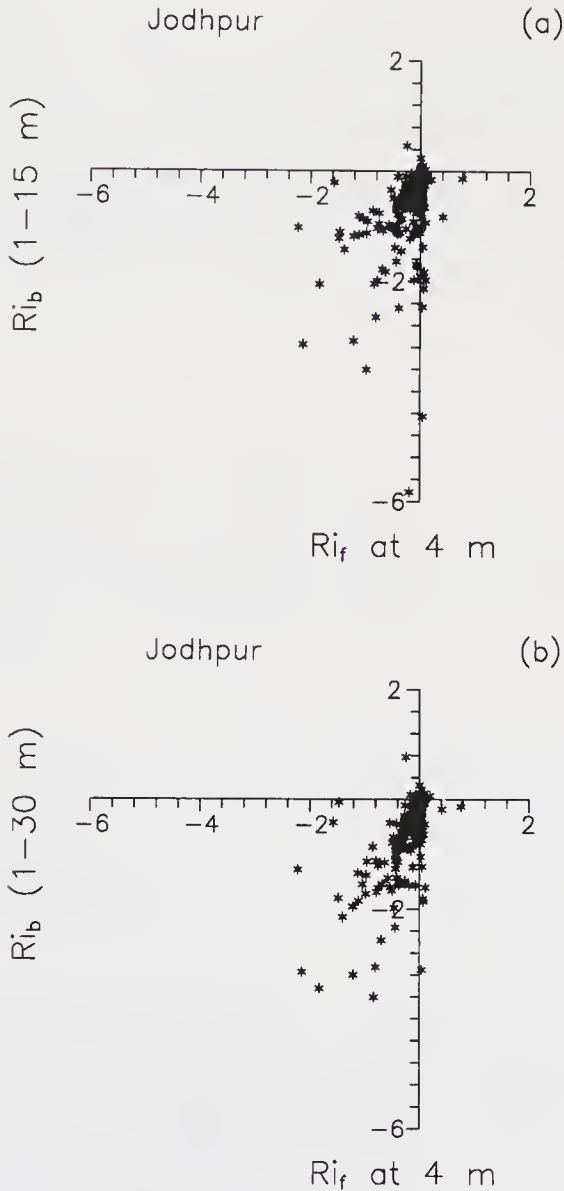


Figure 3(a and b). (a) Comparison between the flux Richardson number Ri_f at 4 m and bulk Richardson number Ri_b (1–15 m); (b) comparison between the flux Richardson number Ri_f at 4 m and bulk Richardson number Ri_b (1–30 m).

measurements made by cup and sonic anemometers and slow temperature sensors, mounted on a 30 m tower at each site. The cup anemometers were placed at six heights on the tower, namely 1, 2, 4, 8, 15 and 30 m above the surface. A sonic anemometer (model: SWS-211/3K orthogonal array, Applied Tech. Inc., Boulder, USA; Kaimal 1988, 1989) was placed at a height of 4 m at Jodhpur and 8 m at Kharagpur. The slow temperature sensors, which were platinum wire thermometers, were placed at 1, 8, 15 and 30 m at Jodhpur and at 1, 4, 15 and 30 m at Kharagpur. High frequency (8 Hz) observations of turbulence and the virtual temperature were obtained from the sonic anemometer. From the rest of the instruments mean wind speed and temperature were obtained. Data from all these instruments were recorded at the rate of 8 samples per second continuously for a sampling period of 15 minutes at pre-determined intervals. The number of data stretches acquired during a day varied from 4 to 24. A PC-based

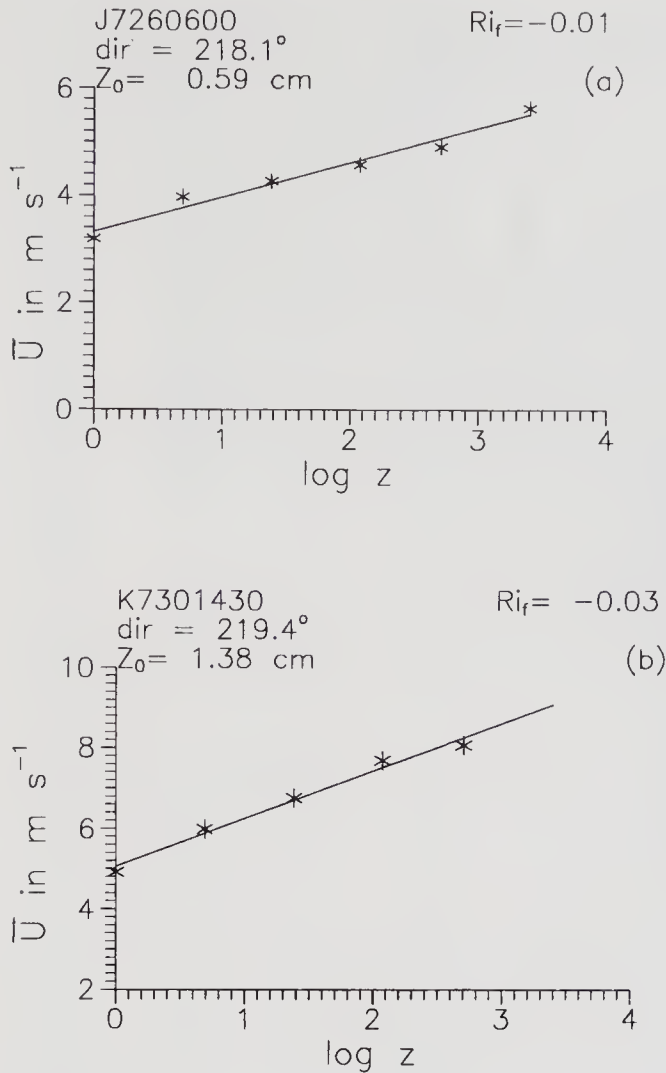


Figure 4(a and b). Variation of cup wind (m s^{-1}) with height for neutral cases (a) at Jodhpur, (b) at Kharagpur. Straight line denotes logarithmic fit.

telemetry system was used to acquire the data. More than 400 observations are available at Jodhpur and about 114 at Kharagpur.

The period from 15th June to 12th July is chosen because it contained two low pressure systems (21st to 30th June and 3rd to 7th July) and included an active monsoon (28th June to 3rd July). During the other period chosen for analysis, namely from 26th July to 10th August the monsoon changed phase from weak (26th July to 1st August) to active (2nd to 10th August), and there were again two low pressure systems (5th to 10th August and 7th to 10th August). For details about the synoptic conditions prevailing during these periods, one can refer to the Weather Summary by Gupta *et al* (1991), Kusuma and Prabhu (1992), Srivastav (1995) and Kusuma *et al* (1995).

4. Roughness length

The roughness lengths for the tower sites are estimated for statically neutral situations as suggested by Wieringa (1993). Initially the flux Richardson number (Ri_f) and the

Table 1. Roughness length for Jodhpur.

N	File name	Dir. (1) (deg.)	Dir. (2) (deg.)	R_f	$U(1)$ (m/s)	z_0 (cm)
14	J6252000	183.5	190.7	0.03	1.9	3.14
19	J6260300	206.2	210.4	0.03	2.9	0.36
20	J6260400	212.0	217.1	0.03	1.8	1.45
41	J6270200	226.2	235.5	0.02	1.8	1.04
58	J6272000	216.2	225.1	0.01	2.0	0.31
59	J6272100	235.1	241.1	0.02	2.0	3.29
60	J6272200	235.7	242.2	0.02	1.7	4.19
61	J6272300	242.6	248.9	0.02	1.3	14.98
64	J6280200	190.6	195.6	0.03	2.2	1.30
65	J6280300	184.4	191.1	0.01	2.3	2.64
66	J6280400	187.4	193.2	0.02	1.8	1.90
67	J6280500	194.4	199.6	0.00	2.7	0.99
68	J6280600	191.0	196.1	0.02	2.3	1.11
78	J6281800	155.2	160.6	-0.03	3.6	2.86
79	J6281900	170.8	174.5	-0.02	2.5	8.40
81	J6282100	106.5	109.7	-0.01	1.4	12.93
82	J6282200	96.2	99.6	-0.02	1.4	14.37
98	J7020600	231.0	235.5	0.00	2.6	0.68
110	J7081800	176.6	174.9	-0.02	2.8	4.03
111	J7090600	209.0	207.1	0.02	2.6	0.57
116	J7092100	197.9	196.6	0.02	2.8	0.83
117	J7100600	186.4	184.5	0.00	3.6	0.78
121	J7101800	180.1	179.7	-0.01	3.6	1.28
122	J7102100	184.2	183.5	0.00	2.3	2.25
128	J7112100	216.3	214.4	0.01	2.9	0.85
140	J7200600	222.0	219.9	-0.01	2.0	2.81
148	J7201500	175.7	175.7	-0.02	2.6	0.95
151	J7201900	211.8	210.4	-0.02	2.8	0.70
157	J7210100	221.2	224.1	0.01	3.1	0.85
158	J7210200	221.3	224.2	0.01	3.3	0.58
159	J7210300	211.1	213.7	0.02	2.3	2.03
172	J7212000	211.3	214.1	0.02	2.1	0.49
173	J7212100	205.9	209.1	0.02	1.8	1.67
181	J7230600	223.2	223.4	0.02	1.2	4.19
187	J7240600	233.5	234.4	0.02	1.2	10.21
201	J7260600	218.1	215.9	-0.01	3.2	0.59
205	J7261800	*	*	-0.02	2.9	0.62
219	J7290600	195.2	195.3	0.02	1.4	2.13
249	J8030600	188.1	192.3	0.00	1.3	2.90
278	J8052000	258.6	256.2	-0.01	1.3	25.69
279	J8052100	226.2	223.4	-0.01	1.3	11.40
281	J8060700	155.1	154.0	0.00	1.4	22.77
282	J8060800	159.0	157.6	0.00	3.2	9.33
283	J8060900	146.0	145.6	0.00	2.8	11.24
284	J8061000	151.0	150.1	0.00	3.3	6.73
285	J8061100	165.7	163.5	-0.01	3.2	10.87
286	J8061200	173.9	172.3	0.00	2.4	6.27
287	J8061300	167.4	165.4	-0.02	2.2	11.64
291	J8061700	171.3	169.9	-0.02	2.4	8.72
292	J8061800	173.4	172.4	0.00	2.6	9.35
302	J8071300	172.4	172.7	-0.01	2.1	9.17

Table 2. Roughness length for Kharagpur.

N	File name	Dir. (1) (deg.)	Dir. (2) (deg.)	R_f	$U(1)$ (m/s)	z_0 (cm)
29	K6211730	160.9	*	0.01	3.0	1.73
34	K6220530	192.8	*	0.00	1.7	3.86
55	K7201432	227.0	*	-0.02	2.4	1.24
68	K7231750	166.3	*	0.02	2.6	1.62
70	K7241751	184.7	*	0.02	2.8	2.84
86	K7301430	219.4	*	-0.03	4.9	1.38
101	K8071730	*	*	-0.03	2.4	1.72
108	K8091730	*	*	0.01	3.4	1.66
110	K8101730	*	*	-0.01	2.9	1.52
114	K8111730	*	*	0.02	2.9	1.80

*No data.

bulk Richardson number (Ri_b) are calculated using the data mentioned above and the formulae

$$Ri_f = (g/\bar{\theta}) \frac{\overline{w'T'_v}}{\overline{U'w'(\partial\bar{U}/\partial z)}}, \tag{1}$$

$$Ri_b = (g/\bar{\theta}) \frac{(\partial T/\partial z) + \gamma_d}{(\partial\bar{U}/\partial z)^2}, \tag{2}$$

where θ represents potential temperature, γ_d the dry adiabatic lapse rate, g the acceleration due to gravity, T the temperature and w the vertical velocity. The momentum and heat fluxes $\overline{U'w'}$ and $\overline{w'T'_v}$ necessary to calculate the flux Richardson number are obtained from sonic anemometer data. U' represents the deviation of U from the mean \bar{U} averaged over 15 minutes in the mean wind direction, similarly w' and T'_v .

The bulk Richardson numbers are calculated for two layers respectively between 1 and 15 m, and 1 and 30 m. Figure 3(a) shows a comparison between Ri_f at 4 m and Ri_b (1–15 m), and similarly figure 3(b) between Ri_f at 4 m and Ri_b (1–30 m). These comparisons indicate that all three Richardson numbers provide roughly compatible measures of stability of the surface layer.

To calculate the roughness length, only those for which the stability conditions are near neutral are now selected from among the data sets chosen above, by restricting the Richardson number Ri_f to be between -0.03 and 0.03 . Panofsky and Dutton (1984) suggest the shorter range $-0.01 < Ri_f < 0.01$, but we have too few points in this range. The roughness length is defined as the height above the surface where the extrapolation of a logarithmic fit to mean winds would assume the value zero. Figures 4(a–b) show the logarithmic fits to cup winds for statically neutral situations at each station. These fits explain fairly well the variation of the wind in the surface layer.

Roughness lengths calculated for various data sets are listed in table 1 for Jodhpur and table 2 for Kharagpur. Values are not presented for those data sets for which the wind speed at the lowest level was less than 1 m/s, as the fit to the log law is not as good in these cases (figure 5a, b) and values of the inferred roughness length from forced log

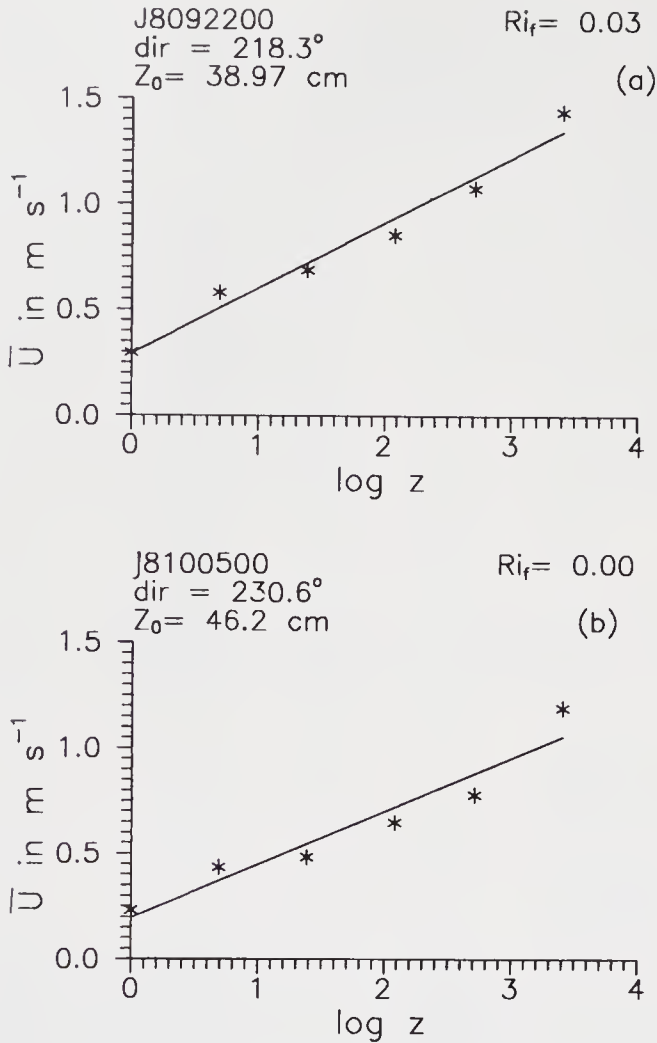


Figure 5(a and b). Variation of cup wind (m s^{-1}) with height at Jodhpur at low winds for neutral cases. Straight line denotes logarithmic fit.

fit can be very large and inconsistent with the roughness elements at the surface. The reason for adopting this criterion is that the mean winds shown in figure 5(a–b) themselves cannot be measured accurately when they are low ($< 0.5 \text{ m s}^{-1}$), due to the inertia of the cup. The first column in tables 1 and 2 represents the data file chosen for the analysis; the file-name is indicated, for example, as J8061000(K8061000) where the first letter J(K) stands for the station name Jodhpur(Kharagpur), the second character (8) represents the month (August), the third and fourth(06) the day (6th) and the last four numbers(1000) the time (10:00 hrs) of the observations at which the data is recorded. In tables 1 and 2, the directions from where the wind blows towards the tower at heights of 1 m and 2 m are given in columns 2 and 3, the flux Richardson number in column 4, mean wind at 1 m height in column 5 and the inferred roughness length z_0 in column 6.

The variation of roughness length with direction at the Jodhpur tower is depicted in figure 6(a). This variation is not unexpected, as the tower site description given above suggests that the roughness elements at the surface differ in size around the tower. We note from figure 6(a) that there are some data points for which the wind is blowing outside the sector $200\text{--}230^\circ$ and z_0 is consistently large varying between 2.86 cm and

more than 20.0 cm, in comparison with the roughness length for the sector between 200° and 230° where the land is entirely flat and obstacle-free. Occasionally (in particular whenever there was a weather system present), the wind blows from southeast. One such occasion was the period from 5th to 10th August when there was a low pressure system located over the Rajasthan region (Kusuma *et al* 1995). The roughness lengths for the subsector 200° to 230° are shown in figure 6(b) and listed in table 3, which shows that the values are between 0.3 and 4.2 cm. There is one data file (J8052100) in this sector for which the inferred z_0 is 11.4 cm which is well outside the range of the rest of the data. On the concerned day (August 5th) a low pressure system was located right over Jodhpur, and presumably produced anomalous velocity profiles. If we slightly increase the sector width to 200°–240°, we see that z_0 varies significantly with values more than 9.0 cm, indicating the influence of the terrain on the west, to be significant. Finally, an average roughness length of 1.23 cm was determined for the subsector between 200° and 230° by averaging the z_0 given in table 3 excluding the file J8052100.

The roughness length at the Kharagpur tower, as listed in table 2 and shown in figure 6(c), varies only between 1.24 and 3.86 cm for almost all the neutrally stable situations; the average turns out to be 1.94 cm. With the prevailing direction of the wind between southeast and southwest, a sector in which the fetch was open, flat and obstacle-free as already pointed out, it is not a surprise that the z_0 values are so consistent.

Both the sites Jodhpur and Kharagpur come under the category of short grass and moss in the terminology of Wieringa (1993). The roughness length validated and listed by him (1993) in table VIII for such a surface lies in the range of 0.8–3.0 cm. Thus the average roughness lengths arrived at here for both the sites agree with values quoted by Wieringa (1993) for similar terrain situations.

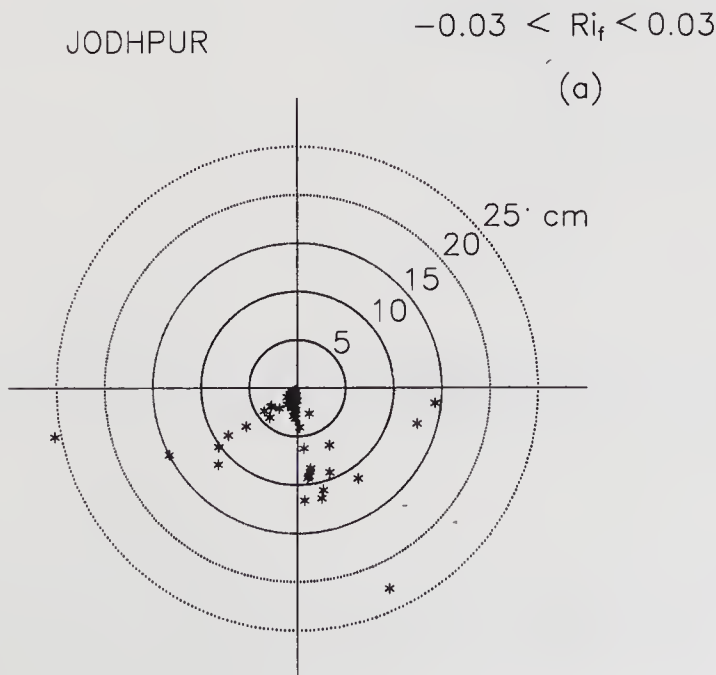


Figure 6.

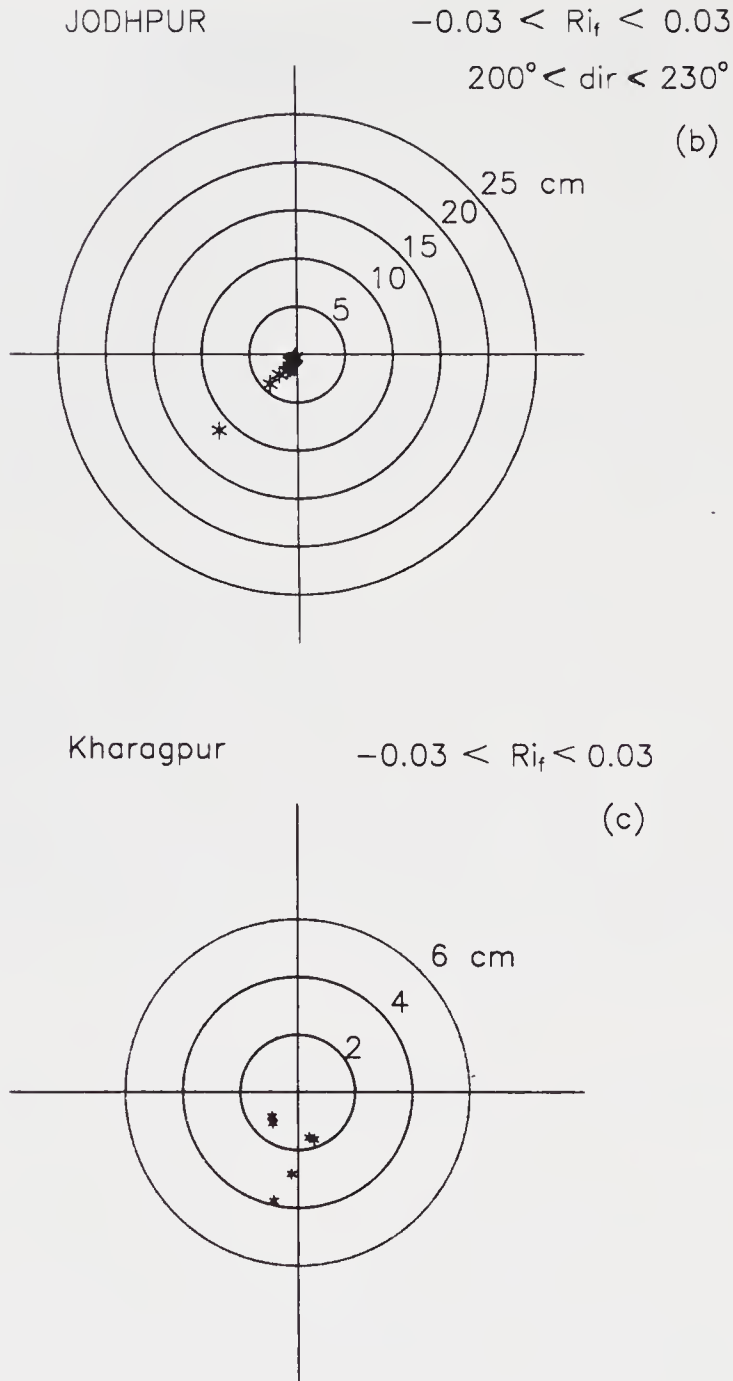


Figure 6(a-c). Variation of roughness length (cm) with direction (a) for the sector outside $200^\circ < Dir < 230^\circ$ at Jodhpur, (b) for the sector between 200° and 230° at Jodhpur, (c) at Kharagpur.

5. Drag coefficient

The drag coefficient is estimated using the formula

$$C_D = \left(\frac{u_*}{\bar{U}_{10}} \right)^2, \tag{3}$$

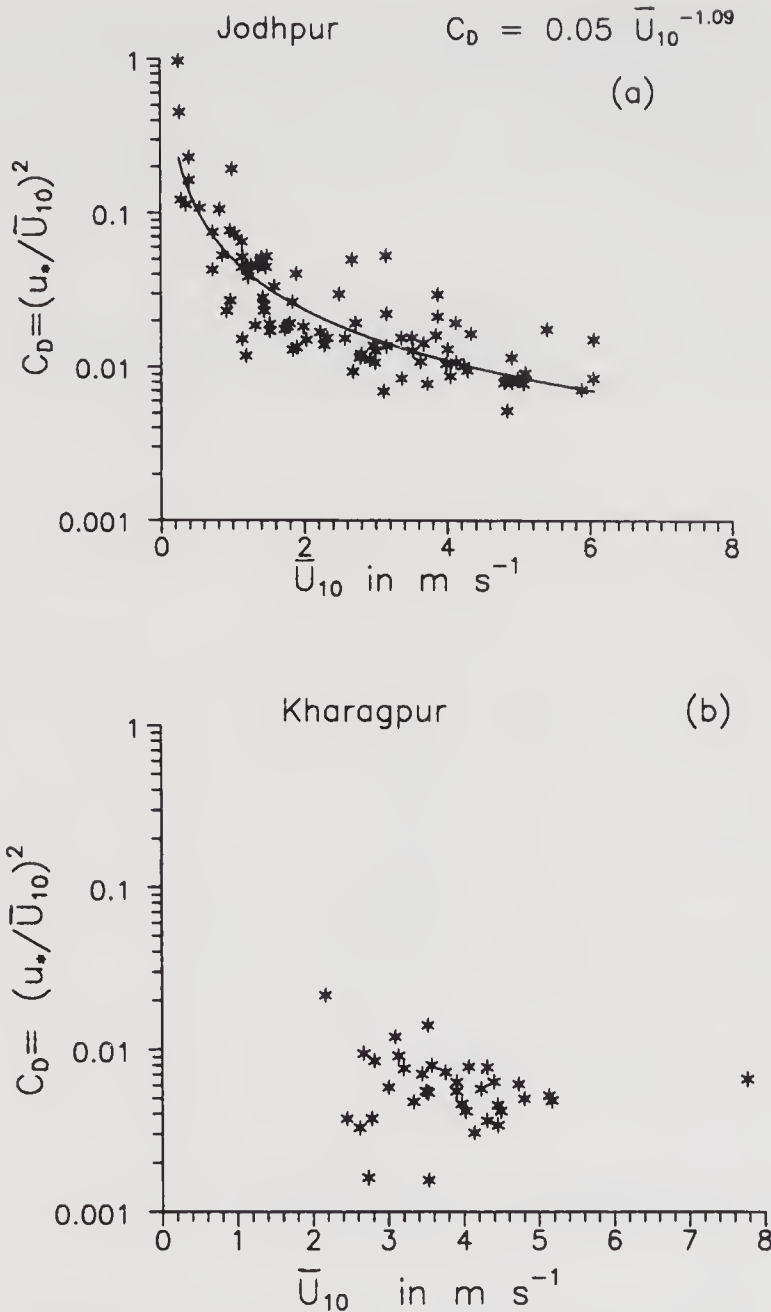


Figure 7(a and b). Variation of drag coefficient with wind at 10m height. (a) Jodhpur, (b) Kharagpur.

where u_* represents the friction velocity calculated from the flux data using the relation

$$u_* = [(\overline{u'w'})^2 + (\overline{v'w'})^2]^{1/4}, \quad (4)$$

and \bar{U}_{10} is the mean wind speed at 10 m height, obtained by reading off from a least squares quadratic curve fitted to the observed wind velocities along the mean wind direction at the six instrumented levels on the tower.

Drag coefficient values estimated for Jodhpur and Kharagpur are shown in figure 7(a and b). At Jodhpur, the drag coefficient varies significantly with wind speed, especially as winds fall below 2 m s^{-1} . At Kharagpur, such low winds were not observed

during the period of analysis. For the same range of wind speeds, C_D at Kharagpur is smaller than at Jodhpur by nearly 50%, suggesting that C_D might be a strong function of roughness and possibly other local surface parameters.

The solid line in figure 7(a) shows the curve fit for the drag coefficient as a function of wind speed from all directions and describes the power law variation

$$C_D = 0.05 \bar{U}_{10}^{-1.09}. \tag{5}$$

The low winds at Jodhpur are found to be blowing from all directions around the tower as shown in figure 8. Since the roughness lengths at Jodhpur vary with sector as demonstrated in section 4, the drag coefficients are plotted as a function of wind speed

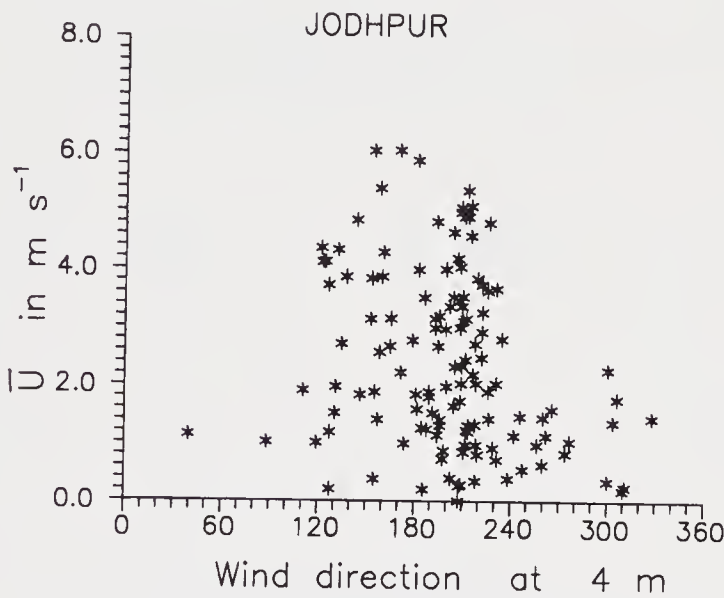


Figure 8. Variation of wind at 10 m height with direction at Jodhpur.

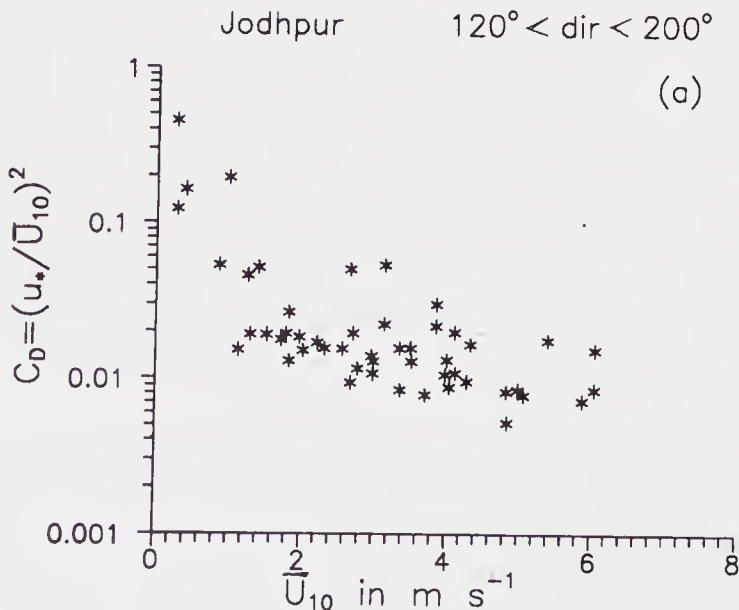


Figure 9.

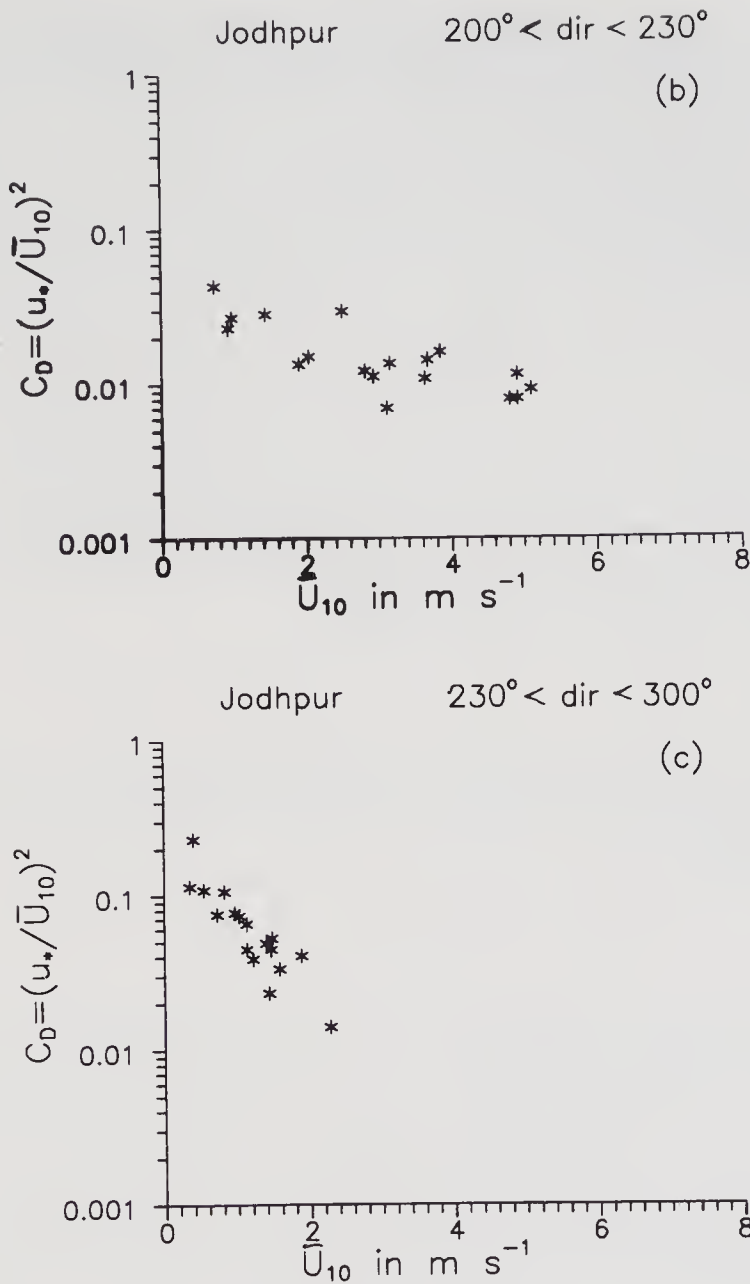


Figure 9(a–c). Variation of drag coefficient with wind at 10m height at Jodhpur for the sectors (a) 120° to 200° (b) 200° to 230° (c) 230° to 300°.

for three different sectors around the tower, namely 120° to 200°, 200° to 230° and 230° to 300°, and are shown in figures 9(a–c) respectively. The drag coefficients assume very large values at low winds in the sectors 120° to 200° and 230° to 300° where the roughness lengths also vary significantly (between 3 and 20 cm). In comparison, in the sector between 200° and 230°, where the land is flat and obstacle-free with a consistent average roughness of 1.23 cm, the drag coefficient does not assume as large values as in the other sectors. Thus, there is an indication that the drag coefficients are significantly influenced by terrain at low winds.

At Kharagpur, for the same range of wind speeds ($> 3 \text{ m s}^{-1}$) the C_D values are smaller than at Jodhpur by nearly 50%. Even at Jodhpur, for high winds ($> 3 \text{ m s}^{-1}$) the C_D values do not show significant variation between the sectors as shown in

figures 9(a–c). This suggests that some local surface parameter other than roughness is responsible for the variation of C_D values between Jodhpur and Kharagpur at high winds ($> 3 \text{ m s}^{-1}$), may be soil moisture! However, with the present data we are unable to make further analysis of this issue.

The variation of the drag coefficient with wind speed is well known over the oceans (Liu *et al* 1979; Large and Pond 1981; Garratt 1993). On land, however, Stull (1988) lists values for the neutral drag coefficient as 3.9×10^{-3} and 27.7×10^{-3} over the Asian continent north of 20°N and south of 20°N respectively. Stull (1988) also gives the formula $C_{DN} = [1.10 + 0.07 M] 10^{-3}$, where M is the wind speed, for neutral drag coefficient over plains and during night time. For instance, if $M = 1.5 \text{ m s}^{-1}$, $C_{DN} = 1.105 \times 10^{-3}$ which is very low when compared to the drag coefficients estimated here at either of the sites. These values of C_{DN} proposed by Stull (1988) are of the same order of magnitude as observed over the oceans (Garratt 1993). However the estimated values of the drag coefficients presented here for the two land stations are not only large compared to the earlier observed values over the land or oceans, but show a strong dependence on wind speed and roughness.

Acknowledgement

The author is grateful to R Narasimha for useful discussions. The author thanks S Ameenulla, Rudra Kumar and A Prabhu for a detailed discussion on the terrain at Jodhpur and Kharagpur.

References

- Businger J A, Wyngaard J C, Izumi Y and Bradley E F 1971 Flux profile relationship in the atmospheric surface layer; *J. Atmos. Sci.* **28** 181–189
- Dyer A J and Hicks B B 1970 Flux gradient relationships in the constant flux layer; *Q. J. R. Meteorol. Soc.* **96** 715–21
- Garratt J R 1993 Sensitivity of climate simulations to land surface and atmospheric boundary layer treatment. A review; *J. Climate* **6** 419–449
- Goel M and Srivastava H N 1990 Monsoon trough boundary layer experiment (MONTBLEX); *Bull. Am. Meteorol. Soc.* **71** 1594–1600
- Gupta G R, Desai D D and Biswas N C 1991 Weather–Summer monsoon season (June–September, 1990); *Mausam.* **42** 3–30
- Kaimal J C 1988 The atmospheric boundary layer – its structure and measurement; Lecture notes, IITM Visiting Professorship Program.
- Kaimal J C 1989 Minimizing flow distortion errors. 5th European Physical Society; Liquid State Conference. Moscow 16th–20th October.
- Kusuma Rao G, Sethu Raman, Prabhu A and Narasimha R 1995 Turbulent heat flux variation over the monsoon trough region during MONTBLEX-90; *Atmos. Environ.* **29** 2113–2129
- Kusuma Rao G and Prabhu A 1992 Computation of sensible heat and momentum fluxes using fast data for Jodhpur during 1st–12th July 1990; Indian Institute of Science Report **92** AS 5
- Large W G and Pond S 1981 Open ocean momentum flux measurements in moderate to strong winds; *J. Phys. Oceanogr.* **11** 324–336
- Liu W T, Katsaros K B and Businger J A 1979 Bulk parameterization of air-sea exchanges of heat and water vapour including the molecular constraints at the interface; *J. Atmos. Sci.* **36** 1722–1735
- Prabhu A, Rao K N, Kusuma Rao G, Kailas S V, Rudra Kumar S, Ameenulla S and Srinivasan H P 1990 MONTBLEX pilot experiment 1989 – Tower component; Indian Institute of Science Report **90** AS 2
- Panofsky H A and Dutton J A 1984 Atmospheric Turbulence – Models and methods for engineering application. (New York: John Wiley and Sons) p. 397

- Rudra Kumar S, Ameenulla S and Prabhu A 1995 MONTBLEX tower observations: Instrumentation, data acquisition and data quality; *Proc. Indian Acad. Sci. (Earth Planet. Sci.)* **104** 221–248
- Srivastav S K 1995 Synoptic meteorological observations and weather conditions during MONTBLEX-90; *Proc. Indian Acad. Sci. (Earth Planet. Sci.)* **104** 189–220
- Stull B 1988 An introduction to boundary layer meteorology. (Dordrecht: Kluwer Academic Publishers) p. 666
- Wieringa J 1993 Representative roughness parameters for homogeneous terrain; *Boundary-Layer Meteorol.* **63** 323–363

Estimation of drag coefficient over the western desert sector of the Indian summer monsoon trough

U C MOHANTY, P S PARIHAR, T VENUGOPAL and
PARASHURAM

Centre for Atmospheric Sciences, Indian Institute of Technology, Hauz Khas, New Delhi
110016, India

Abstract. In the estimation of momentum fluxes over land surfaces by the bulk aerodynamic method, no unique value of the drag coefficient (C_D) is found in the literature. The drag coefficient is generally estimated from special observations at different parts of the world. In this study an attempt is made to estimate drag coefficient over the western desert sector of India using data sets of Monsoon Trough Boundary Layer Experiment (MONTBLEX) during the summer monsoon season of 1990. For this purpose, the fast and slow response data sets obtained simultaneously from a 30 m high micro-meteorological tower at Jodhpur are used. All the observations used in this study are confined to a wind speed regime of $2.5\text{--}9.0\text{ ms}^{-1}$.

A comparison of momentum fluxes computed by eddy correlation (direct estimation) with profile and bulk aerodynamic ($C_D = 3.9 \times 10^{-3}$, Garratt, 1977) methods revealed that though the nature of variation of the fluxes by all these methods is almost similar, both the indirect methods give an under-estimated value of the fluxes. The drag coefficient is estimated as a function of wind speed and surface stability by a multiple regression approach. An average value of the estimated drag coefficient is found to be of the order of 5.43×10^{-3} . The estimated value of C_D is validated with a set of independent observations and found to be quite satisfactory. The recomputed momentum fluxes by bulk aerodynamic method using the estimated drag coefficient are in close agreement with the directly estimated fluxes.

Keywords. Drag coefficient; momentum fluxes; bulk aerodynamic method; eddy correlation method.

1. Introduction

The thermal and dynamic interaction between the atmosphere and the underlying surface (sea or land) occurs through turbulent exchange of momentum, heat and moisture at their interface. The variation of fluxes of momentum, heat and moisture in the surface boundary layer and their distribution in the rest of the planetary boundary layer play a vital role in the energy transport mechanism of the land-atmosphere-ocean system and influence the steady state of the atmosphere.

The surface fluxes are determined by several methods such as eddy correlation, profile, bulk aerodynamic, energy dissipation etc. The bulk aerodynamic method is the most conventional approach and is widely used. In this method, the turbulent transports of momentum, heat and moisture are treated as proportional to the differences of mean meteorological parameters such as wind speed, temperature and moisture between the underlying surface and a reference level. This method is formulated on the basic assumption that the surface wind stress is parallel to the surface wind direction. However, the proportionality constants known as bulk transfer coefficients remain a problem of concern as no unique value is found in the literature.

Most of the studies on the estimation of these transfer coefficients pertain either to open sea, sea-shore, sand-pit or sea-beach interface (Smith and Banke 1975; Sethuraman and Raynor 1975; Francey and Garratt 1978; Vugts and Cannemeijer 1981; Large and Pond 1981 and Tsukamoto *et al* 1990). Only a few works over land regions have been reported in literature.

Garratt (1977) has reported a comprehensive review on the estimation of drag coefficients over ocean and land surfaces. Its dependence on wind speed, stability and nature of the underlying surface has been documented. Beljaars and Holtslag (1991) have briefly described observations and modelling efforts on surface fluxes over land surfaces. However, information on the dependence of drag coefficient over land surfaces on wind speed and stability is still inadequate in many of these reviews.

The most striking feature of all these studies is that there is no unique approach in the estimation of drag coefficient. Garratt (1977) reported average values of neutral drag coefficient over tropical and extra-tropical land surfaces on the basis of the conservation principle of angular momentum. The quoted value of neutral drag coefficient over Asian land mass (20° – 50° N) is of the order of 3.9×10^{-3} .

Over the Asian land mass, the summer monsoon exhibits wide variability from region to region. One of the large scale features of the Indian summer (southwest) monsoon is the persistence of surface low pressure extending from the seasonal desert heat low over Pakistan and north west India through the Indo-Gangetic plains and dipping into the Bay of Bengal on the east of the Indian sub-continent. This surface feature, known as the *monsoon trough*, is quasi-permanent during the Indian summer monsoon. The rainfall activity over the Indian sub-continent is known to be largely associated with the positioning of the monsoon trough (Rao 1976). The monsoon trough is understood to influence the planetary boundary layer over India and other regions of tropics.

Atmospheric boundary layer experiments began during the late sixties. In India for the first time, during the Monsoon Experiment (MONEX-79), a 10 m high mast was installed at a coastal station close to the Bay of Bengal to probe the boundary layer. In the summer monsoon season (June – September) of 1990, the Monsoon Trough Boundary Layer Experiment (MONTBLEX) was designed to carry out exclusive surface boundary layer observations over land surfaces along the monsoon trough (Goel and Srivastava 1990). During this experiment, micro-meteorological towers of 30 m height with slow and fast response sensors fixed at six nearly logarithmic levels were installed at four locations along the monsoon trough. These locations represent the dry-convective to moist-convective nature of the atmosphere along the normal axis of the monsoon trough.

In the present study, an attempt is made to estimate the drag coefficient over land surface on the western desert sector of India and to estimate the surface momentum fluxes by direct and indirect methods using the tower observations of MONTBLEX-90.

2. Methodology

2.1 Determination of surface fluxes

The surface fluxes of momentum, heat and moisture are determined widely by three

methods, viz., eddy correlation, profile and bulk aerodynamic methods. Each of these methods is briefly described below:

2.1.1 *Eddy correlation method*: It is a direct method for determining the surface (momentum, heat and moisture) fluxes in terms of covariances of vertical velocity component with horizontal velocity components, temperature and specific humidity. For this purpose, fast response observations (of frequency 8–10 Hz) are generally used. The fast response sensors placed on stable platforms need a proper levelling and calibration for a better accuracy and reliability.

The surface momentum flux, in particular, is expressed as:

$$\tau = \rho(\overline{u'w'^2} + \overline{v'w'^2})^{1/2}, \tag{1}$$

where ρ is the density of the surface layer.

2.1.2 *Profile method*: It is an indirect method based mainly on Monin-Obukhov's similarity theory for the determination of surface fluxes. For the construction of wind, temperature and moisture profiles, their measures at two levels in the surface layer are required.

The wind and temperature profiles in the surface layer are described in the following forms (Dyer and Hicks 1970; Businger *et al* 1971):

$$\Delta\bar{u} = \frac{u_*}{k} \left(\ln \frac{z_2}{z_1} - \psi_m(\zeta_2) + \psi_m(\zeta_1) \right), \tag{2}$$

$$\Delta\bar{\theta} = R \frac{\theta_*}{k} \left(\ln \frac{z_2}{z_1} - \psi_h(\zeta_2) + \psi_h(\zeta_1) \right), \tag{3}$$

where $\Delta\bar{u} = u_2 - u_1$ and $\Delta\bar{\theta} = \theta_2 - \theta_1$, the subscripts denoting the respective levels. u_* is the friction velocity and θ_* is the temperature scale. ψ_m and ψ_h are the stability functions associated with wind and temperature profiles respectively. $\zeta (= z/L)$ is the stability function where L is the Monin-Obukhov length given by:

$$L = \frac{\bar{T} u_*^2}{g k \theta_*}. \tag{4}$$

$R = 0.74$, a ratio of eddy diffusivities in the neutral limit. $k = 0.4$, the von Karman constant.

The stability functions assume the following form (Paulsen 1970; Barker and Baxter 1975):

In unstable conditions ($\zeta < 0$):

$$\psi_m(\zeta) = \ln \left(\left(\frac{1+x}{2} \right)^2 \frac{1+x^2}{2} \right) - 2 \arctan x + \frac{\pi}{2}, \tag{5}$$

and

$$\psi_h(\zeta) = 2 \ln \left(\frac{1+y}{2} \right), \tag{6}$$

where

$$x = (1 - 15\zeta)^{1/4} \text{ and } y = (1 - 9\zeta)^{1/2}, \tag{7}$$

while in stable conditions ($\zeta > 0$):

$$\psi_m(\zeta) = -4.7\zeta, \quad (8)$$

and

$$\psi_h(\zeta) = \frac{-4.7}{R}\zeta. \quad (9)$$

The friction velocity (u_*) and the temperature scale (θ_*) are computed iteratively through the following steps (Berkowicz and Prahm 1982):

- Step 1: By assuming a large value of L , u_* and θ_* are computed first in neutral limits.
 Step 2: L is recomputed from equation (4) using the neutral estimates of u_* and θ_*
 Step 3: u_* and θ_* are recomputed using equations (2) and (3) and L as recomputed in Step 2.
 Step 4: Steps 2 and 3 are repeated until the value of L does not change in desired accuracy limits.

For the sake of brevity, the moisture scale q_* is not discussed here.

The surface momentum flux, in particular, is expressed as:

$$\tau = \rho u_*^2. \quad (10)$$

2.1.3 Bulk aerodynamic method: This is the most conventional and widely used method for determining the surface fluxes. In this method, the basic assumption is that the surface wind stress is in the direction of surface wind. The surface fluxes are given in terms of the differences in mean meteorological parameters at two lowermost levels in the surface layer.

The surface momentum flux, in particular, is expressed as:

$$\tau = \rho C_D V^2, \quad (11)$$

where C_D is the momentum transfer or drag coefficient and V is the wind speed at a reference height. Over land surfaces, there is no unique value of drag coefficient reported in the literature. It is found to depend on wind, stability and nature of the underlying surface.

2.2 Determination of surface layer parameters

The surface layer parameters, viz., friction velocity and temperature scale have been defined in equations (1) and (2) in terms of profiles of wind and temperature at two levels in the surface layer. These parameters can be directly determined in terms of covariances of vertical velocity component with the horizontal velocity components and temperature through the following relations:

$$u_* = (\overline{u'w'^2} + \overline{v'w'^2})^{1/4}, \quad (12)$$

$$\theta_* = -\frac{\overline{w'\theta'}}{u_*}. \quad (13)$$

The drag coefficient (C_D) can be directly determined from the relation:

$$C_D = \left(\frac{u_*}{V} \right)^2, \quad (14)$$

where u_* is as defined in equation (12).

3. Data used and computational procedure

During MONTBLEX-90, surface boundary layer observations were measured from fast and slow response sensors on 30 m high micro-meteorological towers installed at four locations along the normal position of the monsoon trough. These locations are: Jodhpur on the West, Delhi and Varanasi in the centre, and Kharagpur on the East. Jodhpur (26.3°N, 73°E) represents a dry-convective and semi-arid region in the western desert sector of the monsoon trough. The tower observations at Jodhpur are reported to be continuous and extensive (Rudrakumar *et al* 1991).

The tower observations at Jodhpur consist of slow response data at all six levels (1, 2, 4, 8, 15 and 30 m) and fast response data at two levels (4 and 15 m). The slow data were recorded on Campbell data logger with a sampling frequency of 1 Hz and the fast data were recorded on a computer based telemetry system with a sampling frequency of 8 Hz (Rudrakumar *et al* 1991). Data acquisition from slow response sensors was continuous while from fast response sensors, it was 10–15 min. at each observation time. The interval of observations was 3 hours during the normal period of the experiment and hourly during intensive observation periods (IOP). The IOP correspond to specific synoptic situations.

In the present study on the estimation of drag coefficient and surface momentum fluxes, only simultaneously obtained slow (at 1 and 15 m) and fast (at 4 m) response data sets during the entire MONTBLEX period are considered. From 112 of such observations available with us, about 17% of cases with spikes in the data are rejected as a first step. A further quality check on the data sets is carried out through a comparison of surface momentum fluxes estimated by eddy correlation and profile methods. In order to have a homogeneous data base, 10 cases with a difference in momentum fluxes by direct and indirect estimates exceeding by 50% and 14 cases exceeding by 100% are discarded. Finally, 70 sets of homogeneous and good quality data are used to carry out further study.

4. Results and discussion

4.1 Characteristics of surface layer

The surface layer parameters, viz., the friction velocity (u_*) and the temperature scale (θ_*) are computed directly from equations (12) and (13) using the fast response data at 4 m from the selected 70 sets of observations. The distributions of these parameters are depicted in figures 1 and 2 respectively. The friction velocity varies in the range of 0.2–0.4 m s⁻¹, with extreme values corresponding to relatively high surface winds (of the order of 7–9 m s⁻¹) of an active spell (2nd–12th July). The temperature scale is in the

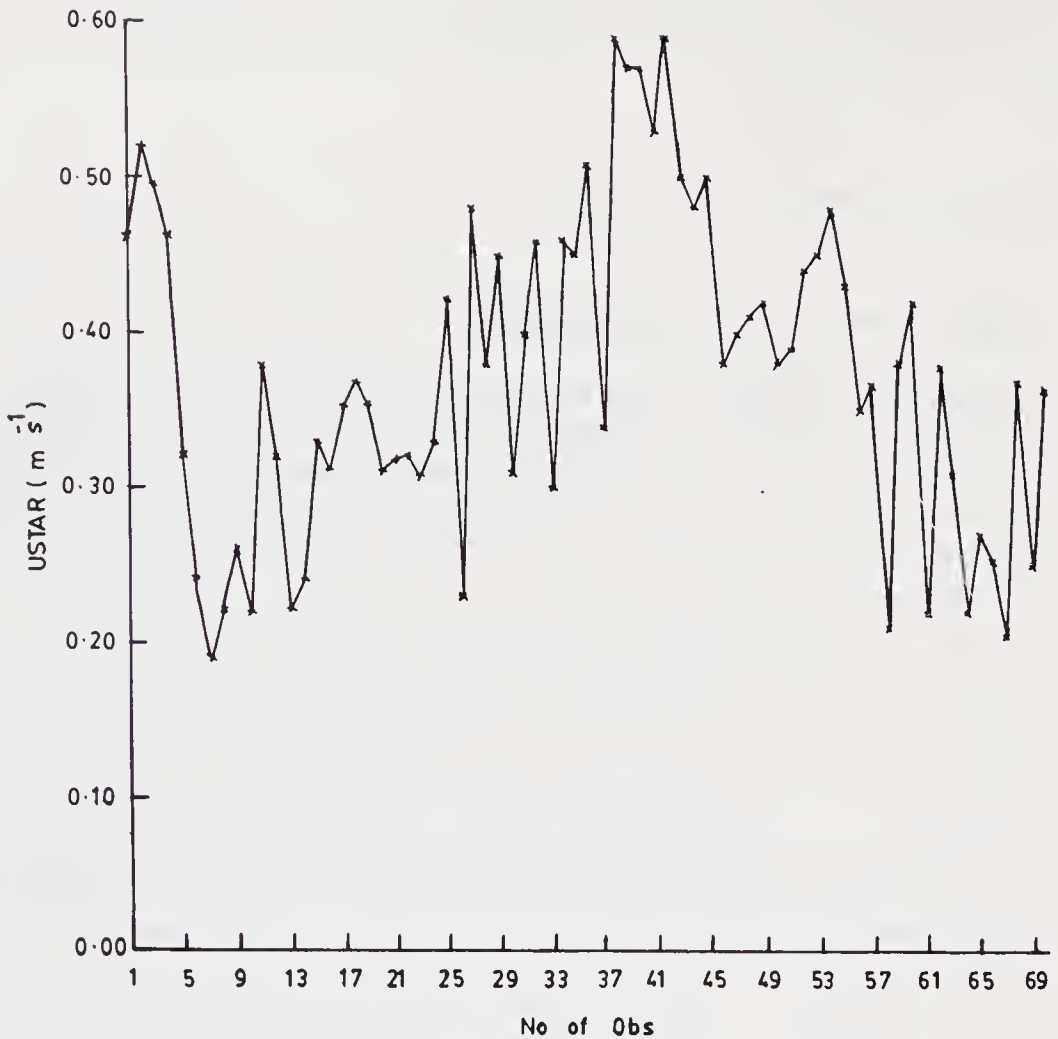


Figure 1. Friction velocity as determined from fast response data at 4 m.

range of -0.2 and -0.6 , indicating that the surface layer remained unstable over a majority of observation hours.

The standard deviations σ_u , σ_v and σ_w of the three velocity components u , v and w are computed and normalized by the friction velocity (figures not presented). The normalized quantities σ_u/u_* and σ_v/u_* are in the range of 1.8 – 2.5 while σ_w/u_* in 1.1 – 1.3 which are nearly in agreement with the general values given by Panofsky and Dutton (1984). They are also comparable with the values obtained by Jiemin *et al* (1990) in their study of surface layer over Gobi desert (39.2°N , 100°E). The fast response observations used in this study are thus of reasonably good quality.

4.2 Computation of surface momentum fluxes

The surface momentum fluxes are first directly estimated by the eddy correlation method and indirectly by the profile method using the 70 sets of observations. As at present a neutral value of drag coefficient over Asian land mass as prescribed by Garratt (1977) is available, the surface momentum fluxes are estimated by bulk aerodynamic method using $C_{DN} = 3.9 \times 10^{-3}$. The distributions of the fluxes computed

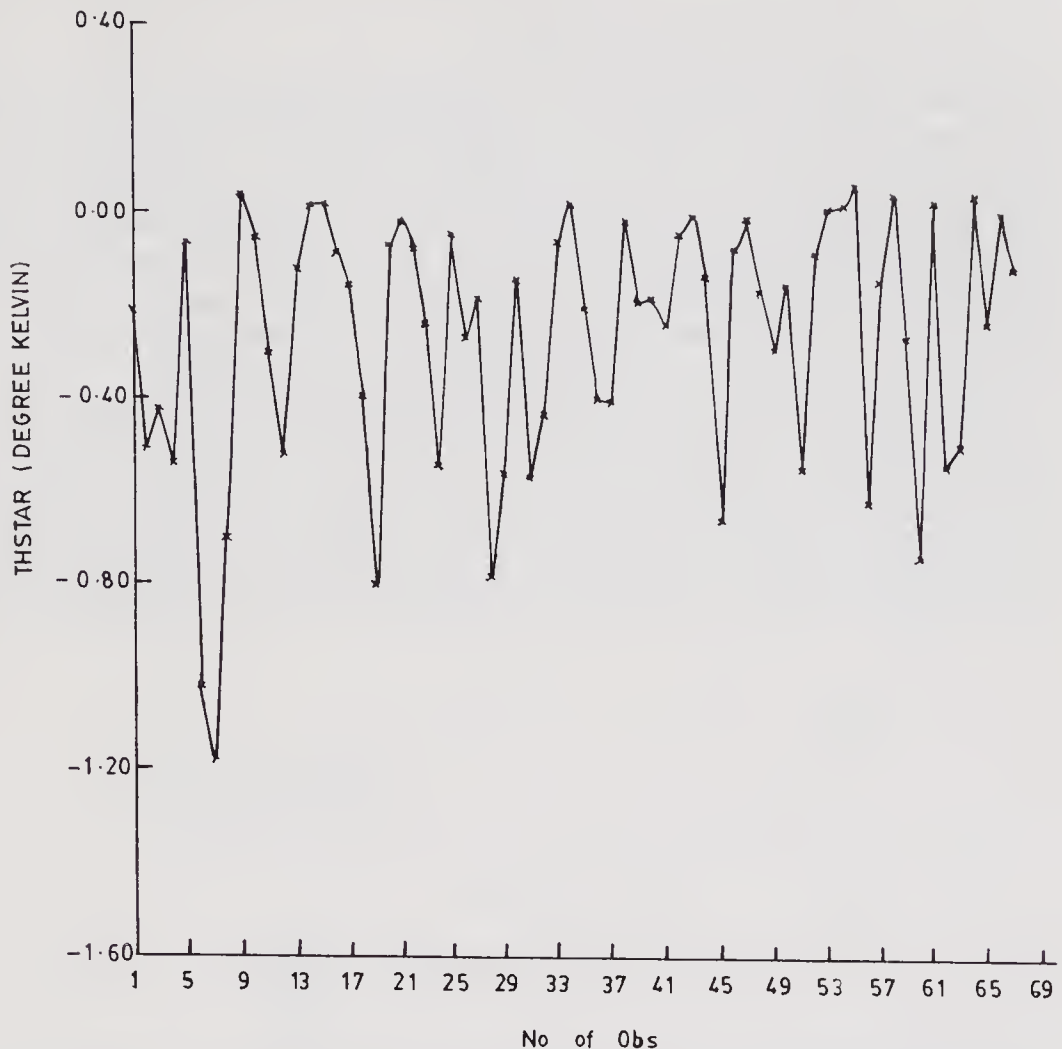


Figure 2. Temperature scale as determined from fast response data at 4 m.

by direct and indirect methods are shown in figure 3. For convenience, the fluxes estimated by the three methods are hereinafter referred to as eddy-fluxes, profile-fluxes and bulk-fluxes and are denoted by MF-E, MF-P and MF-B respectively.

The most striking feature here is that although there is similarity in the nature of variation of these fluxes irrespective of their method of evaluation, the fluxes determined indirectly are under-estimated.

The eddy-fluxes exhibited extreme values during a sequence of observation hours corresponding to an active spell of monsoon rain (2–12 July). The winds in the surface layer during this period are also relatively stronger ($7\text{--}9\text{ m s}^{-1}$) as compared to the winds in any normal period of observation. Such peaks in momentum fluxes are not captured by the profile method and the distribution of profile-fluxes is almost smooth. The standard deviation of profile-fluxes is found to be of lower order (0.05) as compared to that of eddy-fluxes (0.09). As can be seen from figure 3, the bulk-fluxes whose estimation is based on a neutral drag coefficient also exhibited an increasing nature with increasing winds. It is therefore necessary to determine a more realistic drag coefficient from observations and further evaluate it with any statistically significant approach.

4.3 Direct determination of drag coefficient

The under-estimation of bulk-fluxes as compared to eddy-fluxes as seen in § 4.2 may be attributed to the use of a neutral drag coefficient. An alternative approach is to estimate drag coefficient directly, such as by prescribing the observed friction velocity at 4 m level and wind speed at 15 m in equation (14). For convenience, such a directly determined drag coefficient may be referred to as $C_D(\text{dir})$. The estimation gives an average value of the order of 5.43×10^{-3} within a wind speed range of $2-9 \text{ m s}^{-1}$ which is about 35% in excess over Garratt's neutral value of drag coefficient. It is also 3-4 times larger than the normally reported value over ocean surfaces.

In this study, the differences in (potential) temperature between 1 and 15 m levels in the surface layer are in the range of $0.11-3.0^\circ\text{K}$. In the surface layer, the (potential) temperature difference ($\Delta\theta$) between two lowermost levels is sufficient to determine the stability of the surface layer. In this study $\Delta\theta$ is treated as a stability parameter.

Correlation coefficients of $C_D(\text{dir})$ obtained with wind speed and stability parameter are found in the order of -0.39 and 0.12 respectively. Thus a rapid decreasing trend in

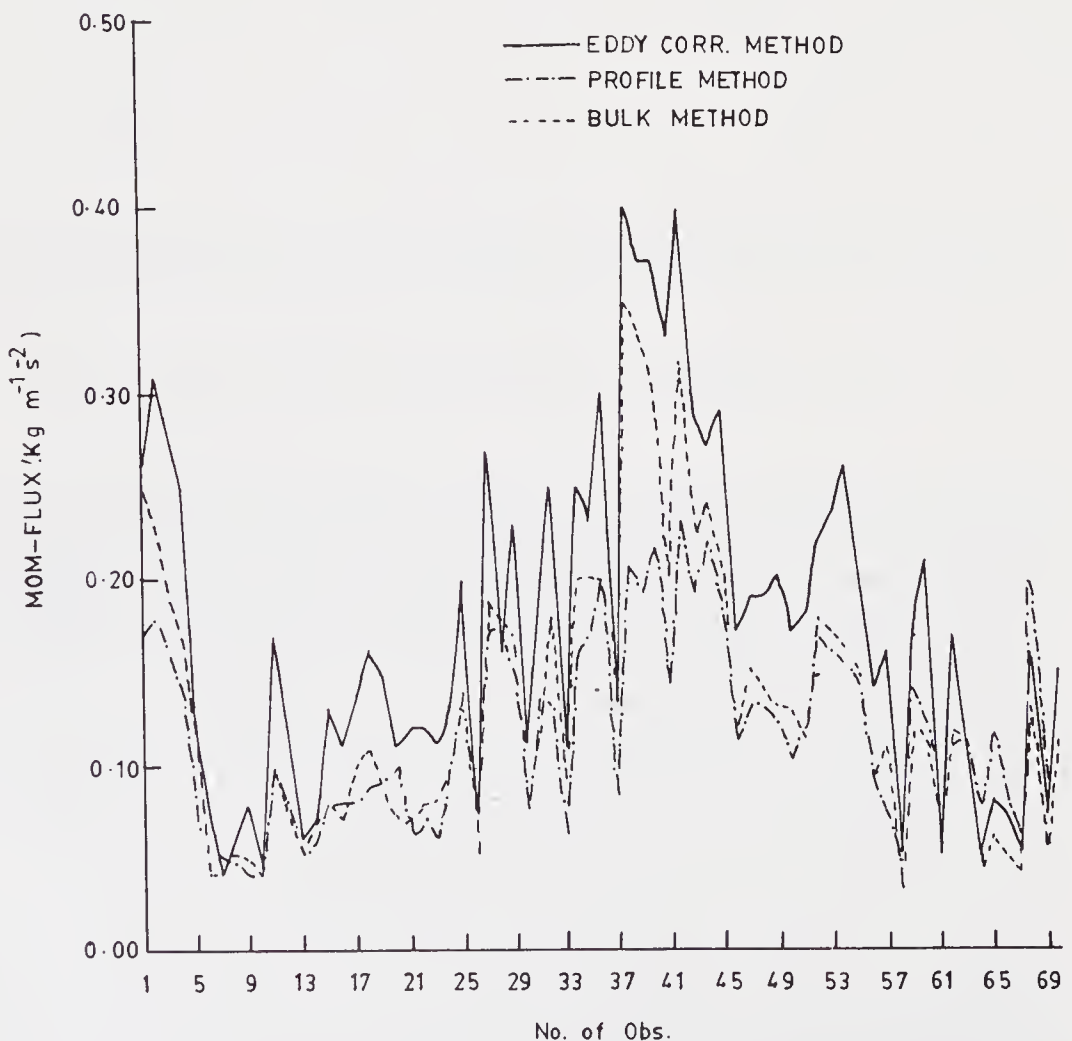


Figure 3. Momentum fluxes computed by eddy correlation, profile and bulk aerodynamic (with C_{DN} , Garratt) methods.

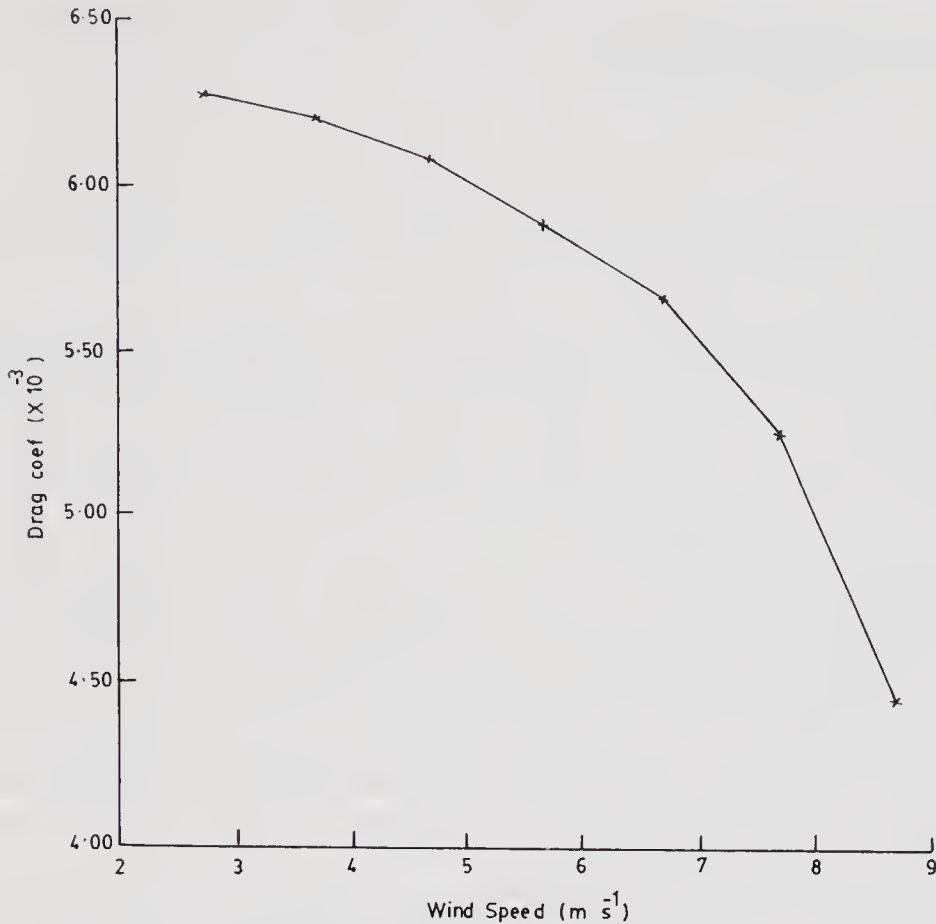


Figure 4. Variation of drag coefficient (direct) with wind speed.

drag coefficient with increasing wind speed, and a slowly increasing trend with increasing instability is evident within the observed ranges of wind speed and (potential) temperature differences. The variation of $C_D(\text{dir})$ with wind speed is shown in figure 4.

The foregoing analysis thus suggests a reexamination of drag coefficient in a more statistically significant approach keeping in view its dependence on wind speed and surface stability.

4.4 Estimation of drag coefficient from wind speed and stability in the surface layer

Over ocean surfaces, the estimation of drag coefficient is normally made considering it either as a linearly varying function or as power function (the power is normally confined to an order of 2) of wind speed at a reference height above the sea surface. Kondo (1975) instead considers a stability parameter in the more generalized form of Richardson number.

In the present study, the estimation of drag coefficient is proposed in the following manner:

- Representing drag coefficient as a function of wind speed alone such that

$$10^3 C_D(V) = a_0 + a_1 V + a_2 V^2. \tag{15}$$

- Representing drag coefficient as a second degree polynomial in both wind speed and stability parameter such that

$$10^3 C_D(V, \Delta\theta) = b_0 + b_1 V + b_2 V^2 + b_3 \Delta\theta + b_4 \Delta\theta^2 + b_5 V \Delta\theta, \quad (16)$$

where V is the wind speed at 15 m and $\Delta\theta$ is the difference in potential temperature at 1 and 15 m levels in the surface layer. a_i ($i = 0$ to 2) and b_j ($j = 0$ to 5) are the regression coefficients to be determined.

The regression coefficients of either form can be obtained by solving equation (15) or (16) by the method of least squares using the wind and temperature data and the directly determined drag coefficients. For the estimation purpose, the first 50 sets of observations out of a total number of 70 are used. The 50 sets of observations are treated as dependent. The remaining 20 sets of observations are treated as independent for validating the estimation.

The regression coefficients a_i and b_j are presented in table 1. The regression coefficients a_0 to a_2 and b_0 to b_2 are nearly of the same order showing that the estimation of drag coefficient is largely influenced by wind speed. The standard error of the estimation of drag coefficient as a function of wind speed alone i.e. $C_D(V)$ is found to be 0.80 while that of $C_D(V, \Delta\theta)$ is 0.72. Equation (16) thus represents a more general variation of drag coefficient applicable under all wind and stability conditions.

The estimated drag coefficient is hereinafter referred to as drag coefficient (regression) and denoted by $C_D(\text{reg})$. The variation of $C_D(\text{reg})$ is shown in figure 5. On the average, $C_D(\text{reg})$ is of the order of 5.38×10^{-3} .

Correlation analysis revealed a correlation coefficient of $C_D(\text{reg})$ with wind speed (V) of the order of -0.76 and with stability parameter ($\Delta\theta$) about 0.24 , indicating a general decreasing trend of drag coefficient with increasing winds and a slowly increasing trend with increasing instability, as were also obtained with $C_D(\text{dir})$ (cf. § 4.3). The trends of $C_D(\text{reg})$ are also in agreement with the analysis of Hsu (1974), Liu *et al* (1979) and Large and Pond (1981) over ocean surfaces.

Interestingly, Kondo (1975) observes two opposite natures of the variation of drag coefficient on sea surface, (i) decreasing under light wind regime ($< 2 \text{ m s}^{-1}$) and (ii) increasing under high wind regime ($> 2 \text{ m s}^{-1}$) in association with the sea surface roughness. In the present study, as mentioned above, light winds ($< 2.5 \text{ m s}^{-1}$) are not found with the data sets and hence the nature of the variation of the drag coefficient under such light winds is not examined.

As a further step, the momentum fluxes are computed by the bulk aerodynamic method using the drag coefficient (regression) corresponding to the 50 dependent sets of observations. A comparative distribution of the bulk-fluxes with the eddy-fluxes is shown in figure 6. It can be noticed that the bulk-fluxes are quantitatively in good agreement with the eddy-fluxes as compared to the bulk-fluxes depicted in figure 3.

Table 1. Regression coefficients in the estimation of drag coefficient.

$C_D(\text{reg})$	a_0/b_0	a_1/b_1	a_2/b_2	b_3	b_4	b_5
$C_D(V)$	5.55345	0.15217	-0.03148	—	—	—
$C_D(V, \Delta\theta)$	5.27371	0.09504	-0.01663	0.68692	0.06837	-0.11917

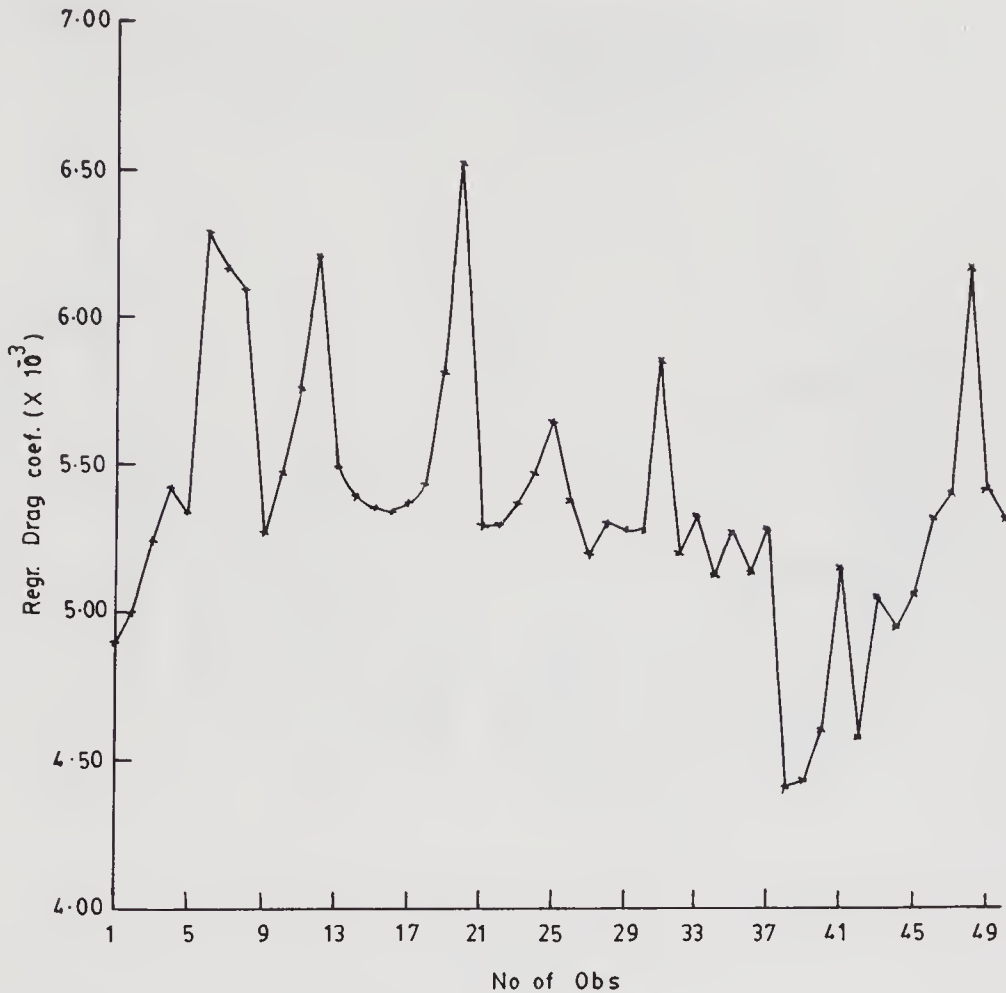


Figure 5. Variation of drag coefficient (regression).

The statistical measures of parameters ($C_D(\text{reg})$, MF-E, MF-P, MF-B) associated with the 50 dependent sets of observations are shown in table 2. The standard deviation of the profile-fluxes is relatively on the lower side (0.05) as compared to that of the eddy-fluxes (0.09).

The lower diagonal matrix of correlation coefficients associated with the dependent sets of observations is presented in table 3. The drag coefficient shows its decreasing tendency with increasing wind and increasing tendency with increasing instability. The bulk fluxes are nearly perfectly correlated with the eddy-fluxes (correlation coefficient is of the order of 0.97).

4.6 Performance with independent data sets

Using wind and temperature data corresponding to 20 independent sets of observations in equation (16) in which the regression coefficients (b_j) are as given in table 1, the drag coefficient at every independent hour of observation is determined. For convenience, the drag coefficient so determined is represented by $C_D(\text{ind})$. The mean value of $C_D(\text{ind})$ over 20 sets of observations is 5.57×10^{-3} which is of comparable magnitude with the mean value of $C_D(\text{reg})$ over 50 (dependent) sets of observations (5.38×10^{-3}).

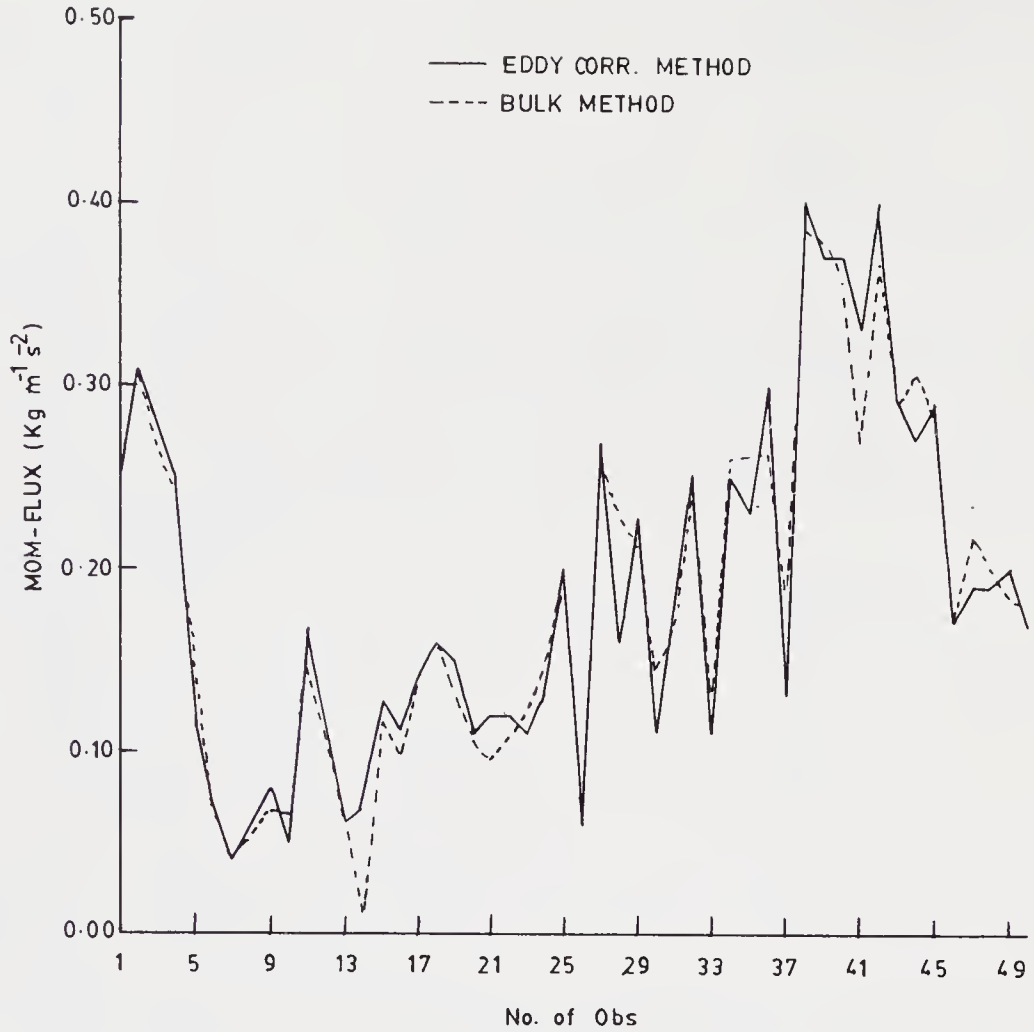


Figure 6. Momentum fluxes computed by eddy correlation and bulk aerodynamic (with $C_D(\text{reg})$) methods (50 dependent cases).

Table 2. Statistical measures of parameters associated with 50 dependent sets of observations.

Parameter	Mean	Std. Dev.	RMS error
$10^3 C_D(\text{reg})$	5.380	0.430	0.723
MF-E	0.186	0.096	—
MF-P	0.120	0.055	0.083
MF-B	0.186	0.093	0.024

Table 3. Lower diagonal matrix of correlation coefficients associated with 50 dependent sets of observations.

	$C_D(\text{reg})$	V	$\Delta\theta$	MF-E	MF-P	MF-B
$C_D(\text{reg})$	1.0					
V	-0.76	1.0				
$\Delta\theta$	0.24	0.34	1.0			
MF-E	-0.70	0.96	1.0			
MF-P	-0.59	0.93	0.48	0.93	1.0	
MF-B	-0.72	0.99	0.41	0.97	0.95	1.0

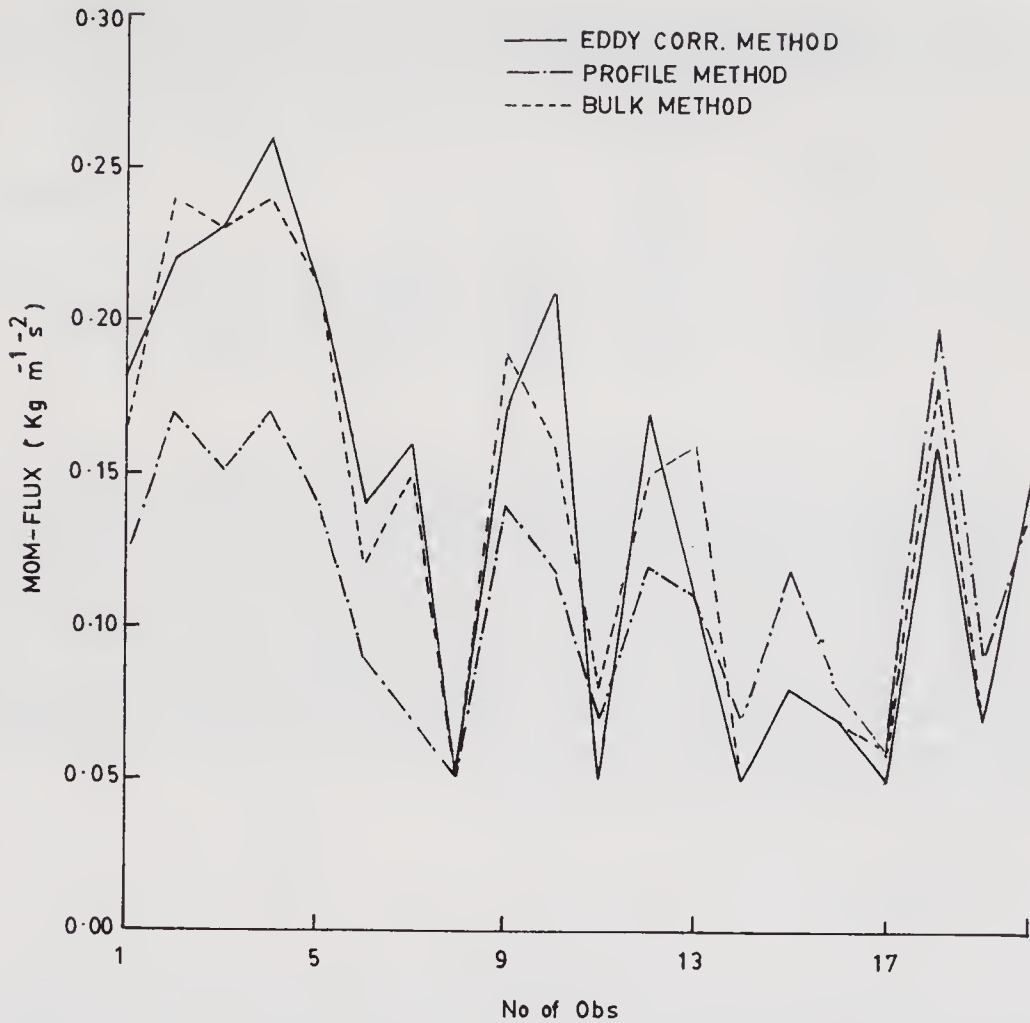


Figure 7. Momentum fluxes computed by eddy correlation, profile and bulk aerodynamic (with $C_D(ind)$) methods (20 independent cases).

Thus the regression coefficients (b_j) and equation (16) may be used for any arbitrary data sets.

The bulk-fluxes (using $C_D(ind)$), the profile-fluxes and the eddy-fluxes are presented in figure 7. The bulk-fluxes are again found to be in good agreement with the eddy-fluxes and the profile-fluxes are again found to be under-estimated in most of the cases.

Table 4. Statistical measures of parameters associated with 20 independent sets of observations.

Parameter	Mean	Std. Dev.	RMS error
$10^3 C_D(ind)$	5.572	0.290	0.842
MF-E	0.140	0.066	—
MF-P	0.107	0.040	0.054
MF-B	0.140	0.062	0.021

Table 5. Lower diagonal matrix of correlation coefficients associated with 20 independent sets of observations.

	$C_D(\text{ind})$	V	$\Delta\theta$	MF-E	MF-P	MF-B
$C_D(\text{ind})$	1.0					
V	-0.25	1.0				
$\Delta\theta$	0.67	0.49	1.0			
MF-E	-0.19	0.94	0.52	1.0		
MF-P	-0.06	0.84	0.59	0.79	1.0	
MF-B	-0.15	0.99	0.60	0.95	0.85	1.0

The statistical measures of parameters ($C_D(\text{reg})$, MF-E, MF-P, MF-B) associated with the independent sets of observations are shown in table 4. The standard deviation of the profile-fluxes is on the lower side (0.04) as compared to that of the eddy- and bulk-fluxes (0.07 and 0.06). A low value of standard error of the bulk-fluxes (0.02) indicates a relatively better performance of the estimated drag coefficient. The lower diagonal matrix of correlation coefficients is shown in table 5. Although stability dominance in the estimation of the drag coefficient is found with the independent sets of observations, the respective decreasing and increasing trends with increasing wind and increasing instability are still persistent.

5. Conclusions

An estimation study on the drag coefficient over the western desert sector of the monsoon trough using simultaneous fast and slow response observations of 30 m high micro-meteorological tower during MONTBLEX-90 brought out the following features:

- The drag coefficient exhibits a decreasing tendency with increasing winds in a wind regime of $2.5\text{--}9\text{ m s}^{-1}$.
- The drag coefficient increases in general with increasing instability of the surface layer. However, the tendency with light winds ($< 2.5\text{ m s}^{-1}$), as they were not available with the present data sets, is not known.
- An average value of the estimated diabatic drag coefficient is found to be of the order of 5.43×10^{-3} which is about 3–4 times larger than the reported average value over ocean surfaces but does not exceed by more than 40% the neutral value (3.9×10^{-3}) prescribed by Garratt (1977) for the Asian region.
- In general, the momentum fluxes computed by the profile method are quantitatively under-estimated as compared to the fluxes directly determined by the eddy correlation method. The fluxes computed by the bulk aerodynamic method using the estimated drag coefficient are in good agreement with the eddy-fluxes.

The conclusions regarding the estimation of drag coefficient are confined to a land region on the western desert sector of the monsoon trough. Similar studies at other major locations along the monsoon trough using MONTBLEX-90 data are desirable to establish the spatial and temporal variation of drag coefficient during the summer monsoon.

The estimation of drag coefficient over tropical land surfaces along the monsoon trough is useful in the parameterization of surface layer in large scale numerical models.

Acknowledgements

The authors would like to acknowledge the support of the Department of Science and Technology in accomplishing this work.

References

- Barker E M and Baxter T L 1975 A note on the computation of atmospheric surface layer fluxes for use in numerical modelling; *J. Appl. Meteorol.* **14** 620–622
- Beljaars A C M and Holtslag A A M 1991 Flux parameterization over land surfaces for atmospheric models; *J. Appl. Meteorol.* **30** 327–341
- Berkowicz R and Prahm L P 1982 Evaluation of the profile method for estimation of surface fluxes of momentum and heat; *Atmos. Environ.* **16** 2809–2819
- Businger J A, Wyngaard J C, Izumi Y and Bradley E E 1971 Flux profile relationships in the atmospheric surface layer; *J. Atmos. Sci.* **28** 181–189
- Dyer A J and Hicks B B 1970 Flux gradient relationships in the constant flux layer; *Q. J. R. Meteorol. Soc.* **96** 715–721
- Francey R J and Garratt J R 1978 Eddy flux measurements over the ocean and related transfer coefficients; *Boundary-Layer Meteorol.* **14** 153–166
- Garratt J 1977 Review of drag coefficients over oceans and continents; *Mon. Weather Rev.* **105** 915–929
- Goel M and Srivastava H N 1990 MONTBLEX; *Bull. Am. Meteorol. Soc.* **71** 1594–1600
- Hsu S A 1974 On the log-linear wind profile and the relationship between shear stress and stability characteristics over the sea; *Boundary-Layer Meteorol.* **6** 509–514
- Jiemin W, Xiaohu L and Yongqiang Q 1990 A preliminary study on characteristics of turbulence transfer over Gobi desert; *Chin. J. Atmos. Sci.* **14** 495–505
- Kondo J 1975 Air-Sea bulk transfer coefficients in diabatic conditions; *Boundary-Layer Meteorol.* **9** 91–112
- Large W G and Pond S 1981 Open ocean momentum flux measurements in moderate to strong winds; *J. Phys. Oceanogr.*, **11** 324–336
- Liu W T, Katsaros K B and Businger J A 1979 Bulk parameterization of air-sea exchanges of heat and water vapour including the molecular constraints at the interface; *J. Atmos. Sci.* **36** 722–735
- Paulsen C A 1970 The mathematical representation of wind and temperature profiles in the unstable atmospheric surface layer; *J. Appl. Meteorol.* **9** 857–861
- Panofsky H S and Dutton J A 1984 *Atmospheric Turbulence*, (Wiley-Interscience Publ.) 379 pp
- Rao Y P 1976 Southwest Monsoon, Meteor. Mono. Synoptic Meteorology, No. 1/1976; *India Meteorol. Dept.*, 1–367
- Rudrakumar S, Srinivasan H P, Satyadev H N, Ameenulla S and Prabhu A 1991 Surface layer data from MONTBLEX-90. Tech. Report, 91 MD 2, Sept., Centre Atmos. Sci., IISc, Bangalore
- Sethuraman S and Raynor G S 1975 Surface drag coefficient dependence on the aerodynamic roughness of the sea; *J. Geophys. Res.* **80** 4983–4988
- Smith S D and Banke E G 1975 Variation of the sea surface drag coefficient with wind speed. *Q. J. R. Meteorol. Soc.* **101** 665–673
- Tsukamoto O, Ohtaki F and Ishida H 1990 On board direct measurements of turbulent fluxes on the Open Sea; *J. Meteorol. Soc. Jpn.* **68** 203–211
- Vuhts H F and Cannemeijer F 1981 Measurements of drag coefficients and roughness length at a sea-beach interface; *J. Appl. Meteorol.* **20** 335–340

An analysis of MONTBLEX data on heat and momentum flux at Jodhpur

KUSUMA G RAO, R NARASIMHA and A PRABHU[†]

Jawaharlal Nehru Centre for Advanced Scientific Research, Bangalore 560 094, India

[†]Centre for Atmospheric Sciences, Indian Institute of Science, Bangalore 560 012, India

Abstract. Parameterization of sensible heat and momentum fluxes as inferred from an analysis of tower observations archived during MONTBLEX-90 at Jodhpur is proposed, both in terms of standard exchange coefficients C_H and C_D respectively and also according to free convection scaling. Both coefficients increase rapidly at low winds (the latter more strongly) and with increasing instability. All the sensible heat flux data at Jodhpur (wind speed at 10 m $\bar{U}_{10} < 8 \text{ ms}^{-1}$) also obey free convection scaling, with the flux proportional to the '4/3' power of an appropriate temperature difference such as that between 1 and 30 m. Furthermore, for $\bar{U}_{10} < 4 \text{ ms}^{-1}$ the momentum flux displays a linear dependence on wind speed.

Keywords. Sensible heat flux; momentum flux; free convection; exchange coefficient of heat; drag coefficient.

1. Introduction

It has been shown by Beljaars and Miller (1990) and Miller *et al* (1992) that the model in use at the European Centre for Medium Range Weather Forecasting produces a more realistic climatological rainfall pattern over India with an improved parameterization for evaporation and sensible heat flux at low winds over the oceans. The improvement seeks to account for an enhancement of the fluxes because of the 'gustiness' due to dry convective motion near the surface, and provides modified transfer coefficients for heat and moisture flux at low winds that are in accord with a scaling law for free convection. At a time when flux data at low winds over the oceans were scarce, the rationale for the modified parameterization adopted by Miller *et al* (1992) was that the evaporation from the ocean cannot be smaller than that from an aerodynamically smooth water surface, i.e., that free convection provided a reliable lower bound. This argument goes back to Deardorff (1972), who recommended that the sensible heat flux in the convective boundary layer should be constrained to be no smaller than that associated with free convection. Following the arguments of Townsend (1964) the heat flux then takes the form

$$Q_s = \overline{(w'\theta')}_s = C_s \left(\frac{g \kappa^2}{\theta_m \nu} \right)^{1/3} (\theta_s - \theta_m)^{4/3}, \quad (1)$$

where κ is the molecular thermal diffusivity, ν is the kinematic viscosity, θ_s is the surface temperature, θ_m is the (constant) potential temperature within the mixed layer, g is the acceleration due to gravity and Q_s represents the surface value of the eddy sensible heat

flux $\overline{w'\theta}$. C_s is a constant whose value was given as 0.20 by Townsend, and as in the range 0.1 to 0.24 by Deardorff and Willis (1985).

The free convection limit has a long history (Prandtl 1932; Priestley 1954). In the corresponding limit of Monin-Obukhov theory, the non-dimensional temperature gradient should approach $(-\zeta)^{-1/3}$ at large negative $\zeta \equiv z/L$ where z is height above ground and L represents the Monin-Obukhov length. That is

$$\phi_\theta \equiv \frac{k}{\theta_*} \frac{\partial \theta}{\partial \log z} \sim (-\zeta)^{-1/3} \quad \text{as} \quad -\zeta \rightarrow \infty, \quad (2)$$

where k represents the von Karman constant (~ 0.4) and θ_* the friction temperature. However Businger *et al* (1971) and Businger (1988), using the well-known Kansas observations, conclude that the non-dimensional temperature gradient approaches $(-\zeta)^{-1/2}$ at large negative ζ . A critical analysis of these two proposals is presented by Tennekes (1973). A different perspective is provided by Schumann (1988), who postulates a simple model for the surface layer of a convective boundary layer at zero mean wind over a homogeneous rough surface. This model suggests that the temperature difference between the ground and the mixed layer increases with the ratio of boundary layer height to roughness length. Schumann concludes that the appropriate heat transfer relationship in terms of Nusselt and Rayleigh numbers is $Nu \sim Ra^{1/2}$ in the rough case (in agreement with the form proposed by Businger), and argues that the relationship $Nu \sim Ra^{1/3}$ (corresponding to (1)) is valid for smooth surfaces at Rayleigh numbers less than a critical value that depends on the ratio of boundary layer thickness to roughness height.

Beljaars and Miller (1990) and Miller *et al* (1992) finally use modified exchange coefficients in the bulk aerodynamic formulae to estimate heat and moisture fluxes. Bulk aerodynamic parameterization of the fluxes is perhaps the most commonly used approach in operational boundary layer and general circulation models. Nevertheless the question of the correct parameterization of fluxes under highly unstable conditions continues to be of great current interest (Beljaars 1994; Stull 1994), and cannot yet be considered to have been satisfactorily resolved.

Most of the observational evidence with regard to heat flux has till recently come from the oceans. Thus Large and Pond (1982) suggest that

$$\begin{aligned} 10^3 C_H &= 1.13, \quad z/L < 0, \quad 4 < \bar{U}_{10} < 25 \text{ ms}^{-1}, \\ &= 0.66, \quad z/L > 0, \quad 6 < \bar{U}_{10} < 20 \text{ ms}^{-1}, \end{aligned} \quad (3)$$

using the temperature differential between sea-surface and 10 m as reference. At low winds there is only the study of Bradley *et al* (1991) over the Pacific warm pool region. There have been very few studies over land and none over the monsoon region.

The main aim of the present paper is to propose a parameterization for the sensible heat flux in terms of temperature differentials between the ground and the air above, as inferred from an analysis of observations archived during the Monsoon Trough Boundary Layer Experiment, 1990 (Goel and Srivastava 1990; Sikka and Narasimha 1995). We report results using both the standard exchange coefficient as it depends on wind speed, stability and roughness, especially at low winds, and also free-convection scaling, along the lines of Townsend (1964) and Schumann (1988).

The results on the exchange coefficient are presented in § 3 and the free convection scaling in § 4. A brief comment on the momentum fluxes at low winds, in the light of the present conclusions on heat flux, is made in § 5.

2. Data analysed

Results are analysed for one station, namely Jodhpur (26.3N, 73E), using micro-meteorological tower observations (Rudra Kumar *et al* 1995). The period chosen for analysis extends from 9th June to 20th August covering almost the entire duration of the experiment. Measurements were made by cup and sonic anemometers and platinum wire resistance thermometers mounted on a 30 m tower. The sonic anemometer was placed at 4 m above the surface, the cup anemometers at six heights namely 1, 2, 4, 8, 15 and 30 m, and the thermometers at four heights namely 1, 8, 15 and 30 m.

High frequency (8 Hz) observations of turbulence and the virtual temperature were obtained from the sonic anemometer. The data are available at hourly intervals during intensive observation periods (Srivastav 1995), otherwise at three-hourly intervals continuously for 10 min (15 min) from 15th June to 7th July (June 6th–14th; July 8th–August 20th). The total number of observations available is 676. Details about the tower site and estimates of the roughness length at site are available in Kusuma (1995). Rudra Kumar *et al* (1995) discuss the instrumentation, the accuracy of the measurements, and the quality control procedures adopted.

The methods used for computing momentum and heat fluxes, the friction velocity u_* and the drag coefficient C_D are described in Kusuma *et al* (1995). The friction temperature θ_* is obtained here as

$$\theta_* = \frac{-\overline{w'\theta'}}{u_*}, \quad (4)$$

and the exchange coefficient for heat (using the velocity \bar{U}_{10} at 10 m as reference) as

$$C_H = \frac{+\overline{w'\theta'}}{\bar{U}_{10}\Delta\theta}, \quad (5)$$

where \bar{U}_{10} is obtained by fitting a least-square quadratic curve to the observed velocities along the mean wind direction at six heights and $\Delta\theta$ is an appropriate temperature differential.

A good candidate for $\Delta\theta$ would appear to be the difference $\theta_g - \theta_{10}$, where θ_{10} can be obtained by curve-fitting to measured temperatures at four heights. As the ground temperature θ_g was unfortunately not measured, we use the values given by Rao (1995) as calculated by solving a heat conduction equation using sub-soil temperatures. A comparison of observed ground temperatures (at a different site) with those estimated by this procedure reveals generally good agreement but differences occasionally as large as 5°C or even more. In general, the use of ground temperatures for defining heat exchange coefficients presents certain problems. Whereas over the oceans the use of the sea-surface temperature is convenient (because of approximate horizontal homogeneity), ground temperature can vary widely and rapidly over land. We shall

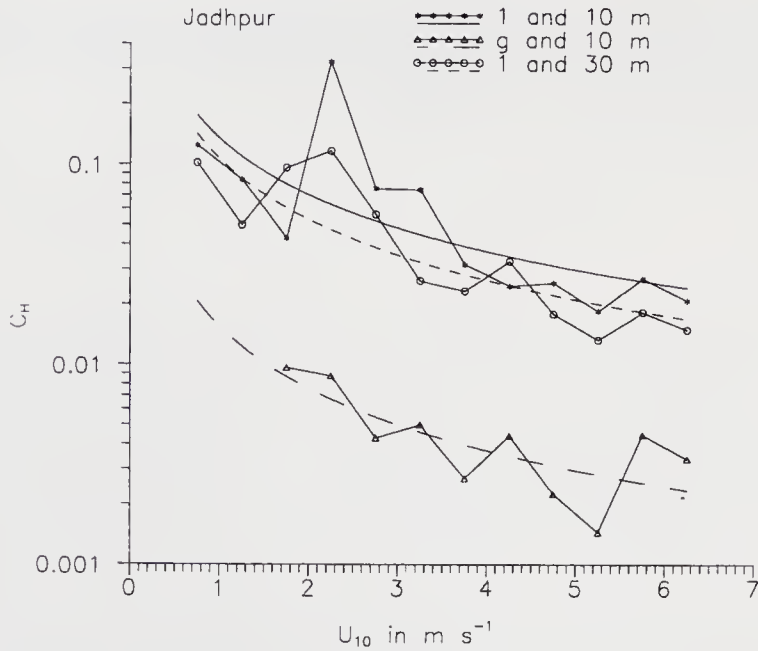


Figure 1. Variation of exchange coefficient of heat, C_H with wind speed for $\Delta\theta = T_g - T_{10}$, $T_1 - T_{10}$ and $T_1 - T_{30}$.

Table 1. Mean and standard deviation (std) of C_H .

N	DT	Mean C_H	Std C_H
1	$T_1 - T_{10}$	0.083	0.037
2	$T_1 - T_{30}$	0.048	0.009
3	$T_g - T_{10}$	0.005	0.001

argue here that for this reason other temperature differentials may be more appropriate in parameterizing heat flux, whether through (1) or (5).

3. Exchange coefficient

3.1 Dependence on wind speed

The exchange coefficient for heat, C_H , estimated according to formula (5), is presented in figure 1 as a function of wind speed for three combinations of temperature differentials: $T_g - T_{10}$, $T_1 - T_{10}$ and $T_1 - T_{30}$, where the subscript denotes height in metres, T_1 and T_{30} are observed temperatures and T_{10} is obtained by fitting a least square quadratic curve to the observed temperatures. Each point in figure 1 is an average over a velocity bin of 0.5 m s^{-1} . All the results presented are for the period 9th June to 2nd July: the data from 3rd July to 20th August present certain difficulties that will be

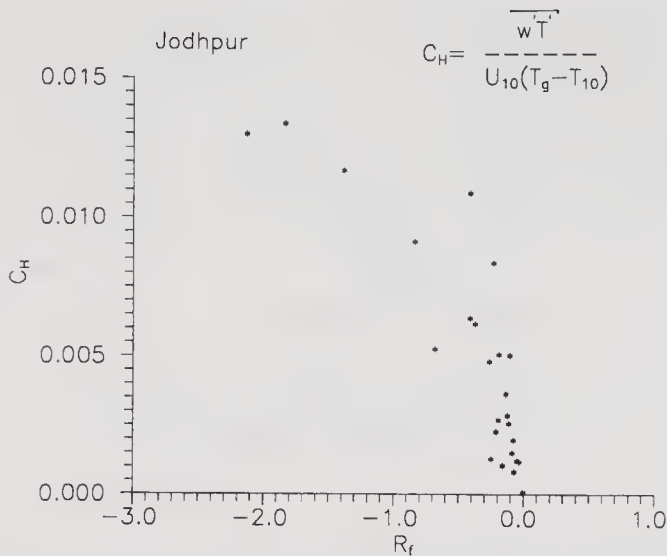


Figure 2. Variation of exchange coefficient of heat, C_H (with $\Delta\theta = T_g - T_{10}$) with flux Richardson number, R_f .

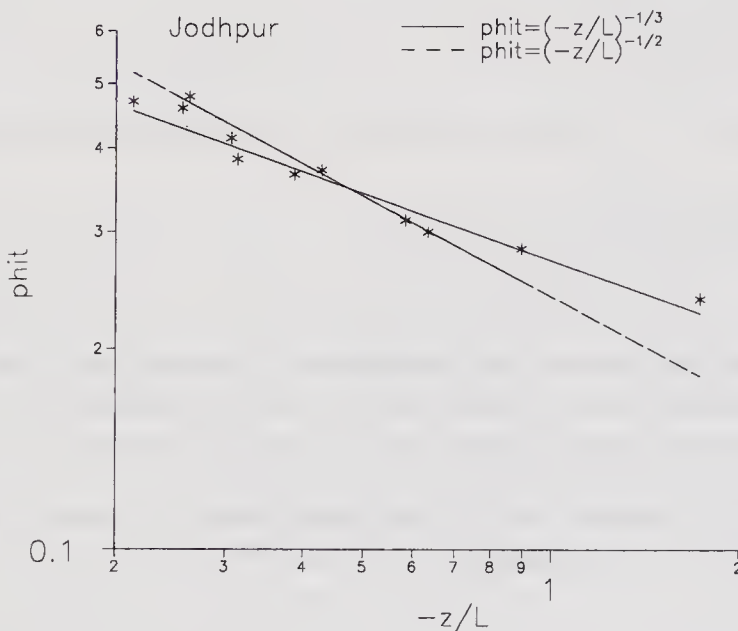


Figure 3. Variation of non-dimensional temperature gradient, ϕ_θ with $-\zeta = -z/L$.

discussed later. A strong dependence of C_H on wind speed is revealed in all the three estimations of C_H in figure 1. However, the absolute values of C_H obtained here cannot be compared directly with other studies as the temperature differentials used here are not the same. The mean and standard deviation (std) for all three estimations of C_H , shown in table 1, suggests that the scatter is much less if the temperature difference between the ground and the 10 m level is chosen as reference. It is interesting that the dependence of C_H on wind speed at low winds is weaker than that of the drag coefficient, as we shall discuss in § 5.

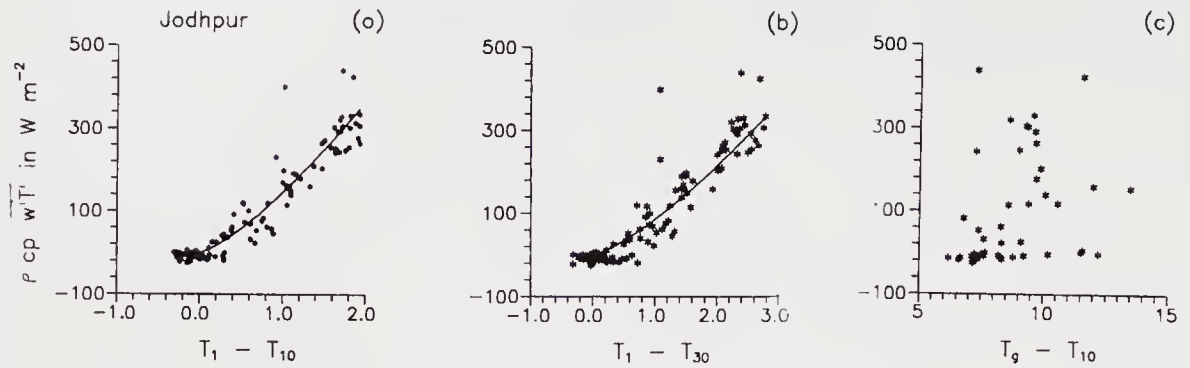


Figure 4. Sensible heat flux (Wm^{-2}) variation with DT taken as (a) $T_1 - T_{10}$, (b) $T_1 - T_{30}$, (c) $T_9 - T_{10}$.

Although in certain models a prescription of C_H on wind speed may be of use, such a relation is not satisfactory (if only for dimensional reasons), and we explore below other methods of analysis of the flux data that may lend themselves to better extrapolation to other situations.

3.2 Dependence on stability

We analyse here the effect of stability through the flux Richardson number, defined as

$$R_f = (g/\bar{\theta}) \frac{\overline{w'T'}}{U'w'(\partial\bar{U}/\partial z)},$$

where U' is the velocity fluctuation along the mean wind direction. Figure 2 shows the dependence of C_H on R_f for the temperature differential between the ground and 10 m. In agreement with earlier studies (Stull 1988), the coefficient increases with increasing instability. The large values of C_H under strongly unstable conditions at low winds suggest free convection, which we study in the next section.

The same tendency is seen even if C_H is calculated with other temperature differentials, namely between 1 and 10 m and between 1 and 30 m.

4. Free convection scaling

4.1 Non-dimensional temperature gradient

The variation of daytime (0700 to 1800IST) sensible heat flux and friction velocity as a function of wind speed, for the period from 9th June to 20th August (figures not shown), suggests that both quantities are significant at low winds, the heat flux going up to values of 300 Wm^{-2} and u_* varying between 0.12 and 0.36 ms^{-1} for winds $< 2 \text{ ms}^{-1}$; u_* increases with wind speed as expected. These large values at low winds suggest that associated convective motions could be the cause. To study this question we construct the non-dimensional temperature gradient according to equation (2) and plot ϕ_θ (labelled phit) versus $-\zeta$ in figure 3. (The temperature gradient is determined by curve

fits to the recorded temperatures, and is evaluated at a height of 4 m). Both the Prandtl and Businger-Dyer limits are shown on the diagram for comparison. It is seen that while a $(-\zeta)^{-1/2}$ law may be valid for $-\zeta < \sim 0.6$, the values at $-\zeta \sim 1$ to 2 are more consistent with a $(-\zeta)^{-1/3}$ law, valid over almost the whole range $-\zeta > 0.2$. It would appear that the condition for the validity of free-convection scaling is much weaker than that quoted by Monin and Yaglom (1975), namely that $-\zeta \gg 1$.

4.2 Sensible heat flux

A plot of heat flux versus the temperature difference between 1 and 10 m is shown in figure 4(a). The solid line here, as represented by

$$Q_s = 145(DT)^{4/3}, \quad (6)$$

where $DT = T_1 - T_{10}$, is the best fit to the Townsend '4/3' power law variation (1). The constant C_s in equation (1) as evaluated with the present data turns out to be 12.3, with an average temperature difference of 1.1°C as given in table 2. Figure 4(b) shows that the heat flux approaches $(DT)^{4/3}$ even when $DT = T_1 - T_{30}$, but with a different constant equal to 85 in (6), and $C_s = 7.2$ in (1), for an average temperature difference of $DT = 1.5^\circ\text{C}$ (table 2). When we use the temperature difference between the ground and 10 m the scatter is too large (figure 4c).

4.3 Dependence on roughness

The roughness length at Jodhpur varies with the sector in which the wind is blowing; in the 'smooth' or open sector (between 200° and 230°) where the terrain is relatively flat and obstacle-free, it is 1.2 cm; and in the sector outside 200° and 230° it is highly variable, with an average value of 6.8 cm. We will call this the 'rough' sector, although it is actually not homogeneous (Kusuma 1995). Plots similar to figure 4 for the heat flux with $DT = T_1 - T_{10}$ are shown in figure 5(a and b) for the smooth and rough sectors separately. Comparing with figure 4(a), we find that figure 5(a) shows much less scatter in the smooth sector; and figure 5(b) shows that the outliers of figure 4(a) are from the rough sector. However figure 5(a and b) depicts the 4/3 power variation irrespective of sector, revealing that the overall variation is independent of roughness. The corresponding C_s values for the smooth and the rough sectors are 11.3 and 13.4 (see table 2).

According to Schumann (1988), the heat flux follows the relation $Nu \sim Ra^{1/3}$ for a smooth surface and $Nu \sim Ra^{1/2}$ for a rough surface; the former is valid for all Rayleigh numbers less than a critical value that depends on the ratio of boundary layer height to

Table 2. C_s values.

N	Levels	$DT(^{\circ}\text{C})$	$Q_s/(DT)^{4/3}$	C_s	Sector
1	1 and 10 m	1.1	144.7	12.28	Entire.
2	1 and 30 m	1.5	85.0	7.22	Entire.
3	1 and 10 m	1.1	133.3	11.3	Smooth.
4	1 and 10 m	1.1	158.0	13.4	Rough.
5	1 and 30 m	1.6	87.8	7.5	Smooth.
6	1 and 30 m	1.5	115.2	9.8	Rough.

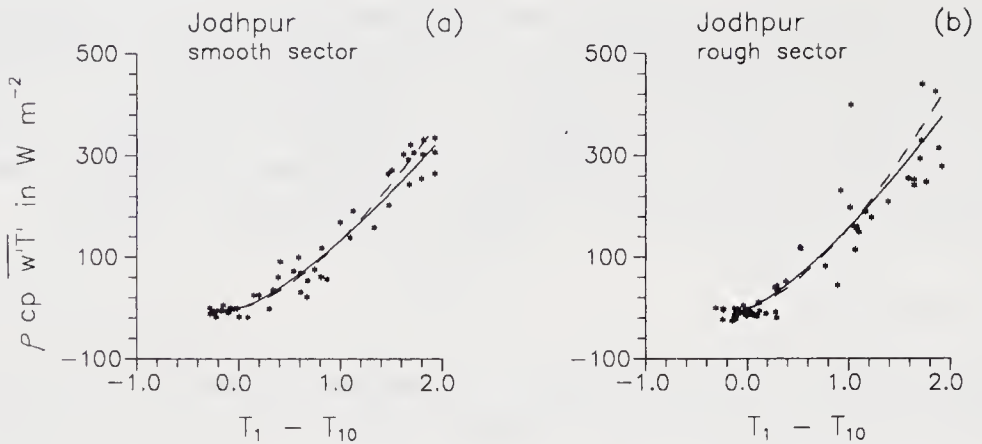


Figure 5. Sensible heat flux (Wm^{-2}) variation with $DT = T_1 - T_{10}$ for (a) smooth sector, (b) rough sector. Dashed line represents '3/2' fit and solid line represents '4/3' fit.

roughness length. Because we do not know the boundary layer height from the present data, a '3/2' power fit (corresponding to the relation for a rough surface) was also made to the data in figure 5(a and b) and is shown by dashed lines. Not surprisingly, the differences between the two fits are not significant.

However, if we assume the boundary layer height h as 1(2)km, the critical Rayleigh number according to Schumann (1988),

$$\text{Ra} = 560(h/20)^{8/3},$$

takes the value of 6.9×10^{15} (4.4×10^{16}) for $\text{Pr} = 0.7$, $(z_0 u_*)/\nu > 10$, where Pr is the Prandtl number. Estimates of the Rayleigh number

$$\text{Ra} = \frac{(g/T)h^3 \Delta\theta}{\kappa\nu}$$

for the present observations may be made using $\Delta\theta = T_1 - T_{10}$, which is usually appreciably less than the differential $\Delta\theta = \theta_g - \theta_m$ used by Schumann. Nevertheless, it turns out that the values of Ra estimated here are larger than the Schumann critical Rayleigh number by two to three orders magnitude. Thus, according to Schumann, the heat flux should obey a '3/2' rather than a '4/3' power law. However we do not see any significant difference between fits assuming either law for the range of temperature differences observed here (which, at $< 2^\circ$, are small compared to the example quoted by Schumann of 9.8 K between θ at roughness height and in the mixed layer). Differences between the two fits will also be larger only if the temperature differences are larger. The value of $z_0 u_*/\nu \sim 160$ suggests that the present data correspond to a convective boundary layer over a rough surface though z_0 is quite small (at 1.2 cm). Thus there is no evidence here to support the dependence of the heat flux relationship on the ratio h/z_0 in the present case. However Schumann's criterion on critical Rayleigh number cannot be subjected to a serious test by the present data as we do not know the boundary layer height or the temperatures at roughness height and in the mixed layer. Nevertheless it is established beyond doubt from the present analysis that the observed

heat flux scales very well according to free convection theory for temperature differentials between 1 and 10 m as well as between 1 and 30 m.

In table 3, the root mean square (rms) deviations of the heat flux from '4/3' and '3/2' laws are presented for both temperature differentials in the two sectors. It is seen that the deviations are smaller for $DT = T_1 - T_{10}$ than for $T_1 - T_{30}$; however we see contrasting differences between the smooth and rough sectors. There is no significant difference in the rms deviations of the heat flux between the two fits.

All the results presented in § 4 are for the period from 9th June to 2nd July. The data between 3rd July and 20th August appear to have been subject to an undocumented change in calibration: the reason for this suspicion is that during this period DT is never negative (as we may expect it to be at least during night), and that in a plot of Q_s vs. DT the best-fit curve is shifted to the right by about 1.5° compared to that in figure 4. A correction by this amount produces excellent agreement between the two data sets, but we have not ventured to present it in the absence of other more direct evidence and calibration data during the period.

5. Momentum flux

The dependence of the drag coefficient on wind speed has been analysed by Mohanty *et al* (1995) and Kusuma *et al* (1996) using somewhat different approaches. The latter work discusses the effect of stability and roughness in detail, so we confine ourselves here to a discussion of the momentum flux in the free-convection regime.

5.1 Drag coefficient

Figure 6 shows a comparison of the dependence of C_D and C_H (with $\Delta\theta = T_g - T_{10}$ on wind speed. The rapid increase of both C_D and C_H at low winds (although at different rates) suggests a need for a drag parameterization that is consistent with the heat flux parameterization of § 4 for application in large-scale models.

Figure 7(a), which shows the drag variation with wind speed for $R_f < 0.03$, suggests that drag is not only significant at low winds but varies nearly linearly with wind speed, i.e., the drag coefficient increases approximately like \bar{U}_{10}^{-1} . However, low winds are not characterized exclusively by a flux Richardson number that takes large negative values, i.e., by strongly unstable situations associated with free convection; there are also

Table 3. Root mean square values.

N	Levels	RMS values for '4/3' law (Wm^{-2})	RMS values for '3/2' law (Wm^{-2})	Sector
1	1 and 10 m	48.0	52.5	Entire.
2	1 and 30 m	51.9	52.3	Entire.
3	1 and 10 m	32.5	35.1	Smooth.
4	1 and 10 m	57.0	62.6	Rough.
5	1 and 30 m	34.3	44.0	Smooth.
6	1 and 30 m	67.1	83.2	Rough.

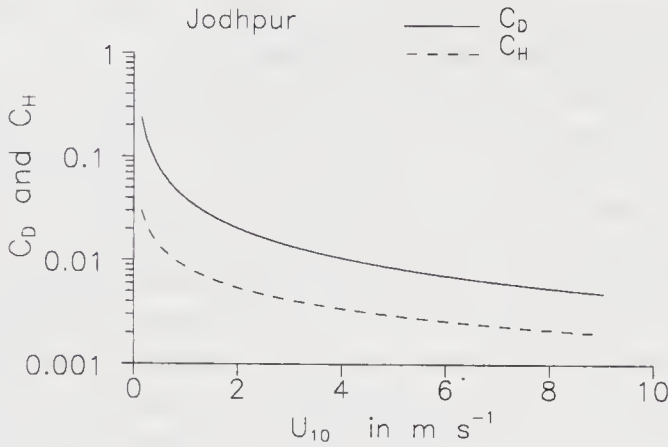


Figure 6. Comparison between drag coefficient, C_D and exchange coefficient of heat, C_H as a function of wind speed.

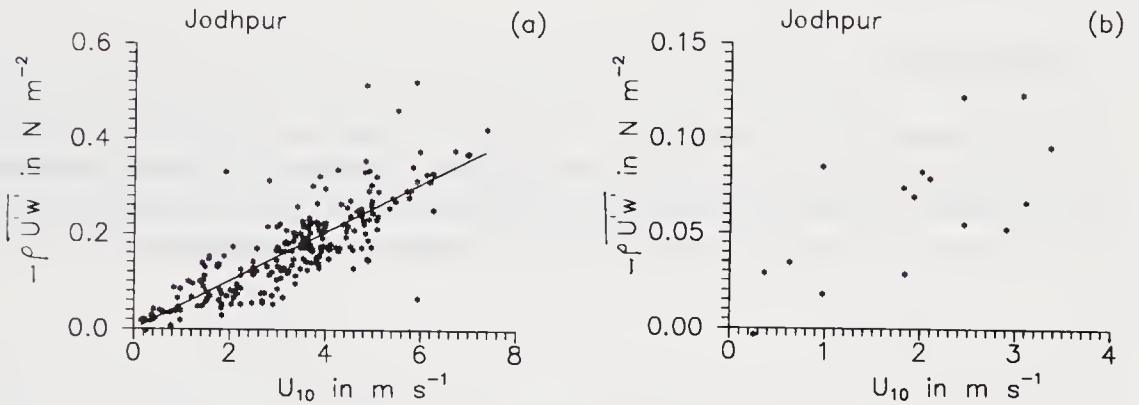


Figure 7. The variation of drag in Nm^{-2} with wind speed for (a) $R_f < 0.03$, (b) strong unstable conditions ($-4.0 < R_f < -1.0$).

situations when conditions can be nearly neutral. If we select data points only for strongly unstable conditions ($-4.0 < R_f < -1.0$), we obtain figure 7(b). It is seen that the data are again consistent with an approximate inverse dependence of C_D on \bar{U}_{10} at low winds, although the number of data points is too small to draw a firm conclusion. We may speculate that, as drag must vanish in true windless free convection, its dependence on wind speed at low winds must be linear. That the same kind of variation holds under near-neutral conditions also suggests that low-wind parameterizations may be more complex than hitherto considered. This must remain a subject for further study.

5.2 Non-dimensional wind shear

The non-dimensional wind shear, $\phi_m = (\kappa z/u_*)\partial\bar{u}/\partial z$, is calculated at two heights, namely 4 m (where the sonic measurements are made) and 30 m. The shear $\partial\bar{u}/\partial z$ is obtained by fitting a least-square curve to cup winds at all six heights, and u_* is estimated from sonic measurements. A comparison of the non-dimensional shear

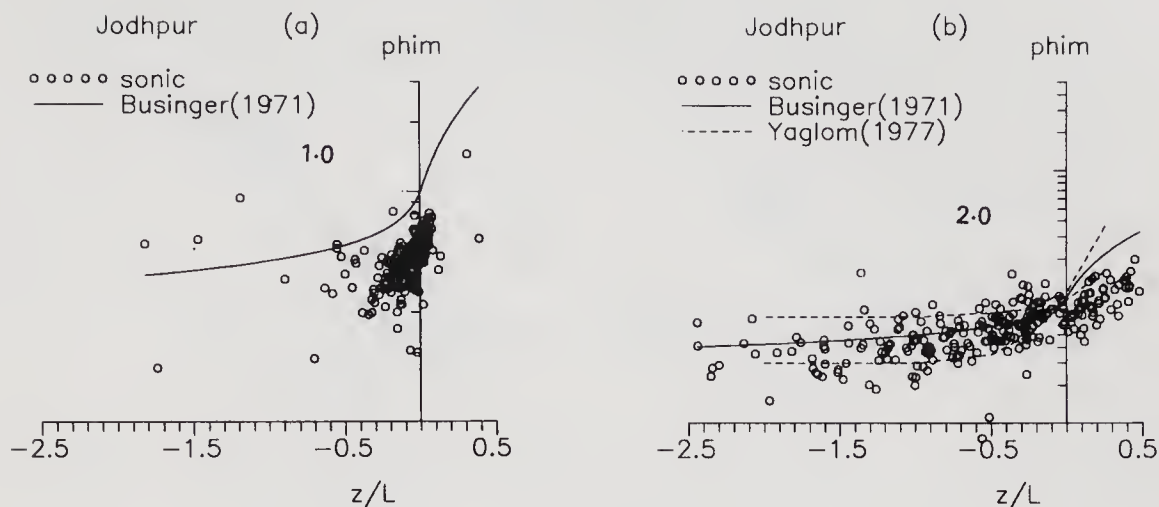


Figure 8. A comparison of non-dimensional wind shear, ϕ_m observed with Businger's expression at (a) 4 m, (b) 30 m.

inferred from the present data with that proposed by Businger *et al* (1971) is presented in figure 8(a and b). The agreement with Businger's curve is not perfect, but the scatter seen here at 30 m is well within the range of ϕ_m recommended by various authors in the near-neutral and unstable regimes, as compiled by Yaglom (1977).

6. Monin-Obukhov similarity

Since exchange coefficients in many general circulation models are based on the Monin-Obukhov theory and Businger *et al*'s (1971) flux-profile relations, we present here a comparison between the values of u_* and θ_* thus estimated with the observed values.

It is seen from figure 9(a-f) that at high winds there is good agreement whereas at low winds and unstable conditions there is substantial disagreement; even under neutral conditions the observed u_* is higher at low winds. (The latter data supplement those in Kusuma G Rao *et al* 1996.)

The flux-profile calculations shown in figure 9 are based on data at roughness height and 10 m level. Further calculations made here suggest that similar conclusions follow even if we choose any level other than 10 m, but that the agreement is poor if the roughness height is not one of the levels. All these results suggest that a careful re-examination of the Monin-Obukhov theory under low wind/free convection conditions is now required, as also recently suggested by Beljaars (1994).*

7. Conclusions

In the light of the analysis made here of heat and momentum flux data acquired at Jodhpur during MONTBLEX, it is concluded that if the fluxes are parameterized by bulk aerodynamic formulae, it is necessary to take dependence on wind speed into

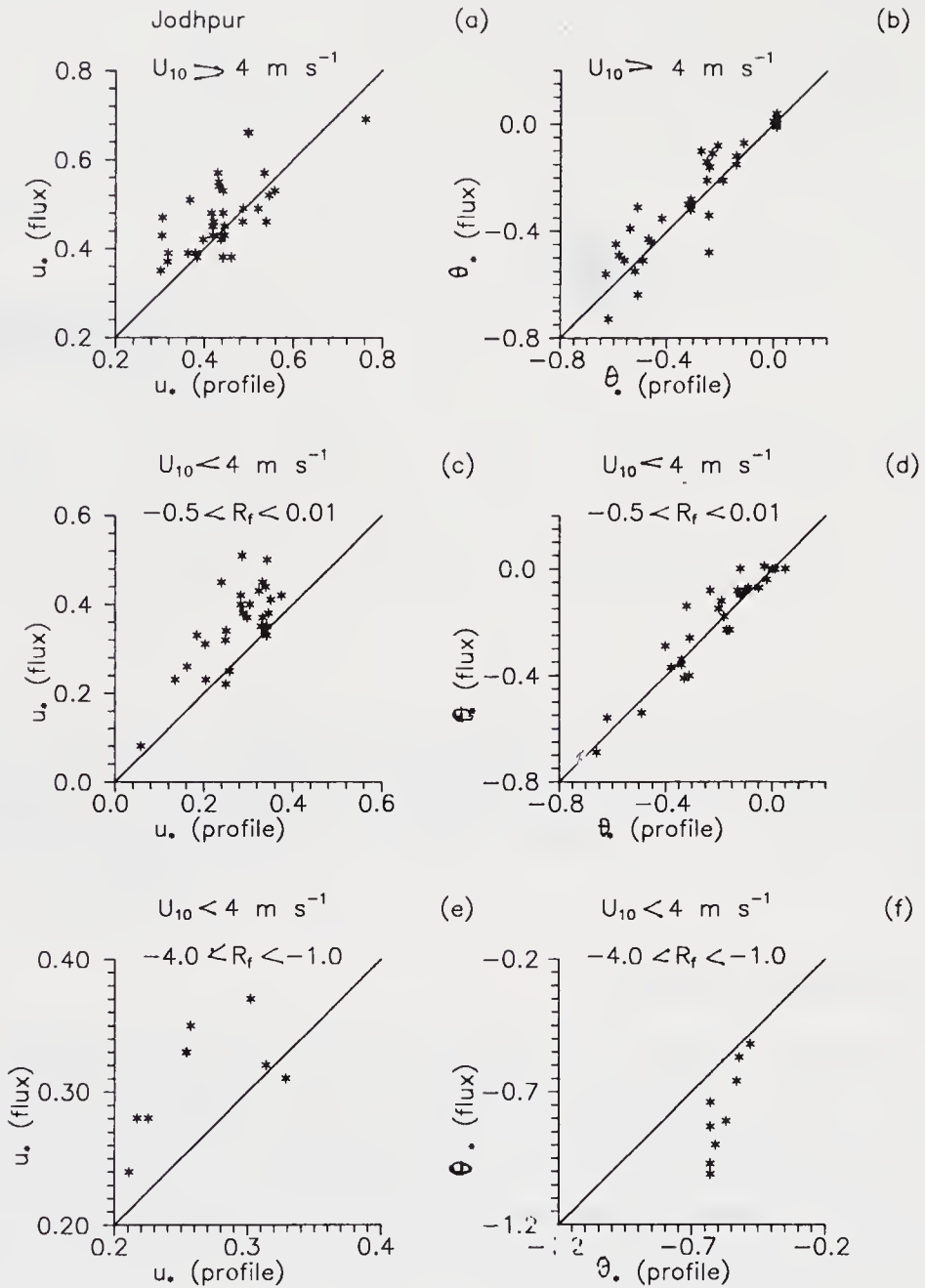


Figure 9. Comparison of u_* and θ_* at Jodhpur obtained by profile and eddy correlation methods: (a, b) for $\bar{U}_{10} > 4 \text{ ms}^{-1}$ and the entire range of stability; (c, d) for $\bar{U}_{10} < 4 \text{ ms}^{-1}$ and near neutral stability; (e, f) for $\bar{U}_{10} < 4 \text{ ms}^{-1}$ and strongly unstable conditions.

account. At Jodhpur the drag data can be represented approximately by the formula

$$C_D = 0.04 \bar{U}_{10}^{-1}, \quad \bar{U}_{10} < 4 \text{ ms}^{-1}.$$

We are unable to confirm this dependence at Kharagpur as wind speeds there rarely fell below 3 ms^{-1} . This parameterization is unsatisfactory if only because it is dimensional. At the present stage both further analysis and observational data are required to arrive at a more satisfactory parameterization. As the above formula suggests that drag

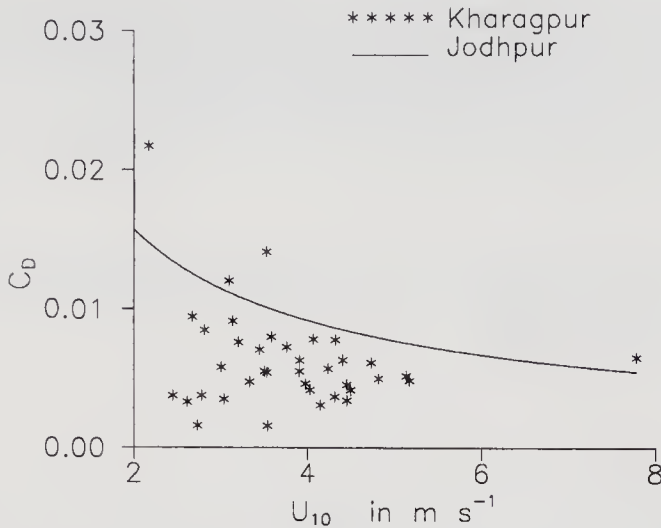


Figure 10. Comparison of drag coefficient between Kharagpur and Jodhpur for the smooth sector.

increases *linearly* with wind speed at low winds, one is tempted to attribute the finding to the dominance of free convection, but this conclusion is not supported by the fact that the linear dependence on velocity seems to characterize the data at nearly neutral conditions as well. (It must be noted that low winds can occur in all stability regimes: highly unstable nearly windless free convection, neutrally stable conditions during daytime associated with rain or cloudiness and also during the transitional epochs (morning and evening), and stable nocturnal conditions). Furthermore, at wind speeds $> 3 \text{ ms}^{-1}$, C_D at Kharagpur is about half that at Jodhpur even in the smooth sector (figure 10), although the roughness heights are comparable (1.2 and 1.9 cm). The evidence therefore suggests that all the variables that are necessary to formulate satisfactory parameterization schemes have not yet been identified.

This conclusion is also supported by the heat flux measurements. However the difference here is that the heat flux is well described by free convection scaling. Indeed we recommend that the sensible heat flux be taken as

$$Q_s = C_s \left(\frac{gK^2}{\theta v} \right)^{1/3} (DT)^{4/3},$$

where DT represents a characteristic temperature differential. We suggest that a convenient measure of DT is the difference in temperature between 1 m and 30 m; for this choice the constant C_s takes the value 7.5 in the smooth sector at Jodhpur (roughness length = 1.2 cm). There is evidence that the constant C_s above varies with roughness, increasing slightly to 9.8 in the rough sector (average roughness length 6.8 cm). While the free convection $4/3$ power law is recommended, the reason for this is chiefly that the argument for the scaling is both plausible and attractive, and is in good accord with observations. However, a $3/2$ power law, which would be consistent with the Businger stability functions, would also perform reasonably well. At the same time estimates of u_* and θ_* using the Businger flux-profile relationships do not agree well with observed values at low winds thus raising questions about the applicability of the Monin-Obukhov theory to conditions actually prevailing in the atmospheric boundary layer.

In spite of the theoretical questions that still need to be tackled, it is believed that the present analysis shows how the parameterization of both momentum and heat flux can be made more realistic for use in large-scale circulation models.

Acknowledgements

This work was carried out as part of a project supported by the Department of Science and Technology, Government of India.

References

- Beljaars A C M 1994 The parameterization of surface flux in large scale models under free convection; *Q. J. R. Meteorol. Soc.* **121** 255–270
- Beljaars A C M and Miller M J 1990 The sensitivity of the ECMWF model to the parameterization of evaporation from the tropical oceans; *ECMWF technical memorandum* no 170
- Bradley E F, Coppin P A and Godfrey J S 1991 Measurements of sensible and latent heat flux in the western equatorial Pacific Ocean; *J. Geophys. Res. (Suppl.)* **96** 3375–3389
- Businger J A 1988 A note on the Businger-Dyer profiles; *Boundary-Layer Meteorol.* **42** 145–151
- Businger J A, Wyngaard J C, Izumi Y and Bradley E F 1971 Flux-profile relationship in the atmospheric surface layer; *J. Atmos. Sci.* **28** 181–189
- Deardorff J W 1972 Parameterization of the planetary boundary layer for use in general circulation models; *Mon. Weather Rev.* **2** 93–106
- Deardorff J W and Willis G E 1985 Further results from a laboratory model of the convective planetary boundary layer; *Boundary-Layer Meteorol.* **32** 205–236
- Goel M and Srivastava H N 1990 Monsoon Trough Boundary Layer Experiment (MONTBLEX); *Bull. Am. Meteorol. Soc.* **71** 1594–1600
- Kusuma G Rao 1996 Roughness length and drag coefficient at two MONTBLEX-90 tower stations; *Proc. Indian Acad. Sci. (Earth Planet. Sci.)* **105** 273–287
- Kusuma G Rao, Narasimha R and Prabhu A 1996 Estimation of drag coefficient at low wind speeds over the monsoon trough land region during MONTBLEX-90; *Geophys. Res. Lett.* (in press)
- Kusuma G Rao, Sethu Raman, Prabhu A and Narasimha R 1995 Surface turbulent heat flux variation over the monsoon trough region during MONTBLEX-90; *Atmos. Environ.* **29** 2113–2129
- Large W G and Pond S 1982 Sensible and latent heat flux measurements over the ocean; *J. Phys. Oceanogr.* **12** 464–482
- Miller M J, Beljaars A C M and Palmer T N 1992 The sensitivity of the ECMWF model to the parameterization of evaporation from the tropical oceans; *J. Climate* **5** 418–434
- Mohanty U C, Parihar P S, Venugopal T and Parashuram 1995 Estimation of the drag coefficient over the western desert sector of the Indian summer monsoon trough; **104** 273–287
- Monin A S and Yaglom A M 1975 *Statistical hydrodynamics.* (Cambridge, MA: MIT Press)
- Prandtl L 1932 Meteorologische Anwendung der stromungslehre; *Beitr Phys. für Atmosph.* **19** 188–202
- Priestley C H B 1954 Convection from a large horizontal surface; *Australian J. Phys.* **7** 176–201
- Rao K Narahari 1995 Estimation of surface temperature from MONTBLEX-data; *Proc. Indian Acad. Sci. (Earth Planet. Sci.)* **104** 257–271
- Rudra Kumar S, Ameenulla S and Prabhu A 1995 MONTBLEX tower observation: Instrumentation, data acquisition and data quality; *Proc. Indian Acad. Sci. (Earth Planet. Sci.)* **104** 221–248
- Schumann U 1988 Minimum friction velocity and heat transfer in the rough surface layer of a convective boundary layer; *Boundary-Layer Meteorology* **44** 311–326
- Sikka D R and Narasimha R 1995 Genesis of the monsoon trough boundary layer experiment (MONTBLEX); *Proc. Indian Acad. Sci. (Earth Planet. Sci.)* **104** 157–187
- Srivastav S K 1995 Synoptic meteorological observations and weather conditions during MONTBLEX-90; *Proc. Indian Acad. Sci. (Earth Planet. Sci.)* **104** 189–220
- Stull R B 1988 An introduction to boundary layer meteorology (Dordrecht, The Netherlands: Kluwer Academic Publishers)

- Stull R B 1994 A convective transport theory for surface fluxes; *J. Atmos. Sci.* **51** 3–22
- Tennekes H 1973 Similarity laws and scale relations in planetary boundary layers. In: *Workshop on micrometeorology* (ed.) D A Hangen (American Met. Soc.) 177–216
- Townsend A A 1964 Natural convection on water over an ice surface; *Q. J. R. Meteorol. Soc.* **90** 248–259
- Yaglom A M 1977 Comments on wind and temperature flux-profile relationship; *Boundary-Layer Meteorol.* **11** 89–102

Estimation of surface heat flux and inversion height with a Doppler acoustic sounder

L K SADANI and B S MURTHY

Indian Institute of Tropical Meteorology, Pune 411 008, India

Abstract. In this paper, acoustic sounder (sodar) derived vertical velocity variance (σ_w^2) and inversion height (Z_i) are used to compute the surface heat flux during the convective activity in the morning hours. The surface heat flux computed by these methods is found to be of the same order of magnitude as that obtained from tower measurements. Inversion heights derived from sodar reflectivity profiles averaged for an hour are compared with those obtained from the σ_w^3/Z profile. Variation of σ_w^2 in the mixed layer is discussed. The data were collected during the Monsoon Trough Boundary Layer Experiment 1990 at Kharagpur. The analysis is made for four days which represent the pre-monsoon, onset, active and relatively weak phases of the summer monsoon 1990. The interaction of the ABL with the monsoon activity is studied in terms of the variation of inversion height, vertical velocity variance and surface heat flux as monsoon progresses from June to August.

Keywords. Sodar; vertical velocity variance; inversion height; surface sensible heat flux.

1. Introduction

Sodar is now widely used to study the thermal as well as the wind structure of the Atmospheric Boundary Layer (ABL). Sodar derived vertical velocity variance (σ_w^2) is of utmost importance in the computation of surface sensible heat flux in the Convective Boundary Layer (CBL). The sodar back-scattered intensity record (echogram) is used to see the erosion of night time ground-based inversion and its uplifting by thermal plumes that originate at the surface during the day time. Sodar estimates of ABL parameters can be even more representative than direct measurements, since they are volume averages which are therefore less sensitive to local conditions (Melas 1990). According to Wyngaard (1986), the accuracy of indirect estimates of ABL parameters can be comparable to that of the underlying similarity relationship. In the present study we have computed surface sensible heat flux by two different similarity methods proposed by Caughey and Readings (1974); McBean and McPherson (1976); and Wyngaard (1986). The analyzed data were taken with a three-axis monostatic Doppler sodar model 2000, manufactured by M/s Aerovironment Inc., USA.

2. Method of computation

2.1 Variance method

Using the similarity theory, McBean and McPherson (1976) and Yokogama *et al* (1977) have shown that vertical velocity variance can be expressed as

$$\sigma_w^2 = \bar{w}'^2 \simeq A \left[Z \left(-\overline{u'w'} \frac{d\bar{U}}{dZ} + \delta \frac{g}{\theta} \cdot \overline{w'\theta'_v} \right) \right], \quad (1)$$

where

- $A =$ universal constant,
- $-\overline{u'w'} dU/dZ =$ local mechanical production of turbulence,
- $dU/dZ =$ mean wind shear,
- $g/\theta \cdot \overline{w'\theta'_v} =$ local buoyancy production of turbulence,
- $Z =$ height,
- $g =$ acceleration due to gravity,
- $\theta'_v =$ virtual potential temperature fluctuation,
- $u' =$ longitudinal velocity fluctuation,
- $w' =$ vertical velocity fluctuation.

In a well-mixed layer, the mechanical production is negligible and equation (1) can be simplified to

$$\sigma_w^2 \simeq \alpha (Z \cdot g/\theta \cdot \overline{w'\theta'_v})^{2/3}, \quad (2)$$

where $\alpha = A\delta^2/3 \simeq 1.4$ (see Caughey and Readings 1974; McBean and McPherson 1976).

Accordingly, a plot of σ_w^3/Z versus Z gives the local heat flux:

$$\frac{\sigma_w^3}{Z} = \alpha^{3/2} \cdot g/\theta \cdot \overline{w'\theta'_v}. \quad (3)$$

Therefore, the local heat flux profile can be determined by using the vertical velocity variance given by sodar (for details see Weill *et al* 1980).

In the well-mixed layer, $d\theta_v/dZ = 0$ and $d\theta_v/dt = -d\overline{w'\theta'_v}/dZ = \text{constant}$ and the heat flux decreases linearly with height. Therefore,

$$\frac{\sigma_w^3}{Z} = \alpha^{3/2} \cdot g/\theta \cdot Q_0 (1 - Z/h_*), \quad (4)$$

where $Q_0 = \overline{(w'\theta')_0}$ at $Z = 0$ is the temperature flux at the surface and h_* is the height at which temperature flux vanishes by linear extrapolation.

The buoyancy flux at the surface $\overline{(w'\theta'_v)_0}$ is related to the temperature flux $\overline{(w'\theta')_0}$ by the equation (see Garratt 1992)

$$\overline{(w'\theta'_v)_0} = \overline{(w'\theta')_0} \left[1 + 0.61 \bar{\theta} \frac{\gamma}{\beta} \right],$$

where β is known as the Bowen ratio and $\gamma = C_p/\lambda$ is called the psychrometer constant. The humidity correction term $\Delta = 1 + 0.61 \bar{\theta} \gamma/\beta$ changes from 1.10 for moist air ($\beta = 0.75$)

to 1.01 for very dry air ($\beta = 10$). At the surface $\theta = T$, so

$$\text{Surface heat flux } H = (\sigma_w^3/Z)_0 (T/g) \alpha^{-3/2} \rho C_p, \quad (5)$$

where ρ is the density of air and C_p is the specific heat at constant pressure. $(\sigma_w^3/Z)_0$ can be obtained by extrapolating the linear part of the profile to the surface. Therefore the surface heat flux can be computed from the vertical velocity variance profile. By this method we get surface heat flux in moist convective conditions whose value is 10% more than the heat flux measured in dry convective conditions (Garratt 1992).

2.2 Inversion height method

Wyngaard (1986) suggested that for the middle-mixed layer,

$$\sigma_w^2/w_*^2 = b, \quad (6)$$

where b is a constant proposed to be 0.4, w_* is the mixed-layer velocity scale given by

$$w_* = \left[\frac{Z_i H g}{\rho C_p T} \right]^{1/3}, \quad (7)$$

and

Z_i = height of the inversion base in CBL.

Melas (1990) estimated that $b = 0.45$ in the height interval $0.1 Z_i$ to $0.7 Z_i$. We have computed b from sonic anemometer and sodar data and found it to be approximately equal to 0.45–0.5 in the same height range $0.1 Z_i$ – $0.7 Z_i$.

From equations (6) and (7), we can write surface heat flux,

$$H = b^{-3/2} (g/\theta)^{-1} \rho C_p \sigma_w^3 / Z_i. \quad (8)$$

Therefore with Z_i (the height of ABL) known from reflectivity profiles and σ_w averaged in the above height interval, the surface heat flux H can be computed.

The H so computed by equations (5) and (8) has been compared with that computed from the tower data by the profile method.

The temperature structure of ABL as inferred from the sodar echogram provides a reliable estimate of mixed layer depth (Z_i) in the convective boundary layer (CBL). The peak in the echo-intensity profile coincides with the bottom of the capping inversion layer on the echogram. Kaimal *et al* (1982) have shown that sodars are able to locate the inversion base with very good accuracy. Melas (1990) has reported that sodar estimates of Z_i are in very good agreement with rawinsonde measurements. In the present analysis, we have used back-scattered intensity profiles averaged over a one-hour period to estimate Z_i . These values are compared with those obtained by linear extrapolation of σ_w^3/Z vs Z profile.

3. Site and its general features

A monostatic three-axis Doppler sodar, model 2000 manufactured by M/s Aerovironment Inc., USA, was installed by the authors at Kharagpur ($22^\circ 25'N$, $87^\circ 18'E$) in the

month of April 1990 for MONTBLEX. The three antennae were configured in an *L* pattern, one pointing towards geographic East and the second pointing towards geographic North. Both antennae are inclined at 30° from the vertical. At the centre the third antenna points exactly vertically up. Tilted antennae are pointed against the prevailing surface wind direction so that the sound pulse reaches a maximum height (1500 m) and gives wind speeds at high levels.

The sodar site enjoys an uninterrupted fetch of more than 500 m towards south, the direction of the summer monsoon wind. The site being a flat fairly open terrain, the influence of topography on wind characteristics is expected to be small.

The mean seasonal weather pattern at this site is determined by the presence of the monsoon trough during the Indian summer monsoon season, i.e., from June to August. Upon the onset of monsoon the dry convection changes over to deep moist convection. One of the objectives of MONTBLEX is to study the diurnal variation of ABL under the monsoon trough. In this paper we attempt to verify whether the similarity methods can be used to compute surface heat flux during the disturbed conditions of ABL.

4. Observed data

The sodar measures vertical velocity W (m/s) until the end of the sampling interval and evaluates the standard deviation by standard software. The manufacturer specified

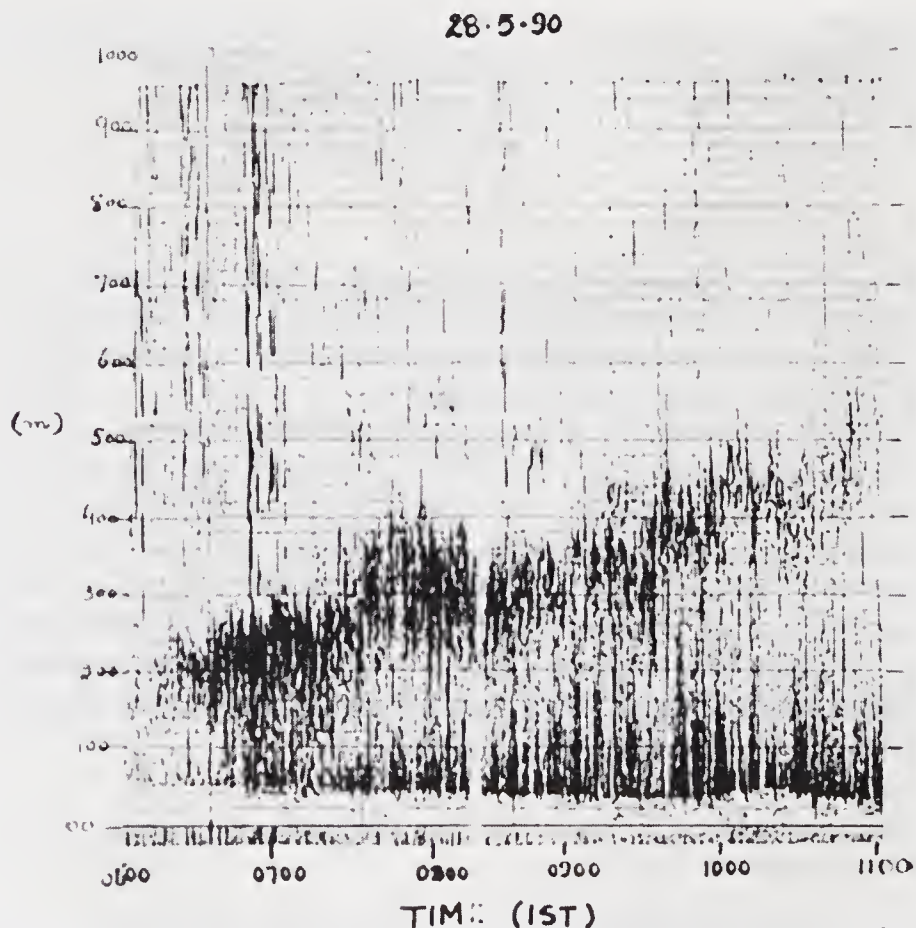


Figure 1(a). Acoustic echo return as a function of height and time on 28th May 1990.

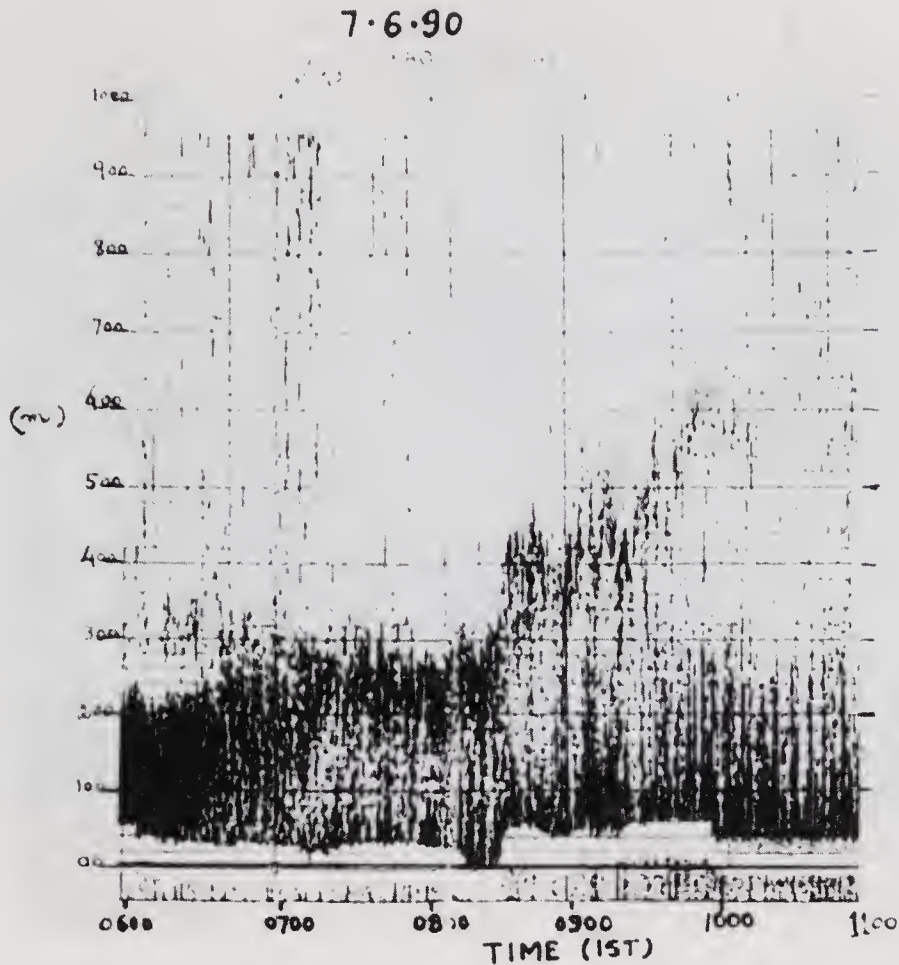


Figure 1(b). Acoustic echo return as a function of height and time on 7th June 1990.

range for W and σ_w is 0–3.7 m/s and 0–1.9 m/s respectively. The vertical velocity accuracy and σ_w resolution are 0.1 m/s. The sodar-observed vertical wind data (from May to August 1990) during the onset and active phases of the monsoon were studied. Our measured value of W lies between 0.16 and 0.48 m/s. Analysis has been done for four representative days of the different phases of monsoon, i.e., 28th May, 7th June, 9th July and 24th August 1990. On these days the CBL had a well-defined capping inversion with rising thermal plumes below (see figures 1a, b, c and d). Heat fluxes and inversion heights have been computed for these four days. The sodar uses a standard electronic filtering process for the good quality of data. The data with zero reliability factor (R) were used for the present study. The data with reliability factors of 0 and 1 are considered best according to the filtering procedure adopted for the data acquired with this instrument. The zero and one-reliability factors are dependent on the return of more than 25% of transmitted sound pulses as acceptable echoes. The data correspond to a sampling interval of one hour.

4.1 Mixing heights

Analysis for onset (May and June) and active (July and August) phases of monsoon is presented separately. Figures 1(a and b) show the time plot of back-scattered sound

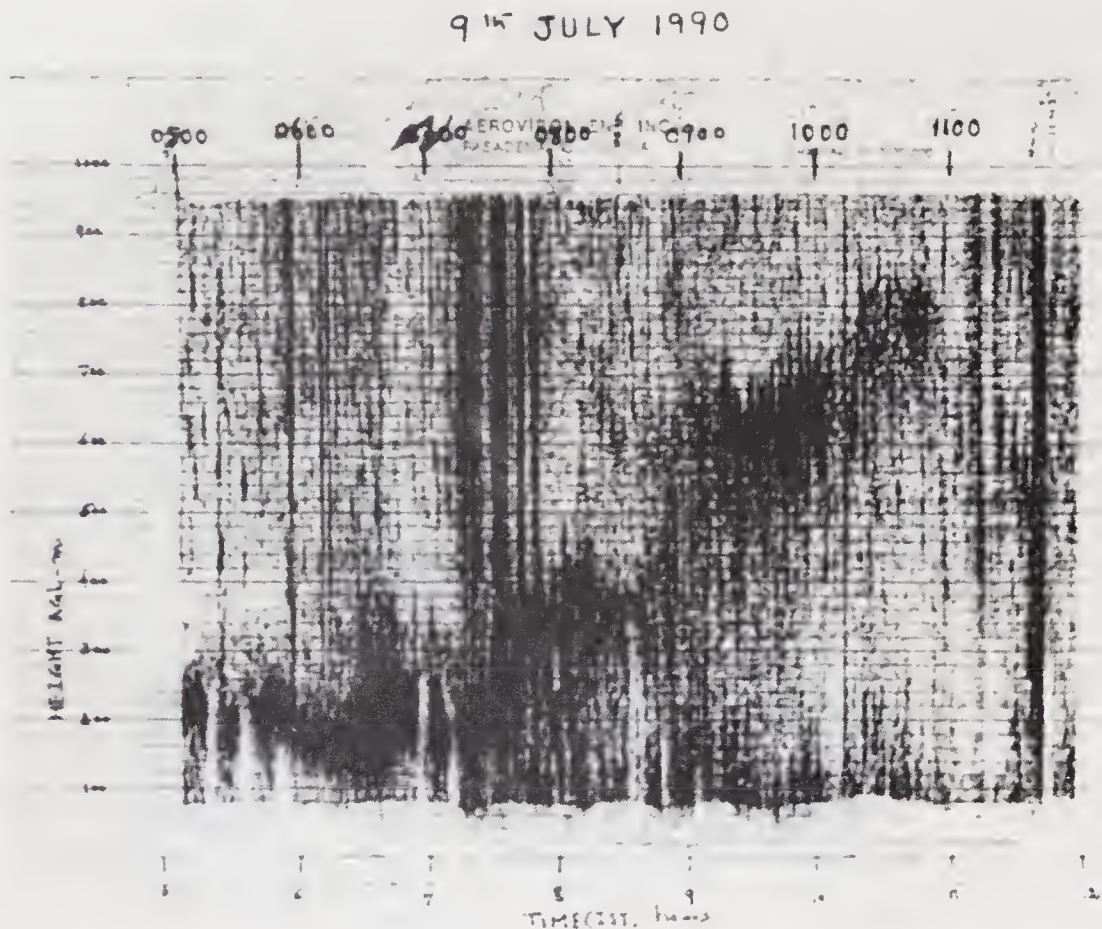


Figure 1(c). Acoustic echo return as a function of height and time on 9th July 1990.

intensity (echogram) versus height. It shows the march of convective activity of ABL for morning hours from 0600 to 1200 hr IST. The rise of the temperature inversion layer capping the CBL is a recognizable atmospheric feature on the plots. From this feature, the height of the inversion layer was obtained for the above period and compared with computed heights from the reflectivity profile and σ_w^3/Z profile. Underneath this capping layer, the start of convective activity is visible at 0700 hr IST in the form of rising thermal plumes. After 1100 hr, the capping inversion layer, having lifted up to more than 1000 m, becomes undetectable by sodar echogram and cannot be seen on the facsimile recorder because the upper maximum limit on the recorder is up to 1000 m and is therefore not seen in the figures. Figures 1(a and b) are facsimile records of convective activity of ABL during the morning hours on 28th May and 7th June respectively. The synoptic condition of the atmosphere over Kharagpur on the four days of analysis, shown in table 1, indicates that 28th May falls in the pre-monsoon period whereas 7th June falls in the monsoon onset phase. A weekly (1st–7th June) cumulative rainfall of 50 mm was reported at Alipore (Calcutta) Observatory (MOCC 1990) during the onset phase.

Figures 1(c and d) show the thermal structure of the ABL during the morning hours on 9th July and 24th August respectively. On 9th July, the inversion height remained stationary at around 200 m during 0500–0800 hr IST and increased suddenly during 0900–1000 hr IST. On 9th July, the capping inversion layer dissipated after 1100 hr IST. On 24th August, the capping inversion layer (figure 1d) remained stationary at

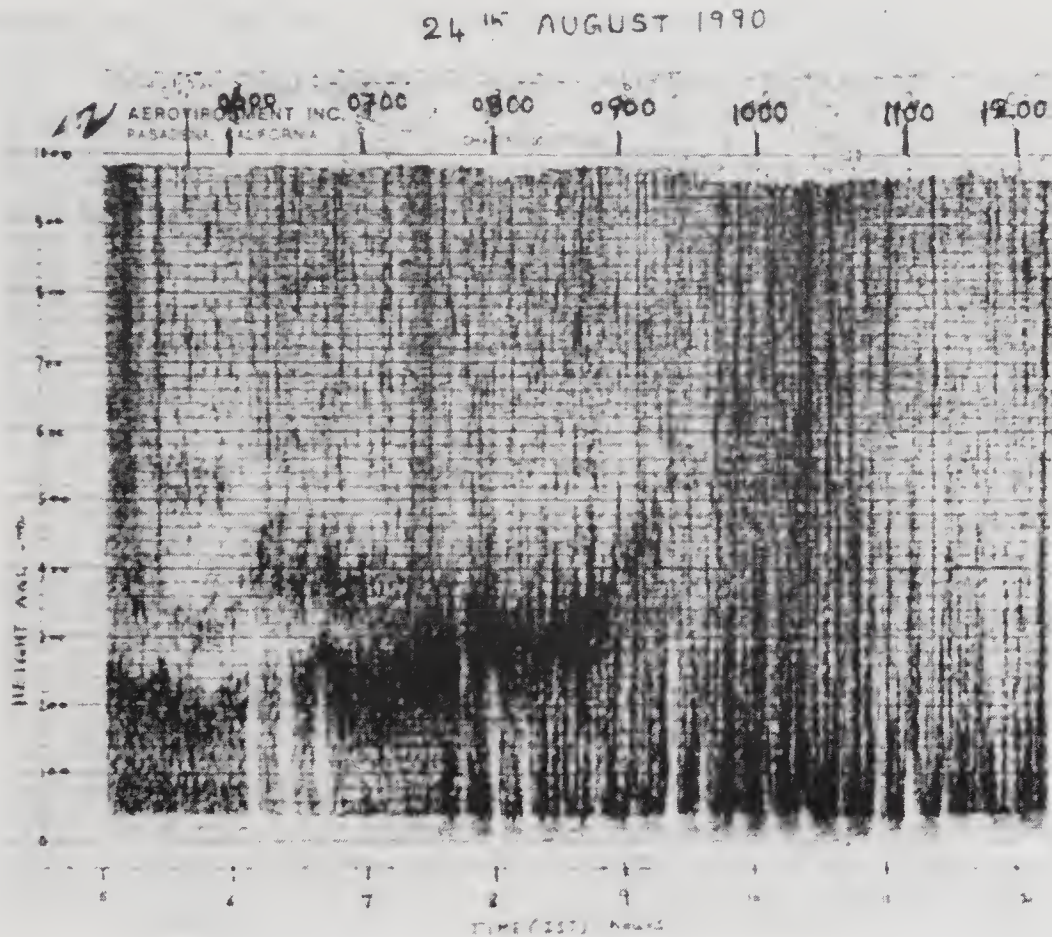


Figure 1(d). Acoustic echo return as a function of height and time on 24th August 1990.

around 300 m during 0500–0900 hr IST and dissipated after 1100 hr IST causing the ABL to grow beyond the detectable range of sodar facsimile (1000 m). The echogram is noisy because of the background noise, during the period 0930–1100 hr IST, making the inversion layer hardly detectable.

5. Discussion and results

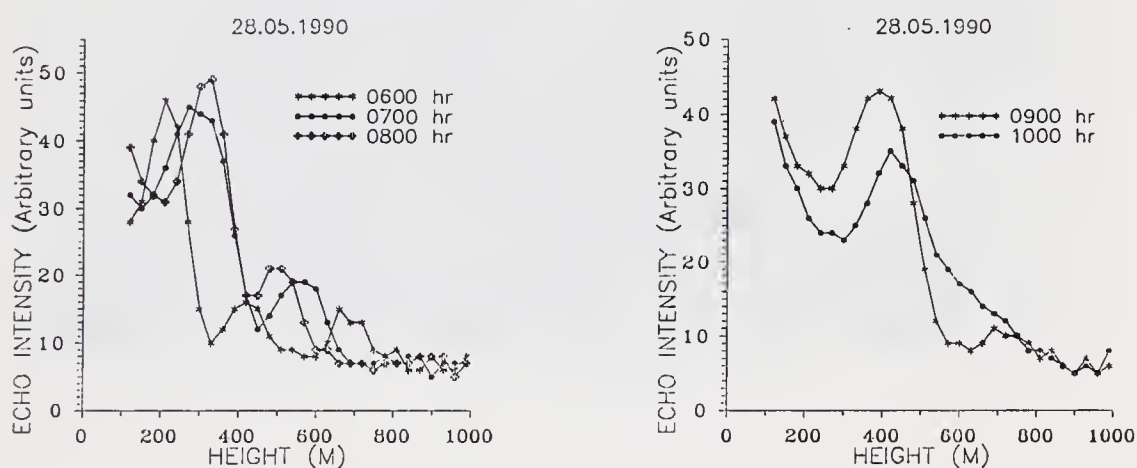
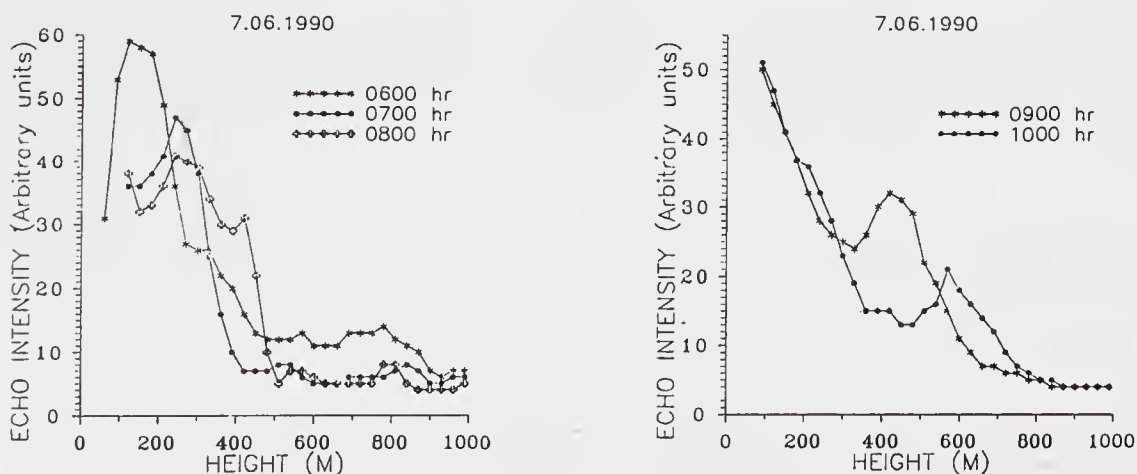
5.1 Vertical reflectivity (back-scatter) analysis

The thermal structure detected by sodar provides a reliable estimation of Z_i . The figures 2(a, b) and 3(a, b) show the graphs of reflectivity vs. height for the days i.e., 28th May, 7th June, 9th July and 24th August during the morning hours i.e., 0600–1000 hr IST respectively for the Kharagpur site. Each profile is averaged over an hour of observation period. The peak in each profile coincides with the bottom of the elevated inversion layer on facsimile record (figures 1a, b, c and d).

In accordance with the results of Kaimal *et al* (1976), our acoustic sounder reflectivity profile results show mean minimum reflectivity height between $0.4 Z_i$ and $0.6 Z_i$ while from 0900 hr IST onward, the profile shows mean minimum reflectivity height of approximately $0.7 Z_i$.

Table 1. Synoptic condition of the atmosphere over Kharagpur on the four representative days during MONTBLEX 1990.

Date	Synoptic state	Weekly cumulative rainfall (mm)
28th May	Pre-monsoon	(Not available)
7th June	Monsoon onset phase	(1st–7th June) 50
9th July	Intense convective clouds and trough fluctuation	(6th–12th July) 235
24th August	Period of monsoon depression/ Low pressure systems	(24th–30th August) 65

**Figure 2(a).** Reflectivity profiles on 28th May 1990.**Figure 2(b).** Reflectivity profiles on 7th June 1990.

The inversion heights are given in column 3 of tables 2–5. The data here show that the increase in the inversion height is associated with an increase in the surface heat flux. This is obvious, because the thermals that originate at the surface traverse larger distances vertically if the surface heat flux is higher and cause more mixing.

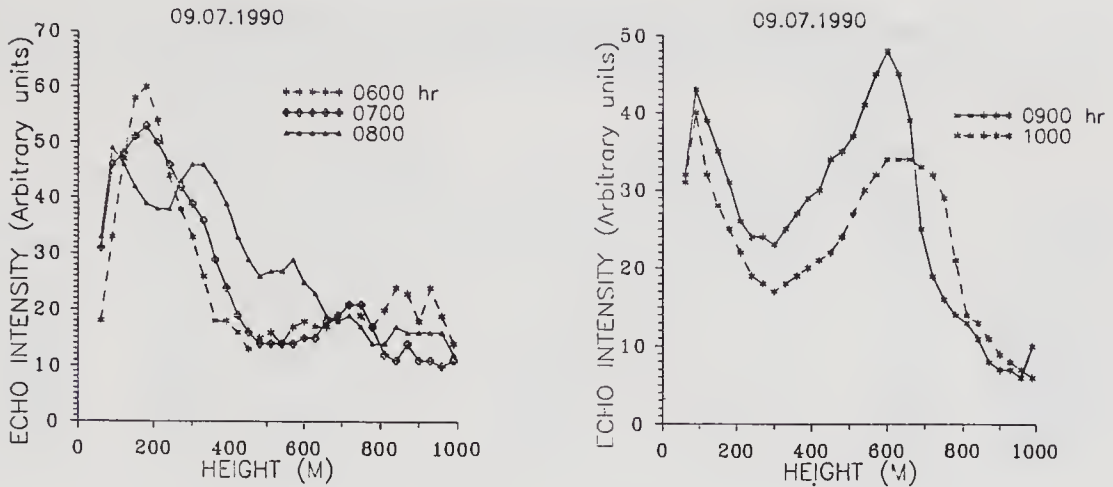


Figure 3(a). Reflectivity profiles on 9th July 1990.

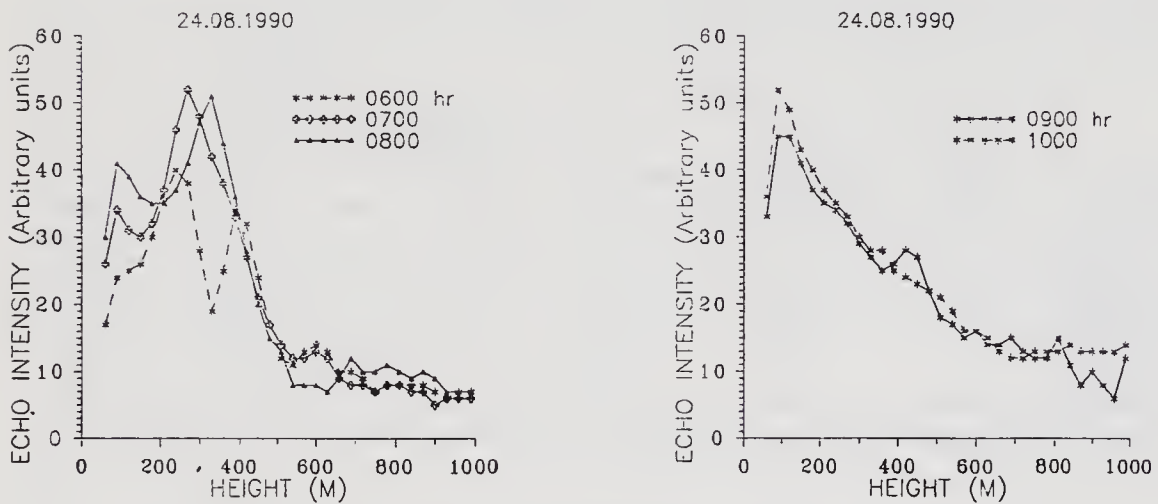


Figure 3(b). Reflectivity profiles on 24th August 1990.

5.2 Heat flux profile and inversion heights

Using sonic anemometer data and sodar measured inversion heights, the computed mixed layer velocity scale w_* for 28th May and 7th June is found to be around 1.15 m/s between 0900 and 1100 hr. Since sonic data are not available for 9th July and 24th August, the w_* , computed using sodar derived heat flux values, are 0.87 m/s and 1.16 m/s respectively between 0900 and 1100 hr IST. This shows that the layer below the capping inversion was well mixed by thermals. So we have used equations (5) and (8) which are applicable to a well-mixed layer for the computation of surface heat flux.

The linear profiles of σ_w^3/Z during the morning hours i.e., from 0600 to 1000 hr IST, are shown in figures 4–7 for 28th May, 7th June, 9th July and 24th August respectively. The linear fit is not always good, because $-dw'\theta'/dZ$ is not constant in the mixed layer, which is an ideal condition. Each profile is an average over an hour's duration. The ordinate intercept is taken as the inversion height and the abscissa intercept $(\sigma_w^3/Z)_0$ is used for computation of surface heat flux for that hour. Using equation 5, the computed heat flux values and inversion heights are given in columns 7 and 2 respectively of

Table 2. Comparison of surface heat flux and inversion height on 28th May 1990.

Time IST	Inversion height Z_i (m)		Surface temperature °C	σ_w^3/Z at surface $\times 10^3$ ($m^2 s^{-3}$)	Surface heat flux H (W/m^2)		Sky condition
	From profile	From reflec- tivity profile			By eq. (8)	By eq. (5)	
0600-0700	260	210	27.54	1.2	51.79	25.03	clear
0700-0800	390	330	28.37	2.5	54.00	52.28	-do-
0800-0900	325	330	29.08	2.8	99.85	58.69	-do-
0900-1000	390	420	29.96	3.6	90.09	75.68	-do-
1000-1100	410	480	31.48	3.5	86.42	73.95	-do-

Table 3. Comparison of surface heat flux and inversion height on 7th June 1990.

Time IST	Inversion height Z_i (m)		Surface temperature °C	σ_w^3/Z at surface $\times 10^3$ ($m^2 s^{-3}$)	Surface heat flux H (W/m^2)		Sky condition
	From profile	From reflec- tivity profile			By eq. (8)	By eq. (5)	
0600-0700	310	180	27.2	0.8	33.55	16.66	7/8 octa
0700-0800	290	270	28.6	3.0	77.92	62.78	-do-
0800-0900	215	300	29.8	4.0	78.22	84.04	-do-
0900-1000	—	480	31.0	—	79.10	—	clear
1000-1100	560	570	32.8	3.6	101.12	76.39	-do-

Table 4. Comparison of surface heat flux and inversion height on 9th July 1990.

Time IST	Inversion height Z_i (m)		Surface temperature °C	σ_w^3/Z at surface $\times 10^3$ ($m^2 s^{-3}$)	Surface heat flux H (W/m^2)		Sky condition
	From profile	From reflec- tivity profile			By eq. (8)	By eq. (5)	
0600-0700	240	180	26.70	0.38	33.50	7.90	over cast
0700-0800	305	180	27.40	0.26	17.90	5.42	-do-
0800-0900	610	330	28.20	0.75	63.67	15.63	-do-
0900-1000	570	600	28.40	1.40	45.27	29.28	-do-
1000-1100	630	700	28.50	1.35	40.77	28.24	-do-

tables 2-5. For 7th June, it is not possible to compute surface heat flux at 0900 hr using equation (5) as unambiguous linearity was not observed in the σ_w^3/Z profile (figure 5).

A comparison of inversion height Z_i as estimated above with values obtained by the reflectivity method is shown in columns 2 and 3 of tables 2-5. The comparison shows

Table 5. Comparison of surface heat flux and inversion height on 24th August 1990.

Time IST	Inversion height Z_i (m)		Surface temperature °C	σ_w^3/Z at surface $\times 10^3$ ($m^2 s^{-3}$)	Surface heat flux H (W/m^2)		Sky condition
	From profile	From reflec- tivity profile			By eq. (8)	By eq. (5)	
0600–0700	160	270	27.8	0.75	24.28	15.65	5/8 octa
0700–0800	350	270	28.7	1.15	66.08	24.08	-do-
0800–0900	450	330	29.4	1.1	44.50	23.08	-do-
0900–1000	550	~ 500	30.4	2.40	37.95	50.53	3/8 octa
1000–1100	550	~ 600	31.6	5.00	85.07	105.68	-do-

that the two estimates of Z_i are in good agreement, especially during the two time periods between 0900 and 1100 hr IST on 28th May. We have computed the surface heat flux (column 6) using the inversion height (column 3) and equation (8) and the values are also shown in the same tables.

The sodar model 2000 measures wind speeds in every 30 m layer of air beginning from 60 to 1500 m or to maximum elevation. The 30 m air layer is nothing but one gate resolution. Hence estimated inversion heights can differ by 30 m and subsequently the surface heat flux obtained from equation (8), which incorporates the Z_i term, varies by 20% between 0600 and 0700 hr IST and by 12% between 0800 and 1000 hr IST; during this time the layer underneath is well mixed.

The surface heat flux computed by equation (5) also depends on the number of points exhibiting linearity in the well-mixed layer, depending upon the ideal condition stated above. Therefore more points on the linear fit indicate the amount of mixing in the layer (figures 4–7).

Bandyopadhyay *et al* (1991) have computed the surface heat flux at the same site by the profile method and the Van Uldan and Holstag method (1985). Their computed heat flux differs from the present values by 36 W/m^2 at 0900 hr IST and by 33 W/m^2 at 1000 hr IST, because the present values are volume averages over the site. Compared with the observed values (Bandyopadhyay *et al* 1991) at the same site, our sodar overestimates the surface heat flux between 0600 and 0800 hr and underestimates it between 0800 and 1000 hr on 28th May and 7th June. Melas (1990) has also reported that sodar derived surface heat flux H (equation 8) overestimates the measured surface heat flux obtained with the direct technique at low values, and underestimates it at high values. However our computed heat flux values and those measured at the site (Bandyopadhyay *et al* 1991) are of the same order.

Surface heat flux has been computed using equations (5) and (8) on 9th July and 24th August from 0600 to 1000 hr IST. As is evident from tables 4 and 5, equation (8) overestimates the surface heat flux compared to that by equation (5). Table 1 shows that 6th–12th July is characterized by intense convective clouds and trough fluctuations. A cumulative weekly rainfall (6th–12th July) of 235 mm was reported. The decrease of surface heat flux from 7th June to 9th July can be attributed to the intensification of the monsoon and increased precipitation over the station (Kharagpur). The surface heat flux on 24th August is nearly of the same magnitude as that observed on 9th July.

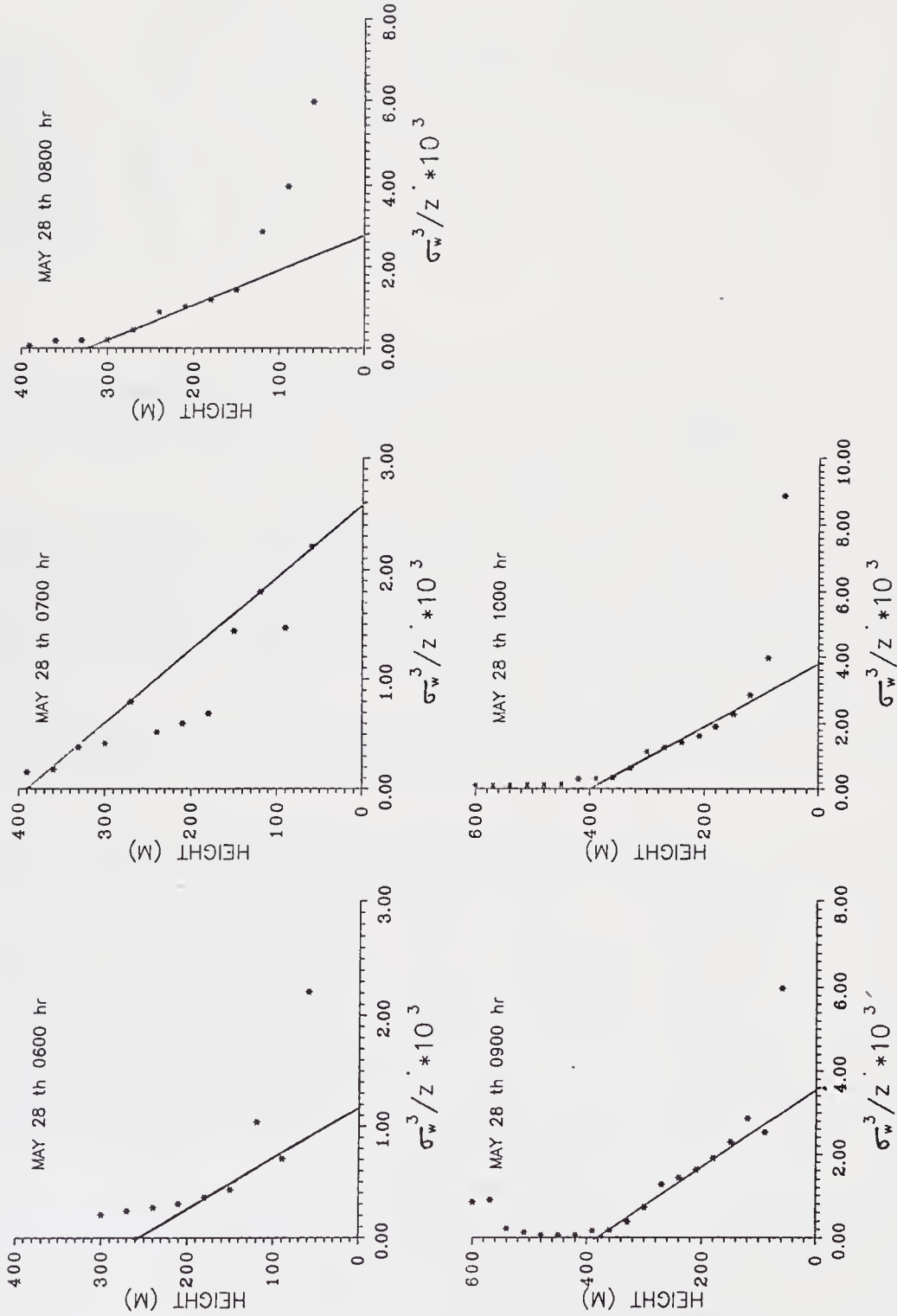


Figure 4. σ_w^3/z profiles on 28th May 1990.

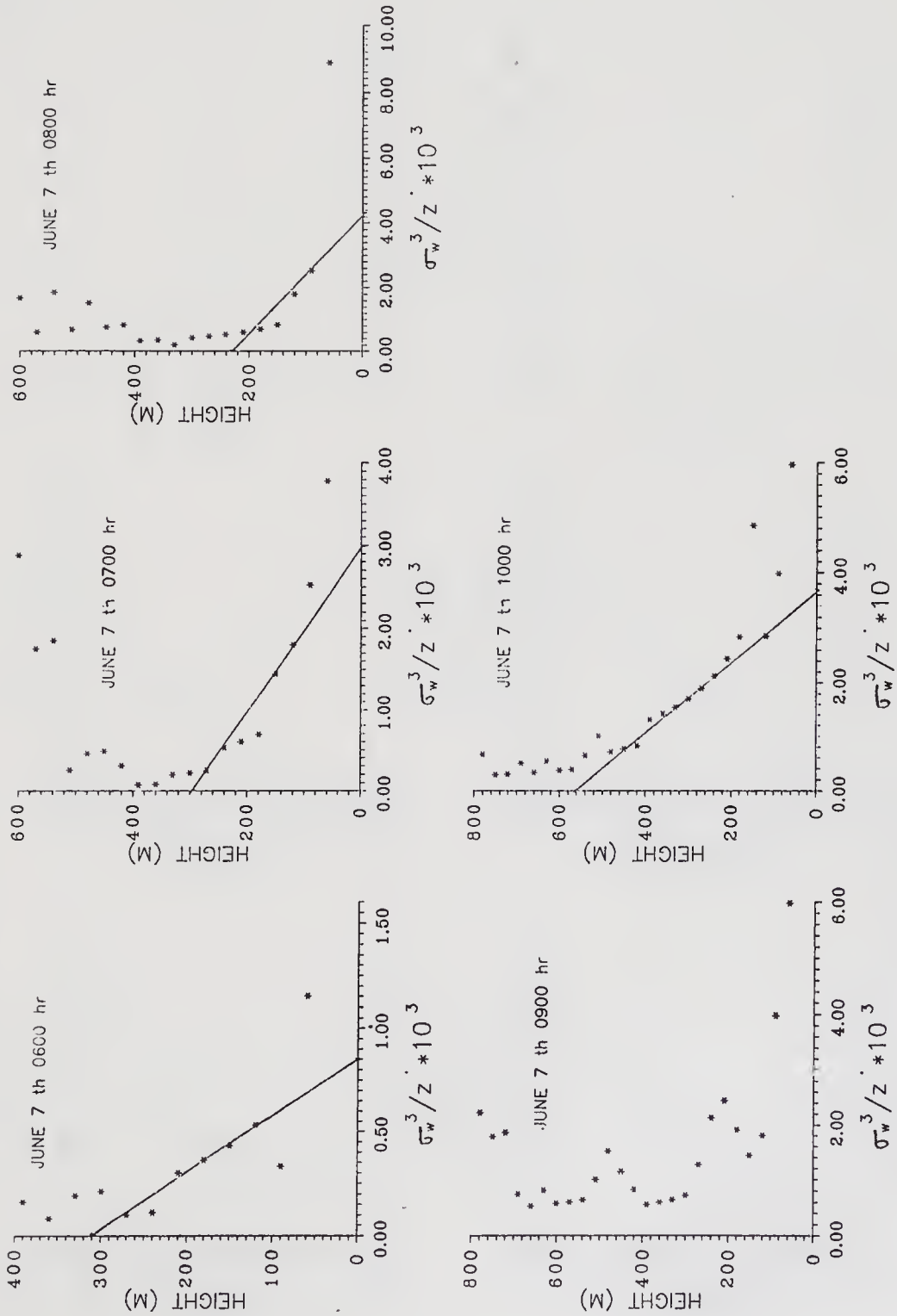


Figure 5. σ_w^3/Z profiles on 7th June 1990.

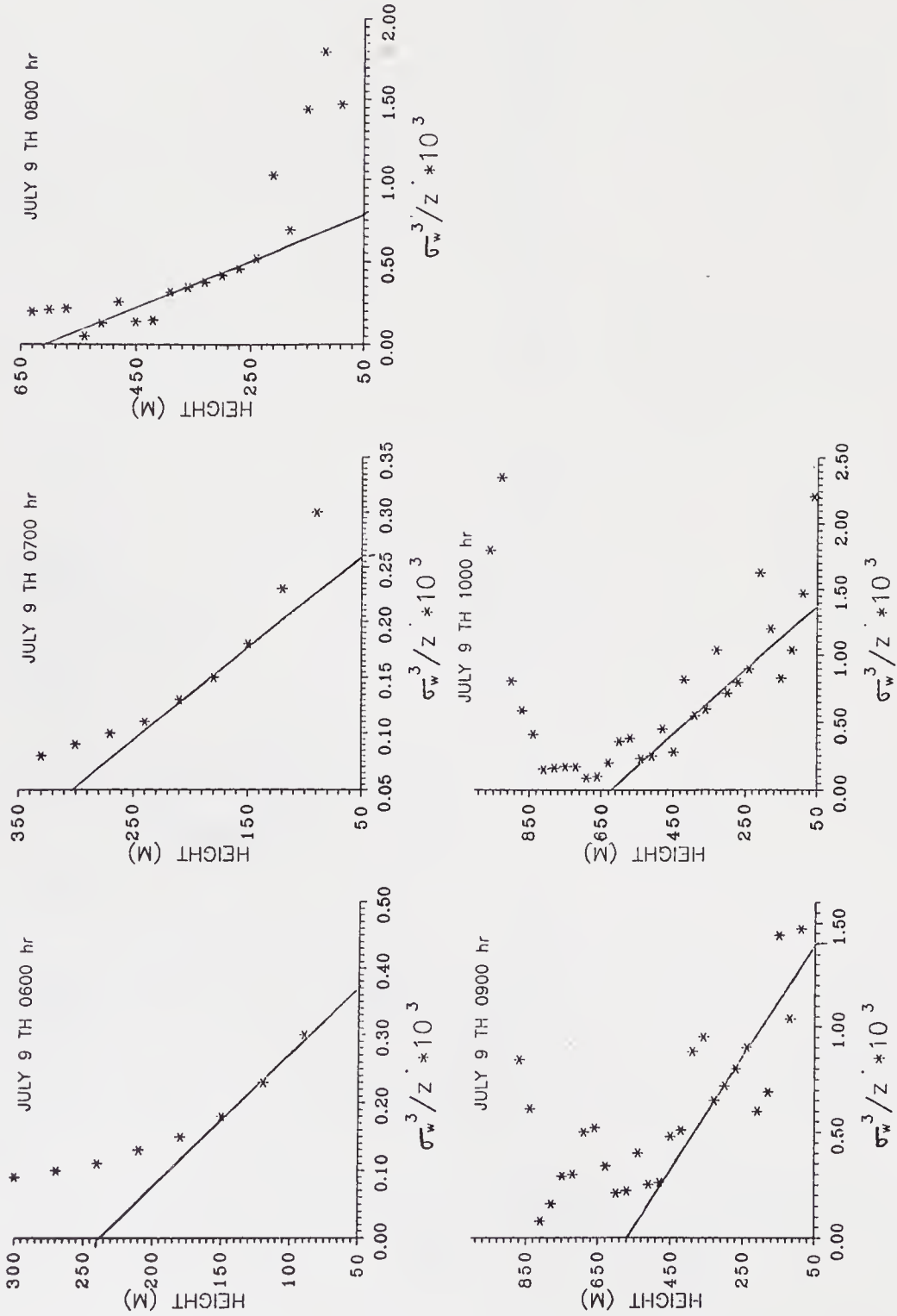


Figure 6. σ_w^3/Z profiles on 9th July 1990.

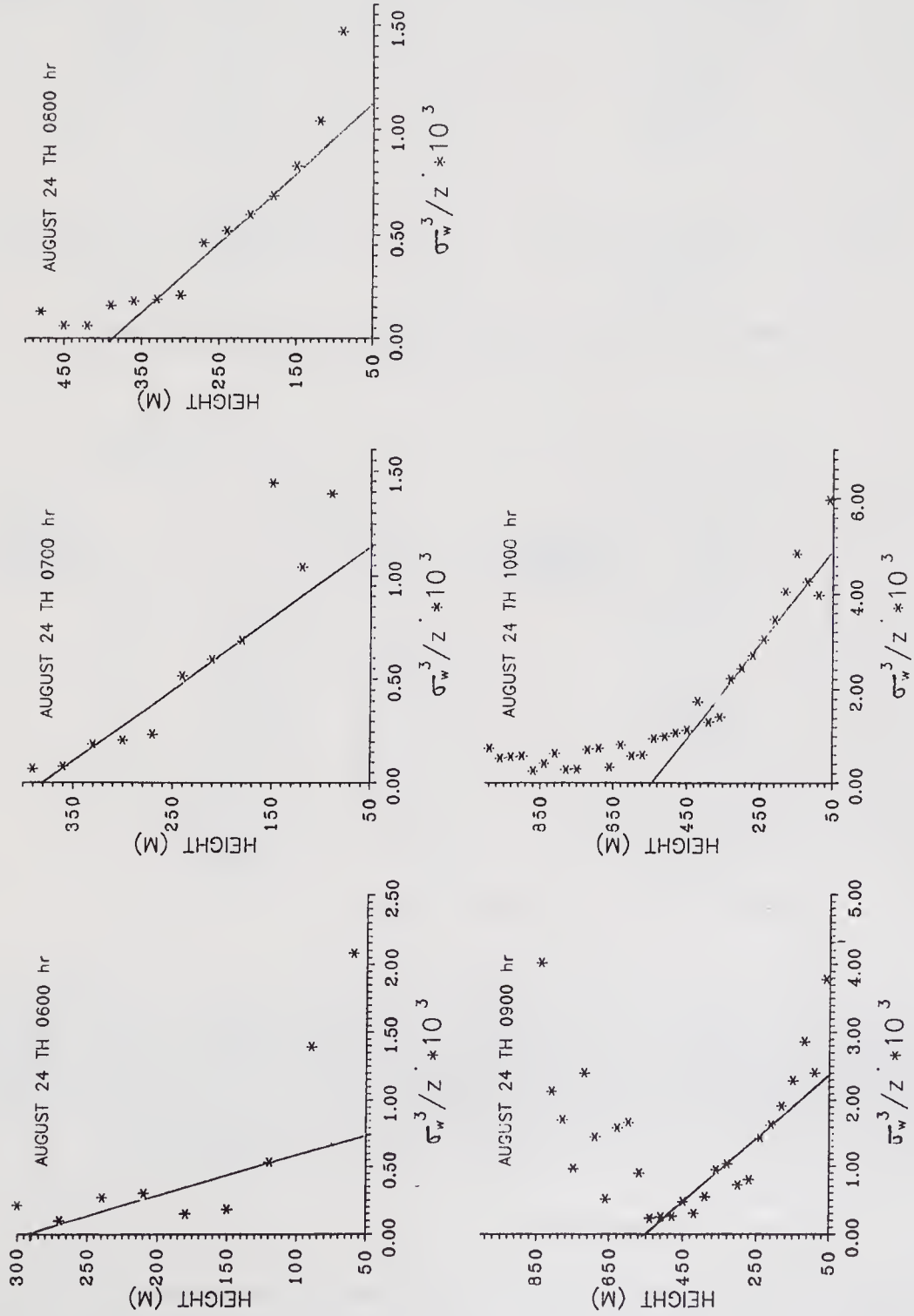


Figure 7. σ_w^3/Z profiles on 24th August 1990.

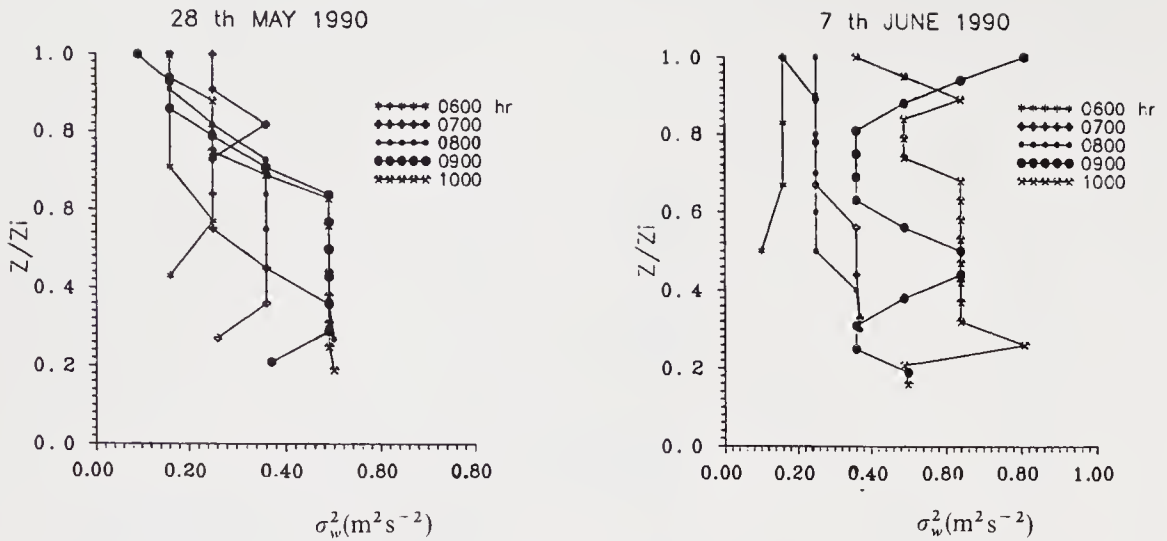


Figure 8(a). Profiles of vertical velocity variance (σ_w^2) on 28.5.90 and 7.6.90.

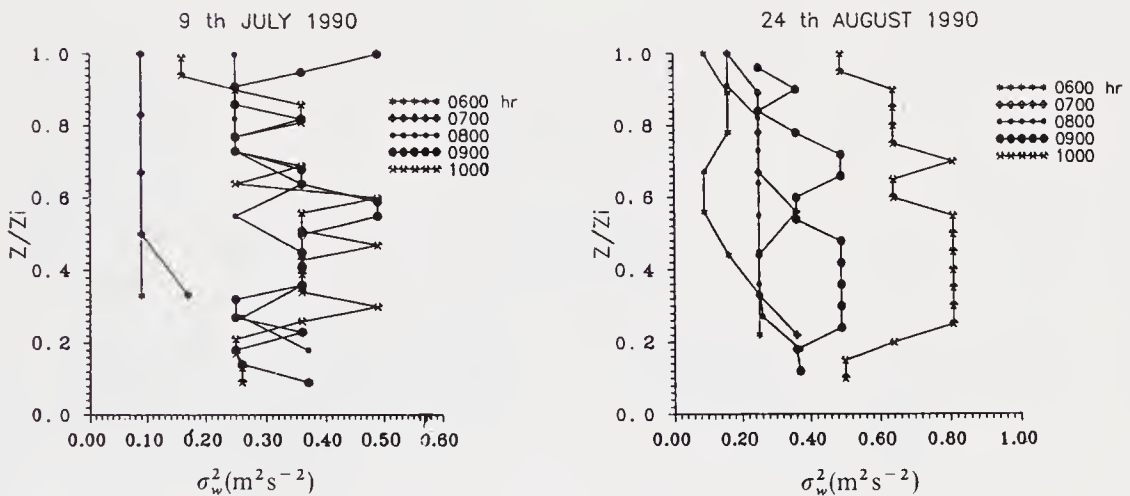


Figure 8(b). Profiles of vertical velocity variance (σ_w^2) on 9.7.90 and 24.8.90.

The inversion height during the late morning hours, i.e., 0900–1100 hr IST, is more during the active monsoon period (July and August) compared to that during the pre-monsoon period (May). The growth rate of the ABL from 0900 to 1000 hr is 270 m/hr during the active phase (24th August) whereas it is 180 m/hr during the onset phase and 170 m/hr during the relatively weak phase of the monsoon.

5.3 Vertical velocity variance profiles

The graphs of vertical velocity variance profiles for 28th May and 7th June (figure 8a) from 0600 to 1000 hr IST correspond to the rise of the temperature inversion layer with the increasing convective activity. Figure 8(a) presents five variance profiles, each being calculated for an hour's period beginning from 0600 hr IST. The altitude is normalized by the height of the inversion evaluated from the reflectivity profile. It should be

Table 6. Hourly averaged normalized heights of maximum variance and their range.

Date	Time IST	Z/Z_i corresponding to maximum variance (σ_w^2)	Z/Z_i range of constant maximum variance (σ_w^2)
28.5.90	0600	0.57	—
	0700	0.36	0.36–0.45
	0800	0.36	0.36–0.37
	0900	0.27	0.27–0.63
	1000	0.19	0.19–0.63
07.06.90	0600	0.67	—
	0700	0.33	0.33–0.55
	0800	0.30	0.30–0.40
	0900	0.38	0.38–0.44
	1000	0.26	0.3–0.68

Table 7. Hourly averaged normalized heights of maximum variance and their range.

Date	Time IST	Z/Z_i corresponding to maximum variance (σ_w^2)	Z/Z_i range of constant maximum variance (σ_w^2)
9.7.90	0600	0.32	—
	0700	0.32	—
	0800	0.36	—
	0900	0.54	0.54–0.60
	1000	0.30	0.30–0.60
24.8.90	0600	0.22	—
	0700	0.56	—
	0800	0.20	—
	0900	0.24	0.24–0.50
	1000	0.26	0.26–0.56

emphasized that the vertical velocity variance is not constant in the mixed layer. The measured value σ_w^2 (figures 8a and b) is small near the surface and increases to a maximum in the middle of the ABL and then decreases with height (Caughey 1982).

From table 6 we see that Z/Z_i corresponding to maximum variance (σ_w^2) decreases while the range of constant maximum variance increases from 0600 to 1000 hr as convective activity increases.

σ_w^2 averaged in the height interval $0.19 Z_i < Z < 0.63 Z_i$ is approximately equal to 0.49 at 1000 hr IST on 28th May and 0.66 at 1000 hr IST on 7th June.

Figure 8(b) presents variance profiles from 0600–1000 hr IST on 9th July and 24th August. The magnitude of variance (σ_w^2) on 24th August is relatively high compared to that on the other three days. On 9th July, σ_w^2 in the mixed layer ($0.1Z_i$ – $0.7Z_i$) has fluctuated much during 0900–1100 hr (figure 8b) whereas it has remained constant on 24th August. As shown in table 7, the ABL below the capping inversion gets well mixed by 0900 hr and remains constant in the height interval $0.2Z_i$ – $0.7Z_i$.

6. Conclusion

In this paper, we have described the measurement of surface heat flux in the CBL using two different methods proposed by Caughey and Readings (1974) and Wyngaard (1986) respectively. These methods are applicable to a well-mixed layer when the capping inversion is underneath the detection range of the sodar. Surface heat fluxes computed by these methods are on the same order of magnitude as those measured by the tower. The peak in the reflectivity profile coincides well with the base of inversion on the echogram. The inversion heights computed from linear extrapolation of σ_w^2/Z vs Z profile agree well with those obtained from the reflectivity profiles. The maximum value of the vertical velocity variance σ_w^2 is reached at a rather low level of $0.2Z_i$. It remains constant in the height interval $0.2Z_i-0.65Z_i$ on the four days during 0900–1100 hr. The height of the ABL in the late morning hours (0900–1100 hr) is greater during the active phase of the monsoon (July–August) than during the pre-monsoon (May) and onset (June) phases, inspite of a decrease in the surface heat flux from May to August. But on each individual day, the ABL height is directly proportional to the surface heat flux. This shows that the interaction between the monsoon and the ABL over the trough region is quite complex and requires the understanding of the physical processes involved. Doppler sodar measured vertical velocity variance can be used to make reliable estimates of the ABL height and surface heat flux in the convective boundary layer.

Acknowledgements

The authors would like to thank their colleagues of the boundary layer group of the Instrumental and Observational Techniques Division for the co-operation they extended during the period of observation of MONTBLEX 1990.

The MONTBLEX-90 was sponsored and supported by the Department of Science and Technology, Government of India. The authors wish to express their thanks to the DST.

References

- Bandyopadhyay P, Chowdhury S and Bandyopadhyay G 1991 Atmospheric surface layer characteristics with MONTBLEX data; *Proc. Indian Acad. Sci. (Earth Planet Sci.)* **100** 219–233
- Caughey S J and Readings C J 1974 Vertical component of turbulence in convective conditions; *Advances in Geophysics* (New York, San Francisco, London: Academic Press) **18** 125–130
- Caughey S J 1982 Observed characteristics of the atmospheric boundary layer. In: *Atmospheric turbulence and air pollution modelling* (eds) F T M Nieuwstadt and H Van Dop, (Dordrecht: D Reidel) pp. 107–158
- Garratt J R 1992 *Atmospheric boundary layer*, Cambridge Atmospheric and Space Science Series, p. 36–37
- Kaimal J C, Wyngaard J C, Haugen D A, Cote O R, Izumi Y, Caughey S J and Readings C J 1976 Turbulence structure in the convective boundary layer; *J. Atmos. Sci.* **33** 2152–2169
- Kaimal J C, Abshire N L, Cladwick R B, Decker M T, Hook W H, Kroffli R A, Neff N D, Pasqualucci F and Hildbrand P H 1982 Estimating the depth of the day time convective boundary layer; *J. Appl. Met.* **21** 1123–1129
- McBean G A and J I McPherson 1976 Turbulence above Lake Ontario; *Velocity and Scalar Statistics Boundary Layer Meteor.* **10** 181–197
- Melas Dimitrio 1990 Sodar estimates of surface heat flux and mixed layer depth compared with direct measurements; *Atmospheric Environment* **24** 2847–2853
- MOCC 1990 Report on MONTBLEX-90 by M G Gupta, IMD

- Van Ulden A P and Holstag A A M 1985 A simple scheme for day time estimates of the surface fluxes from routine weather data; *J. Climate Appl. Meteorol.* **22** 517–529
- Weill A, Klapisz C, Stauss B, Bandin F, Jaupart C, Van Grudeerbeeck P and Goutorbe J P 1980 Measuring heat flux and structure functions of temperature fluctuations with an acoustic Doppler sodar; *J. Appl. Meteorol.* **19** 199–205
- Wyngaard J C 1986 Measurement physics in probing the atmospheric boundary layer (ed.) D H Lenschow (Boston, Massachusetts, USA: AMs), pp. 5–18
- Yokoyama O, Gamo M and Yamamoto S 1977 On the turbulence quantities in the atmospheric mixing layer; *J. Meteorol. Soc. Jpn.*, **55** 182–192

Atmospheric surface layer parameters during different phases of monsoon over Varanasi from MONTBLEX-90

D V VISWANADHAM and A N V SATYANARAYANA

Department of Geophysics, Banaras Hindu University, Varanasi 221 005, India

Abstract. The fast and slow response data (8 Hz and 1 Hz respectively), obtained from the MONTBLEX-90 programme, are analysed for computing various surface layer parameters and the fluxes of sensible heat and momentum. In the present paper these fluxes, the Monin-Obukhov length scale (L), the turbulent kinetic energy (TKE), and the intensity of turbulence (σ_w) over Varanasi have been computed during different phases of monsoon such as dry, weak, moderate and active. Typical days are chosen for studying the above-mentioned parameters.

Keywords. Surface layer; TKE; sensible heat flux.

1. Introduction

The first few tens of meters of the atmosphere, commonly referred to as the surface layer, where most of the interaction takes place between the earth's surface and the overlying atmosphere, has attracted a lot of attention during the last several decades not only because it can be probed thoroughly, but in view of its importance in various exchange processes and its distinct characteristics. This surface layer acts as the main link between the boundary forcings at the surface and the atmosphere above it consisting of the mixed layer and free atmosphere. The energy for the main driving force of the atmosphere is derived mainly from the surface, particularly heat in different forms.

One of the most important features of the monsoon is the presence of a semi-permanent system known as the monsoon trough in the Indo-Gangetic belt normally extending from the Head of the Bay of Bengal to Pakistan, which accounts for rainfall in this part of the country. If the trough is active, low pressure systems such as depressions are generated in the Head of the Bay and move along the trough bringing copious rainfall. It is of interest to study the fluxes and the characteristics of the surface layer during different phases of the monsoon. Some of the earlier studies on the atmospheric surface layer are Businger *et al* (1971), Pruitt *et al* (1973), Champagne *et al* (1977), Holt and Sethuraman (1985) etc., on various aspects of computing the surface layer fluxes and other parameters. In the present paper the fluxes of sensible heat and momentum, the Monin-Obukhov length scale and the intensity of turbulence over Varanasi using fast and slow response data obtained from MONTBLEX-90 during various phases of the monsoon have been studied.

2. Site description

The tower, which is a triangular open lattice structure for free passage of air, is installed in a large agricultural farm at the BHU campus. The farm consists of several fields of

crops of different varieties. Adjacent to the field is a runway extending from the eastern side of the tower. The prevailing wind direction during the monsoon is mostly from SE and S, and sometimes from NW. There is almost an uninterrupted fetch of more than a kilometre in the prevailing sectors, i.e., from West to East through the South. In the NE sector there are, however, trees at a distance of more than 300 m. The receiving unit is located at a distance of 75 m from the western side of the tower. The height of the hut in which the receiving unit was kept is only around 2 m and hence cannot be an obstruction to the observations. The varieties of crops grown had heights of up to 1 m. The site as a whole can be considered one of the best available in Varanasi.

3. Data

The fast response data (8 Hz) were acquired using a sonic anemometer (at 4 m) and a Gill Propellor (at 15 m). The fast response data were collected three-hourly, i.e., at 0530, 0830, 1130, 1430, 1730 and 2330 hrs, for 10 minutes duration. The slow response data (1 Hz) at 1 m, 4 m, and 30 m consist of wind speed, temperature and relative humidity. For the present study, five days i.e., 6th, 27th and 28th July and 18th and 19th August 1990 were chosen.

4. Quality check

Before using the raw fast response data for the final analysis, caution should be exercised since they contain noise in the form of unusually high and low values. So the data are conditioned so as to be usable for statistical purposes since the present study concerns the statistical properties of turbulent quantities. The conditioning has been done as follows.

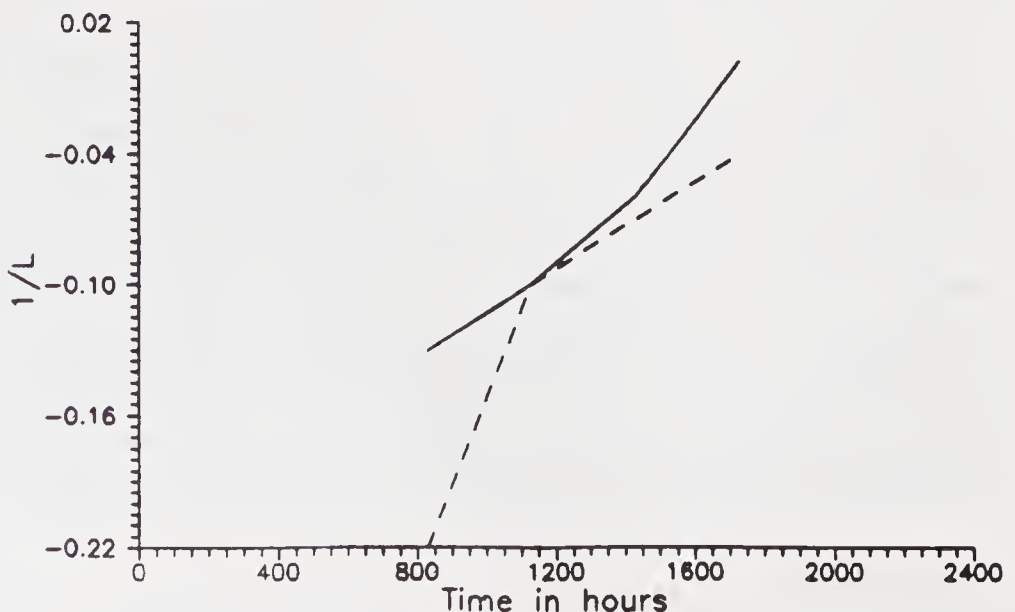


Figure 1. Diurnal variation of $1/L$ on 6th July, 1990; 1–4 m layer (solid line), 4–30 m layer (dashed line).

First a physical check of the whole data set, i.e., for 10 minutes duration, has been made. Any unusual or spurious spikes are removed and replaced by a limited value, taken at par with the highest among other fluctuations. Then its standard deviation is determined. Any individual value falling within ± 3 standard deviations from the mean is retained and the rest are replaced by mean ± 3 standard deviations. Wherever trends are noticed in the data set, they are removed by detrending the data with the least squares technique (Stull 1988) so as to ensure the quasi-random behaviour of turbulence.

The spectral densities of some turbulent parameters have been computed with the auto-correlation technique for the complete data set by the method of Blackman and Tukey (1958). A plot is made for the frequency vs. spectral density on a log-log paper. The best fit lines are obtained to see the general agreement. The analysis is carried out for all the fast data components. (Viswanadham and Satyanarayana 1992). This is one of the quality checks made to ensure the validity of the experimental data. Those cases where the power is between -1.3 and -1.8 only have been retained. There were very few data sets which differed significantly from universality and such data sets are ignored.

5. Methodology

5.1 Flux computation using fast response data

The fluxes from the high frequency data can be determined by the eddy correlation technique.

The fluxes have been computed from the following formulae.

$$\text{momentum flux (MF)} = \rho U_*^2 N \text{ m}^{-2} \quad (1)$$

$$\text{sensible heat flux (SHF)} = -\rho C_{pd}(1 + 0.81q)U_*\theta_* \text{ W m}^{-2}. \quad (2)$$

Where

$$U_* = (\overline{u'w'^2} + \overline{v'w'^2})^{1/4},$$

$$\theta_* = -\overline{w'\theta'}/U_*.$$

The Monin-Obukhov length scale (L) can be obtained as follows.

$$L = TU_*^2/gk\theta_* \text{ (m)}.$$

The turbulent intensity is

$$\sigma_w = (w'^2/N)^{1/2} \text{ ms}^{-1}$$

where N is the number of sample points.

The sonic anemometre data have been sparse due to the non-working of the sensor much of the time. Therefore, only one day i.e., 27th July, is taken to compute surface layer parameters.

5.2 Flux computation using slow response data

Using the slow response data the U_* and θ_* can be computed in the following way. The dimensionless wind shear (ϕ_m) and temperature shear (ϕ_h) are given by $(kz/U_*)(\partial U/\partial z)$ and $(kz/\theta_*)(\partial T/\partial z)$ respectively. These shears are strongly related to the stability. The final relations for the parameters are the following.

For unstable cases:

$$U_* = (U_2 - U_1)/(1/k \ln(z_2/z_1) - \psi_1).$$

$$\theta_* = (T_2 - T_1)/(0.74 \ln(z_2/z_1) - \psi_2).$$

For stable cases:

$$U_* = (U_2 - U_1)/(1/k \ln(z_2/z_1) + 4.7z/L).$$

$$\theta_* = (T_2 - T_1)/(0.74 \ln(z_2/z_1) + 4.7z/L).$$

Here

$$\psi_1 = 2 \ln((1+x)/2) + \ln((1+x)^2/2) - 2 \tan^{-1}x + \pi/2,$$

$$x = (1 - 15z/L)^{1/4} = 1/\varphi_m.$$

$$\psi_2 = \ln(1 + (1 - 9z/L)^{1/2}/2).$$

The three parameters U_* , θ_* and L are not independent and each is a function of at least one other parameter, so their determination requires an iteration technique. The initial guess needed to compute the parameters U_* and θ_* is obtained from the neutral profile. These are substituted in the expression to compute L . The new L is substituted to compute both U_* and θ_* which in turn are made use of to compute new L . This process of iteration is continued till convergence for L is attained. The convergence limit is kept at the fifth decimal. Making use of the gradient observations, the above parameters have been computed for each of the data sets.

Using these parameters the fluxes from the slow response data are computed by (1) and (2). These fluxes are computed for the layers 1–4 m and 4–30 m.

6. Delineation of monsoon phases

The conventional delineation into active and break phases gives rise to some inconsistencies over Varanasi. For example during IOP (Intensive Observational Period) the monsoon was rather weak in some cases. Hence based on the actual observation of rainfall and cloud amount a simple criterion is evolved to delineate the activity of monsoon into four cases viz., dry (D), weak (W), moderate (M) and active (A). Table 1

Table 1. Categorization of various monsoon phases.

Rainfall(mm)	Cloud amount (octas)				
	0	≤2	2–4	4–6	6–8
0	D	D	W	M	A
0–10	—	W	W	M	A
> 10–20	—	W	M	M	A
> 20–30	—	M	M	A	A
> 30–40	—	M	A	A	A
> 40	—	A	A	A	A

D – Dry; W – Weak; M – Moderate; A – Active.

Table 2. Surface layer parameters from sonic data on 27th July.

Time	MF (Nm ⁻²)	SHF Wm ⁻²	U_* ms ⁻¹	θ_* °K	L m	σ_w ms ⁻¹
1030	0.0566	33.00	0.2126	-0.1294	-26.76	0.3138
1330	0.5868	19.44	0.6852	-0.0236	-1515.53	0.1875
1430	0.1125	82.44	0.3000	-0.2290	-30.00	0.2760
2030	0.0118	2.28	0.0979	-0.0194	-37.50	0.1119
2130	0.0131	-1.68	0.1023	0.0131	58.14	0.1287

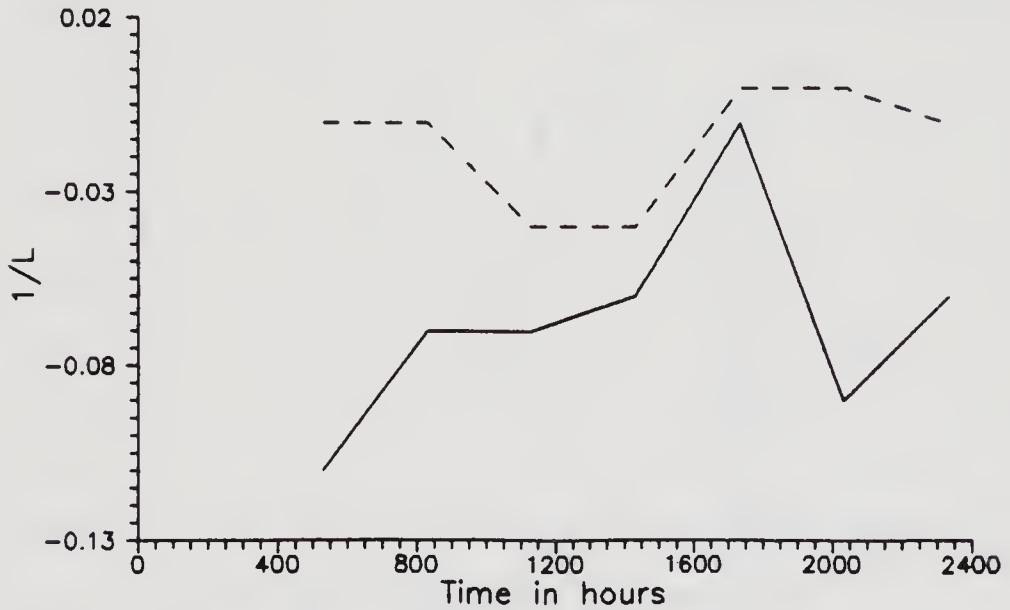


Figure 2. Diurnal variation of $1/L$ on 28th July, 1990; 1–4 m layer (solid line), 4–30 m layer (dashed line).

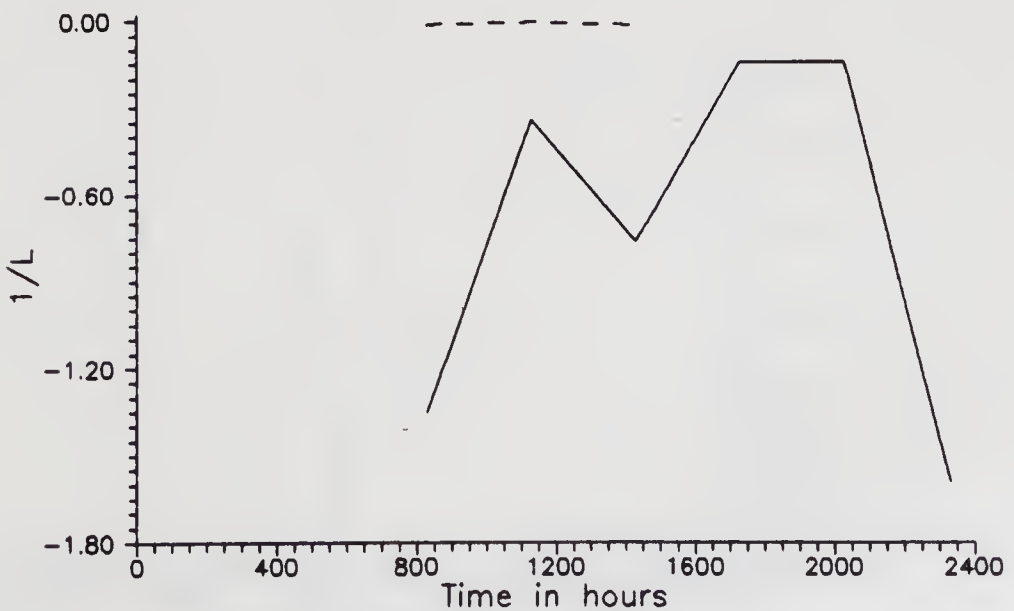


Figure 3. Diurnal variation of $1/L$ on 19th August, 1990; 1–4 m layer (solid line), 4–30 m layer (dashed line).

shows the details. These are evolved for studying only the micrometeorology over Varanasi. Accordingly 6th July represents the moderate and 27th and 28th July the active phases; 18th and 19th August represent the dry case.

7. Results and discussion

Table 2 shows the surface layer parameters obtained at 4 m level from the sonic anemometer during the active phase. The diurnal variation is visible although the magnitudes do not differ significantly.

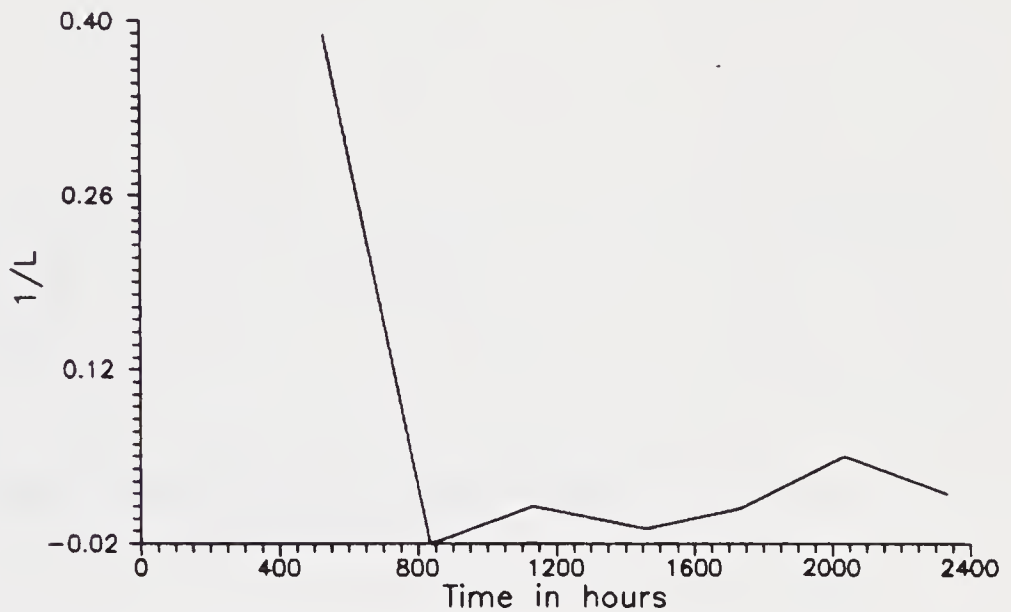


Figure 4. Diurnal variation of $1/L$ on 6th July, 1990 at 15 m height.

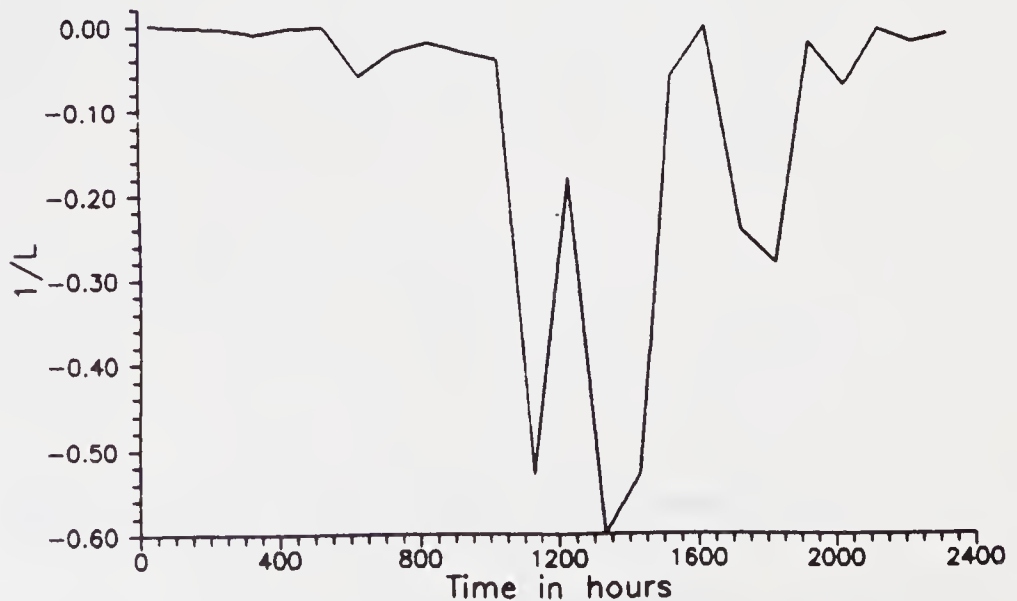


Figure 5. Diurnal variation of $1/L$ on 28th July, 1990 at 15 m height.

The different parameters are discussed hereunder for both the layers and at 15 m level.

7.1 Monin-Obukhov length scale

Figures 1 to 3 indicate the diurnal variation of $1/L$ on 6th July, 28th July and 19th August respectively, for the layers 1–4 m and 4–30 m. Figures 4 to 6 depict $1/L$ at 15 m height for the same dates respectively.

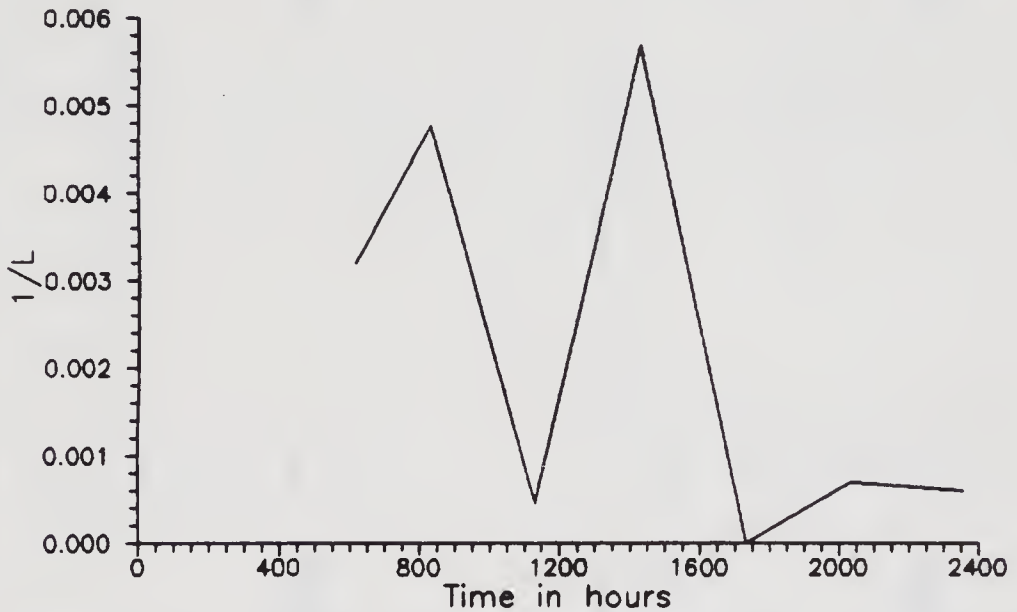


Figure 6. Diurnal variation of $1/L$ on 19th August, 1990 at 15m height.

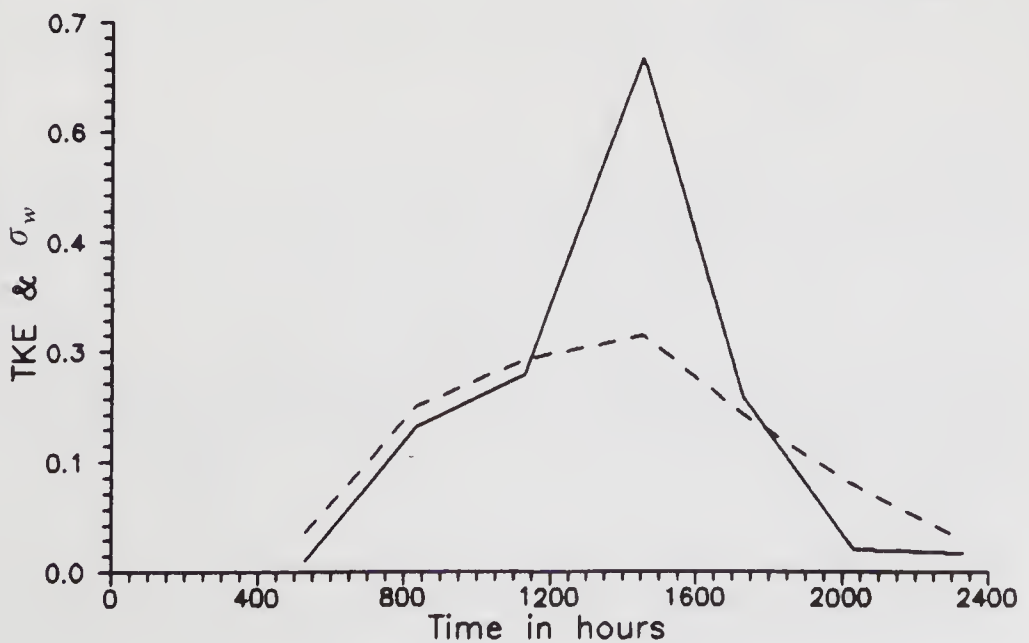


Figure 7. Diurnal variation of TKE (solid line) and σ_w (dashed line) on 6th July, 1990 at 15m height.

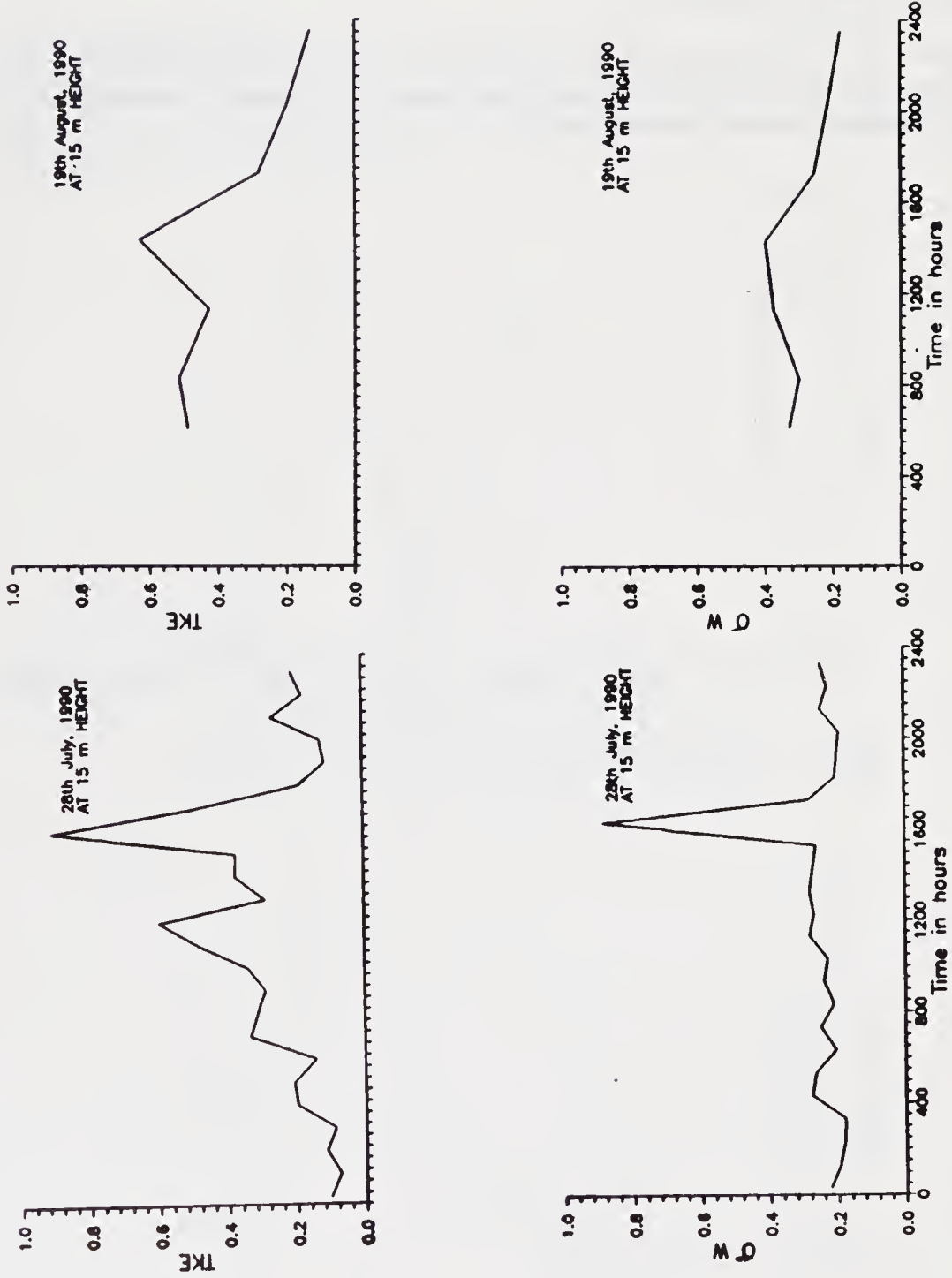


Figure 8. Diurnal variation.

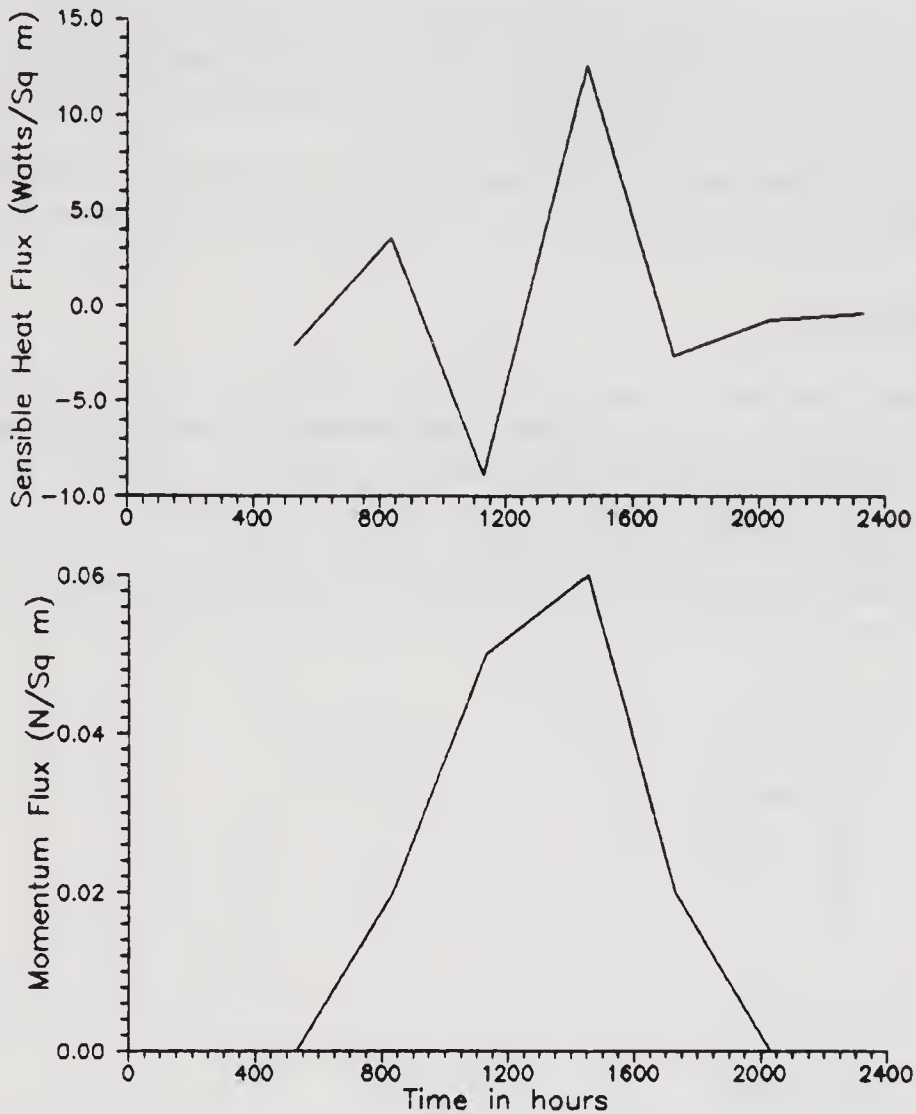


Figure 9. Diurnal variation of fluxes on 6th July, 1990 at 15 m height.

July 28th is considered as part of an active period: one can see the near-neutral conditions prevailing during both day and night. July 6th is neither dry nor active and hence is taken to represent moderate monsoon activity during which the diurnal variation shows a sort of trend tending to attain neutrality from unstable conditions. However the case of 19th August, typical of a dry spell, clearly shows a high degree of instability at least in the 1–4 m layer, although it tends to attain neutrality. The free convective case at 2400 hrs is inconsistent and hence inexplicable. The upper layer, however, shows neutral stability. Examination of the three cases at 15 m reveals very little diurnal variation. Whenever the monsoon is active diurnal variation diminishes, and whenever there is a break or a dry spell it becomes prominent, since in the latter unstable conditions prevail during day-time due to clear skies and stable conditions during night due to clear skies and calm conditions. However, during the active phase, the sky is over-cast and moist winds are present, both of which tend to stabilize the atmosphere from extremes i.e., from instability to less instability and from stable to less stable conditions. This is one of the important points to be borne in mind, that the

activity of the monsoon has a bearing on the surface layer activities at least on stability. The fact that $1/L$ is influenced by the activity of the monsoon suggests the general conclusion that all the activities in the surface layer, particularly energy exchange processes, do get influenced by monsoon activity.

On 19th August at the 15 m level, the conditions obtained from the Gill propeller do coincide with what was observed in the 4–30 m layer centring around 15 m.

7.2 TKE and σ_w

The diurnal variation of these two parameters at the 15 m level, which indicates the turbulence intensity, is shown in figures 7 and 8 respectively for the days mentioned already.

Both parameters exhibit striking variations. In general, the tendency is that relatively high values are noticed during night-time. Whether the monsoon is active or not, the parameters do not show any significant variation. This may be due to the fact that windy conditions induce turbulence during the active phase, and convective conditions during the inactive phase; therefore, there is every possibility of turbulence intensity

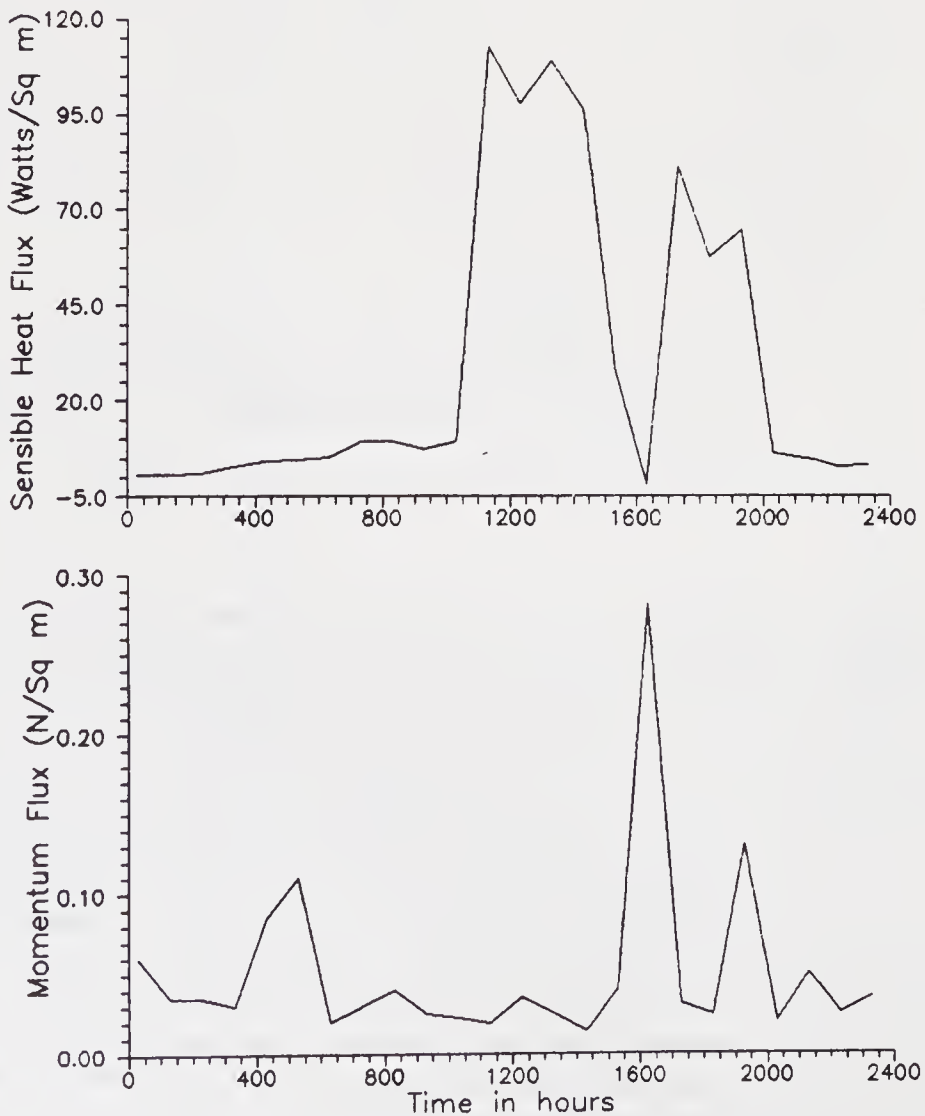


Figure 10. Diurnal variation of fluxes on 28th July, 1990 at 15 m height.

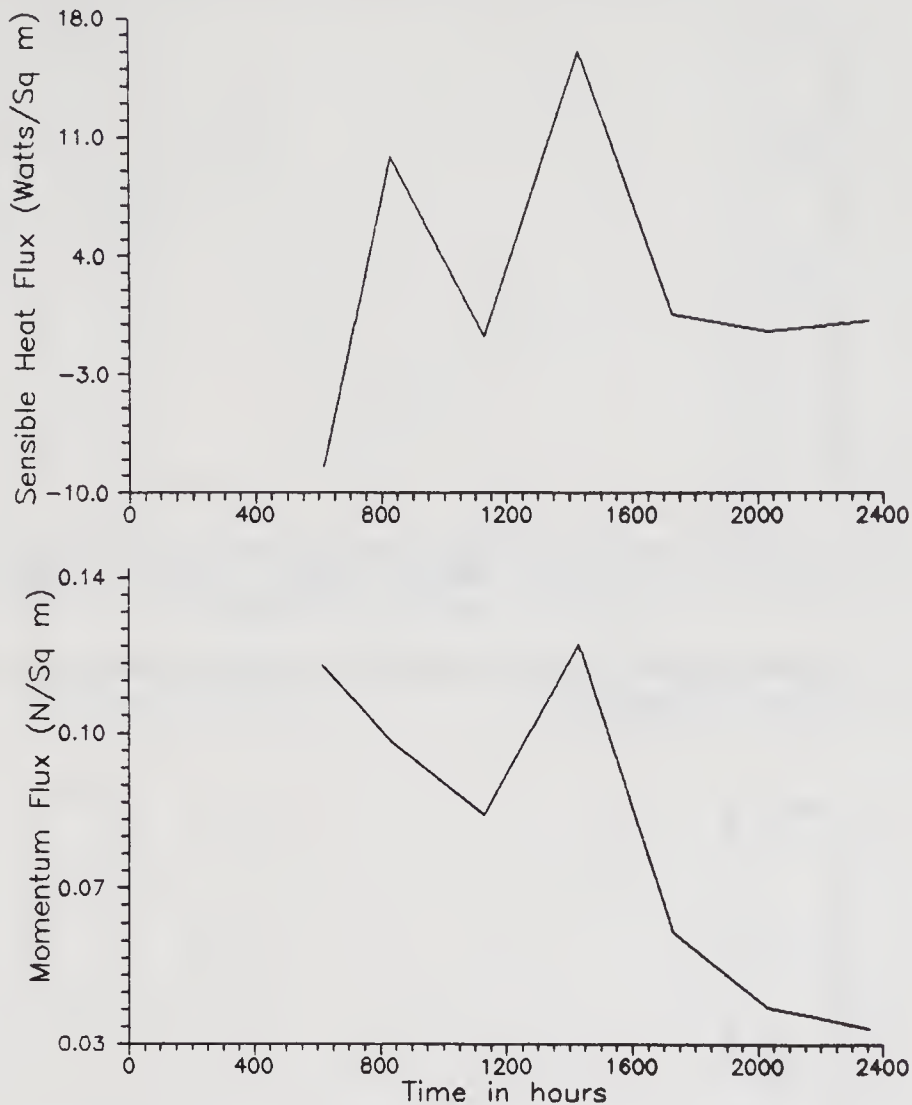


Figure 11. Diurnal variation of fluxes on 19th August, 1990 at 15 m height.

and TKE varying little with the various phases of the monsoon. As mentioned already the diurnal variation is very striking, which can be attributed to individual hourly activities. One important point that comes out of this study is the quasi-randomness of turbulence not only within these micro limits of 10 minutes duration, but even on an hourly basis. In the present study there is a clear revelation that irrespective of day or night, hour-to-hour variations are quite significant although one can visualize a general trend showing relatively greater turbulence during day-time.

7.3 MF and SHF at 15 m height

Figures 9 to 11 depict the diurnal variation on 6th July, 28th July and 19th August respectively.

On 6th July, MF is highest and shows a typical diurnal variation with the peak in the afternoon hours and lowest values during night-time. SHF on the other hand shows very little variation.

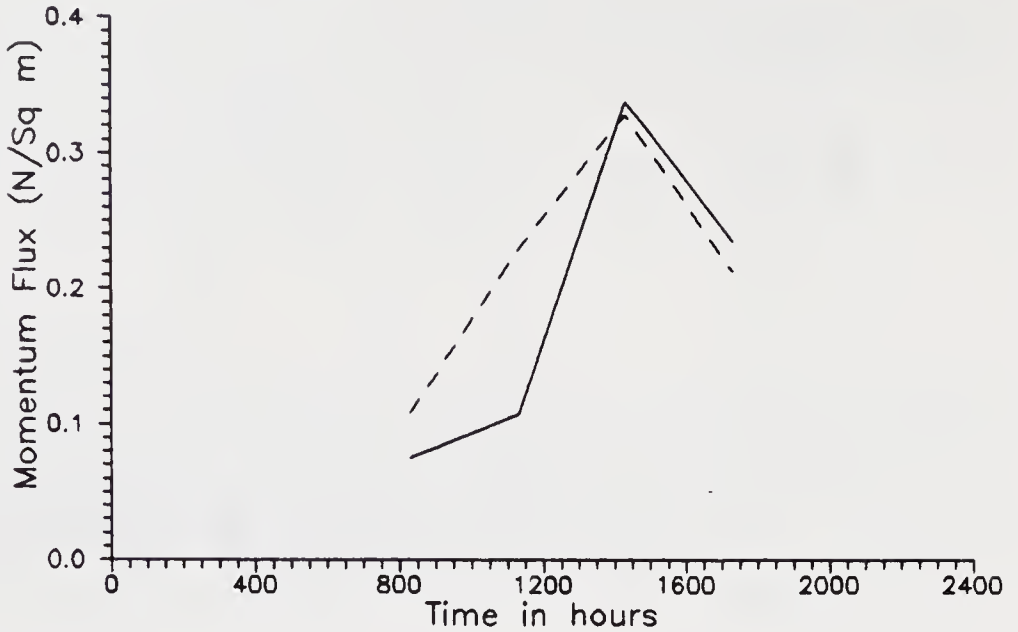


Figure 12. Diurnal variation of momentum flux on 6th July, 1990; 1-4 m layer (solid line), 4-30 m layer (dashed line).

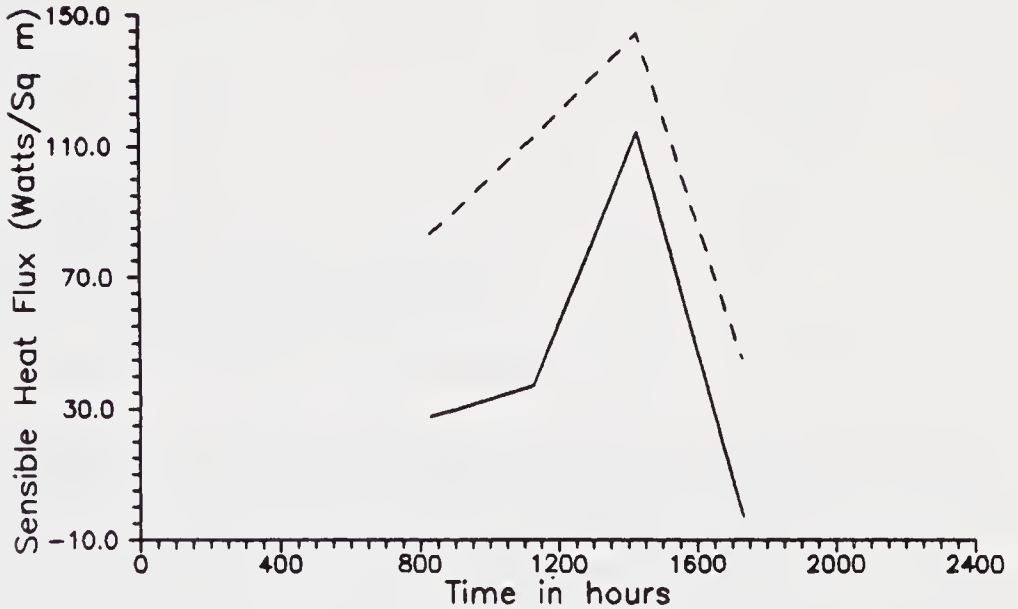


Figure 13. Diurnal variation of sensible heat flux on 6th July, 1990; 1-4 m layer (solid line), 4-30 m layer (dashed line).

On 28th July, MF shows a distinct variation with several peaks. From 1600 to 2400 hrs, the variation is marked in MF. In SHF also, one finds variation from around 1100 to 2000 hrs, while it is invariant during the rest of the time. This is one day when hourly observations are available.

On 19th August, SHF is low and positive. MF decreases generally from early morning hours to midnight, except for a sudden increase at 1300 hrs.

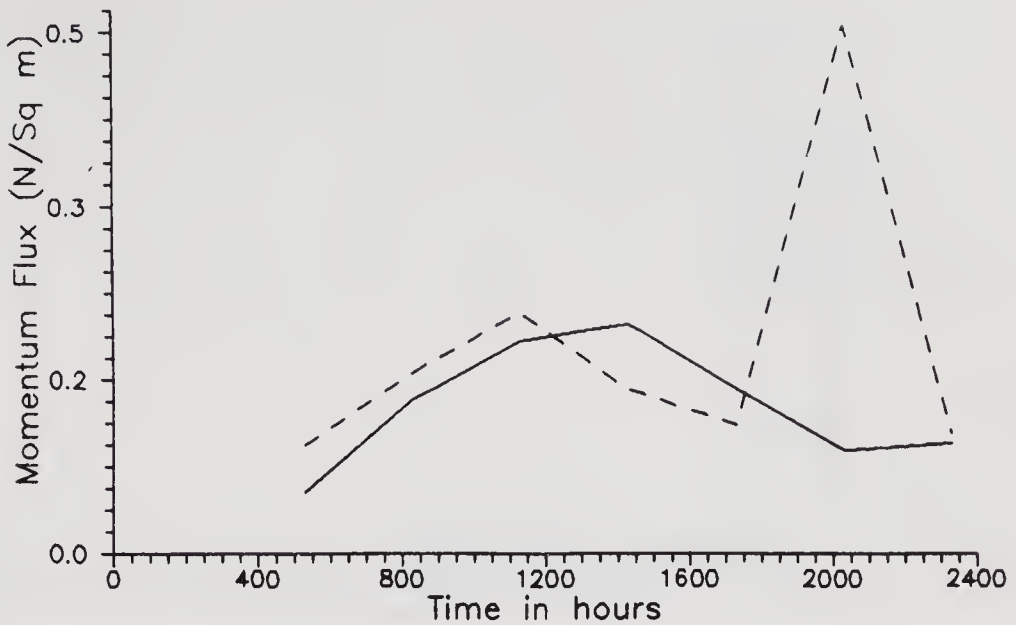


Figure 14. Diurnal variation of momentum flux on 28th July, 1990; 1–4 m layer (solid line), 4–30 m layer (dashed line).

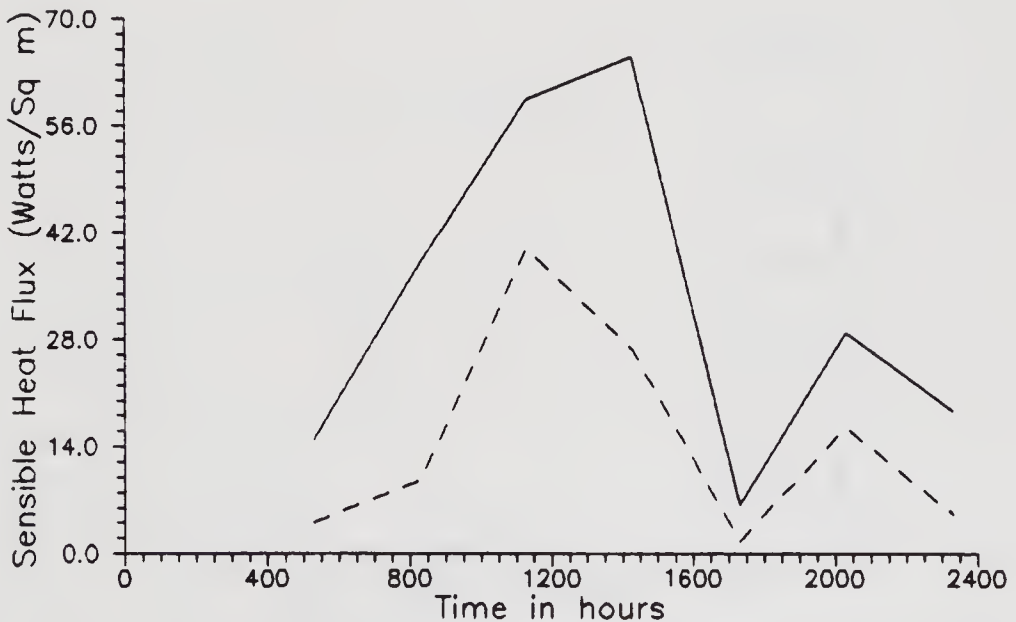


Figure 15. Diurnal variation of sensible heat flux on 28th July, 1990; 1–4 m layer (solid line), 4–30 m layer (dashed line).

7.4 MF and SHF in 1–4 m and 4–30 m layers

Figures 12 and 13 show the diurnal variation on 6th July. MF variation is pronounced in both the layers with the peak being observed at 1300 hrs. SHF also exhibits similar variation. Upward fluxes are recorded almost all the time.

Figures 14 and 15 depict the diurnal variation on 28th July. MF clearly shows the diurnal variation on this day with higher values during day-time and low values during night except for the peak at 2000 hrs in the upper layer. This peak is not very consistent,

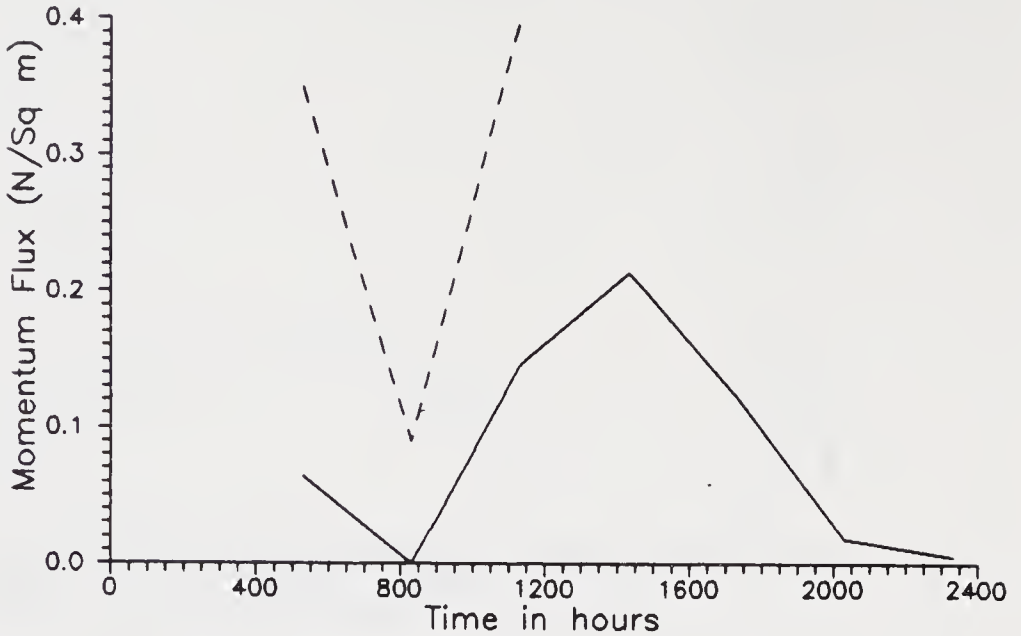


Figure 16. Diurnal variation of momentum flux on 18th August, 1990; 1–4 m layer (solid line), 4–30 m layer (dashed line).

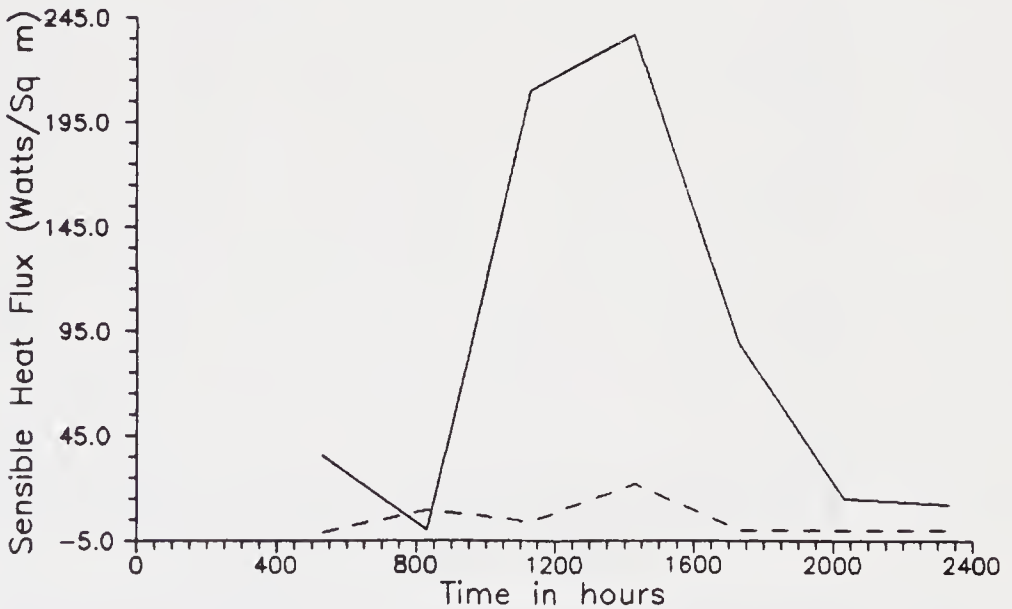


Figure 17. Diurnal variation of sensible heat flux on 18th August, 1990; 1–4 m layer (solid line), 4–30 m layer (dashed line).

keeping the time of the observation in view. The maximum value is around 0.2 N/m^2 barring this unusual peak. SHF also shows diurnal variation but the values are below 60 W/m^2 in the upper layer and below 40 W/m^2 in the lower layer.

Figures 16 and 17 show the variation on 18th August. One finds a strong diurnal variation in the 1–4 m layer. Not many observations are available in the upper layer. The SHF, however, shows strong diurnal variation in the lower layer and very little in the upper layer. Very high SHF is noticed on this day.

It can be seen that whenever the monsoon is active the SHF shows little diurnal variation and also the values are low. If the monsoon is moderate or weak SHF is considerably more. Within the surface layer, differences in fluxes are noticed.

The overall study so far indicates that the stability parameter ($1/L$) shows its relation with the activity of the monsoon. The turbulence intensity parameters such as TKE and σ_w do not show any significant variation with the activity of the monsoon.

The differences in the two layers within the surface layer are significant. Usually a 10% variation of parameters is observed. However, in the present case the variation is significant within the surface layer.

Acknowledgements

The financial support by DST, Govt. of India for carrying out this work is gratefully acknowledged.

List of Symbols

ρ	= Density of air.
g	= Acceleration due to gravity.
k	= Von Karman constant.
C_{pd}	= Specific heat of dry air at constant pressure.
q	= Specific humidity.
$\overline{u'w'}$	= Covariance between u' and w' .
$\overline{v'w'}$	= Covariance between v' and w' .
$\overline{w'\theta'}$	= Covariance between w' and θ' .
U_*	= Friction velocity.
θ_*	= Friction temperature.
L	= Monin-Obukhov length scale.
T	= Atmospheric temperature.
z	= Height above the surface.

References

- Blackman R B and Tukey J W 1958 *The measurement of power spectrum*, (New York: Dover Publications) 190 pp
- Businger J A, Wyngaard J C, Izumi Y and Bradley E F 1971 Flux-profile relationships in the atmospheric surface layer; *J. Atmos. Sci.* **28** 901–917
- Champagne F H, Friche C A and Lague J C 1977 Flux measurements, flux estimation techniques and fine scale turbulence measurements in the unstable surface layer over land; *J. Atmos. Sci.* **30** 568–581
- Holt T and Sethuraman S 1987 A comparison of the significant features of the marine boundary layer over the east central Arabian Sea and north central Bay of Bengal during MONEX-1979; *Mausam* **38** 171–176
- Pruitt W O, Morgan D L and Lourence F J 1973 Momentum and mass transfers in the surface boundary layer; *Q. J. R. Meteorol. Soc.* **99** 370–376

- Stull R B 1988 *An Introduction to Boundary Layer Meteorology* (Dordrecht/Boston/London: Kluwer Publishers) pp 666
- Viswanadham D V and Satyanarayana A N V 1992 Preliminary studies on the surface layer parameters for selected cases over Banaras as revealed by MONTBLEX-90; *Proc. of work shop on preliminary scientific results of MONTBLEX, DST*, 69–82

Fluxes of heat and momentum over sea surface during the passage of a depression in the north Bay of Bengal

S SIVARAMAKRISHNAN, M N PATIL and K G VERNEKAR

Indian Institute of Tropical Meteorology, Pune 411 008, India

Abstract. Time variation of surface fluxes of heat, moisture and momentum over a sea station (20°N, 89°E) in the north Bay of Bengal has been computed by profile method for the period 18th – 25th August 1990 using meteorological data of MONTBLEX-90 from ORV *Sagarkanya*. The fluxes showed synoptic and diurnal variations which are marked during depression (20th – 21st August) compared to their variation prior to and after this period. Variations of heat and water vapour fluxes were in phase. Night time fluxes are relatively high compared to day time. Average momentum transfer during depression was two to three times large. Variations in Bowen ratio were relatively large during day time. During depression, it varied between 0.2 in day time and about 0.3 at night and in the undisturbed period between – 0.1 and 0.2 during day time and 0.2 and 0.25 at night. The study shows that the assumption $C_D = C_H = C_E$ of the exchange coefficients normally used in estimating the fluxes by the bulk aerodynamic method is not appropriate because $C_H/C_D \approx 2$, $C_E/C_D \approx 1.5$ and $C_H/C_E \approx 1.4$.

Keywords. Flux; sea surface; depression; exchange coefficient; Bowen ratio; monsoon.

1. Introduction

Study of surface fluxes during a monsoon disturbance in the summer monsoon in the Indian subcontinent is of interest to both micro- and meso-scale meteorologists. In this paper our objective is to estimate and study the variation of the fluxes of sensible and latent heat, water vapour and momentum for the period 18th – 25th August 1990 from the data collected during observations carried out onboard ORV *Sagarkanya* in the course of the Monsoon Trough Boundary Layer Experiment (MONTBLEX). During August 20th – 21st, a depression passed over the station. The vessel was moored at a sea station (20°N, 89°E) and 3-hourly observations were recorded by the National Institute of Oceanography, Goa, and the data provided to us for analysis.

2. Instrumentation

Surface meteorological observations on wind, temperature and atmospheric pressure were obtained using a wind vane and anemometer (electrical type) installed at 22.6 m above sea level on the radar deck of the ship. Dry and wet bulb temperatures were measured at the deck level (9 m above msl) using an Assman type psychrometer. A bucket thermometer was used to measure the sea surface temperature. In addition the cloud amount and type were observed.

3. Method of analysis

The profile technique has been used to estimate the surface fluxes from wind and temperature data. The temperature difference and measurement of wind speed at only one height combined with roughness length (assumed) over sea surface have been used as input to compute Businger's similarity functions. Numerical iteration procedure is used to compute the friction velocity u_* and temperature scale θ_* for $L = \infty$, L being the Monin-Obukhov length. Details of the profile method and iteration procedure are found in Berkowicz and Prahm (1982). This method is computationally quick and in practical applications needs only a very few steps to achieve the required accuracy. Moreover, wind speed and temperature need not be given at the same height as in other formulations of the profile method (Businger *et al* 1971; Bińkowski 1975; Louis 1979; Blanc 1982). It is argued (Berkowicz and Prahm 1982) that the error arising from the uncertainty in the determination of the roughness length Z_o will be smaller than the error resulting from measurements of wind speed differences when only one speed measured at a height Z such that $Z \gg Z_o$ is used to estimate the fluxes. A wide range of values for Z_o has been reported in the literature: Counihan (1975) has summarised Z_o for the adiabatic atmospheric boundary layer over different terrain types. Based on this we assume a value of $Z_o = 2$ cm over sea which seems plausible in disturbed weather.

4. Results and discussion

4.1 Meteorological conditions

Figures 1(a)–(d) depict the variation of sea surface temperature, surface pressure, wind speed and cloud amount respectively during August 18th–25th, 1990. The maximum SST was observed around 1430–1730 hrs and minimum around midnight to early morning during August 18th–24th. The minimum pressure was mostly observed at 1730 hrs while the maximum was around 1130–1430 and around 2330 hrs during the period. Maximum wind speed occurs around midnight on 21st August and in early morning/late evening on other days, while a minimum occurs around noon/afternoon during the observation period. Cloud amount was maximum around afternoon/evening hours, while it was minimum around midnight/early morning.

Figure 1(a) shows the diurnal and synoptic scale variation of SST (daily mean value indicated at noon of the day). It is observed that the SST shows a smooth synoptic scale variation by 0.2°C during the period. Variation of the order of one degree in SST is seen during intensification of the system (18th–19th August) into a depression. Mean SST decreases smoothly during 18th–22nd August and then rises during 23rd–25th August. Figure 1(b) shows the pressure variation during the period. Pressure is minimum on the evening of 20th August showing the formation of depression, and then rises sharply up to 23rd August showing diurnal oscillations thenceforth. Wind speed in figure 1(c) increases sharply during 18th–21st August, correlating with the pressure drop, and then falls rapidly after 21st–22nd August. The cloud amount in figure 1(d) shows a nearly overcast sky on 20th–21st August. It shows an oscillation between 4 and 6 octas at other times.

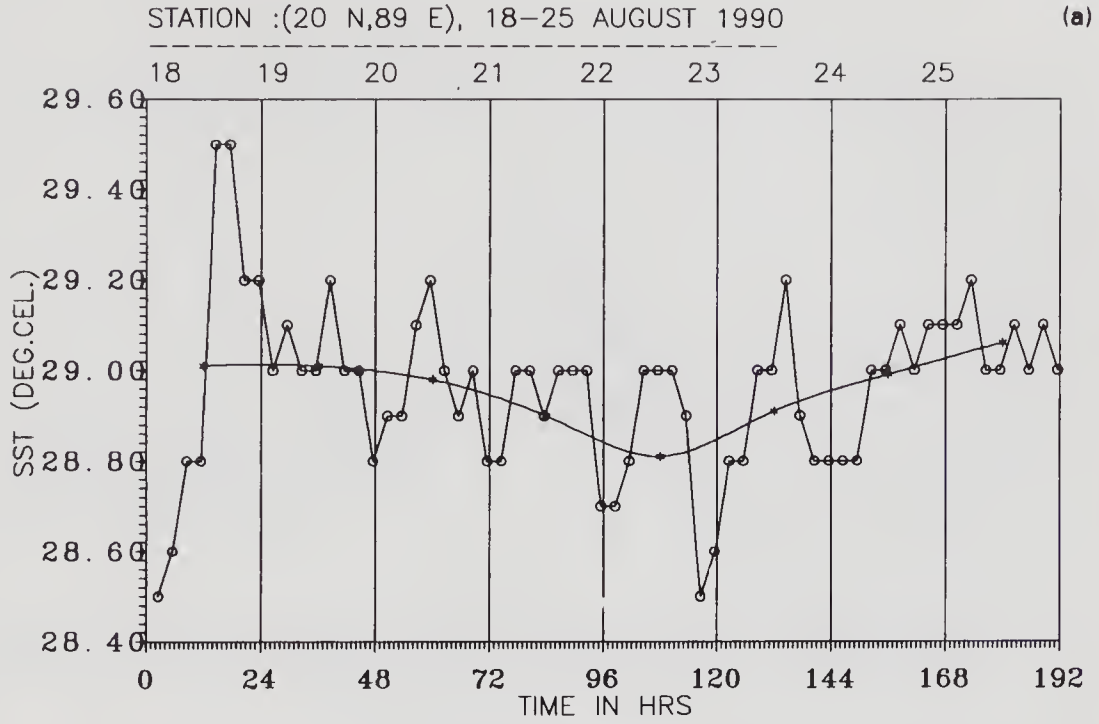


Figure 1(a). Time variation of sea surface temperature over the Bay of Bengal station during 18th - 25th August, 1990.

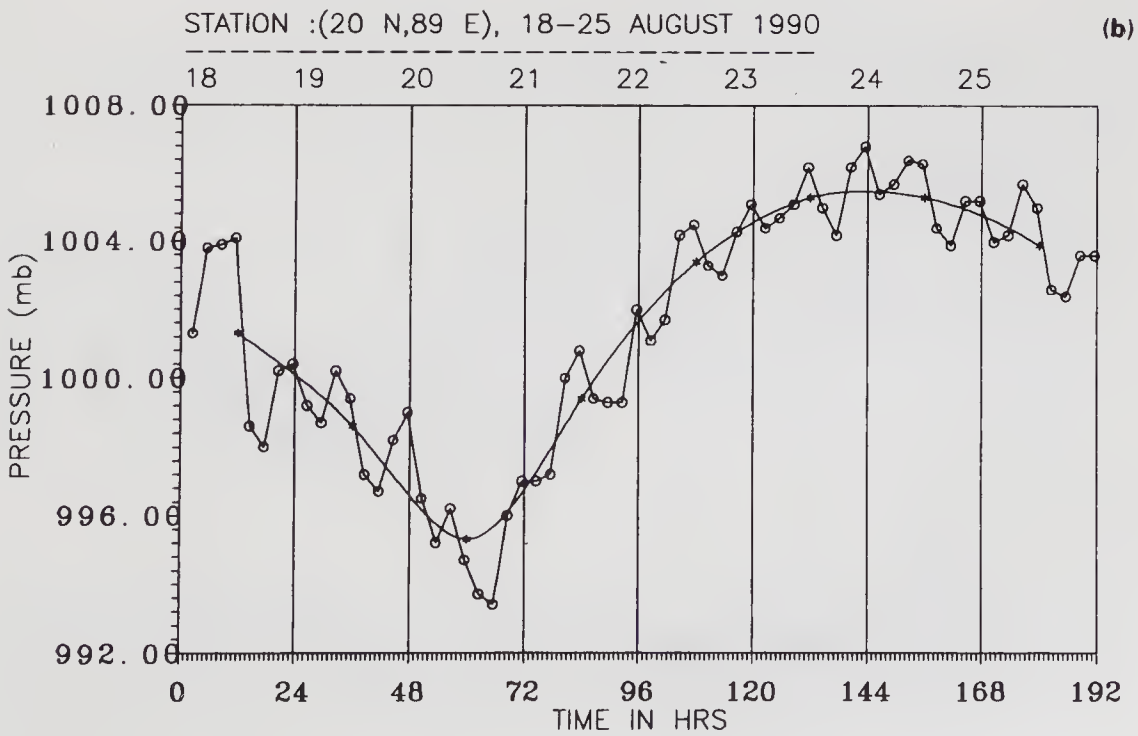


Figure 1(b). Same as in figure 1(a) for pressure.

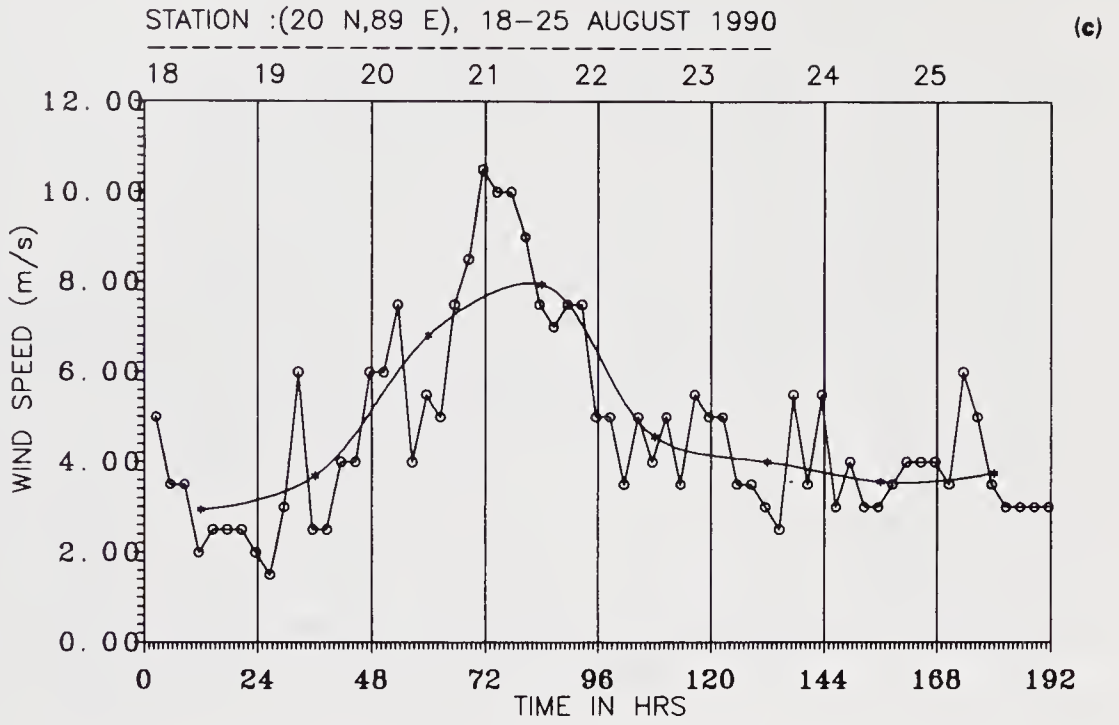


Figure 1(c). Same as in figure 1(a) for wind speed.

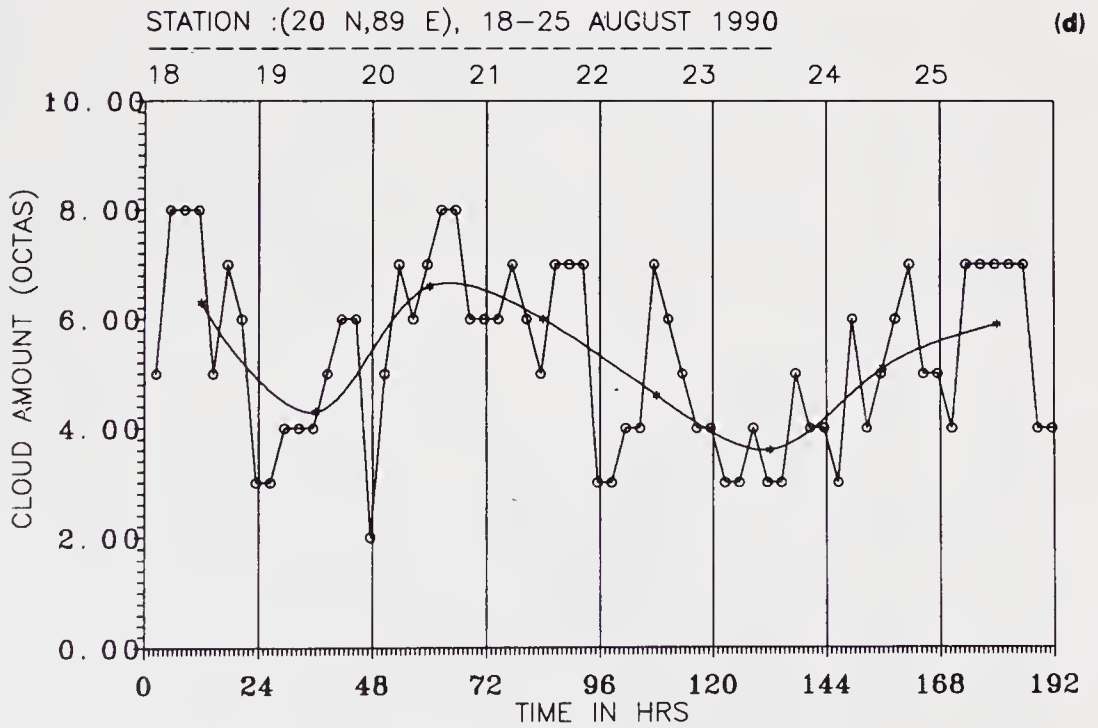


Figure 1(d). Same as in figure 1(a) for cloud amount.

4.2 Surface fluxes

Fluxes of sensible and latent heat, water vapour and momentum are shown in figure 2(a)–(d) respectively for the period (August 18th–25th). It is seen that the time variation of fluxes is nearly in phase. The fluxes of sensible and latent heat, water vapour and momentum were maximum during late evening to midnight and were minimum around noon.

All these fluxes depict a maximum around midnight of August 21st, when wind speeds are high (10 m/s). In figure 2(a)–(d) the fluxes show diurnal variations such that they increase consistently around midnight to early morning hours and decrease around noon or afternoon. Interestingly we observe a diurnal variation of fluxes over this sea station, which is about 150 miles away from the nearest coastal station (Paradeep). Daily mean variation of the fluxes (marked in figure at noon of the day) of sensible and latent heat and water vapour shows a sharp increase from August 19th, attaining a maximum on 20th–21st, then falling on 22nd–23rd, and remaining nearly constant thereafter. The momentum flux shows a steep rise from 18th August reaching maximum on 21st August, and then falls sharply on 22nd–23rd, remaining nearly constant thenceforth. In contrast to the normal feature over land, the fluxes over sea show a minimum around noon/afternoon hours during the entire period. Around 0830–1130 hrs, we observe that the stability of the surface layer as determined by Z/L ($Z = 9$ m) tends towards near neutral conditions. The condition on the whole (18th–25th August) is unstable during day and night; transitions to slightly stable conditions are seen in day time around 0830–1430 hrs IST. Night time instability is due to the sea surface being warmer than the air above. Figure 3 shows the time variation of Bowen ratio.

4.3 Energy exchange coefficients

The exchange coefficients, the heat exchange coefficient or Stanton number (C_H), the drag coefficient (C_D) and the moisture exchange coefficient or Dalton number (C_E) have been estimated from the mean daily fluxes of sensible heat, momentum and latent heat computed by the profile method. The mean C_H , C_D and C_E are estimated as 7.65×10^{-3} , 3.72×10^{-3} and 5.64×10^{-3} respectively during convective conditions. When these estimated mean exchange coefficients were used in the bulk aerodynamic method, it was found that the estimated heat fluxes nearly agree within 10–20% by both methods during 20th–25th August and differ by more than 40% on 18th and 19th August. The momentum flux by the bulk method is less by a factor of 1.2–1.4 compared to the profile method value during 20th–25th August, and by a factor of 1.4 and 1.6 on 18th and 19th August respectively.

4.4 Comparison of fluxes estimated by profile and bulk aerodynamic method

For the period under study, the daily mean fluxes of sensible and latent heat and momentum were estimated independently by Singh (1992) using the bulk aerodynamic method on the assumption that $C_D = C_H = C_E$ (Bunker 1976). These fluxes are compared with those estimated by the profile method and are shown in table 1.

The fluxes estimated by Singh (1992) using the bulk aerodynamic method are less in magnitude by a factor of about 4–10 for sensible heat, and 1.7–2.5 for latent heat, than

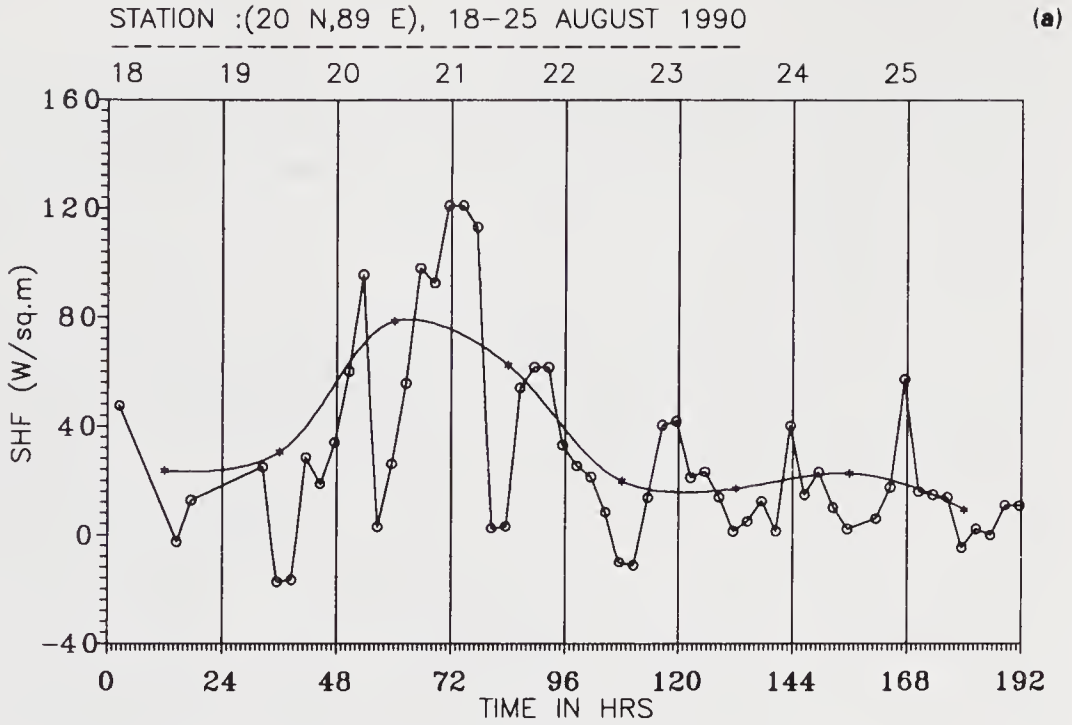


Figure 2(a). Time variation of sensible heat flux during 18th – 25th August, 1990.

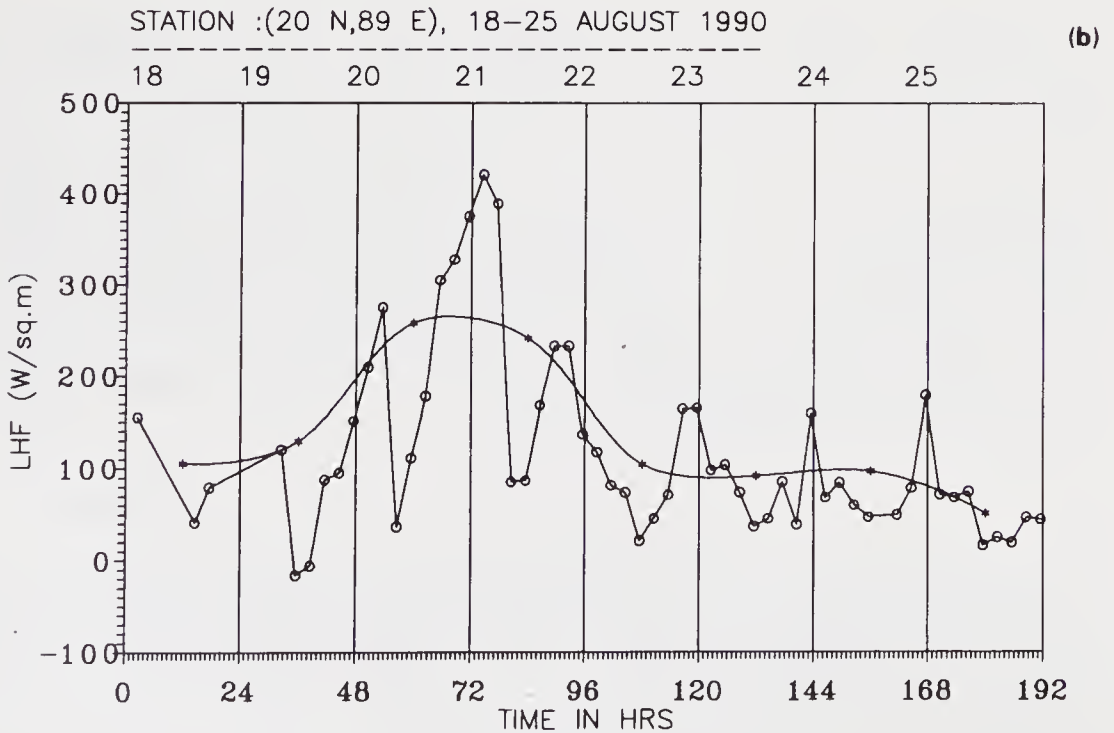


Figure 2(b). Same as in figure 2(a) for latent heat flux.

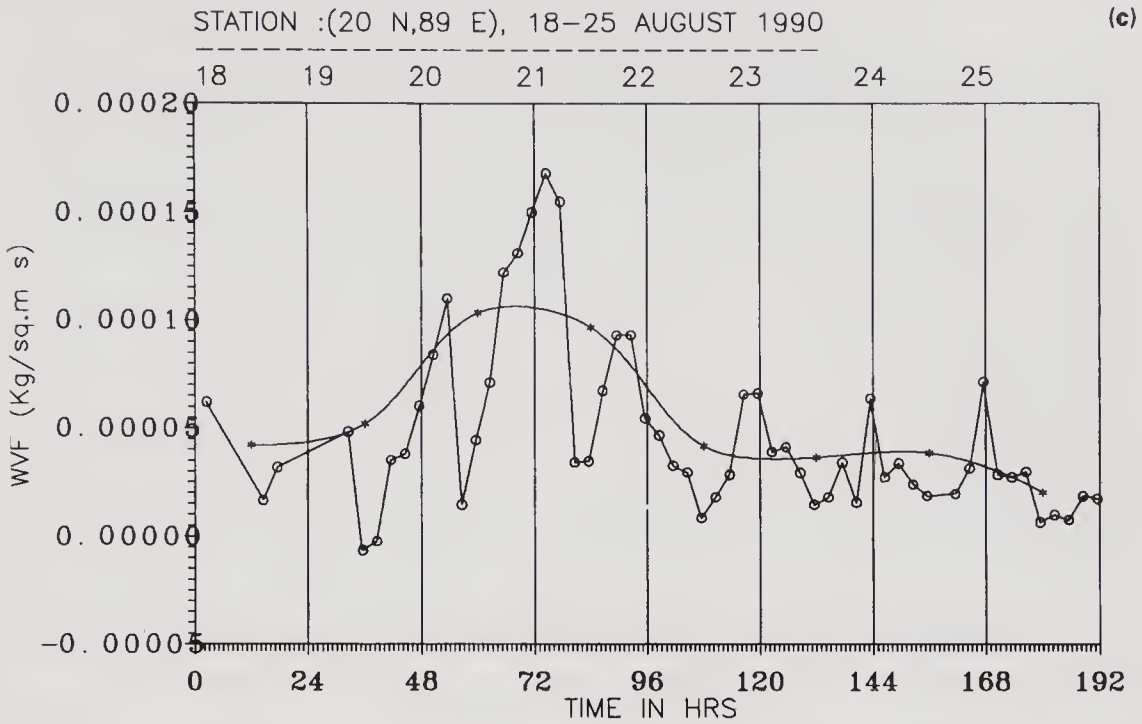


Figure 2(c). Same as in figure 2(a) for water vapour flux.

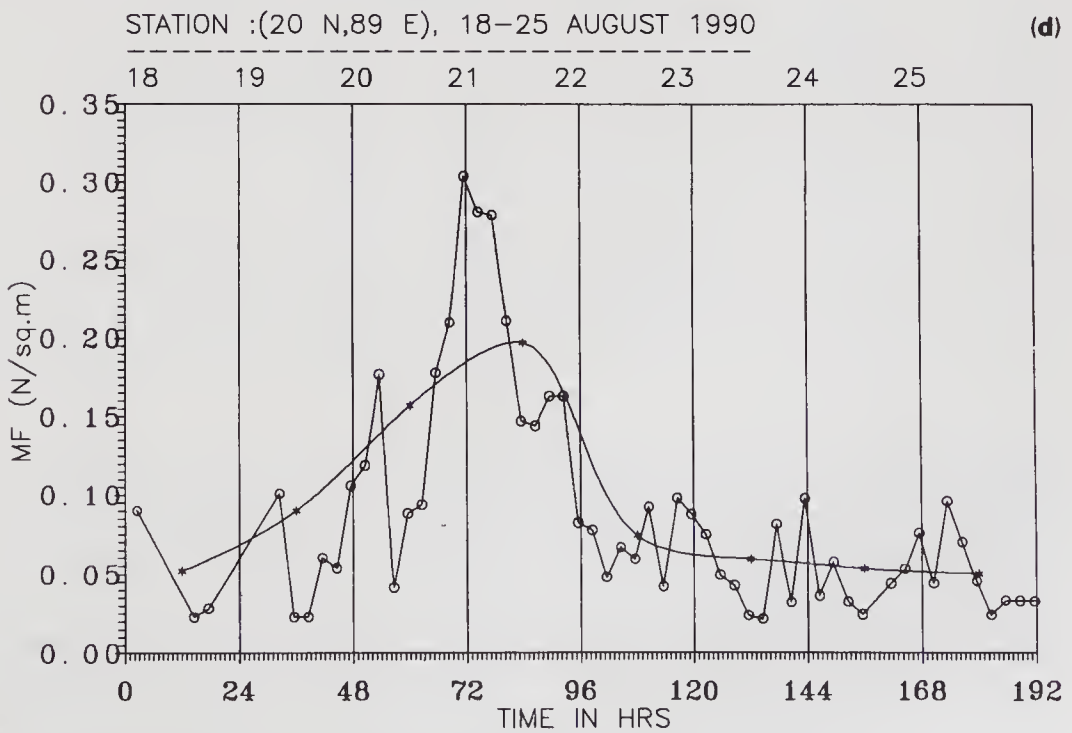


Figure 2(d). Same as in figure 2(a) for momentum flux.

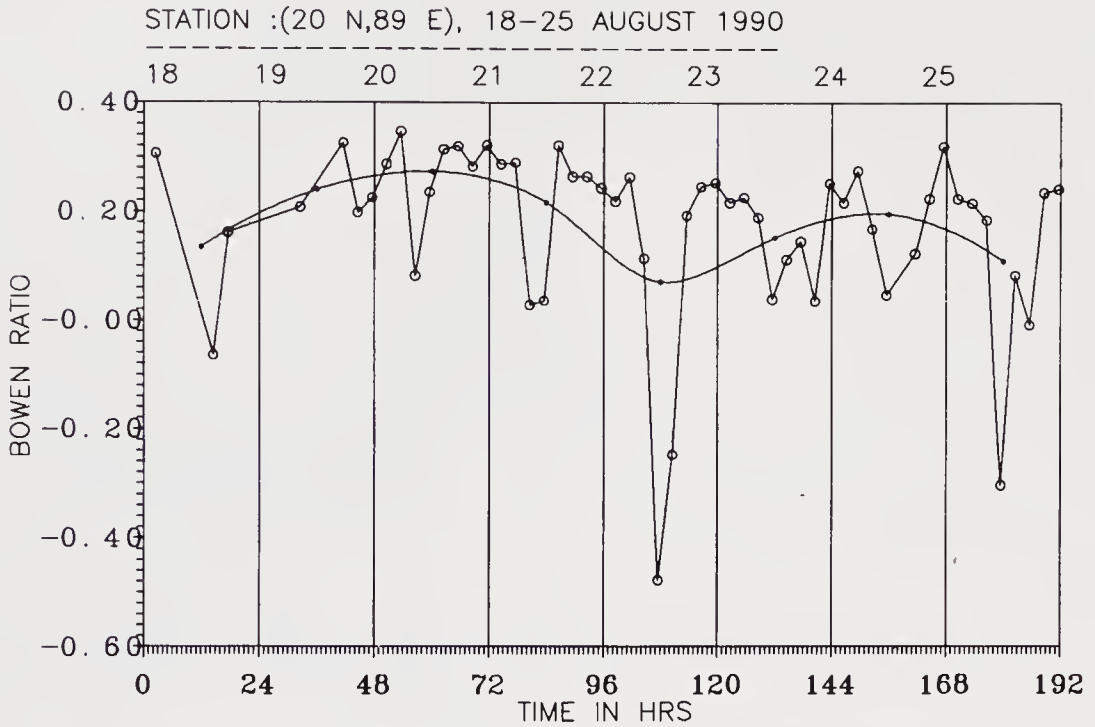


Figure 3. Time variation of Bowen ratio during 18th - 25th August, 1990.

Table 1. Comparison of daily average value of fluxes over Bay of Bengal (20°N, 89°E) during August 18th - 25th, 1990, by profile (P) and bulk aerodynamic (B) method.

Day August 1990	Sensible heat flux (W/m ²)		Latent heat flux (W/m ²)		Momentum flux (N/m ²)	
	P	B	P	B	P	B
18	23.6	5.5	105.3	42.0	0.052	0.007
19	30.6	3.0	129.3	61.0	0.090	0.030
20	78.6	16.0	258.1	109.0	0.157	0.093
21	62.4	9.0	241.3	116.0	0.197	0.088
22	19.9	3.0	104.1	65.6	0.074	0.035
23	17.1	2.0	91.2	50.0	0.059	0.025
24	22.6	3.5	112.7	48.0	0.053	0.020
25	9.2	2.0	50.6	30.0	0.050	0.030

those estimated by the profile method. A detailed study on C_D over the north Bay of Bengal (20°N, 89°E) can be found in Patil and Sivaramakrishnan (1994), which shows that C_D is a strong function of stability, increasing with increasing instability; the C_D under neutral stability (C_{DN}) was found to be 1.45×10^{-3} . When we used this C_{DN} in the computation of momentum flux by the bulk aerodynamic method, we found that its magnitude agrees well with that estimated by Singh (1992). The momentum flux in table 1 calculated by the profile method is higher by a factor of 1.5-3 during 19th - 25th August. Values of fluxes in table 1 clearly imply that the equality $C_D = C_H = C_E$ is not appropriate in disturbed weather (depression) conditions. The ratio of C_H and C_E to C_D is found to be 2.05 and 1.51 respectively and that of C_H to C_E is 1.36.

5. Conclusions

- The fluxes of sensible and latent heat, water vapour and momentum over sea show diurnal and synoptic scale variations due to variability of the weather disturbance near the station.
- The fluxes increase during the depression period and show systematic diurnal trend afterwards.
- Under unstable conditions (disturbance) the assumption $C_D = C_H = C_E$ is not appropriate.

Acknowledgements

The authors are thankful to the Director, Indian Institute of Tropical Meteorology, Pune, for his interest and encouragement and DST for providing the data collected by NIO, Goa, during MONTBLEX-90.

References

- Berkowicz R and Prahm L R 1982 Evaluation of the profile method for estimation of surface fluxes of momentum and heat, *Atmos. Environ.* **16** 2809–2819
- Binkowski F S 1975 On the empirical relationship between the Richardson number and the Monin-Obukhov stability parameter; *Atmos. Environ.* **9** 453–454
- Blanc T V 1982, Profile-bulk method formulas for calculating flux and stability in the marine atmospheric surface layer and a survey of field experiments, NRL Report 8647
- Bunker A F 1976 Computations of surface energy flux and annual air-sea interaction cycle of the North Atlantic Ocean, *Mon. Weather Rev.* **104** 1122–1139
- Businger J A, Wyngaard J C, Izumi Y and Bradley E F 1971 Flux-profile relationship in the atmospheric surface layer; *J. Atmos. Sci.* **28** 181–189
- Counihan J 1975 Adiabatic atmospheric boundary layers: A review and analysis of data from the period 1880–1972, *Atmos. Environ.* **9** 871–905
- Louis J F 1979 A parametric model of the vertical eddy fluxes in the atmosphere; *Boundary-Layer Meteorol.* **17**, 187–202
- Oceanographic and Meteorological data – (ORV *Sagarkanya*) Cruise: 56; MONTBLEX-90, NIO, Goa, Nov. 1990
- Patil M N and Sivaramakrishnan S 1994 Variation of drag coefficient with stability over sea, 8th National Space Science Symposium held at SPL, VSSC, Trivandrum, MT-45, 101–102
- Singh O P 1992 Surface fluxes and the cyclogenesis over north and adjoining central Bay of Bengal during MONTBLEX-1990, *Mausam*, **43** 399–402

Planetary boundary layer over monsoon trough region in a high resolution primitive equation model

K V J POTTY, U C MOHANTY, B NANDI and K J RAMESH[#]

Centre for Atmospheric Sciences, Indian Institute of Technology, Hauz Khas, New Delhi 110016, India

[#]Present Affiliation: National Centre for Medium Range Weather Forecasting (NCMRWF), Mausam Bhavan Complex, Lodi Road, New Delhi 110 003, India

Abstract. Numerical experiment with improved boundary layer physics has been performed to study the Planetary Boundary Layer (PBL) characteristics over the monsoon trough region. Details of the evolution and structure of the associated boundary layer processes in the monsoon trough and adjoining oceanic regions are examined by integrating the model up to a period of 48 hours.

The model used for this study is a high resolution primitive equation, one with 0.5° latitude/longitude horizontal resolution and 16 levels in the vertical (7 levels in the PBL). The boundary layer treatment in the model is based on the Monin-Obukhov similarity theory for the surface layer and Turbulent Kinetic Energy (TKE) formulation based on $E-\epsilon$ approach for the mixed layer. The model is integrated using the FGGE level IIIb analysis of European Centre for Medium Range Weather Forecasts (ECMWF), U.K.

The study shows that the diurnal variation of TKE over land is a dominant feature comparing with that over the ocean. Along the monsoon trough region, TKE increases from the eastern end to the western side which is mainly associated with the enhancement of sensible heat flux as we move from the eastern wet land to the western desert sector. It may be noted that the low level wind maximum, which is a characteristic feature over the monsoon region, is well simulated by this improved model physics.

Keywords. Planetary boundary layer; turbulent kinetic energy; monsoon trough; energy balance.

1. Introduction

The Planetary Boundary Layer (PBL) is that portion of the atmosphere which has close interaction with the underlying earth's surface through the turbulent exchanges of heat, moisture and momentum.

Several observational studies (Palmen 1948; Miller 1958; Tisdale and Clapp 1963; Namias 1973; Gray 1975) and numerical modeling efforts (Anthes and Chang 1978; Krishnamurti *et al* 1989) have demonstrated the importance of the PBL processes in the development and maintenance of the tropical weather systems. In order to include these PBL processes realistically in a numerical model, it is necessary to parameterize the effects of vertical gradients of heat, moisture and momentum in an appropriate manner.

PBL parameterization involves the representation of the effect of unresolvable sub-grid scale processes into the large scale fields. The effects of PBL can be incorporated in an NWP model broadly in two ways. One way is to parameterize the entire PBL as one layer. The complexity of the single layer PBL parameterization lies in the interdependence of various processes acting in different scales. The second approach

would be to include several computational levels in the PBL so that the structure of the PBL can be resolved effectively. Further, it requires some type of closure scheme to relate turbulent characteristics with mean quantities. Presently, closure schemes are limited to first, one and a half (TKE) and higher orders. Higher order schemes involve much detailed treatment of PBL physics and numerical complexity, and are hence computationally expensive. First order closure schemes in multi-level models (though computationally economic) are found to be inadequate in resolving the turbulent characteristics realistically (McBean *et al* 1979). TKE closure is an improvement on the simple first order closure with more physics of the PBL for the estimation of the eddy viscosity coefficient (K).

One dimensional (1-D) multi-level models have been used extensively (Holt and Sethuraman 1988) to understand the PBL characteristics: Due to limitations in incorporating advective and mixing processes, the 1-D models are not so suitable for studying the evolution of PBL and associated characteristics. Hence, the ideal choice would be to have a three-dimensional model having multiple computational levels for resolving PBL characteristics to simulate the PBL effects in the development and maintenance of the tropical weather systems. It is also recognized that increased horizontal resolution together with detailed PBL parameterization would be able to represent the most important characteristics such as moisture convergence and shear zones, which are vital for the development of cumulus convection (Krishnamurti *et al* 1989) in the tropics.

The monsoon trough boundary layer experiment (MONTBLEX) during 1990 was organized basically to study and simulate the dynamical and thermodynamical processes of PBL over the monsoon trough region. Hence, the Limited Area Model (LAM) of the IIT, Delhi (Mohanty *et al* 1987) has been modified suitably and implemented over the monsoon trough region with increased vertical resolution close to the surface for the effective treatment of PBL processes, through the incorporation of TKE closure. In this paper, the evolution of the PBL and its characteristics as simulated by the model are studied over the monsoon trough region.

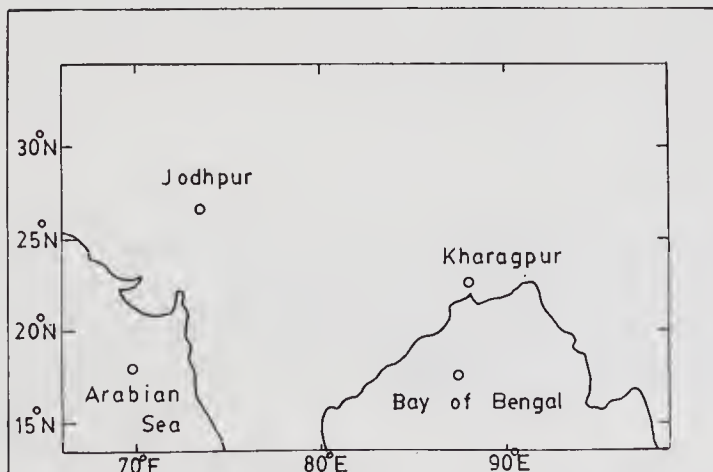
2. The model

A high resolution (0.5° longitude/latitude) hydrostatic, primitive equation model with a terrain following co-ordinate system is used. A brief description of the model is given in table 1. The horizontal domain of the model is from 13.5°N to 34.5°N in the North-South direction and 66°E to 99°E in the East-West direction (figure 1). In the vertical, the model involves 16 levels (7 levels in the PBL) in sigma (σ) co-ordinates. The model uses an envelope topography (mean + 1 standard deviation) based on the U.S. Navy high resolution data set.

The continuous governing equations of horizontal momentum, thermodynamic energy, moisture conservation and surface pressure tendency constitute the set of prognostic equations of the model. The hydrostatic and continuity equations are used as diagnostic equations for evaluating geopotential height and vertical motion and thus form a closed system of the primitive equations (PE) of the atmosphere. The prognostic equations include forcing terms, diabatic heating terms and source/sink terms, which are regarded as physical processes and are treated separately. The primitive equations are written in flux form involving sigma co-ordinates. The Arakawa

Table 1. An overview of the model.

Domain	: 66°–99°E; 13.5°N–34.5°N.
Independent variables	: λ, ϕ, σ, t .
Prognostic variables	: u, v, T, q, P_s .
Diagnostic variables	: ϕ, σ .
Topography	: Envelope (mean + 1 std).
Vertical grid system	: 16 levels (sigma(σ) co-ordinates).
Vertical levels of the model	: 0.05, 0.15, 0.25, 0.35, 0.45, 0.55 0.65, 0.75, 0.82, 0.86, 0.90, 0.935, 0.960, 0.975, 0.987 and 0.997.
Horizontal grid system	: Arakawa C-grid.
Space finite difference scheme	: Second order accuracy.
Time integration scheme	: Split-explicit time integration.
Time step	: $\Delta t = 150$ seconds.
$\Delta\lambda, \Delta\phi$: 0.5 Lat./Long. (50 km).
Horizontal diffusion	: Linear second order.
Initialisation	: Non-linear normal mode.
Physical processes	: Dry convective adjustment; deep cumulus convection 'Kuo Scheme' (Anthes 1977) with convective precipitation. : Large scale stratified precipitation with RH > 95%. : PBL; M-O similarity approach for the surface layer, TKE($E-\epsilon$) for the mixed layer.

**Figure 1.** Model domain and the grid points chosen for the study.

C-grid in spherical co-ordinates is used for horizontal differencing. Time dependent lateral boundary conditions of Perkey and Kreitzberg (1976) are used at the boundary points. A second order diffusion is used in the model to suppress the computational instabilities. The time integration scheme implemented in the model is the split-explicit

method which allows larger time steps by effectively separating various terms of the prognostic equations into parts governing the slow moving Rossby and fast moving gravity waves.

Model physics includes parameterizations of PBL (TKE: $E-\varepsilon$), cumulus convection (Kuo 1974), large scale precipitation and dry convective adjustment.

Details of the model equations and numerics may be obtained from Mohanty *et al* (1987) and Madala *et al* (1987).

3. PBL parameterization scheme of the model

Surface temperature plays an important role in the evolution of PBL processes and hence the prediction of ground temperature is also included in the surface layer for grid points over the land.

3.1 Ground temperature

The ground temperature (T_g) is predicted with the help of surface energy balance equation (Chang 1979):

$$\frac{\delta T_g}{\delta t} = R C_g^{-1} + W(T_m - T_g) + \rho C_p (\overline{w'\theta'})_0 C_g^{-1}. \quad (1)$$

The first term of the right hand side (r.h.s) represents the net radiation, the second term represents the heat exchange with the deep soil and the last term the heat exchange with the overlying atmosphere. Here R is the net radiation, C_g is the heat capacity per unit area of the soil, W is the inverse of the time scale for the heat conduction in the soil ($2\pi/1$ day), T_m is the deep soil temperature. In the last term of equation (1), ρ is the air density, C_p the specific heat at constant pressure and $\overline{w'\theta'}$ the potential temperature flux. The subscript 0 denotes the near surface value.

Net radiation R is given by,

$$R = I_S + I_L - Q_L, \quad (2)$$

I_S = Incoming solar radiation observed at the surface,

I_L = Atmospheric long wave back scattering radiation,

Q_L = Outgoing long wave radiation.

I_S is given by,

$$I_S = S \cos z (1 - A) b^{\sec z}, \quad (3)$$

where S is the solar constant, A is the surface albedo and b is the atmospheric turbidity, which is a function of precipitation.

The zenith angle z is obtained from the local hour angle $h\alpha$, latitude ϕ and declination δ ,

$$\cos z = \cosh\alpha \cos \phi \cos \delta + \sin \phi \sin \delta. \quad (4)$$

Water vapour is ignored in the relationship for net long wave radiation computed using Brunt's equation (Seller 1965),

$$I_L - Q_L = \alpha(1 - 0.61)\beta T_g^{-4}, \quad (5)$$

where α is the soil emissivity which is a function of precipitation and β is the Stefan-Boltzmann constant. Heat capacity of soil slab C_g is approximated as an 80 m deep air layer (Chang 1979). Oceanic grid points use the climatologically averaged sea surface temperature as T_g .

3.2 Surface layer

The surface boundary layer (constant flux layer) is parameterized based on the similarity theory (Monin and Yaglom 1971), using similarity functions (Businger *et al* 1971),

$$\frac{kz}{U_*} \frac{\partial u}{\partial z} = \phi_m(z/L), \quad (6)$$

$$\frac{kz}{\theta_*} \frac{\partial \theta}{\partial z} = \phi_h(z/L), \quad (7)$$

$$\frac{kz}{q_*} \frac{\partial q}{\partial z} = \phi_h(z/L), \quad (8)$$

where the non-dimensional stability parameters ϕ_m and ϕ_h are functions of the Monin-Obukhov length L and k is Von-Karman constant.

3.3 Mixed layer

Treatment of the mixed layer in TKE closure models involves two types of approaches for the evaluation of turbulent dissipation of kinetic energy (ε). The first method is based on mixing length approach ($E-l$) and the second approach ($E-\varepsilon$) involves the time tendency equation for ε evaluation. It was found in the studies of Holt and Sethuraman (1988) using MONEX data sets that TKE closure based on $E-\varepsilon$ formulation performs better than the $E-l$ approach. Therefore in this study the PBL is parameterized by the TKE: $E-\varepsilon$ closure with the constants of Detering and Etling (1985).

The prognostic equation for turbulent kinetic energy (TKE) is derived as (Monin and Yaglom 1971),

$$\frac{\partial E}{\partial t} = -\overline{u'w'} \frac{\partial u}{\partial z} - \overline{v'w'} \frac{\partial v}{\partial z} + \frac{g}{\theta} \overline{w'\theta'} - \frac{\partial}{\partial z} \left(\overline{w'E'} + \frac{\overline{p'w'}}{\rho} \right) - \varepsilon. \quad (9)$$

First two terms on the right hand side represent the shear production, third represents the buoyancy production, the fourth turbulent transport of kinetic energy and pressure, and the fifth dissipation of turbulent kinetic energy. In the above equation several terms have to be parameterized.

Shear terms are related to the vertical gradient of the mean wind by eddy viscosity coefficient K_m which is a property of the turbulent flow,

$$-\overline{u'w'} \frac{\partial u}{\partial z} - \overline{v'w'} \frac{\partial v}{\partial z} = K_m \left[\left(\frac{\partial u}{\partial z} \right)^2 + \left(\frac{\partial v}{\partial z} \right)^2 \right]; \quad (10)$$

similar assumption is valid for heat flux ($\overline{w'\theta'}$) in the buoyancy term and is parameterized as (Deardorff 1966),

$$-\frac{g}{\theta} \overline{w'\theta'} = \frac{g}{\theta} K_h (\partial\theta/\partial z). \quad (11)$$

The kinetic energy and pressure terms which transport stresses from one place to another are small near the surface but become prominent away from the surface. These terms are treated together and assumed to be of the gradient diffusion type (Shir 1973),

$$-\overline{(w'E' + p'w')/\rho} = C_1 \left(K_m \frac{\partial E}{\partial z} \right), \quad (12)$$

where C_1 is a constant.

Substitution of these parameterizations into (9) yields,

$$\frac{\partial E}{\partial t} = K_m \left[\left(\frac{\partial u}{\partial z} \right)^2 + \left(\frac{\partial v}{\partial z} \right)^2 \right] + \frac{g}{\theta} K_h \frac{\partial \theta}{\partial z} + C_1 \frac{\partial}{\partial z} \left(K_m \frac{\partial E}{\partial z} \right) - \varepsilon. \quad (13)$$

The prognostic equation for the dissipation of TKE is given by

$$\frac{\partial \varepsilon}{\partial t} = C_3 \frac{\varepsilon}{E} \left(-\overline{u'w'} \frac{\partial u}{\partial z} - \overline{v'w'} \frac{\partial v}{\partial z} + \frac{g}{\theta} \overline{w'\theta'} \right) - C_4 \frac{\varepsilon^2}{E} + C_5 \frac{\partial}{\partial z} \left(K_m \frac{\partial \varepsilon}{\partial z} \right). \quad (14)$$

The first term on the r.h.s of equation (14) represents the production, second term destruction, and the last term vertical transport of dissipation.

The relationship of eddy viscosity (K_m) and TKE in terms of ε is given by (Daly and Harlow 1970)

$$K_m = C_2 E^2 / \varepsilon. \quad (15)$$

Holt and Sethuraman (1988) have studied the suitability of the values of constants used in the above equations of TKE and dissipation and found that constants of Detering and Etling (1985) suit better. Hence for the present study we used the same constants, which are given by

$$C_1 = 1.35, C_2 = 0.026, C_3 = 1.13, C_4 = 1.9 \text{ and } C_5 = 0.77.$$

Solution of turbulent kinetic energy equation requires the specification of E in the surface layer (Mailhot and Benoit 1982), which should be a function of u_* , w_* and z/L . Based on Deardorff (1974b) and Wyngaard (1975), who give

$$E = 3.75 U_*^2 \quad z/L > 0$$

$$E = 3.75 U_*^2 + 0.2 W_*^2 + (-z/L)^{2/3} U_*^2 \quad z/L < 0$$

$$\varepsilon = U_*^3 / kz$$

where U_* is the frictional velocity and W_* is the convective velocity

$$W_* = [(g/T)h(\overline{w'T'_v})_0]^{1/3}, \quad (16)$$

the subscript zero denotes near-surface values and T_v the virtual temperature. The flux $\overline{w'T'_v}$ is computed as

$$\overline{w'T'_v} = \overline{w'T'} + 0.61 \overline{T'w'q'}$$

where g is the acceleration due to gravity and h is the boundary layer height, which is computed from the TKE of the previous iteration. h is given as the model level height at which TKE reduces to $0.05 \text{ m}^2/\text{s}^2$ or less. Upper boundary condition is taken as $E = \varepsilon = 0$.

The convective velocity scale W_* , which is a measure of the variance of the horizontal velocity components, has been included in the above equation for unstable case to reflect the horizontal motions induced in the lower boundary layer by the vertical motion in the large eddies of the upper boundary layer. The z/L term gives the dependence of $\overline{w'^2}$ on z .

4. Data

FGGE level III-b analysis produced at ECMWF, U.K. for the period from 5th – 7th July 1979 at 1200 UTC has been used. U.S. Navy topography data and climatological sea surface temperature (SST) for July have also been used for the model simulation.

Among the precipitating systems in the monsoon period, the monsoon depression is a major synoptic system. On 5th July 1979 at 1200 UTC a low pressure area was present over north-east Bay of Bengal centred close to 20°N and 90°E , intensified into a depression in 24 hours and further intensified into a deep depression after 48 hours. With the presence of low/depression over northern part of Bay of Bengal, normal monsoon conditions prevailed over the country.

5. Experiment

The objective of the experiment is to study the evolution of the PBL structure over the monsoon trough region. Development of PBL at any surface is determined by thermal and dynamical effects locally. During day time, the land surface gets heated up at a much faster rate than the oceanic surface resulting in a large diurnal variation of surface temperature and surface characteristics. As the western sector of the monsoon trough falls under the dry convective regime, the evolution of the PBL and associated characteristic features are largely controlled by the thermal effects alone. On the other hand, the eastern sector of the monsoon trough is categorized as a moist convective region and hence the turbulent transfer of sensible heat and its diurnal variation is considerably less. At the same time, the local dynamical effects play a significant role in the evolution of PBL over the eastern side of the monsoon trough. Hence we have chosen two grid points of the model close to the stations Jodhpur and Kharagpur representing the western and eastern sectors of the monsoon trough respectively and

one each over the Arabian Sea and Bay of Bengal to study the evolution of the PBL and the associated features over the Indian sub-continent and adjoining oceanic sectors through the incorporation of improved PBL physics in a high resolution LAM (figure 1). The model has been integrated up to 48 hours starting from 1200 UTC on 5th July 1979. Since our aim is to study the PBL characteristics, the discussion of the results is restricted largely up to 24 hours of model simulation.

6. Results and discussion

In this section, results of PBL characteristic features over the monsoon trough region and adjoining oceanic areas as well as simulation of large scale fields are discussed.

6.1 PBL characteristic features

Evaluation of the PBL at various selected points of the model domain is studied through the analysis of the variation of Turbulent Kinetic Energy (TKE) as it is considered as a measure of turbulence intensity. Figure 2 depicts the variation of TKE with height at every hour of the model integration. It is found that, in general, evolution of TKE from day to night conditions over the land points is the most dominant feature. Due to the absence of diurnal variation of surface temperature over the sea points, no significant variations in the TKE magnitudes are observed. Accordingly, the vertical extent of TKE is found to be minimum over the sea points all through the 24 hours of integration. Over the land, TKE magnitudes are found to be more during the evening time (1300–1700 hrs of IST), and the comparison of the relative magnitudes shows that TKE is maximum over the western part of the monsoon trough (Jodhpur) and minimum over the eastern end (Kharagpur) and the diurnal variation of TKE is found to be minimum over the eastern side of the monsoon trough in comparison with the western end. The appearance of maximum TKE magnitudes over the western end of the trough (Jodhpur) could be due to the intense heating during the day followed by cooling in the night. In contrast, over the eastern part of the trough, abundant cloud cover restricts the amount of solar insolation reaching the ground and moist land surface with large evaporation from ground leads to reduced diurnal variation of TKE.

The vertical profiles of TKE (figure 3) and eddy viscosity coefficient (K_m) (figure 3) depicted at 6-hour intervals of the model integration are analysed to study the evolution of PBL characteristics at various selected points of the domain. The profiles of TKE show that TKE values are extremely small at $t + 6$ hours (23:30 hrs of IST) having maximum values close to the ground. With the increase in the intensity of turbulence, the magnitude of TKE increases generally and the level at which maximum TKE is observed moves to higher altitudes. Here again, the maximum value of TKE at $t + 24$ hrs is found to be more at Jodhpur ($1.3 \text{ m}^2/\text{s}^2$) as compared to that of Kharagpur ($0.6 \text{ m}^2/\text{s}^2$). At Jodhpur, the TKE is found to be more at $t + 12$ hrs (05:30 hrs IST) as compared to $t + 18$ hrs (11:30 hrs IST). This could be attributed to the presence of a secondary maximum at this time appearing mainly due to the wind shear. Among the sea points considered, the magnitudes of TKE are found to be more over the Arabian Sea due to the presence of more wind shear over this region than that at the Bay of Bengal. Similar variations of K_m (figure 3) are found at various selected points of the domain.

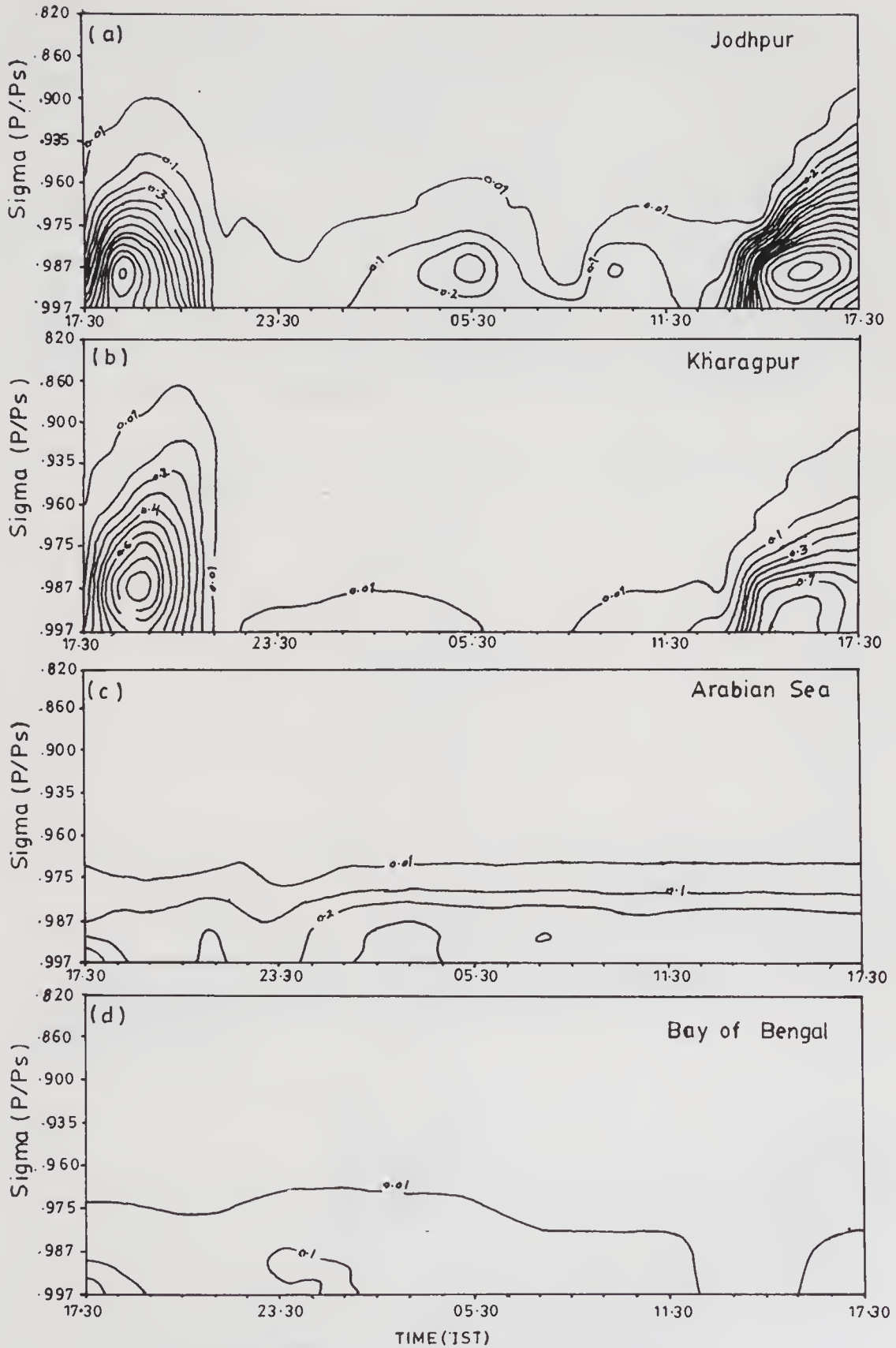


Figure 2. Diurnal variation of TKE (m^2/s^2) with height: (a) Jodhpur; (b) Kharagpur; (c) Arabian Sea; (d) Bay of Bengal.

The height of the planetary boundary layer is an important parameter for the evolution of TKE. In order to assess the planetary boundary layer height, observed virtual potential temperature profile of Calcutta and Jodhpur has been compared with the model simulated profile (figure 4). Observed boundary layer height shows good agreement with the simulated one at Calcutta. But at Jodhpur, the inversion layer is higher than that observed on 6th July, 1979 at 1200 UTC.

The hourly rainfall plots at the four selected points of the domain are illustrated in figure 5. The rainfall variation does not show any significant influence over the diurnal variation of TKE as no explicit treatment of water droplets is included in the PBL parameterization. Due to the dry convective type of PBL over Jodhpur, convective rainfall is not predicted. But over the eastern end of the monsoon trough (Kharagpur) and in the Bay of Bengal due to formation of a depression over the head of the Bay (by 12 Z of 6th July 1979), certain rainfall amounts are predicted by the model. On the other

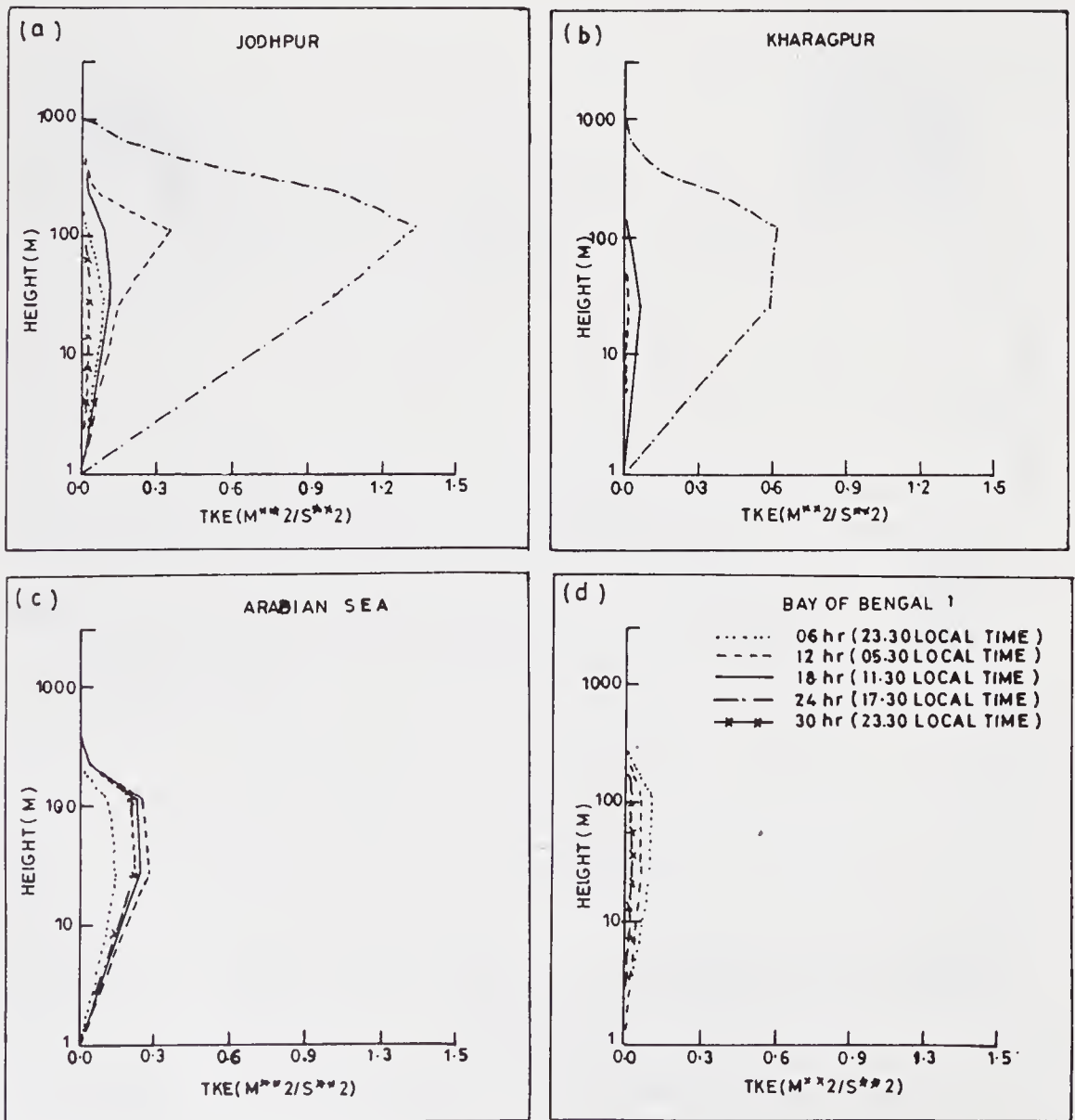


Figure 3. (Continued)

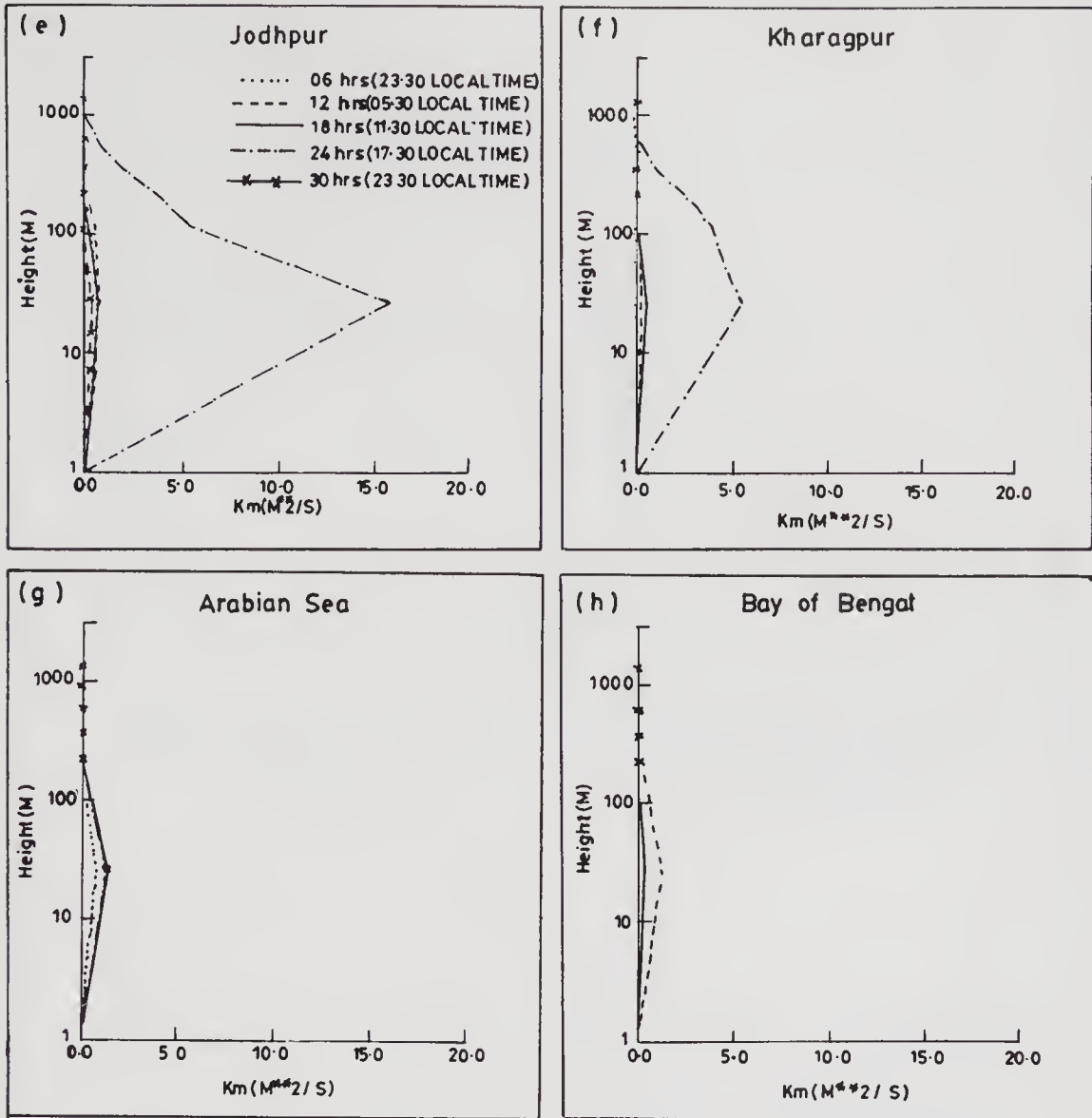


Figure 3. Vertical profiles of TKE and eddy viscosity (K_m) at 6 hours of interval. TKE: (a) Jodhpur; (b) Kharagpur; (c) Arabian Sea; (d) Bay of Bengal. Eddy viscosity: (e) Jodhpur; (f) Kharagpur; (g) Arabian Sea; (h) Bay of Bengal.

hand, rainfall over the Arabian Sea is mainly attributed to the local convective processes.

Latitudinal mean vertical cross-section of wind and temperature fields is analysed over the monsoon trough region to identify the characteristic features of PBL generated by the model physics. Domain of 70°E – 90°E and 22°N – 27°N is chosen, which usually covers the normal monsoon trough region and dominantly covers the land region. Vertical cross-sections of wind and temperature at initial time ($t = 0$) and after 24 hrs of the model integration are shown in figure 6. At the starting time of the model integration (figure 6a) the wind field distribution does not display any variation all along the trough region in the lower-most levels. However, at 0.85σ approximately, the wind is found to be maximum over the western end of the trough as compared to the eastern end. After the integration of the model for 24 hrs (figure 6b), the model could

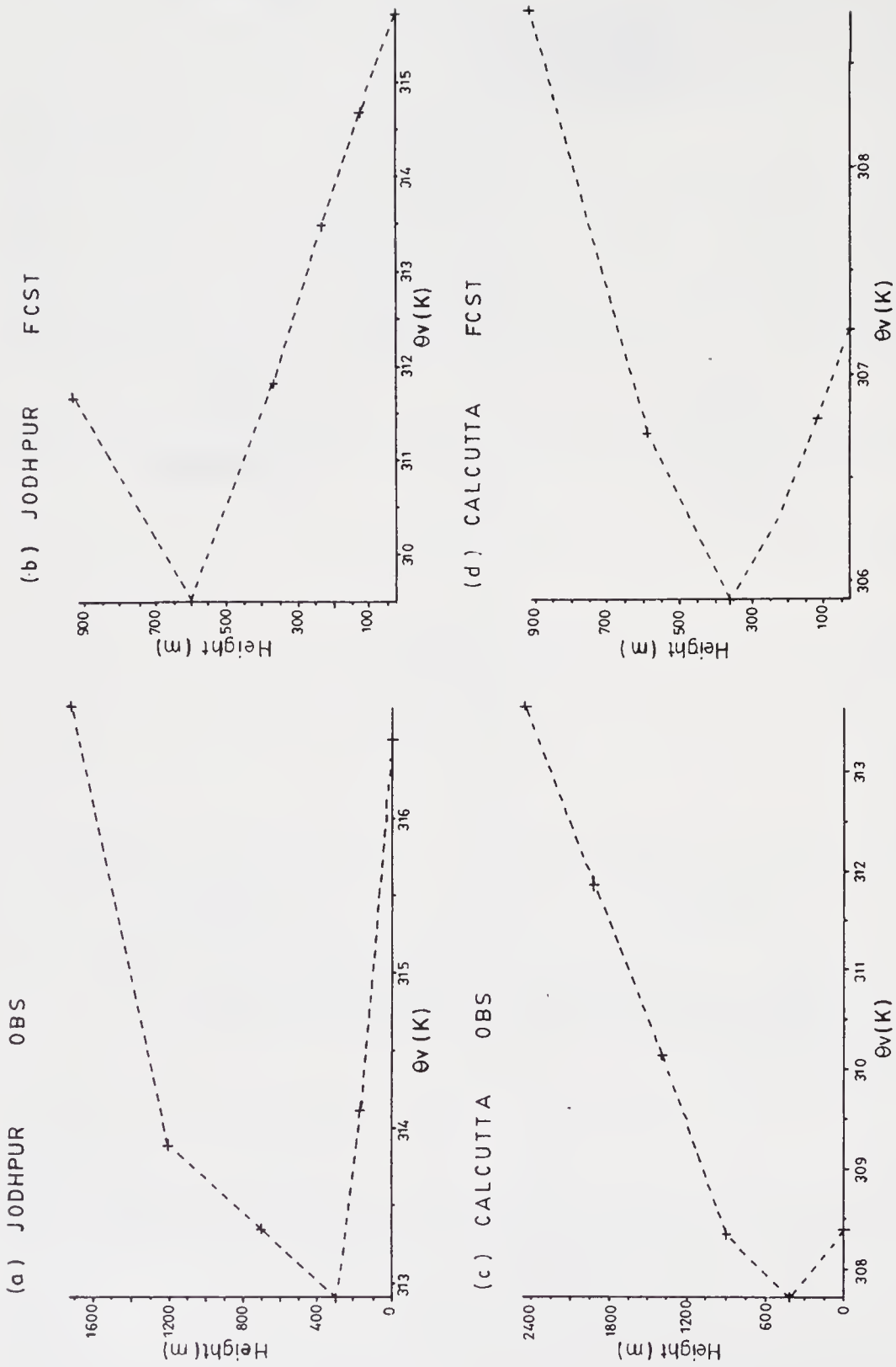


Figure 4. Vertical profiles of virtual potential temperature (θ_v) at 1200 Z on 6th July 1979. (a) Jodhpur-observed; (b) Jodhpur-model forecast; (c) Calcutta-observed; (d) Calcutta-model forecast.

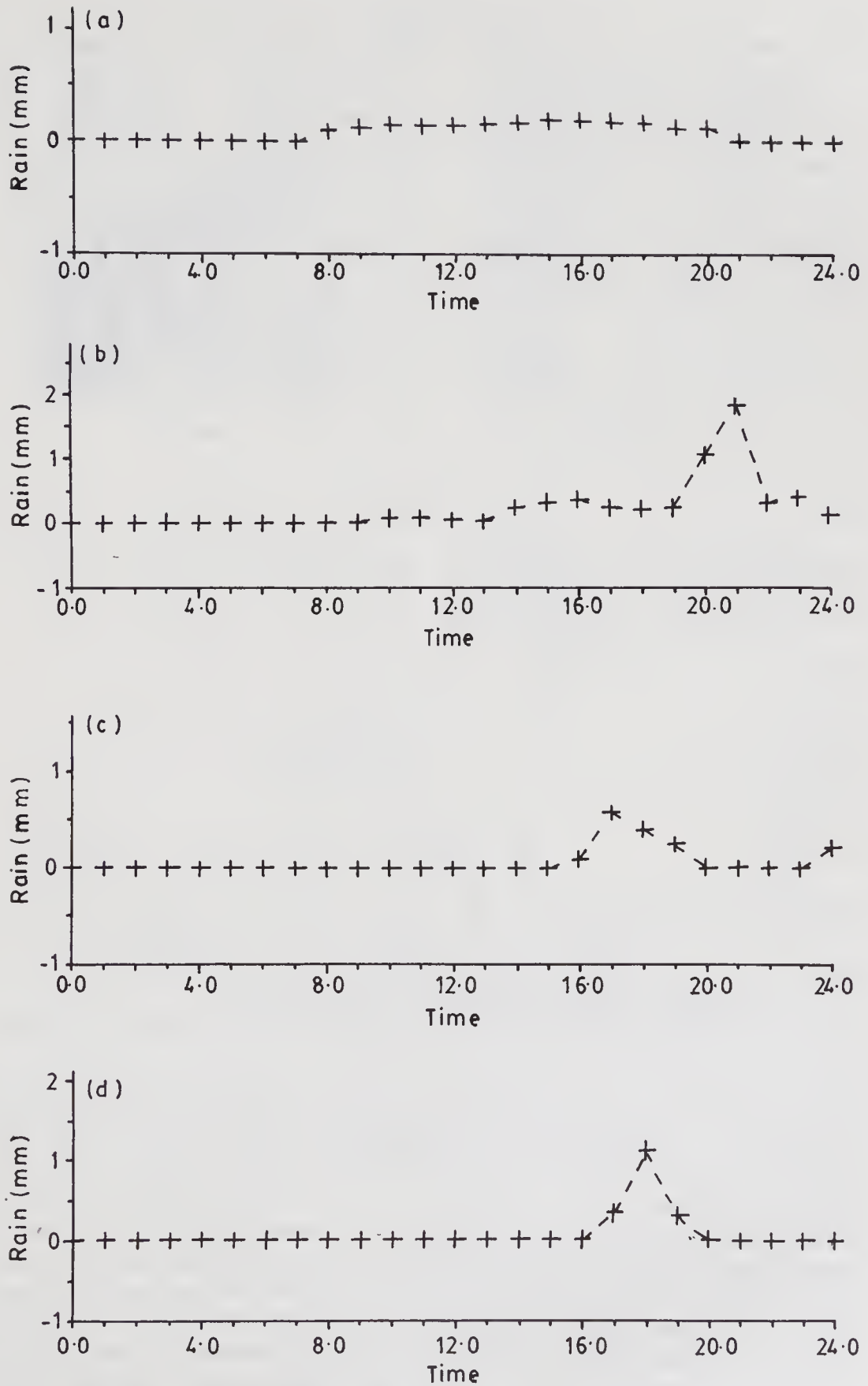


Figure 5. Hourly rainfall.

(a) Jodhpur; (b) Kharagpur; (c) Arabian Sea; (d) Bay of Bengal.

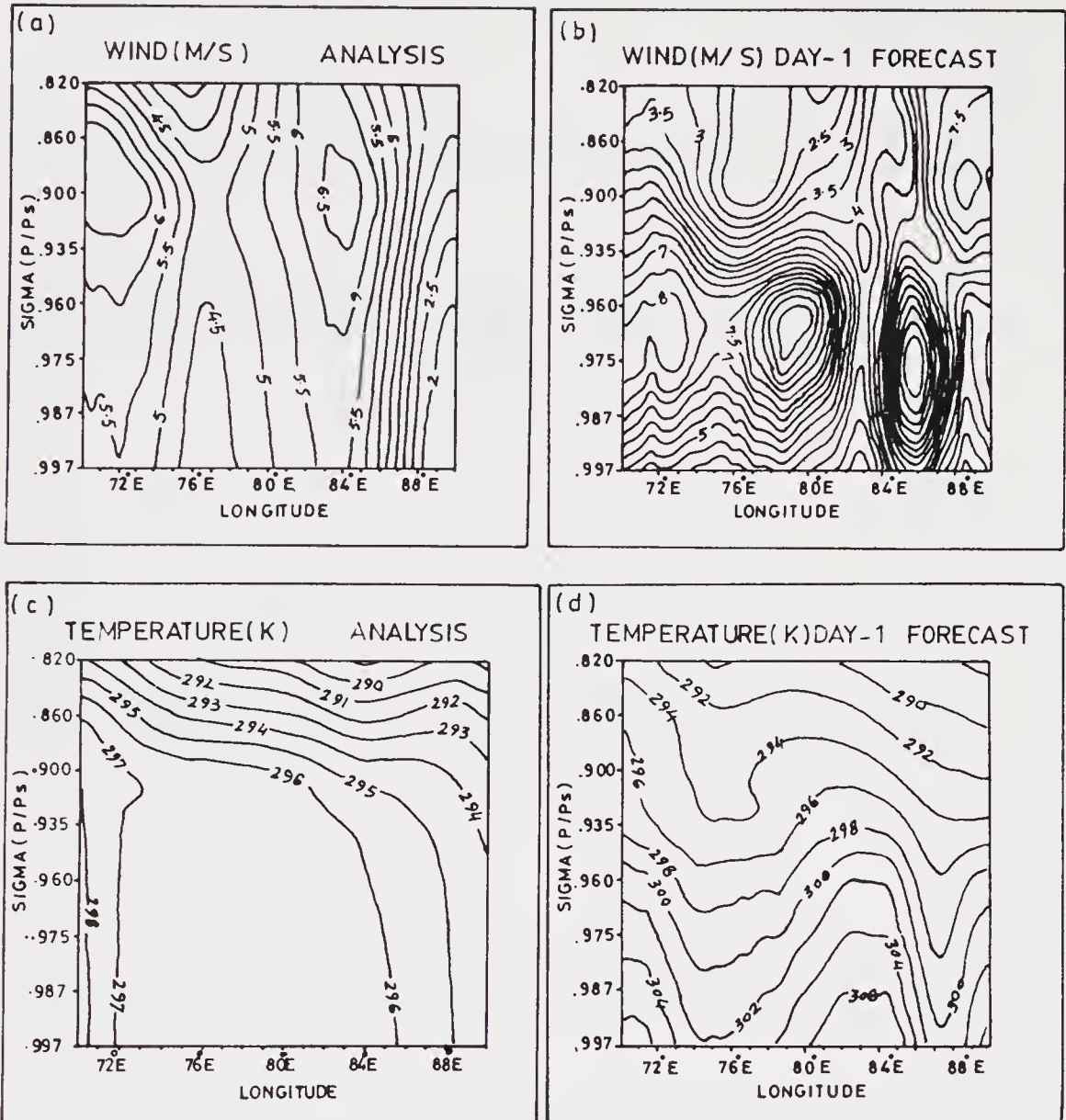


Figure 6. Zonally averaged fields of wind and temperature.

(a) Analysis wind; (b) Forecast wind; (c) Analysis temperature; (d) Forecast temperature.

simulate the low level wind maxima which is a characteristic feature of a turbulent boundary layer. The appearance of wind maxima over the monsoon trough region is also observed in the observational studies (Tyagi *et al* 1994) under the strong and active monsoon conditions. Usually analysis is done for 1000 mb and 850 mb and hence the maxima are seen at about 0.9–0.85 σ level in the analysis field. Since the model has a much higher vertical resolution close to the surface (seven levels), in the simulation the low level wind maxima are found in the column (0.96–0.987 σ) closer to the surface. Hence, such a feature cannot be resolved from the analysed data sets. The existence of such a feature close to the surface (0.15–0.6 km) is also observed at 12 Z on 6th July 1979 over Ranchi, Lucknow, Delhi, Gwalior and Jodhpur stations situated along the monsoon trough (figure 7). It is expected that the analysis of the MONTBLEX-90 data sets would be able to throw some light on the observed structure of PBL in a much

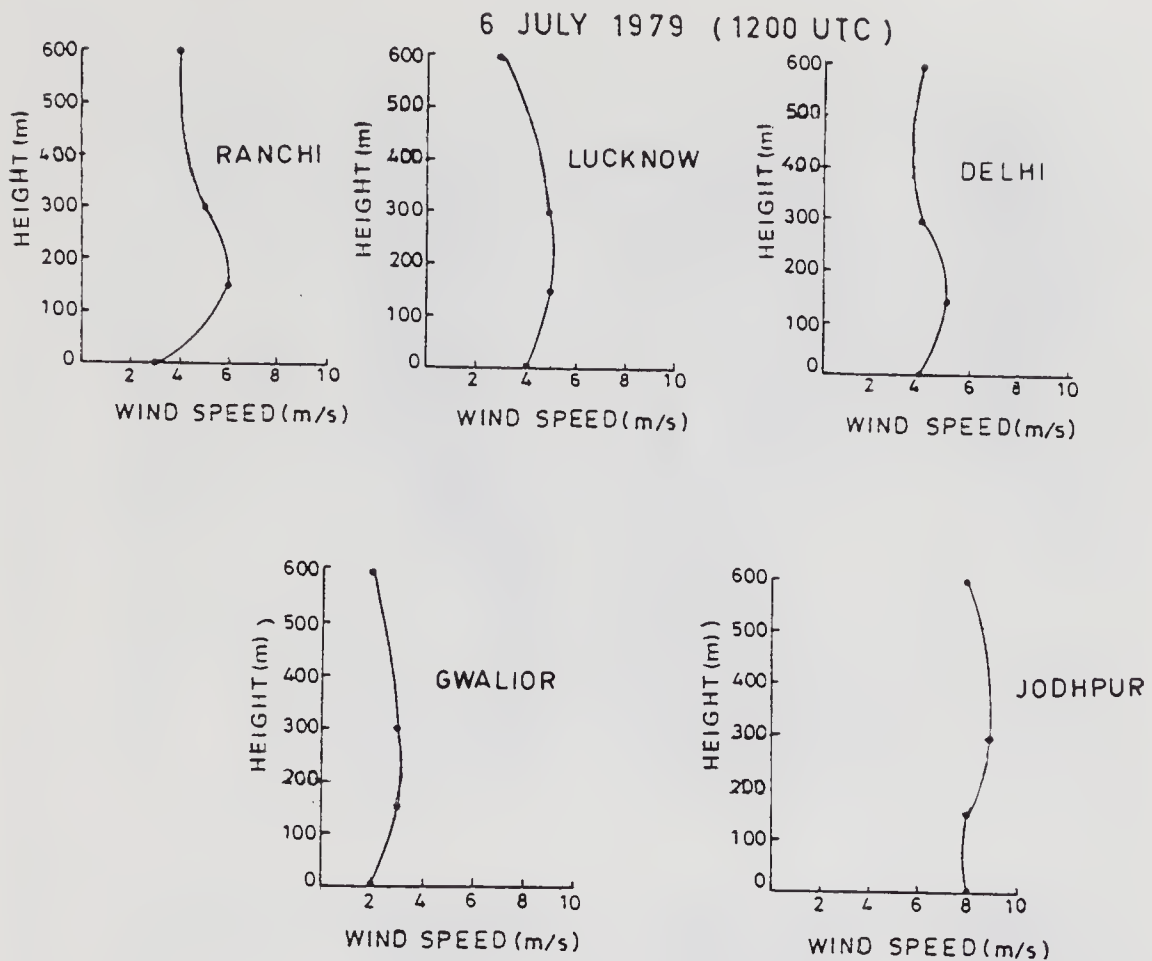


Figure 7. Analysis of wind at 1200 Z on 6th July 1979.

more detailed manner. It is also interesting to note that the level of wind maxima increases from east to west across the monsoon trough region.

In accordance with the increase of turbulence intensity all along the monsoon trough region as seen earlier, the stable atmospheric conditions prevailing over the central parts of the trough (figure 6c) at $t = 0$ transformed into an unstable regime as observed at $t + 24$ hrs of the model integration (figure 6d). Both of these characteristics have been brought out by the model simulation as stated above, as it is apparent that such a feature was not existing at the beginning of the model integration.

6.2 Large scale fields

There was a developing vortex on 5th July 1979 over the north Bay of Bengal and its further developments can be seen in the prediction fields (figure 8) as well as in the verifying analyses (figure 9). The monsoon trough is well-marked to the east of 80°E from central India to the north Bay of Bengal without any significant slope with height. Wind flow analysed at 0.9σ surface indicates that the vortex and associated circulation features over the north Bay of Bengal has been captured reasonably well by the model. Though the predicted center of the vortex lies to the east of its location (about 0.5°

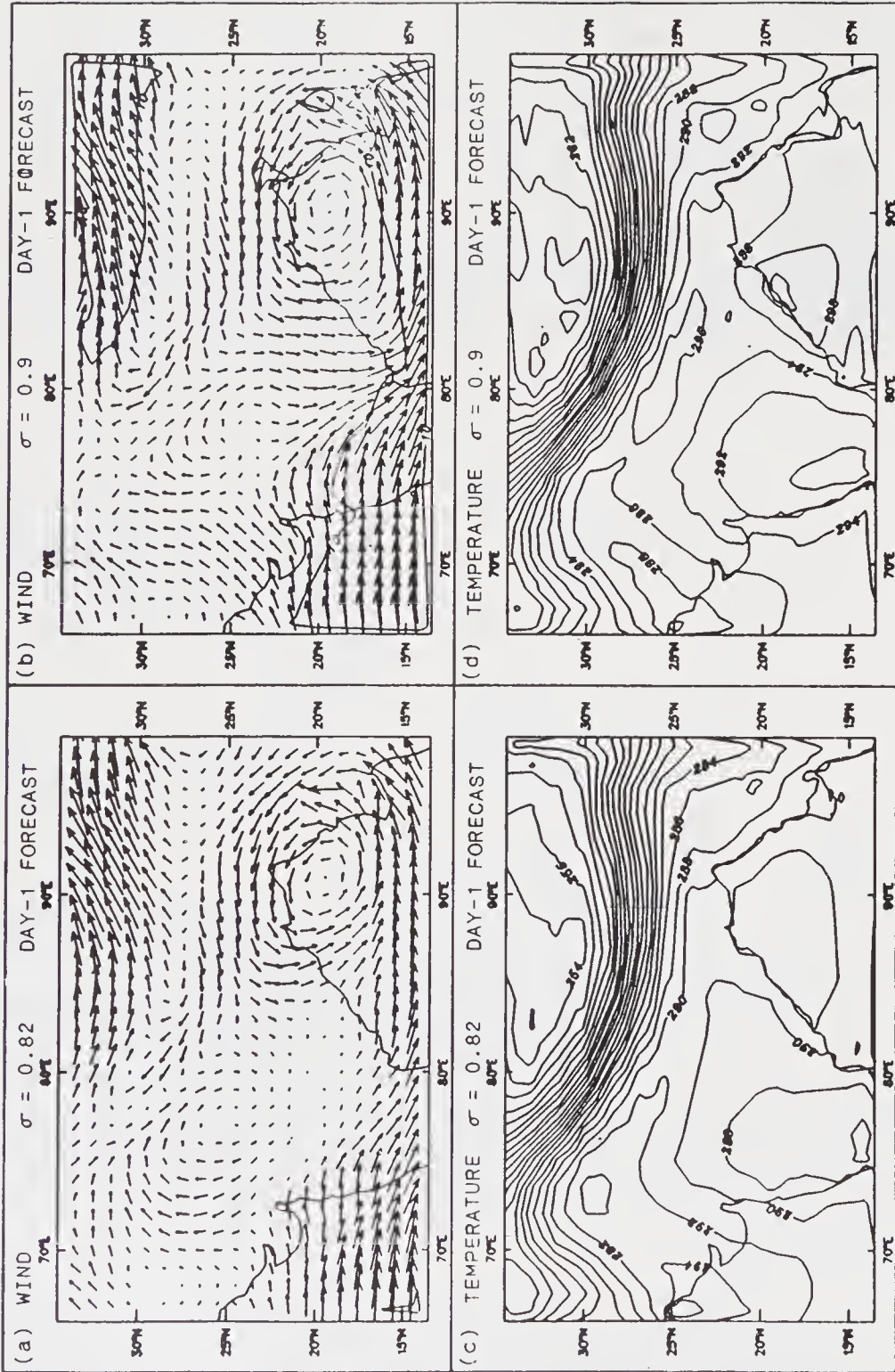


Figure 8. Forecasted large scale fields of wind and temperature. (a) Wind at 0.82 σ level; (b) Wind at 0.9 σ level; (c) Temperature at 0.82 σ level; (d) Temperature at 0.9 σ level.

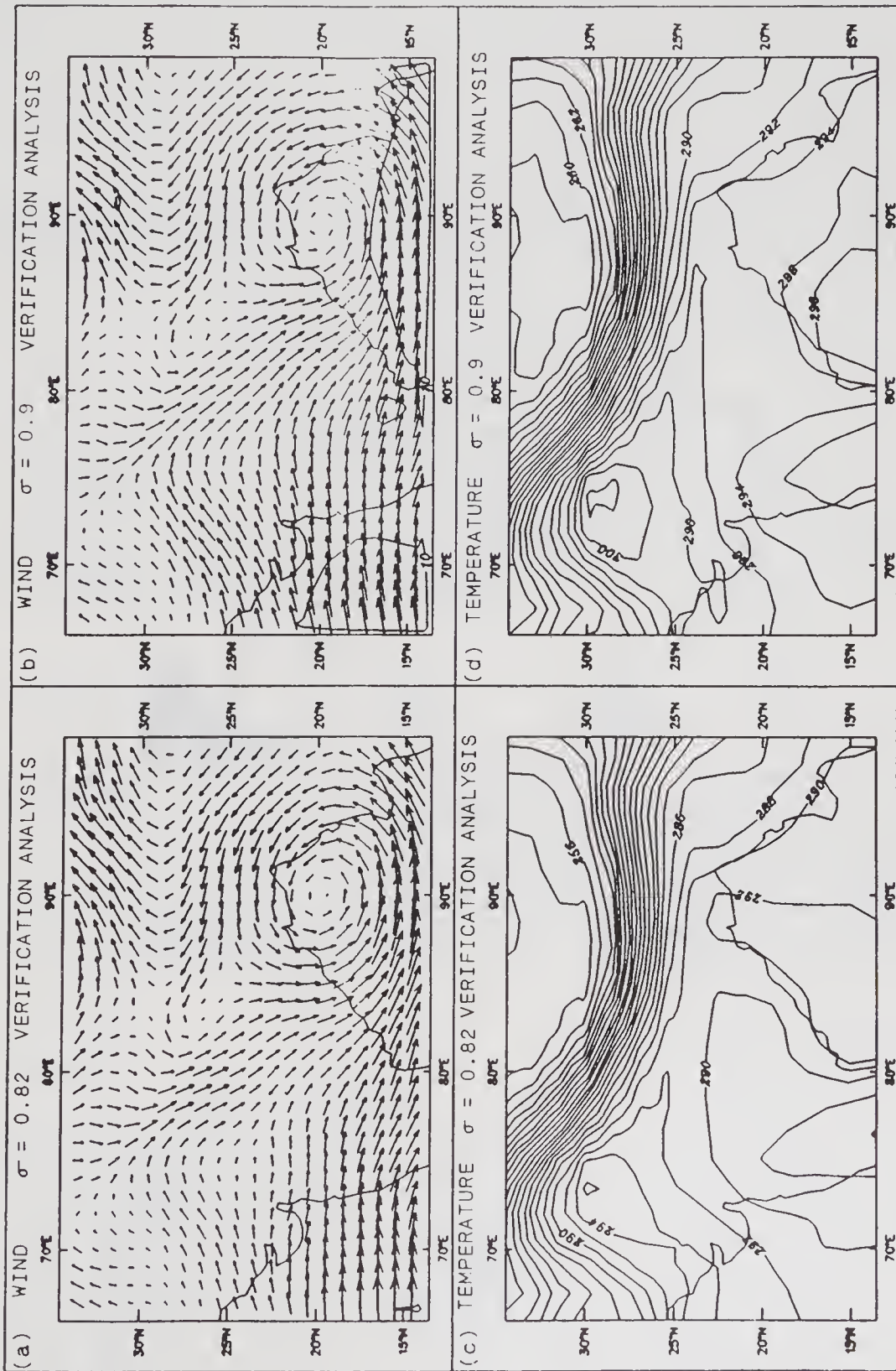


Figure 9. Same as in figure 8, but for verification fields.

latitude eastward), the zone of confluence in the model generated forecasts (figure 8b) is found to be stronger than the verifying analysis. In particular, enhanced westerlies over the peninsular India in the forecasts added to the building up of intense moisture flux convergence surrounding the vortex. But at 0.82 σ level, the wind flow predicted over south Madhya Pradesh and the adjoining region is considerably weaker (figure 8a) when compared to the verifying analysis (figure 9a). However the circulation around the vortex including its center compares well with its verification pattern.

Temperature prediction (figure 8c and d) and corresponding verification fields (figures 9c and d) show that temperature has been predicted reasonably well by the model. The precipitation field for 24 hours (figure 10a) as predicted by the model agrees

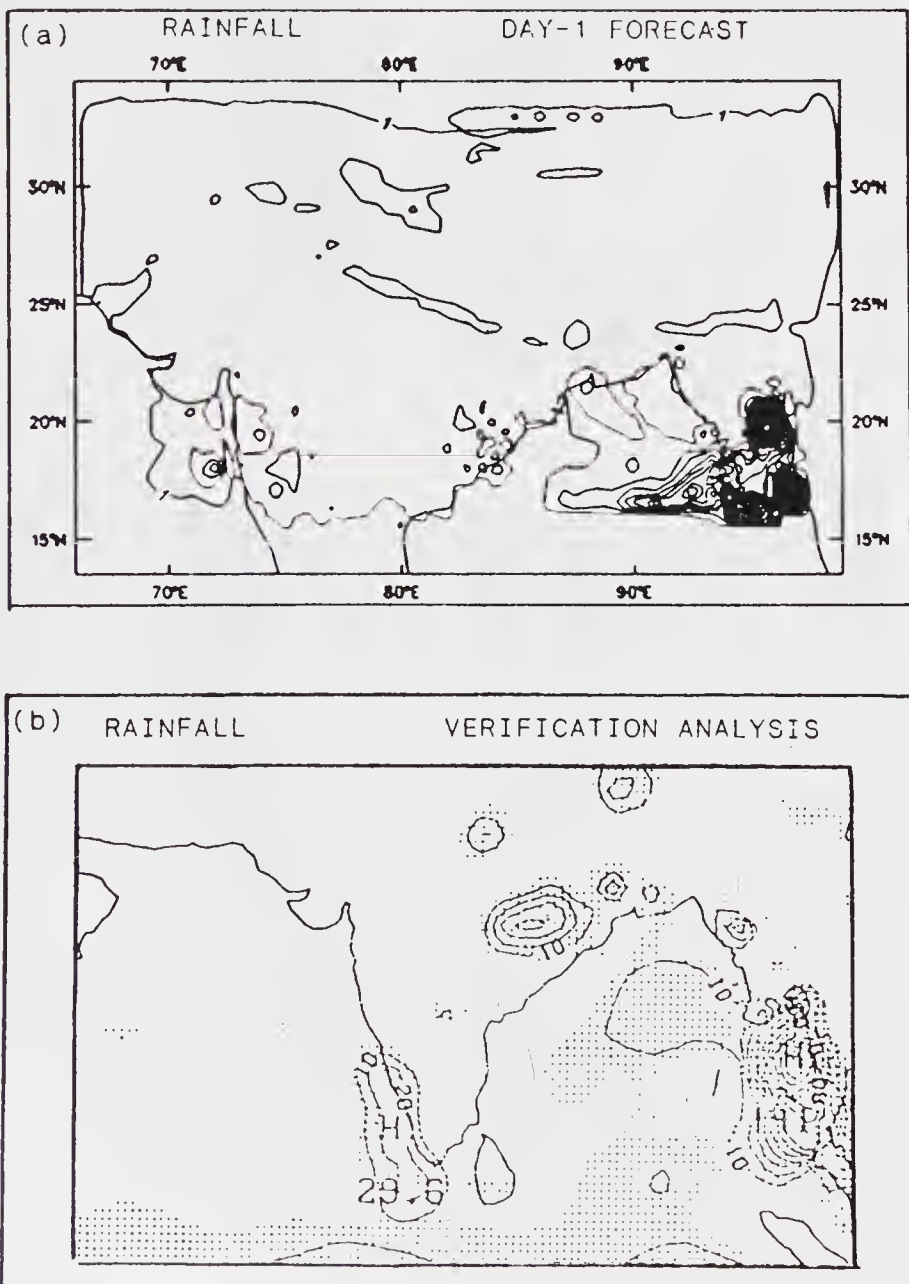


Figure 10. (a) 24 hour forecast of rainfall (mm); (b) Analysis of 24 hour rainfall (mm) ending 00 Z 6th July 1979.

reasonably with the analysis of precipitation field (Krishnamurti *et al* 1983) depicted in figure 10(b). The maximum precipitation field predicted by the model is 74 mm near the Arakan coast.

7. Conclusions

The following conclusions are drawn from this study of PBL characteristics over the monsoon trough region:

- Diurnal variation of TKE is a marked feature over the land compared to ocean. TKE increases from the eastern side of the monsoon trough to the western sector. The maximum magnitude of TKE over land is of the order of $1-1.5 \text{ m}^2/\text{s}^2$ over the desert sector of India.
- Presence of low level wind maxima, which is a characteristic feature of turbulent boundary layer, is well simulated by this improved boundary layer physics.
- The model has been able to predict the large scale fields and the evolution of PBL reasonably well in spite of its limitations of not having radiation parameterization scheme and sophisticated energy balance equation to predict the ground temperature. It may be stated in this regard that for short range simulations (up to 1 day) radiation does not play a very important role.

Acknowledgements

We are thankful to Dr. R V Madala, NRL, Washington DC and Prof. Sethuraman, NCSU, Raleigh, USA for providing an idealized version of the NRL model to our group and for the continued co-operation. We wish to thank NCMRWF, New Delhi for providing the necessary computer facilities. We express our thanks to ECMWF, Reading, UK, for providing the FGGE level III analyses. This work was supported in part by the Office of Naval Research, U.S.A. and the Department of Science and Technology, New Delhi, India.

References

- Anthes R A and Chang S W 1978 Response of the hurricane boundary layer to changes of sea surface temperature; *J. Atmos. Sci.* **35** 1240–1255
- Businger J A, Wyngaard J C, Izumi Y and Bradley E F 1971 Flux-profile relationship in the atmospheric surface layer; *J. Atmos. Sci.* **28** 181–189
- Chang S W 1979 An efficient parameterization of convective and non-convective planetary boundary layers for use in numerical models; *J. Appl. Meteorol.* **18** 1205–1215
- Daly B J and Harlow F H 1970 Transport equations in turbulence; *Phys. Fluids* **13** 2634–2649
- Deardorff J W 1966 The counter gradient heat flux in the lower atmosphere and in the laboratory; *J. Atmos. Sci.* **23** 503–506
- Deardorff J W 1974b Three dimensional numerical study of turbulence in an entraining mixed layer; *Boundary-Layer Meteorol.* **7** 199–226
- Detering H W and Etling D 1985 Application of the $E-\epsilon$ turbulence model to the atmospheric boundary layer; *Boundary-Layer Meteorol.* **33** 113–133
- Gray W M 1975 Tropical cyclone genesis; *Atmos. Sci.* No. 234 (Colorado State University) 119p

- Holt T and Sethuraman 1988 A review and Comparative Evaluation of Multi level Boundary Layer Parameterizations for First-order and Turbulent Kinetic Energy Closure Schemes; *Rev. Geophys.* **26** 761–780
- Krishnamurti T N, Cocke S, Pasch R and Low-Nam S 1983 Precipitation estimates from rain gauge and Satellite observations – Summer MONEX; FSU Report No. 83–7, May 1983, Florida State University, Tallahassee, Florida 373pp.
- Krishnamurti T N, Oosterhot D and Nancy Dignon 1989 Hurricane prediction with a high resolution global model; *Mon. Weather. Rev.* **117** 631–669
- Kuo H L 1974 Further studies of the parameterization of the influence on cumulus convection on large scale flow; *J. Atmos. Sci.* **31** 1232–1240
- Madala R V, Chang S W, Mohanty U C, Madan S C, Paliwal R K, Sarin V B, Holt T and Sethuraman 1987 Description of Naval Research Laboratory Limited Area Dynamical Weather Prediction Model; N R L Tech. Report 5992, Washington D C 131 pp
- Mailhot J and Benoit R 1982 A finite element model of the atmospheric boundary layer suitable for use with numerical weather prediction; *J. Atmos. Sci.* **39** 2249–2266
- McBean G A K, Bernhardt S, Bodin Z, Litynska A P, Van Ulden and Wyngaard J C 1979 The Planetary Boundary Layer; WMO Tech Note 165 World. Met. Org.
- Miller B I 1958 On the maximum intensity of hurricanes; *J. Meteorol.* **15** 184–195
- Mohanty U C, Paliwal R K, Madan S C, Tyagi A, Sarin V B and Ramesh K J 1987 Description of a limited area numerical weather prediction model for India and its neighbourhood; Centre for Atmospheric Sciences, IIT, Delhi.
- Monin A S and Yaglom A M 1971 Statistical Fluid Mechanics; Vol I MIT Press 468–504
- Namias J 1973 Birth of hurricane Agnes-triggered by the trans-equatorial movement of a mesoscale system into a favourable large scale environment; *Mon. Weather Rev.* **101** 177–179
- Palmen E 1948 On the formation and structure of tropical hurricanes; *Geophysics* **3** 26–38
- Perkey D J and Kreitzberg W 1976 A time dependent lateral boundary scheme for limited area primitive equation model; *Mon. Weather Rev.* **104** 744–755
- Seller W D 1965 Physical Climatology; (University of Chicago Press) 53–54
- Shir C C 1973 A preliminary numerical study of atmospheric turbulent flows in the idealized planetary boundary layer; *J. Atmos. Sci.* **30** 1327–1339
- Tisdale C F and Clapp P F 1963 Origin and paths of hurricanes and tropical storms related to certain physical parameters at the air-sea surface; *J. Appl. Meteorol.* **2** 358–367
- Tyagi A, Mohanty U C and Ramesh K J 1994 Structure of the atmospheric boundary layer over the monsoon trough region; *Mausam* (In press)
- Wyngaard J C 1975 Modeling the Planetary boundary layer – extension to the stable case; *Boundary-Layer Meteorol.* **9** 441–460

The mean and turbulence structure simulation of the monsoon trough boundary layer using a one-dimensional model with $e-l$ and $e-\varepsilon$ closures

KUSUMA G RAO, V N LYKOSOV**, A PRABHU*
S SRIDHAR* and E TONKACHEYEV**

Jawaharlal Nehru Centre for Advanced Scientific Research, Jakkur P.O., Bangalore 560 064, India

*Centre for Atmospheric Sciences, Indian Institute of Science, Bangalore 560 012, India

**Institute of Numerical Mathematics, Russian Academy of Sciences, Moscow, Russia

Abstract. An attempt has been made here to study the sensitivity of the mean and the turbulence structure of the monsoon trough boundary layer to the choice of the constants in the dissipation equation for two stations Delhi and Calcutta, using one-dimensional atmospheric boundary layer model with $e-\varepsilon$ turbulence closure. An analytical discussion of the problems associated with the constants of the dissipation equation is presented. It is shown here that the choice of the constants in the dissipation equation is quite crucial and the turbulence structure is very sensitive to these constants. The modification of the dissipation equation adopted by earlier studies, that is, approximating the Tke generation (due to shear and buoyancy production) in the ε -equation by max (shear production, shear + buoyancy production), can be avoided by a suitable choice of the constants suggested here. The observed turbulence structure is better simulated with these constants. The turbulence structure simulation with the constants recommended by Aupoix *et al* (1989) (which are interactive in time) for the monsoon region is shown to be qualitatively similar to the simulation obtained with the constants suggested here, thus implying that no universal constants exist to regulate dissipation rate.

Simulations of the mean structure show little sensitivity to the type of the closure parameterization between $e-l$ and $e-\varepsilon$ closures. However the turbulence structure simulation with $e-\varepsilon$ closure is far better compared to the $e-l$ model simulations. The model simulations of temperature profiles compare quite well with the observations whenever the boundary layer is well mixed (neutral) or unstable. However the models are not able to simulate the nocturnal boundary layer (stable) temperature profiles. Moisture profiles are simulated reasonably better. With one-dimensional models, capturing observed wind variations is not up to the mark.

Keywords. Numerical simulation; monsoon boundary layers; turbulence closure; dissipation equation constants.

1. Introduction

The monsoon trough region (figure 1), being an elongated low pressure region over the central parts of India and the adjoining parts on the west, namely Afghanistan, west Pakistan, and the head of the Bay of Bengal in the east, is of crucial importance in explaining the temporal variability of the southwest monsoon. The monsoon has embedded in it a variety of time scales that are about 3–5 days, quasi bi-weekly, 30–50 days and interannual (Krishnamurti and Bhalme 1976; Murakami 1976; Yasunari 1979, 1980; Sikka and Gadgil 1980; Krishnamurti and Subramanyam 1982) over which it fluctuates. It is very well revealed from the satellite pictures and from the analysis of observed data carried out in some of the above mentioned studies that, whenever the

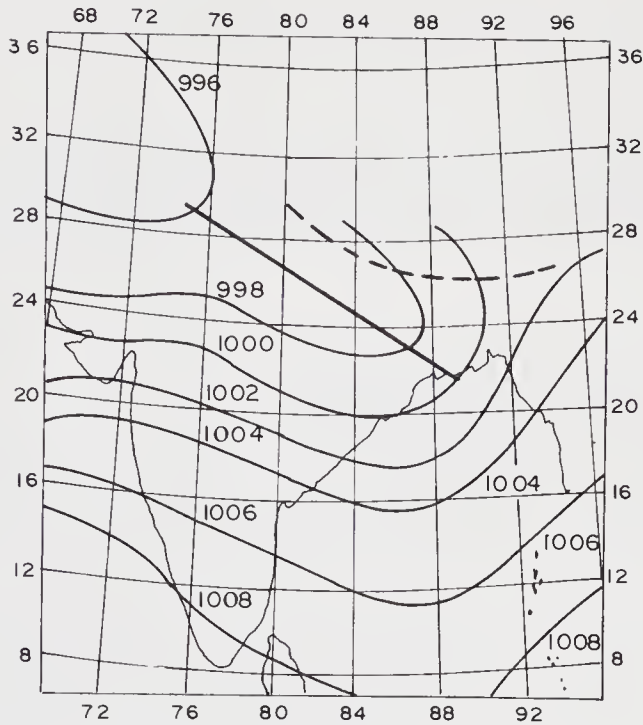


Figure 1. A typical monsoon trough over India. The numbers against the contours indicate the pressure in mbs. Continuous line indicates the trough axis during 'normal' monsoon situations, and the dotted line during 'break' conditions.

monsoon is active, the Continental Intertropical Convergence Zone associated with the monsoon trough region is most intense and well organized spatially; however during the break in the monsoon, it almost disappears. Krishnamurti *et al* (1988) speculated that for the convection to be maintained for long periods of the order of 30–50 days, there must be a steady supply of moisture from the surface of the earth. They noticed that on this time scale, the sensible heat flux and the latent heat flux explain significant amplitudes. In an attempt to understand the cloudiness fluctuations associated with the monsoon trough region between active and break monsoon periods, Kusuma (1988) has shown that during the active spell at levels within the boundary layer of the atmosphere there is a large scale ascent occurring over a large spatial region driven by the dynamic forcing associated with vorticity and temperature advection. However during break monsoon periods such a large scale spatial organization in low level ascent is not seen. Thus the boundary layer processes over the monsoon trough region play a crucial role in driving the monsoon circulation by transporting the moist static energy from the surface into the atmosphere. An attempt has been made here to develop a boundary layer package that may have application in the simulation of monsoon circulation.

There are not many studies reported on the modelling of the monsoon trough boundary layer. Holt and Raman (1988) compared one-dimensional model simulations obtained with various first order closure schemes as well as with Turbulent Kinetic Energy (Tke) closure schemes with the observations over the Bay of Bengal during FGCE, and showed that Tke closure schemes do a better job in simulating the mean structure than the first order; and $e-\epsilon$ closure particularly shows better agreement with observations. Duynkerke and Driedonks (1988) carried out a simulation of

stratocumulus topped boundary layer with a one-dimensional e - ε model. They also conclude that the e - ε model performs better than the Tke model.

In the literature an application of the e - ε closure model to simulate a variety of atmospheric circulation features exist (Detering and Etling 1985; Duynkerke and Driedonks 1987; Duynkerke 1988; Holt and Raman 1988; Huang and Raman 1989). Some studies mentioned above use different values for the constants appearing in the dissipation equation. In fact Holt and Raman (1988) listed different values for the constants chosen by different works (Marchuk *et al* 1977; Detering and Etling 1985; Stublely and Rooney 1986; Beljaars *et al* 1987; Duynkerke and Driedonks 1987). In some of these studies, a further modification of the dissipation equation is done by applying a constraint on the term denoting the generation of dissipation. This term comprises a generation of turbulent kinetic energy (Tke) due to shear and buoyancy. For modelling purposes, the generation of Tke in the dissipation equation due to shear and buoyancy is taken as the maximum of shear production versus a sum of shear and buoyancy production, i.e., maximum (shear, shear + buoyancy). The argument behind such an assumption, stated by the studies mentioned above (e.g. Huang and Raman 1989), is that when the atmosphere is stably stratified, the negative buoyant flux mainly contributes to the re-distribution of heat. Only the energy due to shear production should be cascading down to dissipate. They conclude that this modification reduces mis-representation of dissipation. However, we have shown here how this modification of the dissipation equation can be avoided. Such a modification of the equation seems to be unconvincing. Also it has been shown why the earlier studies (Duynkerke and Driedonks 1987; Duynkerke 1988; Holt and Raman 1988; Huang and Raman 1989) resorted to the above mentioned modification of the dissipation equation.

Here we present a detailed theoretical and physical basis to show how sensitive the turbulence structure is to the constants chosen in the dissipation equation, and also arrive at a particular choice of the constants of the dissipation equation by which any constraint on the Tke generation term in the dissipation equation can be eliminated. The sensitivity of the turbulence structure to the constants of the dissipation equation has been demonstrated by an application of one-dimensional e - ε closure model. The performance of e - ε closure model is estimated in simulating the mean structure of the monsoon trough boundary layer by comparing with both e - l model simulations and observations.

The detailed description of the model adopted here and its validation are described in the next section.

2. Turbulent kinetic energy closure (e - l and e - ε) models

2.1 Model equations

With reference to the list of symbols, the basic equations of the model in (x, y, z, t) system are the following.

u -equation:

$$\frac{\partial u}{\partial t} = -\frac{\partial}{\partial z} \overline{u'w'} - \frac{1}{\rho} \frac{\partial p}{\partial x} + fv. \quad (1)$$

v-equation:

$$\frac{\partial v}{\partial t} = -\frac{\partial \overline{v'w'}}{\partial z} - \frac{1}{\rho} \frac{\partial p}{\partial y} - fu. \quad (2)$$

θ -equation:

$$\frac{\partial \theta}{\partial t} = -\frac{\partial \overline{\theta'w'}}{\partial z} + Q_R + (L/c_p)Q_F. \quad (3)$$

q-equation:

$$\frac{\partial q}{\partial t} = -\frac{\partial \overline{q'w'}}{\partial z} - Q_F. \quad (4)$$

The above equations (1) to (4) form a closed system of equations provided the turbulent fluxes $\overline{u'w'}$, $\overline{v'w'}$, $\overline{\theta'w'}$, $\overline{q'w'}$ are known. These fluxes have been parameterized here, according to the first order closure scheme as originally proposed by Boussinesq (1877), as follows.

Assumption 1:

$$\overline{u'w'} = -K_u(\partial u/\partial z). \quad (5)$$

$$\overline{v'w'} = -K_v(\partial v/\partial z). \quad (6)$$

$$\overline{\theta'w'} = -K_\theta(\partial \theta/\partial z). \quad (7)$$

$$\overline{q'w'} = -K_q(\partial q/\partial z). \quad (8)$$

The eddy exchange coefficients for momentum, K_u and K_v ; for heat K_θ and for moisture, K_q are further assumed to be related as follows.

Assumption 2:

$$\begin{aligned} K_u &= K_v, & K_\theta &= \alpha_\theta K_u, \\ K_q &= \alpha_q K_u, & \alpha_\theta &= \alpha_q. \end{aligned} \quad (9)$$

Thus the emphasis on the fluxes being known in order to close the system of equations (1) to (4) shifts on to the eddy coefficient of viscosity. The eddy coefficient of viscosity is related to turbulent kinetic energy and turbulence length scale according to what is known as 'turbulent kinetic energy closure' or '1/2 closure' scheme (Mellor and Yamada 1974) as follows.

Assumption 3:

$$K_u = l e^{1/2}, \quad (10)$$

where turbulent kinetic energy, e , is prognostically determined and the turbulence length scale, l , is prescribed (in the so-called e - l model) or calculated on the basis of an additional equation for the dissipation rate (e - ϵ model). The turbulent kinetic energy equation (e -equation) (Monin and Yaglom 1971; Busch 1976) is

$$\frac{\partial e}{\partial t} = -\frac{\partial \overline{ew'}}{\partial z} - \frac{\partial}{\partial z} \left(\frac{1}{\rho} \overline{p'w'} \right) - (g/\rho) \overline{\rho'w'} - \overline{u'w'} \frac{\partial u}{\partial z} - \overline{v'w'} \frac{\partial v}{\partial z} - \epsilon, \quad (11)$$

where the buoyant production term can be written as

$$-(g/\bar{\rho})\overline{\rho'w'} = (g/\bar{\theta})\overline{\theta'w'} + 0.61g\overline{q'w'}. \quad (12)$$

The first two terms on the right side of (11), namely vertical turbulent energy transport and pressure transport respectively, are generally included as one and modelled as follows (Monin and Yaglom 1971; Shir 1973; Rodi 1980).

Assumption 4:

$$\frac{\partial}{\partial z} \left(\overline{ew'} + \frac{1}{\rho} \overline{p'w'} \right) = - \frac{\partial}{\partial z} \left(K_e \frac{\partial e}{\partial z} \right), \quad (13)$$

where exchange coefficient K_e is expressed in terms of eddy coefficient of viscosity K_u as $K_e = \alpha_e K_u$, where α_e is a constant.

The dissipation ε can be determined diagnostically (in e - l model) by using the generally accepted relationship of Kolmogorov (1942).

Assumption 5:

$$\varepsilon = C_e e^{3/2}/l, \quad (14)$$

where $C_e = 0.07$.

In e - ε model a prognostic equation for dissipation rate ε is considered as follows, instead of determining it diagnostically as in assumption 5. The concept of using a prognostic equation for energy dissipation ε in the Tke budget equation was first proposed, among others, by Harlow and Nakayama (1967), Daly and Harlow (1970) and Hanjalic and Launder (1972) for fluid engineering applications. The dissipation equation is

$$\begin{aligned} \frac{\partial \varepsilon}{\partial t} = & - \frac{\partial}{\partial z} \overline{\varepsilon w'} - (\varepsilon/e) C_3 [\overline{u'w'}(\partial u/\partial z) + \overline{v'w'}(\partial v/\partial z) + g/\rho(\overline{\rho'w'})] \\ & - C_4 \varepsilon^2/e, \end{aligned} \quad (15)$$

where the diffusion of dissipation is parameterized as follows.

Assumption 6:

$$\frac{\partial}{\partial z} \overline{\varepsilon w'} = - C_5 \frac{\partial}{\partial z} (K_u \partial \varepsilon / \partial z), \quad (16)$$

where $C_5 = 0.77$.

For detailed derivation of the above form of ε -equation (15) from the equations of motion, which is quite involved, one can refer to Marchuk *et al* (1977), Wyngaard (1975) and Lumley (1980). Several assumptions and parameterizations have been made before arriving at the above form of dissipation equation.

The values used for various constants appearing in the above dissipation equation by several researchers have been listed in table 1. The constants quoted by Launder and Spalding (1974) are derived for engineering applications. Detering and Etling (1985) proposed a correction for C_3 by considering the mixing length scale and the height of the boundary layer to better simulate the observed structure of the atmospheric boundary layer, but not based on stringent arguments. A detailed discussion on these constants is presented in the next section.

Table 1. The e - ε model constants.

Author	C_2	C_3	C_4	C_5
Launder and Spalding (1974)		1.44	1.92	0.77
Duynkerke and Driedonks (1987)	0.09	1.44	1.92	0.77
Stublely and Rooney (1986)	0.09	1.44	1.92	0.77
Beljaars <i>et al</i> (1987)	0.032	1.44	1.92	0.54
Detering and Etling (1985)	0.026	1.13	1.90	0.77
Modified Detering and Etling (1985)	0.024	1.13 (l/H)*	1.90	0.77
Marchuk <i>et al</i> (1977)	0.08	1.38	1.40	1.0

* l = mixing length; H = height of the boundary layer.

With relation (12) and assumptions 1 to 6, the equations (11) and (15) can be solved to obtain turbulent kinetic energy and dissipation rate prognostically, hence the eddy coefficient of viscosity as follows

$$K_u = C_e e^2 / \varepsilon.$$

Once the eddy viscosity is known, with the assumptions 1 to 3, the system of equations (1) to (4) form a closed system and a solution can be obtained.

Now regarding the boundary conditions applied to solve equations (1) to (4) and (11) and (15), at the upper boundary it is assumed that the wind approaches observed wind; the temperature and moisture are equal to the observed temperature and moisture respectively at that level and the gradients of Tke and dissipation at that level are zero. That is, at the model top $z = H$

$$\begin{aligned} u &= u_H, & v &= v_H, \\ \theta &= \theta_H, & q &= q_H, \\ K_u(\partial e / \partial z) &= 0, & K_u(\partial \varepsilon / \partial z) &= 0. \end{aligned} \quad (17)$$

At the lower boundary, which is the top of the constant flux layer, the flux continuity conditions are assumed. The Tke at the lower boundary is prescribed according to the relation (10). Therefore

$$\begin{aligned} \text{at } z = h, \quad K_u(\partial u / \partial z) &= C_D |V| u, \\ K_v(\partial v / \partial z) &= C_D |V| v, \\ K_\theta(\partial \theta / \partial z) &= C_D |V| (\theta - \theta_s), \\ K_q(\partial q / \partial z) &= C_\theta |V| (q - q_s), \\ q_s &= r_s q_{\max}(T_s), \end{aligned} \quad (18)$$

where h is the prescribed height of the surface layer. In (18) C_D is drag coefficient, C_θ - heat (moisture) exchange coefficient, suffix 's' stands for the surface, r_s is relative

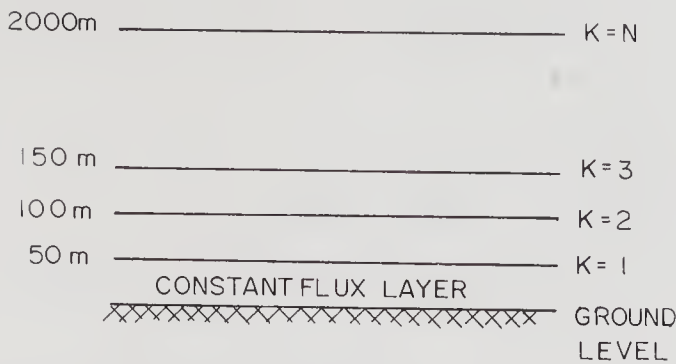


Figure 2(a). Domain of integration.

humidity and q_{\max} – saturated value of specific humidity. It is also assumed that the Tke and dissipation rate at the lower boundary are calculated according to the relations (10) and (14).

$$e = (K_h/\kappa h)^2, \varepsilon = C_e e^2/K_h \quad \text{at } z = h. \tag{19}$$

K_h is calculated on the basis of constant flux layer theory. K_h denotes the eddy coefficient of viscosity at level $z = h$.

Then the equations (1) to (4), (11) and (15) are solved by applying boundary conditions (17) to (19) for the domain extending from surface to a height of 2.0 km as shown in figure 2(a). The lowest level of integration coincides with the top of the constant flux layer. The top-most level represents the top of the boundary layer. The vertical domain has been divided into 40 equidistant levels with a resolution of $\Delta z = 50$ m. Crank Nicholson’s fully implicit scheme is adopted to write the finite difference form of the second order diffusion terms. The technique, namely the tridiagonal matrix method, adopted to solve the finite difference equations is given by Godunov and Ryaberkiy (1962) and Richtmyer and Morton (1967).

The constant flux layer formulation is based on the Monin-Obukov similarity theory which is described in detail in the following section.

2.2 Constant flux layer

The lowest layer which is 50 m thick between the surface and the first level of integration is assumed to be the constant flux layer, as shown in figure 2(a). The constant flux layer formulation has been based on the Monin-Obukov similarity theory. Businger and Dyer universal functions together with ‘ $-1/3$ ’ law asymptotics have been used to describe thermally stratified situations (Kazakov and Lykossov 1982). At the surface, the boundary conditions are $u = u_s = 0; v = v_s = 0; \theta = \theta_s; q = q_s$ where the suffix ‘s’ denotes the surface; u_s, v_s, θ_s, q_s and r_s represent observed values of wind components, potential temperature, moisture and relative humidity respectively.

The constant flux layer prepares the lower boundary conditions necessary for the model integration by calculating the drag coefficient C_D , exchange coefficient for heat C_θ , the eddy coefficient of viscosity K_h and the ratio α_θ between the eddy coefficient of heat, K_θ and K_h at the first level $K = 1$. The formulae used for universal functions are

the following (Kazakov and Lykossov 1982):

$$f_\psi(\zeta, \tilde{\zeta}) = \ln(z_u/z_\psi) + \begin{cases} \ln \tilde{\zeta} + \beta\zeta & \text{when } \zeta > 0, \\ \Phi_\psi(\zeta) - \Phi_\psi(\zeta_u) & \text{when } \zeta^* < \zeta < 0, \\ 3x_\psi^{-1}(\zeta^*)[1 - (\zeta^*/\zeta)^{1/3}] + \phi_\psi(\zeta^*) - \Phi_\psi(\zeta_u) & \text{where } \zeta < \zeta^*, \end{cases} \quad (20)$$

where

$$\phi_u(\zeta) = \ln[(x_u(\zeta) - 1)/(x_u(\zeta) + 1)] + \text{Zarctg}[x_u(\zeta)].$$

$$\Phi_\theta(\zeta) = \ln[(x_\theta(\zeta) - 1)/(x_\theta(\zeta) + 1)],$$

$$x_u(\zeta) = (1 - r_u\zeta)^{1/4}, \quad x_\theta(\zeta) = (1 - r_\theta\zeta)^{1/2}, \quad \zeta_u = z_u/L_v, \quad \tilde{\zeta} = \zeta/\zeta_u,$$

$$\zeta = z/L_v,$$

$$L_v = L[1 + 0.07/B_0]^{-1}, \quad L = u_*^2/\kappa^2\lambda\theta_*, \quad B_0 = H_s/L_x E_s,$$

$$\zeta^* = [2r_\theta - Ar_u - (Ar_u^2 + 4Ar_\theta(r_\theta - r_u))^{1/2}]/2r_\theta^2,$$

$$A = (\alpha_{-\infty}/\alpha_\psi)^4, \quad \alpha_{-\infty} = K_\theta/K_u, \quad \alpha_\psi = 1.15, \quad \alpha_{-\infty} = 3.5,$$

$$r_u = 16.0, \quad r_\theta = 16.0, \quad \beta = 4.7.$$

In (20) ψ stands for u or θ , L_x the latent heat of evaporation, ζ^* is the value of ζ at which Businger and Dyer functions and the '−1/3' asymptotics match. To calculate 'thermal roughness' z_θ the following relations are used.

$$\begin{aligned} \ln(z_u/z_\theta) &= -2.43 \quad \text{when } \text{Re}_* < 0.111, \\ &= 0.83 \ln(\text{Re}_*) - 0.6 \quad \text{when } 0.111 < \text{Re}_* < 16.3, \\ &= 0.49 \text{Re}_*^{0.45} \quad \text{when } \text{Re}_* > 16.3, \end{aligned} \quad (21)$$

where $\text{Re}_* = u_* z_u/\nu_m$ and ν_m is kinematic viscosity. In formulae (20), (21), L, u_*, θ_* are the scales for measuring the length, wind speed and temperature respectively.

2.3 Condensation process

Regarding the heating due to condensation, the convective-adjustment scheme is adopted. That is, whenever super saturation occurs in a moist statically stable atmosphere, the excess moisture is condensed and the latent heat is released. The model has both dry and moist convective adjustment processes.

2.4 Radiation

The model has only long wave cooling effects. The only constituent that takes part in long wave radiative flux calculation is the water vapour. The model does not have solar radiation calculated explicitly. The diurnal cycle in solar radiation is automatically

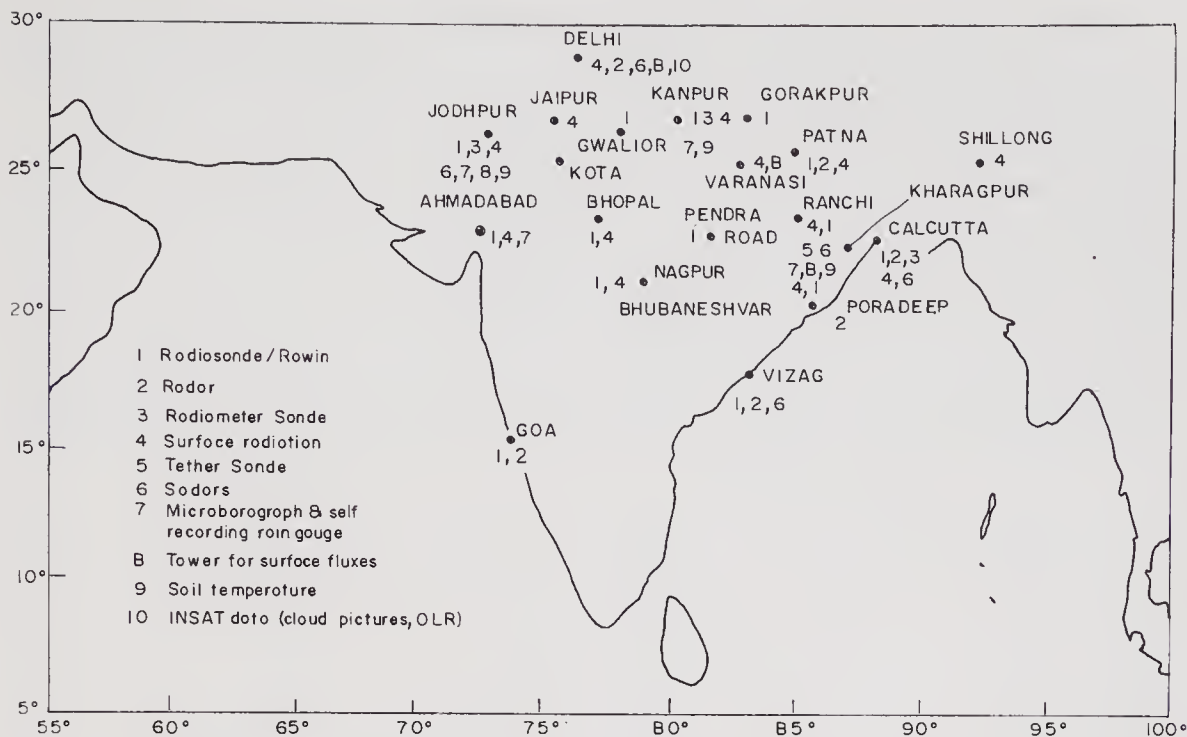


Figure 2(b). 'MONTBLEX' observational platforms.

considered by way of prescribing the surface temperature and surface humidity as boundary conditions.

With these details about the model, we next proceed to describe the data chosen for this study.

3. Data

A national experiment known as Monsoon Trough Boundary Layer Experiment (MONTBLEX) was operational during 1990 (Goel and Srivastava 1990; Sikka and Narasimha 1995). MONTBLEX conducted a pilot experiment during July 1989 for 15 days from 20th July to 3rd August. Figure 2(b) describes the MONTBLEX observational platform. In this study, we have chosen radiosonde data for Calcutta (22°N , 88°E) and New Delhi (28°N , 77°E) stations. Calcutta is a coastal station situated at the head of the Bay of Bengal. New Delhi is situated in the central part of India. Wind data (wind force and magnitude), temperature and dew point temperature data at these stations were available due to radiosonde/rawinsonde and slow ascent balloon techniques. The data were recorded four times a day around 5:30, 10:45, 17:30 and 22:45 IST. The number of data levels at which the observations are recorded varies from 5 to 15 in 2 km of boundary layer. The model input data, namely the zonal and the meridional wind components, the potential temperature and moisture are calculated in turn and these data have been interpolated on to the model grid using cubic-spline interpolation technique. To specify the pressure gradient components in equations (1) and (2) the geostrophic approximation has been used

$$\begin{aligned} -1/\rho(\partial p/\partial x) + fv_g &= 0, \\ -1/\rho(\partial p/\partial y) - fu_g &= 0. \end{aligned} \quad (22)$$

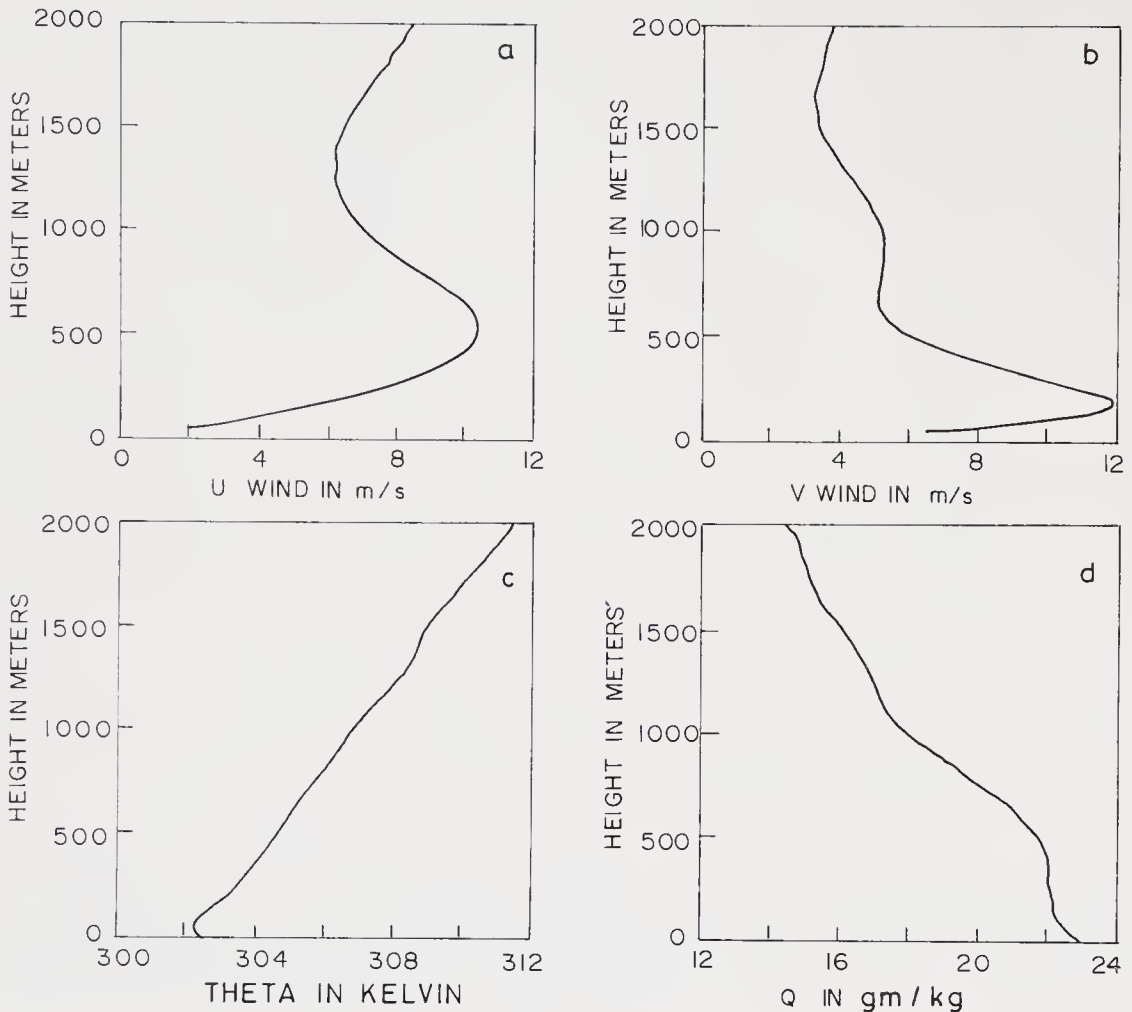


Figure 3. Initial profiles for Calcutta station: (a, b) wind components, u and v in ms^{-1} ; (c) potential temperature, θ in kelvin; (d) moisture q , in gm kg^{-1} .

where u_g and v_g were assumed to be the observed values of real wind velocity at the height H . These profiles of u, v, θ, q taken at 6:00 LST on 20th July for Calcutta are shown in figures 3(a–d) respectively. These profiles have been used as initial data to validate $e-l$ and $e-\varepsilon$ models.

4. Validation of $e-l$ closure model

With the $e-l$ model described in section 2 and data chosen as above, some test experiments are carried out in order to validate the model performance. The first experiment is the steady state and the second experiment compares the model predictions obtained for different time steps.

In the first experiment, the model reaches a steady state when the boundary conditions are fixed invariant with respect to time. The model reaches the steady state in about 7 to 8 hours of model time. In the second experiment, the predictions are obtained for various time steps keeping the initial data and the boundary conditions same in all the model runs. A comparison, of predictions for different time steps at the end of every hour of prediction up to 24 hours of model time, reveals that the predictions

for u, v, θ, q fields agree respectively with each other reasonably well. Further validation of the model has been done by simulating the diurnal cycle of the atmosphere.

In simulation of the diurnal cycle of the atmospheric boundary layer by the $e-l$ model, the initial data recorded at 6 am on 20th July 1988 and shown in figure 3, are used to start the model integration. The model has been integrated for 24 hours with the total physics of the model being considered. The diurnal evolution of the various surface layer characteristics like eddy coefficient of viscosity (K_h), the Richardson number (R_i), the drag coefficient (C_D), surface shear stress (τ_s), the sensible heat flux and the moisture flux are shown in figure 4(a-f). The x-axis indicates the time at which the predictions were made from 9 am on 20th July 1988 to 6 am on 21st July 1988. Figure 4(a-b) indicates the development of day time boundary layer with a large negative Richardson

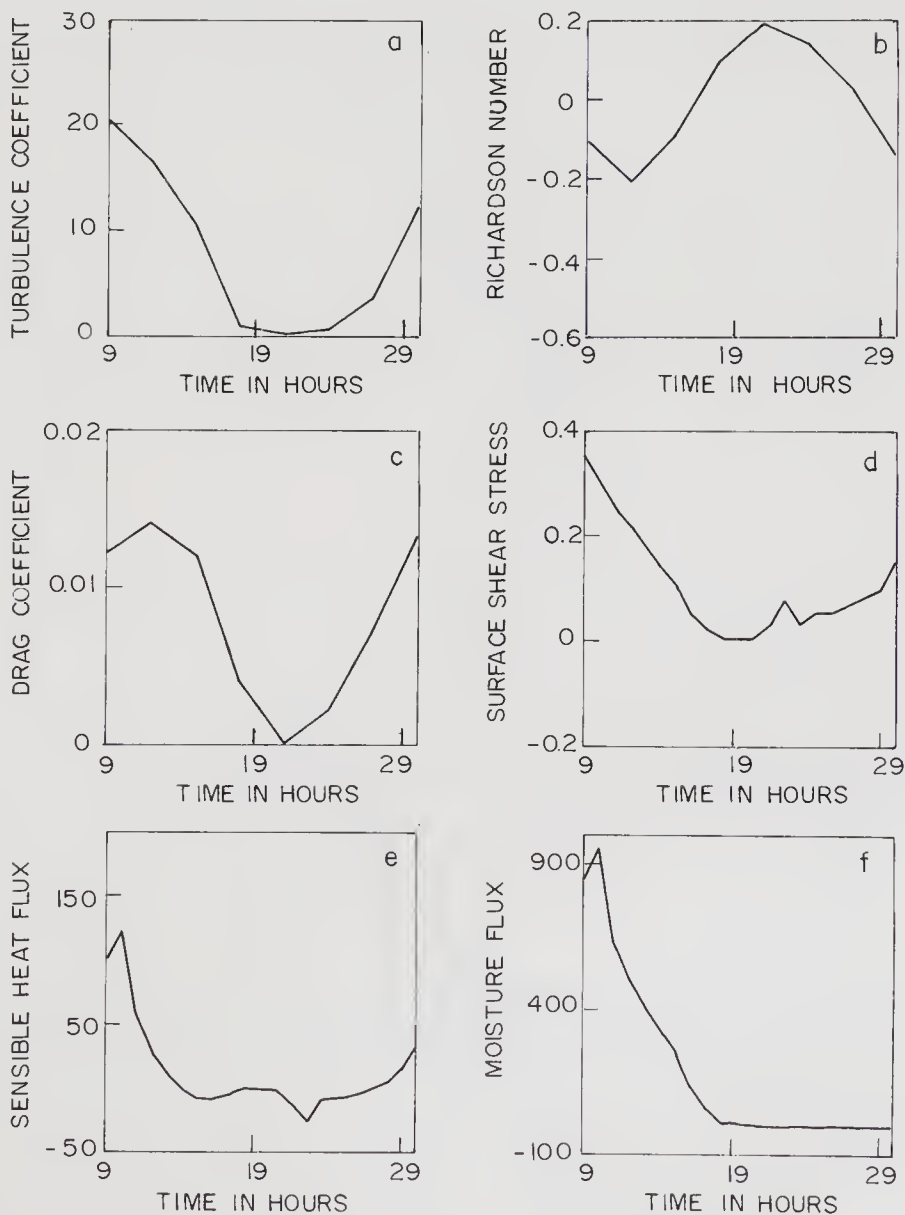


Figure 4. Diurnal evolution of constant flux layer (a) turbulence coefficient, K_h in m^2s^{-1} ; (b) Richardson number, R_i ; (c) drag coefficient, C_D ; (d) surface shear stress, τ_s in Newton m^{-2} ; (e) sensible heat flux, $\rho c_p \overline{w'\theta'}$ in watts m^{-2} ; (f) moisture flux, $\rho_L \overline{w'q'}$ in watts m^{-2} .

number indicating unstable surface layer; and with a large eddy coefficient of viscosity indicating strong mixing. As the night sets in the Richardson number becomes positive, eddy coefficient of viscosity becomes almost zero indicating the decay of turbulence. The surface shear stress, the sensible heat flux and the moisture flux show a similar diurnal trend as shown in figure 4(d-f). The sensible heat flux peaks up in the morning only because the diurnal cycle in surface temperature which is prescribed from observations as the lower boundary condition (17) is not resolved properly as the temperatures were recorded only four times a day at 5.30, 10.45, 17.30 and 22.45 LST. Thus in the surface temperature both the peaks (maximum and minimum) are missing. The vertical profiles of potential temperature are shown every 3 hours from 9 am on 20th July to 6 am on 21st July in figure 5(a-b). To start with the initial θ -profile, figure 3(c) indicates a stable boundary layer. Figure 5(a) shows the day time

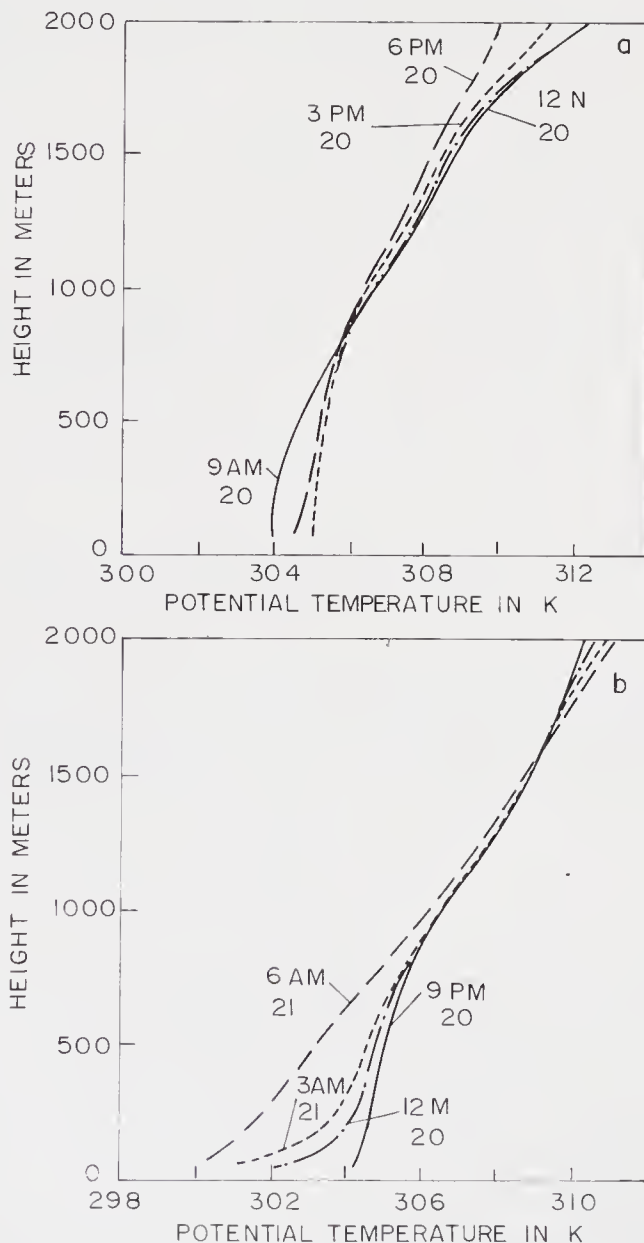


Figure 5. Diurnal evolution of the vertical structure of potential temperature in kelvin. The numbers against the curves indicate the time and day at which the profile is drawn.

development of the boundary layer in potential temperature with the initial input as shown in figure 3(c). As the sun marches, during the day, the θ -profiles on 20th July at 9 am, 12 noon, 3 pm indicate the development of mixed layer clearly as shown in figure 5(a). Further integration of the model (figure 5 b) shows the development of the nocturnal boundary layer. The θ -profiles at 12 midnight on 20th July, and at 3 am and 6 am on 21st July (figure 5b) indicate the development of stable boundary layer as the night sets in. However, the diurnal cycle is not clearly seen in wind as well as in moisture.

5. Validation of e - ε closure model

In this section, initially the problems associated with the modelling of the dissipation equation are dealt with. An analytical discussion on the constants of the dissipation equation is presented. A verification to these analytical results has been demonstrated with the e - ε closure model described in section 2.

5.1 Analytical discussion

The main problem associated with the models based on the dissipation equation is the absence of asymptotics for the decaying turbulence.

Let us assume that the production of the turbulent kinetic energy due to the coupled effect of wind shear and buoyancy is absent and the effects of the turbulent diffusion are negligible corresponding to a situation of self-decaying turbulence. The equations (11) and (15) can be rewritten as follows.

$$\frac{de}{dt} = -\varepsilon, \quad (23)$$

$$\frac{d\varepsilon}{dt} = -C_4(\varepsilon^2/e). \quad (24)$$

As initial data we choose

$$e = e_0, \quad \varepsilon = \varepsilon_0 \quad \text{at } t = 0. \quad (25)$$

It is easy to obtain the solution of the above initial value problem (23)–(24) in the following form

$$e = [e_0^{1-C_4} + ((C_4 - 1)\varepsilon_0/e_0^{C_4})t]^{-1/(C_4-1)}, \quad (26)$$

$$\varepsilon = \varepsilon_0(e/e_0)^{C_4}. \quad (27)$$

From the solution (26) it can be seen that $e \rightarrow 0$, if $t \rightarrow \infty$ and $C_4 > 1$. The turbulence length scale l can be calculated following the assumption 5 (relation 14),

$$\varepsilon = C_e e^{3/2}/l, \quad (28)$$

and using the solutions (26) and (27) as

$$l = (C_e e_0^{C_4}/\varepsilon_0) e^{3/2-C_4}. \quad (29)$$

From (29) one can see that if $C_4 > 3/2$, as $t \rightarrow \infty$, then $l \rightarrow \infty$. In decaying turbulence l tending to $l_0 < \infty$ is possible only if we choose $C_4 < 3/2$. In this case of decaying

turbulence we obtain from the relation (29) that $l_0 = 0$ if $C_4 \leq 3/2$. However in many of the earlier studies (table 1) the constant C_4 is chosen as 1.92 which is greater than $3/2$. With $C_4 = 1.9$, the evolution of the numerical solution with time is shown in the following experiment.

Experiment 1: In order to demonstrate the analytical result that $l \rightarrow \infty$ if $C_4 > 3/2$, we have conducted a numerical experiment with the one-dimensional e - ε closure model as described in section 2 by choosing $C_4 = 1.9$. Initial data chosen are as shown in figure 3 and corresponds to the time instant of 6 am on 20th July. With these initial conditions, with all physics included, the model was integrated for 36 hours. Here we have taken $C_3 = 1.4$. This experiment strictly does not simulate the self-decaying turbulence, because the total Tke and dissipation equations are solved here. The generation terms are kept throughout 36 hours of integration. The time evolution of Tke, K_u , l , dissipation (D), shear production (S) and buoyant production (B) terms are shown in figure 6(a–l) at model heights of 650 m and 1650 m. From figure 6(a–b), we note that Tke assumes very large values at 8 pm on 20th July at the model height of 650 m after approaching very small values before that instant indicating that the turbulence was decaying. From 6(b), we infer that the instability seems to be developing first at higher levels and then descending to the lower levels. From 6(c–d), we see that the eddy coefficient of viscosity values also shoots up at the same instant when Tke shoots up. At this instant, the turbulence length scale (figure 6 e–f) is around 200 m. Even the length scale taking values of 200 m at 8 pm in the night is very large when the atmospheric boundary layer is statically stable. During the day time, when the boundary layer is known to be convectively unstable, the turbulence length scales are even smaller than 200 m. Dissipation as shown in figure 6(g–h) is also high at 8 pm on 20th July since the Tke generation is high and assumes very small value before this instant when Tke is small. Figure 6(i–j) shows that there is a buoyant sink at both the levels of 650 m and 1650 m and figure 6(k) shows that there was very less shear production of Tke at 650 m before the time instant at which the Tke grows rapidly, indicating that the turbulence was decaying. Thus with this choice of constants $C_4 = 1.9$ and $C_3 = 1.4$, the whole model blows up whenever the turbulence is decaying. However since the model is numerically stable, the large K_u produced in the model kills large Tke produced, and hence the model tries to come back to a stable situation.

Thus, it is now very clear to us from the above analysis, why some above-mentioned studies tried to modify the dissipation equation while modelling the atmospheric boundary layer.

In order to avoid this situation of $l \rightarrow \infty$ in the case of nearly decaying turbulence, Duynkerke and Driedonks (1987); Driedonks (1988); Holt and Raman (1988) and Huang and Raman (1989), modified the dissipation equation especially the term denoting the generation of ε . In this term the generation of turbulent kinetic energy due to shear and buoyancy is assumed by the above-mentioned studies to be the maximum of {shear + buoyant} production versus {shear} production. That is

$$\left[-\overline{u'w'} \frac{\partial u}{\partial z} - \overline{v'w'} \frac{\partial v}{\partial z} - \frac{g}{\rho} \overline{w'\rho'} \right] \simeq \text{Max} \left\{ \left(-\overline{u'w'} \frac{\partial u}{\partial z} - \overline{v'w'} \frac{\partial v}{\partial z} \right), \left(-\overline{u'w'} \frac{\partial u}{\partial z} - \overline{v'w'} \frac{\partial v}{\partial z} - \frac{g}{\rho} \overline{w'\rho'} \right) \right\}. \quad (30)$$

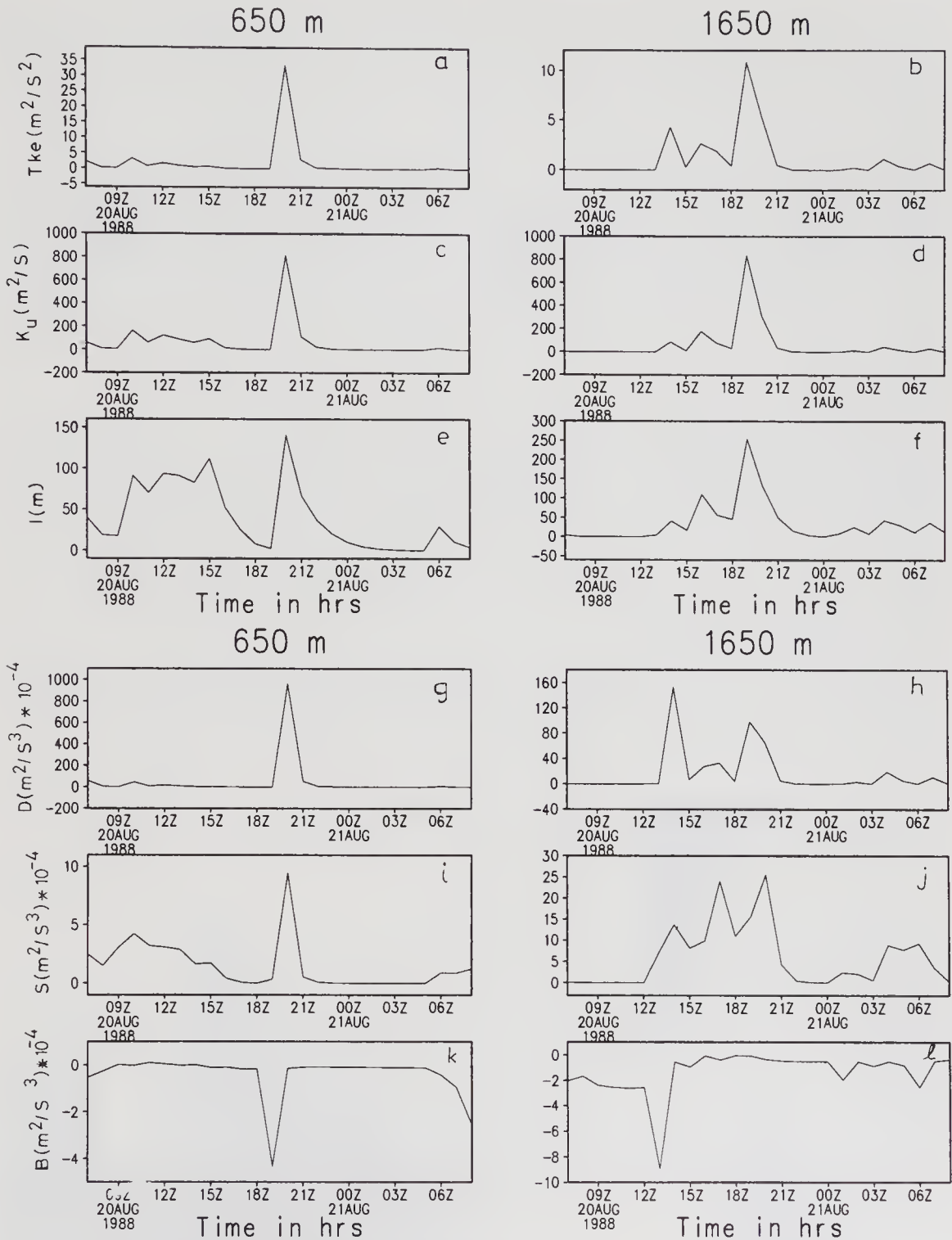


Figure 6. Time evolution of: (a–b) T_{ke} in m^2s^{-2} ; (c–d) turbulence coefficient in m^2 ; (e–f) turbulence length scale in m ; (g–h) dissipation in m^2s^{-3} ; (i–j) shear production in m^2s^{-3} ; (k–l) buoyant production in m^2s^{-3} . Here $C_4 = 1.9$, $C_3 = 1.4$.

Experiment 2: Similar to experiment 1, another numerical experiment was run with the same initial conditions and the same model physics as in experiment 1 but for the modification of dissipation equation (15). The evolution of T_{ke} for 72 hours is shown in

figure 7. Here again we have chosen the constants of dissipation equation as $C_3 = 1.4$ and $C_4 = 1.9$ as in experiment 1 with the modification of dissipation generation term according to (30). The Tke evolution (figure 7), is more stable as compared with its evolution in the earlier experiment (figure 6a–b). This modification of dissipation equation has reduced the large Tke values seen in experiment 1 to very small values except at the upper boundary around 2 pm on 20th July. Large Tke values around 2 pm at the upper most levels are due to large shear production (figures not shown) occurring there. However there is a strong buoyant sink at these levels at that instant (figures not shown) which is not considered in the dissipation calculation. Therefore the dissipation is over-estimated which kills large Tke production at that instant and hence the Tke values beyond 3 pm on 20th July are reasonable. The Tke values evolving in this experiment at the upper boundaries are high compared to the observed values noted in the literature (Stull 1988).

Thus such an assumption on the generation of turbulent kinetic energy in dissipation equation over-estimates the dissipation. Because in a situation where the shear production is positive (which can be negative when the counter gradients in momentum exist) and buoyant production is negative in a statically stable situation which is seen in the above experiment, the above mentioned assumption (30) will over-estimate the generation of Tke and hence the dissipation. This is also true when there is negative shear production and positive buoyant production of Tke which can happen in a statically unstable situation.

Let us consider this problem in more detail. To get the constant C_4 for the decaying turbulence situation, the turbulent kinetic energy spectra are chosen as follows

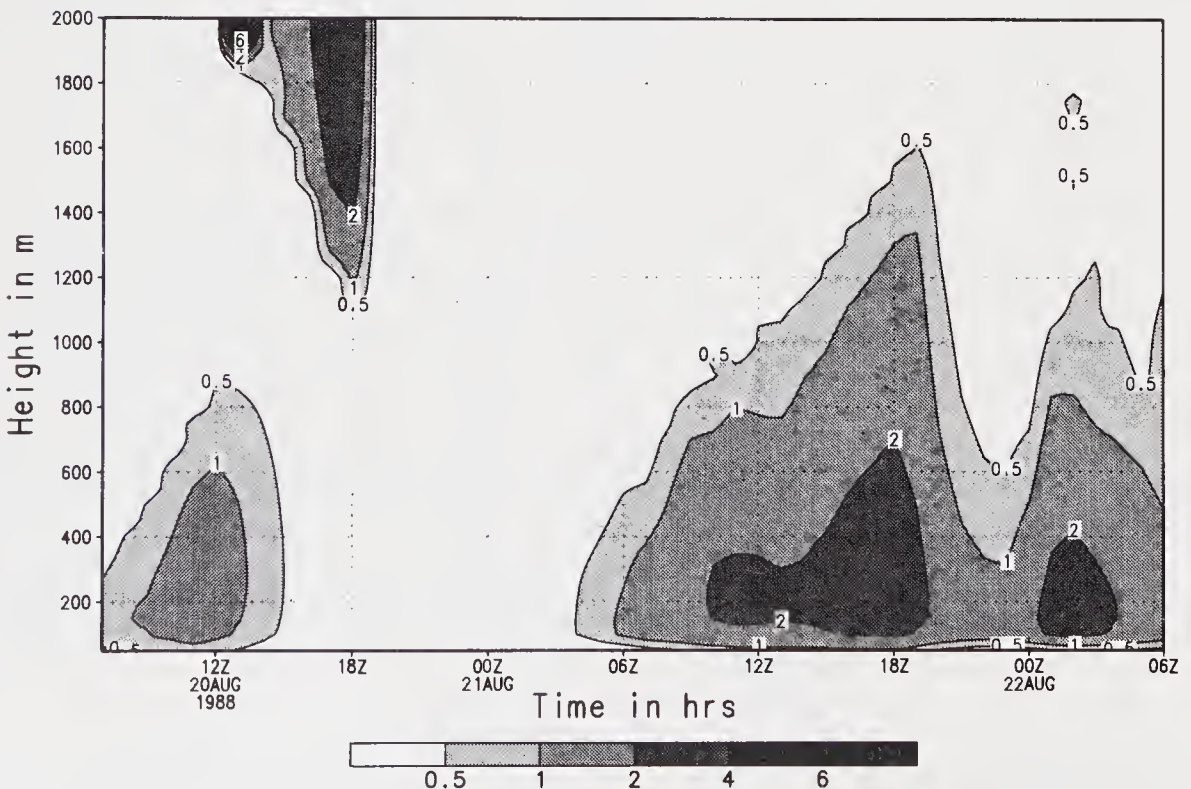


Figure 7. Time evolution of Tke in m^2s^{-2} . $C_4 = 1.9$, $C_3 = 1.4$. In ε -equation, Tke generation is $\max(\text{shear}, \text{shear} + \text{buoyancy})$.

(Reynolds 1974; Aupoix *et al* 1989)

$$E(K) \sim \begin{cases} K^s & \text{for } K \leq K_m, \\ \varepsilon^{2/3} K^{-5/3} & \text{for } K \geq K_m, \end{cases} \quad (31a)$$

$$(31b)$$

where parameter K_m is the wavenumber which separates conditionally two spectral intervals. In the above relations, the first relation (31a) represents the contribution from very large eddies and the second relation (31b) describes the so-called inertial subrange. Then the turbulent kinetic energy can be expressed in the following form

$$e = \int_0^\infty E(K) dK \sim \varepsilon^{2(s+1)/(3s+5)}. \quad (32)$$

For the homogeneous isotropic decaying turbulence the Tke equation takes the form of (23), which together with relation (32) and the dissipation equation (24), leads to a relation in which the constant C_4 can be expressed as a function of the parameter S

$$C_4 = (3s + 5)/2(s + 1), \quad (33)$$

where s can take the value between 1 and 4, Aupoix *et al* (1989). If we choose $s = 1.5$, then it is easy to obtain from (33) that $C_4 = 1.9$.

From our point of view the effect of very large eddies is probably over-estimated in such an approach where we choose $C_4 = 1.9$ and this leads to the unrealistic values of l and hence necessitates an artificial correction of the term representing generation of ε in equation (15).

We preferred to use only inertial subrange of spectra 31(b). In this case it is easy to obtain that $C_4 = 3/2$ and for the decaying turbulence, we have from (29) that l is constant and $< \infty$.

Once again with the same model physics and initial conditions as described in earlier experiments, an experiment has been run with $C_4 = 3/2$ and $C_3 = 1.4$, but without any modification of dissipation equation. Once again we note that the Tke evolution with these constants (figure not shown here) is stable as in experiment 2 but the Tke values are still on the higher side at the upper levels of the domain when compared with observations (Stull 1988). We note that in the present experiment there is no modification of the dissipation equation as done in experiment 2.

Let us consider a more general case where we again neglect the turbulent diffusion in equations (11) and (15), but include the energy generation term. Hence the equations (11) and (15) can be generalized as follows,

$$de/dt = -\varepsilon + (e^2/\varepsilon)F, \quad (34)$$

$$d\varepsilon/dt = (\varepsilon/e)(-C_4\varepsilon + C_3(e^2/\varepsilon)F), \quad (35)$$

where $(e^2/\varepsilon)F$ is the source (or sink) of turbulent kinetic energy due to dynamics and/or buoyancy. Hereafter we assume that $C_4 = 1.5$. From these equations (34) and (35), it is easy to show that e and ε should satisfy the following equation

$$(e/\varepsilon)(d\varepsilon/de) = (C_3e^2F - C_4\varepsilon^2)/(e^2F - \varepsilon^2). \quad (36)$$

The above equation (36) can be reduced by the transformation

$$y = (\varepsilon/e)^2, \tag{37}$$

to the following one

$$[(F - y)/((C_3 - 1)F - (C_4 - 1)y)] dy/y = 2de/e. \tag{38}$$

Solution of the above equation when F is treated constant in time, is the following

$$|(C_3 - 1)Fe^2 - (C_4 - 1)\varepsilon^2|^r \varepsilon^{2/(C_3 - 1)} = Ce^{2C_4/(C_4 - 1)}, \tag{39}$$

where $C > 0$ is the constant of integration, depending on initial data (25) and

$$r = (C_3 - C_4)/[(C_3 - 1)(C_4 - 1)]. \tag{40}$$

Taking into consideration the relation (28), the above relation (39) takes the form

$$|F^*l^2 - \alpha e|^r = C^*l^{\beta_1} e^{\beta_2}, \tag{41}$$

where

$$F^* = (C_3 - 1)F, \alpha = C_e^2(C_4 - 1), \beta_1 = 2/(C_4 - 1), \beta_2 = (2C_3 - 3)/(C_3 - 1), \tag{42}$$

and $C^* > 0$ is a modified constant of integration. For the chosen $C_4 = 3/2$ and $C_e = 0.07$ we obtain that $\alpha = 0.00245$ and $\beta_1 = 4$.

Let us consider first the case $F^* < 0$. In this case relation (41) can be rewritten in the following form

$$(\alpha e + |F^*|^2)^r = C^*l^{\beta_1} e^{\beta_2}. \tag{43}$$

If we assume that $\beta_2 > 0$ then from the last relation (42), it is seen that $C_3 > 3/2$ and consequently $r > 0$. For the case $\beta_2 = 0$ (hence $r = 0$), we immediately obtain that

$$l = (1.0/C^*)^{1/4}, \quad \varepsilon \sim e^{3/2} \tag{44}$$

are the zeroth order solutions of equations (34) and (35).

If $\beta_2 > 0$ and also if we assume that $e \rightarrow 0$ as $t \rightarrow \infty$, it follows in this case for the small enough values of e that the following asymptotic for l must be satisfied.

$$l^{2r - \beta_1} \sim e^{\beta_2}. \tag{45}$$

Taking into account definitions of r and β_1 (as in (40) and (42)) we obtain that

$$2r - \beta_1 = -2/(C_3 - 1) < 0$$

for the assumed value of $C_3 > 3/2$. It means that $l \rightarrow \infty$ if $e \rightarrow 0$.

If we choose $\beta_2 < 0$, then $r < 0$ and an asymptotic behaviour to l should be as follows

$$l^{2|r| - \beta_1} \sim e^{-\beta_2}. \tag{46}$$

Then l tends to 0, if e tends to 0 and $C_3 > 1$. Taking for example, $C_3 = 4/3$, we get $r = -1, \beta_2 = -1$ and therefore the relationship (46) leads to the l and ε asymptotics to be as follows

$$l \sim e^{1/6}, \quad \varepsilon \sim e^{4/3}. \tag{47}$$

The above asymptotic relation implies that in the case of $F^* < 0$ a stationary solution of problem (34)–(35) should be zero. It is natural to assume that $e \neq 0$ and $\varepsilon \neq 0$ in the

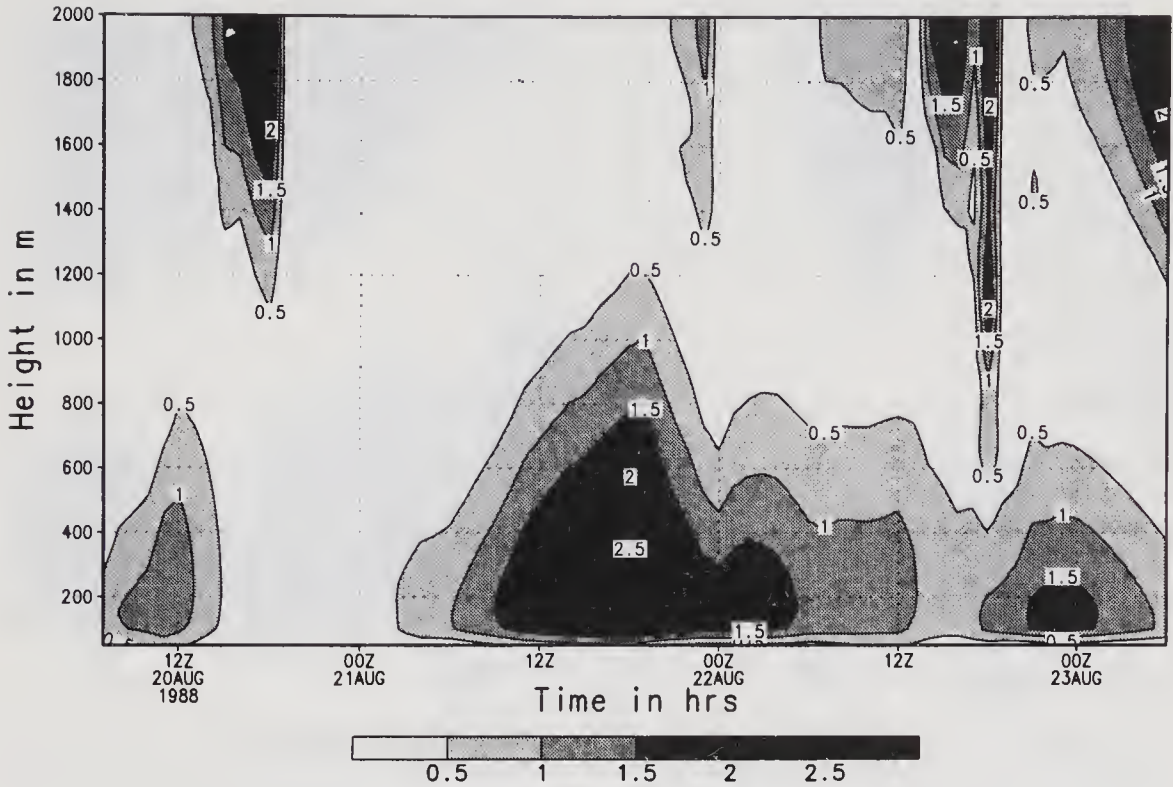


Figure 8. Time evolution of Tke in m^2s^{-2} . $C_4 = 1.5$, $C_3 = 4/3$.

case of $F^* > 0$. However one can easily see from equations (34) and (35) that non-zero stationary solution of the problem does not exist if C_3 is not equal to C_4 . If we assume that the constants C_3 and C_4 are the same as $C_3 = 4/3$ and $C_4 = 3/2$ for this case also, the solution of the problem (34) and (35) can be expressed in phase space (e, y) by the curve, the equation of which follows from the relation (39),

$$y^3 + 3/2Ce^2y \mp CFe^2 = 0, \tag{48}$$

where the upper (lower) sign stands for the case of positive (negative) difference $(F - (3/2)y)$. We are interested in the positive solution only of algebraic equation (48). It is necessary to be reminded here that $C > 0$, $F > 0$.

Let us consider first the case of the upper signs in the equation (48). It is well known from the theory of cubic algebraic equations that equation (48) has, for the parameters C and F under consideration, a single positive solution for every value of e . In the case of the lower sign in the relation (48), this algebraic equation does not have positive solutions. We conclude therefore that

$$(\varepsilon/e)^2 < 2/3F, \tag{49}$$

of course initial conditions must also satisfy the above inequality (49).

However the solution of problems (34) and (35) can tend to zero or to infinity depending on parameters C_3 , C_4 and F (Kochergin and Sklyar 1992). Particularly, they have shown that in case $F > 0$, the solution tends to zero when $C_4 < C_3$ and tends to infinity when $C_4 > C_3$. The greater the difference $C_4 - C_3$, the faster the solution tends to infinity. To show this experimentally, we have done experiments 3 and 4.

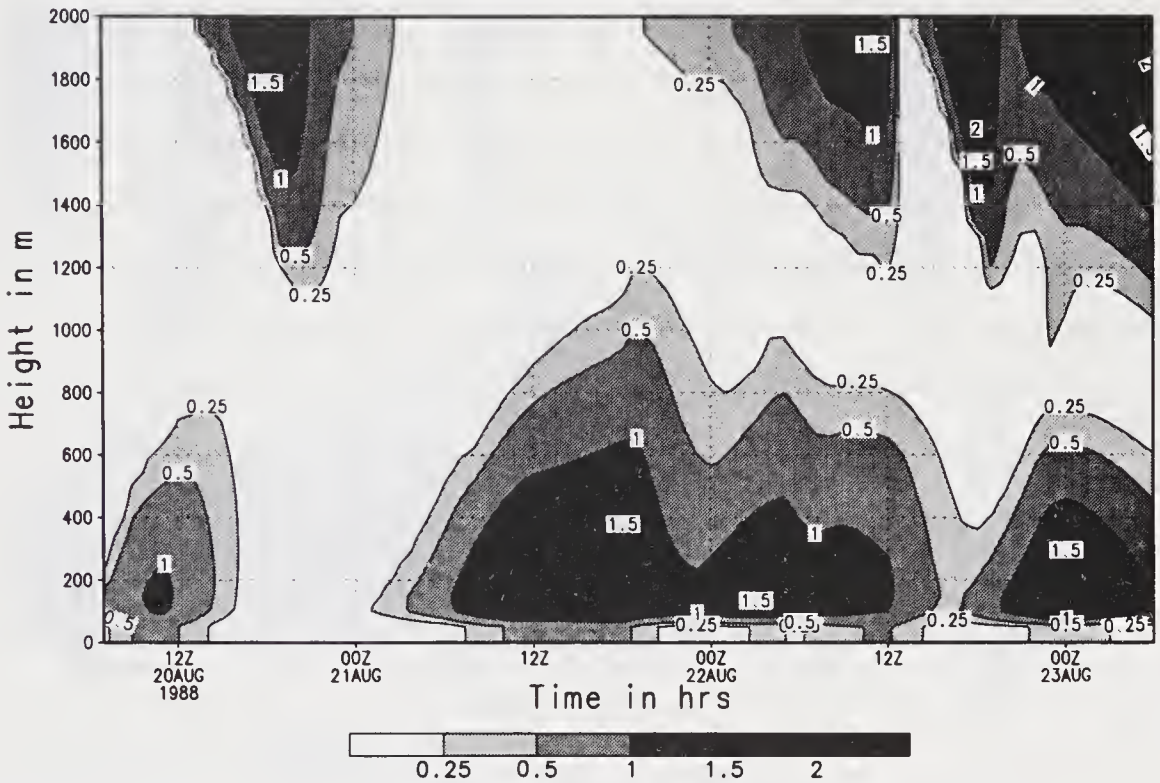


Figure 9. Time evolution of Tke in m^2s^{-2} . $C_4 = 1.4$, $C_3 = 1.38$.

Experiment 3: This experiment is again similar to the earlier experiments. Here we have chosen $C_4 = 3/2$ and $C_3 = 4/3$; and no modification to dissipation equation is being done. The Tke evolution for 72 hours is shown in figure 8. Here also the Tke evolution is quite stable and not very different in strength and pattern compared to Tke evolution of the earlier experiment. However the Tke evolution in the present experiment is much closer to the observations everywhere (Stull 1988). When compared with experiment 2, the Tke values seen here are very reasonable.

Another aspect is that these constants $C_3 = 4/3$ and $C_4 = 3/2$ are very close to the set of constants used by Marchuk (1977) namely $C_4 = 1.4$, $C_3 = 1.38$.

Experiment 4: In this experiment everything is the same as in the earlier experiment but for the constants. Here we have chosen the same set of constants as given by Marchuk *et al* (1977), that is $C_4 = 1.4$ and $C_3 = 1.38$. With this choice of constants, the difference $C_4 - C_3$ is very small. The 72 hours of Tke evolution has been shown in figure 9. The Tke evolution (figure 9) of the present experiment compares much better with the observations, Stull (1988) and the comparison seen in this experiment is as good as it is in the earlier experiment. As noted by Kochergin and Sklyar (1992), the smaller the differences $C_4 - C_3$, the smaller the Tke values. Thus in the last two experiments we note that the Tke evolution agrees with observations (Stull 1988), if the constants chosen are those we have arrived at, namely $C_4 = 3/2$ and $C_3 = 4/3$ as well as with those proposed by Marchuk *et al* (1977).

Thus from the discussion that we have presented so far, it is evident that Tke-dissipation closure is very sensitive to the choice of constants in the dissipation equation. So far we have not considered the dissipative range in the representation of

turbulent kinetic energy spectrum. Aupoix *et al* (1989) proposed a new approach known as the ‘MIS approach’ to obtain the dissipation equation wherein assumptions are made about the shape of the turbulent kinetic energy spectrum and its evolution. In accounting for low Reynold’s number influences in the derivation of dissipation equation, he has taken into account the dissipative range in assuming the energy spectrum shape. That is the representation of the spectrum as in (31) but with reduced inertial sub-range, containing however, the energy over the entire inertial sub-range (Saffman 1963), that is

$$\int_{K_i}^{\infty} \kappa \varepsilon^{2/3} K^{-5/3} f(K/K_D) dK = \int_{K_i}^{\alpha K_D} \kappa \varepsilon^{2/3} K^{-5/3} dK. \quad (50)$$

Where K_i is an arbitrary wave number from inertial sub-range; $K_D = (\varepsilon/\nu^3)^{1/4}$ is Kolmogorov’s wave number, ν molecular diffusion coefficient; α is close to 1.0, f is some function which corrects spectrum shape in inertial sub-range, then expression C_4 is modified as follows

$$C_4 = C_4^*/(1 + (2 - C_4^*)(\beta/3)\text{Re}_t^{-1/2}), \quad (51)$$

where C_4^* is the same as C_4 in the equation (35). β is some constant which depends on α and function f ($\beta = 2.047$ for Saffman’s spectrum), Re_t stands for the turbulent Reynolds number

$$\text{Re}_t = 4(e^2)/9(\nu\varepsilon). \quad (52)$$

For large enough Re_t , C_4 tends to C_4^* , but for small Re_t coefficient C_4 also becomes small. According to Aupoix *et al* (1989) let us suppose constant C_3 to be in this case equal to C_4 . Note that C_3 and C_4 are interactive in time but not fixed. That is when the turbulence is decaying, that is when $\text{Re}_t \rightarrow 0$, the constant C_4 becomes small and hence, since $C_3 = C_4$, the generation of dissipation terms also becomes automatically small thereby avoiding the misrepresentation of dissipation. Also when the turbulence is developing the constants C_4 and hence C_3 get modified according to (51) thereby once again avoiding the misrepresentation of dissipation.

Experiment 5: Thus the last sensitivity experiment that we have conducted with the e - ε closure model is with this new set of interactive constants as defined in (51). The model physics and the initial conditions are the same as in the earlier experiments. The evolutions of Tke, the eddy coefficient of viscosity and turbulence length scales, Tke dissipation, shear production and buoyant production are shown in figures 10(a–f) respectively. From the figures 10(a–c), we notice that the Tke evolution is highly stable as in experiment 4 and also the Tke, the eddy coefficient of viscosity and turbulence length scales are of the orders observed in the atmospheric boundary layer (Stull 1988). Also the Tke evolution shows three distinct diurnal cycles with large energy prevailing during day time associated with buoyancy as the sun rises; and the minimum prevailing during night as the sun sets.

Thus the constants as given by Aupoix *et al* (1989) being interactive in time can automatically take care of the dissipation during both decaying and developing turbulence. The values of C_4 as found throughout the integration, at every three time steps and at all levels in the domain are presented in table 2. Also in table 2 turbulence

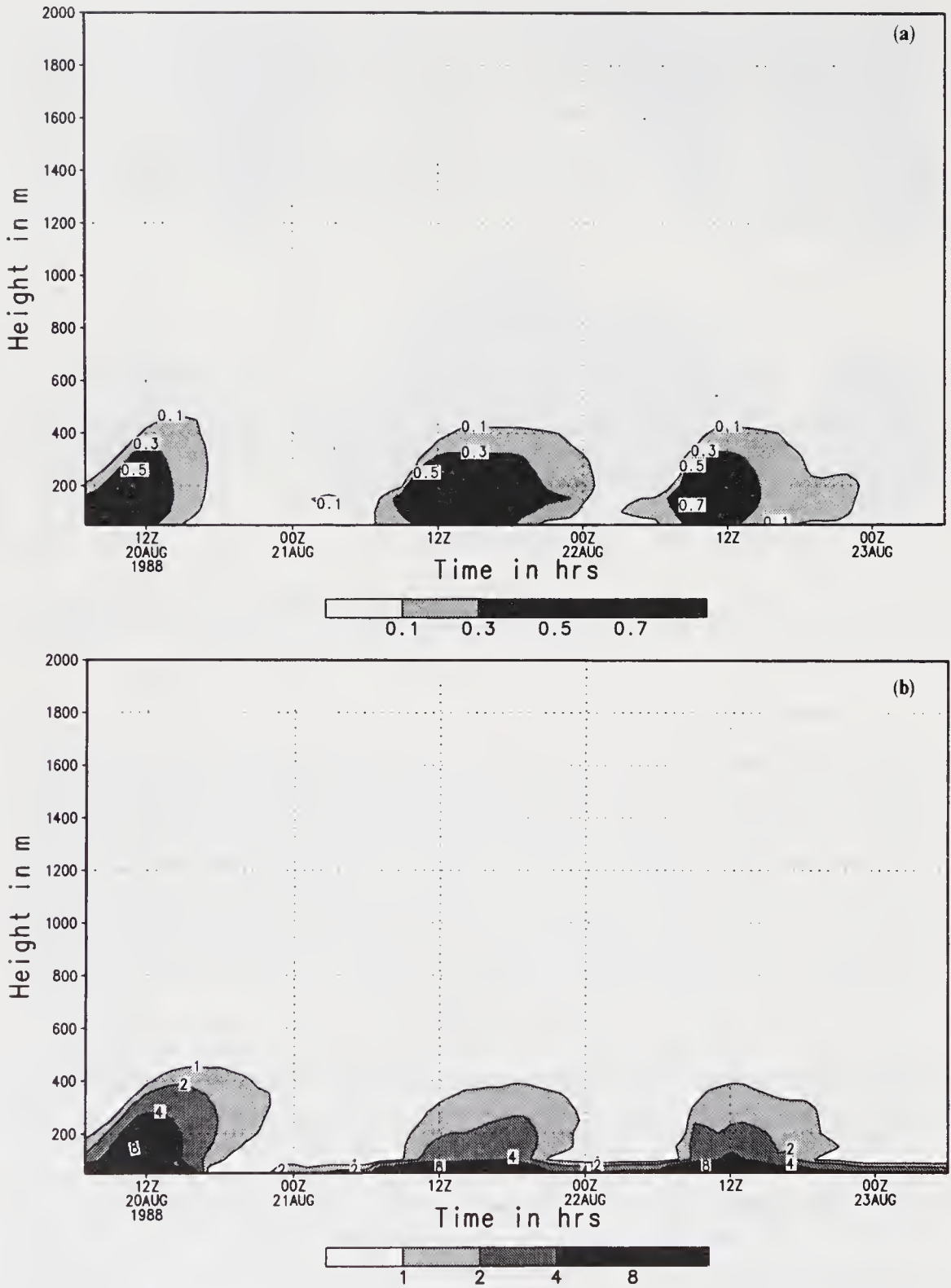


Figure 10. Time evolution of (a) Tke in $m^2 s^{-2}$; (b) eddy coefficient of viscosity in $m^2 s^{-1}$; (c) turbulence length scale in m; (d) dissipation in $m^2 s^{-3}$; (e) shear production in $m^2 s^{-3}$; (f) buoyant production in $m^2 s^{-3}$, C_4 and C_3 are calculated interactively with time.

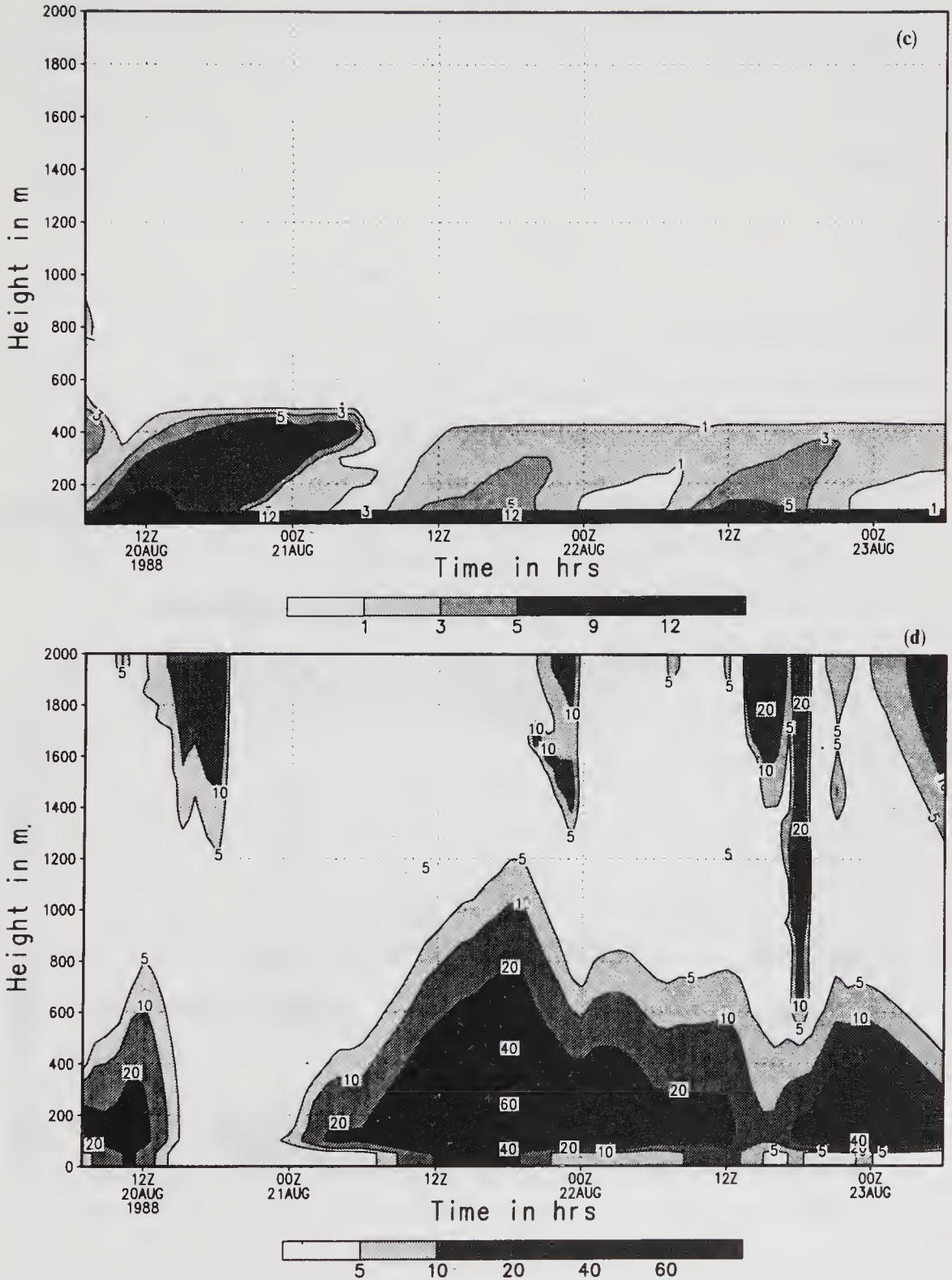


Figure 10(c-d).

Reynolds number and the corresponding Tke at every three time steps and at every point in the domain are given. It is very interesting to note from this table that whenever Tke tends to zero, and hence the turbulence Reynolds number, the constant C_4 also tends to be smaller, thus automatically reducing the generation of dissipation

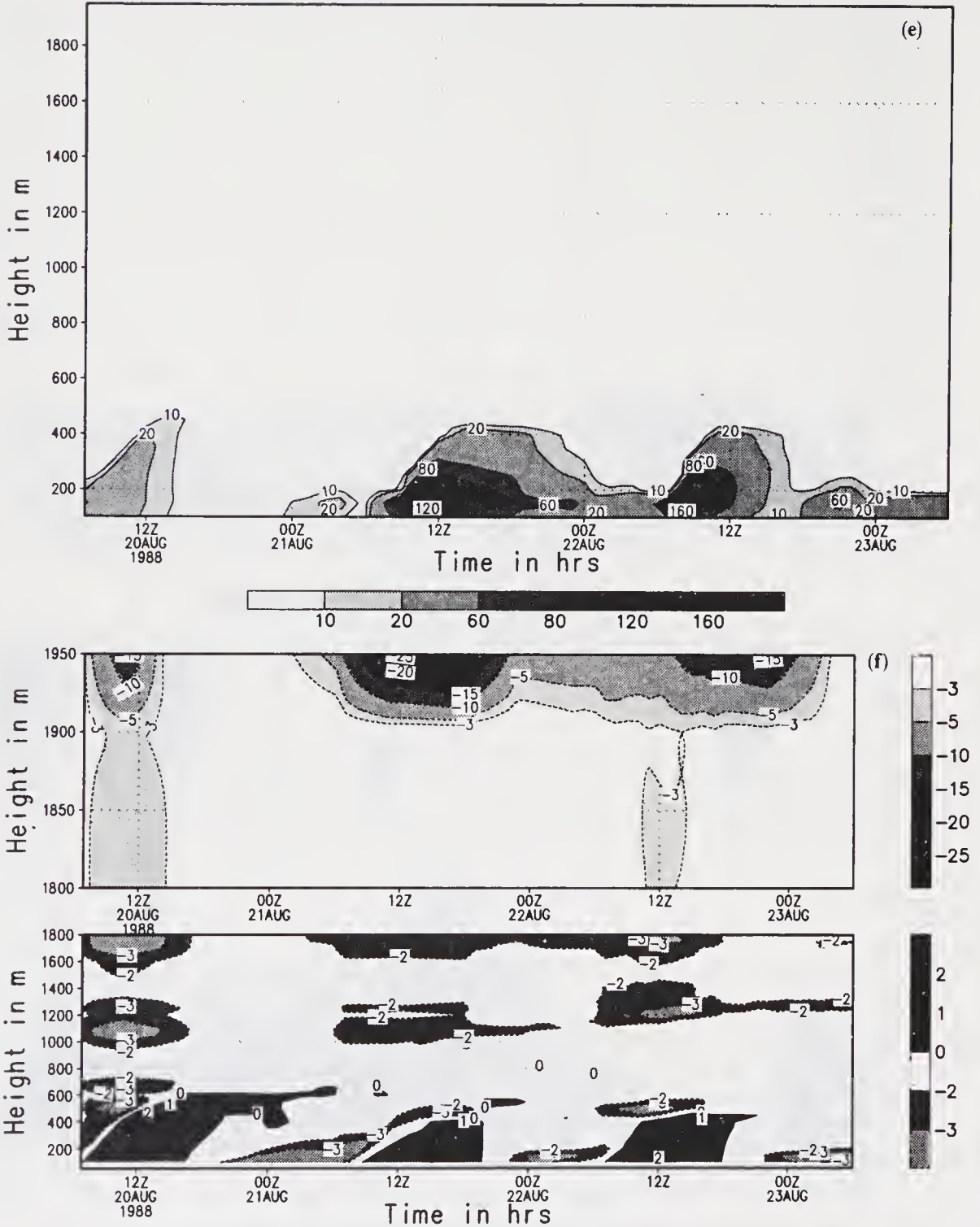


Figure 10(e-f).

thereby avoiding misrepresentation of dissipation during decaying turbulence. For instance at many points in the domain, we see Tke approaching smaller values, the Reynolds number tends to zero and the constant C_4 takes a relatively smaller value. When the turbulence is developing, the constant C_4 remains the same, at whatever the initial value assigned to it.

So far, the sensitivity of turbulent structure with e - ε closure model was discussed. Further an attempt has been made to study the improvement achieved with this improved e - ε closure model in simulating the mean structure of the monsoon trough boundary layer in the next section. By choice the constants in the dissipation equation are calculated according to the relation (51) as given by Aupoix *et al* (1989) in all the experiments in the next section.

5.2 Comparison of e - l and e - ε model simulations with observations

Here an attempt is made to compare the simulations of the mean structure of the monsoon trough boundary layer with the e - l and e - ε closure models for two stations, Delhi and Calcutta. Also the performance of the models are evaluated by making a comparison of these model simulations with the observations.

Calcutta: With the initial data as described in figures 3(a–d), the e - l and e - ε models were integrated for 24 hours with a time step of 15 minutes from 6 am on 20th July to 6 am on 21st July. A comparison of model simulations with observations is carried out and figure 11(a–d) describes these comparisons of vertical profiles of potential temperature with observations available at 11 am, 6 pm and 10 pm on 20th July and 6 am on 21st July; similarly for moisture in figure 12(a–d). Various profiles obtained at 11 am on 20th July, that is after 5 hours of model integration, as shown in figure 11(a) do not compare very well with the observations. At 11 am the observed θ profile shows a statically stable structure, figure 11(a). The reason for large departure between the observations and simulations at 11 am could be due to the fact that the model has been integrated only for five hours which is well within the model's spin-up time. Spin-up time is the time required for the model to arrive at a consistent solution. Although the initial profiles of u , v , θ , q are known, because the initial profiles of turbulent kinetic energy, eddy coefficient of viscosity and dissipation are not known from observations, it requires some time known as 'spin-up time' for these T_{ke} , K_u and ε profiles to be consistent with observed u , v , θ , q fields. However actual spin-up time can be arrived at by conducting a number of prediction experiments. From figure 11(b), we see that the θ simulations at 6 pm on 20th July is in good agreement with the observations. The observed θ profile at 6 pm (figure 11b) indicates that the boundary layer is well mixed. The maximum difference between the prediction and the observations is less than half a degree. Figure 11(c and d) shows comparisons at 10 pm on 20th July and 6 am on 21st July. Once again we see that there is a large departure between observations and simulations. The observed θ profiles indicate a statically stable boundary layer at 10 pm and 6 am. By comparisons made later on we learn that whenever the observed θ profile describes a stable atmospheric boundary layer, e - l and e - ε models are incapable of simulating. Moisture profile simulations shown in figure 12(a–d) compare reasonably well with the observations around 11 am and 10 pm on 20th July. Wind profile simulations (figures not shown) are more complicated and do not agree with the observations.

In all these simulations of θ , q , u , v there are no significant differences in the performance between e - l and e - ε models.

Delhi: The initial profiles of wind, temperature and humidity taken at 7 am on 19th August at Delhi are shown in figure 13(a–d). The initial profiles of u and v ,

Table 2. Variation of C_4 and Reynolds number (Re) every three hours.

Time(hrs)	3:0		6:0		9:0		12:0		15:0		18:0		21:0		24:0	
Height	C_4	Re														
50	1.9	0.4E+07	1.9	0.6E+07	1.9	0.5E+07	1.9	0.2E+07	1.9	0.9E+05	1.9	0.1E+06	1.9	0.5E+06	1.9	0.9E+06
100	1.9	0.1E+07	1.9	0.3E+07	1.9	0.3E+07	1.9	0.1E+07	1.9	0.4E+06	1.9	0.2E+05	1.9	0.1E+05	1.9	0.2E+05
150	1.9	0.7E+06	1.9	0.3E+07	1.9	0.3E+07	1.9	0.1E+07	1.9	0.7E+06	1.9	0.2E+06	1.9	0.4E+05	1.9	0.4E+05
200	1.9	0.4E+06	1.9	0.2E+07	1.9	0.3E+07	1.9	0.2E+07	1.9	0.8E+06	1.9	0.4E+06	1.9	0.2E+04	1.9	0.6E+02
250	1.9	0.5E+06	1.9	0.1E+07	1.9	0.2E+07	1.9	0.2E+07	1.9	0.9E+06	1.9	0.5E+06	1.9	0.2E+06	1.9	0.1E+05
300	1.9	0.6E+06	1.9	0.9E+06	1.9	0.2E+07	1.9	0.1E+07	1.9	0.9E+06	1.9	0.6E+06	1.9	0.3E+06	1.9	0.1E+05
350	1.9	0.7E+06	1.9	0.4E+06	1.9	0.2E+07	1.9	0.1E+07	1.9	0.9E+06	1.9	0.6E+06	1.9	0.3E+06	1.9	0.3E+05
400	1.9	0.6E+06	1.9	0.4E+05	1.9	0.1E+07	1.9	0.1E+07	1.9	0.8E+06	1.9	0.5E+06	1.9	0.3E+06	1.9	0.8E+04
450	1.9	0.5E+06	1.9	0.1E+03	1.9	0.1E+07	1.9	0.1E+07	1.9	0.7E+06	1.9	0.5E+06	1.9	0.3E+06	1.9	0.3E+02
500	1.9	0.3E+06	0.5	0.7E-03	1.9	0.6E+06	1.9	0.7E+06	1.9	0.5E+06	1.9	0.3E+06	1.9	0.2E+06	1.9	0.6E+03
550	1.9	0.2E+05	0.0	0.6E-07	0.0	0.1E-34										
600	1.9	0.1E+04	0.0	0.1E-34												
650	1.9	0.1E+03	0.0	0.1E-34												
700	1.9	0.3E+03	0.0	0.1E-34												
750	1.9	0.8E+04	0.0	0.3E-09	0.0	0.1E-34										
800	1.9	0.2E+05	0.0	0.9E-08	0.0	0.1E-34										
850	1.9	0.9E+04	0.0	0.4E-09	0.0	0.1E-34										
900	1.9	0.3E+04	0.0	0.1E-10	0.0	0.1E-34										
950	1.9	0.1E+04	0.0	0.1E-34												
1000	1.9	0.7E+02	0.0	0.1E-34												
1050	1.9	0.8E+01	0.0	0.1E-34												

(Continued)

Table 2. (Continued)

Time (hrs)	3:0		6:0		9:0		12:0		15:0		18:0		21:0		24:0	
Height	C ₄	Re														
1100	1.8	0.5E+01	0.0	0.1E-34												
1150	1.9	0.1E+02	0.0	0.1E-34												
1200	1.9	0.2E+02	0.0	0.1E-34												
1250	1.9	0.8E+01	0.0	0.1E-34												
1300	1.9	0.2E+02	0.0	0.1E-34												
1350	1.9	0.9E+02	0.0	0.1E-34												
1400	1.9	0.2E+03	0.0	0.1E-34												
1450	1.9	0.2E+03	0.0	0.1E-34												
1500	1.9	0.4E+02	0.0	0.1E-34												
1550	1.9	0.3E+02	0.0	0.1E-34												
1600	1.9	0.2E+02	0.0	0.1E-34												
1650	1.9	0.9E+01	0.0	0.1E-34												
1700	1.8	0.4E+01	0.0	0.1E-34												
1750	1.8	0.3E+01	0.0	0.1E-34												
1800	1.8	0.3E+01	0.0	0.1E-34												
1850	1.8	0.3E+01	0.0	0.1E-34												
1900	1.8	0.5E+01	0.0	0.1E-34												
1950	1.9	0.7E+01	1.2	0.2E-01	1.5	0.7E-01	1.6	0.1E+00	1.6	0.1E+00	1.6	0.1E+00	1.6	0.2E+00	1.7	0.2E+00
2000	1.9	0.7E+01	1.2	0.2E-01	1.5	0.7E-01	1.6	0.1E+00	1.6	0.1E+00	1.6	0.1E+00	1.6	0.2E+00	1.7	0.2E+00

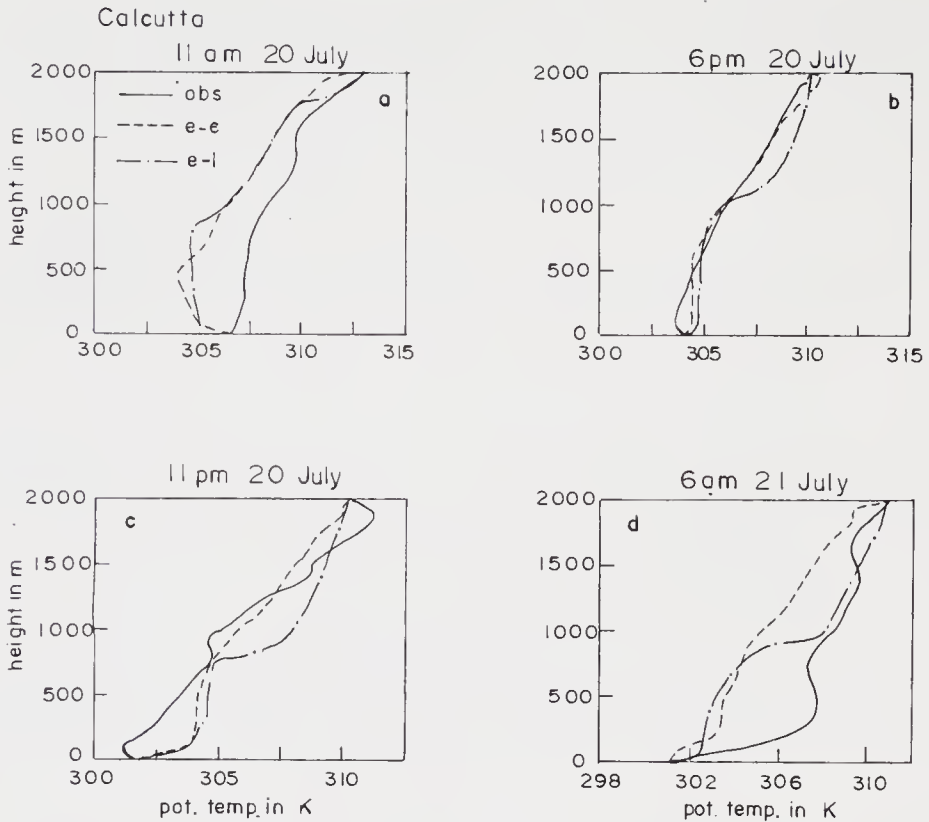


Figure 11. Comparison of simulations of vertical profile of θ in kelvin by $e-l$ and $e-\epsilon$ models with observations for Calcutta station at (a) 11 am on 20th July; (b) 6 pm on 20th July; (c) 11 pm on 20th July and (d) 6 am on 21st July.

(figure 13a–b), imply that at Delhi, winds are from southeast on 19th August. The θ -profile, figure 13(c), describes a stable boundary layer and the q -profile (13d) describes the moisture decreasing continuously in the vertical.

With this initial data of u, v, θ, q (figure 13a–d), the models with $e-l$ and $e-\epsilon$ closure were integrated for 24 hours from 7 am on 19th August to 7 am on 20th August as was carried out for Calcutta. These model simulations of vertical profiles of temperatures and humidity are compared with the observations as described in figures 14 and 15. Figure 14(a–c) describes a comparison of model simulations of potential temperature variation in the vertical with observations available at 11 am, 4 pm and 12 pm on 19th August, similarly figure 14(d) at 7 am on 20th August. Similarly figure 15(a–d) describes the moisture profile simulations. In figure 14(a), the observed θ profile indicates an unstable boundary layer and the model predictions show reasonable agreement with the θ -observed. The model simulations shown in figure 14(a) are obtained only after 4 hours of integration which is well within the spin-up time. In figure 14(b), which compares the model simulations with observations at 4 pm on 19th August, once again we notice that there is good agreement between simulations and observations and the boundary layer continued to be unstable. The maximum difference between $e-l$ model simulations and observations is less than half a degree except near the top boundary. Figure 14(c and d) shows the comparison in θ -profiles at 12 midnight on 19th August and 7 am on 20th August respectively. Observed profiles in figure 14(c–d) describe nocturnal stable boundary layers. We

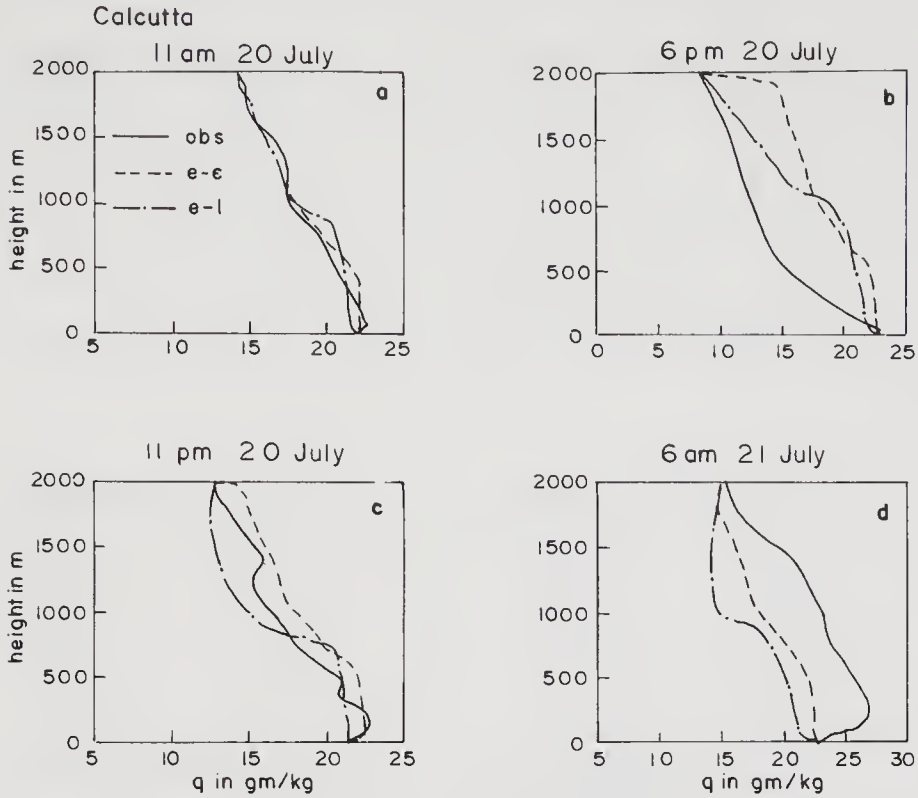


Figure 12. Comparison of simulations of vertical profile of q in gm kg^{-1} by $e-l$ and $e-\epsilon$ models with observations for Calcutta station at (a) 11 am on 20th July; (b) 6 pm on 20th July; (c) 11 pm on 20th July and; (d) 6 am on 21st July.

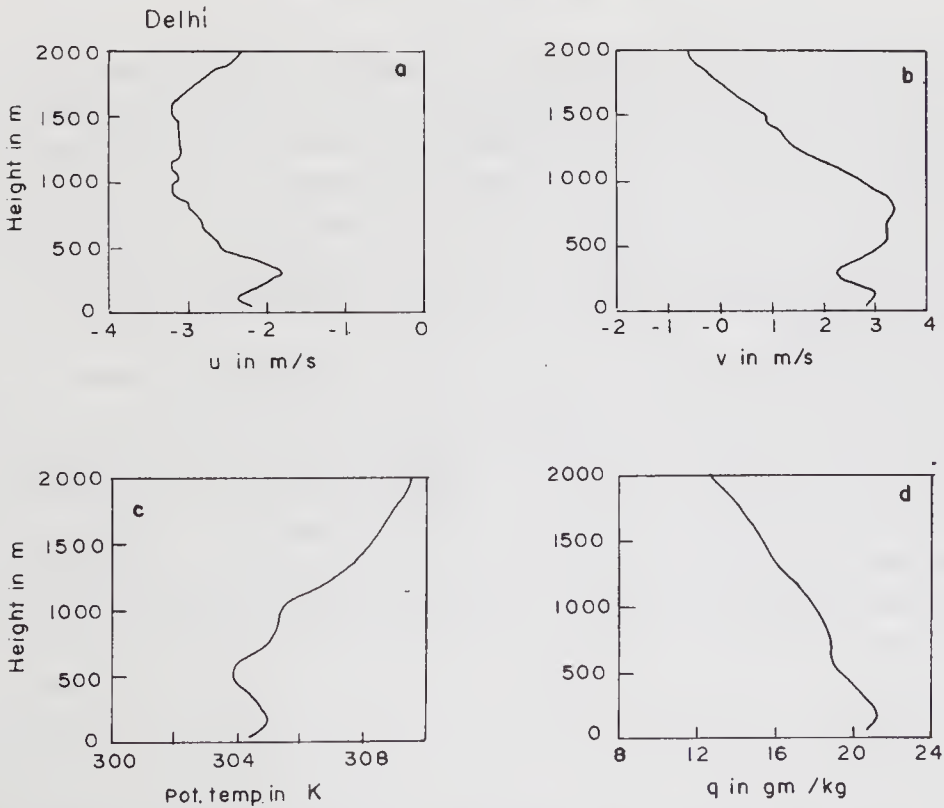


Figure 13. Initial profiles for Delhi station of (a, b) wind components, u and v in ms^{-1} ; (c) potential temperature, θ in kelvin; (d) moisture q , in gm kg^{-1} .

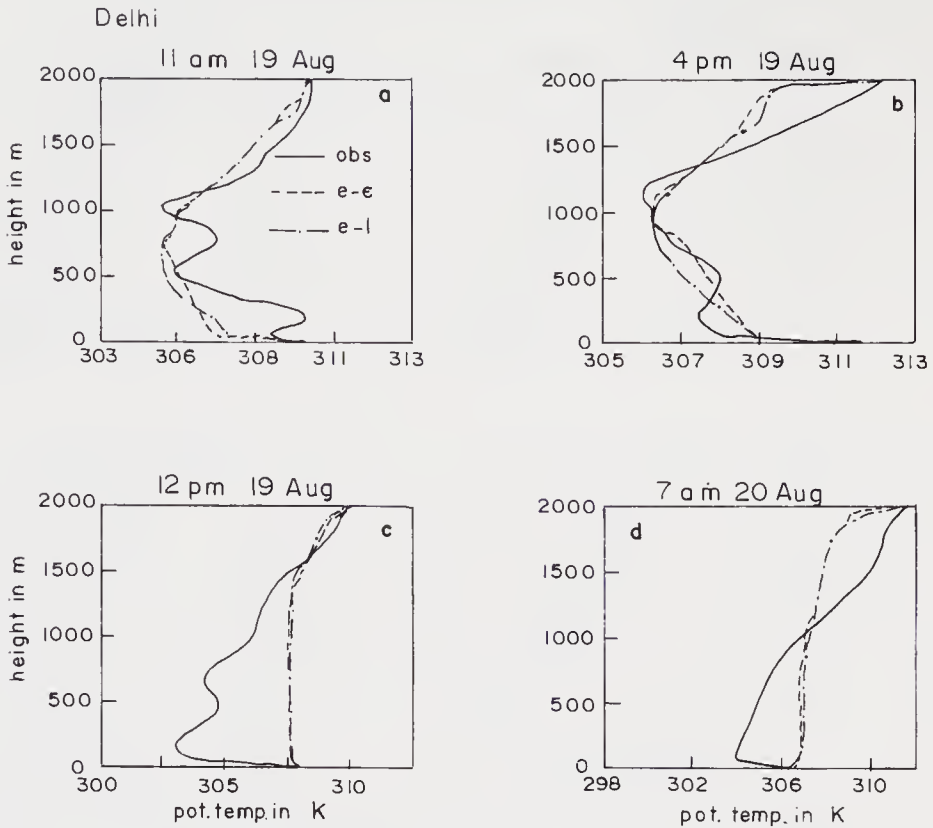


Figure 14. Comparison of simulations of vertical profile of θ in kelvin by $e-l$ and $e-\epsilon$ models with observations for Delhi station at (a) 11 am on 19th August; (b) 4 pm on 19th August; (c) 12 midnight on 19th August and; (d) 7 am on 20th August.

see from these figures that there are large differences between the observations and simulations. Similar kind of comparison tests made for Calcutta above suggest that models are not able to simulate the nocturnal boundary layer temperature profiles. However the model simulations compare very well with observations whenever the boundary layer is well mixed (figure 11b) or unstable (figure 14b). Moisture profiles are simulated reasonably well as shown in figure 15(a–d). Regarding the wind simulation, as seen earlier, model simulations do not compare well with the observations.

In all the above simulations of u , v , θ , and q , we see that one-dimensional numerical model with improved $e-\epsilon$ turbulence closure does no better when compared with the $e-l$ model simulations in simulating the monsoon trough boundary layer as far as the mean structure is concerned. Similar conclusions were arrived at by Holt and Raman (1988) though they use a modified dissipation rate equation (as done in experiment 2). However, as seen earlier the turbulence structure is better simulated by the model which has $e-\epsilon$ closure as they show closer agreement with the observed turbulence structure in the boundary layer than the $e-l$ closure.

6. Conclusions

In several earlier studies, simulating various atmospheric phenomena with $e-\epsilon$ turbulence closure model, a modification of the dissipation equation is done by

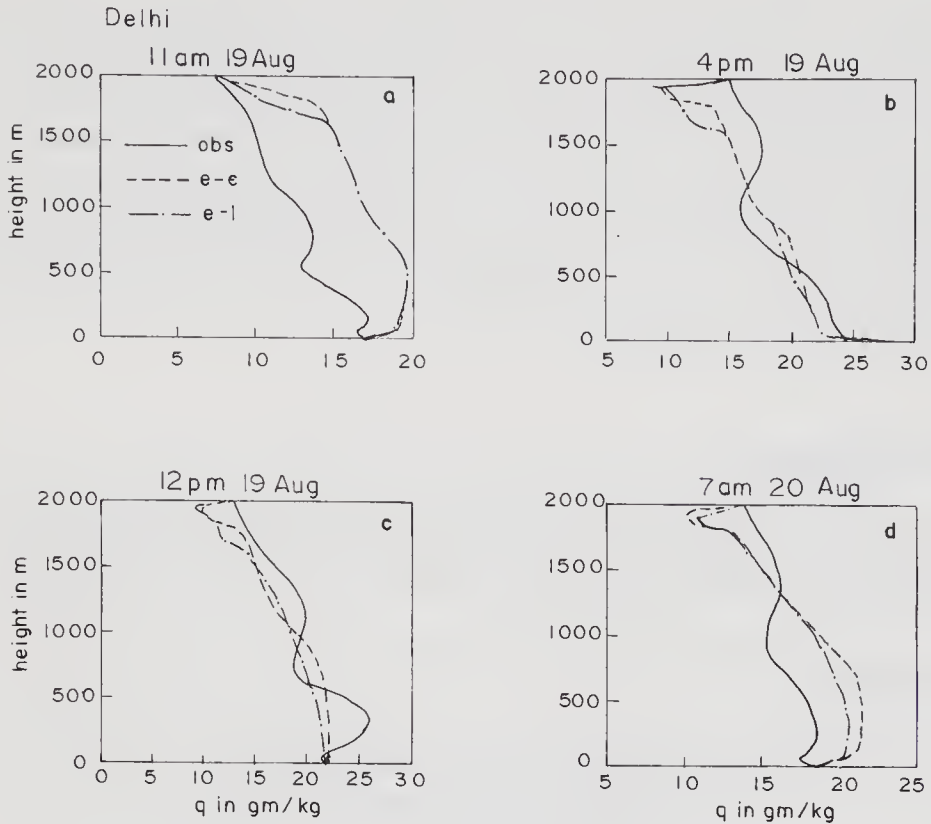


Figure 15. Comparison of simulations of vertical profile of q in gm kg^{-1} by $e-l$ and $e-\epsilon$ models with observations for Delhi station at (a) 11 am on 19th August; (b) 4 pm on 19th August; (c) 12 midnight on 19th August and; (d) 7 am on 20 August.

applying a constraint on the term denoting the generation of dissipation; that is, the Tke generation due to shear and buoyancy production in the dissipation equation is approximated as the maximum of shear production versus the sum of shear and buoyancy production. In an attempt to simulate the mean and the turbulence structure of the monsoon trough boundary layer with $e-\epsilon$ closure model, it is shown here that such a modification of the dissipation equation, which is unconvincing, can be avoided by a suitable choice of the constants suggested here, namely $C_4 = 3/2$ and $C_3 = 4/3$; and with these constants the observed turbulence structure is better simulated. While carrying out the experiments to study the sensitivity of the mean and turbulence structure to a different choice of the constants, we came across the constants given by Aupoix *et al* (1989) which are interactive in time and can automatically take care of the dissipation during both decaying and developing turbulence. The turbulence structure simulation with the constants recommended by Aupoix *et al* (1989) is shown to concur with the simulations obtained with the constants suggested here for the monsoon region. Also the turbulence structure simulation with $e-\epsilon$ model is far better when compared to the $e-l$ model simulations.

Thus we conclude that no universal constants exist to regulate the dissipation rate in the regime of homogeneous isotropic decaying turbulence and the choice of some value of C_4 is defined totally by assumptions about energy spectrum shape. The analysis which we have conducted here allows us to choose some reasonable values for the constants C_3 and C_4 to simulate the atmospheric boundary layer by an $e-\epsilon$ model without any modification of the standard dissipation rate equation.

Further, a comparison of the simulations of one-dimensional mean structure of the monsoon trough boundary layer with the $e-l$ and $e-\varepsilon$ closure models with the observations for two stations, Delhi and Calcutta, shows little sensitivity to the type of closure parameterization. That is for the simulation of mean profiles of u , v , θ and q , determination of K_m using a diagnostic formulation of ε or a prognostic determination of ε makes little difference. However the temperature profiles which show neutral and unstable situations are better simulated, but not the nocturnal stable temperature profiles. Moisture profiles are also simulated reasonably well, but the wind profiles simulation is more complicated.

Acknowledgements

The authors thank the Department of Science and Technology, India, and Academy of Sciences, Russia for supporting this work under an Indo-Russia long term project.

List of symbols

x	= coordinate directed towards east.
y	= coordinate directed towards north.
z	= coordinate directed vertically upwards.
t	= time.
p	= pressure.
$(\bar{\quad})$	= time mean.
$(\quad)'$	= $(\quad) - (\bar{\quad}) =$ deviation from time mean.
u	= velocity in x direction.
v	= velocity in y direction.
w	= velocity in z direction.
θ	= potential temperature.
T	= temperature.
q	= moisture.
q_s	= moisture at saturation.
ρ	= density.
Q_R	= rate of heating due to radiation.
Q_F	= source (sink) of moisture.
R	= universal gas constant.
C_p	= specific heat at constant pressure.
e	= turbulent kinetic energy.
g	= acceleration due to gravity.
$\overline{u'w'}, \overline{v'w'}$	= turbulent fluxes of momentum.
$\overline{\theta'w'}$	= turbulent flux of heat.
$\overline{v'w'}$	= turbulent flux of moisture.
K_u, K_v, K_θ, K_q	= eddy exchange coefficients corresponding to u -momentum, v -momentum, heat, moisture respectively.
ε	= dissipation.
u_g, v_g	= geostrophic winds in x and y directions.

l	=	turbulent length scale.
$\partial/\partial z$	=	differential operator.
C_e	=	dissipation constant.
L	=	latent heat of condensation.
κ	=	Karman constant.
H_s	=	sensible heat flux.
E_s	=	moisture flux.

References

- Aupoix B, Cousteix J and Liandrat J 1989 MIS: a way to derive the dissipation equation. Turbulent shear flows-6. Selected papers from the sixth International Symposium on turbulent shear flows: (ed) J C Andre, J Cousteix, F Durst, B E Launder, F W Schmidt, J H Whitelaw (Springer-Verlag) pp. 6–17
- Beljaars A C M, Walmsley J L and Taylor P A 1987 A mixed spectral finite-difference model for neutrally stratified boundary layer flow over roughness changes and topography; *Boundary-Layer Meteorol.*, **38** 273–303
- Boussinesq J 1877 Essai sur la theorie des courantes; *Mem Pres Divers Savant Acad Sci.* **23** 46
- Busch N E 1976 On the mechanisms of atmospheric turbulence. Workshop on micro-meteorology (ed.) D A Haugen, *American Meteor. Soc.* pp. 1–65
- Daly B J and Harlow F H 1970 Transport equations in turbulence; *Phys. Fluids* **13** 2634–2649
- Detering H W and Etling D 1985 Application of the E - ϵ turbulence model to the atmospheric boundary layer; *Boundary-Layer Meteorol* **33** 113–133
- Duykerke P G and Driedonks A G M 1987 A model for the turbulent structure of the strato-cumulus topped atmospheric boundary layer; *J. Atmos. Sci.* **44** 43–64
- Duykerke P G 1988 Application of E - ϵ turbulence closure model to the neutral and stable atmospheric boundary layer; *J. Atmos. Sci.* **45** 865–880
- Duykerke P G and Driedonks A G M 1988 Turbulent structure of shear driven stratus-topped atmospheric boundary layer; A comparison of model results with observations; *J. Atmos. Sci.* **45** 2343–2351
- Goel M and Srivastava H N 1990 Monsoon Trough Boundary Layer Experiment (MONTBLEX); *Bull. Am. Meteorol. Soc.* **71** 1594–1600
- Godunov S K and Ryaberkij V S 1962 Introduction to theory of finite difference schemes, Moscow FIZMATGIZS.
- Hanjalic K and Launder B E 1972 A Reynolds stress model of turbulence and its application to thin shear flows; *J. Fluid Mechanics* **52** 609–638
- Harlow F H and Nakayama P I 1967 Turbulence transport equations; *Phys. Fluids* **10** 2323–2332
- Holt T and Raman S 1988 A review and comparative evaluation of multi-level boundary layer parameterizations for first order and turbulent kinetic energy closure schemes; *Reviews of geophysics* **26** 761–780
- Huang C Y and Raman S 1989 Application of E - ϵ closure model to simulations of mesoscale topographic effects; *Boundary-layer Meteorol.* **49** 169–195
- Kazakov A L and Lykossov V N 1982 On parameterization of the interaction between the atmosphere and the underlying surface in the numerical modelling of atmospheric processes; *Proc. Zap Sib NII, Gidrometeoi Zdat, Moscow* **55** 3–20 (in Russian)
- Kochergin V P and Sklyar S N 1992 A semi-empirical variant of the equation approximation in 'b- ϵ ' model of the turbulence; *Russ. J. Numerical and Maths Modelling*, **7**
- Kolmogorov A N 1942 The equation of turbulent motion in an incompressible fluid (in Russian); *Izv. Akad. Nauk. SSSR, Ser Fiz* **6**(1–2) 56–58
- Krishnamurti T N and Bhalme H N 1976 Oscillations of a monsoon system part-1; observational aspects; *J. Atmos. Sci.* **33** 1937–1954
- Krishnamurti T N and Subrahmanyam D 1982 The 30–50 day mode at 850 mb during MONEX; *J. Atmos. Sci.* **39** 2088–2095
- Krishnamurti T N, Oosterhof D K and Mehta A V 1988 Air-sea interaction on the time-scale of 30 to 50 days; *J. Atmos. Sci.* **45** 1304–1322
- Kusuma G Rao 1988 Diagnosis of dominant forcing factors for large scale vertical velocities during active and break phases of the monsoon; *PAGEOPH* **127** 669–693

- Launder B E and Spalding D B 1974 The numerical computations of turbulent flows; *Comput. Methods Appl. Mech. Eng.* **3** 269–289
- Lumley J L 1980 Second order modelling of turbulent flows in prediction methods for turbulent flows: (ed.) W Kollman 1–31 Hemisphere, London
- Marchuk G I, Kochergin V P, Klimok V I and Sukhorukov V A 1977 On the dynamics of the ocean surface mixed layer; *J. Phys. Oceanogr.* **7** 865–875
- Mellor C L and Yamada T 1974 A hierarchy of turbulence closure models for planetary boundary layers; *J. Atmos. Sci.* **31** 1791–1806
- Monin A S and Yaglom A M 1971 *Statistical Fluid Mechanics 1*, MIT Press, Cambridge, Mass
- Murakami 1976 Cloudiness fluctuations during the summer monsoon; *J. Meteorol. Soc. Japan* **54** 175–181
- Reynolds W C 1974 Computation of turbulent flows; *AIAA paper* 74–556
- Richtmyer R D and Morton K N 1967 *Difference methods for initial value problems*. Inter Science Publishers, pp. 405
- Rodi W 1980 *Turbulence models and their application in hydraulics* (Delft: International Association for Hydraulic Research)
- Saffman P G 1963 On the fine scale structure of vector fields convected by a turbulent field; *J. Fluid Mech.* **16** pp 545
- Shir C C 1973 A preliminary numerical study of atmospheric turbulent flows in the idealized planetary boundary layer; *J. Atmos. Sci.* **30** 1327–1329
- Sikka D R and Gadgil S 1980 On the maximum cloud zone and the ITCZ over the Indian longitudes during the south west monsoon; *Mon. Weather Rev.* **108** 1840–1853
- Sikka D R and Narasimha R 1995 Genesis of the monsoon trough boundary layer experiment (MON-TBLEX); *Proc. Indian Acad. Sci. (Earth Planet. Sci.)* **104** 157–187
- Stubley G D and Rooney D R 1986 The sensitivity of k - ϵ model computations of the neutral planetary boundary layer to baroclinicity; *Boundary-Layer Meteorol.* **37** 53–70
- Stull R B 1988 *An introduction to boundary layer meteorology* (Dordrecht: Kluwer Academic Publishers)
- Wyngaard J C 1975 Modelling the planetary boundary layer – extension to the stable case; *Boundary-Layer Meteorol.* **9** 441–460
- Yasunari T 1979 Cloudiness fluctuations associated with the northern hemisphere summer monsoon; *J. Meteorol. Soc. Jpn.* **57** 227–242
- Yasunari T 1980 A quasi-stationary appearance of 30–40 day period in the cloudiness fluctuations during the summer monsoon over India; *J. Meteorol. Soc. Jpn.* **58** 225–229

Understanding the turbulent structure of the atmospheric boundary layer: A diagnostic approach

M CHATTERJEE, G K SEN and D K SINHA

Centre for Atmospheric Sciences, University of Calcutta, 92, A.P.C. Road, Calcutta 700 009, India

Abstract. In this paper, we have attempted a diagnostic study of the turbulence characteristics of the ABL by means of two one-dimensional models. The first model uses a first order non-local closure, based on the Transilient Turbulence Theory, for parameterizing turbulent fluxes, while the second model uses second order local closure for parameterizing these. The models have been applied to conduct case studies using the Kytton data taken at Kharagpur, during 17th – 21st June, 1990, as part of the MONTBLEX programme.

Our findings bring out various interesting features regarding the non-local and local turbulent statistics such as kinematic fluxes, turbulence kinetic energy, vertical velocity variance, the contribution of the eddies of various sizes to the fluxes at different levels and the mixing lengths. The one-dimensional anisotropy of the turbulent eddies has been revealed by the findings from the transilient model. The vertical variation of the turbulence kinetic energy, as computed directly by the second order model, is found to be strongly correlated with the vertical velocity variance. In particular, for stably stratified boundary layers, identification of two distinct zones of the turbulence kinetic energy and corresponding vertical velocity maxima is possible, which has been interpreted as positive evidence of patchy turbulence in the boundary layer.

Keywords. Atmospheric boundary layer; non-local closure; local closure; turbulence structure.

1. Introduction

The most important and interesting feature within the atmospheric boundary layer (ABL) is the turbulent eddies that are generated due to external forcings such as solar heating of the earth's surface and the frictional drag it exerts on the layers of air above it, radiative cooling, wind shear, etc. Depending on the existing mean flow conditions within the ABL, turbulence increases or decays with time and the eddies interact with the surrounding air and with each other, thereby transporting and exchanging mass, momentum, heat, moisture and energy at various levels.

The wide range or spectrum of the turbulent eddy sizes is difficult to take into account completely in observational and theoretical investigations attempting in-depth studies of the various ABL processes. Simplifying assumptions, such as concentrating on a particular range of eddy sizes and employing statistical methods for quantifying turbulence, have been adopted. These lead us to a set of equations governing ABL flow which, in addition to the mean flow terms, now contain non-linear turbulence terms. These non-linear terms are the statistical moments of various orders involving the turbulent components of wind, temperature and moisture, and mathematically represent processes such as turbulent fluxes, turbulence kinetic energy (TKE) etc. As first recognised by Keller and Friedman (1924), the number of equations governing

ABL flow is less than the number of unknowns contained in them. This has resulted in the well-known closure problem in which the unknown turbulent quantities have to be specified in terms of known parameters in order to obtain solutions of these equations.

Two principal classes of closure methods are usually used in order to solve the ABL equations (Stull 1988). Local closure methods are based on analogy with the process of molecular diffusion and assume that turbulent transport is a diffusive process. The unknown turbulent quantities at any point in space are parameterized in terms of the known quantities such as the observed wind, temperature, humidity or their gradients at that point. The well-known bulk methods and K-theory methods are examples of local closure parameterization. Local closure methods have been used extensively over a long period of time by investigators, and references become too numerous to cite. Thus it may be appropriate to refer to reviews by Bhumralkar (1976), McBean *et al* (1979), Nieuwstadt and van Dop (1984), Stull (1988) and others.

The non-local closure methods of parameterization are based on the idea that turbulent processes are advective rather than diffusive and the unknown quantities at any point in space are expressed in terms of known quantities at various points in space. Large eddy simulation techniques (Deardorff (1972), Wyngaard and Brost (1984)) and the transilient turbulence theory (Stull 1984, 1988, 1992), hereafter referred to as Stull (a, b, c), are examples of non-local closure methods.

However, none of these closure methods, or the parameterization schemes adopted in them, are exact. Both have advantages and disadvantages and their applications are dictated by the particular physical processes being investigated. It has been observed (Stull 1988) that local closure methods of second and higher orders, and the non-local closure methods in general, provide more accurate and realistic descriptions of turbulence within the ABL.

In the present paper, we have attempted to investigate turbulence within the ABL through two numerical models. Both are diagnostic, one-dimensional models. For parameterizing turbulent fluxes, one of them uses a first order, non-local closure method based on transilient turbulence theory, and the other model uses second order local closure method for doing the same. Using the available Kytoon data for Kharagpur, taken as part of the MONTBLEX programme, we have applied these two models to study the structure of the ABL during 17th – 21st June, 1990.

The findings from these models reveal various interesting aspects of the turbulent transports in the ABL, such as non-local and local kinematic fluxes of heat and momentum, the contribution of eddies of different sizes to the non-local fluxes at each level, the mixing length profiles and the one-dimensional anisotropy of the turbulent eddies. An interesting feature revealed from the results of the second order model is the strong correlation between the TKE and the vertical velocity variance maxima. Interestingly, for stable boundary layers, we could distinguish clearly between two separate zones within the ABL where these peaks lie. These zones may be interpreted as zones of patchy turbulence, a commonly observed feature in the stable boundary layer.

2. The non-local closure model: Transilient turbulence theory

Detailed description of the transilient turbulence theory (TTT) is available in Stull (a, b, c). Briefly stated, TTT is based on the fact that the larger turbulent eddies are organised,

coherent structures, which transport turbulent properties such as momentum, heat, moisture, pollutants etc, across finite distances in space, in a manner analogous to the process of advection, before the smaller sized eddies begin to do so. TTT thus allows the incorporation of the effects of turbulent mixing not only between adjacent layers or grid boxes (as in the local closure methods), but also between grid points separated by finite distances, which is extremely advantageous.

Proceeding as in Stull (a, b, c), we discretize the vertical column of air over the observing station (Kharagpur) into N not necessarily equal-sized grid boxes of length ΔZ . Grid indices are placed at the box centres with i denoting a reference (destination) box and j denoting other source boxes.

At any instant of time t (seconds), all the grid boxes contain air which have some average property of state $\bar{\xi}_i(t)$, which may physically represent its mass, momentum, temperature, humidity etc. After a small interval of time Δt , turbulence, if present, will cause mixing of air between boxes i and j . If $c_{ij}(t, \Delta t)$ denotes the fraction of air in box i after it has mixed with air from box j , and assuming that during the time Δt air from the box j retains and carries its original state property $\bar{\xi}_j(t)$ into box i , the average property of state $\bar{\xi}_i(t)$ will change to $\bar{\xi}_i(t + \Delta t)$ according to the relation:

$$\bar{\xi}_i(t + \Delta t) = \sum_{j=1}^N c_{ij}(t, \Delta t) \bar{\xi}_j(t). \quad (2.1)$$

The elements $c_{ij}(t, \Delta t)$ of the transient matrix $C(t, \Delta t)$ are the unknown quantities which must be parameterized in terms of the known mean flow variables. To make the parameterization more realistic, the continuous response of the ABL flow to the external forcings and conditions at the earth's surface should be taken into account. Any external or dynamical forcing at the earth's surface such as insolation, frictional drag, wind shear, etc., causes destabilization of the mean flow in the ABL and generation of turbulence. Turbulent mixing then tends to restabilize the flow to a new equilibrium state. Mathematically this concept is written as (Stull (c)):

$$\bar{\xi}_i^*(t + \Delta t) = \bar{\xi}_i(t) + \Delta t \cdot (\text{net source at } Z = i\Delta Z), \quad (2.2)$$

$$\bar{\xi}_i(t + \Delta t) = \sum_{j=1}^N c_{ij}(t, \Delta t) \bar{\xi}_j^*(t + \Delta t),$$

with $c_{ij}(t, \Delta t) = \text{function}(u_i, u_j, v_i, v_j, \theta_i, \theta_j, \dots)$.

In the present study, the responsive parameterization scheme used is known as the mixing potential approach and had been proposed by Stull and Driedonks (1987). The mixing potential Y_{ij} for each source destination box is computed from the TKE budget equation which in the non-local framework has the form:

$$Y_{ij} = \left[\frac{\Delta t \cdot T_0}{(\Delta_{ij} Z)^2} (\Delta_{ij} u)^2 + (\Delta_{ij} v)^2 - \frac{g(\Delta_{ij} Z)(\Delta_{ij} \theta)}{\bar{\theta} R_c} \right] - \frac{D_y \cdot \Delta t}{T_0} \quad \forall i \neq j, \quad (2.3)$$

where the notation $\Delta_{ij} X = X_i - X_j$ implies the non-local difference between X_i and X_j . In (2.3), the last term represents the TKE dissipation. Also, the parameters $T_0 (= 1000 \text{ s})$ and $R_c (= 0.25)$ represent the time scale and the critical Richardson number respectively. Observed values of the wind and temperature are used to compute the Y_{ij} .

The elements $c_{ij}(t, \Delta t)$ are then computed from:

$$c_{ij} = \frac{Y_{ij}}{\|Y\|}, \quad i \neq j, \quad (2.4)$$

$$c_{ii} = 1 - \sum_{\substack{j=1 \\ j \neq i}}^N c_{ij},$$

where $\|Y\|$ is the maximum row norm of the matrix Y_{ij} .

The non-local flux $F_k(t, \Delta t)$ across the level k (that is at height $Z = k\Delta Z$) is computed from (Stull and Driedonks 1987):

$$F_k(t, \Delta t) = F_{k-1}(t, \Delta t) + \frac{\Delta Z}{\Delta t} \cdot \sum_{j=1}^N c_{kj}(t, \Delta t) [\bar{\xi}_k(t) - \bar{\xi}_j(t)], \quad (2.5)$$

with $F_k(t, \Delta t) = 0$ at $k = 0$ (that is across the earth's surface) and also at $k = N$ (at the model top).

The transport spectral components $F_{k/m}(t, \Delta t)$ give the contribution of the eddies of size $m\Delta Z$ to the total flux across the level k (that is at $Z = k\Delta Z$). These may be computed from Stull (b, c):

$$F_{k/m}(t, \Delta t) = \frac{\Delta Z}{\Delta t} \cdot \sum_{i=1}^k \sum_{j=k+1}^N \delta_{m, |i-j|} [c_{ij}(t, \Delta t) \bar{\xi}_i(t) - c_{ji}(t, \Delta t) \bar{\xi}_j(t)], \quad (2.6)$$

where $\delta_{m,n}$ denotes the Kronecker delta function.

The mixing length at any level k ($Z = k\Delta Z$) is given by:

$$l_k = 0.5 \Delta Z \cdot \sum_{i=1}^N [c_{ik}(t, \Delta t) + c_{ki}(t, \Delta t) \cdot |i - k|]. \quad (2.7)$$

To get some idea about the one-dimensional anisotropy of turbulence in the ABL, the mixing length l_k is separated into upward and downward transport from the source box j :

$$l_j \uparrow(t, \Delta t) = \frac{\Delta Z \cdot \sum_{i=j}^N c_{ij}(t, \Delta t) \cdot |i - j|}{\sum_{i=j}^N c_{ij}(t, \Delta t)},$$

$$l_j \downarrow(t, \Delta t) = \frac{\Delta Z \cdot \sum_{i=1}^j c_{ij}(t, \Delta t) \cdot |i - j|}{\sum_{i=1}^j c_{ij}(t, \Delta t)}, \quad (2.8)$$

and an upward and downward transport to the destination box i :

$$l_i \uparrow(t, \Delta t) = \frac{\Delta Z \cdot \sum_{j=1}^i c_{ij}(t, \Delta t) \cdot |i - j|}{\sum_{j=1}^i c_{ij}(t, \Delta t)},$$

$$l_i \downarrow (t, \Delta t) = \frac{\Delta Z \cdot \sum_{j=i}^N c_{ij}(t, \Delta t) \cdot |i-j|}{\sum_{j=i}^N c_{ij}(t, \Delta t)}. \quad (2.9)$$

The transient model was run with a vertical grid resolution of $\Delta Z = 10$ m and a time interval of $\Delta t = 600$ s. Model results have been discussed in § 4.

3. The second order local closure model

The second order local closure model used in this study is a simplified version of the model given by Donaldson (1973). The simplifying assumptions we have adopted are briefly described below.

Being primarily concerned with a diagnostic study, the steady state version of the prognostic equations of turbulence variances have been used. The triple correlation term $\overline{w'\theta'^2}$ has been omitted following arguments by Hogstorm (1990) that suggest that this term is usually negligible near the surface and throughout the ABL. Furthermore, in the case studies attempted here, the ABL usually had a very weak or nearly neutral stratification and turbulence was weak. We have thus neglected the triple correlation terms $\overline{u'w'^2}$ and $\overline{v'w'^2}$ in the equations for $\overline{u'^2}$ and $\overline{v'^2}$. Terms such as $\overline{u'\theta'}$, $\overline{v'\theta'}$, and $\overline{u'v'}$ occurring in these equations have also been neglected. These simplifications enable us to obtain a set of coupled, first order ordinary differential equations:

$$\frac{\partial u}{\partial t} = -f(v - v_g) + \frac{\partial}{\partial Z}(\overline{w'u'}), \quad (3.1)$$

$$\frac{\partial v}{\partial t} = f(u - u_g) + \frac{\partial}{\partial Z}(\overline{w'v'}), \quad (3.2)$$

$$\frac{\partial \theta}{\partial t} = \frac{\partial}{\partial Z}(\overline{w'\theta'}), \quad (3.3)$$

$$u' \frac{\partial u}{\partial Z} + \overline{w'v'} \frac{\partial v}{\partial Z} - \frac{g}{\theta} \overline{w'\theta'} + \frac{\partial}{\partial Z} \left(\Lambda_e e^{1/2} \frac{\partial e}{\partial Z} \right) + \frac{e^{3/2}}{\Lambda_1} = 0, \quad (3.4)$$

$$\overline{w'^2} \frac{\partial u}{\partial Z} + \frac{e^{1/2}}{\Lambda_2} \overline{w'u'} = 0, \quad (3.5)$$

$$\overline{w'^2} \frac{\partial v}{\partial Z} + \frac{e^{1/2}}{\Lambda_2} \overline{w'v'} = 0, \quad (3.6)$$

$$\frac{2g}{\theta} \overline{w'\theta'} + \frac{e^{1/2}}{\Lambda_3} \left(\overline{w'^2} - \frac{2}{3}e \right) = 0, \quad (3.7)$$

$$\overline{w'^2} \frac{\partial \theta}{\partial Z} - \frac{g}{\theta} \overline{\theta'^2} + \frac{e^{1/2}}{\Lambda_3} \overline{w'\theta'} = 0, \quad (3.8)$$

$$2 \overline{w'\theta'} \frac{\partial \theta}{\partial Z} + \frac{e^{1/2}}{\Lambda_4} \overline{\theta'^2} = 0, \quad (3.9)$$

with

$$\begin{aligned}\Lambda_1 &= 5.75\Lambda, \Lambda_2 = 2.08\Lambda, \Lambda_3 = 2.14\Lambda, \\ \Lambda_4 &= 7.44\Lambda \text{ and } \Lambda_e = 0.2\Lambda\end{aligned}\quad (3.10)$$

(Donaldson (1973)).

The system of equations (3.1) – (3.9) has been solved numerically, at first keeping the turbulence length scale Λ constant and then allowing it to vary with height. The vertical grid chosen for both cases is identical to the one used for the transilient model.

For the second case, the simplest method for estimating the variation of Λ with height is based on the comparison of the grid point values of the turbulent fluxes, $\overline{w'\theta'}$, $\overline{w'u'}$, $\overline{w'v'}$, obtained by numerically solving the diagnostic equations (3.4) – (3.9) with those obtained from the transilient model. In this case, it is to be expected that a single grid point value of Λ will not reproduce all the three fluxes simultaneously. In order to assess the profiles of Λ for the case (A) where the effect of surface frictional drag is large and case (B) where the surface heat flux is dominant, two numerical experiments were performed. In experiment (A), a surface heat flux $\overline{w'\theta'} = -0.004 \text{ K m/s}$ and a drag coefficient $C_D = 0.0039$ was provided. These inputs are the same as the ones used for the case study for 20th June with the transilient model. In experiment (B), the prescribed surface heat flux is $\overline{w'\theta'} = -0.006 \text{ K m/s}$ with a drag coefficient $C_D = 0.0015$. The results have been discussed in § 4.

4. Case studies

The non-local closure model described in § 2 has been used to compute the vertical profiles of various ABL parameters over Kharagpur (22.30 N, 87.2 E) during 19th – 21st June, 1990. The second order local closure model described in § 3 has been used to obtain estimates of the TKE and turbulent vertical velocity variance at the same location for the period 17th – 21st June, 1990.

The data used are Kytoon observations of pressure, pressure height, dry and wet bulb temperatures, wind speed and direction taken at Kharagpur during the MON-TBLEX programme. The time of observation for 17th – 20th June was 00 GMT (0530 local time) and 1130 GMT (1700 local time) for 21st June. These different timings enable us to study the early morning ABL (17th – 20th June) which is a continuation of the nocturnal stable boundary layer, and also the late afternoon ABL (21st June, 1990) as it changes from the daytime convective boundary layer to the nocturnal one.

The basic inputs to the transilient model are the observed potential temperature θ ($^{\circ}\text{K}$) and the zonal and meridional wind components u and v (m/s) at 10 m intervals. These initial profiles of θ , u , v , for 19th – 21st June have been shown in figure 1. In figure 2(a), the vertical variation of the Richardson numbers computed from the observations for these three days have been shown. It is seen that on 19th June, the lowest 15 m of the ABL is unstable above which lies a stable layer, with highly stable zones around 70–80 m, 100–120 m and 155–211 m and the ABL top around 200 m. On 20th and 21st June, the ABL stratification was weaker, with the lowest 15 m having a weakly stable or near neutral stratification on 20th June and a weakly unstable or near neutral stratification on 21st June. On 20th June, stable stratification existed above this level, with the height of the ABL top around 175 m, while on 21st June the

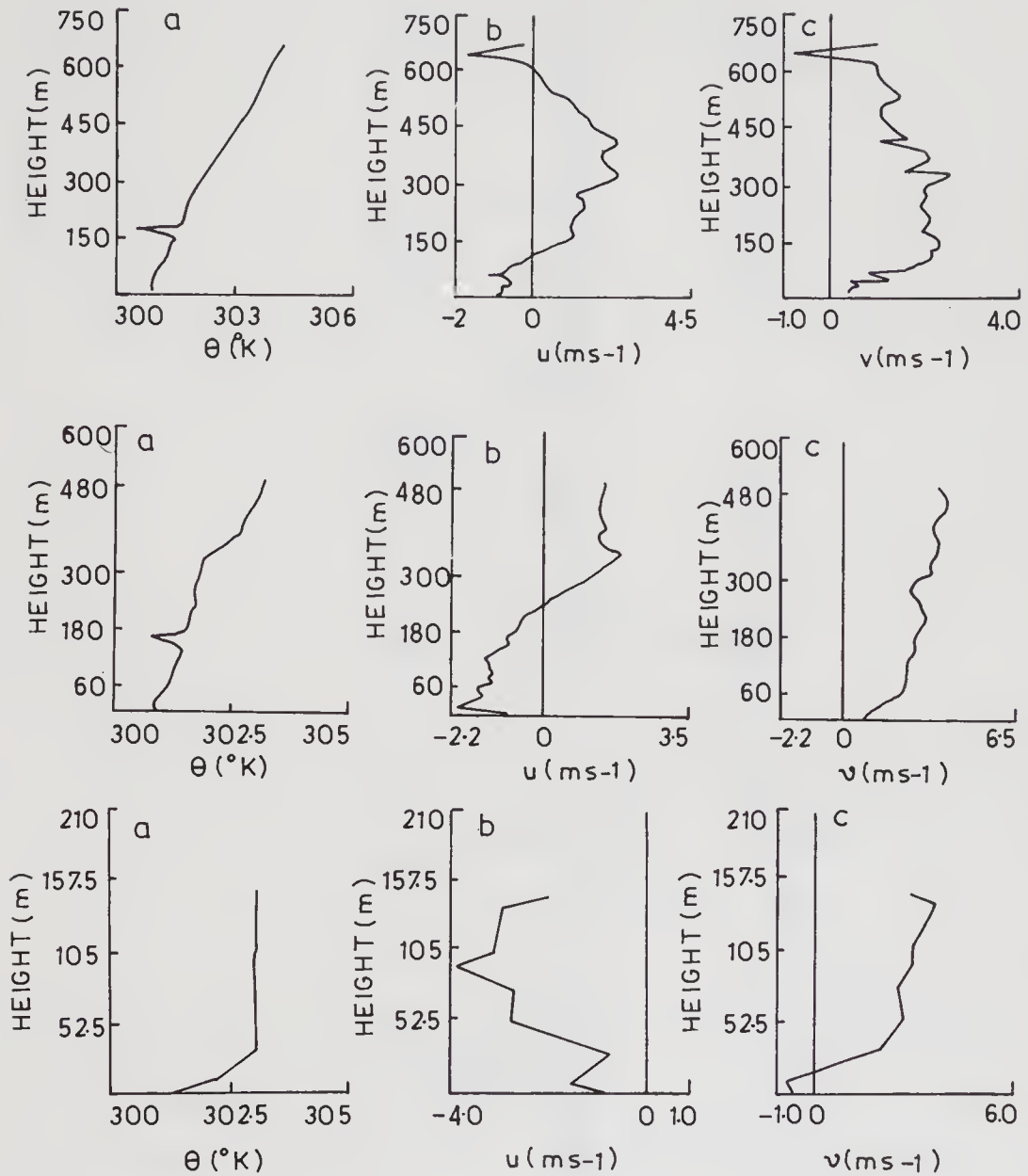


Figure 1. Observed profiles of: a) θ , b) u and c) v for Kharagpur.

Top panel : 19th June, 1990, 00 GMT.

Middle panel : 20th June, 1990, 00 GMT.

Bottom panel : 21st June, 1990, 1130 GMT.

layers between 40–90 m were neutrally stratified, with the ABL top around 125 m. In this connection, we mention that discussions on local vis-a-vis non-local stability can be found in Stull (1991) and Stull (c).

In addition to these basic inputs, prescribed heat and momentum fluxes were provided at the lowest model level. These were estimated in the usual manner from the first two levels of observations, namely 3 m and 15 m. After 10 minutes of transient mixing, the model outputs consisting of vertical profiles of θ , u , v and fluxes $\overline{w'\theta'}$, $\overline{w'u'}$, $\overline{w'v'}$ have been displayed in figures 3, 4 and 5.

The Richardson number variation with height as computed from the model outputs has been shown in figure 2(b). This may be compared with figure 2(a) to get an idea

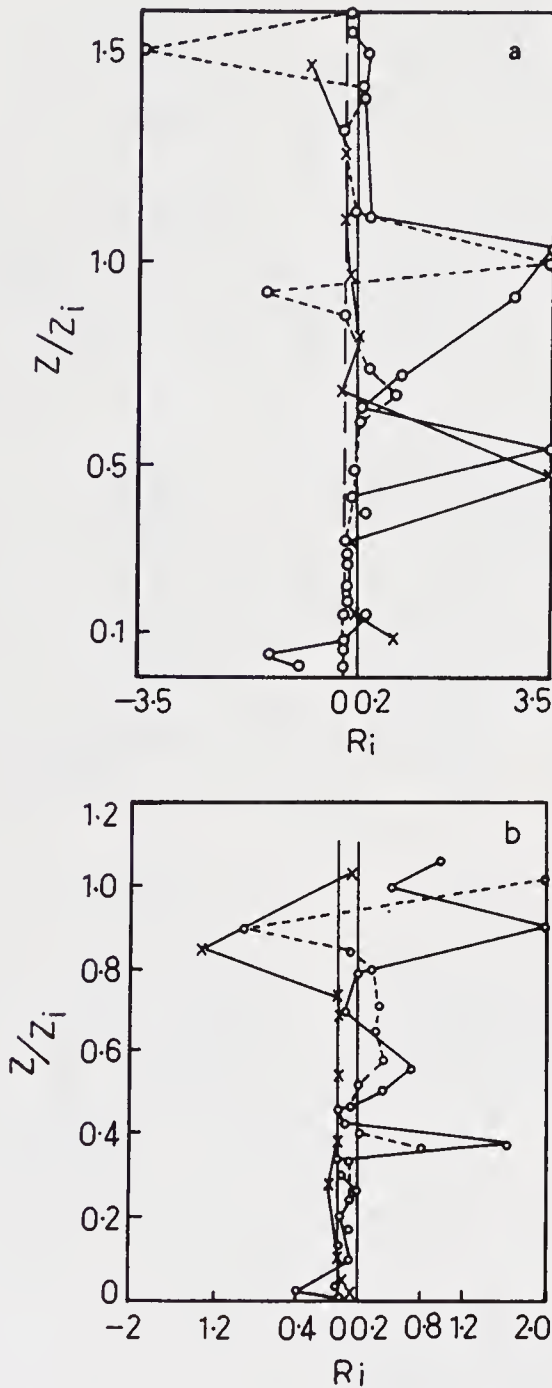


Figure 2. Richardson numbers computed from: a) Observed profiles and b) transient model outputs. $\circ-\circ-\circ$ 19th June; $\circ--\circ--\circ$ 20th June and $\times--\times--\times$ 21st June.

about how the turbulent zones have changed within these 10 minutes. The heat flux, as seen from figures 3(d), 4(d) and 5(d) is negative up to a considerable height for all three days. This implies subsidence and downward transport of heat which is not uncommon in stably stratified zones. The ABL tops on these days have been estimated to be around $Z_i = 230$ m, 178 m and 85.5 m respectively. Thus for the early morning case studies, 19th – 20th June, the ABL has warmed up as observed also from figures 3(a) and 4(a), and the tops have risen. As seen from figure 5(a), on 21st June, although the temperature

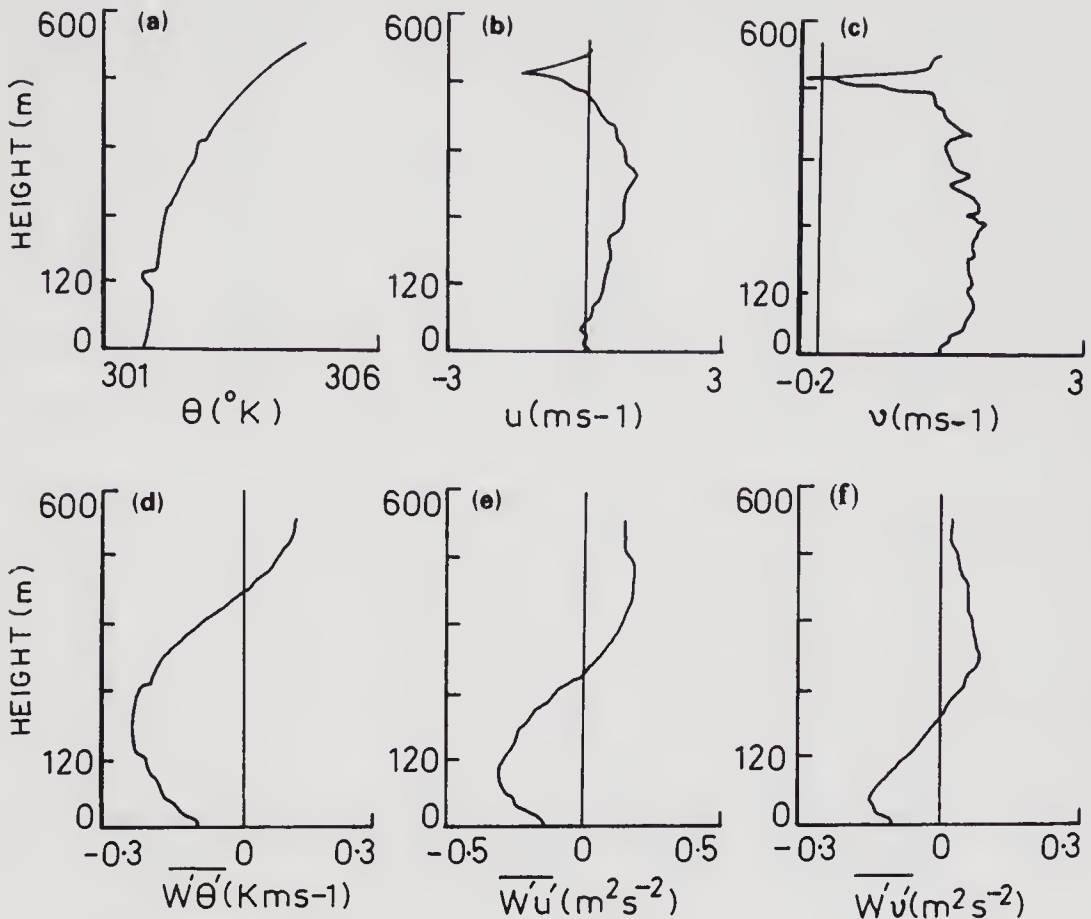


Figure 3. Transilient model outputs for 19th June, 1990 – θ , u , v , $\overline{w'\theta'}$, $\overline{w'u'}$ and $\overline{w'v'}$.

has risen at the lowest level, temperature has decreased above this. This cooling of the upper layers has brought down the ABL top.

To gain some insight into the TKE, the contribution of the various terms in the TKE budget equation, namely $\overline{w'u'} \frac{\partial u}{\partial Z}$, $\overline{w'v'} \frac{\partial v}{\partial Z}$ and $-(g/\bar{\theta}) \overline{w'\theta'}$ have been plotted in figures 6 (a–c), in which the variation of the computed sum of the above three terms has also been shown. It is seen that on all the days, the mechanical shear production terms are dominating, particularly the term $\overline{w'u'} \frac{\partial u}{\partial Z}$, which is mostly a negative term. This suggests that TKE is being produced due to wind shear. The buoyant production term $(g/\bar{\theta}) \overline{w'\theta'}$ representing the rate of working against buoyancy forces is negative on all the three days indicating that TKE production due to this is suppressed. The sum of these three terms represents the excess of TKE production over consumption. In this case, it should be noted that we have not considered the turbulent transport and pressure correlation terms in the TKE budget equation. These terms are thought to have significant contributions, at least in the surface layer (Wyngaard and Cote 1971). These terms have been included, however, in the second order model, which gives a direct estimate of the TKE. Thus, from figure 6(a), we find that on 19th June, there is a net production of TKE in the shaded zones in the figure, viz. between 50–90 m, 110–130 m and 150–200 m. In between these layers TKE is lost, but as

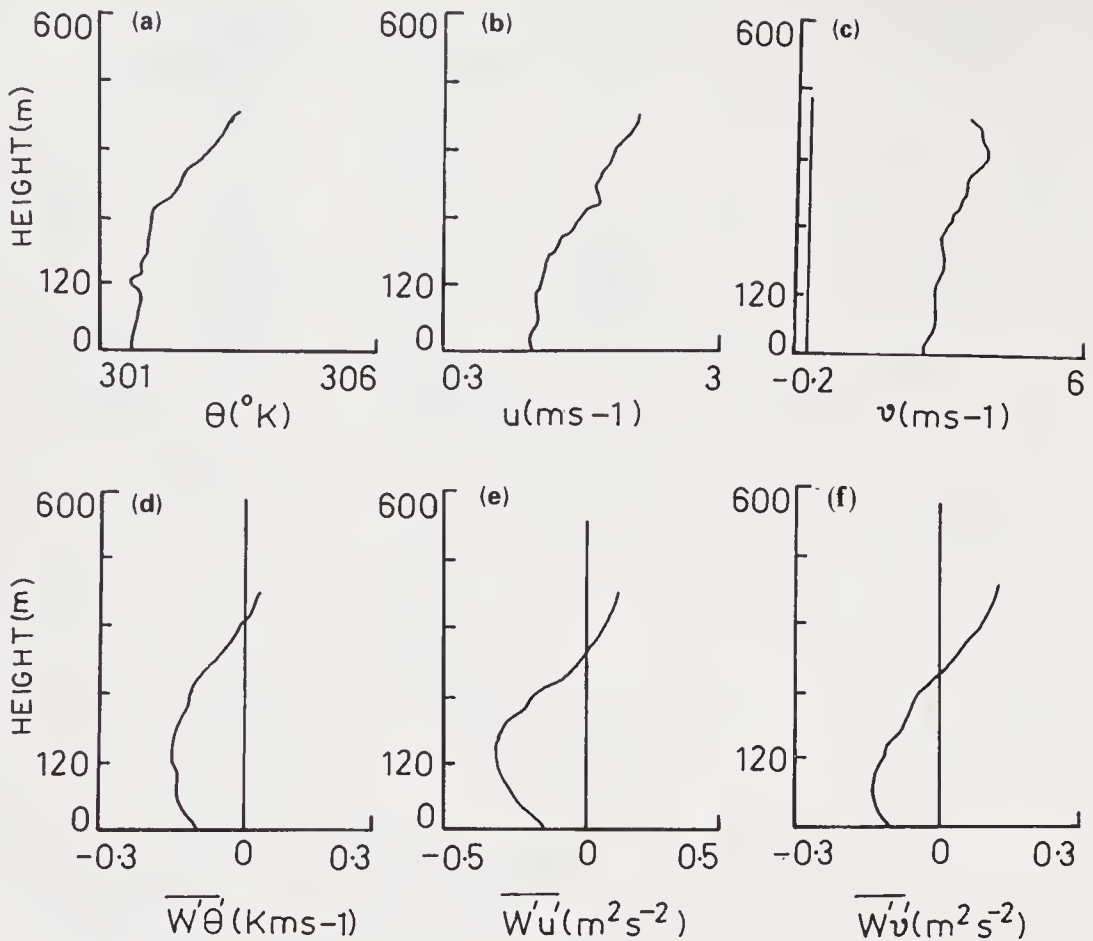


Figure 4. Same as in figure 3 but for 20th June, 1990.

seen from the figure the gain exceeds the loss. The build up of TKE between 110–130 m and above 160 m is quite significant on this day. At the lowest levels, gain and loss almost balance each other.

On 20th June, as may be observed from figure 6(b), a large build up of TKE occurs below 60 m, with significant gain between 40–60 m. A considerable amount of TKE seems to be lost above 140 m. On 21st June, as seen from figure 6(c), where we are dealing with a transition boundary layer, the TKE consumption always exceeds production, with significant losses below 60 m. It may be noted that as defined in the parameterization for turbulent fluxes (equation (2.3)), the potential for mixing is related to the excess of TKE production over consumption and dissipation. So, the shaded zones in figures 6(a) and 6(b) are zones of vigorous turbulent mixing. In contrast, on 21st June (figure 6c) the potential for mixing is quite low, particularly in the lower levels.

At this point, it would be useful to obtain some information regarding the turbulent eddies that are involved in the mixing process. The transport spectra and the mixing length are two important parameters in this connection. The transport spectra give an idea about the contribution of eddies of various sizes to the flux across any level. The mixing length at any level is a measure of the mean distance moved by the air parcels during the mixing process.

The contribution of the eddies ranging in size between 10–30 m, 40–100 m, 120–170 m and 180–230 m to the heat flux across different levels has been illustrated in

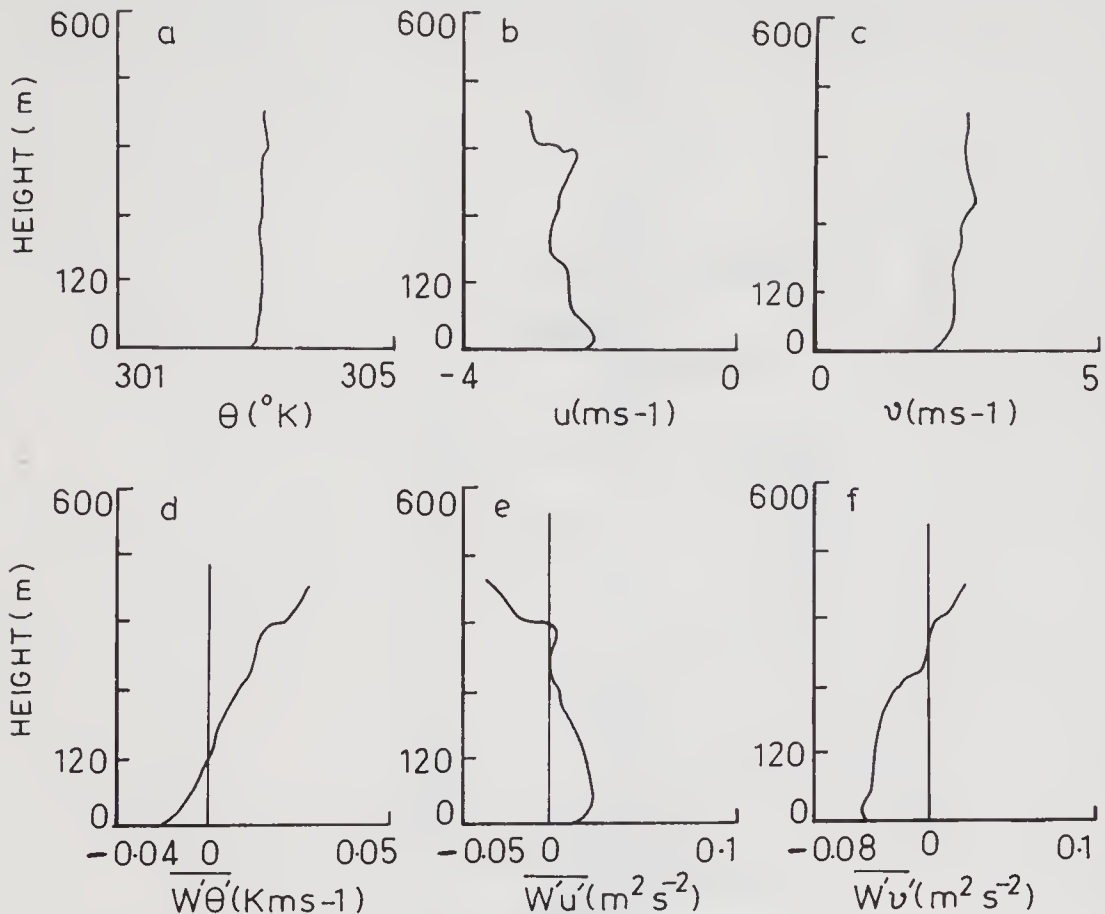


Figure 5. Same as in figure 3 but for 21st June, 1990.

figures 7(a–b), for 19th and 20th June respectively, In figure 7(c), the contribution to the heat flux by eddies ranging in sizes between 10–40 m, 50–70 m and 80–100 m has been shown for 21st June. Recalling that the heat fluxes (figures 3(d), 4(d) and 5(d)) are all negative at least up to the ABL top on all three days, we may conclude that all eddies being considered in figure 7(a–c) are transporting heat downwards.

The major contribution to the downward heat flux throughout the ABL comes from the 120–230 m eddies for 19th and 20th June. The largest contribution up to the level $1.1Z_i$ on both days is from the 180–230 m eddies. At this level, the contribution from the 120–170 m eddies begins to dominate. The contribution of the 180–230 m eddies remains nearly constant (but less than that from the 120–170 m eddies), between $0.9Z_i - 0.5Z_i$ on 19th June (figure 7a). On 20th June, as figure 7(b) indicates, the contribution of these eddies keeps on increasing till $0.8Z_i$, although this contribution is less than that of the 120–170 m eddies at these levels. Below $0.5Z_i$ ($0.8Z_i$) on 19th June (20th June), the contribution to the heat flux by the 180–230 m class of eddies becomes weaker but increases again below $0.4Z_i$ ($0.5Z_i$) where it once more exceeds the contribution from the 120–170 m class.

The 120–170 m eddies dominate between $0.9Z_i - 0.5Z_i$ ($1.04Z_i - 0.72Z_i$) on 19th June (20th June). The smaller eddies belonging to the 40–100 m class contribute less significantly than the above two classes all throughout the ABL on 19th June. On 20th June however, the contribution of the 40–100 m eddies follows a different pattern, showing increasing contributions at $1.4Z_i$ and again at $0.6Z_i$. Figure 7(c), for 21st June,

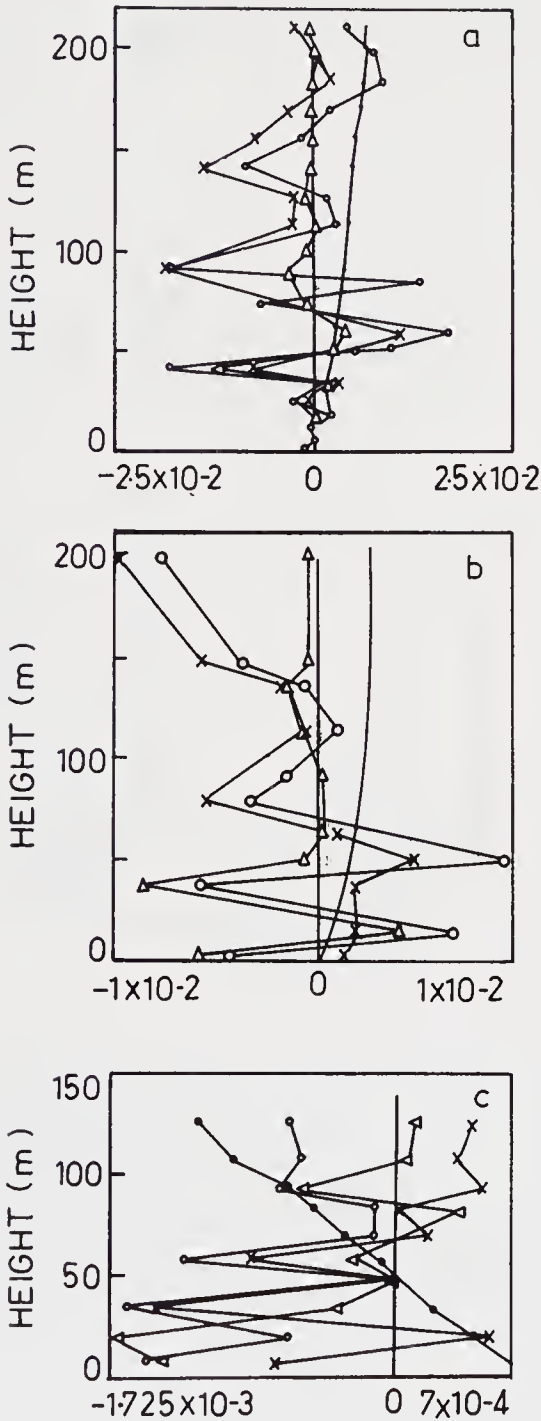


Figure 6. Turbulence kinetic energy budgets for: **a)** 19th June, **b)** 20th June and **c)** 21st June. ●—●—● buoyant production; ×—×—× mechanical shear production (zonal); △—△—△ mechanical shear production (meridional); ○—○—○ total of all terms.

reveals much the same pattern. However, on this day, the largest class of eddies, 80–100 m, contributed significantly to the heat flux as low as $0.2Z_i$. The major contribution (between $0.7Z_i - 0.4Z_i$) comes from the 50–70 m eddies on this day. Below this, all the eddies are seen to contribute to the heat flux with the 10–40 m eddies dominating below $0.25Z_i$. Thus only on 21st June, when we are dealing with a transition boundary layer in the late afternoon, we find that the smallest class of eddies contributes largely in the downward

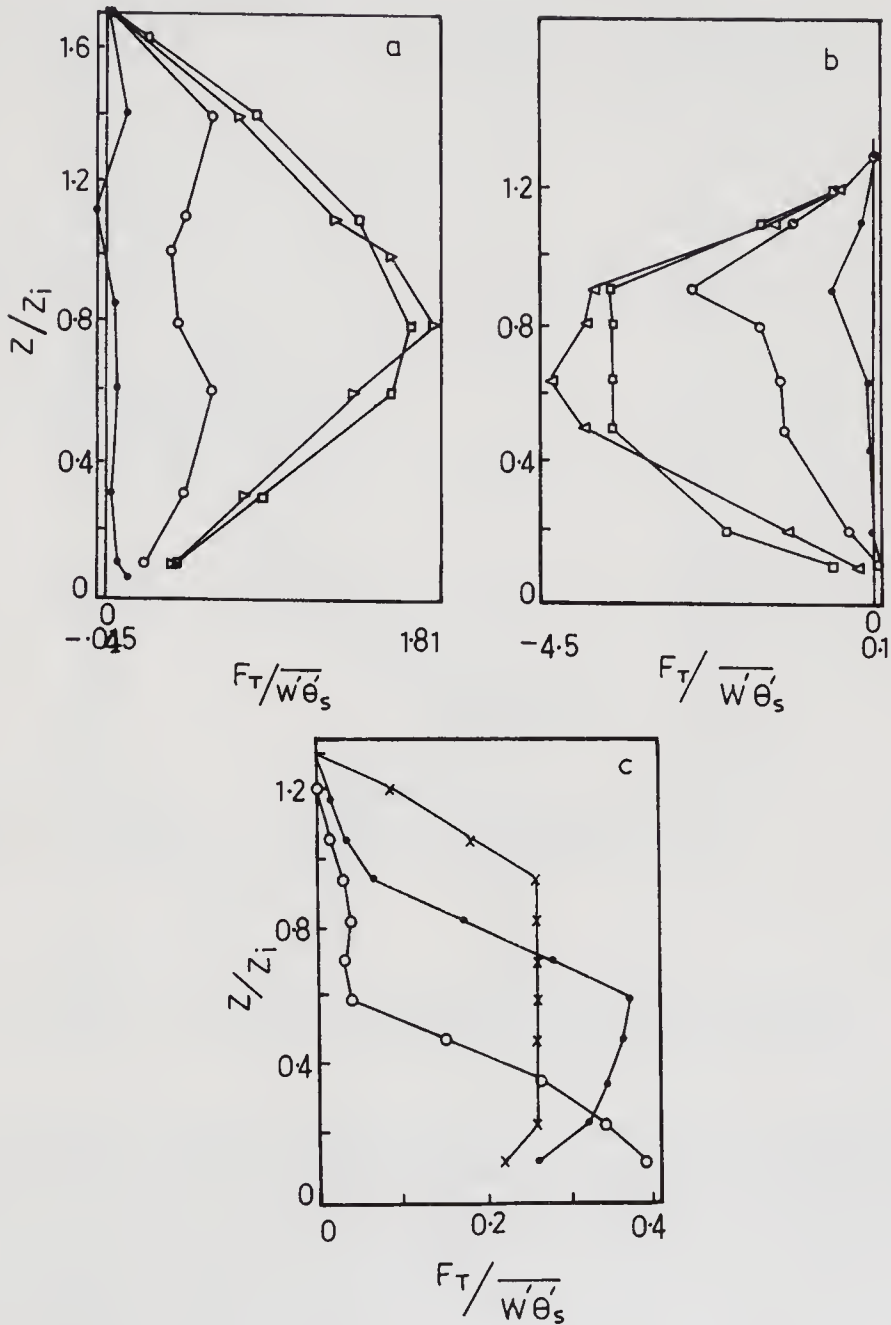


Figure 7. Contribution of turbulent eddies of various sizes to the heat flux across any level: **a)** 19th June, **b)** 20th June, **c)** 21st June. In **a)** and **b)**: ●—●—● 10–30 m, ○—○—○ 40–100 m, △—△—△ 120–170 m, □—□—□ 180–230 m. In **c)**: ○—○—○ 10–40 m, ●—●—● 50–70 m, ×—×—× 80–100 m.

heat transfer in the surface layer, whereas, in the early morning ABL's of 19th and 20th June, all eddy sizes considered, contribute in the surface layer.

We next consider the mixing length profiles for 19th – 20th June, illustrated in figure 8. A zone of vigorous mixing exists in the lowest 50 m of the ABL on both these days. This agrees with the earlier finding that the zone below 60 m is a zone of TKE production and vigorous mixing (figures 6a and b). Above this level, on 19th June, the vigour of mixing decreases around the 55 m level, which again corresponds to the zone of TKE consumption shown in figure 6(a). The largest values of the mixing length occur

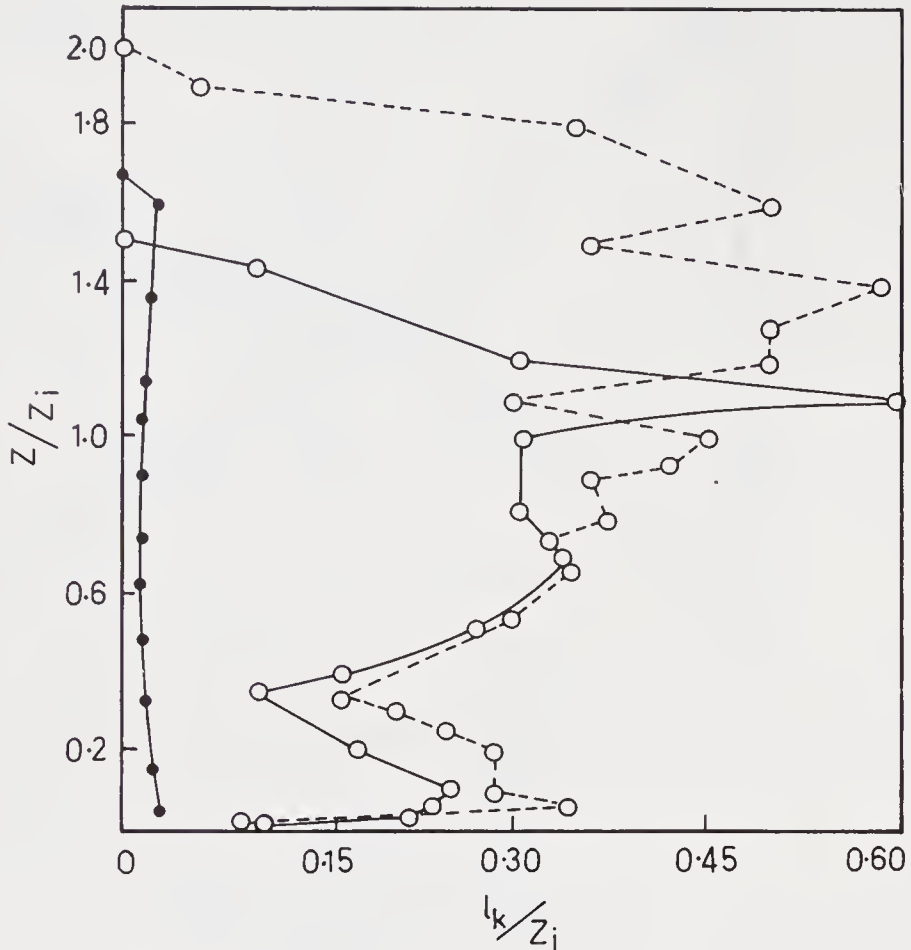


Figure 8. Total mixing length profiles for Kharagpur. $\circ-\circ-\circ$ 19th June, $\circ--\circ--\circ$ 20th June, $\bullet-\bullet-\bullet$ 21st June.

near the ABL tops on both the days. The mixing also appears to be more intense on 20th June than on 19th June. The mixing length profiles for 21st June, again display a different pattern. The amount of mixing is relatively more below 35 m although far less than that on 19th, 20th June, and increases again near the ABL top, after which it decreases steadily. In between, mixing is highly suppressed. This can perhaps be attributed to the TKE consumption exceeding production throughout the ABL on this day.

Finally, we have shown the one-dimensional anisotropy of turbulence in figures 9(a-c). We recall that on all three days, the lowest levels in the ABL had a very weak or near-neutral stratification with stable layers above. The transilient matrix obtained in this situation was symmetric, in contrast to the matrices obtained in convective situations. Consequently, partitioning of the mixing length into upward and downward components for each source-destination box, resulted in $l_j^\uparrow = l_j^\downarrow$ and $l_j^\downarrow = l_j^\uparrow$. Nevertheless, since l_j^\uparrow is not equal to l_j^\downarrow , the anisotropic structure of the turbulent eddies is highlighted.

Figures 9(a and b) reveal that for the early morning boundary layers on 19th and 20th June, the downward transport dominates the upward transport at all but the lowest levels. The maximum downward transport occurs from the level $0.9Z_i$ on 19th June, upward transport on that day being confined mostly to below $0.4Z_i$. On 20th June, downward transport is maximum from the $1.5Z_i$ level and the ABL top. Upward

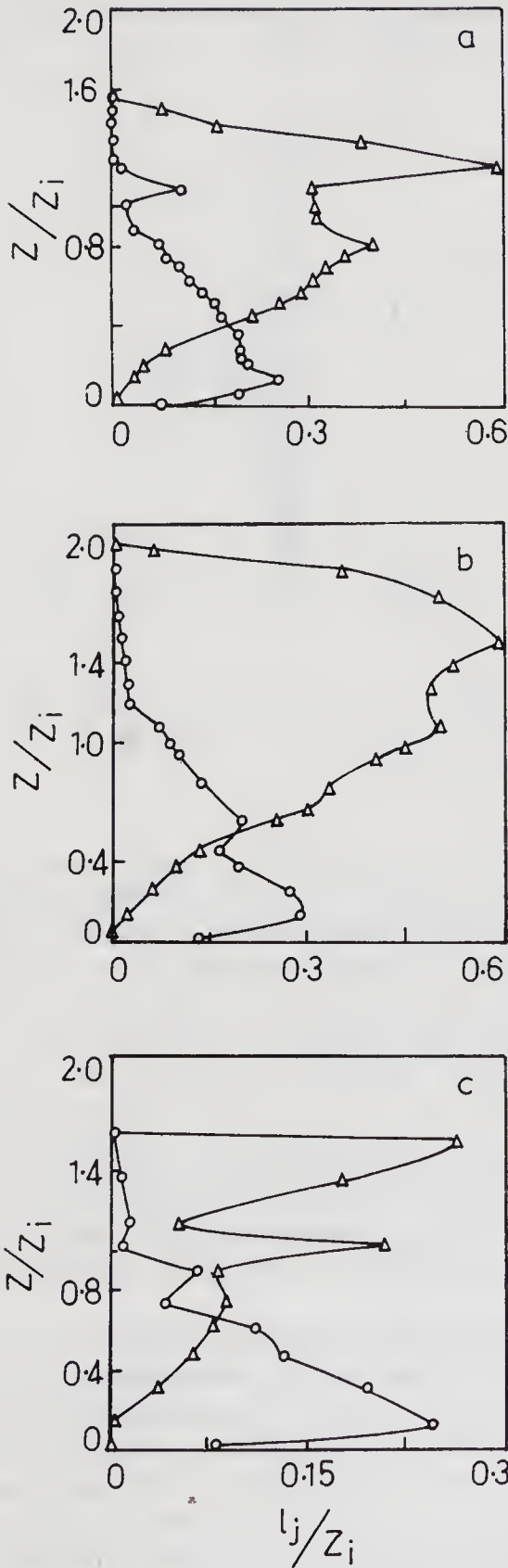


Figure 9. One-dimensional anisotropy of turbulent eddies over Kharagpur: a) 19th June, b) 20th June and c) 21st June. $\circ-\circ-\circ$ $l_j \uparrow$ $\triangle-\triangle-\triangle$ $l_j \downarrow$.

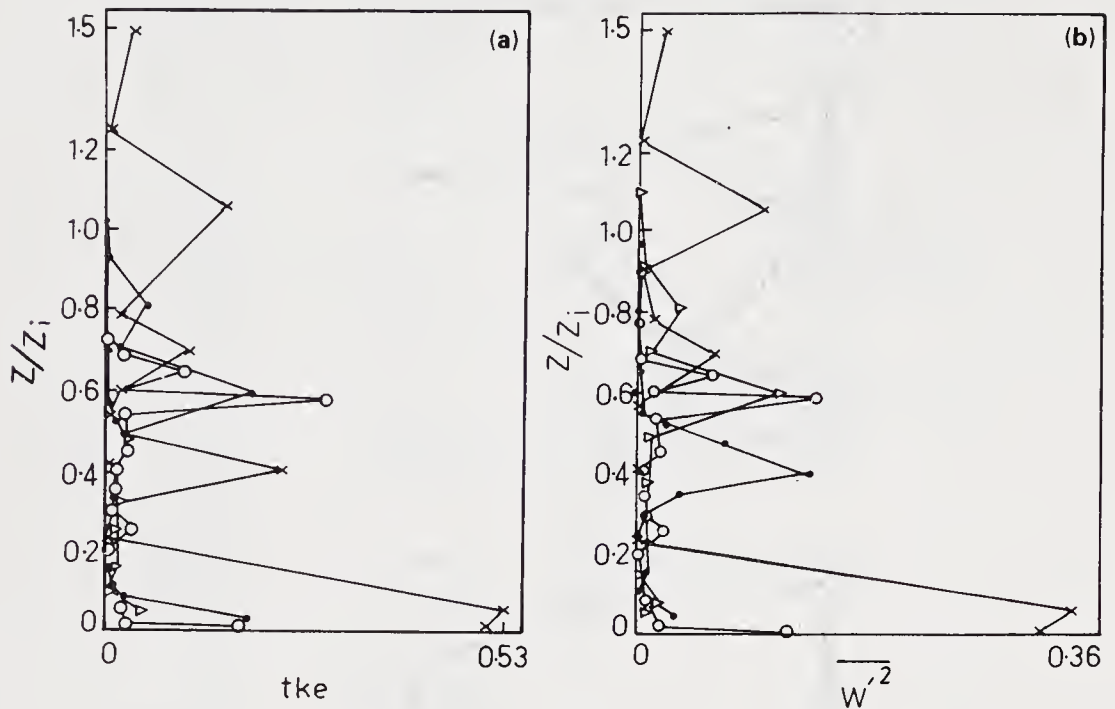


Figure 10. Outputs from the second order model. a) Turbulence kinetic energy and b) Turbulent vertical velocity variance. \circ — \circ — \circ 17th June, \bullet — \bullet — \bullet 18th June, \triangle — \triangle — \triangle 19th June, \times — \times — \times 21st June.

transport is quite strong for this day and exceeds the downward component below $0.23Z_i$, and equals it around $0.23Z_i - 0.27Z_i$. As figure 9(c) indicates, for the late afternoon transition boundary layer on 21st June, the upward transport dominates up to $0.73Z_i$, above which downward transport dominates between $1.6Z_i$ and the ABL top.

We now discuss some of the results obtained from the second order closure model. With the turbulence length scale Λ kept constant, the profiles of the TKE and turbulence vertical velocity variance $\overline{w'^2}$ obtained for 17th, 18th, 19th and 21st June, 1990 have been displayed in figures 10 (a and b) respectively. The most interesting feature observed here is the one-to-one correspondence of the TKE and $\overline{w'^2}$ profiles. In particular, the profiles for 17th, 18th and 21st June indicate distinct and separate zones of TKE and corresponding $\overline{w'^2}$ maxima. This indicates the existence of zones of turbulence, in other words, patchy turbulence, a common and well-known feature in stable boundary layers.

For 20th June, the second numerical experiment mentioned in §3 was conducted. Two model runs were made, one (experiment A) using prescribed inputs of heat and momentum, exactly similar to the ones provided in the transient model run for that day. In the second experiment (experiment B) a higher value of heat flux and lower momentum flux were used. The profile of the length scale Λ that agrees well with the mixing length profiles from the transient model has been plotted in figure 11. Turbulence is seen to be most vigorous at the lower levels, namely $0.14Z_i$ and $0.23Z_i$ for the experiments A and B respectively. Another turbulent zone occurs around $0.4Z_i$ (experiment A) and $0.63Z_i$ (experiment B). Above these levels, turbulence decreases to a minimum at the ABL top and increases above it. Comparison of figure 11 with figures 6(b) and 8 shows that the levels of turbulent activity below $0.5Z_i$ agree fairly

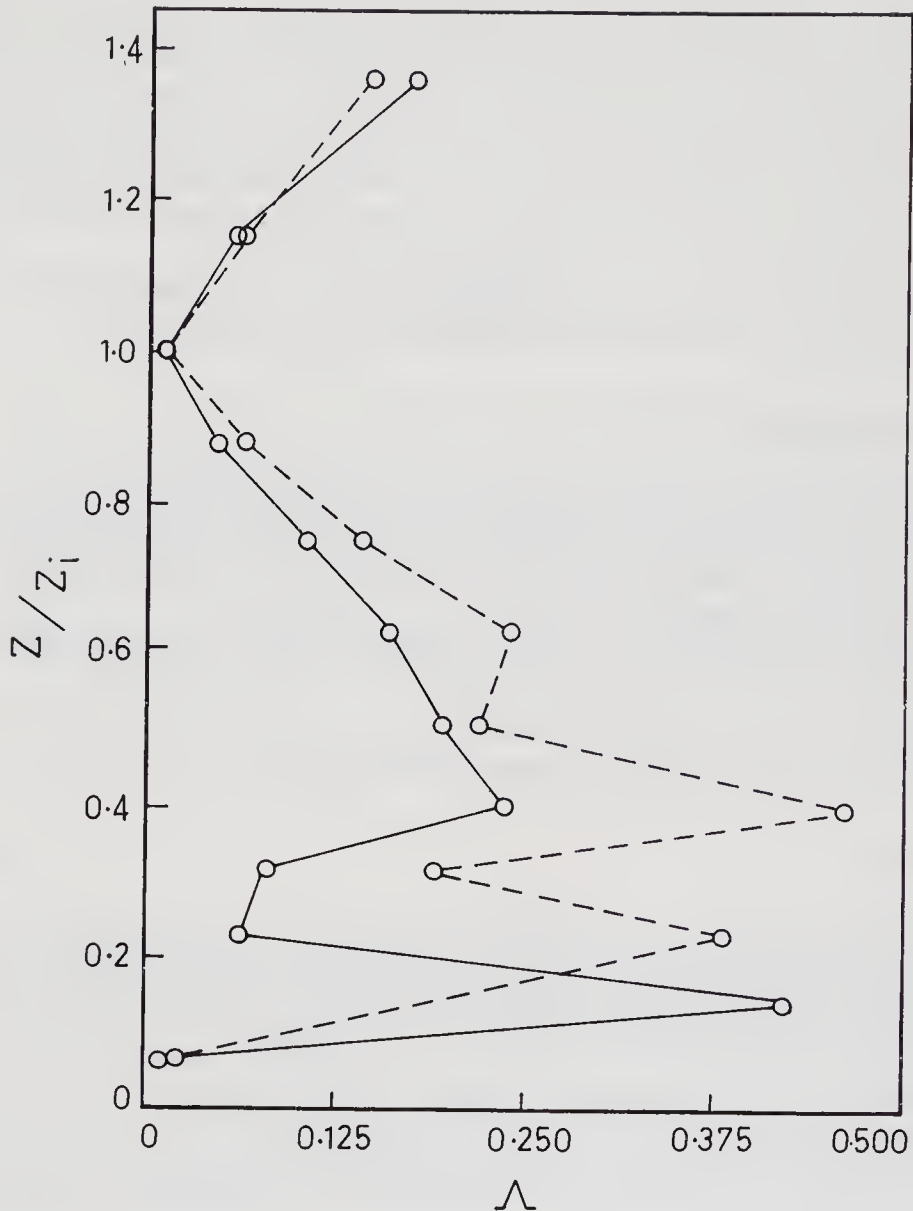


Figure 11. Profiles of the characteristic turbulent length scale Λ , obtained from the second order model for 20th June.

○—○—○ Experiment A: Prescribed heat flux:- .004 K m/s, drag coefficient $C_D = 0.0039$.

○--○--○ Experiment B: Prescribed heat flux:- .006 K m/s, drag coefficient $C_D = 0.0015$.

well. It is also interesting to note that at higher levels, the profile for the two experiments come close to each other whereas at lower levels, their difference is significant.

5. Conclusion

The case studies for 17th – 21st June, 1990 reveal certain interesting features as a result of this diagnostic study on the turbulent transport within the ABL. Using the transient model, the case studies for the early morning ABL's of 19th – 20th June indicate that distinct zones exist where TKE production exceeds consumption and thus support turbulent activity. In contrast, in the late-afternoon transition boundary layer (21st June),

turbulence is suppressed due to the TKE consumption exceeding production all throughout the ABL. The contribution to the downward heat flux by several classes of eddies indicates that, for 19th–20th June, eddies of all sizes between 40–230 m contribute up to and within the surface layer, while for 21st June, only the smallest eddies dominate within the surface layer. The early morning boundary layers are characterised by downward turbulent transport dominating over upward transport while for the late afternoon case, the reverse is true.

The results from the second order model provide diagnostic evidence of zones of patchy turbulence which is another significant upshot of this study.

Acknowledgement

The authors gratefully thank the Department of Science and Technology, Government of India for providing financial support. The help and suggestions given by Prof. D K Rakshit of Jadavpur University and Dr. K G Verneker of IITM, Pune, are gratefully acknowledged.

The authors also thank Prof. A Prabhu of IISc, Bangalore, and Dr. S Shivramakrishnan of IITM, Pune, for helpful discussions.

Finally we express our thanks to Prof. R Narasimha of IISc, Bangalore for his helpful criticisms regarding the improvement of the manuscript.

References

- Bhumralkar C M 1976 A survey of parameterization techniques for the planetary boundary layer in atmospheric circulation models. Report R-1653-ARPA JULY 1976. ARPA Order No. 189-1. 6P10 Information Processing Technique Office, Rand Corp. Santa Monica, CA 90406, 84 pp.
- Deardorff J W 1972 Numerical investigation of neutral and unstable planetary boundary layers. *J. Atmos. Sci.* **29** 91–115
- Deardorff J W 1974: Three dimensional numerical study of turbulence in an entraining mixed layer. *Boundary-Layer Meteorol.* **7** 199–226
- Donaldson C duP 1973 Construction of a dynamic model of the production of atmospheric turbulence and dispersal of atmospheric pollutants. Workshop on Micrometeorology: (ed) D A Haugen (AMS, Boston) pp. 313–392
- Hogstrom U 1990 Analysis of turbulence structure in the surface layer with a modified similarity formulation for near neutral conditions. *J. Atmos. Sci.* **47** 1949–1972
- Keller L V and Friedman A A 1924 Differentialgleichung fur die turbulente Bewegung einer Kompressiblen Flussigkeit. *Proc. 1st Int. Cong. Appl. Mech.*, Delft. pp. 345–405
- McBean G A (ed.) 1979 The Planetary Boundary Layer. WMO Technical Note No. 165, 201 pp.
- Neuwstadt F T M and Van Dop H (eds) 1984 Atmospheric Turbulence and Air Pollution Modelling (Dordrecht, Holland: D Reidel Publishing Company) 358 pp.
- Stull R B 1984 Transient turbulence theory, Part 1: The concept of eddy mixing across finite distances. *J. Atmos. Sci.* **41** 3351–3367
- Stull R B and Driedonks A G M 1987 Applications of the transient turbulence parameterization to atmospheric boundary layer simulations. *Boundary-Layer Meteorol.* **40** 209–239
- Stull R B 1988 An Introduction to Boundary Layer Meteorology (Dordrecht, Holland: Kluwer Academic Publishers) pp. 666
- Stull R B 1991 Static stability – An update. *Bull. Am. Meteorol. Soc.*, **72** 1521–1529
- Stull R B 1992 Review of transient turbulence theory and non-local mixing. *Boundary-Layer Meteorol.* **45**
- Wyngaard J C and Cote O R 1971 Budgets of turbulent kinetic energy and temperature variance in the atmospheric surface layer. *J. Atmos. Sci.* **28** 190–201
- Wyngaard J C and Brost R A 1984 Top-down and bottom-up diffusion of a scalar in the convective boundary layer. *J. Atmos. Sci.* **41** 102–112

MONTBLEX data archival centre

K G VERNEKAR and S S ARALIKATTI

Indian Institute of Tropical Meteorology, Pune 411 008, India

Abstract. A co-ordinated project Monsoon Trough Boundary Layer Experiment (MONTBLEX) to study the atmospheric boundary layer in the monsoon trough region was taken up during 1990. 30-m high instrumented towers were erected at Kharagpur, Banaras, Delhi and Jodhpur. Sophisticated equipment like Doppler sodar and Kytton were used at Kharagpur. Sodars were exposed at Calcutta, Delhi and Jodhpur. ORV *Sagarkanya* cruises were arranged in the Bay of Bengal. The India Meteorological Department set up new surface and radiation observatories and released special radio-sonde, pilot balloons. Using the above mentioned platforms, data were collected during April – September 1990 and after proper editing the entire data were archived at the Indian Institute of Tropical Meteorology, Pune. The DST-MONTBLEX data bank was started at IITM on 25th November 1991. The paper contains the details of this data.

Keywords. Data centre; MONTBLEX data; boundary layer data.

1. Introduction

The main aim of the co-ordinated project on Monsoon Trough Boundary Layer Experiment was to study the land-locked monsoon trough dynamics. The core measurements included the evaluation of surface fluxes at Kharagpur, Varanasi, New Delhi and Jodhpur using tower-based data. The large scale atmospheric parameters in the monsoon trough region were monitored by the India Meteorological Department and Indian Air Force. The ship observations near the head of the Bay of Bengal, a potential site for development of monsoon depressions, were arranged by the National Institute of Oceanography. Details of the observational programme can be seen in figure 1.

2. Special observations

2.1 Doppler sodar monostatic sodar observations

A Doppler sodar was operated by the Indian Institute of Tropical Meteorology, Pune at Kharagpur during April 28th – Sept. 15th, 1990. Monthwise number of observations are as follows.

Month	May	June	July	Aug.	Sept.
Duration in hours	97	206	124	336	99

Frequency of observations of Doppler sodar is as follows.

Hours per day	20	15–20	10–15	5–10	1–5
Number of days	2	11	34	33	13

Monostatic sodars, one each at Calcutta, Banaras, Delhi, Jodhpur, were operated during the MONTBLEX period.

2.2 *Kytoon observations*

A 2.3 m³ Kytoon was operated by the Indian Institute of Tropical Meteorology, Pune on 28 occasions. Though the Kytoon has the capability to reach 1500 m, the maximum height reached during the course of experimental phase was only 840 m. This constraint was due to high winds prevailing at Kharagpur.

2.3 *Minisonde observations*

Slow-rising minisondes were released by the Indian Institute of Tropical Meteorology to record temperature fluctuations in the boundary layer. During IOP about 7–8 minisondes were released per day. A total of 45 minisondes were released.

2.4 *Marine boundary layer observations*

The National Institute of Oceanography, operated its research vessel *Sagarkanya* during the months of Aug. – Sept. 1990 over Bay of Bengal. The ship was stationed at a fixed point 20°N–89°E for over fifteen days and routine marine observations were collected along with micrometeorological observations arranged by IITM, Pune. The routes of *Sagarkanya* are shown in figure 2.

3. **Data archival programme**

After successful completion of the Monsoon Trough Boundary Layer Experiment, it was decided that the vast data collected during the main campaign should be archived at one place, and accordingly the Department of Science and Technology sanctioned the proposal on archival of MONTBLEX data at the Indian Institute of Tropical Meteorology, Pune. All the project leaders who actively participated in the experiment were required to transfer their data to the data bank. The data bank became fully operational during February 1992.

3.1 *Data dissemination*

The data from instrumented towers are stored on cartridge tapes. Most of the remaining data are stored on floppies (1.2 MB, DSHD). A small amount of data is held in

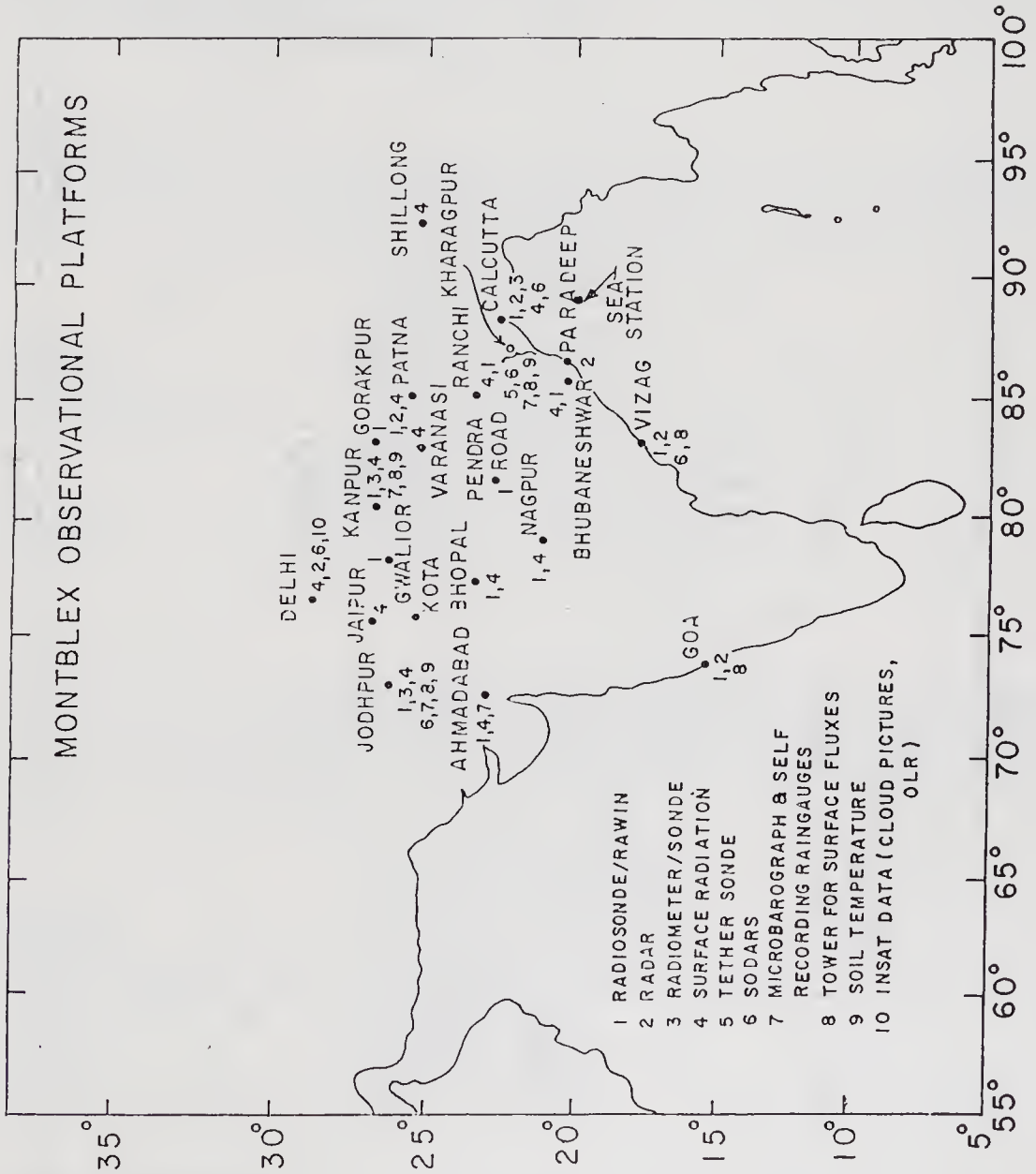


Figure 1.

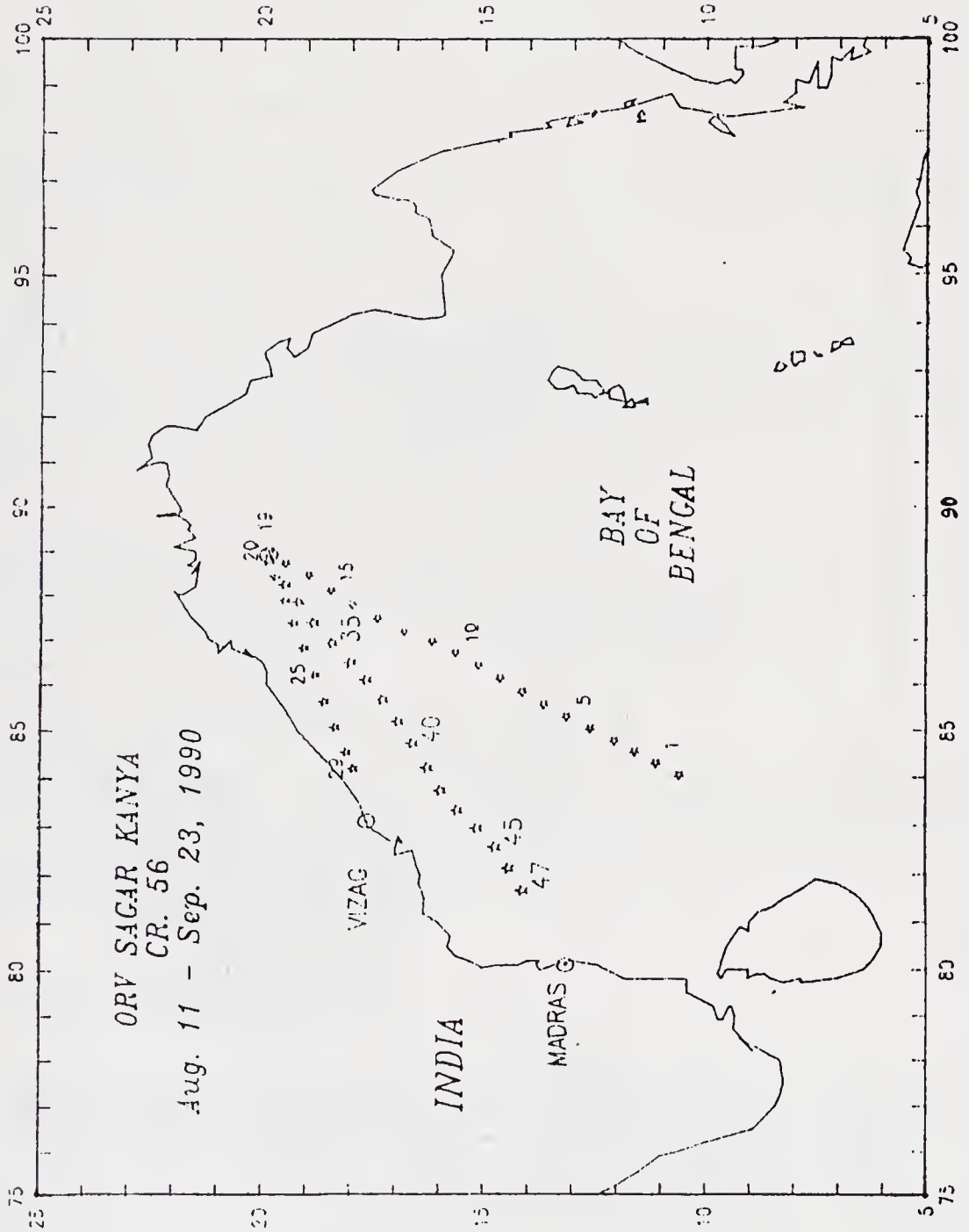


Figure 2. MONTBLEX-90 station locations; ★ - XBT Stations; ○ - Stationary position.

manuscript form only. Research scientists interested in availing the MONTBLEX data can obtain them by supplying the appropriate magnetic media. Two workshops on the results of the MONTBLEX experiment were held; first at IISc, Bangalore during 16th–17th January 1992 and the second at IITM, Pune during 16th–17th March 1993.

MONTBLEX data has been supplied to the following organizations: DST New Delhi, IITM Pune, IMD Pune, IISc Bangalore, BARC Bombay, NPOL Cochin, JNU New Delhi, ISI Calcutta, NCMRWF New Delhi, BHU Banaras, IAF New Delhi, IIT New Delhi and Jadhavpur University, Calcutta.

3.2 Details of the data

The bulk of the data is from instrumented towers. The entire slow and fast data are held on 65 cartridges of 40 MB each. The details of this data can be obtained from the authors. The details of other data archived at Data Centre are as follows.

Doppler sodar data

- 1) Scientist : K G Vernekar, IITM, Pune.
- 2) Data type : Doppler sodar data.
- 3) Brief description of the data : Wind components (u, v, w) at 30 m interval up to 1500 m. Reliability assessment for wind components.
- 4) Period : 15th May – 8th Sept. 1990.
- 5) Station : Kharagpur.

Details of the data

The entire data are available on 7 floppies of 1.2 MB capacity. Data contain information on all the three components of winds up to 1500 m at an interval of 30 m. Standard deviation of all the three components is also available. The data reliability for each component of wind is specified.

Monostatic sodar data

- 1) Scientist : S P Singal, NPL, New Delhi.
- 2) Data type : Monostatic sodar data.
- 3) Brief description of the data : Inversion height, types of inversions and thermals.
- 4) Period : 30th May – 30th Aug. 1990.
- 5) Station : Jodhpur.

Details of the data

The quantized data are available on one (360 KB) floppy. The fascimile records are available on 10 pages.

IITM – Sagarkanya data

- 1) Scientist : K G Vernekar, IITM, Pune.
- 2) Data type : Ship tower data.
- 3) Brief description : Wind speed, temperature, at two levels

- of the data : and sea surface temperature (SST).
- 4) Period : 11th Aug. – 22nd Sept. 1990.
- 5) Stations : 48 stations in Bay of Bengal.

Details of the data

The data are available on 13 floppies (360 KB each) for wind speeds and temperatures at two levels (bow level and 1.65 m above). Reliability of the data is poor.

Kytoon data

- 1) Scientist : K G Vernekar, IITM, Pune.
- 2) Data type : Kytoon data.
- 3) Brief description of the data : Wind speed, direction, dry bulb temperature, wet bulb temperature and mixing ratio profiles.
- 4) Period : 22nd May – 28th June 1990.
- 5) Station : Kharagpur.

Details of the data

In all, 26 kytoon flights were conducted at Kharagpur. The data contain profiles of dry bulb temperature, wet bulb temperature, wind speed, wind direction, relative humidity and mixing ratio. The printed data are available on 100 pages (120 columns, 60 lines/page).

Minisonde data

- 1) Scientist : K G Vernekar, IITM, Pune.
- 2) Data type : Minisonde data.
- 3) Brief description of the data : Temperature profile data.
- 4) Period : 26th May – 12th July 1990.
- 5) Station : Kharagpur.

Details of the data

The data contain profiles of 46 minisonde flights. Four to six sondes were released per day during IOP periods. As there was no height sensor, a constant ascent rate was assumed during day time. The printed data are available on 21 pages.

NIO – Sagarkanya data

- 1) Scientist : Panakkala Rao, NIO, Goa.
- 2) Data type : Oceanic data and surface data.
- 3) Brief description of the data : Conductivity, salinity, surface meteorological data, SST data and upper air data.
- 4) Period : 11th Aug. – 22nd Sept. 1990.
- 5) Station : Over Bay of Bengal.

Details of the data

- 1) Conductivity, temperature and depth (CTD) up to 1000 m.
- 2) Salinity, temperature and depth (STD) up to 300 m.
- 3) Surface meteorological observations.
- 4) Upper air observation at synoptic hours in August 1990.

The data are available on 2 floppies (360 KB each).

Tower data

- 1) Scientist : A Prabhu, IISc, Bangalore.
- 2) Data type : 30m tower data at 6 levels
- 3) Brief description of the data : Tower data at 1, 2, 4, 8, 15, and 30 m levels.
- 4) Period : Mid May – mid Sept. 1990.
- 5) Stations : Kharagpur, Varanasi, Jodhpur and Delhi.

Details of the data

Tower data at 1, 2, 4, 8, 15 and 30 m on wind speed, wind direction, dry temperature (slow response), dry temperature (rapid response), wet bulb temperature are recorded. Data from Gill propeller, soil temperature at 10, 20, 60 cm below the surface and sonic anemometer (at 8 m at Kharagpur, 4 m at Jodhpur and Varanasi) are also recorded. The tower data for Kharagpur, Varanasi, Jodhpur and Delhi stations are available on 65 cartridges (40 MB capacity).

RS/RW low level, pilot balloon and surface data (IMD)

- 1) Scientist : S K Srivastava, IMD, New Delhi.
- 2) Data type : Surface data.
- 3) Description : All elements covered under surface data.
- 4) Period : 25th May – 15th Sept. 1990.
- 5) Stations : Stations covered under MONTBLEX area.

Details of the data

	Calcutta	Bhubaneshwar	Ranchi	Delhi	Jodhpur
Total observations	116	139	109	82	79
Routine	65	78	55	42	44
Low level sondes	51	61	54	40	35

Pilot balloon data for Gaya, Jamshedpur, Raipur, Bhubaneshwar, Gopalpur, Jharsuguda, Balasore and Panagarh along with surface data are available. This data from India Meteorological Department are available in 7 bound volumes and also available on 1 floppy (1.2 MB).

Indian Air Force data

- 1) Scientist : N. Natarajan.
- 2) Brief description of the data : Air-borne meteorological parameters and surface observations.

- 3) Period : 1st May – 15th Sept. 1990.
- 4) Stations : Bhatinda, Kalaikunda, Gwalior, Bareilly, Hindon, Bombrauli, Agra, Lucknow, Jodhpur, Gorakhpur, Suratgarh and Kanpur.

Details of the data

The following data are available: 1) The take-off time, 2) time of observations, 3) station co-ordinates, 4) height above mean sea level, 5) wind speed and direction, 6) temperature, 7) cloud observations. Pilot balloon observations and surface observations for a few stations are also available. The data are recorded on 5 floppies (1.2 MB).

Monostatic sodar data

- 1) Scientist : J Das.
- 2) Type of data : Monostatic sodar data.
- 3) Brief description of the data : Inversion heights, types of inversions and thermals.
- 4) Period : 28th May – 3rd Sept. 1990.
- 5) Station : Varanasi.

Details of the data

The complete quantized data are on 50 typed pages.

SUBJECT INDEX

- Acoustic
 Study of horizontal scales of motion observed over Kharagpur during MONTBLEX-1990 185
- Atmosphere
 Atmospheric boundary layer studies at Jodhpur during MONTBLEX using sodar and tower 141
- Atmospheric boundary layer
 Genesis of the monsoon trough boundary layer experiment (MONTBLEX) 1
 Thermal and wind structure of the monsoon trough boundary layer 153
 Wind profiles in the boundary layer over Kharagpur associated with synoptic scale systems 199
 Understanding the turbulent structure of the atmospheric boundary layer: A diagnostic approach 393
- Atmospheric sensing
 Planning MONTBLEX – An overview 33
- Atmospheric surface layer
 MONTBLEX tower observations: Instrumentation, data acquisition and data quality 97
- Back-scatter intensity
 Some observations from the data taken in and around Kharagpur during the onset of the monsoon, 1990 209
- Backscatter
 Study of horizontal scales of motion observed over Kharagpur during MONTBLEX-1990 185
- Bay of Bengal
 Variability of the oceanic boundary layer characteristics in the northern Bay of Bengal during MONTBLEX-90 223
- Boundary layer
 Atmospheric boundary layer studies at Jodhpur during MONTBLEX using sodar and tower 141
 Some observations from the data taken in and around Kharagpur during the onset of the monsoon, 1990 209
 Roughness length and drag coefficient at two MONTBLEX-90 tower stations 245
- Boundary layer data
 MONTBLEX data archival centre 411
- Bowen ratio
 Fluxes of heat and momentum over sea surface during the passage of a depression in the north Bay of Bengal 329
- Bulk aerodynamic method
 Estimation of drag coefficient over the western desert sector of the Indian summer monsoon trough 261
- Convective instability
 Some observations from the data taken in and around Kharagpur during the onset of the monsoon, 1990 209
- Cyclone detection radars
 Synoptic meteorological observations and weather conditions during MONTBLEX-90 51
- Data centre
 MONTBLEX data archival centre 411
- Data quality
 MONTBLEX tower observations: Instrumentation, data acquisition and data quality 97
- Depression
 Fluxes of heat and momentum over sea surface during the passage of a depression in the north Bay of Bengal 329
- Display memory equation constants
 The mean and turbulence structure simulation of the monsoon trough boundary layer using a one-dimensional model with $e-l$ and $e-\varepsilon$ closures 359
- Dissipation equation constants
 The mean and turbulence structure simulation of the monsoon trough boundary layer using a one-dimensional model with $e-l$ and $e-\varepsilon$ closures 359
- Diurnal variation
 Estimation of surface temperature from MONTBLEX data 125
- Doppler
 Study of horizontal scales of motion observed over Kharagpur during MONTBLEX-1990 185
- Drag coefficient
 Roughness length and drag coefficient at two MONTBLEX-90 tower stations 245
 Estimation of drag coefficient over the western desert sector of the Indian summer monsoon trough 261
 An analysis of MONTBLEX data on heat and momentum flux at Jodhpur 277

- Eddy correlation method
 Estimation of drag coefficient over the western desert sector of the Indian summer monsoon trough 261
- Energy balance
 Planetary boundary layer over monsoon trough region in a high resolution primitive equation model 339
- Exchange coefficient
 Fluxes of heat and momentum over sea surface during the passage of a depression in the north Bay of Bengal 329
- Exchange coefficient of heat
 An analysis of MONTBLEX data on heat and momentum flux at Jodhpur 277
- Flux
 Fluxes of heat and momentum over sea surface during the passage of a depression in the north Bay of Bengal 329
- Free convection
 An analysis of MONTBLEX data on heat and momentum flux at Jodhpur 277
- Heat budget
 Variability of the oceanic boundary layer characteristics in the northern Bay of Bengal during MONTBLEX-90 223
- Heat content
 Variability of the oceanic boundary layer characteristics in the northern Bay of Bengal during MONTBLEX-90 223
- INSAT
 Synoptic meteorological observations and weather conditions during MONTBLEX-90 51
- Intensive observation periods
 Synoptic meteorological observations and weather conditions during MONTBLEX-90 51
- Inversion height
 Some observations from the data taken in and around Kharagpur during the onset of the monsoon, 1990 209
 Estimation of surface heat flux and inversion height with a Doppler acoustic sounder 293
- Local closure
 Understanding the turbulent structure of the atmospheric boundary layer: A diagnostic approach 393
- Low level cloud-base height
 Some observations from the data taken in and around Kharagpur during the onset of the monsoon, 1990 209
- MONTBLEX
 Genesis of the monsoon trough boundary layer experiment (MONTBLEX) 1
- Planning MONTBLEX – An overview 33
- Synoptic meteorological observations and weather conditions during MONTBLEX-90 51
- Statistical analysis of the position of the monsoon trough 83
- Atmospheric boundary layer studies at Jodhpur during MONTBLEX using sodar and tower 141
- Study of horizontal scales of motion observed over Kharagpur during MONTBLEX-1990 185
- MONTBLEX data
 MONTBLEX data archival centre 411
- MONTBLEX-90
 Variability of the oceanic boundary layer characteristics in the northern Bay of Bengal during MONTBLEX-90 223
- Micrometeorological
 Study of horizontal scales of motion observed over Kharagpur during MONTBLEX-1990 185
- Micrometeorological towers
 Planning MONTBLEX – An overview 33
- Mixing ratio
 A study of turbulent characteristics of atmospheric boundary layer over monsoon trough region using Kytton and Doppler sodar 171
- Momentum flux
 An analysis of MONTBLEX data on heat and momentum flux at Jodhpur 277
- Momentum fluxes
 Estimation of drag coefficient over the western desert sector of the Indian summer monsoon trough 261
- Monsoon
 Study of horizontal scales of motion observed over Kharagpur during MONTBLEX-1990 185
 Fluxes of heat and momentum over sea surface during the passage of a depression in the north Bay of Bengal 329
- Monsoon trough
 Genesis of the monsoon trough boundary layer experiment (MONTBLEX) 1
 Planning MONTBLEX – An overview 33
- Monsoon trough
 Statistical analysis of the position of the monsoon trough 83
 Atmospheric boundary layer studies at Jodhpur during MONTBLEX using sodar and tower 141
 Roughness length and drag coefficient at two MONTBLEX-90 tower stations 245
 Planetary boundary layer over monsoon trough region in a high resolution primitive equation model 339
- Monsoon trough boundary layers
 The mean and turbulence structure simulation of the monsoon trough boundary layer using a one-dimensional model with $e-l$ and $e-e$ closures 359

- Monsoons
 Thermal and wind structure of the monsoon trough boundary layer 153
- Non-local closure
 Understanding the turbulent structure of the atmospheric boundary layer: A diagnostic approach 393
- Numerical simulation
 The mean and turbulence structure simulation of the monsoon trough boundary layer using a one-dimensional model with $e-l$ and $e-\varepsilon$ closures 359
- Observational programme
 Genesis of the monsoon trough boundary layer experiment (MONTBLEX) 1
- Ocean boundary layer
 Variability of the oceanic boundary layer characteristics in the northern Bay of Bengal during MONTBLEX-90 223
- Phase and amplitude of temperature waves
 Estimation of surface temperature from MONTBLEX data 125
- Pilot balloon
 Synoptic meteorological observations and weather conditions during MONTBLEX-90 51
- Planetary boundary layer
 Planetary boundary layer over monsoon trough region in a high resolution primitive equation model 339
- Radiometersonde
 Synoptic meteorological observations and weather conditions during MONTBLEX-90 51
- Radiosonde/radiowind
 Synoptic meteorological observations and weather conditions during MONTBLEX-90 51
- Rainfall
 Atmospheric boundary layer studies at Jodhpur during MONTBLEX using sodar and tower 141
- Range
 Study of horizontal scales of motion observed over Kharagpur during MONTBLEX-1990 185
- Range-bin
 Study of horizontal scales of motion observed over Kharagpur during MONTBLEX-1990 185
- Roughness length
 Roughness length and drag coefficient at two MONTBLEX-90 tower stations 245
- Sea surface
 Fluxes of heat and momentum over sea surface during the passage of a depression in the north Bay of Bengal 329
- Sensible heat flux
 An analysis of MONTBLEX data on heat and momentum flux at Jodhpur 277
- Atmospheric surface layer parameters during different phases of monsoon over Varanasi from MONTBLEX-90 313
- Sensors
 MONTBLEX tower observations: Instrumentation, data acquisition and data quality 97
- Sodar
 Atmospheric boundary layer studies at Jodhpur during MONTBLEX using sodar and tower 141
 Study of horizontal scales of motion observed over Kharagpur during MONTBLEX-1990 185
 Estimation of surface heat flux and inversion height with a Doppler acoustic sounder 293
- Soil and surface temperature
 Estimation of surface temperature from MONTBLEX data 125
- Southwest monsoon
 Variability of the oceanic boundary layer characteristics in the northern Bay of Bengal during MONTBLEX-90 223
- Spectrum
 Statistical analysis of the position of the monsoon trough 83
- Statistics
 Statistical analysis of the position of the monsoon trough 83
- Storm detection radars
 Synoptic meteorological observations and weather conditions during MONTBLEX-90 51
- Surface layer
 Atmospheric surface layer parameters during different phases of monsoon over Varanasi from MONTBLEX-90 313
- Surface parameters
 Some observations from the data taken in and around Kharagpur during the onset of the monsoon, 1990 209
- Surface sensible heat flux
 Estimation of surface heat flux and inversion height with a Doppler acoustic sounder 293
- Synoptic systems
 Wind profiles in the boundary layer over Kharagpur associated with synoptic scale systems 199
- TKE
 Atmospheric surface layer parameters during different phases of monsoon over Varanasi from MONTBLEX-90 313
- Temperature structure parameter (C_T^2)
 A study of turbulent characteristics of atmospheric boundary layer over monsoon trough region using Kytoon and Doppler sodar 171
- Thermal diffusivity
 Estimation of surface temperature from MONTBLEX data 125
- Thermal structure
 Atmospheric boundary layer studies at Jodhpur during MONTBLEX using sodar and tower 141

- Thermodynamic structure
 Thermal and wind structure of the monsoon trough boundary layer 153
- Tower instrumentation
 MONTBLEX tower observations: Instrumentation, data acquisition and data quality 97
- Turbulence closure
 The mean and turbulence structure simulation of the monsoon trough boundary layer using a one-dimensional model with $e-l$ and $e-\varepsilon$ closures 359
- Turbulence structure
 Understanding the turbulent structure of the atmospheric boundary layer: A diagnostic approach 393
- Turbulent dissipation (ε)
 A study of turbulent characteristics of atmospheric boundary layer over monsoon trough region using Kytoon and Doppler sodar 171
- Turbulent kinetic energy
 Planetary boundary layer over monsoon trough region in a high resolution primitive equation model 339
- Velocity structure parameter (C_v^2)
 A study of turbulent characteristics of atmospheric boundary layer over monsoon trough region using Kytoon and Doppler sodar 171
- Vertical velocity variance
 Estimation of surface heat flux and inversion height with a Doppler acoustic sounder 293
- Veering
 Wind profiles in the boundary layer over Kharagpur associated with synoptic scale systems 199
- Warm core eddy
 Variability of the oceanic boundary layer characteristics in the northern Bay of Bengal during MONTBLEX-90 223
- Wind profile
 Wind profiles in the boundary layer over Kharagpur associated with synoptic scale systems 199

Journals Published by the Academy

Sl No.	Name of Journal	ISSN No.	Vol. No. (1997)	No. of issues	No. of pages (app.)	Annual subscription rate	
						India Rs.	Abroad US \$
1.	<i>Pramana – J. Phys.</i>	0304-4289	48,49	12	1200	200	200
2.	<i>Journal of Astrophysics and Astronomy</i>	0250-6335	18	4	400	150	100
3.	<i>Proceedings (Mathematical Sciences)</i>	0253-4142	107	4	400	150	100
4.	<i>Proceedings (Earth and Planetary Sciences)</i>	0253-4126	106	4	400	150	100
5.	<i>Proceedings (Chemical Sciences)</i>	0253-4134	109	6	600	150	150
6.	<i>Bulletin of Materials Science</i>	0250-4707	20	6	600	150	150
7.	<i>Sadhana (Engg. Sci)</i>	0256-2499	22	6	600	150	100
8.	<i>Journal of Biosciences</i>	0250-5991	22	4	500	150	100
9.	<i>Journal of Genetics</i>	0022-1333	76	3	400	150	100
10.	<i>Resonance – Journal of Science Education</i>	0971-8044	2	12	1200	400	100*
11.	<i>Current Science</i> (fortnightly)	0011-3891	72,73	24	1500	350 [†]	200

* *Resonance*: US \$ 50 for third world countries.

[†] *Current Science*: Rs. 700 for industries & commercial establishments.